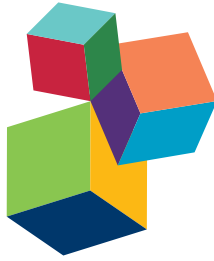




# DEVELOPMENT OF MICROBIAL ECOLOGICAL THEORY: STABILITY, PLASTICITY, AND EVOLUTION OF MICROBIAL ECOSYSTEMS

EDITED BY : Shin Haruta, Yasuhisa Saito and Hiroyuki Futamata  
PUBLISHED IN : *Frontiers in Microbiology*





# frontiers

## Frontiers Copyright Statement

© Copyright 2007-2017 Frontiers Media SA. All rights reserved.

All content included on this site, such as text, graphics, logos, button icons, images, video/audio clips, downloads, data compilations and software, is the property of or is licensed to Frontiers Media SA ("Frontiers") or its licensees and/or subcontractors. The copyright in the text of individual articles is the property of their respective authors, subject to a license granted to Frontiers.

The compilation of articles constituting this e-book, wherever published, as well as the compilation of all other content on this site, is the exclusive property of Frontiers. For the conditions for downloading and copying of e-books from Frontiers' website, please see the Terms for Website Use. If purchasing Frontiers e-books from other websites or sources, the conditions of the website concerned apply.

Images and graphics not forming part of user-contributed materials may not be downloaded or copied without permission.

Individual articles may be downloaded and reproduced in accordance with the principles of the CC-BY licence subject to any copyright or other notices. They may not be re-sold as an e-book.

As author or other contributor you grant a CC-BY licence to others to reproduce your articles, including any graphics and third-party materials supplied by you, in accordance with the Conditions for Website Use and subject to any copyright notices which you include in connection with your articles and materials.

All copyright, and all rights therein, are protected by national and international copyright laws.

The above represents a summary only. For the full conditions see the Conditions for Authors and the Conditions for Website Use.

ISSN 1664-8714

ISBN 978-2-88945-169-2

DOI 10.3389/978-2-88945-169-2

## About Frontiers

Frontiers is more than just an open-access publisher of scholarly articles: it is a pioneering approach to the world of academia, radically improving the way scholarly research is managed. The grand vision of Frontiers is a world where all people have an equal opportunity to seek, share and generate knowledge. Frontiers provides immediate and permanent online open access to all its publications, but this alone is not enough to realize our grand goals.

## Frontiers Journal Series

The Frontiers Journal Series is a multi-tier and interdisciplinary set of open-access, online journals, promising a paradigm shift from the current review, selection and dissemination processes in academic publishing. All Frontiers journals are driven by researchers for researchers; therefore, they constitute a service to the scholarly community. At the same time, the Frontiers Journal Series operates on a revolutionary invention, the tiered publishing system, initially addressing specific communities of scholars, and gradually climbing up to broader public understanding, thus serving the interests of the lay society, too.

## Dedication to Quality

Each Frontiers article is a landmark of the highest quality, thanks to genuinely collaborative interactions between authors and review editors, who include some of the world's best academicians. Research must be certified by peers before entering a stream of knowledge that may eventually reach the public - and shape society; therefore, Frontiers only applies the most rigorous and unbiased reviews.

Frontiers revolutionizes research publishing by freely delivering the most outstanding research, evaluated with no bias from both the academic and social point of view.

By applying the most advanced information technologies, Frontiers is catapulting scholarly publishing into a new generation.

## What are Frontiers Research Topics?

Frontiers Research Topics are very popular trademarks of the Frontiers Journals Series: they are collections of at least ten articles, all centered on a particular subject. With their unique mix of varied contributions from Original Research to Review Articles, Frontiers Research Topics unify the most influential researchers, the latest key findings and historical advances in a hot research area! Find out more on how to host your own Frontiers Research Topic or contribute to one as an author by contacting the Frontiers Editorial Office: [researchtopics@frontiersin.org](mailto:researchtopics@frontiersin.org)

# DEVELOPMENT OF MICROBIAL ECOLOGICAL THEORY: STABILITY, PLASTICITY, AND EVOLUTION OF MICROBIAL ECOSYSTEMS

Topic Editors:

**Shin Haruta**, Tokyo Metropolitan University, Japan

**Yasuhisa Saito**, Shimane University, Japan

**Hiroyuki Futamata**, Shizuoka University, Japan



As Antoni Gaudi skillfully employed beautiful mosaic tiles to represent nature and creatures, we are trying to assemble a variety of research articles into a comprehensive picture representing general rules of microbial ecosystems.

Photo credit: Sawa Arai & Miwa Arai

“How can we develop microbial ecological theory?” The development of microbial ecological theory has a long way to reach its goal. Advances in microbial ecological techniques provide novel insights into microbial ecosystems. Articles in this book are challenging to determine the central and general tenets of the ecological theory that describes the features of microbial ecosystems. Their achievements expand the frontiers of current microbial ecology and propose the next step. Assemblage of these diverse articles hopefully helps to go on this long journey with many avenues for advancement of microbial ecology.

**Citation:** Haruta, S., Saito, Y., Futamata, H., eds. (2017). Development of Microbial Ecological Theory: Stability, Plasticity, and Evolution of Microbial Ecosystems. Lausanne: Frontiers Media. doi: 10.3389/978-2-88945-169-2

# Table of Contents

- 05 Editorial: Development of Microbial Ecological Theory: Stability, Plasticity, and Evolution of Microbial Ecosystems**  
Shin Haruta, Yasuhisa Saito and Hiroyuki Futamata
- Extensive characterization of microbial ecosystems**
- 07 Dynamic Transition of Chemolithotrophic Sulfur-Oxidizing Bacteria in Response to Amendment with Nitrate in Deposited Marine Sediments**  
Tomo Aoyagi, Makoto Kimura, Namiha Yamada, Ronald R. Navarro, Hideomi Itoh, Atsushi Ogata, Akiyoshi Sakoda, Yoko Katayama, Mitsuru Takasaki and Tomoyuki Hori
- 19 Bacterial Population Succession and Adaptation Affected by Insecticide Application and Soil Spraying History**  
Hideomi Itoh, Ronald Navarro, Kazutaka Takeshita, Kanako Tago, Masahito Hayatsu, Tomoyuki Hori and Yoshitomo Kikuchi
- 31 Survival of Free-Living Acholeplasma in Aerated Pig Manure Slurry Revealed by <sup>13</sup>C-Labeled Bacterial Biomass Probing**  
Dai Hanajima, Tomo Aoyagi and Tomoyuki Hori
- 41 The Effects of Elevated CO<sub>2</sub> Concentration on Competitive Interaction Between Aceticlastic and Syntrophic Methanogenesis in a Model Microbial Consortium**  
Souichiro Kato, Rina Yoshida, Takashi Yamaguchi, Tomoyuki Sato, Isao Yumoto and Yoichi Kamagata
- 49 Recombination Does Not Hinder Formation or Detection of Ecological Species of Synechococcus Inhabiting a Hot Spring Cyanobacterial Mat**  
Melanie C. Melendrez, Eric D. Becraft, Jason M. Wood, Millie T. Olsen, Donald A. Bryant, John F. Heidelberg, Douglas B. Rusch, Frederick M. Cohan and David M. Ward
- 69 Characterization of a Single Mutation in TraQ in a Strain of Escherichia Coli Partially Resistant to Q $\beta$  Infection**  
Akiko Kashiwagi, Hikari Kitamura and Fumie Sano Tsushima
- 76 Complexities of Cell-to-Cell Communication Through Membrane Vesicles: Implications for Selective Interaction of Membrane Vesicles with Microbial Cells**  
Yusuke Hasegawa, Hiroyuki Futamata and Yosuke Tashiro
- Mathematical modeling and simulations**
- 81 Mathematical Modeling of Dormant Cell Formation in Growing Biofilm**  
Kotaro Chihara, Shinya Matsumoto, Yuki Kagawa and Satoshi Tsuneda

**89 *Interspecies Interactions are an Integral Determinant of Microbial Community Dynamics***

Fatma A. A. Aziz, Kenshi Suzuki, Akihiro Ohtaki, Keita Sagegami, Hidetaka Hirai, Jun Seno, Naoko Mizuno, Yuma Inuzuka, Yasuhisa Saito, Yosuke Tashiro, Akira Hiraishi and Hiroyuki Futamata

**100 *Estimating and Mapping Ecological Processes Influencing Microbial Community Assembly***

James C. Stegen, Xueju Lin, Jim K. Fredrickson and Allan E. Konopka

**115 *What Difference Does it Make if Viruses are Strain-, Rather than Species-Specific?***

T. Frede Thingstad, Bernadette Pree, Jarl Giske and Selina Våge

**Theoretical frameworks**

**125 *A Generalized Spatial Measure for Resilience of Microbial Systems***

Ryan S. Renslow, Stephen R. Lindemann and Hyun-Seob Song

**134 *Integrating Ecological and Engineering Concepts of Resilience in Microbial Communities***

Hyun-Seob Song, Ryan S. Renslow, Jim K. Fredrickson and Stephen R. Lindemann

**141 *Incorporating the Soil Environment and Microbial Community into Plant Competition Theory***

Po-Ju Ke and Takeshi Miki



# Editorial: Development of Microbial Ecological Theory: Stability, Plasticity, and Evolution of Microbial Ecosystems

Shin Haruta<sup>1\*</sup>, Yasuhisa Saito<sup>2</sup> and Hiroyuki Futamata<sup>3,4</sup>

<sup>1</sup> Department of Biological Sciences, Tokyo Metropolitan University, Hachioji, Japan, <sup>2</sup> Department of Mathematics, Shimane University, Matsue, Japan, <sup>3</sup> Research Institute of Green Science and Technology, Shizuoka University, Shizuoka, Japan, <sup>4</sup> Department of Applied Chemistry and Biochemical Engineering, Shizuoka University, Hamamatsu, Japan

**Keywords:** ecological theory, mathematical modeling, diversity, stability, evolution, interspecies interaction, resilience

## Editorial on the Research Topic

### Development of Microbial Ecological Theory: Stability, Plasticity, and Evolution of Microbial Ecosystems

We initiated this research topic based on the question “how can we develop microbial ecological theory?” We incorporated three important aspects, stability, plasticity, and evolution, which are key areas for progress in microbial ecological theory. Advances in microbial ecological techniques have allowed us to meticulously consider the dynamics of community structures, interspecies networks, and metabolic flux of microbial ecosystems. Studies using these techniques have demonstrated the stability (i.e., resistance, resilience, and persistence), dynamic equilibrium, and self-organizing ability of micro-ecosystems. Here, the fine contributors in this volume aimed to determine the central and general tenets of the ecological theory that describes the features of microbial ecosystems.

Analyses of the microflora in static-state conditions are insufficient to understand microbial ecosystems even if advanced omics techniques are used. Studies described in the included articles in this volume have tested several factors to elucidate how they affect the structures and functions of microbial communities. As external factors, the effects of temperatures (Melendrez et al.), nutrients (Aoyagi et al.; Aziz et al.; Itoh et al.; Kato et al.), and viruses (Kashiwagi et al.; Thingstad et al.) were intensively investigated. Internal factors, such as dormancy (Chihara et al.; Thingstad et al.), genetic modifications (Kashiwagi et al.; Melendrez et al.; Thingstad et al.), distribution (Chihara et al.; Melendrez et al.; Stegen et al.; Thingstad et al.), and interspecies interactions (Aoyagi et al.; Fatma et al.; Hanajima et al.; Hasegawa et al.; Kato et al.) were widely examined and discussed. Kashiwagi et al. and Melendrez et al. enlightened us about the genetic and physiological plasticity of microbes in microbial communities. The articles mentioned above successfully provided information that has not been observed in microbial communities, suggesting unknown characteristics of microbial ecosystems.

To unveil complex microbial ecosystems, it is desirable to strategically apply stimuli (i.e., perturbation) and comprehensively examine the microbial response. Mathematical modeling and simulations are powerful tools to develop a strategy to interpret comprehensive data and predict unknown characteristics of ecosystems (Chihara et al.; Fatma et al.; Haruta et al., 2013; Melendrez et al.; Stegen et al.; Thingstad et al.).

## OPEN ACCESS

### Edited by:

George Tsiamis,  
University of Patras, Greece

### Reviewed by:

Spyridon Ntougias,  
Democritus University of Thrace,  
Greece

### \*Correspondence:

Shin Haruta  
sharuta@tmu.ac.jp

### Specialty section:

This article was submitted to  
Systems Microbiology,  
a section of the journal  
Frontiers in Microbiology

**Received:** 27 September 2016

**Accepted:** 07 December 2016

**Published:** 21 December 2016

### Citation:

Haruta S, Saito Y and Futamata H  
(2016) Editorial: Development of  
Microbial Ecological Theory: Stability,  
Plasticity, and Evolution of Microbial  
Ecosystems. *Front. Microbiol.* 7:2069.  
doi: 10.3389/fmicb.2016.02069

Relationships between the “*diversity*” and “*stability*” of ecosystems have been extensively discussed so far. Some researchers stated that high *diversity* is beneficial for high *stability*, whereas others stated that higher *diversity* reduces *stability*. Clear definition and evaluation scale for these claims are still lacking due to technical limitations. Omic analysis cannot completely grasp all elements of microbial communities, and the stability of the community must depend on the strength and duration of perturbations. Theoretical frameworks are important to generalize microbial ecological observations. Song et al. systematically redefined “resilience” as an intrinsic property of complex microbial ecosystems by integrating ecological and engineering concepts in their perspective article. Renslow et al. developed a new method that broadens the use of spatial data for assessing “resilience” in general and reported its applicability using a simulated microbial community. Ke and Miki comparatively summarized theoretical frameworks for close interactions between organisms and environments by reviewing studies on plant-soil feedback. Their review article provides various aspects for the development and applicability of ecological theories. In other words, these theoretical frameworks hopefully help to interpret big data from multi-omics approaches.

The development of sophisticated microbial ecological theory still has a long way to reach its goal. We believe that this volume is a constructive step toward expanding the frontiers of current microbial ecology. Furthermore, the articles in this volume propose the next step we will need for this long journey with many avenues for advancement. SH said the following; this volume reminds us that microorganisms are totally different from macro-organisms, i.e., microorganisms are physiologically versatile, show high heterogeneity even in clonal population, frequently change genetic elements, and have close cell-to-cell interactions. It may be necessary to recognize microbial ecosystems as a huge gene network, as proposed by Song et al. and refurbish ecological theories that have been established for macro-ecosystems. To discover a novel theory, I would like to put another question “are there any ecological theories applicable to complex microbial ecosystems?” YS said the following; it is crucial to study how parts of a system give rise to the collective behaviors of the system and how the system interacts with its environment to understand the features of microbial ecosystems. Developing mathematical something helpful (or as powerful as

possible) for this problem has a quite long journey and is more challenging than developing those for macrobial ecosystems. HF said the following; the phrases of “population dynamics,” “community succession,” and “interspecies interactions” always make me imagine the breath of microbial ecosystems. Microbial ecosystems seemingly change with utter abandon; however, there should be any yet-to-be-discovered rules in their behavior. Through this volume, I recognize that consideration of time scales is indispensable to exactly understand the dynamics of microbial ecosystems. Mathematical modeling research of the resilience focusing on recovery time and length by Renslow et al. breaks through to approach to ecological theory. It has been developing to understand microbial ecosystems integrally by linking gene expression, metabolisms, and interspecies interactions with the aid of mathematics. I believe that the microbial ecological theory emerges through these integral analyses.

We acknowledge the talented group of researchers who have contributed to this volume. They have aggressively addressed the critical issues in microbial ecology and have presented research, which can be a foundation for future studies. While initiating this research topic, we aimed to gather diverse research articles and assemble all of them into a comprehensive picture representing the general rules of microbial ecosystems. Actually, however, it was difficult for us to sufficiently assemble the wide variety of the great achievements. We hope you enjoy this unfinished but vivid and entrancing picture and this volume will help to find other pieces of the puzzle obtaining complete picture of microbial ecosystems.

## AUTHOR CONTRIBUTIONS

SH drafted the manuscript. All authors wrote, revised, and approved the final version.

## FUNDING

This work was supported by KAKENHI Grant Numbers 15K12228, 26281038, and 26800080, Japan. It was also partially supported by ALCA project, Japan Science and Technology Agency.

## REFERENCES

- Haruta, S., Yoshida, T., Aoi, Y., Kaneko, K., and Futamata, H. (2013). Challenges for complex microbial ecosystems: combination of experimental approaches with mathematical modeling. *Microb. Environ.* 28, 285–294. doi: 10.1264/jsme2.ME13034

**Conflict of Interest Statement:** The authors declare that the research was conducted in the absence of any commercial or financial relationships that could be construed as a potential conflict of interest.

Copyright © 2016 Haruta, Saito and Futamata. This is an open-access article distributed under the terms of the Creative Commons Attribution License (CC BY). The use, distribution or reproduction in other forums is permitted, provided the original author(s) or licensor are credited and that the original publication in this journal is cited, in accordance with accepted academic practice. No use, distribution or reproduction is permitted which does not comply with these terms.

# Dynamic transition of chemolithotrophic sulfur-oxidizing bacteria in response to amendment with nitrate in deposited marine sediments

Tomo Aoyagi<sup>1†</sup>, Makoto Kimura<sup>1†</sup>, Namiha Yamada<sup>1</sup>, Ronald R. Navarro<sup>1</sup>, Hideomi Itoh<sup>2</sup>, Atsushi Ogata<sup>1</sup>, Akiyoshi Sakoda<sup>3</sup>, Yoko Katayama<sup>4</sup>, Mitsuru Takasaki<sup>5</sup> and Tomoyuki Hori<sup>1\*</sup>

## OPEN ACCESS

### Edited by:

Hiroyuki Futamata,  
Shizuoka University, Japan

### Reviewed by:

Paul Richard Himes,  
University of Louisville, USA  
Michael Pester,  
University of Konstanz, Germany

### \*Correspondence:

Tomoyuki Hori,  
Environmental Management Research  
Institute, National Institute  
of Advanced Industrial Science  
and Technology, Onogawa 16-1,  
Tsukuba, Ibaraki 305-8569, Japan  
hori-tomo@aist.go.jp

† These authors have contributed  
equally to this work.

### Specialty section:

This article was submitted to  
Systems Microbiology,  
a section of the journal  
Frontiers in Microbiology

Received: 13 March 2015

Paper pending published:  
27 March 2015

Accepted: 22 April 2015

Published: 18 May 2015

### Citation:

Aoyagi T, Kimura M, Yamada N,  
Navarro RR, Itoh H, Ogata A,  
Sakoda A, Katayama Y, Takasaki M  
and Hori T (2015) Dynamic transition  
of chemolithotrophic sulfur-oxidizing  
bacteria in response to amendment  
with nitrate in deposited marine  
sediments.  
Front. Microbiol. 6:426.  
doi: 10.3389/fmicb.2015.00426

<sup>1</sup> Environmental Management Research Institute, National Institute of Advanced Industrial Science and Technology, Tsukuba, Japan, <sup>2</sup> Bioproduction Research Institute, National Institute of Advanced Industrial Science and Technology, Sapporo, Japan, <sup>3</sup> Institute of Industrial Science, The University of Tokyo, Tokyo, Japan, <sup>4</sup> Graduate School of Agriculture, Tokyo University of Agriculture and Technology, Tokyo, Japan, <sup>5</sup> Department of Food and Environmental Sciences, Faculty of Science and Engineering, Ishinomaki Senshu University, Ishinomaki, Japan

Although environmental stimuli are known to affect the structure and function of microbial communities, their impact on the metabolic network of microorganisms has not been well investigated. Here, geochemical analyses, high-throughput sequencing of 16S rRNA genes and transcripts, and isolation of potentially relevant bacteria were carried out to elucidate the anaerobic respiration processes stimulated by nitrate (20 mM) amendment of marine sediments. Marine sediments deposited by the Great East Japan Earthquake in 2011 were incubated anaerobically in the dark at 25°C for 5 days. Nitrate in slurry water decreased gradually for 2 days, then more rapidly until its complete depletion at day 5; production of N<sub>2</sub>O followed the same pattern. From day 2 to 5, the sulfate concentration significantly increased and the sulfur content in solid-phase sediments significantly decreased. These results indicated that denitrification and sulfur oxidation occurred simultaneously. Illumina sequencing revealed the proliferation of known sulfur oxidizers, i.e., *Sulfurimonas* sp. and Chromatiales bacteria, which accounted for approximately 43.5% and 14.8% of the total population at day 5, respectively. These oxidizers also expressed 16S rRNA to a considerable extent, whereas the other microorganisms, e.g., iron(III) reducers and methanogens, became metabolically active at the end of the incubation. Extinction dilution culture in a basal-salts medium supplemented with sulfur compounds and nitrate successfully isolated the predominant sulfur oxidizers: *Sulfurimonas* sp. strain HDS01 and *Thioalkalispira* sp. strain HDS22. Their 16S rRNA genes showed 95.2–96.7% sequence similarity to the closest cultured relatives and they grew chemolithotrophically on nitrate and sulfur. Novel sulfur-oxidizing bacteria were thus directly involved in carbon fixation under nitrate-reducing conditions, activating anaerobic respiration processes and the reorganization of microbial communities in the deposited marine sediments.

**Keywords:** marine sediment, sulfur-oxidizing bacteria, environmental stimuli, high-throughput sequencing, the Great East Japan Earthquake in 2011

## Introduction

Environmental stimuli affect the structure and function of microbial communities in natural environments. Numerous investigations have employed artificial stimulations by temperature, pH, NaCl, and electron donors and acceptors to clarify which microorganisms play important roles in the development and functioning of microbial communities (Hori et al., 2006; Kotsyurbenko et al., 2007; Lydmark et al., 2007; Ontiveros-Valencia et al., 2012). For instance, in terrestrial ecosystems, the supplementation with inorganic electron acceptors, e.g., nitrate, iron(III), and sulfate, has been shown to change the metabolic pathway and/or strengthen the degradation capability of indigenous microbial communities (Lueders and Friedrich, 2002; Labrenz et al., 2005; Hori et al., 2010), which in turn provides an opportunity to study the relationship among biogeochemical cycles of nitrogen, iron, sulfur, and carbon. However, the microbial community adaptation and development in response to environmental stimuli remain to be delineated because of the limited information concerning microbial population dynamics, rather than the dynamics of a particular taxon or a specific trophic group.

Marine sediment is commonly found on the sea floor below fish farms and in closed water areas throughout the world (Pearson and Rosenberg, 1978; Kemp et al., 1990; Armenteros et al., 2010; Kunihiro et al., 2011). A large quantity of marine sediment was deposited by the tsunami originating from the Great East Japan Earthquake in 2011, and the study of this material has shed light on the vast accumulation of marine sediments in not only closed sea areas but also coastal marine regions facing the open ocean (Inui et al., 2012). The geochemical cycles of elements in marine sediments have attracted much attention because of their possible association with coastal biotic activities. In a recent study, we reported that only limited degradation of organic matter occurred in association with the sulfate reduction in deposited marine sediments, even though the 16S rRNA transcripts detected were mainly from sulfate reducers (Hori et al., 2014). In the same report, we found that ferric iron amendment had little effect on the structure and activity of the sediment microorganisms. Marine sediments have been accumulating in the past few decades, possibly due to their resistance to the degradation abilities of sulfate and iron reducers. For this reason, biostimulation with energetically more favorable electron acceptors such as nitrate is considered more effective in facilitating degradation processes in the marine sediments. This is particularly relevant because nitrate pollution from farm run-off and/or other sources may currently be contributing to the nitrate amendment of marine sediments. However, the precise effects of such biostimulation and the responsible microorganisms are largely unknown.

The advent of high-throughput DNA sequencing technologies has revolutionized approaches to the study of microbial community structure and function (Caporaso et al., 2011; Miller et al., 2013). One of these technologies, the Illumina platform for 16S rRNA amplicon sequencing, has made it possible to comprehensively screen microbial communities at high resolution and

high sensitivity (Caporaso et al., 2012). In addition, the comparative analysis of 16S rRNA genes and transcripts has enabled the fine-scale identification of metabolically active microorganisms. The resulting phylogenetic information is useful for the isolation of key microorganisms, which is one of the exclusive means of accessing their ecophysiological roles.

The objective of this study was to amend deposited marine sediments with an energetic electron acceptor, nitrate, and investigate the impact of this amendment on the structure and activity of microbial communities by using a combination of geochemical analyses, high-throughput Illumina sequencing of 16S rRNA genes and transcripts, and isolation.

## Materials and Methods

### Anaerobic Incubation of the Deposited Marine Sediments

Marine sediments deposited by the tsunami that originated from the Great East Japan Earthquake in 2011 were collected on September 2011. The sampling site was located on the coast of Higashi-matsushima, Miyagi, Japan (38°25'N, 141°14'E). The samples were stored at 4°C prior to experimental use. Sediment slurry was prepared by mixing the deposited sediment with artificial seawater (Daigo; Nihon Pharmaceutical) at a ratio of 1:4 (v/v). Aliquots (20 ml) of the homogenized slurry were transferred anaerobically into 50-ml serum vials, which were then sealed with butyl rubber septa. The samples were pre-incubated in the dark at 25°C for more than 30 days in order to activate the sediment microorganisms. After pre-incubation, the headspace of each sample vial was flushed with N<sub>2</sub>. Three sediments were produced: (i) a non-autoclaved sediment amended with nitrate to a final concentration of 20 mM, (ii) a non-autoclaved sediment with addition of sterilized water in place of nitrate (control sediment), and (iii) an autoclaved sediment amended with nitrate to a final concentration of 20 mM. Sterilization of the sediment microorganisms was performed three times at 121°C for 1 h. All treatments were run in triplicate with static incubation for 5 days at 25°C in the dark.

### Geochemical Analyses for Gas, Liquid, and Solid Phases of the Sediment Incubation

Samples of the headspace gas, slurry water and solid-phase sediment were taken at day 0, 2, and 5 from each vial of each of the triplicate replications of the two treatments (i.e., the nitrate and non-amended control treatments) performed in triplicate. Total CO<sub>2</sub>, N<sub>2</sub>O, and CH<sub>4</sub> in the headspace gas were analyzed by a gas chromatograph (GC-14B; Shimadzu) equipped with a packed column (ShinCarbon ST; Shinwa). Concentrations of NO<sub>3</sub><sup>-</sup>, NO<sub>2</sub><sup>-</sup>, NH<sub>4</sub><sup>+</sup>, PO<sub>4</sub><sup>2-</sup>, and SiO<sub>2</sub> in the slurry water were determined by the colorimetric method (Hansen and Koroleff, 2007) with an auto-analyzer (QuA Atrio 2-HR; BLTEC). This colorimetric analysis was also conducted on the nitrate-amended sterilized sediments after a 5-day incubation. The sulfate concentration in the slurry water was determined by using an ion chromatograph (DX-500; Dionex) equipped with

an IonPac AS11 column (Dionex) and an ED40 electrochemical detector (Dionex). The total organic carbon (TOC) concentration from the slurry water was determined by the non-purgeable organic carbon method with a TOC analyzer (TOC-L; Shimadzu). The concentration of volatile fatty acids (VFAs) from the slurry water was measured by a high-pressure liquid chromatograph (Alliance e26951; Waters) equipped with an RSpak KC-811 column (Shodex) and a photodiode array (2998; Waters). Ferrous iron ( $\text{Fe}^{2+}$ ) and total iron in the slurry were determined using 6N HCl extraction and the ferrozine method as described previously (Braunschweig et al., 2012). The content ratio of elements (i.e., carbon, hydrogen, nitrogen, and sulfur) in the solid-phase sediment was determined by using a CHNS analyzer (FLASH 2000 Organic Elemental analyzer; Thermo Scientific). The thermogravimetry (TG) and differential thermal analysis (DTA) curves of the solid-phase sediment were determined by using a simultaneous differential thermo gravimetric analyzer (DTG-60; Shimadzu). The sediment slurry samples were stored at  $-80^{\circ}\text{C}$  for subsequent molecular analyses.

### Nucleic Acid Extraction and Amplification of 16S rRNA Genes and Transcripts

Nucleic acids were extracted from each sample from one replication of the nitrate and control treatments at day 0, 2, and 5 using a direct lysis protocol involving bead beating (Noll et al., 2005). Total DNA and RNA were prepared by digestion with RNase (Type II-A; Sigma-Aldrich) and DNase (RQ1; Promega), respectively. The PCR was performed with a high-fidelity DNA polymerase (Q5; New England Biolabs). Reverse transcription PCR (RT-PCR) was carried out using a one-step RT-PCR system (Access Quick; Promega). The universal primer set 515F/806R was modified to contain an Illumina adaptor region, and the reverse primer was encoded with 6-bp barcodes (Caporaso et al., 2012). The thermal profile of PCR was as follows: an initial denaturation at  $98^{\circ}\text{C}$  for 90 s; followed by 25 cycles of denaturation at  $98^{\circ}\text{C}$  for 10 s, annealing at  $54^{\circ}\text{C}$  for 30 s, and extension at  $72^{\circ}\text{C}$  for 30 s; and a final extension step at  $72^{\circ}\text{C}$  for 2 min. For RT-PCR, RT was performed at  $48^{\circ}\text{C}$  for 45 min, and the thermal profile of the subsequent PCR consisted of a denaturation at  $94^{\circ}\text{C}$  for 3 min; followed by 30 cycles of 30 s at  $94^{\circ}\text{C}$ , 45 s at  $52^{\circ}\text{C}$ , and 90 s at  $72^{\circ}\text{C}$ ; with a final extension of 5 min at  $72^{\circ}\text{C}$ . The absence of the DNA contamination was confirmed by RT-PCR without reverse transcriptase.

### Illumina Sequencing and Data Processing

The amplicons were purified first with an AMPure XP Kit (Beckman Coulter) and then a second time with a QIAquick gel extraction kit (QIAGEN). The barcode-encoded DNA library and an initial control (PhiX; Illumina) were subjected to paired-end sequencing with a 300-cycle MiSeq Reagent kit (Illumina) on a MiSeq sequencer (Illumina). The PhiX, low-quality ( $Q < 30$ ), and chimeric sequences were removed and the paired-end sequences were assembled as described previously (Itoh et al., 2014). The sequences in each library were characterized phylogenetically using the QIIME software package version 1.7.0 (Caporaso et al., 2010). The operational taxonomic units (OTUs) were grouped

using a 97% sequence identity cut-off. Representative sequences for each OTU were assigned with the BLAST program in the DDBJ nucleotide sequence database. Using the program QIIME (Caporaso et al., 2010),  $\alpha$ -diversity indices (i.e., Chao1, Shannon, and Simpson reciprocal) and the weighted UniFrac distances for principal coordinate analysis (PCoA) were calculated.

### Isolation and Phylogenetic Analysis of the Dominant Sulfur Oxidizers

For isolation and cultivation of the dominant sulfur-oxidizing bacteria from the deposited marine sediments, the incubated slurry was transferred to a slightly modified Widdel medium (pH 7.0; Kanno et al., 2013) containing NaCl,  $\text{MgCl}_2 \cdot 6\text{H}_2\text{O}$ ,  $\text{KH}_2\text{PO}_4$ , and  $\text{NH}_4\text{Cl}$  at concentrations of 20.5, 3, 0.136, and 0.005 g/l, respectively. In this protocol, 2 ml of the incubated slurry and 18 ml of basal medium were first distributed into 50 ml glass serum vials with butyl rubber septa. Then the solutions were further amended with nitrate (20 mM) as an electron acceptor and elemental sulfur (20 mM) or thiosulfate (20 mM) as an electron donor. After flushing the vial headspace with  $\text{N}_2/\text{CO}_2$  (80:20, v/v), enrichment was performed at  $25^{\circ}\text{C}$  in the dark. After 1 week, 5% of the enrichment cultures were transferred to fresh media, and the subculturing process was carried out four times. Thereafter, extinction dilution culture was conducted for the isolation of sulfur oxidizers. The purification of isolates was checked by microscopic observation and Illumina sequencing of 16S rRNA genes.

For the phylogenetic analysis of isolates, nucleic acids were extracted from the pure cultures as described above. Nearly the full length of the 16S rRNA gene sequences was amplified with PCR using a Q5 DNA polymerase (New England Biolabs) and the primer set B27f/B1525r (Lane, 1991). The thermal conditions of PCR were as described above, except that an annealing temperature of  $52^{\circ}\text{C}$  and an extension time of 1 min were employed. The PCR products were purified and ligated into the plasmid vector pGEM-T Easy (Promega), and the ligation mixture was used to transform *Escherichia coli* JM109 supercompetent cells (Nippon Gene) according to the manufacturer's instructions. The plasmid DNA was sequenced using a BigDye Terminator v3.1 Cycle Sequencing kit (Applied Biosystems) and a 3730xl DNA Analyzer (Applied Biosystems). A phylogenetic tree was constructed by the neighbor-joining and maximum likelihood methods using the program MEGA, version 5.2 (Tamura et al., 2011). The robustness of the tree topology was assessed by the bootstrap value based on 1,000 replications. For physiological characterization, the sulfate concentrations during the incubation with sulfur compounds (i.e., elemental sulfur and thiosulfate) and nitrate were determined to assess the chemolithotrophic growth of the isolates.

### Nucleotide Sequence Accession Numbers

The nucleotide sequence data obtained from Illumina sequencing analyses based on the 16S rRNA genes and transcripts have been deposited in the MG-RAST database<sup>1</sup> under the project title "Dynamic transition of chemolithotrophic sulfur oxidizers

<sup>1</sup><http://metagenomics.anl.gov/>

in deposited marine sediments in 2015<sup>2</sup> with the ID numbers 4620652.3–4620661.3 (10 libraries), and those obtained from the phylogenetic analysis of isolates have been deposited in the DDBJ nucleotide sequence database<sup>2</sup> under accession numbers LC029406 to LC029408 (three isolates).

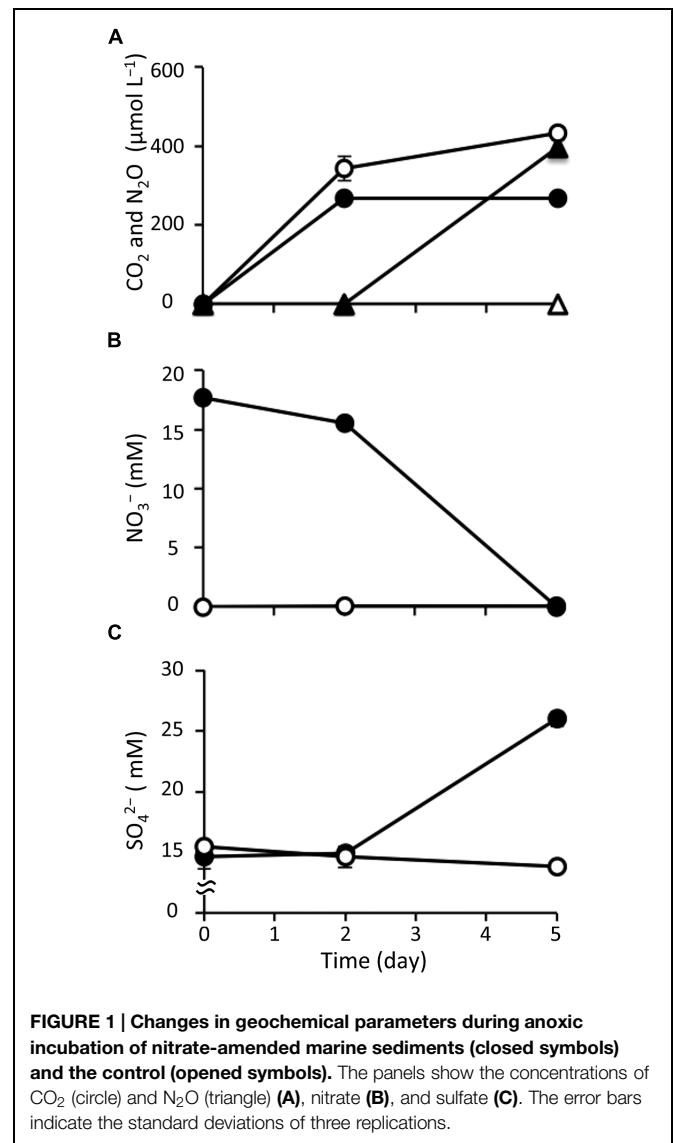
## Results

### Biogeochemical Activities in the Nitrate-Amended Marine Sediments

After amending with nitrate at a concentration of 20 mM, marine sediment slurries were anaerobically incubated for 5 days; this was designated the nitrate treatment. In parallel, the incubation of non-amended slurries was conducted as a control. Geochemical analysis showed significant differences in the biological activity under the different incubation conditions. First, based on the gaseous phase analysis of the samples (Figure 1A), N<sub>2</sub>O was produced from day 2 in the nitrate-amended sediment but it was not detected in the control. Under both conditions, CO<sub>2</sub> was generated from the start of the incubations. In both cases the CO<sub>2</sub> concentrations increased to 258–378 μM at day 2, suggesting that the CO<sub>2</sub> production was caused by degassing and establishment of a CO<sub>2</sub>-bicarbonate equilibrium. After 2 days, the CO<sub>2</sub> concentration stabilized at 255–285 μM under the nitrate treatment, while it increased to 434 μM at day 5 in the control. CH<sub>4</sub> was not detected under either condition throughout the incubation (data not shown).

With respect to the analysis of slurry water in the nitrate-amended samples, the nitrate concentration decreased to 15.5 mM at day 2 and was completely depleted at the end of the incubation (Figure 1B). Nitrite was not detected during the 5-day incubation (data not shown). The ammonium concentration increased slightly to 1.25 mM at day 2, and then decreased to 0.78 mM at day 5 (Supplementary Figure S1A). Sulfate concentrations were maintained at 14.6–15.5 mM during the first 2 days, but they increased remarkably to 26.0 mM at day 5 (Figure 1C). This suggests that sulfur components originally present in the sediment were gradually being oxidized to sulfate. TOC was kept at a constant level of 22.6 mg l<sup>-1</sup> during the incubation (Supplementary Figure S1B). Since VFAs were absent in the slurry water, they were considered not to have contributed to the TOC content. The concentrations of silicate and phosphate, which are known nutrients for microbial growth, decreased throughout the incubation period (Supplementary Figures S1C,D). It was interesting to note that these geochemical parameters did not change in the control (Figure 1 and Supplementary Figure S1). In addition, decreases in nitrate, silicate, and phosphate were also not observed in the nitrate-amended sterilized sediments (data not shown). These findings indicate that the apparent denitrification and sulfur oxidation under the nitrate treatment were microbially mediated processes.

With respect to the analysis of solid-phase sediments, the content ratio of the sulfur moiety decreased to 1.1 wt% at day 5 under the nitrate treatment, and this value was significantly lower

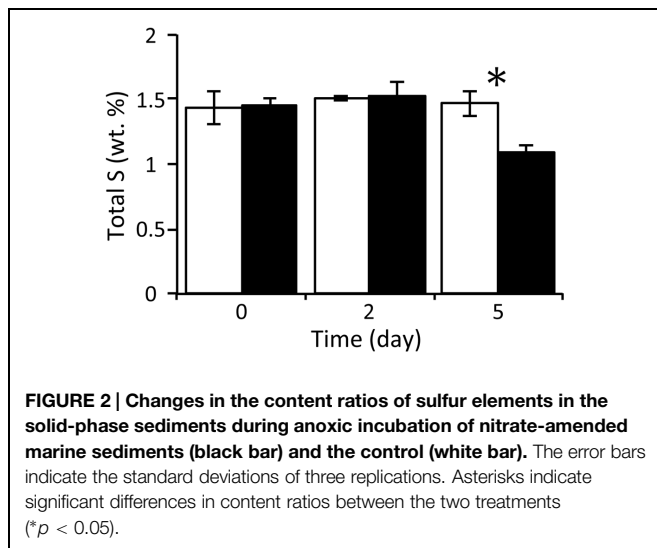


than that in the control ( $P < 0.05$ ; Figure 2). Combined with the results from the slurry water analyses, this strongly suggests that the reduced sulfur components in the nitrate-amended sediments were oxidized to sulfate which was then released to the liquid phase. No significant differences in the content ratios of the other elements (i.e., carbon, hydrogen, and nitrogen) were observed between the nitrate treatment and the control (Supplementary Figure S2). The TG/DTA curves also showed that there were no significant differences in these ratios from the beginning (Supplementary Figure S3A) until the end of the incubation under either set of conditions (Supplementary Figures S3B,C), which suggests that the major components of the sediments were little changed by nitrate amendment.

### Changes in Microbial Communities Based on 16S rRNA Genes and Transcripts

Illumina sequencing on the basis of the 16S rRNA genes and transcripts demonstrated the dynamic transition of whole

<sup>2</sup><http://www.ddbj.nig.ac.jp>



and metabolically active microbial communities in the nitrate-amended sediments (Figure 3 and Supplementary Table S1). A total of 10 Illumina sequence libraries were constructed from 16S rRNA genes ('G') and transcripts ('T') at day 2 and 5 for both the nitrate ('N') treatment and the control ('C'). For instance, the library built from 16S rRNA genes at day 2 of the nitrate treatment was designated as the NG2 library. The NG5, NT2, NT5, CG2, CG5, CT2, and CT5 libraries were defined in the same manner. The libraries from 16S rRNA genes and transcripts at day 0 were presented as a consensus between the two conditions, and were designated as the G0 and T0 libraries, respectively. A total of 280,651 sequences (i.e., a mean of 28,065 sequences per library) were characterized phylogenetically. The numbers of sequences in all the libraries are shown in Supplementary Table S1.

Alpha-diversity indices (i.e., Chao1, Shannon, and Simpson reciprocal) of the Illumina libraries were determined on the basis of equal numbers of sequences ( $n = 7,374$ ; Supplementary Table S1). The Chao1 values in the NG2, NG5, NT2, and NT5 libraries were significantly lower than those in the CG2, CG5, CT2, and CT5 libraries, respectively, which indicates that the richness of microbial communities decreased in response to nitrate amendment. Further, the values of the indices Shannon and Simpson reciprocal were in the order  $G0 > NG2 > NG5$  libraries, while those for the G0, CG2, and CG5 libraries were at similar levels. A decreasing trend was also observed in the T0, NT2, and NT5 libraries but not in the T0, CT2, and CT5 libraries. These facts show that the even distribution of microbial communities significantly decreased with time following the nitrate treatment. The decrease in the evenness of the distribution was more obvious in the whole microbial populations (i.e., at the gene level) than in metabolically active microorganisms (at the transcript level). Taken together, these results showed that the microbial diversity was remarkably lowered by nitrate amendment and thus indicated that particular species dominated the microbial communities. In order to compare the community structures in all the libraries, a PCoA plot was generated from the weighted UniFrac

distance analysis using equal numbers of sequences ( $n = 9,336$ ; Supplementary Figure S4). In the nitrate treatment, distance was maintained between all the libraries on the plot, while in the control treatment, the libraries were in close proximity. This suggests that the microbial communities shifted progressively with time in the nitrate-amended sediments. A considerably greater degree of change in the community was observed from days 2–5 compared to days 0–2. In addition, the libraries of 16S rRNA genes were located far from those of the transcripts, implying that only selected members of the microbial communities expressed 16S rRNA.

Phylogenetic analyses of the Illumina sequence libraries revealed the drastic changes in microbial community structures following the nitrate treatment (Figure 3). Notably, the Epsilon- and Gamma-proteobacteria classes increased drastically from 2% and 5% of the whole microbial population at day 0 to 44% and 17% at day 5, respectively (G0 and NG5 libraries in Figure 3A). Significant increases in these classes were also found in the metabolically active microbial communities (T0 and NT5 libraries in Figure 3B). The most abundant OTUs of these classes in the NG5 library are shown in Figure 4. Within the class Epsilonproteobacteria, OTU 4053 became the most predominant, accounting for 42.7% and 14.7% of the total NG5 and NT5 libraries, respectively (Figures 4A,B). This OTU was phylogenetically related to *Sulfurimonas denitrificans* (NR074133; 98.4% sequence similarity). Concerning the Gammaproteobacteria, the Chromatiales OTUs 5722 and 3944 accounted for 12.5% and 1.9%, respectively, of the total in the NG5 library (Figure 4C). The closely related species of these OTUs were *Thioalkalispira microaerophila* (NR025239; 96.8% sequence identity) and *Thioalbus denitrificans* (NR122087; 100% sequence identity), respectively. On the other hand, the epsilon- and gamma-proteobacterial OTUs are listed in descending order of relative abundance in the NT5 library (Supplementary Figure S5). Only small differences in the abundant epsilonproteobacterial OTUs were observed between the NT5 and NG5 libraries (Figure 4A and Supplementary Figure S5B), indicating that 16S rRNA expression was mostly originated from the major members, more specifically the OTU 4053, within the Epsilonproteobacteria. Meanwhile, the abundant gamma-proteobacterial OTUs in the NT5 library were remarkably distinct from those in the NG5 library (Figure 4C and Supplementary Figure S5D). The metabolic activity of the community members appeared not to be linked with the population size, and a variety of minor microorganisms within the Chromatiales highly expressed 16S rRNA. Consequently, the high-resolution dynamics of microbial communities on the basis of the 16S rRNA genes and transcripts revealed that the specific members within the genus *Sulfurimonas* and the order Chromatiales, hitherto known as sulfur-oxidizing bacteria (Friedrich et al., 2001; Nakagawa et al., 2005; Campbell et al., 2006; Nakagawa and Takai, 2008), drastically proliferated and/or were metabolically activated in the nitrate-amended sediments. Moreover, additional quantification assays, e.g., quantitative PCR, of 16S rRNA genes and transcripts are effective for verifying the relationship between the population sizes and metabolic activities of the sulfur-oxidizing bacteria.

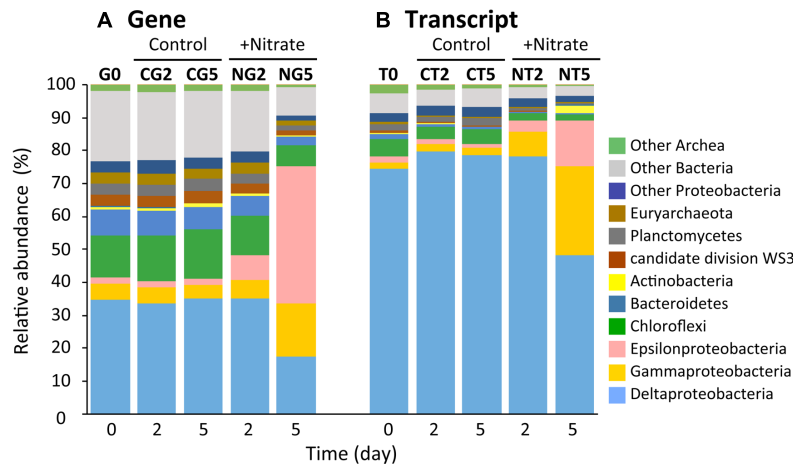


**FIGURE 3 | Dynamic transition of microbial communities during anoxic incubation of marine sediments as determined by Illumina sequencing of 16S rRNA genes (A) and transcripts (B).** Relative abundances of 16S rRNA genes ('G') and transcripts ('T') defined phylogenetically are represented by the colors shown at the right side of the graph. The

sequence libraries were obtained from the incubation at day 0 (designated the G0 and T0 libraries) and at days 2 and 5 in the nitrate-amended sediment ('N'; designated the NG2, NG5, NT2, and NT5 libraries) and in the control ('C'; designated the CG2, CG5, CT2, and CT5 libraries). The sequence library is indicated at the top of each bar.

Some OTUs outside the Epsilon- and Gamma-proteobacteria exhibited higher levels of 16S rRNA expression in the NT5 library than in the CT5 library. The OTUs with more than five-fold increases in relative abundance are shown in **Table 1**. The metabolic activation of anaerobically respiring microorganisms other than sulfur oxidizers was observed at the end of the incubation. In particular, the 16S rRNA expression level of the fermentative and heterotrophically nitrate-reducing *Cellulomonas* sp. (OTU: 566) in the NT5 library was 430-fold higher than that in the CT5 library. The iron(III)-reducing bacteria such as the *Geobacter* spp. (OTUs: 8007, 425, and 3917), *Pelobacter* sp. (OTU: 2865), and *Geothrix* sp. (OTU: 2401) showed 13–94-fold increases in relative abundance. In addition, the 16S rRNA expressions from the syntrophically VFA-oxidizing Syntrophobacteriaceae bacterium (OTU: 11860) and the aceticlastic methanogen *Methanosaeta* sp. (OTU: 3178) increased to some extent in the NT5 library compared to those in the CT5 library (data not shown).

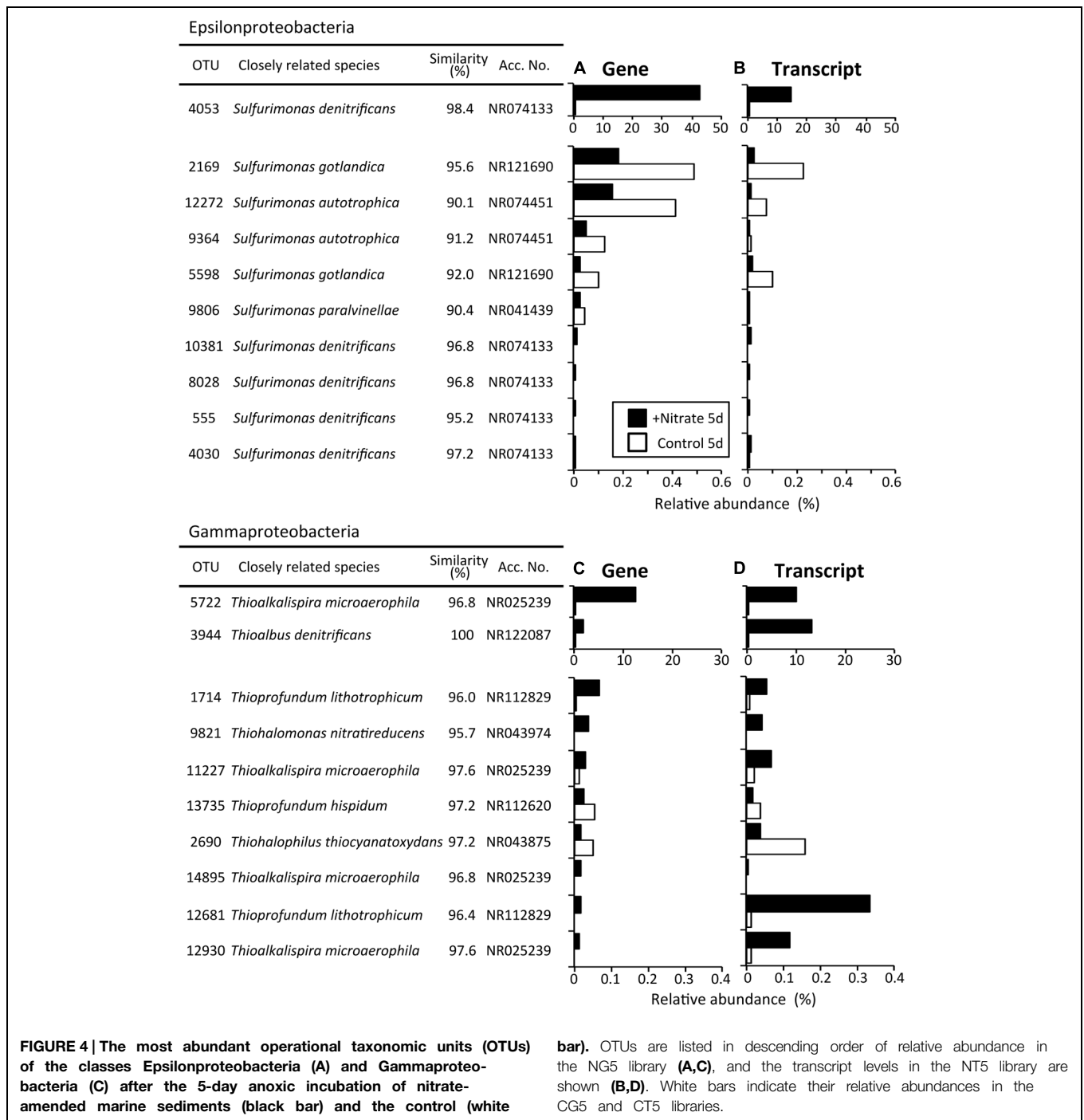
Regarding the composition of microbial communities in the control, the relative abundances in the main phyla or classes were not changed throughout the incubation (G0, CG2, CG5, T0, CT2, and CT5 libraries in **Figure 3**). Deltaproteobacterial sulfate reducers, i.e., Desulfobacteraceae and Desulfobulbaceae bacteria, were dominant. They occupied 11.5% and 7.7% of the CG5 library and 6.3% and 50.3% of the CT5 library, respectively. The dominance of sulfate reducers was consistent with the results from previous studies (Holmer and Kristensen, 1992; Habicht and Canfield, 1997). This suggests that these sulfate-reducing bacteria were originally present in the marine sediments and maintained their predominance throughout the control incubation. Although they expressed most of 16S rRNA under in situ conditions (at day 0) and at days 2 and 5, their contribution to sulfate reduction was small, as indicated by the constant sulfate concentration over time (**Figure 1C**).

### Isolation of the Dominant Sulfur Oxidizers and Their Chemolithotrophic Growth

Through extinction dilution culture by using a liquid medium supplemented with nitrate and sulfur compounds, three strains, HDS01, HDS22, and HDSN4, were successfully isolated from the deposited sediments. The phylogenetic analysis based on the nearly full-length 16S rRNA genes indicated that the isolates formed two novel clusters in the phylogenetic tree and the strains HDS01 and HDSN4 were related to *S. denitrificans* (NR074133; 96.7% and 95.8% sequence similarities, respectively), while the strain HDS22 had 95.2% sequence similarity to *Thioalkalispira microaerophila* (NR025239; **Figure 5**). The strains HDS01 and HDS22 corresponded to the OTUs 4053 and 5722, and were identified as the most predominant sulfur oxidizers in the nitrate-amended sediments (**Figures 4A,C**). During the incubation of these two strains (HDS01 and HDS22) with elemental sulfur and thiosulfate as electron donors and nitrate as electron acceptor, the sulfate concentration significantly increased, which indicates that both strains were able to grow chemolithotrophically on these compounds. Because of their low sequence similarities, we consider that these three isolates are novel species in the genera *Sulfurimonas* and *Thioalkalispira*. Further characterizations of these isolates are in progress.

### Discussion

In this study, we investigated microbial community succession stimulated by nitrate amendment of deposited marine sediments. Geochemical analyses were used to monitor the change in the physicochemical parameters of the nitrate-amended sediments (e.g., consumption of nitrate, and production of  $N_2O$  and sulfate). High-throughput Illumina sequencing based on the 16S rRNA genes and transcripts revealed the proliferation



and metabolic activation of sulfur-oxidizing bacteria. In addition, isolation of the dominant sulfur oxidizers demonstrated their chemolithotrophic growth on nitrate, which suggests that the biotically fixed carbon was further available for growth of the other anaerobic microorganisms. Actually, at the end of the incubation, Illumina sequencing detected the expression of 16S rRNA from fermentative bacteria, ferric iron reducers, and acetilastic methanogens. The combination of geochemical analyses, high-throughput sequencing, and isolation was proven to be a

powerful approach to comprehensively characterize microbial communities affected by environmental stimuli and their trophic interaction in the marine sediments.

The amendment with nitrate initiated the co-occurrence of sulfur oxidation and denitrification during anoxic incubation of marine sediment slurries (Figure 1). Since the concentration of TOC in slurry waters changed little during the incubation (Supplementary Figure S1B), it was suggested that little or no heterotrophic denitrification occurred. There have been

TABLE 1 | Operational taxonomic units (OTUs) highly expressing 16S rRNA after the 5-day anoxic incubation of nitrate-amended marine sediments.

OTU ID	Closely related species	Similarity (%)	Accession number	Phylum/Class	Family	Relative abundance (%) <sup>a</sup>	Increasing ratio (fold) <sup>b</sup>	Putative function <sup>c</sup>
4053	<i>Sulfurimonas denitrificans</i>	98.4	NR121690	Epsilonproteobacteria	Helicobacteraceae	14.64	2421.7	Sulfur oxidation
566	<i>Cellulomonas oligotrophica</i>	98.8	KF817659	Actinobacteria	Cellulomonadaceae	2.60	430.2	Fermentation, nitrate reduction
13536	<i>Thioalkalispira microaerophila</i>	97.6	NR025239	Gammmaproteobacteria	Thioalkalispiraceae	0.82	269.8	Sulfur oxidation
11183	<i>Thioalbus denitrificans</i>	96.8	NR122087	Gammmaproteobacteria	Ectothiorhodospiraceae	0.43	143.1	Sulfur oxidation
8007	<i>Geobacter bremensis</i>	100	KF800712	Deltaproteobacteria	Geobacteraceae	6.78	93.5	Iron(III) reduction
3944	<i>Thioalbus denitrificans</i>	100	NR122087	Gammmaproteobacteria	Ectothiorhodospiraceae	13.37	38.8	Sulfur oxidation
2401	<i>Geothrix fermentans</i>	99.2	NR036779	Acidobacteria	Holophagae	0.21	34.7	Iron(III) reduction
14834	<i>Thioalbus denitrificans</i>	96.8	NR122087	Gammmaproteobacteria	Ectothiorhodospiraceae	0.20	33.7	Sulfur oxidation
7917	<i>Thioprotundum lithotrophicum</i>	95.2	NR112829	Gammmaproteobacteria	Thioalkalispiraceae	0.09	30.7	Sulfur oxidation
2865	<i>Pelobacter carbinolicus</i>	95.2	NR075013	Deltaproteobacteria	Pelobacteraceae	0.09	28.6	Iron(III) reduction, sulfate reduction
425	<i>Geobacter luticola</i>	99.6	NR114303	Deltaproteobacteria	Geobacteraceae	6.02	26.5	Iron(III) reduction
20	<i>Thioprotundum lithotrophicum</i>	94.5	NR112829	Gammmaproteobacteria	Thioalkalispiraceae	0.07	22.5	Sulfur oxidation
12681	<i>Thioprotundum lithotrophicum</i>	96.4	NR112829	Gammmaproteobacteria	Thioalkalispiraceae	0.33	22.1	Sulfur oxidation
5722	<i>Thioalkalispira microaerophila</i>	96.8	NR025239	Gammmaproteobacteria	Thioalkalispiraceae	10.17	21.4	Sulfur oxidation
15348	<i>Thioprotundum lithotrophicum</i>	95.3	NR112829	Gammmaproteobacteria	Thioalkalispiraceae	0.31	17.4	Sulfur oxidation
13687	<i>Desulfovibrio butyratiphilus</i>	95.3	NR112679	Deltaproteobacteria	Desulfovibrionales	0.09	15.3	Butyrate oxidation, sulfate reduction
3917	<i>Geobacter pelophilus</i>	97.6	NR026077	Deltaproteobacteria	Geobacteraceae	0.12	12.9	Iron(III) reduction
14604	<i>Desulfocapsa sulfexigens</i>	93.3	KF952439	Deltaproteobacteria	Desulfobacterales	0.06	10.2	Sulfur disproportionation
12930	<i>Thioalkalispira microaerophila</i>	97.6	NR025239	Gammmaproteobacteria	Thioalkalispiraceae	0.12	9.7	Sulfur oxidation
17265	<i>Desulfomonile tiedjei</i>	98.4	NR074118	Deltaproteobacteria	Syntrophaceae	0.09	7.7	Sulfate reduction
9626	<i>Desulfobulbus mediterraneus</i>	94.5	NR025150	Deltaproteobacteria	Desulfobulbaceae	4.05	6.2	Sulfate reduction
1714	<i>Thioprotundum lithotrophicum</i>	96.0	NR112829	Gammmaproteobacteria	Thioalkalispiraceae	0.06	6.1	Sulfur oxidation

<sup>a</sup>The relative abundance of the 16S rRNA transcripts in the NTS library. More than 0.05% of the abundance is shown.

<sup>b</sup>The increasing ratio was calculated from the relative abundance in the NTS library to that in the CT5 library.

<sup>c</sup>The putative function was determined by the reported physiology of the closely related species.

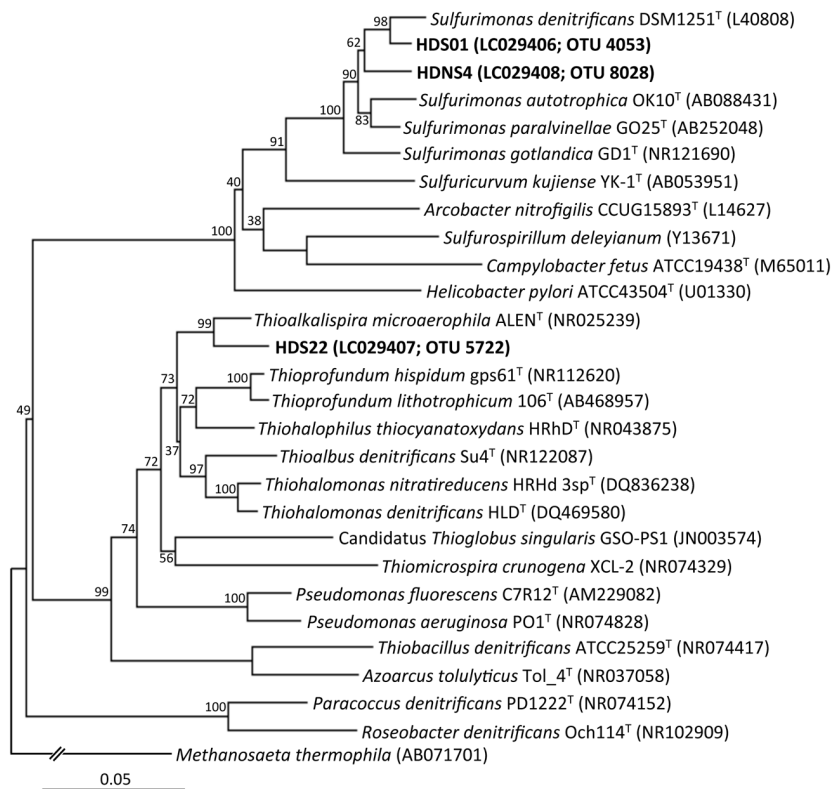
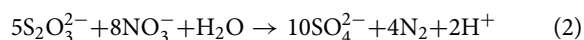


**FIGURE 5 | Phylogenetic tree showing the taxonomic distribution of 16S rRNA genes from isolates (the strains HDS01, HDNS4, and HDS22), and their known cultivated relatives.** The tree was constructed by the

neighbor-joining method using the nearly full-length 16S rRNA gene sequences. Bootstrap values were obtained from 1,000 replications. The scale bar represents 5% sequence divergence.

reports showing that, in the absence of organic matter as a carbon source, denitrification was coupled with sulfur oxidation in anoxic marine sediments in the Black Sea and the Baltic Sea (Böttcher and Lepland, 2000; Zopfi et al., 2004; Thang et al., 2013). Sulfur compounds that were originally present in the sediments may have served as the electron donor. In this study, the content ratios of sulfur significantly decreased with time in solid-phase sediments amended with nitrate (Figure 2). This strongly suggests that certain sulfur compounds such as zerovalent sulfur, thiosulfate, and hydrosulfide ion were oxidized to sulfate in association with denitrification. The oxidation of these compounds and its coupling with denitrification are expressed by the following equations (Cardoso et al., 2006; Zhang et al., 2015):



Indeed, throughout the incubation of nitrate-amended sediments, the concentration of nitrate decreased by 17.7 mM, while that of sulfate increased by 11.3 mM (Figures 1B,C). The ratio of

$NO_3^-/SO_4^{2-}$  was 1.57, which is close to the expected stoichiometric value from the equilibrium (3). The accumulation of hydrogen sulfide, the end product of sulfate reduction, has frequently been observed in anoxic marine sediments (Holmer and Kristensen, 1992; Zopfi et al., 2004). This implies that hydrogen sulfide was most likely the electron donor utilized for the redox reaction with denitrification in such environments.

The sulfur oxidizers affiliated with the classes Epsilon- and Gamma-proteobacteria were drastically proliferated in the nitrate-amended sediments, as revealed by Illumina sequencing of 16S rRNA genes and transcripts (Figure 3). The predominant OTUs 4053 and 5722 were successfully isolated and were designated as *Sulfurimonas* sp. strain HDS01 and *Thioalkalispira* sp. strain HDS22, respectively. The 16S rRNA genes of these isolates had 95.2–96.7% sequence similarities to those of cultured relatives and were able to grow chemolithotrophically on nitrate and sulfur compounds such as elemental sulfur and thiosulfate. These chemolithotrophic sulfur oxidizers drastically increased during the incubation; the relative abundances of the OTU 4053 (strain HDS01) and the OTU 5722 (strain HDS22) increased from 0.03% and 0.5% at day 0 to 42.7% and 12.5% at day 5, respectively. In addition, the expression levels of the bacterial rRNA were clearly enhanced by nitrate (Figures 4B,D). Furthermore, lower  $CO_2$  concentrations were found in the nitrate-amended

sediments than in the non-amended controls, suggesting the occurrence of CO<sub>2</sub> fixation in the former (**Figure 1A**). These results strongly suggest that the OTUs 4053 and 5722 (i.e., the strains HDS01 and HDS22, respectively) were directly involved in chemolithotrophic denitrification-dependent sulfur oxidation in the marine sediments. High-resolution microbial analysis further indicated that, aside from these two isolates, the order Chromatiales proliferated and became metabolically active (**Figure 4** and Supplementary Figure S5). This phylogenetic group may have played a complementary role in the geochemical cycles of sulfur and nitrogen in the marine sediments. On the other hand, the filamentous sulfur-oxidizing Desulfobulbaceae bacteria, which originally dominated the sediment microbial communities, did not increase under nitrate amendment, indicating that they played only minor roles in the redox process.

Notably, anaerobic microorganisms in addition to the chemolithotrophic sulfur oxidizers were metabolically activated at the end of the nitrate-amended incubation (**Table 1**). Sulfate, iron(III), and CO<sub>2</sub> were originally present in the marine sediments (**Figures 1A,C** and Supplementary Figure S1E) and thus were available as electron acceptors for anaerobic respiration processes. Fine-scale analyses of Illumina sequence data successfully detected the increases in 16S rRNA transcripts from fermentative and nitrate-reducing bacteria (i.e., *Cellulomonas* sp.), iron(III) reducers (e.g., *Geobacter* spp., *Pelobacter* sp., and *Geothrix* sp.), and acetate-clastic methanogens (i.e., *Methanoseta* sp.) at day 5 (**Table 1**), although no changes in geochemical parameters such as the concentrations of TOC, iron(II), and CH<sub>4</sub> were found (Supplementary Figures S1B,F). It is tempting to speculate that the carbon fixed by the chemolithotrophic sulfur oxidizers might be utilized as an electron donor by these anaerobically respiring microorganisms. In order to clarify the trophic relationships of anaerobic microorganisms in the marine sediments, isotope-tracing assays such as ultra-high-sensitivity stable isotope probing (Aoyagi et al., 2015) should be applied.

It is also noteworthy that two different types of chemolithotrophic sulfur-oxidizing bacteria (i.e., the genus *Sulfurimonas* and the order Chromatiales) coexisted in our experiments (**Figure 4**). Niche differentiation of these physiologically similar microorganisms developed during the incubation, and was a potential driving force in shaping the sediment microbial communities. A single species [the OTU 4053 (strain HDS01)] of the genus *Sulfurimonas* increased exclusively (**Figures 4A,B**), while a wide variety of species [e.g., OTUs 5722 (strain HDS22), 3944, and 1143] within the order Chromatiales became metabolically active. Almost all of the top Chromatiales bacteria in terms of 16S rRNA transcript expression levels, with the exception of the OTUs 5722 and 6560 (Supplementary Figure S5D), accounted for quite low percentages of the total microbial populations at the gene level (Supplementary Figure S5C), suggesting that these minor Chromatiales members actively dissimilated sulfur and nitrate but only marginally assimilated carbon for their growth in the sediments. Recently,

genomics-based studies have reported that bacteria belonging to the genus *Sulfurimonas* and those belonging to the order Chromatiales employed different metabolic pathways for sulfur oxidation, nitrate reduction, and carbon fixation (Sievert et al., 2008; Kovaleva et al., 2011; Grote et al., 2012; Handley et al., 2014; Thomas et al., 2014). Further, some Chromatiales bacteria have been reported to be capable of growing specifically at low concentrations (i.e., 1–2 mM) of nitrate, and thereby adapting to energy-limiting conditions (Sorokin et al., 2006). These metabolic types and capacities might have triggered the distinct responses of these two sulfur oxidizers to nitrate amendment. More detailed physiological characterization and investigation into the competitive mechanism of these two isolates (the strains HDS01 and HDS22) may lead to a better understanding of the niche differentiation of sulfur-oxidizing bacteria in marine sediments.

## Conclusion

The results of this study demonstrated that the novel microorganisms *Sulfurimonas* sp. strain HDS01 and *Thioalkalispira* sp. strain HDS22 were directly involved in the chemolithotrophic denitrification-dependent sulfur oxidation in nitrate-amended marine sediments. In addition to these two sulfur-oxidizers, a variety of the Chromatiales bacteria, including minor but metabolically active microorganisms, might also play important roles in the geochemical cycles of sulfur, nitrogen, and carbon. High-resolution analyses of 16S rRNA transcripts implicated trophic interaction and niche differentiation of key microorganisms as the ecological principles underlying the reorganization of microbial communities. The two different types of sulfur oxidizers stably co-existed in the sediments and complementarily fixed carbon, leading to the metabolic activation of fermentative bacteria, ferric iron reducers, and acetate-clastic methanogens. The mechanisms underlying the community reorganization should be studied to gain deeper insight into the stability and flexibility of microbial ecosystems.

## Acknowledgments

We thank Akemi Katayama and Yumiko Kayashima for technical assistance. This study was supported by Japan Society for the Promotion of Science (JSPS) KAKENHI Grants Number 24651089 (Grant-in-Aid for Challenging Exploratory Research) and 25701003 [Grant-in-Aid for Young Scientists (A)].

## Supplementary Material

The Supplementary Material for this article can be found online at: <http://journal.frontiersin.org/article/10.3389/fmicb.2015.00426/abstract>

## References

- Aoyagi, T., Hanada, S., Itoh, H., Sato, Y., Ogata, A., Friedrich, M. W., et al. (2015). Ultra-high-sensitivity stable-isotope probing of rRNA by high-throughput sequencing of isopycnic centrifugation gradients. *Environ. Microbiol. Rep.* 7, 282–287. doi: 10.1111/1758-2229.12243
- Armenteros, M., Pérez-García, J. A., Ruiz-Abierno, A., Diaz-Asencio, L., Helguera, Y., Vincx, M., et al. (2010). Effects of organic enrichment on nematode assemblages in a microcosm experiment. *Mar. Environ. Res.* 70, 374–382. doi: 10.1016/j.marenvres.2010.08.001
- Böttcher, M. E., and Lepland, A. (2000). Biogeochemistry of sulfur in a sediment core from the west-central Baltic Sea: evidence from stable isotopes and pyrite textures. *J. Mar. Syst.* 25, 299–312. doi: 10.1016/S0924-7963(00)00023
- Braunschweig, J., Bosch, J., Heister, K., Kuebeck, C., and Meckenstock, R. U. (2012). Reevaluation of colorimetric iron determination methods commonly used in geomicrobiology. *J. Microbiol. Methods* 89, 41–48. doi: 10.1016/j.mimet.2012.01.021
- Campbell, B. J., Engel, A. S., Porter, M. L., and Takai, K. (2006). The versatile epsilon-proteobacteria: key players in sulphidic habitats. *Nat. Rev. Microbiol.* 4, 458–468. doi: 10.1038/nrmicro1414
- Caporaso, J. G., Kuczynski, J., Stombaugh, J., Bittinger, K., Bushman, F. D., Costello, E. K., et al. (2010). QIIME allows analysis of high-throughput community sequencing data. *Nat. Methods* 7, 335–336. doi: 10.1038/nmeth.f.303
- Caporaso, J. G., Lauber, C. L., Walters, W. A., Berg-Lyons, D., Huntley, J., Fierer, N., et al. (2012). Ultra-high-throughput microbial community analysis on the Illumina HiSeq and MiSeq platforms. *ISME J.* 6, 1621–1624. doi: 10.1038/ismej.2012.8
- Caporaso, J. G., Lauber, C. L., Walters, W. A., Berg-Lyons, D., Lozupone, C. A., Turnbaugh, P. J., et al. (2011). Global patterns of 16S rRNA diversity at a depth of millions of sequences per sample. *Proc. Natl. Acad. Sci. U.S.A.* 108(Suppl. 1), 4516–4522. doi: 10.1073/pnas.1000080107
- Cardoso, R. B., Sierra-Alvarez, R., Rowlette, P., Flores, E. R., Gomez, J., and Field, J. A. (2006). Sulfide oxidation under chemolithoautotrophic denitrifying conditions. *Biotechnol. Bioeng.* 95, 1148–1157. doi: 10.1002/bit.21084
- Friedrich, C. G., Rother, D., Bardischewsky, F., Quentmeier, A., and Fischer, J. (2001). Oxidation of reduced inorganic sulfur compounds by bacteria: emergence of a common mechanism? *Appl. Environ. Microbiol.* 67, 2873–2882. doi: 10.1128/aem.67.7.2873-2882.2001
- Grote, J., Schott, T., Bruckner, C. G., Glockner, F. O., Jost, G., Teeling, H., et al. (2012). Genome and physiology of a model Epsilonproteobacterium responsible for sulfide detoxification in marine oxygen depletion zones. *Proc. Natl. Acad. Sci. U.S.A.* 109, 506–510. doi: 10.1073/pnas.1111262109
- Habicht, K. S., and Canfield, D. E. (1997). Sulfur isotope fractionation during bacterial sulfate reduction in organic-rich sediments. *Geochim. Cosmochim. Acta* 61, 5351–5361. doi: 10.1016/S0016-7037(97)00311-6
- Handley, K. M., Bartels, D., O’Loughlin, E. J., Williams, K. H., Trimble, W. L., Skinner, K., et al. (2014). The complete genome sequence for putative H<sub>2</sub>- and S-oxidizer *Candidatus Sulfuricurvum* sp., assembled de novo from an aquifer-derived metagenome. *Environ. Microbiol.* 16, 3443–3462. doi: 10.1111/1462-2920.12453
- Hansen, H. P., and Koroleff, F. (2007). “Determination of nutrients,” in *Methods of Seawater Analysis*, eds K. Grasshoff, K. Kremling, and M. Ehrhardt (Weinheim: Wiley-VCH), 159–228. doi: 10.1002/9783527613984.ch10
- Holmer, M., and Kristensen, E. (1992). Impact of marine fish cage farming on metabolism and sulphate reduction of under-lying sediment. *Mar. Ecol. Progr. Ser.* 80, 191–201. doi: 10.3354/meps080191
- Hori, T., Haruta, S., Ueno, Y., Ishii, M., and Igarashi, Y. (2006). Dynamic transition of a methanogenic population in response to the concentration of volatile fatty acids in a thermophilic anaerobic digester. *Appl. Environ. Microbiol.* 72, 1623–1630. doi: 10.1128/aem.72.2.1623-1630.2006
- Hori, T., Kimura, M., Aoyagi, T., R. Navarro, R., Ogata, A., Sakoda, A., et al. (2014). Biodegradation potential of organically enriched sediments under sulfate- and iron-reducing conditions as revealed by the 16S rRNA deep sequencing. *J. Water Environ. Technol.* 12, 357–366. doi: 10.2965/jwet.2014.357
- Hori, T., Muller, A., Igarashi, Y., Conrad, R., and Friedrich, M. W. (2010). Identification of iron-reducing microorganisms in anoxic rice paddy soil by <sup>13</sup>C-acetate probing. *ISME J.* 4, 267–278. doi: 10.1038/ismej.2009.100
- Inui, T., Yasutaka, T., Endo, K., and Katsumi, T. (2012). Geo-environmental issues induced by the 2011 off the Pacific Coast of Tohoku Earthquake and tsunami. *Soils Found.* 52, 856–871. doi: 10.1016/j.sandf.2012.11.008
- Itoh, H., Aita, M., Nagayama, A., Meng, X. Y., Kamagata, Y., Navarro, R., et al. (2014). Evidence of environmental and vertical transmission of *Burkholderia* symbionts in the oriental chinch bug, *Cavelerius saccharivorus* (Heteroptera: Blissidae). *Appl. Environ. Microbiol.* 80, 5974–5983. doi: 10.1128/aem.01087-4
- Kanno, M., Katayama, T., Tamaki, H., Mitani, Y., Meng, X. Y., Hori, T., et al. (2013). Isolation of butanol- and isobutanol-tolerant bacteria and physiological characterization of their butanol tolerance. *Appl. Environ. Microbiol.* 79, 6998–7005. doi: 10.1128/aem.02900-3
- Kemp, W. M., Sampou, P., Caffrey, J., Mayer, M., Henriksen, K., and Boynton, W. R. (1990). Ammonium recycling versus denitrification in Chesapeake Bay sediments. *Limnol. Oceanogr.* 35, 1545–1563. doi: 10.4319/lo.1990.35.7.1545
- Kotsyurbenko, O. R., Friedrich, M. W., Simankova, M. V., Nozhevnikova, A. N., Golyshin, P. N., Timmis, K. N., et al. (2007). Shift from acetoclastic to H<sub>2</sub>-dependent methanogenesis in a west Siberian peat bog at low pH values and isolation of an acidophilic *Methanobacterium* strain. *Appl. Environ. Microbiol.* 73, 2344–2348. doi: 10.1128/aem.02413-6
- Kovaleva, O. L., Tourova, T. P., Muzyer, G., Kolganova, T. V., and Sorokin, D. Y. (2011). Diversity of RuBisCO and ATP citrate lyase genes in soda lake sediments. *FEMS Microbiol. Ecol.* 75, 37–47. doi: 10.1111/j.1574-6941.2010.00996.x
- Kunihiro, T., Takasu, H., Miyazaki, T., Uramoto, Y., Kinoshita, K., Yodnasari, S., et al. (2011). Increase in Alphaproteobacteria in association with a polychaete, *Capitella* sp. I, in the organically enriched sediment. *ISME J.* 5, 1818–1831. doi: 10.1038/ismej.2011.57
- Labrenz, M., Jost, G., Pohl, C., Beckmann, S., Martens-Habben, W., and Jurgens, K. (2005). Impact of different in vitro electron donor/acceptor conditions on potential chemolithoautotrophic communities from marine pelagic redoxclines. *Appl. Environ. Microbiol.* 71, 6664–6672. doi: 10.1128/aem.71.11.6664-6672.2005
- Lane, D. J. (1991). “16S/23S rRNA sequencing,” in *Nucleic Acid Techniques in Bacterial Systematics*, eds E. Stackebrandt M. Goodfellow (Chichester: John Wiley and Sons), 115–175.
- Lueders, T., and Friedrich, M. W. (2002). Effects of amendment with ferrihydrite and gypsum on the structure and activity of methanogenic populations in rice field soil. *Appl. Environ. Microbiol.* 68, 2484–2494. doi: 10.1128/AEM.68.5.2484-2494.2002
- Lydmark, P., Almstrand, R., Samuelsson, K., Mattsson, A., Sorensson, F., Lindgren, P. E., et al. (2007). Effects of environmental conditions on the nitrifying population dynamics in a pilot wastewater treatment plant. *Environ. Microbiol.* 9, 2220–2233. doi: 10.1111/j.1462-2920.2007.01336.x
- Miller, C. S., Handley, K. M., Wrighton, K. C., Frischkorn, K. R., Thomas, B. C., and Banfield, J. F. (2013). Short-read assembly of full-length 16S amplicons reveals bacterial diversity in subsurface sediments. *PLoS ONE* 8:e56018. doi: 10.1371/journal.pone.0056018
- Nakagawa, S., and Takai, K. (2008). Deep-sea vent chemoautotrophs: diversity, biochemistry and ecological significance. *FEMS Microbiol. Ecol.* 65, 1–14. doi: 10.1111/j.1574-6941.2008.00502.x
- Nakagawa, S., Takai, K., Inagaki, F., Hirayama, H., Nunoura, T., Horikoshi, K., et al. (2005). Distribution, phylogenetic diversity and physiological characteristics of epsilon-Proteobacteria in a deep-sea hydrothermal field. *Environ. Microbiol.* 7, 1619–1632. doi: 10.1111/j.1462-2920.2005.00856.x
- Noll, M., Matthies, D., Frenzel, P., Derakhshani, M., and Liesack, W. (2005). Succession of bacterial community structure and diversity in a paddy soil oxygen gradient. *Environ. Microbiol.* 7, 382–395. doi: 10.1111/j.1462-2920.2005.00700.x
- Ontiveros-Valencia, A., Ziv-El, M., Zhao, H. P., Feng, L., Rittmann, B. E., and Krajmalnik-Brown, R. (2012). Interactions between nitrate-reducing and sulfate-reducing bacteria coexisting in a hydrogen-fed biofilm. *Environ. Sci. Technol.* 46, 11289–11298. doi: 10.1021/es302370t
- Pearson, T. H., and Rosenberg, R. (1978). Macrobenthic succession in relation to organic enrichment and pollution of the marine environment. *Oceanogr. Mar. Biol.* 16, 229–311. doi: 10.2983/035.034.0121ü1.10
- Sievert, S. M., Scott, K. M., Klotz, M. G., Chain, P. S., Hauser, L. J., Hemp, J., et al. (2008). Genome of the epsilonproteobacterial chemolithoautotroph

- Sulfurimonas denitrificans*. *Appl. Environ. Microbiol.* 74, 1145–1156. doi: 10.1128/aem.01844-7
- Sorokin, D. Y., Tourova, T. P., Lysenko, A. M., and Muyzer, G. (2006). Diversity of culturable halophilic sulfur-oxidizing bacteria in hypersaline habitats. *Microbiology* 152, 3013–3023. doi: 10.1099/mic.0.29106-0
- Tamura, K., Peterson, D., Peterson, N., Stecher, G., Nei, M., and Kumar, S. (2011). MEGA5: molecular evolutionary genetics analysis using maximum likelihood, evolutionary distance, and maximum parsimony methods. *Mol. Biol. Evol.* 28, 2731–2739. doi: 10.1093/molbev/msr121
- Thang, N., Brüchert, V., Formolo, M., Wegener, G., Ginters, L., Jørgensen, B., et al. (2013). The impact of sediment and carbon fluxes on the biogeochemistry of methane and sulfur in littoral Baltic Sea Sediments (Himmerfjärden, Sweden). *Estuaries Coasts* 36, 98–115. doi: 10.1007/s12237-012-9557-0
- Thomas, F., Giblin, A. E., Cardon, Z. G., and Sievert, S. M. (2014). Rhizosphere heterogeneity shapes abundance and activity of sulfur-oxidizing bacteria in vegetated salt marsh sediments. *Front. Microbiol.* 5:309. doi: 10.3389/fmicb.2014.00309
- Zhang, Z., Lo, I. C., Zheng, G., Woon, K., and Rao, P. (2015). Effect of autotrophic denitrification on nitrate migration in sulfide-rich marine sediments. *J. Soils Sediments* 15, 1019–1028. doi: 10.1007/s11368-015-1078-6
- Zopfi, J., Ferdelman, T. G., and Fossing, H. (2004). Distribution and fate of sulfur intermediates—sulfite, tetrathionate, thiosulfate, and elemental sulfur—in marine sediments. *Geol. Soc. Am. Special Pap.* 379, 97–116. doi: 10.1130/0-8137-2379-5.97

**Conflict of Interest Statement:** The authors declare that the research was conducted in the absence of any commercial or financial relationships that could be construed as a potential conflict of interest.

Copyright © 2015 Aoyagi, Kimura, Yamada, Navarro, Itoh, Ogata, Sakoda, Katayama, Takasaki and Hori. This is an open-access article distributed under the terms of the Creative Commons Attribution License (CC BY). The use, distribution or reproduction in other forums is permitted, provided the original author(s) or licensor are credited and that the original publication in this journal is cited, in accordance with accepted academic practice. No use, distribution or reproduction is permitted which does not comply with these terms.



# Bacterial population succession and adaptation affected by insecticide application and soil spraying history

Hideomi Itoh<sup>1</sup>, Ronald Navarro<sup>2</sup>, Kazutaka Takeshita<sup>1</sup>, Kanako Tago<sup>3</sup>, Masahito Hayatsu<sup>3</sup>, Tomoyuki Hori<sup>2</sup> and Yoshitomo Kikuchi<sup>1\*</sup>

<sup>1</sup> Bioproduction Research Institute, National Institute of Advanced Industrial Science and Technology (AIST), Sapporo, Japan

<sup>2</sup> Research Institute for Environmental Management Technology, National Institute of Advanced Industrial Science and Technology (AIST), Tsukuba, Japan

<sup>3</sup> Environmental Biofunction Division, National Institute for Agro-Environmental Sciences, Tsukuba, Japan

## Edited by:

Shin Haruta, Tokyo Metropolitan University, Japan

## Reviewed by:

Raffaella Balestrini, Consiglio Nazionale delle Ricerche, Italy  
Joerg Graf, University of Connecticut, USA  
Satoshi Ishii, Hokkaido University, Japan

## \*Correspondence:

Yoshitomo Kikuchi, Bioproduction Research Institute, National Institute of Advanced Industrial Science and Technology (AIST), 2-17-2-1, Tsukisamu-higashi, Toyohira-ku, Sapporo, Hokkaido 062-8517, Japan  
e-mail: y-kikuchi@aist.go.jp

Although microbial communities have varying degrees of exposure to environmental stresses such as chemical pollution, little is known on how these communities respond to environmental disturbances and how past disturbance history affects these community-level responses. To comprehensively understand the effect of organophosphorus insecticide application on microbiota in soils with or without insecticide-spraying history, we investigated the microbial succession in response to the addition of fenitrothion [*O,O*-dimethyl *O*-(3-methyl-*p*-nitrophenyl) phosphorothioate, abbreviated as MEP] by culture-dependent experiments and deep sequencing of 16S rRNA genes. Despite similar microbial composition at the initial stage, microbial response to MEP application was remarkably different between soils with and without MEP-spraying history. MEP-degrading microbes more rapidly increased in the soils with MEP-spraying history, suggesting that MEP-degrading bacteria might already exist at a certain level and could quickly respond to MEP re-treatment in the soil. Culture-dependent and -independent evaluations revealed that MEP-degrading *Burkholderia* bacteria are predominant in soils after MEP application, limited members of which might play a pivotal role in MEP-degradation in soils. Notably, deep sequencing also revealed that some methylotrophs dramatically increased after MEP application, strongly suggesting that these bacteria play a role in the consumption and removal of methanol, a harmful derivative from MEP-degradation, for better growth of MEP-degrading bacteria. This comprehensive study demonstrated the succession and adaptation processes of microbial communities under MEP application, which were critically affected by past experience of insecticide-spraying.

**Keywords:** fenitrothion, organophosphorus insecticide, soil microbes, deep sequencing, *Burkholderia*, methylotroph

## INTRODUCTION

Biological communities are exposed to varying levels of environmental stresses or disturbances such as global warming, typhoon, drought, and bush fire (Phillips et al., 2009; O'Connell and Nyman, 2011; Peñuelas et al., 2013; Rota et al., 2014), and little is known about community succession and adaptation processes under such environmental stimuli. In addition to naturally occurring environmental disturbances, chemical insecticides have been developed and used worldwide to control agricultural, hygienic, and household pest insects. Although insecticides have revolutionized modern agriculture and sanitation in terms of pest management, abuse of usage sometimes causes serious problems including environmental pollution from its residues, health hazard, unexpected effects on non-targeted organisms, and evolution of insecticide-resistant insects (Whalon et al., 2008; Diez, 2010). Thus, insecticide-spraying is thought to be a man-made, yet strong, environmental stress on natural organisms.

Organophosphorus insecticide, a general name referring to insecticides containing a phosphoester bond, is one of the most widely used insecticides. It includes a number of commercially available chemicals such as diazinon, malathion, and dichlorvos (Singh and Walker, 2006; Singh, 2009). The chemical compounds found in organophosphorus insecticide show high mammalian toxicity as well as insecticidal activity by inhibiting acetylcholinesterase (AChE), causing overstimulation of the cholinergic synapses by the overaccumulation of acetylcholine (da Silva et al., 2013). Fenitrothion [*O,O*-dimethyl *O*-(3-methyl-*p*-nitrophenyl) phosphorothionate, abbreviated as MEP] is one of the organophosphorus compounds commonly used because of its broad-spectrum activity and less mammal toxicity. In natural fields, MEP can be degraded photochemically, but is mainly degraded by soil bacteria. Biodegradation pathways of MEP were first investigated in forest soils using C<sup>14</sup>-labeled MEP (Spillner et al., 1979) and are currently described in the International Programme on Chemical Safety IPCS (1992). In

microorganisms, MEP is hydrolyzed to 3-methyl-4-nitrophenol and then finally decomposed to CO<sub>2</sub> through a phenol ring cleavage pathway (IPCS, 1992). Previous culture-dependent studies reported that members of the genera *Burkholderia*, *Pseudomonas*, *Cupriavidus*, *Corynebacterium*, *Arthrobacter*, and *Sphingomonas* have been identified as MEP-degraders, some of which use the compound as a sole carbon source (Tago et al., 2006; Zhang et al., 2006; Kim et al., 2009). Considering that only a tiny fraction of environmental bacteria is culturable (Wilson and Piel, 2013), culture-independent as well as culture-dependent approaches are pivotal to comprehensively understand microbial dynamics in soils after spraying with MEP, as previously mentioned (Jacobsen and Hjelmsø, 2014).

Recent advances in sequence technologies, the so-called next generation sequencing (NGS), provide a faster and simpler alternative to previously established techniques for the comprehensive investigation of microbial community structures (Moorthie et al., 2011). Fairly recent works using NGS include the evaluation of microbial community compositions of soils polluted with organochlorine pesticides including Dichlorodiphenyltrichloroethane (DDT), hexachlorocyclohexane (HCH), and 2-chloro-4-ethylamino-6-isopropylamino-s-triazine (ATZ) (Fang et al., 2014). Based on the metagenomic survey of functional genes, these studies have suggested that diverse bacterial species complement one another to degrade these organochlorides (Fang et al., 2014).

In crop fields, biodegradation of the insecticides is one of the pivotal factors affecting the recovery and sustainability of soil ecosystems. Furthermore, it has been reported that one or more previous applications of the same insecticides and/or other structurally-analogous insecticides frequently result to less persistence of the insecticide in the environment (Felsot, 1989). In soil environments where the same insecticide has been continuously sprayed, it has been hypothesized that insecticide-degrading microbes grow by assimilating the insecticide and are enriched in the soil, which cause excessively enhanced biodegradation of the sprayed insecticides (Arbeli and Fuentes, 2007). However, it remains unclear how microbial communities transit under and adapt to insecticide-spraying and how the history of insecticide-spraying affects these succession and adaptation processes of soil microbial communities.

By combining the culture-independent approach using the NGS technique with culture-dependent isolation of MEP-degrading bacteria, we investigated the detailed process of microbial succession when MEP was sprayed on field-collected soils with or without a history of MEP-spraying prior to collection. Among the collected soils, one has been sprayed with MEP at least for 4 years and the other has never been sprayed with MEP nor with other organophosphorus compounds. The NGS analysis combined with culture-dependent approach clearly demonstrates previously unseen dynamics of soil microbiota during MEP-spraying, highlighting the different responses of microbiota against the experimental MEP-spraying in the different types of soil, and identifying the key players of MEP-degradation in soil environments.

## MATERIALS AND METHODS

### SOILS

We collected two andisol soils from agricultural fields located at the National Institute for Agro-Environmental Sciences (Tsukuba, Ibaraki, Japan; 36°0'N, 140°1'E): *soil S* (Sprayed soil) was collected from a crop field that had been sprayed with MEP for at least 4 years [pH(H<sub>2</sub>O), 6.3; water content (w/w), 35.2%; total carbon, 5.0%; total nitrogen, <0.3%]; *soil N* (Naive soil) was collected from a field that had never been sprayed with MEP and other organophosphorus compounds [pH(H<sub>2</sub>O), 6.6; water content (w/w), 33.7%; total carbon, 4.4%; total nitrogen, <0.3%]. Characterization of these soil samples is summarized in Table S1. Each soil was passed through a 2 mm sieve to remove large organic litters like leaves and roots.

### INSECTICIDE-SPRAYING EXPERIMENTS

Experimental design of the insecticide-spraying test is shown in Figure S1. Approximately 150 g (dry weight) of each of the sieved soils were transferred into plastic pots (10 × 8 cm; opening diameter × depth). The potted soils were incubated at 25°C with weekly application of MEP solution (diluted by distilled water) at a specific loading of 50 mg kg<sup>-1</sup>-dry soil (Tago et al., 2006). For both soils S and N, duplicate runs (pot 1 and pot 2) were prepared and individually subjected to experiments and further analyses. Control treatments were conducted under the same conditions, but the addition of MEP solution was replaced by equal amount of distilled water only once a week. These pots were covered with a sheet of aluminum foil during incubation to prevent water evaporation and photodegradation of MEP. Soil samples from the surface layer up to a depth of 1 cm were collected 1 week after the final spraying, e.g., soil samples treated three times with MEP were collected 1 week after the 3rd MEP-spraying (see Figure S1), and then subjected to the various analyses described below.

### CFU COUNTING OF MEP-DEGRADING BACTERIA

The total CFU (colony forming units) counts of MEP-degrading bacteria was measured by plating serial dilutions of soil samples [1% (w/w) diluted in distilled water] on 1.5% agar plates of MEP medium [0.08% MEP, 20 mM potassium phosphate (pH 7.0), 0.1% (NH<sub>4</sub>)<sub>2</sub>SO<sub>4</sub>, 0.02% NaCl, 0.01% MgSO<sub>4</sub>•7H<sub>2</sub>O, 0.05% CaCl<sub>2</sub>•2H<sub>2</sub>O, 0.0002% FeSO<sub>4</sub>•7H<sub>2</sub>O, 0.1% yeast extract] and incubated for 4 days at 25°C, as previously described (Tago et al., 2006). The CFU of MEP-degrading bacteria were determined by counting the colonies with a halo on the MEP plates. In the halo-forming assay, the bacteria that are capable of degrading MEP to 3-methyl-4-nitrophenol were detected.

### ISOLATION AND IDENTIFICATION OF MEP-DEGRADING BACTERIA

Isolated colonies were identified based on the partial sequences (c.a. 600 bp) of their 16S rRNA genes. During isolation, each of the colonies was picked with a sterile toothpick and then suspended in 35 μl TE buffer [10 mM Tris-HCl, 1 mM EDTA (pH 8.0)] in each well of a 96 well titer plate. The cells were subjected to heat shock treatment (98°C for 3 min) in order to extract the genomic DNA, which was used as template for PCR amplification. The PCR amplification of bacterial 16S rRNA gene was performed with the use of a KOD Fx

Neo polymerase (TOYOBO, Tokyo, Japan), a universal primer set, 16SA1 [5'-AGAGTTTGATCMTGGCTCAG-3'] and 16SB1 [5'-TACGGYTACCTTGTACGACTT-3'] (Fukatsu and Nikoh, 1998), and the template DNA extracted as described above. The temperature program for PCR is as follows: 94°C for 2 min, followed by 20 cycles of 98°C for 10 s, 55°C for 30 s, and 68°C for 90 s. The resulting 1.5 kb amplicons were used as templates of sequencing reaction conducted with a universal primer 357F [5'-CCTACGGGAGGCAGCAG-3'] (Muyzer et al., 1993). Taxonomic assignment of the resulting sequences was double checked by the RDP multiclassifier ver. 1.1 (Wang et al., 2007) and BLASTN-search (<http://ncbi.nlm.nih.gov/blast/>) against GreenGene database (DeSantis et al., 2006).

### DEEP SEQUENCING

DNA was extracted from soil S and soil N samples before treatment (S0, N0), after the 2nd (S2) and 3rd (S3, N3) MEP-treatments, and after the 3rd control treatment (S3C, N3C) by using a slightly modified published protocol (Noll et al., 2005). Briefly, 0.5 g wet soil was combined with 0.08 g skim milk, 700  $\mu$ l extraction buffer [50 mM Tris-HCl (pH 8.0), 1.7% Polyvinylpyrrolidone, 20 mM MgCl<sub>2</sub>], and 0.5 ml zirconia/silica beads (0.1 mm diameter, Biospec, OK, USA), and blended in a Multi-Beads Shocker (Yasui Kikai, Osaka, Japan) at 2000 rpm for 60 s. Crude extracts were purified by phenol/chloroform/isoamyl alcohol (25:24:1) treatment followed by isopropanol precipitation. Contaminating RNA was digested with Ribonuclease (Nippon Gene, Toyama, Japan). The prepared DNA was subjected to PCR amplification of 16S rRNA gene for deep sequencing. The variable region (V4) of bacterial 16S rRNA gene was amplified using universal primers 515F [5'-GTGCCAGCMGCCGCGGTAA-3'] and 806R [5'-GGACTACHVGGGTWTCTAAT-3'] (Caporaso et al., 2012). The PCR reaction mixture comprised of 50  $\mu$ M each dNTP, 0.4  $\mu$ M 515F with Illumina P5 sequences, 0.4  $\mu$ M 806R with 6-bases indexes and Illumina P7 sequences (Caporaso et al., 2012) (Illumina, San Diego, CA, USA), Q5 High-Fidelity DNA polymerase with Q5 reaction buffer (New England BioLabs, Ipswich, MA, USA) and the extracted soil DNA template. The PCR conditions were as follows: initial denaturation at 98°C for 90 s, followed by 25 cycles of 98°C for 10 s, 54°C for 30 s, 72°C for 30 s, and a final extension at 72°C for 2 min. The PCR amplicons were purified as described previously (Itoh et al., 2014). DNA libraries containing all tagged-amplicons and internal control phiX were generated for paired-end sequencing by the MiSeq sequencer using MiSeq Reagent kit v2 (Illumina, San Diego, CA, USA) according to the manufacturer's instruction.

### QUANTITATIVE PCR

Quantitative PCR (qPCR) of bacterial 16S rRNA gene was performed to amplify bacterial 16S rRNA genes using a Power SYBR Green PCR Master Mix (Applied Biosystems, Foster City, CA, USA) and the LightCycler 96 System (Roche Applied Science, Indianapolis, IN, USA). The reaction mixture was comprised of 2 $\times$  SYBR Green PCR Master Mix, 0.2  $\mu$ M 515F and 806R primer pairs (Caporaso et al., 2012), 0.5  $\mu$ g/ $\mu$ l BSA, and soil DNA as a template. The PCR conditions were as follows: initial

denaturation at 95°C for 10 min, followed by 45 cycles of 95°C for 30 s, 57°C for 30 s, and 72°C for 30 s. The amount of bacterial 16S rRNA gene copies was calculated on the basis of the standard curve constructed using a dilution series of the target PCR product of *Burkholderia* sp. SFA1 (DDBJ accession no. AB232333).

### DATA ANALYSIS

Internal control phiX sequences and low-quality sequences were removed, and paired sequences were joined as described previously (Itoh et al., 2014). Chimeric sequences were removed using uchime algorithm on Mothur program ver. 1.29.2 (Schloss et al., 2009) through the alignment with Greengene database (DeSantis et al., 2006). The resulting sequences were subjected to taxonomic assignment by using RDP multiclassifier ver. 1.1 (Wang et al., 2007) with an 80% confidence threshold. Operational taxonomic units (OTU) based analyses, including estimation of diversity indices and Principal Coordinate Analysis (PCoA) based on OTUs with 3% differences, were performed by using the macqiime ver. 1.6.0 (Caporaso et al., 2010). Phylogenetic tree was constructed by the neighbor-joining method with the bootstrap test (1000 replicates) under MEGA ver. 4.0.2 (Tamura et al., 2007). Analysis of variance (ANOVA) was performed using R software ver. 3.0.1 (R Development Core Team, 2008) to analyze differences in qPCR data among samples.

### NUCLEOTIDE SEQUENCE ACCESSION NUMBER

The nucleotide sequences reported in this study were deposited in the DDBJ/Genbank/EBI databases under the accession numbers: AB904935–AB905196 (16S rRNA gene sequences of isolates, Table S2) and the MG-RAST database (<http://metagenomics.anl.gov/>, Meyer et al., 2008) as a “Microbial succession under MEP-spraying in 2012” project under the ID: 4562358.3–4562369.3 (deep sequencing, Table 1).

## RESULTS

### POPULATION DYNAMICS OF MEP-DEGRADING BACTERIA IN MEP-SPRAYED SOILS

Abundance changes of MEP-degrading strains by a culture-dependent method were investigated using two types of soils with different MEP-spraying histories: MEP-sprayed “soil S” and MEP-naïve “soil N” (Table S1). Although the CFU of MEP-degrading bacteria were below the detectable level (<10<sup>3</sup> cfu g<sup>-1</sup> dry soil) even 1 week after the insecticide application, they became detectable after the 2nd and 3rd treatments in soil S and soil N, respectively, (Figure 1). In the control, with only the addition of distilled water, no MEP-degraders were detected even after the 3rd treatment (Figure 1). These results indicate that the repeated spraying of MEP acts as a strong selective pressure on soil microbiota, confirming our findings from previous studies (Tago et al., 2006; Kikuchi et al., 2012). It has also been reported that some bacteria are capable of utilizing MEP as a sole carbon source, fostering their population increase (Hayatsu et al., 2000; Tago et al., 2006; Zhang et al., 2006; Kim et al., 2009), which likely explains the above-observed population dynamics of MEP-degrading strains in soil environments.

**Table 1 | Summary of deep sequencing and qPCR.**

Soil	No. of spraying	Pot No.	Library ID	No. of sequences <sup>b</sup>	No. of OTU <sub>0.03</sub> <sup>c</sup>	Cx <sup>d</sup>	Diversity indices <sup>e</sup>			No. of copies <sup>f</sup>
							chao1	shannon	1/simpson	
S	0	1	S0p1	13,202	1,206	0.97	1,944 ± 107	7.98 ± 0.04	65 ± 2.7	3.6 ± 0.1 × 10 <sup>8</sup>
S	2	1	S2p1	13,346	796	0.99	1,188 ± 103	5.9 ± 0.03	15 ± 0.3	4.5 ± 0.3 × 10 <sup>8</sup>
S	3	1	S3p1	14,600	575	0.99	813 ± 79	3.86 ± 0.05	4.5 ± 0.1	4.7 ± 0.2 × 10 <sup>8</sup>
S	0	2	S0p2	6,218	1,062	0.93	2,446 ± 78	8.62 ± 0.01	109 ± 0.7	4.6 ± 0.2 × 10 <sup>8</sup>
S	2	2	S2p2	10,223	1,154	0.94	2,324 ± 116	7.72 ± 0.03	42 ± 0.8	4.0 ± 0.6 × 10 <sup>8</sup>
S	3	2	S3p2	8,213	897	0.96	1,731 ± 100	6.43 ± 0.03	13 ± 0.3	4.4 ± 0.5 × 10 <sup>8</sup>
S	0 <sup>a</sup>	control	S3C	17,933	1,533	0.94	2,260 ± 123	8.6 ± 0.04	124 ± 2.8	4.8 ± 1.2 × 10 <sup>8</sup>
N	0	1	N0p1	13,540	1,500	0.85	3,268 ± 190	9.07 ± 0.04	138 ± 5.8	5.5 ± 1.8 × 10 <sup>8</sup>
N	3	1	N3p1	10,171	1,028	0.95	1,919 ± 114	7.3 ± 0.03	36 ± 0.8	6.3 ± 0.9 × 10 <sup>8</sup>
N	0	2	N0p2	15,054	1,747	0.87	3,655 ± 180	9.1 ± 0.02	151 ± 3.4	6.3 ± 0.2 × 10 <sup>8</sup>
N	3	2	N3p2	34,865	1,970	0.90	2,977 ± 187	7.78 ± 0.04	33 ± 1.2	6.8 ± 0.5 × 10 <sup>8</sup>
N	0 <sup>a</sup>	control	N3C	72,066	2,459	0.90	3,470 ± 139	9.06 ± 0.04	149 ± 9.3	8.6 ± 1.0 × 10 <sup>8</sup>

<sup>a</sup> Control pots received distilled water (DW) once a week; soils were collected 1 week after 3rd DW-spraying.

<sup>b</sup> Number of sequences after removal of low-quality, chimeric, and archaeal sequences.

<sup>c</sup> Clustered at the 3% distance level.

<sup>d</sup> Calculated from the equation,  $Cx = 1 - (n/N)$ , where "n" is the number of OTUs composed of only one sequence (singleton) and N is the total number of sequences.

<sup>e</sup> Each index was calculated based on the same amount of sequences (5174) sub-sampled from original libraries (Mean ± SDs of 10 time sub-samplings is shown).

<sup>f</sup> Copy numbers (copies g<sup>-1</sup>-dry soil) of 16S rRNA genes estimated by qPCR (Mean ± SDs of three time measurements of the same DNA sample is shown).

Analysis of variance (ANOVA) was performed using R software ver. 3.0.1 (R Development Core Team, 2008), showing the copy numbers were not significantly different between samples that were originated from the same field soil.

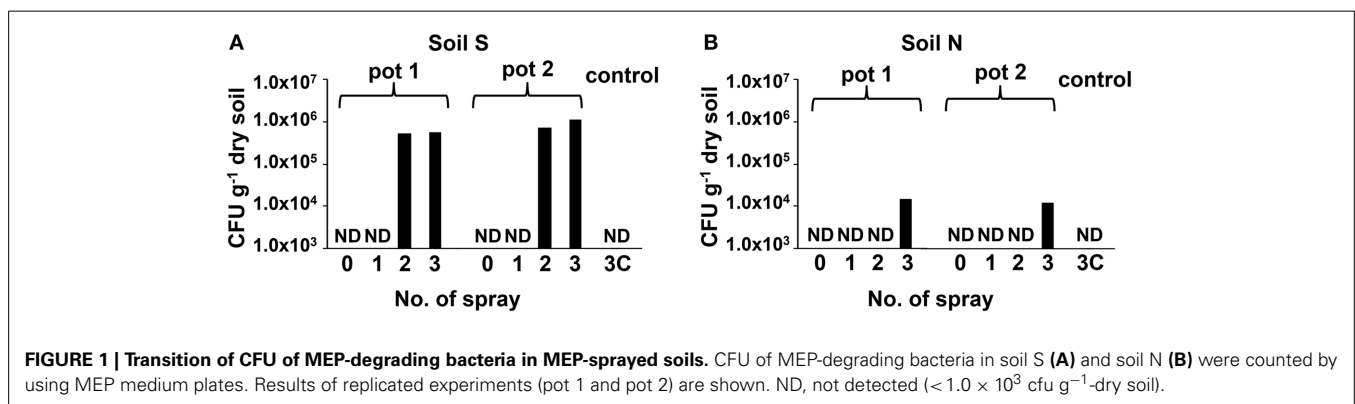


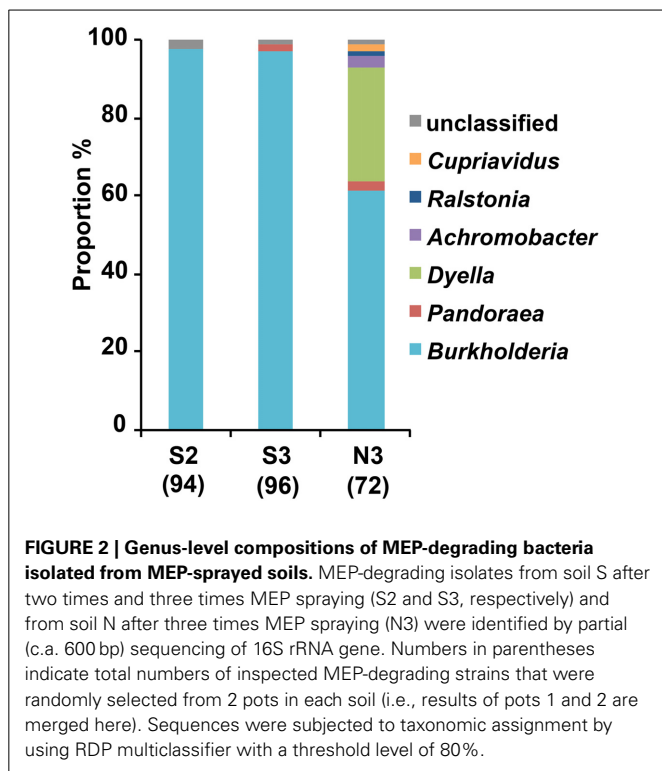
**FIGURE 1 | Transition of CFU of MEP-degrading bacteria in MEP-sprayed soils.** CFU of MEP-degrading bacteria in soil S (A) and soil N (B) were counted by using MEP medium plates. Results of replicated experiments (pot 1 and pot 2) are shown. ND, not detected (< 1.0 × 10<sup>3</sup> cfu g<sup>-1</sup>-dry soil).

### ISOLATION AND IDENTIFICATION OF MEP-DEGRADING BACTERIA

From the soil S after the 2nd and 3rd MEP-treatments (S2 and S3), and soil N after the 3rd MEP-treatment (N3), colonies of the MEP-degrading bacteria were isolated and identified based on the partial sequences of 16S rRNA gene. The sequence analyses demonstrated that the majority belonged to the betaproteobacterial genus *Burkholderia*. Specifically, they occupied around 97.9, 96.9, and 61.1% of the total sequenced-bacteria isolated from the S2, S3, and N3 soils, respectively, (Figure 2; Table S2). Notably, in contrast to the predominance of *Burkholderia* strains in the S2 and S3 samples, MEP-degraders from the N3 sample were more phylogenetically diverse with the presence of strains from the genera *Dyella*, *Ralstonia*, *Pandoraea*, *Achromobacter*, and *Cupriavidus*.

### SUCCESSION OF MICROBIOTA IN MEP-SPRAYED SOILS AS REVEALED BY DEEP SEQUENCING

For comprehensive understanding of the temporal dynamics of microbiota in the MEP-sprayed soils, we performed deep sequencing of bacterial 16S rRNA genes from both soils before treatment (S0 and N0), after the 2nd (S2) and 3rd (S3 and N3) MEP-treatments, and after the 3rd control-treatment (S3C and N3C). The sequencing of PCR amplicons of partial 16S rRNA genes produced > 2 × 10<sup>5</sup> sequences in total (Table 1). The qPCR data showed that the amount of bacterial 16S rRNA genes was stable at around 4 × 10<sup>8</sup> and 6 × 10<sup>8</sup> g<sup>-1</sup>-dry soil in soil S and soil N, respectively, during the treatments (Table 1). Meanwhile, in both soils S and N, diversity indices, chao1, Shannon, and reciprocal simpson decreased after MEP-spraying (Table 1), suggesting



that MEP treatment caused the decrease of soil microbial diversity.

Similarities among the sequence libraries of each soil sample were analyzed by PCoA based on weighted unifracc distance (Figure S2). The results suggest that the bacterial compositions of S2, S3, and N3 were distinct from those of S0 and N0 samples, although the shift direction was different between the soil S and soil N. The controls, S3C and N3C, were closely related to the soils before treatments, S0 and N0. These results also clearly demonstrate that MEP-spraying dramatically altered the community structure of soil microbiota.

#### BACTERIAL GROUPS RESPONDING TO MEP-SPRAYING

Figures 3A,B show the phylum-level (class-level in the *Proteobacteria*) distribution of sequences obtained from the deep sequence libraries. Among the diverse bacterial groups, *Betaproteobacteria* drastically increased after MEP-spraying in all samples from both soils S and N. Especially in soil S, the relative abundance of *Betaproteobacteria* was over 40% (80.4% in pot 1 and 49.8% in pot 2) after the 3rd MEP-treatment (Figure 3A). In the control samples (S3C and N3C), the bacterial composition appeared to be stable based from the initial states (S0 and N0), as also supported by the PCoA profile (Figure S2).

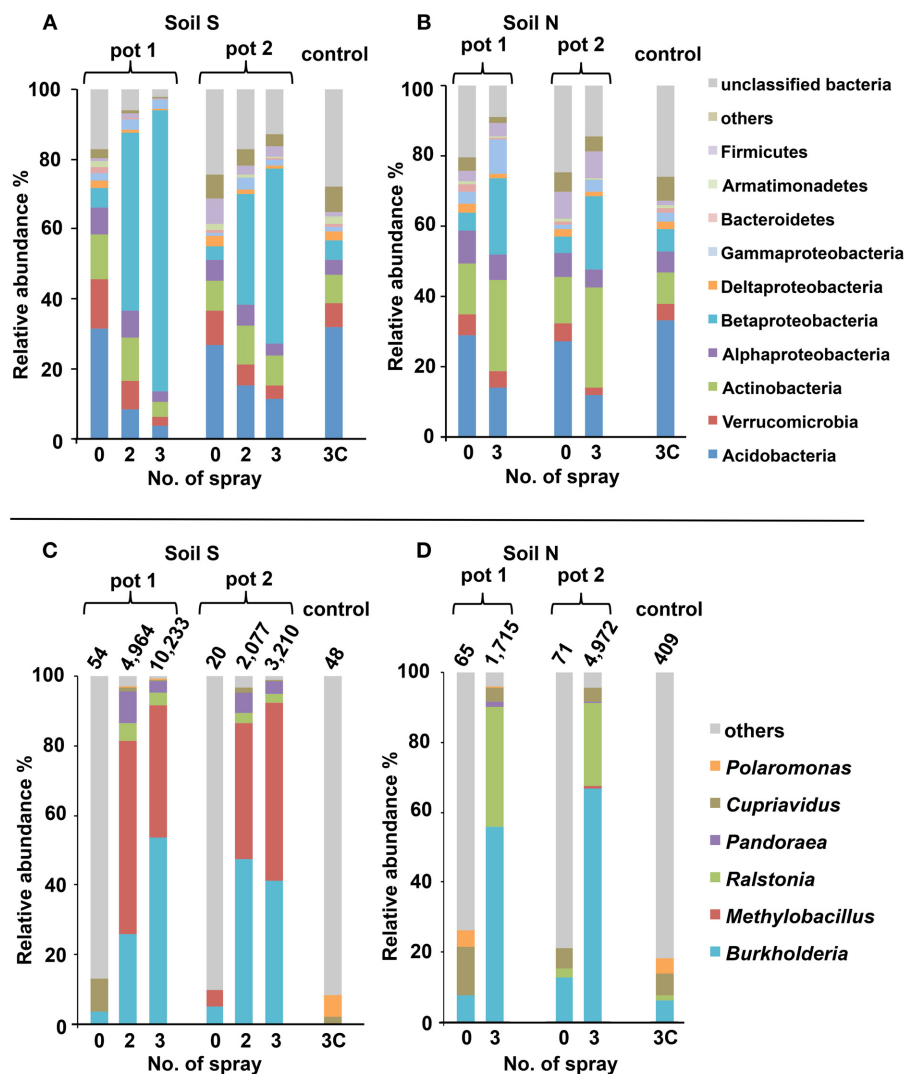
Within the increasing community of *Betaproteobacteria*, the genus *Burkholderia* was the most abundant, followed by *Ralstonia* and *Pandoraea* (Figures 3C,D). Before MEP treatment, few *Burkholderia* sequences were detected. However, after the 3rd treatment, the frequencies of *Burkholderia* drastically increased up to 53.8% in soil S pot 1, 41.1% in soil S pot 2, 55.7% in soil N pot 1, and 66.9% in soil N pot 2.

Figure 4 shows increase in the relative proportion of specific bacteria genera during the MEP-spraying experiments. It depicts the top 10 genera with the higher frequency after the 3rd treatment. From the list, the *Burkholderia*, *Cupriavidus*, *Pseudomonas*, and *Arthrobacter* are already well-known MEP-degrading strains (Tago et al., 2006; Zhang et al., 2006; Kim et al., 2009). Furthermore, the genera *Pandoraea*, *Ralstonia*, and *Dyella*, which were additionally identified earlier as MEP-degrading group (Figure 2), were also included in the top 10 genera that highly responded to MEP (Figure 4). In both soils S and N, the frequencies of *Burkholderia* and *Ralstonia* drastically increased in response to MEP-spraying at two to three orders of magnitude, suggesting that these genera might possess a strong MEP-assimilation ability to highly adapt to the biological niche resulting from MEP-sprayed soils. Other bacterial groups, such as *Rhodanobacter*, *Nevskia*, and *Methylobacillus*, were also included in the top 10 (Figure 4), although they were not detected through the culture-dependent approach (Figure 2). These strains might assimilate the intermediates of MEP degradation such as 3-methyl-4-nitrophenol and p-nitrophenol (Hayatsu et al., 2000; Arora et al., 2013), and thus proliferate under the MEP treatment. The frequencies of these bacterial groups with high increasing ratios after MEP treatment were almost stable in the control set-ups in both of soils S and N (Fold: 0.2~3.4), emphasizing that these bacteria respond to MEP-spraying.

#### BURKHOLDERIA STRAINS RESPONDING TO MEP-SPRAYING

To clarify the diversity of *Burkholderia* strains in the MEP-sprayed soils, 16S rRNA gene sequences of *Burkholderia* derived from the MEP-degrading isolates and the deep sequencing libraries of the soils treated with MEP three times (i.e., S3 and N3 soils) were classified into OTUs defined by 100% sequence identity. In the MEP-degrading isolates, 4 and 8 OTUs were identified from the S3 and N3 soils, respectively, in which a single and distinct OTU dominantly occupied at >70–90% frequency (Figures 5A,B). Although >100 OTUs were determined from all of the S3p1, S3p2, N3p1, and N3p2 libraries, a single and distinct OTU was dominant with >40% frequency in each soil sample (Figures 5C–F). In sequence libraries of both soil S and soil N, the dominant OTUs were not detected or a few sequences were detected before the MEP-treatment (Figure S3). These culture-dependent and -independent studies strikingly demonstrated that a particular phylotype of *Burkholderia* dominantly responds in soil environments in the presence of MEP.

We then estimated the phylogenetic relationship of these dominant *Burkholderia* strains based on 255 bp sequences of the V4 region of 16S rRNA gene (Figure 6). Regardless of whether the strain was identified by the culture-dependent or -independent method, each of the dominant *Burkholderia* OTUs derived from isolates and deep sequences was clustered together with the OTUs detected from the soil of the same origin (Figure 6), strongly indicating that our isolates are representative strains of MEP-degrading *Burkholderia* dominating the MEP-sprayed soils. This also indicates that the *Burkholderia* frequently detected from deep sequencing in MEP-sprayed soils are most likely to have MEP-degrading activity. The most dominant OTUs in soil S samples were related to pathogenic *Burkholderia* such as *B. cepacia*,



**FIGURE 3 | Structural changes of microbial communities in MEP-sprayed soils.** Soil S (A,C) and soil N (B,D) were analyzed by deep sequencing of 16S rRNA gene. For each soil, results of replicated experiments (pot 1 and pot 2) are shown. Relative distributions of the sequences at (A,B) phylum-level (class-level in the *Proteobacteria*) and

(C,D) genus-level within *Betaproteobacteria* are shown. In (C,D), total numbers of betaproteobacterial sequences excluding those of unclassified genus are depicted on the bars. Sequences were subjected to taxonomic assignment by using RDP multiclassifier with a threshold level of 80%.

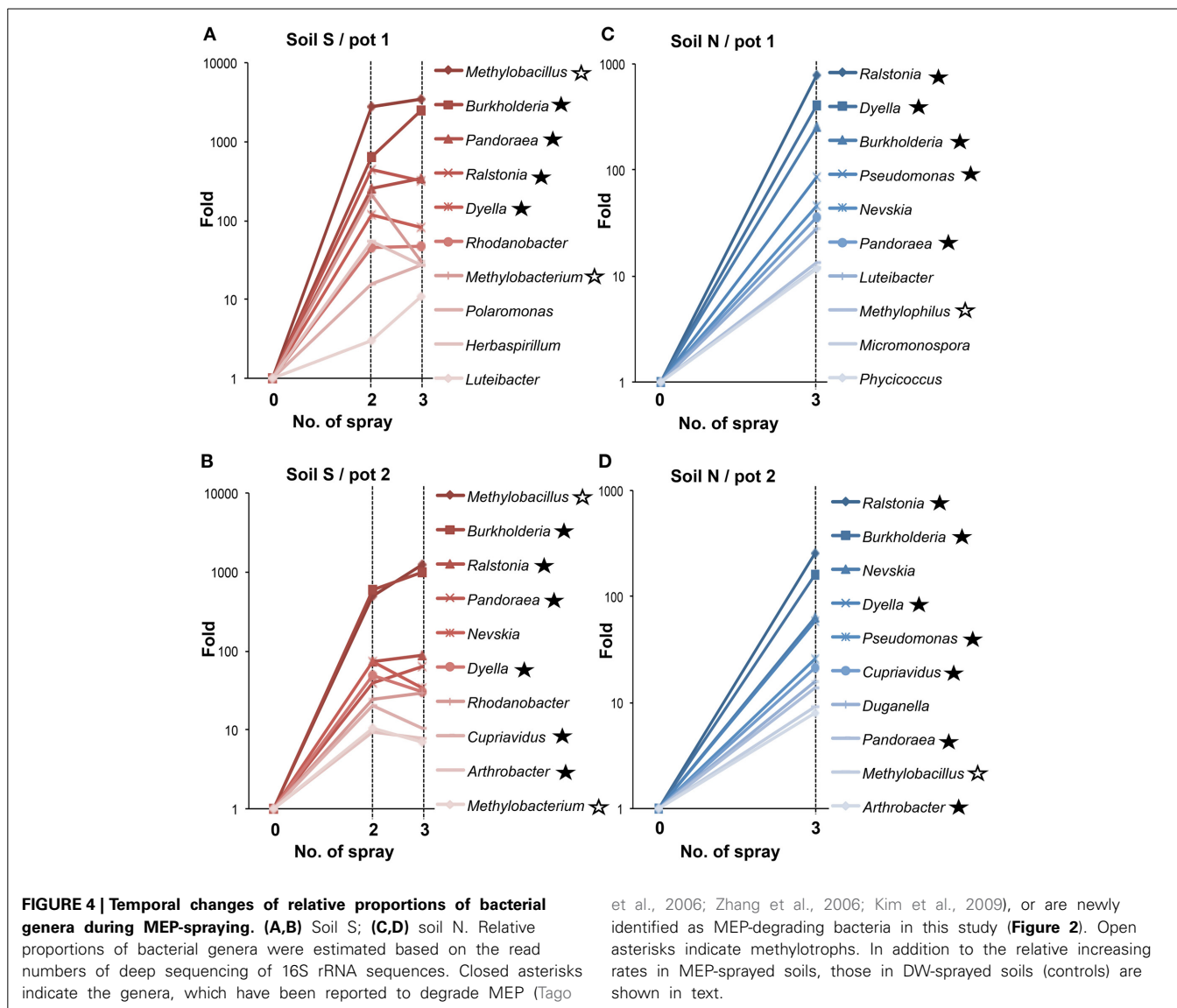
*B. glumae*, and *B. pseudomallei* of the *Burkholderia cepacia* complex (Bcc) group (Coenye et al., 2001), while those in soil N samples were related to known MEP-degrading bacteria isolated from soils and symbiotic *Burkholderia* in stinkbugs (Tago et al., 2006; Kikuchi et al., 2011). These results suggest that the phylogenetic lineage of *Burkholderia* responding to MEP-spraying appears likely to not be general, but specific for each soil environment.

## DISCUSSION

### EFFECTS OF FIELD-USE HISTORY ON SOIL MICROBIOTA RESPONDING TO MEP TREATMENT

Deep sequencing combined with culture-dependent approach clearly demonstrated that soil microbiota is strongly affected by the application of MEP, and furthermore, bacterial communities

responding to MEP-spraying were remarkably different between the two andisol soils (soil S and soil N) (Figures 3, 4, 6 and Figure S2) despite their almost similar origin and chemical properties (Table S1). Notably, the two soils have different histories of insecticide application: the agricultural field where soil S was obtained had experienced at least 4 years of MEP spraying; the field where soil N was collected was not subjected to such insecticide application (Table S1). Therefore, in soil S, MEP-degrading bacteria (i.e., *Burkholderia* species) might already exist at a certain level, thus allowing them to respond quickly to the presence of the chemical. Meanwhile, the greater variety of MEP-degrading bacteria in soil N may be due to the absence of selection pressure from MEP. Although the enhanced biodegradation caused by repeated treatment with the same insecticide were reported from the 1970s



(Felsot, 1989), little is known about the relation between soil microbial succession/adaptation and insecticide-spraying history. This is the first report to show the different microbial-community responses against insecticide re-treatment in soils that previously experienced such chemical application vs. naive soil with no such treatment prior to the experiment.

It should be noted that the bacterial composition of the initial states in both soils S and N was similar to each other (Figure S2) despite their different MEP-spraying history. This result strongly suggests that, although speculative, microbial community-structure disturbed by insecticide-spraying could recover to an initial community composition once the insecticide application is terminated. To clarify the plasticity of microbial community in more detail, it would be of great interest to investigate succession process of insecticide-enriched microbiota after terminating insecticide spraying. Interestingly, our results demonstrated that soil diagnostics of biological activity should not be inferred only based on a snapshot of environmental

microbial community. To estimate potentials of a soil (microbiota) more precisely, it may be more important to trace the microbial succession under environmental stimuli.

#### BURKHOLDERIA IS A KEY PLAYER IN MEP-DEGRADATION

Among the bacterial groups that dominantly responded to this insecticide, the genus *Burkholderia* was the most abundant after MEP-treatment (Figures 3C,D) and included a number of MEP-degrading isolates (Figure 2). Previous studies from China, Japan, and South Korea that were based on culture-dependent methods have repeatedly isolated MEP-degrading *Burkholderia* strains from MEP-contaminated soils at a higher frequency relative to other genera (Tago et al., 2006; Zhang et al., 2006; Kim et al., 2009). Taken together, our findings from both culture-dependent and -independent approaches strongly suggest that *Burkholderia* is a key bacterial group for MEP-degradation in soil environments. Remarkably, *Burkholderia* species were also found to degrade other organophosphorus insecticides, which includes

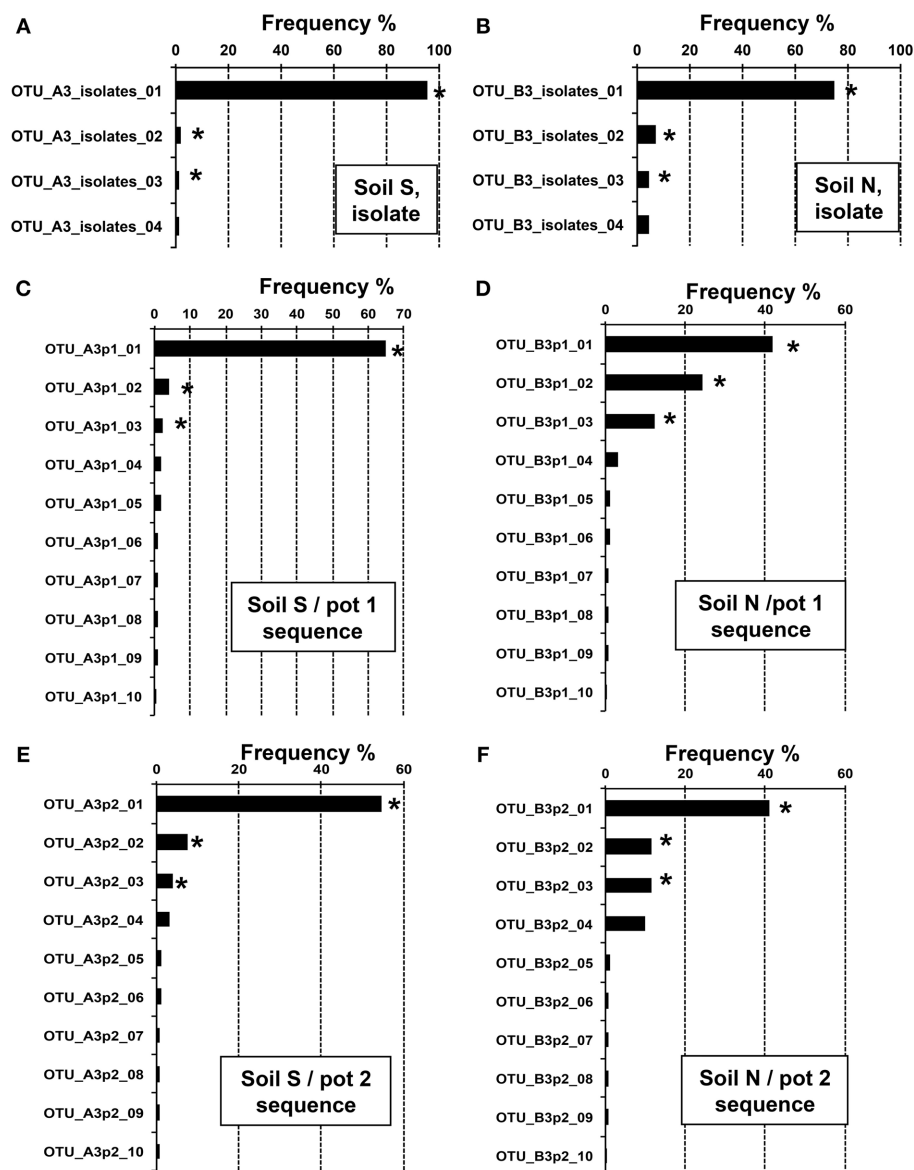


**FIGURE 5 | Relative abundance of *Burkholderia* OTUs in MEP-sprayed soils.** Relative abundance of 16S rRNA gene sequences assigned to different OTUs (100% sequence identity thresholds) of the genus *Burkholderia* in the MEP-degrading isolates (A,B) and the deep sequence

libraries (C–F). (A,C,E) Soil S; (B,D,F) soil N. Data showed the top 4 or 10 OTUs with high frequency in *Burkholderia* isolates or sequences, respectively. OTUs with asterisks were subjected to phylogenetic analysis (see Figure 6).

parathion, methyl parathion, glyphosate, and chlorpyrifos-methyl (Keprasertsupa et al., 2001; Kuklinsky-Sobral et al., 2005; Kim et al., 2007b, 2009). Considering that MEP-degrading strains of *Burkholderia* frequently show cross-acclimation against other organophosphorus compounds (Hayatsu et al., 2000; Kim and Ahn, 2009; Kim et al., 2009; Kikuchi et al., 2012), *Burkholderia* might have a pivotal role in the degradation of various insecticides. To clarify this point, it would be of great interest to also employ a deep sequencing survey of 16S rRNA genes for various types of organophosphorus insecticide-contaminated soils.

#### OTHER BACTERIAL GROUPS RESPONDING TO MEP-SPRAYING

Previous studies have isolated and characterized MEP-degrading bacteria from genera *Cupriavidus*, *Pseudomonas*, *Sphingomonas*, *Corynebacterium*, *Arthrobacter*, and *Burkholderia* (Tago et al., 2006; Zhang et al., 2006; Kim et al., 2009). In addition to *Burkholderia*, members of genera *Dyella*, *Ralstonia*, *Pandoraea*, and *Achromobacter* were also isolated as MEP-degrading bacteria in our culture-dependent experiments (Figure 2). Hence, this is the first record of MEP-degrading strains from these four genera, suggesting that broader taxonomic groups could contribute to MEP-degradation in natural soil environments. Some

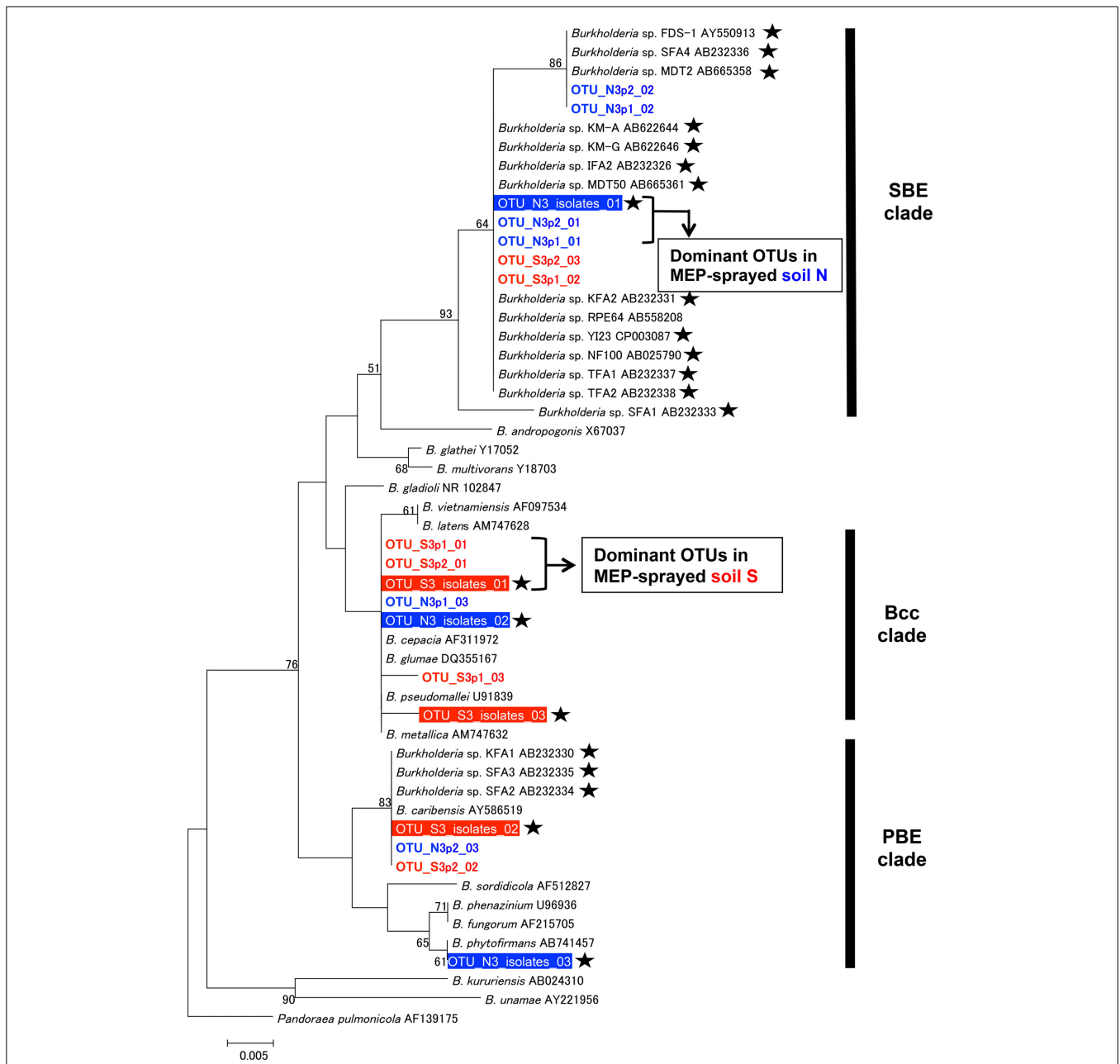


**FIGURE 6 | Phylogenetic analysis of *Burkholderia* strains dominating in MEP-sprayed soils.** A neighbor-joining tree inferred from aligned 255bp sequences of 16S rRNA gene is shown. Phylogenetic placements of OTUs (OTUs at 100% identity thresholds) of *Burkholderia*, identified from the MEP-degrading isolates and deep sequences, were estimated. Among dominant OTUs in each soil samples, top 3 OTUs (see **Figure 5**) were included in the analysis. Red and blue colored OTUs are detected from soil S and soil N, respectively. Outline letters on a filled background indicate OTUs determined by the isolation. Colored letters on a white

background indicate OTUs detected by the deep sequencing. Asterisks indicate MEP-degrading *Burkholderia* strains. Clade names of SBE (stinkbug-associated beneficial and environmental group), Bcc (*Burkholderia cepacia* complex), and PBE (plant-associated beneficial and environmental group), respectively, according to Itoh et al. (2014), Coenye et al. (2001), and Suárez-Moreno et al. (2012), are shown on the right side. Bootstrap values higher than 50% are depicted at the nodes. The 16S rRNA sequence of *Pandoraea pulmonicola* (AF139175) was used as an outgroup.

strains of *Ralstonia* and *Achromobacter* have already been reported to degrade organophosphorus compounds that are analogous to MEP, particularly fenamifos (organophosphorus nematocide) and methyl parathion (organophosphorus insecticide), respectively, (Zhang et al., 2005; Cabrera et al., 2010). Similar to

*Burkholderia* strains, these bacteria probably have an ability for cross-acclimation toward other organophosphorus compounds.

In addition to the complete degradation of MEP by a single bacterium, the cooperative degradation of MEP has also been reported *in vitro*. In this case, MEP-hydrolyzing

and MEP-hydrolysate-degrading bacteria cooperate for complete consumption of the chemical compound (Katsuyama et al., 2009). Previous studies have shown that some *Burkholderia* strains, though ineffective against MEP, are able to degrade its hydrolysate, 3-methyl-4-nitrophenol (Kim et al., 2007a; Katsuyama et al., 2009). Hence, some of the increasing bacteria identified by deep sequencing (Figure 4) from the MEP-sprayed soils might be directly involved in the hydrolysis of MEP, while others might contribute to the degradation of the resulting hydrolysates. Such a synergistic interaction among bacterial species could promote efficient degradation of MEP in soils.

### METHYLOTROPHS COULD PLAY A ROLE IN MEP-DEGRADATION

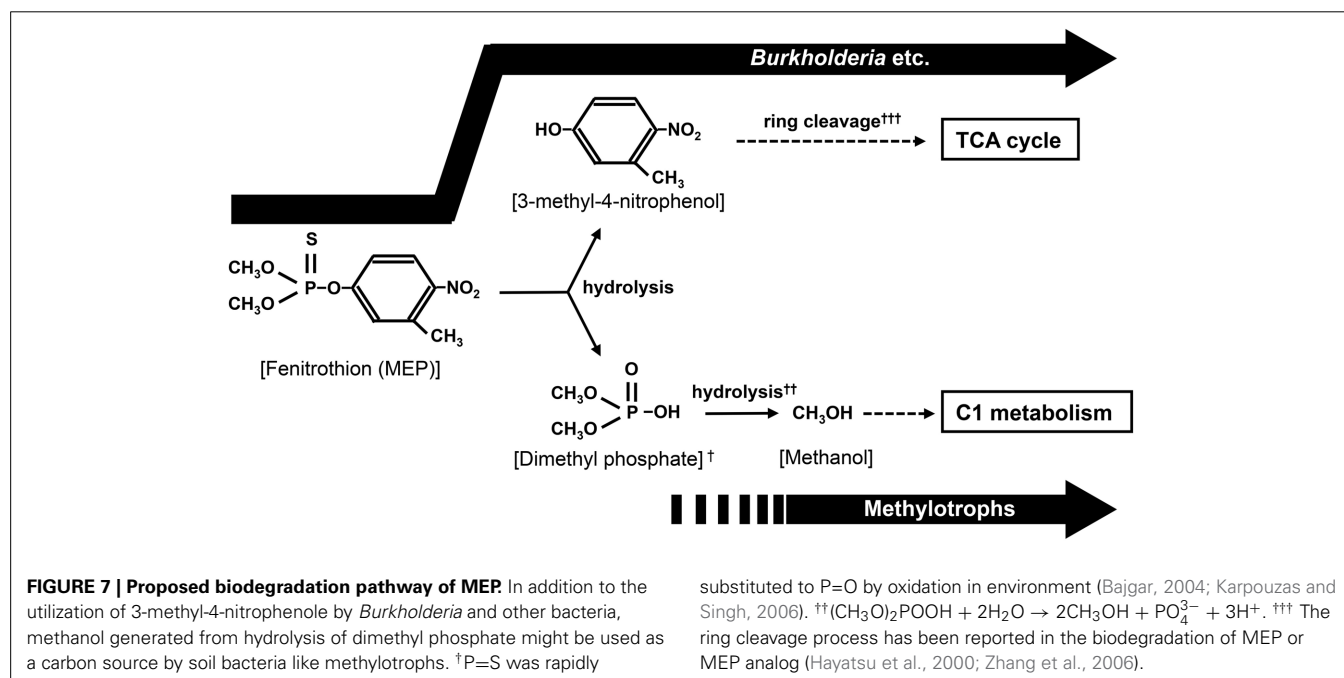
Notably, deep sequencing revealed that the frequency of *Methylobacillus*, *Methylobacterium*, and *Methylophilus*, which were never detected by the culture-dependent approach in this study and from previous researches (Tago et al., 2006; Zhang et al., 2006; Kim et al., 2009), also dramatically increased in soils after MEP-spraying (Figure 4). Most members of these genera are methylotrophic, that is, they actively use one-carbon compounds such as methanol as a sole carbon source (Kolb and Stacheter, 2013). Past studies have demonstrated that bacteria break down MEP into 3-methyl-4-nitrophenol and dimethyl phosphate during the initial hydrolysis step (Spillner et al., 1979; IPCS, 1992) (Figure 7). Though the succeeding stages for biodegrading the former aromatic compound have been described in detail (Spillner et al., 1979; IPCS, 1992; Hayatsu et al., 2000), the fate of dimethyl phosphate in soil still remains unclear. In the case of the degradation of paraoxon, an analog of MEP, the initial hydrolysis process produces diethyl phosphate, which is then further hydrolyzed into two molecules of ethanol by *Delftia acidovorans* and *Pseudomonas putida* through phosphodiesterase and phosphatase enzymes (Tehara and Keasling, 2003).

Although speculative, dimethyl phosphate may also be hydrolyzed into two molecules of methanol by a similar route during MEP-degradation. If so, the methylotrophs detected in this study may consume and utilize such generated methanol for growth (Figure 7).

It has been reported that accumulated methanol is harmful to organisms that are unable to metabolize it (Martin-Amat et al., 1978). In fact, growth of MEP-degrading *Burkholderia* strains isolated in this study was depressed by a tiny amount of methanol contamination (Figure S4). If methylotrophs rapidly consume any methanol generated during MEP-degradation, they might protect other bacteria involved in the overall degradation process from the toxicity of this by-product. This could probably lead to better growth of such relevant bacterial communities, thus contributing to more efficient and complete mineralization of MEP. This hypothesis could be verified through future evaluations on the (1) degradability of dimethyl phosphate by methylotrophs and (2) co-culture of MEP-degrading bacteria and methylotrophs.

### CONCLUDING REMARKS

This study demonstrated the effect of MEP-spraying history to the microbial succession under MEP application and identified key bacteria for MEP-degradation by performing both culture experiments and high-throughput sequencing. Owing to the enormous information generated by the deep sequencing of bacterial 16S rRNA gene, we comprehensively revealed the community structures of bacterial species responding to MEP, and found previously unseen members, methylotrophs, that may play an important role in the complete degradation of MEP in soil environments. In contrast, it should be noted that the partial sequencing of 16S rRNA gene gave us only indirect information about the MEP-degrading strains. In fact, our previous study



reported that even *Burkholderia* strains exhibiting high (>99.8%) sequence similarities in 16S rRNA gene possess quite different MEP-degrading activities (Kikuchi et al., 2012). Sequencing of functional genes involved in the MEP-degradation pathway might give more direct information for MEP-degradation in environmental soils, although MEP-degradation genes are not well understood (Singh, 2009). In addition, fungal biodegradation of MEP has been also reported (Baarschers and Heitland, 1986), although here we focused only on bacteria. Metagenomic approaches of functional genes and more comprehensive survey including fungal communities in soils should improve our knowledge of MEP-degradation by soil microorganisms.

## ACKNOWLEDGMENTS

We appreciate Tomo Aoyagi and Natsuki Nakamura (AIST) for technical assistance, and Mia Terashima (Hokkaido University) for English correction. This study was supported by the Program for Promotion of Basic and Applied Researches for Innovations in Bio-oriented Industry, the Ministry of Education, Culture, Sports, Science and Technology (MEXT) KAKENHI Grant number 24117525, and Grant-in-Aid for Scientific Research (B).

## SUPPLEMENTARY MATERIAL

The Supplementary Material for this article can be found online at: <http://www.frontiersin.org/journal/10.3389/fmicb.2014.00457/abstract>

## REFERENCES

- Arbeli, Z., and Fuentes, L. C. (2007). Accelerated biodegradation of pesticides: an overview of the phenomenon, its basis and possible solutions; and a discussion on the tropical dimension. *Crop Protect.* 26, 1733–1746. doi: 10.1016/j.cropro.2007.03.009
- Arora, P. K., Srivastava, A., and Singh, V. P. (2013). Bacterial degradation of nitrophenols and their derivatives. *J. Hazard. Mater.* 266C, 42–59. doi: 10.1016/j.jhazmat.2013.12.011
- Baarschers, H. W., and Heitland, S. H. (1986). Biodegradation of fenitrothion and fenitrooxon by the fungus *Trichoderma viride*. *J. Agric. Food Chem.* 34, 707–709. doi: 10.1021/jf00070a029
- Bajgar, J. (2004). Organophosphates/nerve agent poisoning: mechanism of action, diagnosis, prophylaxis, and treatment. *Adv. Clin. Chem.* 38, 151–216. doi: 10.1016/S0065-2423(04)38006-6
- Cabrera, J. A., Kurtz, A., Sikora, R. A., and Schouten, A. (2010). Isolation and characterization of fenamiphos degrading bacteria. *Biodegradation* 21, 1017–1027. doi: 10.1007/s10532-010-9362-z
- Caporaso, J. G., Kuczynski, J., Stombaugh, J., Bittinger, K., Bushman, F. D., Costello, E. K., et al. (2010). QIIME allows analysis of high-throughput community sequencing data. *Nat. Methods* 7, 335–336. doi: 10.1038/nmeth.f.303
- Caporaso, J. G., Lauber, C. L., Walters, W. A., Berg-Lyons, D., Huntley, J., Fierer, N., et al. (2012). Ultra-high-throughput microbial community analysis on the Illumina HiSeq and MiSeq platforms. *ISME J.* 6, 1621–1624. doi: 10.1038/ismej.2012.8
- Coenye, T., Vandamme, P., Govan, J. R., and LiPuma, J. J. (2001). Taxonomy and identification of the *Burkholderia cepacia* complex. *J. Clin. Microbiol.* 39, 3427–3436. doi: 10.1128/JCM.39.10.3427-3436.2001
- da Silva, N. A., Birolli, W. G., Selegim, M. H. R., and Porto, A. L. M. (2013). “Biodegradation of the organophosphate pesticide profenofos by Marine Fungi,” in *Applied Bioremediation-Active and Passive Approaches*, eds Y. B. Patil and P. Rao (Rijeka: InTechWeb), 149–180. doi: 10.5772/56372
- DeSantis, T. Z., Hugenholtz, P., Larsen, N., Rojas, M., and Brodie, E. L. (2006). Greengenes, a chimera-checked 16S rRNA gene database and workbench compatible with ARB. *Appl. Environ. Microbiol.* 72, 5069–5072. doi: 10.1128/AEM.03006-05
- Diez, M. C. (2010). Biological aspects involved in the degradation of organic pollutants. *J. Soil. Sci. Plant Nutr.* 10, 244–267. doi: 10.4067/S0718-95162010000100004
- Fang, H., Cai, L., Yang, Y., Ju, F., Li, X., Yu, Y., et al. (2014). Metagenomic analysis reveals potential biodegradation pathways of persistent pesticides in freshwater and marine sediments. *Sci. Total Environ.* 1, 983–992. doi: 10.1016/j.scitotenv.2013.10.076
- Felsot, A. S. (1989). Enhanced biodegradation of insecticides in soil: implications for agroecosystems. *Ann. Rev. Entomol.* 34, 453–476. doi: 10.1146/annurev.en.34.010189.002321
- Fukatsu, T., and Nikoh, N. (1998). Two intracellular symbiotic bacteria from the mulberry psyllid *Anomoneura mori* (Insecta, Homoptera). *Appl. Environ. Microbiol.* 64, 3599–3606.
- Hayatsu, M., Hirano, M., and Tokuda, S. (2000). Involvement of two plasmids in MEP degradation by *Burkholderia* sp. strain NF100. *Appl. Environ. Microbiol.* 66, 1737–1740. doi: 10.1128/AEM.66.4.1737-1740.2000
- International Programme on Chemical Safety (IPCS). (1992). “Environmental health criteria 133: fenitrothion,” in *World Health Organization* (Accessed December 22, 2013). <http://www.inchem.org/documents/ehc/ehc/ehc133.htm>
- Itoh, H., Aita, M., Nagayama, A., Meng, X. Y., Kamagata, Y., Navarro, R., et al. (2014). Evidence of environmental and vertical transmission of *Burkholderia* symbionts in the oriental chinch bug *Cavelerius saccharivorus* (Heteroptera: Blissidae). *Appl. Environ. Microbiol.* doi: 10.1128/AEM.01087-14. (in press).
- Jacobsen, C. S., and Hjelmsø, M. H. (2014). Agricultural soils, pesticides and microbial diversity. *Curr. Opin. Biotech.* 27, 15–20. doi: 10.1016/j.copbio.2013.09.003
- Karpouzias, D. G., and Singh, B. K. (2006). Microbial degradation of organophosphorus xenobiotics: metabolic pathways and molecular basis. *Adv. Microb. Physiol.* 51, 119–185. doi: 10.1016/S0065-2911(06)51003-3
- Katsuyama, C., Nakaoka, S., Takeuchi, Y., Tago, K., Hayatsu, M., and Kato, K. (2009). Complementary cooperation between two syntrophic bacteria in pesticide degradation. *J. Theor. Biol.* 256, 644–654. doi: 10.1016/j.jtbi.2008.10.024
- Keprasertsupa, C., Upathamb, E. S., Sukhapanthb, N., and Prempreed, P. (2001). Degradation of methyl parathion in an aqueous medium by soil Bacteria. *Scienceasia* 27, 261–270. doi: 10.2306/scienceasia1513-1874.2001.27.261
- Kikuchi, Y., Hayatsu, M., Hosokawa, T., Nagayama, A., Tago, K., and Fukatsu, T. (2012). Symbiont-mediated insecticide resistance. *Proc. Natl. Acad. Sci. U.S.A.* 109, 8618–8622. doi: 10.1073/pnas.1200231109
- Kikuchi, Y., Hosokawa, T., and Fukatsu, T. (2011). An ancient but promiscuous host-symbiont association between *Burkholderia* gut symbionts and their heteropteran hosts. *ISME J.* 5, 446–460. doi: 10.1038/ismej.2010.150
- Kim, J. R., and Ahn, Y. J. (2009). Identification and characterization of chlorpyrifos-methyl and 3,5,6-trichloro-2-pyridinol degrading *Burkholderia* sp. strain KR100. *Biodegradation* 20, 487–497. doi: 10.1007/s10532-008-9238-7
- Kim, K. D., Ahn, J. H., Kim, T., Park, S. C., Seong, C. N., Song, H. G., et al. (2009). Genetic and phenotypic diversity of fenitrothion-degrading bacteria isolated from soils. *J. Microbiol. Biotechnol.* 19, 113–120. doi: 10.4014/jmb.0808.467
- Kim, S. H., Park, M. R., Han, S., Whang, K., Shim, J. H., and Kim, I. S. (2007a). Degradation of 3-Methyl-4-nitrophenol, a Main Product of the Insecticide Fenitrothion, by *Burkholderia* sp. SH-1 Isolated from Earthworm (*Eisenia fetida*) Intestine. *J. Appl. Biol. Chem.* 50, 281–287.
- Kim, T., Ahn, J. H., Choi, M. K., Weon, H. Y., Kim, M. S., Seong, C. N., et al. (2007b). Cloning and expression of a parathion hydrolase gene from a soil bacterium, *Burkholderia* sp. JBA3. *J. Microbiol. Biotechnol.* 17, 1890–1893.
- Kolb, S., and Stacheter, A. (2013). Prerequisites for amplicon pyrosequencing of microbial methanol utilizers in the environment. *Front. Microbiol.* 4:268. doi: 10.3389/fmicb.2013.00268
- Kuklinsky-Sobral, J., Araújo, W. L., Mendes, R., Pizzirani-Kleiner, A., and Azevedo, J. (2005). Isolation and characterization of endophytic bacteria from soybean (*Glycine max*) grown in soil treated with glyphosate herbicide. *Plant Soil* 273, 91–99. doi: 10.1007/s11104-004-6894-1
- Martin-Amat, G., McMartin, K. E., Hayreh, S. S., Hayreh, M. S., and Tephly, T. R. (1978). Methanol poisoning: ocular toxicity produced by formate. *Toxicol. Appl. Pharmacol.* 45, 201–208. doi: 10.1016/0041-008X(78)90040-6
- Meyer, F., Paarmann, D., D’Souza, M., Olson, R., Glass, E. M., Kubal, M., et al. (2008). The metagenomics RAST server – a public resource for the automatic phylogenetic and functional analysis of metagenomes. *BMC Bioinformatics* 9:386. doi: 10.1186/1471-2105-9-386

- Moorthie, S., Mattocks, C. J., and Wright, C. F. (2011). Review of massively parallel DNA sequencing technologies. *Hugo J.* 5, 1–12. doi: 10.1007/s11568-011-9156-3
- Muyzer, G., de Waal, E. C., and Uitterlinden, A. G. (1993). Profiling of complex microbial populations by denaturing gradient gel electrophoresis analysis of polymerase chain reaction-amplified genes coding for 16S rRNA. *Appl. Environ. Microbiol.* 59, 695–700.
- Noll, M., Matthies, D., Frenzel, P., Derakshani, M., and Liesack, W. (2005). Succession of bacterial community structure and diversity in a paddy soil oxygen gradient. *Environ. Microbiol.* 7, 382–395. doi: 10.1111/j.1462-2920.2005.00700.x
- O'Connell, J. L., and Nyman, J. A. (2011). Effects of marsh pond terracing on coastal wintering waterbirds before and after Hurricane Rita. *Environ. Manage.* 48, 975–984. doi: 10.1007/s00267-011-9741-1
- Peñuelas, J., Sardans, J., Estiarte, M., Ogaya, R., Carnicer, J., Coll, M., et al. (2013). Evidence of current impact of climate change on life: a walk from genes to the biosphere. *Glob. Chang. Biol.* 19, 2303–2338. doi: 10.1111/gcb.12143
- Phillips, O. L., Aragão, L. E., Lewis, S. L., Fisher, J. B., Lloyd, J., López-González, G., et al. (2009). Drought sensitivity of the Amazon rainforest. *Science* 323, 1344–1347. doi: 10.1126/science.1164033
- R Development Core Team. (2008). *R: A Language and Environment for Statistical Computing*. R Foundation for Statistical Computing. <http://www.R-project.org>
- Rota, C. T., Millsbaugh, J. J., Rumble, M. A., Lehman, C. P., and Kesler, D. C. (2014). The role of wildfire, prescribed fire, and mountain pine beetle infestations on the population dynamics of black-backed woodpeckers in the black hills, South Dakota. *PLoS ONE* 9:e94700. doi: 10.1371/journal.pone.0094700
- Schloss, P. D., Westcott, S. L., Ryabin, T., Hall, J. R., Hartmann, M., Hollister, E. B., et al. (2009). Introducing mothur: open-source, platform-independent, community-supported software for describing and comparing microbial communities. *Appl. Environ. Microbiol.* 75, 7537–7541. doi: 10.1128/AEM.01541-09
- Singh, B. K. (2009). Organophosphorus-degrading bacteria: ecology and industrial applications. *Nat. Rev. Microbiol.* 7, 156–164. doi: 10.1038/nrmicro2050
- Singh, B. K., and Walker, A. (2006). Microbial degradation of organophosphorus compounds. *FEMS Microbiol. Rev.* 30, 428–471. doi: 10.1111/j.1574-6976.2006.00018.x
- Spillner, C. J., DeBaun, J. R., and Menn, J. J. (1979). Degradation of fenitrothion in forest soil and effects on forest soil microbes. *J. Agric. Food Chem.* 27, 1054–1060. doi: 10.1021/jf60225a009
- Suárez-Moreno, Z. R., Caballero-Mellado, J., Coutinho, B. G., Mendonça-Previato, L., and James, E. K. (2012). Common features of environmental and potentially beneficial plant-associated *Burkholderia*. *Microb. Ecol.* 63, 249–266. doi: 10.1007/s00248-011-9929-1
- Tago, K., Sekiya, E., Kiho, A., Katsuyama, C., Hoshito, Y., Yamada, N., et al. (2006). Diversity of fenitrothion-degrading bacteria in soils from distant geographical areas. *Microbes Environ.* 21, 58–64. doi: 10.1264/jsme2.21.58
- Tamura, K., Dudley, J., Nei, M., and Kumar, S. (2007). MEGA4: molecular Evolutionary Genetics Analysis (MEGA) software version 4.0. *Mol. Biol. Evol.* 24, 1596–1599. doi: 10.1093/molbev/msm092
- Tehara, S. K., and Keasling, J. D. (2003). Gene cloning, purification, and characterization of a phosphodiesterase from *Delftia acidovorans*. *Appl. Environ. Microbiol.* 9, 504–508. doi: 10.1128/AEM.69.1.504-508.2003
- Wang, Q., Garrity, G. M., Tiedje, J. M., and Cole, J. R. (2007). Naive bayesian classifier for rapid assignment of rRNA Sequences into the new bacterial taxonomy. *Appl. Environ. Microbiol.* 73, 5261–5267. doi: 10.1128/AEM.00062-07
- Whalon, M. E., Monte-Sanchez, D., and Hollingworth, R. M. (2008). *Global Pesticide Resistance in Arthropods*. London: CAB International. doi: 10.1079/9781845933531.0000
- Wilson, M. C., and Piel, J. (2013). Metagenomic approaches for exploiting uncultivated bacteria as a resource for novel biosynthetic enzymology. *Chem. Biol.* 20, 636–647. doi: 10.1016/j.chembiol.2013.04.011
- Zhang, R., Cui, Z., Jiang, J., He, J., Gu, X., and Li, S. (2005). Diversity of organophosphorus pesticide-degrading bacteria in a polluted soil and conservation of their organophosphorus hydrolase genes. *Can. J. Microbiol.* 51, 337–343. doi: 10.1139/w05-010
- Zhang, Z., Hong, Q., Xu, J., Zhang, X., and Li, S. (2006). Isolation of fenitrothion-degrading strain *Burkholderia* sp. FDS-1 and cloning of mpd gene. *Biodegradation* 17, 275–283. doi: 10.1007/s10532-005-7130-2

**Conflict of Interest Statement:** The authors declare that the research was conducted in the absence of any commercial or financial relationships that could be construed as a potential conflict of interest.

Received: 08 May 2014; accepted: 12 August 2014; published online: 29 August 2014.

Citation: Itoh H, Navarro R, Takeshita K, Tago K, Hayatsu M, Hori T and Kikuchi Y (2014) Bacterial population succession and adaptation affected by insecticide application and soil spraying history. *Front. Microbiol.* 5:457. doi: 10.3389/fmicb.2014.00457

This article was submitted to *Systems Microbiology*, a section of the journal *Frontiers in Microbiology*.

Copyright © 2014 Itoh, Navarro, Takeshita, Tago, Hayatsu, Hori and Kikuchi. This is an open-access article distributed under the terms of the Creative Commons Attribution License (CC BY). The use, distribution or reproduction in other forums is permitted, provided the original author(s) or licensor are credited and that the original publication in this journal is cited, in accordance with accepted academic practice. No use, distribution or reproduction is permitted which does not comply with these terms.



# Survival of free-living *Acholeplasma* in aerated pig manure slurry revealed by $^{13}\text{C}$ -labeled bacterial biomass probing

Dai Hanajima<sup>1\*</sup>, Tomo Aoyagi<sup>2</sup> and Tomoyuki Hori<sup>2</sup>

<sup>1</sup> Dairy Research Division, Hokkaido Agricultural Research Center, National Agricultural and Food Research Organization, Sapporo, Japan, <sup>2</sup> Environmental Management Research Institute, National Institute of Advanced Industrial Science and Technology, Tsukuba, Japan

## OPEN ACCESS

### Edited by:

Shin Haruta,  
Tokyo Metropolitan University, Japan

### Reviewed by:

Tsukasa Ito,  
Gunma University, Japan  
Deborah A. Neher,  
University of Vermont, USA

### \*Correspondence:

Dai Hanajima  
hanadi@affrc.go.jp

### Specialty section:

This article was submitted to  
Systems Microbiology,  
a section of the journal  
Frontiers in Microbiology

**Received:** 30 May 2015

**Accepted:** 16 October 2015

**Published:** 31 October 2015

### Citation:

Hanajima D, Aoyagi T and Hori T  
(2015) Survival of free-living  
*Acholeplasma* in aerated pig manure  
slurry revealed by  $^{13}\text{C}$ -labeled  
bacterial biomass probing.  
*Front. Microbiol.* 6:1206.  
doi: 10.3389/fmicb.2015.01206

Many studies have been performed on microbial community succession and/or predominant taxa during the composting process; however, the ecophysiological roles of microorganisms are not well understood because microbial community structures are highly diverse and dynamic. Bacteria are the most important contributors to the organic-waste decomposition process, while decayed bacterial cells can serve as readily digested substrates for other microbial populations. In this study, we investigated the active bacterial species responsible for the assimilation of dead bacterial cells and their components in aerated pig manure slurry by using  $^{13}\text{C}$ -labeled bacterial biomass probing. After 3 days of forced aeration,  $^{13}\text{C}$ -labeled and unlabeled dead *Escherichia coli* cell suspensions were added to the slurry. The suspensions contained  $^{13}\text{C}$ -labeled and unlabeled bacterial cell components, possibly including the cell wall and membrane, as well as intracellular materials. RNA extracted from each slurry sample 2 h after addition of *E. coli* suspension was density-resolved by isopycnic centrifugation and analyzed by terminal restriction fragment length polymorphism, followed by cloning and sequencing of bacterial 16S rRNA genes. In the heavy isotopically labeled RNA fraction, the predominant  $^{13}\text{C}$ -assimilating population was identified as belonging to the genus *Acholeplasma*, which was not detected in control heavy RNA. *Acholeplasma* spp. have limited biosynthetic capabilities and possess a wide variety of transporters, resulting in their metabolic dependence on external carbon and energy sources. The prevalence of *Acholeplasma* spp. was further confirmed in aerated pig manure slurry from four different pig farms by pyrosequencing of 16S rRNA genes; their relative abundance was ~4.4%. Free-living *Acholeplasma* spp. had a competitive advantage for utilizing dead bacterial cells and their components more rapidly relative to other microbial populations, thus allowing the survival and prevalence of *Acholeplasma* spp. in pig manure slurry.

**Keywords:** stable isotope probing, dead bacterial biomass, assimilation, heterotroph, aerated slurry, *Acholeplasma*

## INTRODUCTION

Composting is a waste treatment process by which organic material is degraded and stabilized to produce fertilizer and amend soil. Aerobic bacteria are the most important decomposers during the composting process; they obtain energy by oxidizing organic material, especially the carbon fraction. Composting is typically applied to solid waste; however, aerobic treatment is also effective for liquid waste. Animal manure slurry consisting of a mixture of feces and urine is normally stored in a manure pit until land application. During storage, malodorous compounds such as volatile fatty acids and amines, indoles, phenols, ammonia, and sulfur-containing compounds accumulate due to the anaerobic degradation of organic matter (Zhu, 2000). When the stored slurry is then directly applied to agricultural fields, it often leads to complaints from residents of surrounding areas. In addition, the application of excessive amounts of easily digestible organic matter is phytotoxic to plants. Forced aeration of manure slurry has been employed to mitigate slurry odor and stabilize its quality.

In batch solid/liquid composting, the majority of organic carbon is derived from a single initial input present within the substrate itself. Labile substrates are consumed first by copiotrophic microbial taxa, which are later replaced by more oligotrophic taxa that metabolize the remaining more recalcitrant organic carbon pools (Fierer et al., 2010). It is hypothesized that microbial populations that arise due to slurry aeration are responsible for degrading the complex mixture of organic matter such as intestinal cells, microbial cells, undigested feed, or soluble organic carbons, including odorous substances. Within several hours of initiating aeration, a distinct shift in bacterial community structure occurs, accompanied by drastic changes in slurry conditions, including physicochemical parameters such as pH, oxidation-reduction potential (ORP), and reducing organic carbon (Hanajima et al., 2009, 2011). Bacteria act as important decomposers in an aerated slurry environment, while decayed bacterial cells can serve as readily digested substrates for other microbial populations. Biomass accumulation is often highest in the earlier stages of the composting process, tapering off as succession progresses (Fierer et al., 2010). Decay of the accumulated biomass releases ammonia during the decomposition process and may trigger the regrowth of unfavorable microbial populations (e.g., pathogens).

There have been many studies on microbial community succession and/or predominant taxa during the composting process (Ishii and Takii, 2003; Danon et al., 2008; Hanajima et al., 2009, 2011). However, the ecophysiological roles of microorganisms are not well understood because microbial community structures are highly diverse and dynamic. Stable isotope probing (SIP) has been used to investigate the link between the metabolic functions and phylogenetic identities of uncultured microorganisms in natural environments (Hori et al., 2007; Lee et al., 2011). For instance, SIP of rRNA has been used to trace the incorporation of  $^{13}\text{C}$ -labeled substrates by microorganisms, which has advanced our understanding of metabolically active microbial species in a particular

environment. Isotopically labeled rRNA is density-resolved by isopycnic centrifugation, and the density fraction of rRNA is analyzed by fingerprinting techniques and subsequently identified by cloning and sequencing. It was previously reported that carbon from bacterial biomass is incorporated into a soil microbial food web (Lueders et al., 2006; Murase et al., 2011); however, carbon flow mediated by microbial communities has been poorly studied in copiotrophic environments such as solid/liquid compost.

The objective of the present study was to identify active heterotrophic bacteria that are able to directly incorporate the dead *Escherichia coli* cells and their components present in aerated pig manure slurry. To achieve this objective, *E. coli* cells were cultivated with  $^{13}\text{C}$ -labeled and unlabeled glucose to prepare  $^{13}\text{C}$ -labeled and unlabeled bacterial biomass, respectively. These cells were heat-inactivated and dead cells and their components were added as substrates to aerated pig manure slurry. To clarify the fate of dead cells and their components, the incorporation of the substrate-derived  $^{13}\text{C}$  into bacterial rRNA was investigated. After identifying the microorganisms that assimilated carbon from dead bacterial cells and their components by using SIP of rRNA, their widespread distribution in several pig manure slurry was examined by pyrosequencing of 16S rRNA genes.

## MATERIALS AND METHODS

### SIP with $^{13}\text{C}$ -labeled Bacterial Biomass in Aerated Pig Manure Slurry

#### Preparation of Pig Manure Slurry

Fresh pig feces were collected from a pig fattening house at the National Institute of Livestock and Grassland Science (Tsukuba, Japan). The feces were transported to Hokkaido Agricultural Research Center (Sapporo, Japan) in a cold box, and mixed with distilled water (dry weight of feces:weight of distilled water = 1:14). The mixture was filtered through a metallic sieve (0.5-mm mesh size) to remove large suspended solids that resist biological degradation. We simulated the actual content of pig manure slurry by adding 2 g urea instead of urine to 1 l of the filtered mixture.

#### Preparation of $^{13}\text{C}$ -labeled Bacterial Cells as a Substrate for SIP

To obtain  $^{13}\text{C}$ -labeled bacterial biomass, *E. coli* strain NBRC 3301 was cultured on mineral medium [(6.97 g  $\text{l}^{-1}$   $\text{Na}_2\text{HPO}_4$ , 3.42 g  $\text{l}^{-1}$   $\text{KH}_2\text{PO}_4$ , 0.2 g  $\text{l}^{-1}$   $\text{MgCl}_2 \cdot 7\text{H}_2\text{O}$ , 1.0 g  $\text{l}^{-1}$   $\text{NH}_4\text{Cl}$ , 0.1 g  $\text{l}^{-1}$   $\text{CaCl}_2$ , 0.01 g  $\text{l}^{-1}$   $\text{FeSO}_4$ , 0.2 mg  $\text{l}^{-1}$   $\text{ZnSO}_4$ , and 0.2 mg  $\text{l}^{-1}$   $\text{MnSO}_4$  (pH 7.2)] (Kindler et al., 2006) containing 2 g  $\text{l}^{-1}$   $^{13}\text{C}$ -labeled glucose (D-glucose- $^{13}\text{C}_6$ , min. 99 atom%  $^{13}\text{C}$ ; Sigma-Aldrich, St. Louis, MO, USA). Unlabeled cells for the control experiment were obtained by cultivation on the same medium except for containing unlabeled glucose in place of  $^{13}\text{C}$ -labeled glucose. Cultures were incubated on a rotary shaker at 37°C and 200 rpm. *E. coli* cultures were incubated for 16 h and cells were harvested by centrifugation (4,000  $\times$  g, 10 min, 4°C) and washed three times with phosphate-buffered saline (PBS; pH 7.2). The labeling of *E. coli* cells was 97.5  $^{13}\text{C}$  atom%.

$^{13}\text{C}$ -labeled or unlabeled *E. coli* cell pellets were resuspended in 35-ml PBS and the number of viable cells in the suspension was counted by plating on LB agar (BD Biosciences, Franklin Lakes, NJ, USA).  $^{13}\text{C}$ -labeled and unlabeled *E. coli* suspensions ( $2.2 \times 10^{10}$  CFU/ml) were inactivated by heating at  $90^\circ\text{C}$  for 30 min and stored at  $-20^\circ\text{C}$  until use. The suspensions contained  $^{13}\text{C}$ -labeled and unlabeled bacterial cell components possibly including cell wall and membrane, as well as intracellular materials (e.g., amino acids and fatty acids).

### Batch Treatment of Aerated Pig Manure Slurry Supplemented with $^{13}\text{C}$ -labeled Biomass

Two batch aerobic treatments were carried out in a 5-l jar fermenter (TJM-502WS; Takasaki Scientific Instruments Corp., Saitama, Japan) containing 1.5-l manure slurry and equipped with a foam cutter. The liquid was maintained at  $40^\circ\text{C}$  and stirred at 350 rpm. Constant airflow at  $50 \text{ ml min}^{-1} \text{ l}^{-1}$  was provided from the bottom of the jar fermenter through a ceramic stone diffuser (1.2 cm inner diameter  $\times$  5.5 cm) for 5 days. This airflow rate corresponds to the average value used by farmers in Japan ( $1\text{--}5 \text{ m}^3 \text{ air h}^{-1} \text{ m}^{-3}$  slurry) (Japan Livestock Industry Association, 1989). On day 3 after aeration was initiated, 30-ml suspensions of  $^{13}\text{C}$ -labeled dead *E. coli* and unlabeled dead *E. coli* (control) were added to the aerated slurry. Every 30 min, the ORP and pH of the slurry were automatically measured and recorded (Thermocac EF, Model 5020A; Eto Electrics, Tokyo, Japan). The slurry in the reactor was periodically sampled using a syringe. Samples were stored at  $-80^\circ\text{C}$  for subsequent molecular analyses.

### Physicochemical Analyses of Aerated Slurry

Moisture content was determined by drying samples for 24 h at  $105^\circ\text{C}$ . Chemical oxygen demand ( $\text{COD}_{\text{Cr}}$ ) was measured using the closed reflux colorimetric method in reaction tubes with prepared reagents provided by Hach Company (Loveland, CO, USA), according to the manufacturer's instructions. Analysis of  $\delta^{13}\text{C}$  was carried out at the International Research Center for Agricultural Sciences (Tsukuba, Japan) using an infrared mass spectrometer (Finnigan Delta PLUS XP; Thermo Scientific, Hamburg, Germany) connected to an element analyzer (EA Flash 1112; Carlo Erba, Milan, Italy). To detect total carbon, freeze-dried slurry samples were incinerated in the element analyzer furnace and separated as pure  $\text{CO}_2$  gas, a small quantity of which was used to measure the ratio of  $^{13}\text{CO}_2/^{12}\text{CO}_2$  as different mass weights of 45/44 to obtain  $\delta^{13}\text{C}$  (‰).

### RNA Extraction and Density Gradient Centrifugation

RNA was extracted from 0.5 ml of slurry samples that were obtained after 2- and 6-h incubations with  $^{13}\text{C}$ -labeled and unlabeled dead *E. coli* cells using a direct lysis protocol involving bead beating (Noll et al., 2005). Total RNA was quantified using the Ribogreen RNA quantification kit (Invitrogen, Karlsruhe, Germany) according to the manufacturer's instructions. RNA extracts (500 ng RNA) from  $^{13}\text{C}$ -labeled and unlabeled samples were mixed with cesium trifluoroacetate (CsTFA) (Wako Pure Chemical Industries Ltd., Osaka, Japan) solution. The mixture was subjected to equilibrium density gradient centrifugation as previously described (Lueders et al., 2004). The RNA density

gradients were fractionated, and their CsTFA buoyant density (BD) was determined (Lueders et al., 2004).

### Reverse Transcription (RT)-PCR and Terminal Restriction Fragment Length Polymorphism (T-RFLP) Analysis

Each density fraction of RNA from  $^{13}\text{C}$ -labeled and unlabeled samples was subjected to RT-PCR using a PrimeScript RT-PCR kit (Takara Bio, Otsu, Japan) for T-RFLP fingerprinting. The PCR primer set 27f (5'-AGA GTT TGA TCM TGG CTC AG-3'-6-carboxyfluorescein) and 926r (5'-CCG TCA ATT CCT TTRAGT TT-3') was used to amplify bacterial 16S rRNA genes. RT was carried out at  $65^\circ\text{C}$  for 5 min for annealing, followed by  $42^\circ\text{C}$  for 30 min and  $95^\circ\text{C}$  for 5 min for transcription. The thermal profile for PCR amplification consisted of 20 cycles of  $94^\circ\text{C}$  for 30 s,  $52^\circ\text{C}$  for 30 s, and  $72^\circ\text{C}$  for 1 min under stringent conditions, followed by final extension at  $72^\circ\text{C}$  for 5 min. RT-PCR products were verified by electrophoresis on a 1.5% agarose gel and were purified using the MonoFas DNA purification kit (GL Sciences, Tokyo, Japan). Two hundred nanograms of the amplicon was digested with *MspI* (Nippon Gene, Tokyo, Japan) and then desalted by ethanol precipitation. Prior to electrophoresis,  $1 \mu\text{l}$  of the digests was resuspended in  $12 \mu\text{l}$  Hi-Di formamide (Applied Biosystems, Foster City, CA, USA) and  $0.5 \mu\text{l}$  of GeneScan 600 LIZ Size Standard (Applied Biosystems). The mixture was denatured at  $95^\circ\text{C}$  for 3 min and cooled immediately on ice. Size separation of T-RFs was performed using an ABI 310 genetic analyzer (Applied Biosystems).

### Cloning and Sequencing of the RNA Density Fractions

Selected density fractions of RNA were amplified for cloning using the primer set 27f/926r under the thermal conditions described above. RT-PCR products were ligated into the pGEM-T Easy vector (Promega, Madison, WI, USA) and the ligated product was used to transform ECOS competent *E. coli* JM109 cells (Nippon Gene, Tokyo, Japan) according to the manufacturer's instructions. We randomly selected 63 clones from  $^{13}\text{C}$ -labeled samples and 92 clones from unlabeled samples. The 16S rRNA segments were sequenced on a 3130xl Genetic Analyzer (Applied Biosystems) using the BigDye Terminator V3.1 cycle sequencing kit (Applied Biosystems). The 16S rRNA gene sequences obtained was compared with those in the nucleotide sequence database by using the BLAST program<sup>1</sup>. Chimeric structures were detected by separately analyzing the phylogenies of terminal stretches at the 5' and 3' ends, known as fractional treeing (Ludwig et al., 1998).

### Analysis of Bacterial Communities in Pig Manure Slurry Samples using Pyrosequencing

#### Preparation of Aerated Pig Manure Slurry from Different Pig Farms

To analyze bacterial communities in aerated pig manure slurry, samples from four different locations (designated as R, N, O,

<sup>1</sup><http://ddbj.nig.ac.jp/blast/>

and K) were collected. N corresponded to a pig fattening house at the National Institute of Livestock and Grassland Science, and R, O, and K were pig farms located in various areas of Japan separated by a distance of at least 300 km. Pig feces were transported to Hokkaido Agricultural Research Center in a cold box and slurry samples were prepared as described above. Batch aerobic treatment of the slurry was also performed as described, except that a 3-l volume was used. To prevent bacterial cross-contamination between samples, the jar fermenter including sensors and air inlet were autoclaved prior to each batch aerobic treatment. Air was supplied through a filter with a pore size of 0.22  $\mu\text{m}$ .

### Barcoded Pyrosequencing of Bacterial 16S rRNA Genes

Total genomic DNA from pig manure slurry was extracted using the UltraClean Fecal DNA Isolation kit (MO BIO, Carlsbad, CA, USA) according to the manufacturer's instructions. The V4–V5 regions of the bacterial 16S rRNA gene were amplified using primers T6m563F (5'-NNNNNN-AYTGGGYDTAAAGNG-3') and T6m926R (5'-NNNNNN-CCGTC AATTCMTTTRAGT-3'), where NNNNNN denotes a unique 6-mer barcode. PCR amplification was performed on a T100 thermal cycler (Bio-Rad, Hercules, CA, USA) in a 50- $\mu\text{l}$  reaction volume containing the BIOTAQ HS DNA Polymerase mixture (Bioline, London, UK), 1  $\mu\text{l}$  genomic DNA, and 20 pmol of each primer. The reaction conditions were as follows: 95°C for 10 min; 20 cycles of 94°C for 30 s, 52°C for 30 s, and 72°C for 1 min; and 72°C for 5 min. PCR products were resolved by electrophoresis on a 1.5% agarose gel and the DNA band of the correct size was excised and purified using the MonoFas DNA purification kit. Equal amounts of purified PCR product were pooled and ligated with adapters using the GS Titanium Rapid Library Preparation kit (Roche, Mannheim, Germany). Pyrosequencing was carried out on a 454 GS Junior instrument (Roche) following the Roche Amplicon Lib-L protocol, and the resulting sequencing reads were analyzed using the Ribosomal Database Project (RDP) pyrosequencing pipeline<sup>2</sup> (Wang et al., 2007) with default parameters (maximum number of Ns = 0 and minimum average quality score = 20). Pyrosequencing reads were assigned to specific samples based on their unique bar codes; these as well as primers were then trimmed off. DECIPHER was used to identify chimeric sequences<sup>3</sup> (Wright et al., 2012). Taxonomic assignment of bacterial high quality reads was performed using the RDP naive Bayesian rRNA Classifier with 80% confidence thresholds.

### Phylogenetic Analyses and Deposition of Identified 16S rRNA Genes

**Phylogenetic Analyses of 16S rRNA Gene Sequences**  
Phylogenetic analyses were carried out using MEGA software version 6 (Tamura et al., 2013). Phylogenetic trees with reference 16S rRNA sequences (>1,400 nucleotides) and representative partial 16S rRNA sequences (i.e., ~850 bp from clone analysis

or 325 bp from pyrosequencing) obtained in this study were analyzed using the neighbor-joining method. Bootstrap values were obtained from 1,000 replicates.

### Nucleotide Sequence Accession Numbers

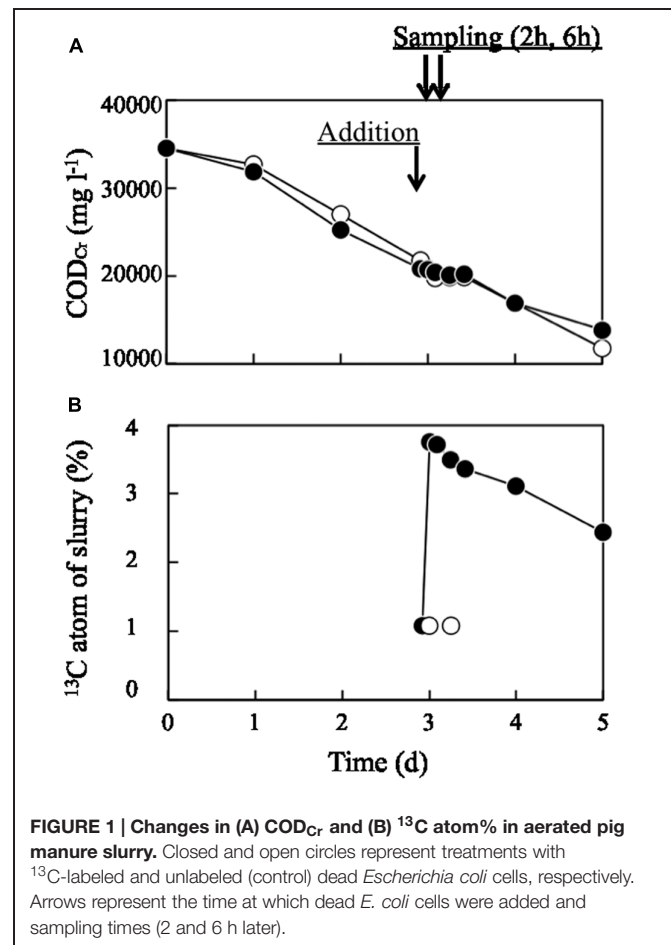
Nucleotide sequence data obtained in this study have been deposited in the DNA Data Bank of Japan<sup>4</sup> under accession numbers LC055721–LC055728.

## RESULTS

### Aerated Slurry Conditions and Addition of Labeled Biomass

Organic matter in pig manure slurry decreased linearly from 35,000 to 15,000  $\text{mg l}^{-1}$  over 5 days of aeration, as evaluated by  $\text{COD}_{\text{Cr}}$  (Figure 1A). <sup>13</sup>C-labeled or unlabeled dead *E. coli* cell suspension was added on day 3; at this point, the  $\text{COD}_{\text{Cr}}$  value was approximately 21,000  $\text{mg l}^{-1}$ , while the value for <sup>13</sup>C-labeled or unlabeled dead *E. coli* cell suspension was 34,510  $\text{mg l}^{-1}$ . Hence, the bacterial suspension (30 ml) corresponded to 3.3% of the total  $\text{COD}_{\text{Cr}}$  of the bulk slurry. Immediately after adding

<sup>4</sup><http://www.ddbj.nig.ac.jp>



<sup>2</sup><http://pyro.cme.msu.edu/>

<sup>3</sup><http://decipher.cce.wisc.edu/>

$^{13}\text{C}$ -labeled bacterial biomass, the  $\text{COD}_{\text{Cr}}$  value of the slurry did not change significantly, while  $^{13}\text{C}$  atom% increased from 1.07 to 3.76% (Figure 1B) and then decreased to 2.44% on day 5. The ORP decreased to less than  $-400$  mV within 12 h of the operation (Supplementary Figure S1A). This low ORP value lasted through day 3. After day 3, ORP began to increase and finally reached  $-30$  mV on day 5. The pH fluctuated between 8.1 and 8.6 during the process (Supplementary Figure S1B). The time courses of ORP and pH were similar between runs incubated with  $^{13}\text{C}$ -labeled and unlabeled dead *E. coli* cells and their components.

## Bacterial Community Structures in RNA Density Gradients

RNA-based SIP was performed to identify bacterial populations capable of assimilating bacterial biomass in aerated pig manure slurry 2 and 6 h after adding dead *E. coli* cell suspension. Bacteria-specific amplicons were obtained from density fractions with the highest BD ( $> 1.811$  g  $\text{ml}^{-1}$ ) obtained for the  $^{13}\text{C}$ -labeled sample, while no amplicons were obtained in this fraction ( $> 1.811$  g  $\text{ml}^{-1}$ ) in unlabeled control samples. T-RFLP fingerprinting patterns were similar in light fractions of RNA (BD: 1.760–1.786 g  $\text{ml}^{-1}$ ) after a 2-h incubation (Figure 2). The community profiles changed with increasing BD in  $^{13}\text{C}$ -labeled samples, in which two major T-RFs (277 and 278 bp in length) predominated in heavy fractions (BD:  $> 1.811$  g  $\text{ml}^{-1}$ ), accounting for  $\sim 71\%$  of total peak heights. However, this predominance was not observed either in light fractions (BD  $< 1.786$  g  $\text{ml}^{-1}$ ) of  $^{13}\text{C}$ -labeled samples or in entire-range fractions of unlabeled samples. In addition, the two T-RF peaks differed from that of the 16S rRNA from  $^{13}\text{C}$ -labeled dead *E. coli* cells (Figure 2). Although several minor T-RFs (94, 96, 151, 296, and 300 bp) were detected in heavy fractions, most of these were also present in light fractions. A high relative abundance of the two major peaks, reaching  $\sim 62\%$  of total peak heights, was still detected in heavy fractions after 6 h (Supplementary Figure S2).

## Phylogenetic Identification of Bacteria Incorporating $^{13}\text{C}$ -labeled Bacterial Biomass

Major populations found in heavy fractions by T-RFLP were identified by cloning and sequencing their 16S rRNAs from  $^{13}\text{C}$ -labeled and unlabeled samples. Phylogenetic affiliation and number of 16S rRNA clones are shown in Table 1. A high relative abundance of *Acholeplasma* sequences was present in heavy fractions of  $^{13}\text{C}$ -labeled sample as compared to unlabeled sample (63% of total clones). T-RF sizes of the sequences were estimated to be 277 and 278 bp, which corresponded to the major peaks in the T-RFLP fingerprint (Figure 2). These clones were related to *Acholeplasma axanthum* (90–94% sequence identity, 850 bp in length); two representative sequences, AS1 and AS2, were obtained (Figure 3) that belonged to clades that were distinct from the only free-living *Acholeplasma*, *A. laidlawii* ( $\sim 88\%$  sequence identity, 850 bp in length). Besides *Acholeplasma*, specific sequences of Clostridia or Bacteroidia were obtained from the heavy fraction in  $^{13}\text{C}$ -labeled samples. However, some of these were also detected as minor T-RFs in the unlabeled T-RFLP fingerprint. A large fraction of clones in the unlabeled sample library was related to Bacilli (57% of total clones), Clostridia (12%),  $\gamma$ -Proteobacteria (11%), and *Corynebacterium* (11%); only one clone related to *Acholeplasma* was obtained.

## Prevalence of *Acholeplasma* in Different Sources of Aerated Pig Manure Slurry

To evaluate the prevalence of *Acholeplasma* bacteria, pig manure slurry was obtained from four different locations (R, N, O, and K) in Japan. The pig manure slurry was sampled 3 days after the start of aeration; the sampling time was same as for SIP. Bacterial community composition was analyzed by pyrosequencing of 16S rRNA genes. The relative abundances of the *Acholeplasma* sequences (323 or 325 bp in length) in the four sample libraries were as follows: R, 4.5% (29 out of 649 sequences); N, 0.6% (10

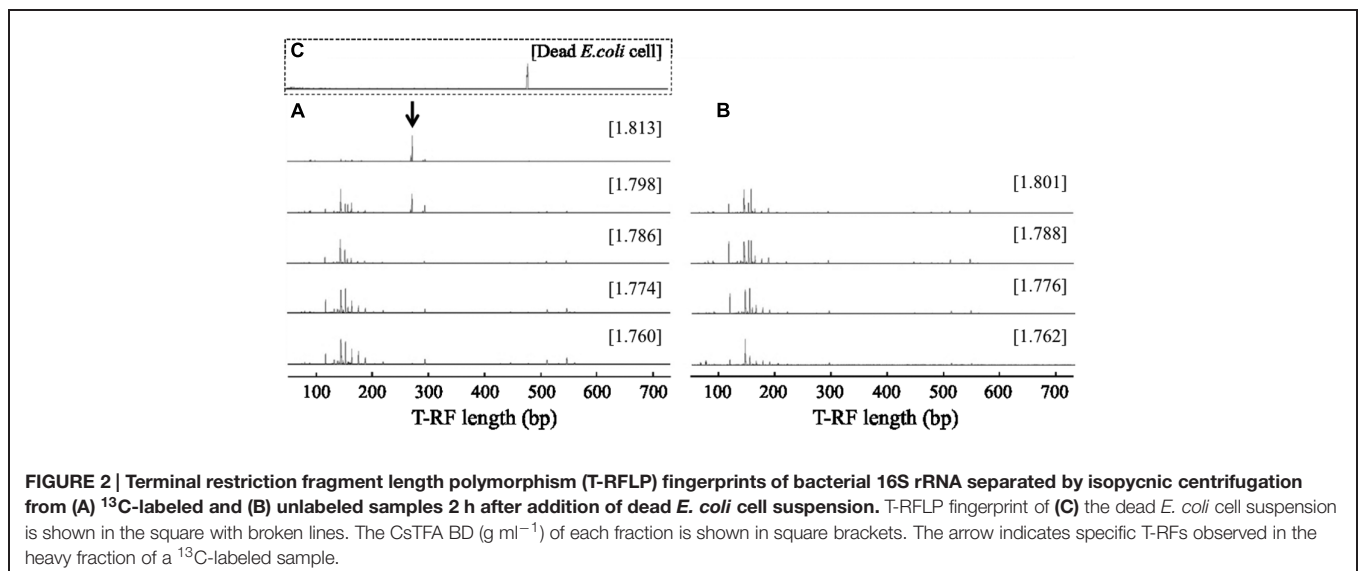


**FIGURE 2 | Terminal restriction fragment length polymorphism (T-RFLP) fingerprints of bacterial 16S rRNA separated by isopycnic centrifugation from (A)  $^{13}\text{C}$ -labeled and (B) unlabeled samples 2 h after addition of dead *E. coli* cell suspension. T-RFLP fingerprint of (C) the dead *E. coli* cell suspension is shown in the square with broken lines. The CsTFA BD (g  $\text{ml}^{-1}$ ) of each fraction is shown in square brackets. The arrow indicates specific T-RFs observed in the heavy fraction of a  $^{13}\text{C}$ -labeled sample.**

**TABLE 1 | Phylogenetic affiliations, T-RF length, and number of 16S rRNA clones obtained from the highest-density fraction of bacterial RNA following addition of <sup>13</sup>C-labeled and unlabeled bacterial biomass.**

Phylogenetic group	<sup>13</sup> C-labeled		Unlabeled	
	Clones (n)	T-RF (bp)	Clones (n)	T-RF (bp)
<i>Acholeplasma</i>	39	<b>277, 278 (71%)</b> , 279	1	278
Bacilli				
<i>Bacillus</i>	3	153, 165, 168	11	155, 167, <b>169 (4%)</b>
Planococcaceae	1	151	25	145, 147, <b>151 (25%)</b> , 159, 558
<i>Lactobacillus</i>	–	–	10	29, <b>181 (2%)</b>
<i>Streptococcus</i>	–	–	6	<b>555 (3%)</b>
Clostridia				
<i>Sporanaerobacter</i>	4	296	–	–
<i>Tissierella</i>	2	300	–	–
<i>Proteiniborus</i>	1	167	–	–
<i>Clostridium XI</i>	–	–	6	<b>195 (5%)</b>
<i>Clostridium sensu stricto</i>	–	–	2	520
<i>Cryptanaerobacter</i>	–	–	2	508
<i>Clostridium XIVa</i>	–	–	1	287
Bacteroidia				
<i>Petrimonas</i>	6	<b>94 (3%)</b>	–	–
<i>Proteiniphilum</i>	2	96	1	96
α-Proteobacteria	2	150	2	439
β-Proteobacteria	–	–	4	129, 488, 496
γ-Proteobacteria	1	123	10	<b>123 (10%)</b> , 226
<i>Erysipelothrix</i>	1	173	–	–
<i>Corynebacterium</i>	–	–	10	<b>165 (25%)</b>
<i>Flavobacterium</i>	–	–	1	29
<b>Total</b>	<b>62</b>		<b>92</b>	

T-RF detected for more than five clones within a group is indicated in boldface. Relative abundance of corresponding peaks in the T-RFLP profile is presented in parentheses.

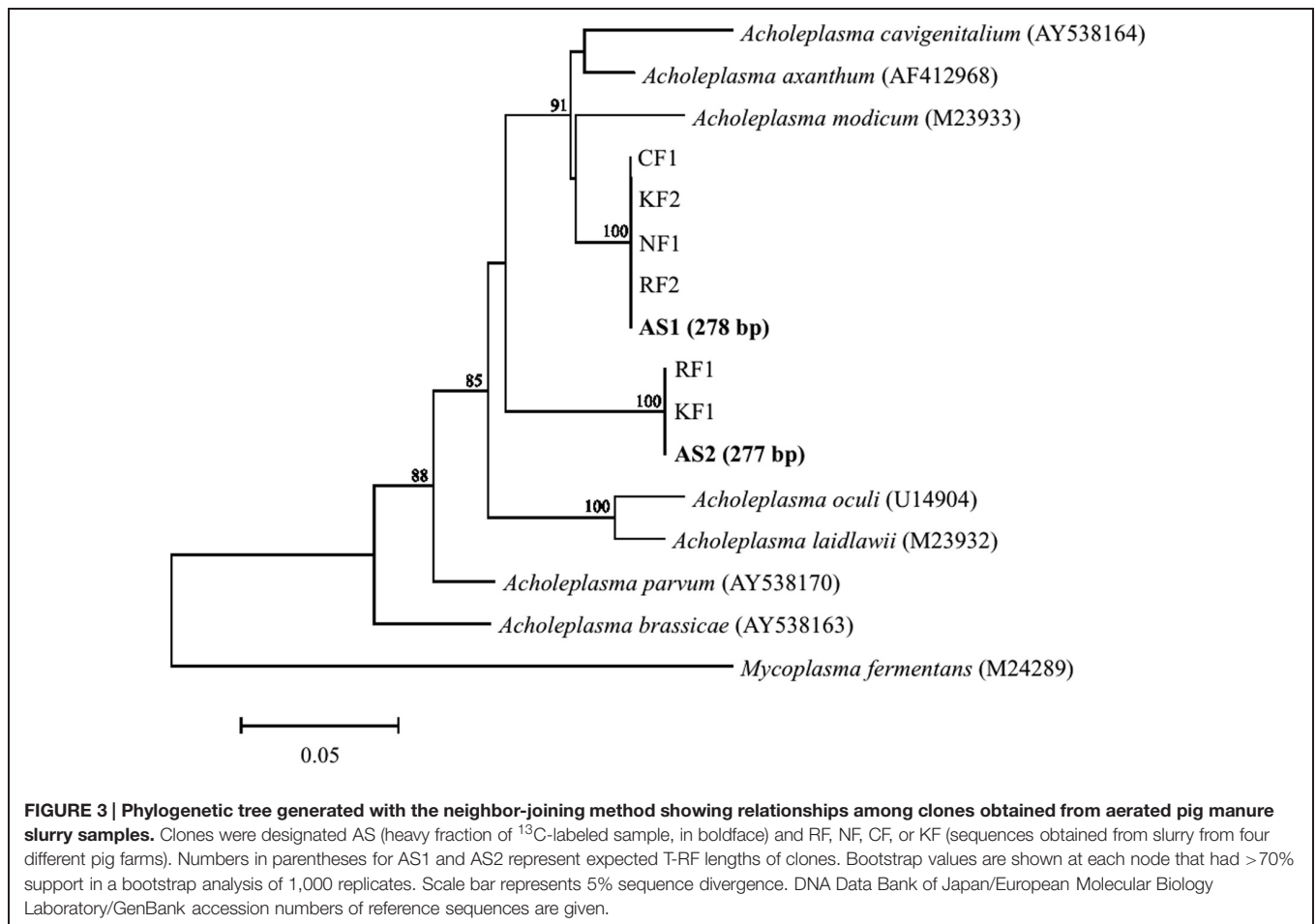
out of 1583 sequences); O, 0.2% (3 out of 1431 sequences); and K, 3.9% (44 out of 1128 sequences). All representative sequences obtained from these libraries were similar to the bacteria (i.e., AS1 or AS2) obtained in the <sup>13</sup>C-labeled sample (100% sequence identity, 323 or 325 bp in length) (Figure 3).

## DISCUSSION

Forced aeration of pig manure slurry has been used to mitigate odor emission and stabilize slurry quality. During this process, the bacterial community—mainly comprising pig gastrointestinal bacteria in raw manure—immediately shifts to become predominantly composed of Bacilli (Hanajima et al., 2009). *Bacillus* species are ubiquitous and are typically but variably capable of growing aerobically on complex, low molecular mass substrates (Sneath, 1986). These bacteria are implicated in organic matter degradation under aeration, which converts a portion of decayed bacterial biomass to carbon dioxide, ammonia, and/or water; however, it was assumed that a significant fraction of decayed bacterial biomass is recycled by newly proliferating populations. If the slurry is mixed thoroughly under stirring and forced aeration within the reactor, most microorganisms have access to

bacterial cell components (e.g., cell wall and membrane, as well as intracellular materials) from decayed bacterial cells. However, with longer incubation times, carbon derived from labeled microbial products rapidly spread throughout the slurry microorganisms via trophic interactions. We therefore focused on identifying the first-to-arrive scavengers in the aerated slurry, and demonstrated by SIP of rRNA that dead cells and their components were incorporated specifically by *Acholeplasma*.

Dead cells and their components were added just prior to ORP elevation. ORP is closely linked to the level of dissolved oxygen (DO) in slurry, and a decline in ORP has been attributed to increased DO consumption by microorganisms (Hanajima et al., 2009). In contrast, a reduction in available carbon in slurry decreases the requirement for oxygen in the decomposition of carbon substrates. This fluctuation in ORP is generally observed during aerated slurry treatment, and drastic shifts in bacterial community composition occur along with changes in ORP (Hanajima et al., 2009, 2011). Under these conditions, a certain amount of dead bacterial cells is likely produced in response to drastic shifts in the bacterial community. To prevent the continued existence and/or proliferation of <sup>13</sup>C-labeled *E. coli* in aerated slurry, cell cultures were inactivated before their addition as substrate. Given that the bacterial suspension



was <3.3% of the total  $\text{COD}_{\text{Cr}}$  of bulk slurry, it had little influence on the aerobic treatment process. Moreover, *E. coli* suspensions were not contaminated with *Acholeplasma* and none of the T-RFs derived from  $^{13}\text{C}$ -labeled *E. coli* were detected in the T-RFLP fingerprint. Therefore, sequences enriched in heavy fractions of RNA were derived from metabolically active bacteria that assimilated the  $^{13}\text{C}$ -labeled dead cells and their components. It was noted that these heavy fractions contained *Acholeplasma* sequences. Because none of the *Acholeplasma*-related T-RFs were observed in the unlabeled control or light fractions of the  $^{13}\text{C}$ -labeled sample, it was concluded that *Acholeplasma* was directly involved in the utilization of the dead cells and their components, albeit at a small population size.

Bacteria of the class *Mollicutes*, which includes the genus *Acholeplasma*, are widespread in nature and engage in a parasitic lifestyle; they are characterized by the absence of a cell wall and drastic reduction of genome size (Razin et al., 1998). *Acholeplasma* spp. possessing relatively large genomes of 1.5–1.8 Mbp (Lazarev et al., 2011), do not require sterols for cultivation, and are able to synthesize fatty acids from precursors, unlike other mycoplasma (Saito et al., 1977). *Acholeplasma* members have been detected as parasitic bacteria in nearly all organisms, including plants, crustaceans, mammals, and insects

(Atobe et al., 1983; Clark et al., 1986; Tully et al., 1994; Chen et al., 2011). One of the best-characterized species is *A. laidlawii*, which is regarded as a universalist that adapts to various environmental conditions. It was isolated from wastewater and is the only known *Acholeplasma* capable of surviving and reproducing in animals and plants through a parasitic lifestyle and in wastewaters through a free-living lifestyle (Lazarev et al., 2011). However, *Acholeplasma* sequences obtained in this study constituted a clade distinct from that of *A. laidlawii*, demonstrating for the first time that another free-living *Acholeplasma* species exists and is metabolically active in aerated slurry. *Acholeplasma* sequences have been previously detected in swine waste lagoons (Goh et al., 2009), aerated pig manure slurry (Hanajima et al., 2009), and pigpen pit slurry (Hwang et al., 2014). The latter study found a relative abundance of 3.5% from *Acholeplasma* in pig manure slurry, which is in accordance with results from our survey of four different farm samples (~4.4%). These results strongly suggest that *Acholeplasma* is prevalent in the pig manure slurry environment. In addition to these environments, *Acholeplasma* were found in marine sediments (Masui et al., 2008; Imachi et al., 2011), suggesting that these organisms are concentrated in copiotrophic environments in which bacterial cell components released from decayed microbial biomass accumulate.

It is widely known that Mollicutes have limited biosynthetic capabilities (Fraser et al., 1995; Sasaki et al., 2002; Vasconcelos, 2005); these are primarily for energy acquisition, with synthetic pathways being considerably reduced or absent. As such, many nutrients must be obtained from external sources (e.g., the host organism). Metabolic and genomic analyses have been carried out to elucidate the principles of metabolic regulation and adaptation to environmental conditions by Mollicutes (Lazarev et al., 2011; Kube et al., 2014; Vanyushkina et al., 2014). The *Acholeplasma* genome encodes a wide variety of ATP-binding cassette (ABC) transporters, and most genetic modules are implicated in the conversion of intermediates and are linked to ABC transporter genes for the uptake of oligopeptides and amino acids (Kube et al., 2014). This demonstrates that *Acholeplasma* are capable of incorporating oligopeptides and amino acids released from dead cells and their components. However, this raises questions about the assimilation of labile carbon sources by heterotrophic bacteria in slurry, such as why only the rRNA recovered from *Acholeplasma* was  $^{13}\text{C}$ -labeled despite most heterotrophic bacteria having access to dead cells and their components, and why  $^{13}\text{C}$ -labeled rRNA was recovered after a very short (2-h) incubation period. *Acholeplasma* has the capacity to generate dNTPs from adenosine, guanosine, uracil, and thymine (Kube et al., 2014), and *A. laidlawii* was reported to incorporate nucleic acid precursors during the first 4 h of incubation in medium (McIvor and Kenny, 1978). The detection of  $^{13}\text{C}$ -labeled rRNA within a 2-h incubation period leads us to speculate that *Acholeplasma* incorporated  $^{13}\text{C}$ -labeled nucleic acid precursors released by dead *E. coli* cells. Although most heterotrophic bacteria may incorporate  $^{13}\text{C}$ -labeled dead cells and their components, a longer incubation time would be required to obtain  $^{13}\text{C}$ -labeled rRNA from these bacteria, with the exception of *Acholeplasma*.

*Acholeplasma axanthum*, the closest relative to metabolically active bacteria identified in our study, has been isolated from a variety of habitats and hosts, including the lung of swine (Stipkovits et al., 1974). The genotypic patterns of these strains differed markedly from one another, suggesting considerable heterogeneity within the same species (Razin et al., 1983). Growth in varied environments requires regulatory switches and cross-talk between metabolic pathways to allow rapid adaptation to environmental changes in nutritional flux. The *A. laidlawii* genome contains genes encoding components of signal transduction pathways and the SOS response system, which are closely related to the regulation of gene expression and mutagenic response to stress (Lazarev et al., 2011). These functions allow *A. laidlawii* to adapt to various environmental conditions. It is unclear whether the *Acholeplasma* spp. detected in this study originated from the body of pigs or from the manure slurry itself; nonetheless, the results suggest that

*Acholeplasma* has a competitive advantage for utilizing dead bacterial biomass more rapidly relative to other microbial populations.

Linking the phylogeny and function of microorganisms is one of the most fundamental challenges in microbial ecology. Generating defined mixed cultures of isolated microorganisms is one promising approach to achieve this end (Kato et al., 2005, 2014). However, in natural and engineered environments, unidentified microbial components may nonetheless play critical ecophysiological roles. In this study, we identified the first-to-arrive scavengers in aerated pig manure slurry by  $^{13}\text{C}$ -labeled bacterial biomass probing of rRNA. *Acholeplasma* spp. were identified for the first time as a major heterotroph that assimilates the dead cells and their components in pig manure slurry. Substrate competition has been found in many types of biological processes, in which physiologically similar microorganisms co-exist and fill ecological niches owing to the difference in the substrate availability and affinity (Hori et al., 2006; Aoyagi et al., 2015). Due to the limited biosynthetic capabilities, free-living *Acholeplasma* spp. most likely require biomolecules released from dead bacterial cells as substrates. Actually, they were capable of incorporating the dead cells and their components more rapidly than the other microbial populations, which allowed the survival and prevalence of *Acholeplasma* spp. in pig manure slurry. These findings provide deeper understanding of carbon flow mediated by microorganisms in copiotrophic environments and unveil one of the mechanisms underlying the microbial ecosystem development.

## AUTHOR CONTRIBUTIONS

DH designed the research. DH and TH wrote the manuscript. DH, TA, and TH carried out the experiments and analyzed the data.

## ACKNOWLEDGMENTS

This work was supported by a Japan Society for the Promotion of Science KAKENHI (grant number 21580338). We thank Dr. Satoshi Tobita and Dr. Kenji Fujieda for  $\delta^{13}\text{C}$  analysis of slurry samples by isotope ratio mass spectrometry.

## SUPPLEMENTARY MATERIAL

The Supplementary Material for this article can be found online at: <http://journal.frontiersin.org/article/10.3389/fmicb.2015.01206>

## REFERENCES

- Aoyagi, T., Kimura, M., Yamada, N., Navarro, R. R., Itoh, H., Ogata, A., et al. (2015). Dynamic transition of chemolithotrophic sulfur-oxidizing bacteria in response to amendment with nitrate in deposited marine sediments. *Front. Microbiol.* 6:426. doi: 10.3389/fmicb.2015.00426
- Atobe, H., Watabe, J., and Ogata, M. (1983). *Acholeplasma parvum*, a new species from horses. *Int. J. Syst. Bacteriol.* 33, 344–349. doi: 10.1099/00207713-33-2-344
- Chen, J. G., Lou, D., and Yang, J. F. (2011). Isolation and identification of *Acholeplasma* sp. from the mud crab, *Scylla serrata*. *Evid. Based Complement. Alternat. Med.* 2011, 209406. doi: 10.1155/2011/209406

- Clark, T. B., Tully, J. G., Rose, D. L., Henegar, R., and Whitcomb, R. F. (1986). Acholeplasmas and similar nonsterol-requiring mollicutes from insects—missing link in microbial ecology. *Curr. Microbiol.* 13, 11–16. doi: 10.1007/BF01568152
- Danon, M., Franke-Whittle, I. H., Insam, H., Chen, Y., and Hadar, Y. (2008). Molecular analysis of bacterial community succession during prolonged compost curing. *FEMS Microbiol. Ecol.* 65, 133–144. doi: 10.1111/j.1574-6941.2008.00506.x
- Fierer, N., Nemergut, D., Knight, R., and Craine, J. M. (2010). Changes through time: integrating microorganisms into the study of succession. *Res. Microbiol.* 161, 635–642. doi: 10.1016/j.resmic.2010.06.002
- Fraser, C. M., Gocayne, J. D., White, O., Adams, M. D., Clayton, R. A., Fleischmann, R. D., et al. (1995). The minimal gene complement of *Mycoplasma genitalium*. *Science* 270, 397–403. doi: 10.1126/science.270.5235.397
- Goh, S. H., Mabbett, A. N., Welch, J. P., Hall, S. J., and McEwan, A. G. (2009). Molecular ecology of a facultative swine waste lagoon. *Lett. Appl. Microbiol.* 48, 486–492. doi: 10.1111/j.1472-765X.2009.02560.x
- Hanajima, D., Fukumoto, Y., Yasuda, T., Suzuki, K., Maeda, K., and Morioka, R. (2011). Bacterial community dynamics in aerated cow manure slurry at different aeration intensities. *J. Appl. Microbiol.* 111, 1416–1425. doi: 10.1111/j.1365-2672.2011.05151.x
- Hanajima, D., Haruta, S., Hori, T., Ishii, M., Haga, K., and Igarashi, Y. (2009). Bacterial community dynamics during reduction of odorous compounds in aerated pig manure slurry. *J. Appl. Microbiol.* 106, 118–129. doi: 10.1111/j.1365-2672.2008.03984.x
- Hori, T., Haruta, S., Ueno, Y., Ishii, M., and Igarashi, Y. (2006). Dynamic transition of a methanogenic population in response to the concentration of volatile fatty acids in a thermophilic anaerobic digester. *Appl. Environ. Microbiol.* 72, 1623–1630. doi: 10.1128/AEM.72.2.1623-1630.2006
- Hori, T., Noll, M., Igarashi, Y., Friedrich, M. W., and Conrad, R. (2007). Identification of acetate-assimilating microorganisms under methanogenic conditions in anoxic rice field soil by comparative stable isotope probing of RNA. *Appl. Environ. Microbiol.* 73, 101–109. doi: 10.1128/AEM.01676-06
- Hwang, O. H., Raveendar, S., Kim, Y. J., Kim, J. H., Kim, T. H., Choi, D. Y., et al. (2014). Deodorization of pig slurry and characterization of bacterial diversity using 16S rDNA sequence analysis. *J. Microbiol.* 52, 1056–1056. doi: 10.1007/s12275-014-4251-5
- Imachi, H., Aoi, K., Tasumi, E., Saito, Y., Yamanaka, Y., Saito, Y., et al. (2011). Cultivation of methanogenic community from seafloor sediments using a continuous-flow bioreactor. *ISME J.* 5, 1913–1925. doi: 10.1038/ismej.2011.64
- Ishii, K., and Takii, S. (2003). Comparison of microbial communities in four different composting processes as evaluated by denaturing gradient gel electrophoresis analysis. *J. Appl. Microbiol.* 95, 109–119. doi: 10.1046/j.1365-2672.2003.01949.x
- Japan Livestock Industry Association (1989). *Facility of Liquid Composting*. Tokyo: Japan Livestock Industry Association.
- Kato, S., Haruta, S., Cui, Z. J., Ishii, M., and Igarashi, Y. (2005). Stable coexistence of five bacterial strains as a cellulose-degrading community. *Appl. Environ. Microbiol.* 71, 7099–7106. doi: 10.1128/AEM.71.11.7099-7106.2005
- Kato, S., Yoshida, R., Yamaguchi, T., Sato, T., Yumoto, I., and Kamagata, Y. (2014). The effects of elevated CO<sub>2</sub> concentration on competitive interaction between acetoclastic and syntrophic methanogenesis in a model microbial consortium. *Front. Microbiol.* 5:575. doi: 10.3389/fmicb.2014.00575
- Kindler, R., Miltner, A., Richnow, H. H., and Kastner, M. (2006). Fate of gram-negative bacterial biomass in soil—mineralization and contribution to SOM. *Soil Biol. Biochem.* 38, 2860–2870. doi: 10.1016/j.soilbio.2006.04.047
- Kube, M., Siewert, C., Migdoll, A. M., Duduk, B., Holz, S., Rabus, R., et al. (2014). Analysis of the complete genomes of *Acholeplasma brassicae*. *A. palmae* and *A. laidlawii* and their comparison to the obligate parasites from ‘*Candidatus Phytoplasma*’. *J. Mol. Microbiol. Biotechnol.* 24, 19–36. doi: 10.1159/000354322
- Lazarev, V. N., Levitskii, S. A., Basovskii, Y. I., Chukin, M. M., Akopian, T. A., Vereshchagin, V. V., et al. (2011). Complete genome and proteome of *Acholeplasma laidlawii*. *J. Bacteriol.* 193, 4943–4953. doi: 10.1128/JB.05059-11
- Lee, C. G., Watanabe, T., Sato, Y., Murase, J., Asakawa, S., and Kimura, M. (2011). Bacterial populations assimilating carbon from <sup>13</sup>C-labeled plant residue in soil: analysis by a DNA-SIP approach. *Soil Biol. Biochem.* 43, 814–822. doi: 10.1016/j.soilbio.2010.12.016
- Ludwig, W., Strunk, O., Klugbauer, S., Klugbauer, N., Weizenegger, M., Neumaier, J., et al. (1998). Bacterial phylogeny based on comparative sequence analysis. *Electrophoresis* 19, 554–568. doi: 10.1002/elps.1150190416
- Lueders, T., Kindler, R., Miltner, A., Friedrich, M. W., and Kaestner, M. (2006). Identification of bacterial micropredators distinctively active in a soil microbial food web. *Appl. Environ. Microbiol.* 72, 5342–5348. doi: 10.1128/AEM.00400-06
- Lueders, T., Manefield, M., and Friedrich, M. W. (2004). Enhanced sensitivity of DNA- and rRNA-based stable isotope probing by fractionation and quantitative analysis of isopycnic centrifugation gradients. *Environ. Microbiol.* 6, 73–78. doi: 10.1046/j.1462-2920.2003.00536.x
- Masui, N., Morono, Y., and Inagaki, F. (2008). Microbiological assessment of circulation mud fluids during the first operation of riser drilling by the deep-earth research vessel Chikyū. *Geomicrobiol. J.* 25, 274–282. doi: 10.1080/01490450802258154
- McIvor, R. S., and Kenny, G. E. (1978). Differences in incorporation of nucleic acid bases and nucleosides by various *Mycoplasma* and *Acholeplasma* species. *J. Bacteriol.* 135, 483–489.
- Murase, J., Hordijk, K., Tayasu, I., and Bodelier, P. L. (2011). Strain-specific incorporation of methanotrophic biomass into eukaryotic grazers in a rice field soil revealed by PLFA-SIP. *FEMS Microbiol. Ecol.* 75, 284–290. doi: 10.1111/j.1574-6941.2010.01007.x
- Noll, M., Matthies, D., Frenzel, P., Derakshani, M., and Liesack, W. (2005). Succession of bacterial community structure and diversity in a paddy soil oxygen gradient. *Environ. Microbiol.* 7, 382–395. doi: 10.1111/j.1462-2920.2005.00700.x
- Razin, S., Tully, J. G., Rose, D. L., and Barile, M. F. (1983). DNA cleavage patterns as indicators of genotypic heterogeneity among strains of *Acholeplasma* and *Mycoplasma* species. *J. Gen. Microbiol.* 129, 1935–1944.
- Razin, S., Yogeve, D., and Naot, Y. (1998). Molecular biology and pathogenicity of mycoplasmas. *Microbiol. Mol. Biol. Rev.* 62, 1094–1156.
- Saito, Y., Silvius, J. R., and McElhaney, N. (1977). Membrane lipid biosynthesis in *Acholeplasma laidlawii* B: de novo biosynthesis of saturated fatty acids by growing cells. *J. Bacteriol.* 132, 497–504.
- Sasaki, Y., Ishikawa, J., Yamashita, A., Oshima, K., Kenri, T., Furuya, K., et al. (2002). The complete genomic sequence of *Mycoplasma penetrans*, an intracellular bacterial pathogen in humans. *Nucl. Acids Res.* 30, 5293–5300. doi: 10.1093/nar/gkf667
- Sneath, P. H. A. (1986). “Endospore-forming Gram-Positive Rods and Cocci,” in *Bergey’s Manual of Systematic Bacteriology*, Vol.2, eds P. H. A. Sneath, N. S. Mair, M. E. Sharpe, and J. G. Holt (Baltimore: Williams & Wilkins Co), 1104–1207.
- Stipkovits, L., Romvary, J., Nagy, Z., Bodon, L., and Varga, L. (1974). Studies on the pathogenicity of *Acholeplasma axanthum* in swine. *J. Hyg.* 72, 289–296. doi: 10.1017/S0022172400023500
- Tamura, K., Stecher, G., Peterson, D., Filipiński, A., and Kumar, S. (2013). MEGA6: molecular evolutionary genetics analysis version 6.0. *Mol. Biol. Evol.* 30, 2725–2729. doi: 10.1093/molbev/mst197
- Tully, J. G., Whitcomb, R. F., Rose, D. L., Bove, J. M., Carle, P., Somerson, N. L., et al. (1994). *Acholeplasma brassicae* sp. nov. and *Acholeplasma palmae* sp. nov., two non-sterol-requiring mollicutes from plant surfaces. *Int. J. System. Bacteriol.* 44, 680–684. doi: 10.1099/00207713-44-4-680
- Vanyushkina, A. A., Fisunov, G. Y., Gorbachev, A. Y., Kamashev, D. E., and Govorun, V. M. (2014). Metabolomic analysis of three mollicute species. *PLoS ONE* 9:e89312. doi: 10.1371/journal.pone.0089312
- Vasconcelos, A. T. R. (2005). Swine and poultry pathogens: the complete genome sequences of two strains of *Mycoplasma hyopneumoniae* and a strain of *Mycoplasma synoviae*. *J. Bacteriol.* 187, 7548–7548. doi: 10.1128/JB.187.16.5568-5577.2005

- Wang, Q., Garrity, G. M., Tiedje, J. M., and Cole, J. R. (2007). Naive Bayesian classifier for rapid assignment of rRNA sequences into the new bacterial taxonomy. *Appl. Environ. Microbiol.* 73, 5261–5267. doi: 10.1128/AEM.00062-07
- Wright, E. S., Yilmaz, L. S., and Noguera, D. R. (2012). DECIPHER, a search-based approach to chimera identification for 16S rRNA sequences. *Appl. Environ. Microbiol.* 78, 717–725. doi: 10.1128/AEM.06516-11
- Zhu, J. (2000). A review of microbiology in swine manure odor control. *Agric. Ecosyst. Environ.* 78, 93–106. doi: 10.1016/S0167-8809(99)00116-4

**Conflict of Interest Statement:** The authors declare that the research was conducted in the absence of any commercial or financial relationships that could be construed as a potential conflict of interest.

Copyright © 2015 Hanajima, Aoyagi and Hori. This is an open-access article distributed under the terms of the Creative Commons Attribution License (CC BY). The use, distribution or reproduction in other forums is permitted, provided the original author(s) or licensor are credited and that the original publication in this journal is cited, in accordance with accepted academic practice. No use, distribution or reproduction is permitted which does not comply with these terms.



# The effects of elevated CO<sub>2</sub> concentration on competitive interaction between acetoclastic and syntrophic methanogenesis in a model microbial consortium

Souichiro Kato<sup>1,2,3\*</sup>, Rina Yoshida<sup>4</sup>, Takashi Yamaguchi<sup>4</sup>, Tomoyuki Sato<sup>1</sup>, Isao Yumoto<sup>1</sup> and Yoichi Kamagata<sup>1,2</sup>

<sup>1</sup> Bioproduction Research Institute, National Institute of Advanced Industrial Science and Technology, Sapporo, Japan

<sup>2</sup> Division of Applied Bioscience, Graduate School of Agriculture, Hokkaido University, Sapporo, Japan

<sup>3</sup> Research Center for Advanced Science and Technology, The University of Tokyo, Tokyo, Japan

<sup>4</sup> Department of Civil and Environmental Engineering, Nagaoka University of Technology, Nagaoka, Japan

## Edited by:

Shin Haruta, Tokyo Metropolitan University, Japan

## Reviewed by:

Hans Karl Carlson, University of California, Berkeley, USA

Spyridon Ntougias, Democritus University of Thrace, Greece

Shawn E. McGlynn, Tokyo Metropolitan University, Japan

## \*Correspondence:

Souichiro Kato, Bioproduction Research Institute, National Institute of Advanced Industrial Science and Technology, 2-17-2-1

Tsukisamu-Higashi, Toyohira-ku, Sapporo, Hokkaido 062-8517, Japan  
e-mail: s.katou@aist.go.jp

Investigation of microbial interspecies interactions is essential for elucidating the function and stability of microbial ecosystems. However, community-based analyses including molecular-fingerprinting methods have limitations for precise understanding of interspecies interactions. Construction of model microbial consortia consisting of defined mixed cultures of isolated microorganisms is an excellent method for research on interspecies interactions. In this study, a model microbial consortium consisting of microorganisms that convert acetate into methane directly (*Methanosaeta thermophila*) and syntrophically (*Thermacetogenium phaeum* and *Methanothermobacter thermautotrophicus*) was constructed and the effects of elevated CO<sub>2</sub> concentrations on intermicrobial competition were investigated. Analyses on the community dynamics by quantitative RT-PCR and fluorescent *in situ* hybridization targeting their 16S rRNAs revealed that high concentrations of CO<sub>2</sub> have suppressive effects on the syntrophic microorganisms, but not on the acetoclastic methanogen. The pathways were further characterized by determining the Gibbs free energy changes ( $\Delta G$ ) of the metabolic reactions conducted by each microorganism under different CO<sub>2</sub> concentrations. The  $\Delta G$  value of the acetate oxidation reaction (*T. phaeum*) under high CO<sub>2</sub> conditions became significantly higher than  $-20$  kJ per mol of acetate, which is the borderline level for sustaining microbial growth. These results suggest that high concentrations of CO<sub>2</sub> undermine energy acquisition of *T. phaeum*, resulting in dominance of the acetoclastic methanogen. This study demonstrates that investigation on model microbial consortia is useful for untangling microbial interspecies interactions, including competition among microorganisms occupying the same trophic niche in complex microbial ecosystems.

**Keywords:** model consortia, methanogenesis, acetate, thermodynamics, CO<sub>2</sub> concentration

## INTRODUCTION

In natural and engineered environments, many species of microorganisms coexist by interacting with each other. Comprehension of interspecies interactions is essential for describing the features of complex microbial ecosystems, and competition among microorganisms occupying similar trophic niches is a conventional and significant aspect of such interspecies interaction. Coexistence of multiple microorganisms with similar trophic niches is regarded as one of the major factors to confer functional stability and resiliency on microbial ecosystems (Loreau et al., 2001; Deng, 2012). It is important to grasp how the population of each microorganism changes depending on a specific environmental disturbance. Most microbial ecological research has assessed the effects of specific environmental factors on competitive interactions among multiple microbial species by observing the transition of abundances of each microorganism responding to environmental disturbances. Although this approach has produced

many excellent outcomes, existence of non-target microorganisms and uncontrollable environmental factors in the systems often hamper precise understanding of the effects of specific environmental factors on the competitive interactions among target microorganisms.

Construction of microbial model consortia, in which interspecies interactions in ecosystems are reproduced by defined co-culture of isolated microorganisms, is appreciated as a worthwhile method to investigate microbial interactions (Haruta et al., 2009; De Roy et al., 2014; Großkopf and Soyer, 2014). For instance, the complex phenomenon of bacterial competition as being similar to rock-paper-scissors among colicin-producing, colicin-resistant, and colicin-sensitive strains was untangled by constructing model co-culture systems (Kerr et al., 2002; Nahum et al., 2011). Kato et al. (2005, 2008) constructed model microbial consortia composed of 4–5 bacterial strains, in which all members stably coexisted for long period of time, and demonstrated

that existence of both positive and negative interspecies interactions among the members make these consortia stable. The construction of model consortia is a specific and beneficial feature of microbiological research fields, which will also be effective for proof-of-concept studies for theories in the field of macro-ecology (Haruta et al., 2009, 2013).

Methanogenesis from organic compounds is a complex microbial process accomplished by catabolic interactions among different trophic levels of microorganisms (Schink, 1997; Jones et al., 2008; Kato and Watanabe, 2010). Among the sequential biodegradation processes, acetate is the most important intermediary metabolite (Schink, 1997). Methanogenic acetate degradation proceeds by either acetoclastic methanogenesis or syntrophic acetate oxidation. The acetoclastic pathway is solely mediated by acetoclastic methanogens (Jetten et al., 1992). On the contrary, syntrophic acetate oxidation pathway requires cooperative interactions of two different types of microorganisms: acetate is first oxidized to H<sub>2</sub> and CO<sub>2</sub> by syntrophic acetate-oxidizing bacteria (SAOB), and then hydrogenotrophic methanogens convert the products to CH<sub>4</sub> (Zinder and Koch, 1984). As the acetate oxidation reaction is endergonic under the standard conditions and is feasible only under extremely low H<sub>2</sub> partial pressure, acetate oxidation by SAOB requires H<sub>2</sub> elimination by hydrogenotrophic methanogens (Karakashev et al., 2006; Hattori, 2008). These two different acetate-degrading methane-producing pathways and organisms involved can co-exist, but diverse environmental factors, such as temperature, pH, salinity, toxic compounds, and concentrations of substrates determine one pathway and organisms to dominate over the other (Nüsslein et al., 2001; Shigematsu et al., 2004; Karakashev et al., 2006; Hao et al., 2013; Kato et al., 2014).

In our previous studies, we demonstrated that the syntrophic pathway is the dominant methanogenic acetate degradation pathway in underground, thermophilic petroleum reservoirs (Mayumi et al., 2011). We further demonstrated that acetoclastic pathway becomes dominant under high CO<sub>2</sub> concentrations, which mimicked carbon capture and storage field conditions (Mayumi et al., 2013), whereas syntrophic acetate oxidation dominated over acetoclastic reactions under low CO<sub>2</sub> concentrations. Since CO<sub>2</sub> is either substrate or product of acetoclastic methanogenesis, acetate oxidation, and hydrogenotrophic methanogenesis, high CO<sub>2</sub> concentration alters the thermodynamics of each methanogenic reaction, which may cause the observed transition between syntrophic and acetoclastic methanogenic pathways. However, all the data were based on the analyses of complex microbial communities in field samples thus many other factors that affect the community shift could not be ruled out.

In the present study, the effect of CO<sub>2</sub> concentrations on methanogenic microorganisms were assessed by using a defined inorganic medium and a defined methanogenic consortium which is comprised of three organisms, i.e., SAOB, hydrogenotrophic methanogen and acetoclastic methanogen, namely, which contains two different acetate-degrading methanogenic pathways. The experiments allowed to precisely show the CO<sub>2</sub> concentrations to be a crucial factor affecting the dominance of respective pathways and organisms.

## MATERIALS AND METHODS

### MICROORGANISMS AND CULTURE CONDITIONS

*Methanosaeta thermophila* DSM6194<sup>T</sup> (Kamagata and Mikami, 1991) and *Thermacetogenium phaeum* DSM12270<sup>T</sup> (Hattori et al., 2000) were obtained from the Deutsche Sammlung von Mikroorganismen und Zellkulturen GmbH (Braunschweig, Germany). *Methanothermobacter thermautotrophicus* strain TM was isolated from a thermophilic anaerobic methanogenic reactor in Japan (Hattori et al., 2000). Routine cultivations were conducted at 55°C with 68-ml capacity serum vials containing 20 ml of a bicarbonate-buffered inorganic medium (pH 7.0; Kato et al., 2014) under an atmosphere of N<sub>2</sub>-CO<sub>2</sub> [80/20 (v/v)] without shaking. Pyruvate (40 mM) or 200 kPa H<sub>2</sub>-CO<sub>2</sub> [80/20 (v/v)] was supplemented as energy and carbon sources for the pure cultures of *T. phaeum* and *Methanothermobacter thermautotrophicus*, respectively. Sodium acetate (40 mM) was utilized as an energy and carbon source for the pure culture of *Methanosaeta thermophila*, the defined co-culture of *T. phaeum* and *Methanothermobacter thermautotrophicus*, and the tri-culture of the three strains. The tri-culture was constructed by simultaneously inoculating 1 and 2 ml of the early-stationary phases of pure culture of *Methanosaeta thermophila* and the defined co-culture of *T. phaeum* and *Methanothermobacter thermautotrophicus*, respectively, into the 20 ml of the medium. Although the long term stability of the tri-culture was not been tested, coexistence of the three microorganisms in the batch culture was confirmed.

### CULTURES WITH DIFFERENT CO<sub>2</sub> CONCENTRATIONS

Three culture conditions were prepared to examine the effects of CO<sub>2</sub> concentrations on the microorganisms. For each condition, the media were supplemented with different concentrations of sodium bicarbonate and the gas phases were replaced with N<sub>2</sub>/CO<sub>2</sub> mixed gas with different volume ratios, as described in **Table 1**. The medium was bubbled with the respective deoxygenated gas with 100 ml min<sup>-1</sup> for 5 min and immediately capped with a butyl rubber stopper and an aluminum cap. The medium pH was adjusted to 7.0 by adding 1N NaOH solution before the cultivation, and the fluctuation of pH value throughout the cultivation was less than 0.2. For pH measurement, 100 μl of the medium was sampled with syringes and the pH value was determined using a compact pH meter B-212 (Horiba). The concentration of CO<sub>2</sub> in the aqueous phase [*c*<sub>aq</sub> (M)] was calculated according to Henry's law (*c*<sub>aq</sub> = *k**p*), where *k* is the Henry's law constant (0.019 for CO<sub>2</sub> at 55°C) and *p* is the partial pressure of CO<sub>2</sub> in the gas phase (atm). Then the bicarbonate concentrations were calculated based on the equilibrium formula (H<sub>2</sub>CO<sub>3</sub> = H<sup>+</sup> + HCO<sub>3</sub><sup>-</sup>) with the

**Table 1 | Media with different initial [ΣCO<sub>2</sub>] used in this study.**

[ΣCO <sub>2</sub> ] <sub>initial</sub> (mmol l <sup>-1</sup> )	NaHCO <sub>3</sub> added (mM)	Partial pressure of the gas phase CO <sub>2</sub> (atm)	Calculated [HCO <sub>3</sub> <sup>-</sup> ] <sub>initial</sub> (mM)
5.0	5	0	0.8
50.7	35	0.2	8.1
113.4	35	1	18.1

equilibrium constant of  $4.47 \times 10^7$ . The culture experiments were conducted in triplicate and the student's *t*-test was used for the statistical analyses.

Growth of *Methanosaeta thermophila* and *Methanothermobacter thermautotrophicus* in pure and mixed cultures was determined by measuring methane production. Growth of *T. phaeum* pure culture was determined by measuring acetate production from pyruvate. The partial pressure of CH<sub>4</sub> was determined using a gas chromatograph GC-2014 (Shimadzu) as described previously (Kato et al., 2014). The partial pressure of H<sub>2</sub> was determined using a trace reduction gas analyzer TRA-1000 (ACE Inc.) according to the manufacturer's instruction. The concentrations of organic acids were determined using a high performance liquid chromatography (D-2000 LaChrom Elite HPLC system, HITACHI) equipped with Aminex HPX-87H Ion Exclusion column (BIO-RAD) and L2400 UV detector (HITACHI).

### FLUORESCENT *IN SITU* HYBRIDIZATION (FISH)

Microbial cells of the tri-cultures in the early stationary phases were collected by centrifugation, fixed with 4% paraformaldehyde in phosphate buffered saline (PBS; 137 mM NaCl, 2.7 mM KCl, 8.1 mM Na<sub>2</sub>HPO<sub>4</sub>, 1.5 mM KH<sub>2</sub>PO<sub>4</sub>, pH 7.2) and left for 6 h at 4°C. The samples were washed three times with PBS, immobilized on glass slides, and dehydrated by successive passages through 50, 70, 80, 90, and 100% ethanol (3 min each). The following oligonucleotide probes complementary to specific regions of 16S rRNA were utilized for hybridizations: (i) Alexa488-labeled EUB338, specific for the domain *Bacteria* (Amann et al., 1990) and (ii) TexRed-labeled ARCH917, specific for the domain *Archaea* (Loy et al., 2002), (iii) Alexa594-labeled MSMX860, specific for the order *Methanosarcinales* (Raskin et al., 1994), and (iv) Alexa488-labeled MB311, specific for the order *Methanobacteriales* (Crocetti et al., 2006). Hybridizations were performed at 46°C for 3 h with hybridization buffer (0.9 M NaCl, 0.1 M Tris-HCl, pH 7.5) containing 5 ng μl<sup>-1</sup> of each labeled probe. The specificity of each probe was confirmed by FISH observations using pure cultures of the three microorganisms used in this study even with the hybridization buffer not containing formamide. The washing step was done at 48°C for 30 min with washing buffer (0.2 M NaCl, 0.1 M Tris-HCl, pH 7.5). The samples hybridized with the probes were observed with a fluorescent microscope Provis AX70 (Olympus).

### QUANTITATIVE RT-PCR (qRT-PCR)

Microbial cells were harvested from the mid-logarithmic phases by centrifugation at 10,000 X *g* and 4°C. Total RNA was isolated using ISOGEN II reagent (Nippon Gene, Japan) combined with a bead-beating method, as described previously (Kato et al., 2014). Total RNA was purified using an RNeasy Mini kit (Qiagen) with DNase treatment (RNase-free DNase set, Qiagen) as described in the manufacturer's instructions. The purified RNA was spectroscopically quantified using a NanoDrop ND-1000 spectrophotometer (NanoDrop Technologies). The PCR primers used for quantitative RT-PCR (qRT-PCR) were designed with Primer3 software (<http://simgene.com/Primer3>) and are listed in **Table 2**. Quantification of 16S rRNA copy numbers in the defined mixed culture

**Table 2 | Quantitative RT-PCR (qRT-PCR) primers designed and used in this study.**

Primer name	Sequence (5'-3')	Target
PT387f	GATAAGGGGACCTCGAGTGCT	<i>Methanosaeta thermophila</i>
PT573r	GGCCGGCTACAGACCT	<i>Methanosaeta thermophila</i>
PB486f	ACGGGACGAAGGGAGTGACGG	<i>Thermacetogenium phaeum</i>
PB646r	CTCCTCCCCTCAAGTCATCCAGT	<i>Thermacetogenium phaeum</i>
TM1139f	TTACCAGCGGAACCCTTATGG	<i>Methanothermobacter thermautotrophicus</i>
TM1275r	ACCTGGTTTAGGGGATTACCTCC	<i>Methanothermobacter thermautotrophicus</i>

were performed by one-step real-time RT-PCR using a Mx3000P QPCR System (Stratagene) and RNA-direct SYBR Green Realtime PCR Master Mix (Toyobo) as described previously (Kato et al., 2014). At least three biological replicates were subjected to qRT-PCR analysis, and at least two separate trials were conducted for each sample. Standard curves were generated with serially diluted PCR products ( $10^3$ – $10^8$  copies ml<sup>-1</sup>) amplified using the respective primer sets and were used to calculate the copy number of rRNA in the total RNA samples.

## RESULTS AND DISCUSSION

### EFFECTS OF CO<sub>2</sub> CONCENTRATIONS ON THE MODEL METHANOGENIC CONSORTIUM

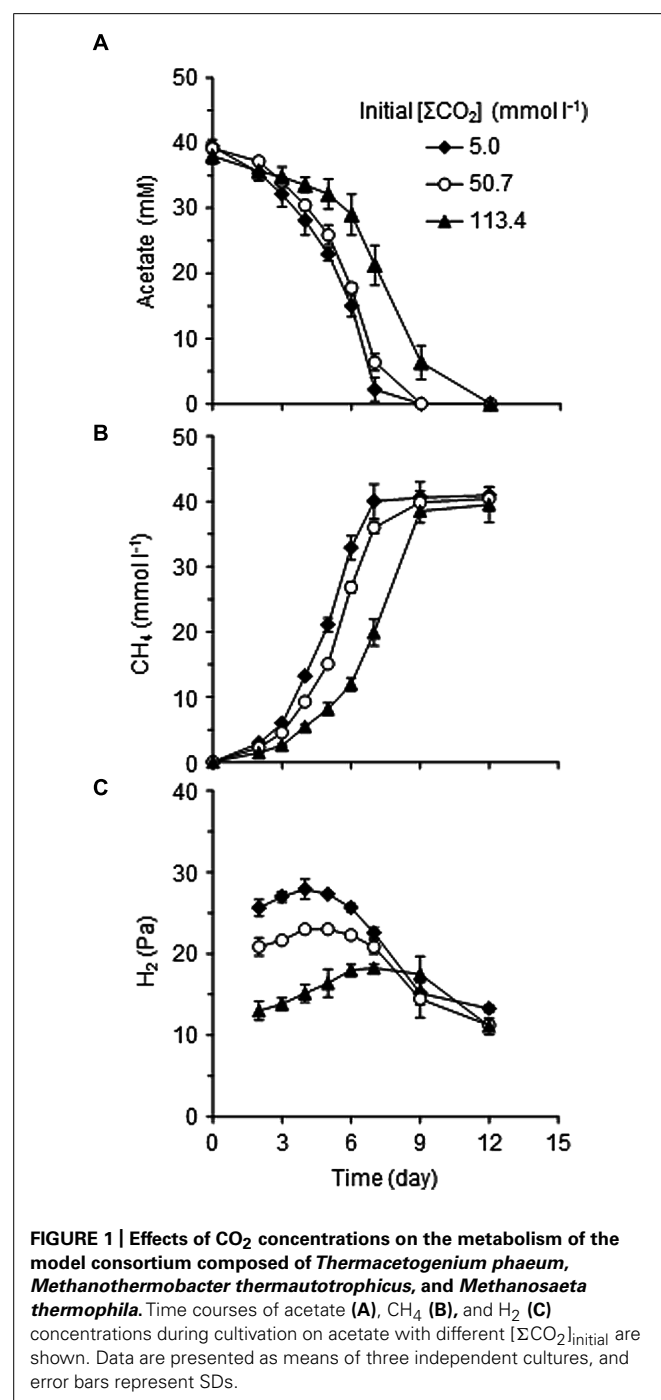
As the model consortium performing methanogenic acetate degradation, we utilized a defined mixed culture of an aceticlastic methanogen (*Methanosaeta thermophila*), a hydrogenotrophic methanogen (*Methanothermobacter thermautotrophicus*), and a SAOB (*T. phaeum*; **Table 3**). These microbial species were originally isolated from a thermophilic methanogenic digester (Kamagata and Mikami, 1991; Hattori et al., 2000) and are regarded as representative species for the methanogenic acetate degradation reactions that occur in various natural environments such as high-temperature petroleum reservoirs (Pham et al., 2009; Mayumi et al., 2011, 2013) and thermophilic methanogenic digesters (Sekiguchi et al., 1998; McHugh et al., 2003; Hori et al., 2011).

To adequately assess the effects of CO<sub>2</sub> concentration itself, media with different supplementation of CO<sub>2</sub>/HCO<sub>3</sub><sup>-</sup> were prepared (**Table 1**). The initial concentrations of total CO<sub>2</sub>/HCO<sub>3</sub><sup>-</sup> in the cultures, designated as [ΣCO<sub>2</sub>]<sub>initial</sub>, were 5.0, 50.7, or 113.4 mmol l<sup>-1</sup>. The model consortium composed of *Methanosaeta thermophila*, *Methanothermobacter thermautotrophicus*, and *T. phaeum* was cultivated under the three different [ΣCO<sub>2</sub>]<sub>initial</sub> conditions to evaluate their methanogenic acetate degradation abilities (**Figure 1**). A stoichiometric production of CH<sub>4</sub> from acetate in a 1:1 molar ratio was observed in all culture conditions tested. Both acetate consumption and CH<sub>4</sub> production rates slightly decreased with increasing the [ΣCO<sub>2</sub>]<sub>initial</sub> (**Figures 1A,B**). Interestingly, the partial pressure of H<sub>2</sub>, which is an important intermediate of syntrophic

**Table 3 | The metabolic reactions and the respective standard Gibbs free energy changes ( $\Delta G^\circ$ ) of the microorganisms utilized in this study.**

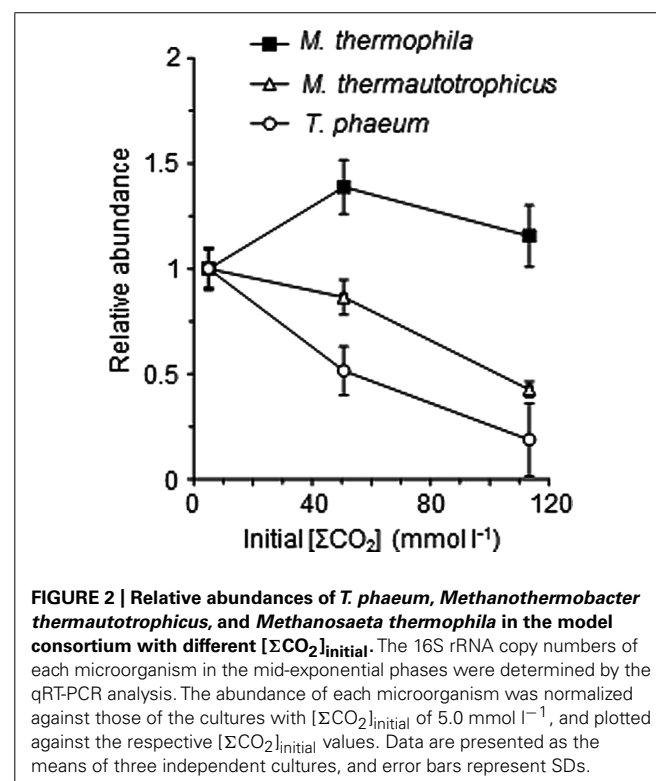
Microbial species	Metabolic reactions	$\Delta G^\circ$ (kJ mol <sup>-1</sup> ) <sup>a</sup>
<i>Methanosaeta thermophila</i>	$\text{CH}_3\text{COO}^- + \text{H}_2\text{O} \rightarrow \text{CH}_4 + \text{HCO}_3^-$	-31.0
<i>Thermacetogenium phaeum</i>	$\text{CH}_3\text{COO}^- + 4\text{H}_2\text{O} \rightarrow 2\text{HCO}_3^- + 4\text{H}_2 + \text{H}^+$	+104.6
<i>Methanothermobacter thermautotrophicus</i>	$4\text{H}_2 + \text{HCO}_3^- + \text{H}^+ \rightarrow \text{CH}_4 + 3\text{H}_2\text{O}$	-135.6

<sup>a</sup>The  $\Delta G^\circ$  values were calculated according to the reference (Thauer et al., 1977).



acetate degradation, significantly decreased with increasing the [ΣCO<sub>2</sub>]<sub>initial</sub> (Figure 1C). This observation suggests that syntrophic methanogenic microorganisms are influenced by elevated CO<sub>2</sub> concentrations.

To assess the influence of the elevated CO<sub>2</sub> concentrations on each methanogenic pathway, the relative abundances of each microorganism in the exponentially growing cultures of the model consortium with the different [ΣCO<sub>2</sub>]<sub>initial</sub> were evaluated by FISH and qRT-PCR analyses. The qRT-PCR analysis clearly demonstrated the decrease of the abundances of *Methanothermobacter thermautotrophicus* and *T. phaeum* in the higher [ΣCO<sub>2</sub>]<sub>initial</sub> cultures (Figure 2). The FISH analysis also demonstrated that the relative abundances of *Methanothermobacter thermautotrophicus* and *T. phaeum* in the cultures with higher CO<sub>2</sub> concentrations are significantly lower than those in the low CO<sub>2</sub> cultures (Figure 3). These results indicate that the syntrophic methanogenic pathway is more strongly influenced by the elevation of CO<sub>2</sub> concentrations compared to the aceticlastic pathway.



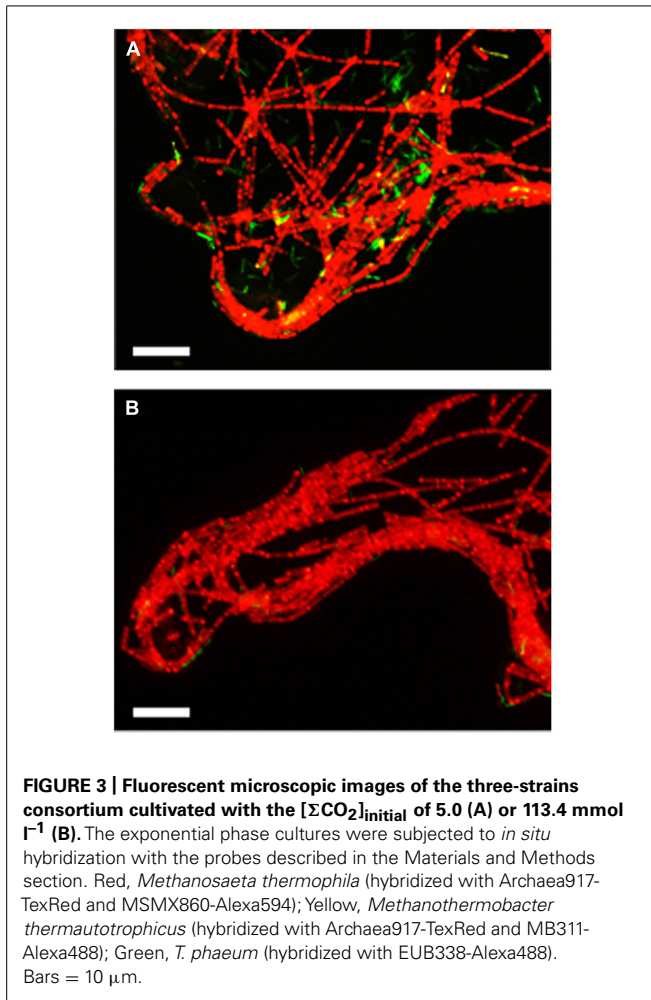


**FIGURE 3 |** Fluorescent microscopic images of the three-strains consortium cultivated with the  $[\Sigma\text{CO}_2]_{\text{initial}}$  of 5.0 (A) or 113.4  $\text{mmol l}^{-1}$  (B). The exponential phase cultures were subjected to *in situ* hybridization with the probes described in the Materials and Methods section. Red, *Methanosaeta thermophila* (hybridized with Archaea917-*TexRed* and MSMX860-Alexa594); Yellow, *Methanothermobacter thermautotrophicus* (hybridized with Archaea917-*TexRed* and MB311-Alexa488); Green, *T. phaeum* (hybridized with EUB338-Alexa488). Bars = 10  $\mu\text{m}$ .

### EFFECTS OF $\text{CO}_2$ CONCENTRATIONS ON THE ACETICLASTIC AND SYNTROPHIC PATHWAYS

To confirm the differences in the suppressive effects of elevated  $\text{CO}_2$  concentrations on the two methanogenic pathways, the pure culture of *Methanosaeta thermophila* and the defined co-culture of *Methanothermobacter thermautotrophicus* and *T. phaeum* were separately cultivated in the media with the different  $[\Sigma\text{CO}_2]_{\text{initial}}$  (Figure 4). The growth of *Methanosaeta thermophila* was barely affected by the elevated  $\text{CO}_2$  concentration: the methanogenic rate in the  $[\Sigma\text{CO}_2]_{\text{initial}}$  of 113.4  $\text{mmol l}^{-1}$  cultures decreased only about 10% compared to the cultures with  $[\Sigma\text{CO}_2]_{\text{initial}}$  of 5.0  $\text{mmol l}^{-1}$  (Figures 4A,C). On the contrary, the methanogenic rate of the syntrophic co-culture in the  $[\Sigma\text{CO}_2]_{\text{initial}}$  of 113.4  $\text{mmol l}^{-1}$  dropped to less than half of that in the cultures with  $[\Sigma\text{CO}_2]_{\text{initial}}$  of 5.0  $\text{mmol l}^{-1}$  (Figures 4B,C). These observations confirm the assumption that the syntrophic acetate degradation pathway is more susceptible to elevated  $\text{CO}_2$  concentrations than the aceticlastic pathway.

### EFFECTS OF $\text{CO}_2$ CONCENTRATIONS ON THE PURE CULTURES OF *Methanothermobacter thermautotrophicus* AND *T. phaeum*

One possible explanation for the suppressive effects of  $\text{CO}_2$  on the syntrophic methanogenesis is the susceptibility of

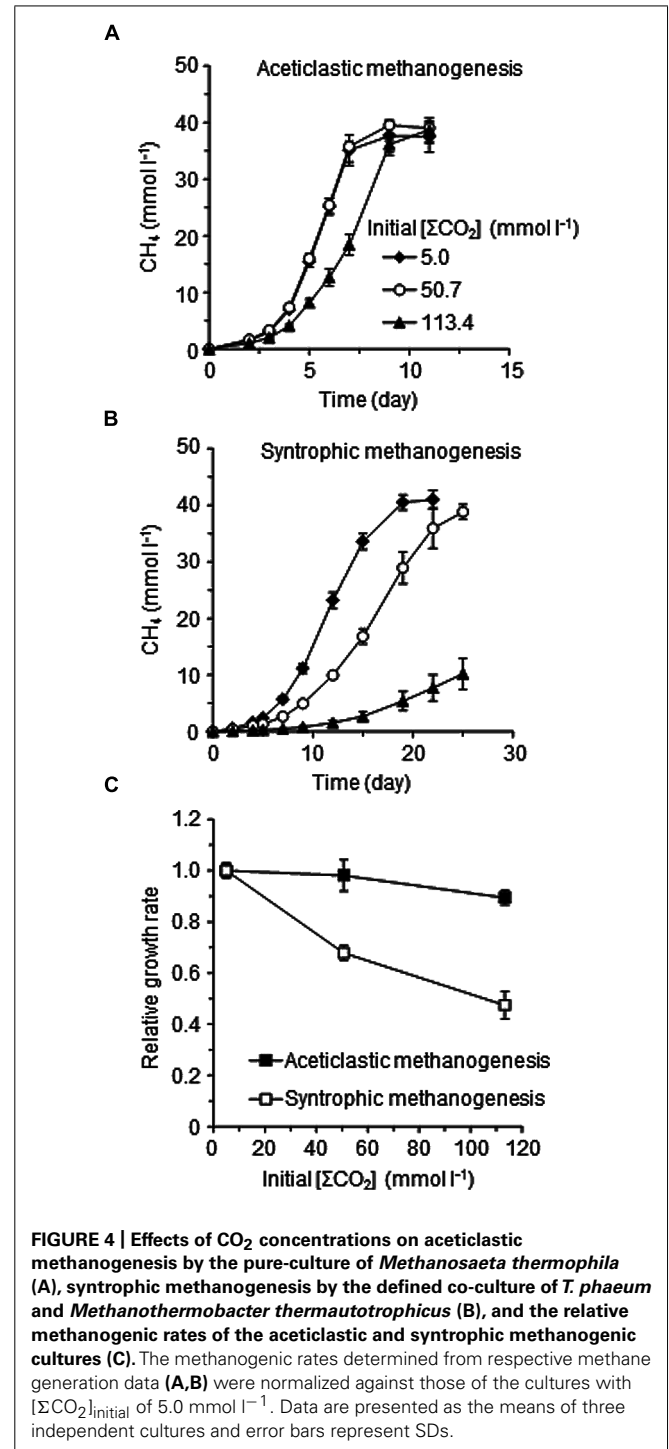


**FIGURE 4 |** Effects of  $\text{CO}_2$  concentrations on aceticlastic methanogenesis by the pure-culture of *Methanosaeta thermophila* (A), syntrophic methanogenesis by the defined co-culture of *T. phaeum* and *Methanothermobacter thermautotrophicus* (B), and the relative methanogenic rates of the aceticlastic and syntrophic methanogenesis cultures (C). The methanogenic rates determined from respective methane generation data (A,B) were normalized against those of the cultures with  $[\Sigma\text{CO}_2]_{\text{initial}}$  of 5.0  $\text{mmol l}^{-1}$ . Data are presented as the means of three independent cultures and error bars represent SDs.

*Methanothermobacter thermautotrophicus* and/or *T. phaeum* to some environmental alterations induced by increased  $\text{CO}_2$  or to  $\text{CO}_2$  itself. To evaluate this possibility, pure cultures of *Methanothermobacter thermautotrophicus* and *T. phaeum* were cultivated in media with different  $[\Sigma\text{CO}_2]_{\text{initial}}$  (Figure 5). No significant differences were observed for the growth of both *Methanothermobacter thermautotrophicus* and *T. phaeum* under the different  $\text{CO}_2$  conditions tested. These results suggest that elevated  $\text{CO}_2$

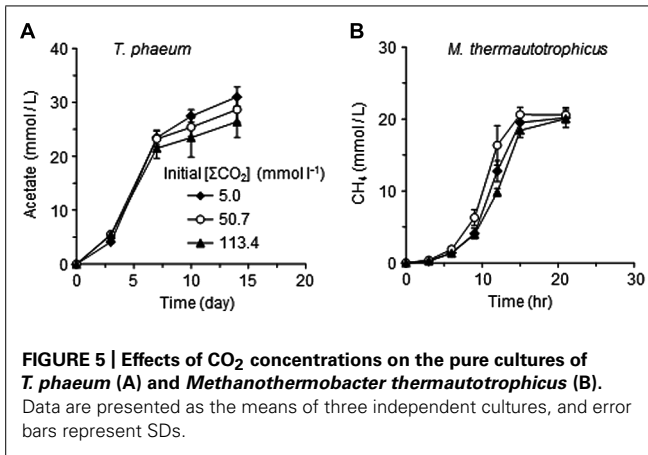


**FIGURE 5 | Effects of CO<sub>2</sub> concentrations on the pure cultures of *T. phaeum* (A) and *Methanothermobacter thermautotrophicus* (B).** Data are presented as the means of three independent cultures, and error bars represent SDs.

concentrations negatively affect the microbial activity only when *Methanothermobacter thermautotrophicus* and *T. phaeum* are in a syntrophic relationship.

#### EFFECTS OF CO<sub>2</sub> CONCENTRATIONS ON THE THERMODYNAMICS OF EACH REACTION

The other possible explanation for the suppression of syntrophic methanogenesis by elevated CO<sub>2</sub> concentration is alterations of thermodynamic conditions of each microbial reaction. A minimum energy required for biochemical energy conversion is estimated at around  $-20 \text{ kJ mol}^{-1}$  (Schink, 1997), while some anaerobic microorganisms have been reported to thrive under more thermodynamically restricted conditions (Jackson and McInerney, 2002; Nauhaus et al., 2002). The value was estimated from the energetics of ATP formation (around  $-70 \text{ kJ mol}^{-1}$  under the physiological conditions; Jetten et al., 1991; Tran and Uden, 1998) and the number of protons transported to ATP formation (between 3 and 4; Maloney, 1983; Stock et al., 1999). Since syntrophic methanogenesis from acetate

is one of the least exergonic microbial metabolisms (Schink, 1997), it is no wonder that only slight perturbations on the thermodynamics induce deteriorations of the syntrophic methanogenesis.

To evaluate the influences of elevated CO<sub>2</sub> concentrations on the thermodynamic properties,  $\Delta G$  values of metabolic reactions conducted by each microorganism in the model consortium were determined using the data-set of metabolite concentrations shown in Figure 1. The  $\Delta G$  values of the acetoclastic methanogenesis conducted by *Methanosaeta thermophila* were not significantly influenced by the elevated CO<sub>2</sub> concentrations (Figure 6). The average  $\Delta G$  values during the logarithmic growth phase (day 2–5) with the  $[\Sigma\text{CO}_2]_{\text{initial}}$  of 5.0, 50.7 and 113.4 mmol l<sup>-1</sup> were  $-47.7 \pm 3.5$ ,  $-44.9 \pm 2.6$ , and  $-44.6 \pm 2.0 \text{ kJ mol}^{-1}$ , respectively, which are substantially lower than the  $\Delta G$  value required for microbial energy acquisition.

The  $\Delta G$  values of the hydrogenotrophic methanogenesis catalyzed by *Methanothermobacter thermautotrophicus* were also largely not altered with different CO<sub>2</sub> settings and were constantly lower than  $-20 \text{ kJ mol}^{-1}$  (Figure 6). The average  $\Delta G$  values during the logarithmic growth phases with the  $[\Sigma\text{CO}_2]_{\text{initial}}$  of 5.0, 50.7, and 113.4 mmol l<sup>-1</sup> were  $-24.6 \pm 1.0$ ,  $-27.2 \pm 1.0$ , and  $-26.0 \pm 1.2 \text{ kJ mol}^{-1}$ , respectively. Since CO<sub>2</sub> is the substrate for hydrogenotrophic methanogenesis, lower  $\Delta G$  values under the higher CO<sub>2</sub> conditions are expected. However, the decrease in H<sub>2</sub> partial pressures under the higher CO<sub>2</sub> conditions (Figure 1C) compensates for the positive effects of increase in CO<sub>2</sub> concentration.

On the contrary, elevation of CO<sub>2</sub> concentrations significantly influenced the  $\Delta G$  values of the acetate oxidation reaction performed by *T. phaeum* (Figure 6). While the average  $\Delta G$  value during the logarithmic growth phases with the  $[\Sigma\text{CO}_2]_{\text{initial}}$  of 5.0 mmol l<sup>-1</sup> ( $-23.1 \pm 2.7 \text{ kJ mol}^{-1}$ ) was less than the borderline  $\Delta G$  value of  $-20 \text{ kJ mol}^{-1}$ , those with the  $[\Sigma\text{CO}_2]_{\text{initial}}$  of 50.7 and 113.4 mmol l<sup>-1</sup> ( $-17.8 \pm 1.3$  and  $-18.7 \pm 1.4 \text{ kJ mol}^{-1}$ )

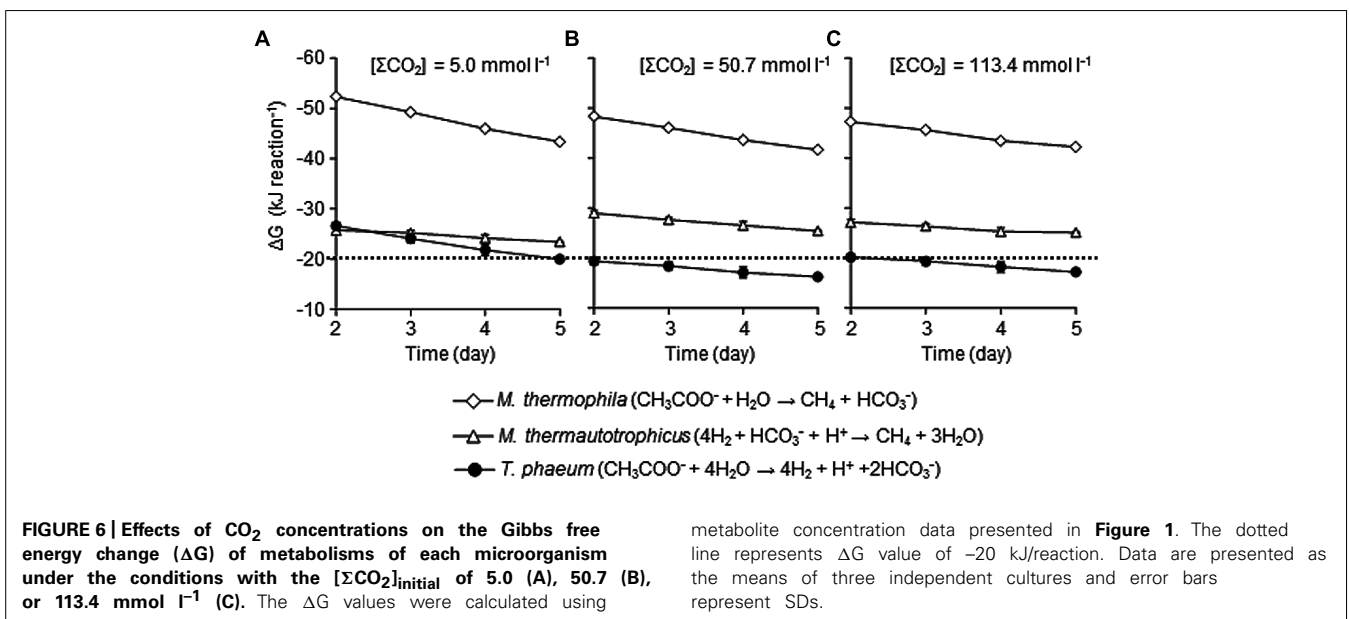


**FIGURE 6 | Effects of CO<sub>2</sub> concentrations on the Gibbs free energy change ( $\Delta G$ ) of metabolisms of each microorganism under the conditions with the  $[\Sigma\text{CO}_2]_{\text{initial}}$  of 5.0 (A), 50.7 (B), or 113.4 mmol l<sup>-1</sup> (C).** The  $\Delta G$  values were calculated using

metabolite concentration data presented in Figure 1. The dotted line represents  $\Delta G$  value of  $-20 \text{ kJ/reaction}$ . Data are presented as the means of three independent cultures and error bars represent SDs.

mol<sup>-1</sup>, respectively) exceeded the borderline. As acetate oxidation reaction produces 2 mol of CO<sub>2</sub> from 1 mol of acetate, it is rational that this reaction is strongly influenced by the elevation of CO<sub>2</sub> concentration. The decrease in the partial pressure of H<sub>2</sub>, the other metabolic product of acetate oxidation, is expected to compensate for the negative effects of increase in CO<sub>2</sub>. However, the decrease in H<sub>2</sub> partial pressure would be limited by the minimum threshold for H<sub>2</sub> consumption by *Methanothermobacter thermautotrophicus*. The minimum thresholds for H<sub>2</sub> utilization by hydrogenotrophic methanogens have been reported as around 5–10 Pa (Lovley, 1985; Thauer et al., 2008). However, considering the energy required for active growth, H<sub>2</sub> partial pressure of around 10–15 Pa observed in the increased CO<sub>2</sub> conditions in this study may be the minimum H<sub>2</sub> threshold for the syntrophic interaction. Actually, if the H<sub>2</sub> partial pressure in the cultures with [ΣCO<sub>2</sub>]<sub>initial</sub> of 113.4 mmol l<sup>-1</sup> at the logarithmic growth phase (day 5) becomes 10 Pa, the ΔG value becomes > -20 kJ mol<sup>-1</sup> (-19.7 ± 0.3 kJ mol<sup>-1</sup>) from the actual value of -25.1 ± 1.4 kJ mol<sup>-1</sup> (with H<sub>2</sub> partial pressure of 16.4 ± 1.7 Pa). These results clearly demonstrated that high concentrations of CO<sub>2</sub> thermodynamically constrain the acetate oxidizing reaction, which results in the deterioration of syntrophic methanogenesis from acetate.

## CONCLUSION

This is the first paper to evaluate the influence of elevated CO<sub>2</sub> concentration on the two different methanogenic acetate degradation pathways, namely aceticlastic and syntrophic pathways, using a model microbial consortium. As expected from the observations based on *in situ* environments with complex microbial communities, high concentrations of CO<sub>2</sub> suppressed the syntrophic pathway rather than the aceticlastic pathway. Thermodynamic calculations revealed that the acetate oxidation reaction is more intensely constrained by elevated CO<sub>2</sub> concentrations. This study exemplified the importance of even slight changes in the ΔG values of microbial metabolisms in anaerobic biota. Furthermore, this study demonstrated that the construction of model microbial consortia is useful for assessing competitive interspecies interactions even in anaerobic, methanogenic environments.

## AUTHOR CONTRIBUTIONS

Souichiro Kato, Tomoyuki Sato, and Yoichi Kamagata designed the research. Souichiro Kato, Rina Yoshida, Takashi Yamaguchi, Tomoyuki Sato, and Isao Yumoto carried out the experiments and analyzed the data. Souichiro Kato and Yoichi Kamagata wrote the manuscript.

## ACKNOWLEDGMENTS

This work was supported by grants from the Japan Society for the Promotion of Science (JSPS). We thank Dr. Mia Terashima and Hiromi Ikebuchi for helpful comments by critical reading and technical assistance, respectively.

## REFERENCES

Amann, R. I., Krumholz, L., and Stahl, D. A. (1990). Fluorescent-oligonucleotide probing of whole cells for determinative, phylogenetic, and environmental studies in microbiology. *J. Bacteriol.* 172, 762–770.

- Crocetti, G., Murto, M., and Björnsson, L. (2006). An update and optimization of oligonucleotide probes targeting methanogenic Archaea for use in fluorescence *in situ* hybridisation (FISH). *J. Microbiol. Methods* 65, 194–201. doi: 10.1016/j.mimet.2005.07.007
- Deng, H. (2012). A review of diversity-stability relationship of soil microbial community: what do we not know? *J. Environ. Sci.* 24, 1027–1035. doi: 10.1016/S1001-0742(11)60846-2
- De Roy, K., Marzorati, M., Van den Abbeele, P., Van de Wiele, T., and Boon, N. (2014). Synthetic microbial ecosystems: an exciting tool to understand and apply microbial communities. *Environ. Microbiol.* 16, 1472–1481. doi: 10.1111/1462-2920.12343
- Großkopf, T., and Soyer, O. S. (2014). Synthetic microbial communities. *Curr. Opin. Microbiol.* 18, 72–77. doi: 10.1016/j.mib.2014.02.002
- Hao, L., Lü, F., Li, L., Wu, Q., Shao, L., and He, P. (2013). Self-adaptation of methane-producing communities to pH disturbance at different acetate concentrations by shifting pathways and population interaction. *Bioresour. Technol.* 140, 319–327. doi: 10.1016/j.biortech.2013.04.113
- Haruta, S., Kato, S., Yamamoto, K., and Igarashi, Y. (2009). Intertwined interspecies relationships: approaches to untangle the microbial network. *Environ. Microbiol.* 11, 2963–2969. doi: 10.1111/j.1462-2920.2009.01956.x
- Haruta, S., Yoshida, T., Aoi, Y., Kaneko, K., and Futamata, H. (2013). Challenges for complex microbial ecosystems: combination of experimental approaches with mathematical modeling. *Microbes Environ.* 28, 285–294. doi: 10.1264/jsm.2013.03.034
- Hattori, S. (2008). Syntrophic acetate-oxidizing microbes in methanogenic environments. *Microbes Environ.* 23, 118–127. doi: 10.1264/jsm.2.23.118
- Hattori, S., Kamagata, Y., Hanada, S., and Shoun, H. (2000). *Thermacetogenium phaeum* gen. nov., sp. nov., a strictly anaerobic, thermophilic, syntrophic acetate-oxidizing bacterium. *Int. J. Syst. Evol. Microbiol.* 50, 1601–1609. doi: 10.1099/00207713-50-4-1601
- Hori, T., Sasaki, D., Haruta, S., Shigematsu, T., Ueno, Y., Ishii, M., et al. (2011). Detection of active, potentially acetate-oxidizing syntrophs in an anaerobic digester by flux measurement and formyltetrahydrofolate synthetase (FTHFS) expression profiling. *Microbiology* 157, 1980–1989. doi: 10.1099/mic.0.049189-0
- Jackson, B. E., and McInerney, M. J. (2002). Anaerobic microbial metabolism can proceed close to thermodynamic limits. *Nature* 415, 454–456. doi: 10.1038/415454a
- Jetten, M. S. M., Stams, A. J. M., and Zehnder, A. J. B. (1991). Adenine nucleotide content and energy charge of *Methanotheroxobacterium* during acetate degradation. *FEMS Microbiol. Lett.* 84, 313–318. doi: 10.1111/j.1574-6968.1991.tb04616.x
- Jetten, M. S. M., Stams, A. J. M., and Zehnder, A. J. B. (1992). Methanogenesis from acetate: a comparison of the acetate metabolism in *Methanotheroxobacterium* and *Methanosarcina* spp. *FEMS Microbiol. Lett.* 88, 181–197. doi: 10.1111/j.1574-6968.1992.tb04987.x
- Jones, D. M., Head, I. M., Gray, N. D., Adams, J. J., Rowan, A. K., Aitken, C. M., et al. (2008). Crude-oil biodegradation via methanogenesis in subsurface petroleum reservoirs. *Nature* 451, 176–180. doi: 10.1038/nature06484
- Kamagata, Y., and Mikami, E. (1991). Isolation and characterization of a novel thermophilic *Methanosarcina* strain. *Int. J. Syst. Bacteriol.* 41, 191–196. doi: 10.1099/00207713-41-2-191
- Karakashev, D., Batstone, D. J., Trably, E., and Angelidaki, I. (2006). Acetate oxidation is the dominant methanogenic pathway from acetate in the absence of Methanosarcinaceae. *Appl. Environ. Microbiol.* 72, 5138–5141. doi: 10.1128/AEM.00489-06
- Kato, S., Haruta, S., Cui, Z. J., Ishii, M., and Igarashi, Y. (2005). Stable coexistence of five bacterial strains as a cellulose-degrading community. *Appl. Environ. Microbiol.* 71, 7099–7106. doi: 10.1128/AEM.71.11.7099-7106.2005
- Kato, S., Haruta, S., Cui, Z. J., Ishii, M., and Igarashi, Y. (2008). Network relationships of bacteria in a stable mixed culture. *Microb. Ecol.* 56, 403–411. doi: 10.1007/s00248-007-9357-4
- Kato, S., Sasaki, K., Watanabe, K., Yumoto, I., and Kamagata, Y. (2014). Physiological and transcriptomic analyses of a thermophilic, aceticlastic methanogen *Methanosarcina thermophila* responding to ammonia stress. *Microbes Environ.* 29, 162–167. doi: 10.1264/jsm.2014.02.021
- Kato, S., and Watanabe, K. (2010). Ecological and evolutionary interactions in syntrophic methanogenic consortia. *Microbes Environ.* 25, 145–151. doi: 10.1264/jsm.2010.02.021

- Kerr, B., Riley, M. A., Feldman, M. W., and Bohannon, B. J. (2002). Local dispersal promotes biodiversity in a real-life game of rock-paper-scissors. *Nature* 418, 171–174. doi: 10.1038/nature00823
- Loreau, M., Naeem, S., Inchausti, P., Bengtsson, J., Grime, J. P., Hector, A., et al. (2001). Biodiversity and ecosystem functioning: current knowledge and future challenges. *Science* 294, 804–808. doi: 10.1126/science.1064088
- Lovley, D. R. (1985). Minimum threshold for hydrogen metabolism in methanogenic bacteria. *Appl. Environ. Microbiol.* 49, 1530–1531.
- Loy, A., Lehner, A., Lee, N., Adamczyk, J., Meier, H., Ernst, J., et al. (2002). Oligonucleotide microarray for 16S rRNA gene-based detection of all recognized lineages of sulfate-reducing prokaryotes in the environment. *Appl. Environ. Microbiol.* 68, 5064–5081. doi: 10.1128/AEM.68.10.5064-5081.2002
- Maloney, P. (1983). Relationship between phosphorylation potential and electrochemical H<sup>+</sup> gradient during glycolysis in *Streptococcus lactis*. *J. Bacteriol.* 153, 1461–1470.
- Mayumi, D., Dolfing, J., Sakata, S., Maeda, H., Miyagawa, Y., Ikarashi, M., et al. (2013). Carbon dioxide concentration dictates alternative methanogenic pathways in oil reservoirs. *Nat. Commun.* 13:1998. doi: 10.1038/ncomms2998
- Mayumi, D., Mochimaru, H., Yoshioka, H., Sakata, S., Maeda, H., Miyagawa, Y., et al. (2011). Evidence for syntrophic acetate oxidation coupled to hydrogenotrophic methanogenesis in the high-temperature petroleum reservoir of Yabase oil field (Japan). *Environ. Microbiol.* 13, 1995–2006. doi: 10.1111/j.1462-2920.2010.02338.x
- McHugh, S., Carton, M., Mahony, T., and O'Flaherty, V. (2003). Methanogenic population structure in a variety of anaerobic bioreactors. *FEMS Microbiol. Lett.* 219, 297–304. doi: 10.1016/S0378-1097(03)00055-7
- Nahum, J. R., Harding, B. N., and Kerr, B. (2011). Evolution of restraint in a structured rock-paper-scissors community. *Proc. Natl. Acad. Sci. U.S.A.* 108, 10831–10838. doi: 10.1073/pnas.1100296108
- Nauhaus, K., Boetius, A., Krüger, M., and Widdel, F. (2002). In vitro demonstration of anaerobic oxidation of methane coupled to sulphate reduction in sediment from a marine gas hydrate area. *Environ. Microbiol.* 4, 296–305. doi: 10.1046/j.1462-2920.2002.00299.x
- Nüsslein, B., Chin, K. J., Eckert, W., and Conrad, R. (2001). Evidence for anaerobic syntrophic acetate oxidation during methane production in the profundal sediment of subtropical Lake Kinneret (Israel). *Environ. Microbiol.* 3, 460–470. doi: 10.1046/j.1462-2920.2001.00215.x
- Pham, V. D., Hnatow, L. L., Zhang, S., Fallon, R. D., Jackson, S. C., Tomb, J. F., et al. (2009). Characterizing microbial diversity in production water from an Alaskan mesothermic petroleum reservoir with two independent molecular methods. *Environ. Microbiol.* 11, 176–187. doi: 10.1111/j.1462-2920.2008.01751.x
- Raskin, L., Poulsen, L. K., Noguera, D. R., Rittmann, B. E., and Stahl, D. A. (1994). Quantification of methanogenic groups in anaerobic biological reactors by oligonucleotide probe hybridization. *Appl. Environ. Microbiol.* 60, 1241–1248.
- Schink, B. (1997). Energetics of syntrophic cooperation in methanogenic degradation. *Microbiol. Mol. Biol. Rev.* 61, 262–280.
- Sekiguchi, Y., Kamagata, Y., Syutsubo, K., Ohashi, A., Harada, H., and Nakamura, K. (1998). Phylogenetic diversity of mesophilic and thermophilic granular sludges determined by 16S rRNA gene analysis. *Microbiology* 144, 2655–2665. doi: 10.1099/00221287-144-9-2655
- Shigematsu, T., Tang, Y., Kobayashi, T., Kawaguchi, H., Morimura, S., and Kida, K. (2004). Effect of dilution rate on metabolic pathway shift between acetate and nonacetate methanogenesis in chemostat cultivation. *Appl. Environ. Microbiol.* 70, 4048–4052. doi: 10.1128/AEM.70.7.4048-4052.2004
- Stock, D., Leslie, A. G. W., and Walker, J. E. (1999). Molecular architecture of the rotary motor in ATP synthase. *Science* 286, 1700–1705. doi: 10.1126/science.286.5445.1700
- Thauer, R. K., Jungermann, K., and Decker, K. (1977). Energy conservation in chemotrophic anaerobic bacteria. *Bacteriol. Rev.* 41, 100–180.
- Thauer, R. K., Kaster, A. K., Seedorf, H., Buckel, W., and Hedderich, R. (2008). Methanogenic archaea: ecologically relevant differences in energy conservation. *Nat. Rev. Microbiol.* 6, 579–591. doi: 10.1038/nrmicro1931
- Tran, Q. H., and Uden, G. (1998). Changes in the proton potential and the cellular energetics of *Escherichia coli* during growth by aerobic and anaerobic respiration or by fermentation. *Eur. J. Biochem.* 251, 538–543. doi: 10.1046/j.1432-1327.1998.2510538.x
- Zinder, S. H., and Koch, M. (1984). Non-acetate methanogenesis from acetate: acetate oxidation by a thermophilic syntrophic coculture. *Arch. Microbiol.* 138, 263–272. doi: 10.1007/BF00402133

**Conflict of Interest Statement:** The authors declare that the research was conducted in the absence of any commercial or financial relationships that could be construed as a potential conflict of interest.

Received: 28 August 2014; accepted: 13 October 2014; published online: 30 October 2014.

Citation: Kato S, Yoshida R, Yamaguchi T, Sato T, Yumoto I and Kamagata Y (2014) The effects of elevated CO<sub>2</sub> concentration on competitive interaction between acetate and syntrophic methanogenesis in a model microbial consortium. *Front. Microbiol.* 5:575. doi: 10.3389/fmicb.2014.00575

This article was submitted to *Systems Microbiology*, a section of the journal *Frontiers in Microbiology*.

Copyright © 2014 Kato, Yoshida, Yamaguchi, Sato, Yumoto and Kamagata. This is an open-access article distributed under the terms of the Creative Commons Attribution License (CC BY). The use, distribution or reproduction in other forums is permitted, provided the original author(s) or licensor are credited and that the original publication in this journal is cited, in accordance with accepted academic practice. No use, distribution or reproduction is permitted which does not comply with these terms.



# Recombination Does Not Hinder Formation or Detection of Ecological Species of *Synechococcus* Inhabiting a Hot Spring Cyanobacterial Mat

Melanie C. Melendrez<sup>1\*</sup>, Eric D. Becraft<sup>1</sup>, Jason M. Wood<sup>1</sup>, Millie T. Olsen<sup>1</sup>, Donald A. Bryant<sup>2</sup>, John F. Heidelberg<sup>3</sup>, Douglas B. Rusch<sup>4</sup>, Frederick M. Cohan<sup>5</sup> and David M. Ward<sup>1</sup>

<sup>1</sup> Department of Land Resources and Environmental Science, Montana State University, Bozeman, MT, USA, <sup>2</sup> Department of Biochemistry and Molecular Biology, Pennsylvania State University, University Park, PA, USA, <sup>3</sup> Department of Biological Sciences, College of Letters, Arts and Sciences, University of Southern California, Los Angeles, CA, USA, <sup>4</sup> Informatics Group, J. Craig Venter Institute, Rockville, MD, USA, <sup>5</sup> Department of Biology, Wesleyan University, Middletown, CT, USA

## OPEN ACCESS

### Edited by:

Hiroyuki Futamata,  
Shizuoka University, Japan

### Reviewed by:

Kim Marie Handley,  
University of Chicago, USA  
Michael Kevin Watters,  
Valparaiso University, USA

### \*Correspondence:

Melanie C. Melendrez  
mmelendrez@gmail.com

### Specialty section:

This article was submitted to  
Systems Microbiology,  
a section of the journal  
Frontiers in Microbiology

**Received:** 31 August 2015

**Accepted:** 21 December 2015

**Published:** 14 January 2016

### Citation:

Melendrez MC, Becraft ED, Wood JM, Olsen MT, Bryant DA, Heidelberg JF, Rusch DB, Cohan FM and Ward DM (2016) Recombination Does Not Hinder Formation or Detection of Ecological Species of *Synechococcus* Inhabiting a Hot Spring Cyanobacterial Mat. *Front. Microbiol.* 6:1540. doi: 10.3389/fmicb.2015.01540

Recent studies of bacterial speciation have claimed to support the biological species concept—that reduced recombination is required for bacterial populations to diverge into species. This conclusion has been reached from the discovery that ecologically distinct clades show lower rates of recombination than that which occurs among closest relatives. However, these previous studies did not attempt to determine whether the more-rapidly recombining close relatives within the clades studied may also have diversified ecologically, without benefit of sexual isolation. Here we have measured the impact of recombination on ecological diversification within and between two ecologically distinct clades (A and B') of *Synechococcus* in a hot spring microbial mat in Yellowstone National Park, using a cultivation-free, multi-locus approach. Bacterial artificial chromosome (BAC) libraries were constructed from mat samples collected at 60°C and 65°C. Analysis of multiple linked loci near *Synechococcus* 16S rRNA genes showed little evidence of recombination between the A and B' lineages, but a record of recombination was apparent within each lineage. Recombination and mutation rates within each lineage were of similar magnitude, but recombination had a somewhat greater impact on sequence diversity than mutation, as also seen in many other bacteria and archaea. Despite recombination within the A and B' lineages, there was evidence of ecological diversification within each lineage. The algorithm Ecotype Simulation identified sequence clusters consistent with ecologically distinct populations (ecotypes), and several hypothesized ecotypes were distinct in their habitat associations and in their adaptations to different microenvironments. We conclude that sexual isolation is more likely to follow ecological divergence than to precede it. Thus, an ecology-based model of speciation appears more appropriate than the biological species concept for bacterial and archaeal diversification.

**Keywords:** population genetics, speciation, *Synechococcus*, cyanobacteria, multi-locus sequence typing, Ecotype Simulation, ecotype, recombination

## INTRODUCTION

For much of the last century, theories of the origin of species have revolved around genetic exchange (Mayr, 1942, 1963; Dobzhansky, 1951; Coyne and Orr, 2004). In highly sexual organisms such as animals and plants, genetic exchange is frequently seen as a cohesive force holding together the individuals within a species population, thus preventing divergence into irreversibly separate lineages (Cohan, 2013). The role of genetic exchange in bacteria and archaea, where recombination is not connected to reproduction (Levin and Bergstrom, 2000), has been vigorously debated. Recombination has been viewed by some as a rampant process that can erode the distinctness of nascent species (Doolittle and Zhaxybayeva, 2009); moreover, recombination is seen as a cohesive force binding a species together, as in the case of sexual species. Speciation theories based on Mayr's Biological Species Concept see the breaking of recombination between populations as a critical step in population divergence; in this view, populations can diverge ecologically and irreversibly only after their genetic exchange is blocked (Coyne and Orr, 2004).

On the other hand, theories of ecological speciation hold that ecological divergence is the critical step in the origin of diversity, and that recombination plays only a minor role in the subsequent fate of newly split, ecologically distinct populations (Van Valen, 1976; Mallet, 2008; Schluter, 2009). According to a theory developed long ago by Haldane, rare introduction of genes from one population to another cannot reverse the adaptive divergence between populations (Haldane, 1932). This is because natural selection against niche-specifying genes from other populations can limit these foreign genes to negligible frequencies, especially if the rate of recombination between populations is very low. The equilibrium frequency of a recombinant niche-specifying gene is equal to the rate of recombination between populations ( $c_b$ ) divided by the intensity of selection ( $s$ ) against the gene (Mallet, 2008; Wiedenbeck and Cohan, 2011). The equilibrium frequency of recombinant genes is thus extremely low, as recombination rates are not known to exceed the mutation rate by more than a factor of 10 (Vos and Didelot, 2009), and mutation rates are known to be very low in nearly all bacteria and archaea studied (about  $10^{-6}$  per gene per generation; Drake, 2009). It can therefore be inferred that recombination rates are much too low to reverse adaptive divergence of microbial populations, and that recombination is unlikely to prevent ecological divergence among the most closely related bacteria and archaea (Wiedenbeck and Cohan, 2011).

The conflict between recombination-based and ecology-based theories of speciation has motivated several recent studies on the role of recombination in the evolution of bacterial and archaeal species. In a study of coexisting strains of *Sulfolobus islandicus* isolated from the same hot spring, Cadillo-Quiroz and colleagues found depressed rates of recombination between two major clades formed by these organisms compared to recombination within either clade (Cadillo-Quiroz et al., 2012). Inter-clade recombination was taken to be insufficient to prevent the divergence of the clades into easily distinguishable clusters, and the authors claimed this as support for the Biological

Species Concept in archaeal speciation. Ellegaard et al. came to a similar conclusion based on comparison of genomes derived from closely related *Wolbachia* strains (97–98% 16S rRNA identity) isolated from the same host fly (Ellegaard et al., 2013). Shapiro et al. obtained similar results for closely related clades of marine *Vibrio cyclitrophicus* strains that may be ecologically distinct, based on their isolation from particles of different sizes (Shapiro et al., 2012). They proposed a model in which ecological specialization, based on horizontal genetic transfer, leads to occupancy of different habitats; this causes a decrease in recombination between the ecologically distinct populations, allowing the ecological populations to further diverge (Shapiro et al., 2012; see also Retchless and Lawrence, 2010; Polz et al., 2013). In all these studies the reduced recombination between the clades under investigation was taken as evidence that recombination must be lowered to allow irreversible divergence among close relatives into stably coexisting, ecologically distinct populations. However, these studies did not address whether ecological divergence may have also occurred *within* each clade, where recombination rates are higher.

Here we test whether ecological divergence can occur among organisms so closely related that recombination between them is not reduced. Our model system is the set of unicellular cyanobacteria (*Synechococcus*) inhabiting the microbial mats of Mushroom Spring, Yellowstone National Park. This hypothesis emerged from a series of studies based on variation found in single genetic loci (Ferris and Ward, 1997; Ramsing et al., 2000; Ferris et al., 2003; Melendrez et al., 2011). First, closely related 16S rRNA genotypes were distributed differently along the effluent channel (genotypes A, A', A, B, and B along a temperature gradient from  $\sim 72$ – $74^\circ\text{C}$  to  $\sim 50^\circ\text{C}$  Ferris and Ward, 1997) and with depth in the photic zone (Ramsing et al., 2000), suggesting differential adaptations to temperature and light that were later confirmed by studying isolates with genotypes representative of *in situ* populations (Allewalt et al., 2006). Second, analyses based on the internal transcribed spacer separating 16S and 23S rRNA genes revealed that 16S rRNA sequence variation was insufficient to detect all ecologically distinct populations (Ferris et al., 2003; Ward et al., 2006), limiting the utility of 16S rRNA-based methods for detecting closely related ecotypes (e.g., Eren et al., 2013). Third, analyses of several more rapidly evolving protein-encoding genes revealed numerous closely related and ecologically distinct populations, the number of which depended on the depth of coverage and on the degree of sequence divergence of the gene used (Becraft et al., 2011; Melendrez et al., 2011). It is clearly important to appreciate that the amount of molecular divergence between these closely related species is very small (see Discussion).

Our aim in these studies has been to discover the fundamental “ecotypes” within the A and B' clades (originally demarcated as 16S rRNA clusters), where we define an *ecotype* as a group of organisms that is ecologically distinct from other ecotypes and whose members are ecologically interchangeable (Kopac and Cohan, 2011). More specifically, different ecotypes are expected to coexist indefinitely owing to their ecological distinctness, while lineages within an ecotype are too similar to be able to coexist indefinitely (Kopac et al., 2014). In our recent work

we hypothesized the demarcations of putative ecotypes (PEs) from sequence clusters using a theory-based algorithm (Ecotype Simulation, based on the Stable Ecotype Model of species and speciation, Kopac et al., 2014; Cohan, 2016), which simulates the evolutionary dynamics of ecotype formation and the forces that purge sequence diversity within ecotypes (Koeppel et al., 2008). Unlike other studies that have used traditional or intuitive sequence cutoffs to define sequence clusters of interest (e.g., “main cloud” roughly equivalent to 3% 16S rRNA cutoff, see Rosen et al., 2015), we have used this dynamic approach to let the natural variation, itself, reveal the clusters that most likely fit the dynamic properties of species, given the resolution allowed by the sequence data. In recent pyrosequencing analyses of a gene encoding an essential photosynthesis protein (PsaA), Ecotype Simulation demarcated 18 B'-like, 14 A-like, and 5 A'-like *Synechococcus* PEs (Becraft et al., 2015). Importantly, these analyses demonstrated the ecological distinctness of the PEs: (i) the most abundant PEs had unique environmental distributions, (ii) the PEs showed unique gene expression patterns, (iii) cultivated strains with identical 16S rRNA sequences (see Nowack et al., 2015) from PEs with different depth distributions showed different light adaptations and acclimation responses (Nowack et al., 2015), and (iv) comparative genomic analyses of these strains are beginning to reveal the genetic mechanisms underlying these adaptations (Olsen et al., 2015). Moreover, the membership within PEs was shown to be ecologically interchangeable: (v) individuals predicted to belong to the same PE were distributed similarly along ecological gradients and (vi) the membership within a PE showed coordinated responses to environmental change (Becraft et al., 2015; Olsen et al., 2015).

Recently, Rosen et al. (2015) presented a view of the same Mushroom Spring *Synechococcus* populations that suggests recombination prevents the formation of such PEs. These authors pyrosequenced numerous PCR-amplified genes to study the genetic diversity within the A and B' lineages of the present model system (that is, the A and B' lineages of *Synechococcus* in Mushroom Spring) Although, Rosen et al. described their study as a multi-locus sequence analysis, any given organism was sampled for only one locus (i.e., multiple loci were unlinked in these analyses). Rosen et al. (2015) inferred from patterning of single-nucleotide polymorphisms (SNPs) in individual amplicons that recombination and mutation occur at similar rates within the sampled population. Viewing recombination to be “ubiquitous” and, based on comparison of neutral drift and sexual recombination models, they inferred that their “results were inconsistent with the presence of multiple ecotypes” within the A and B' lineages and conjectured that the A and B' lineages of *Synechococcus* were each behaving “as effectively [a] quasisexual species... occupying a broad environmental niche.” However, as noted above we previously showed these lineages to each contain multiple, ecologically distinct populations (Becraft et al., 2015; Nowack et al., 2015; Olsen et al., 2015). Clearly, these *Synechococcus* populations provide a test case for understanding the roles of recombination and ecological specialization in speciation within these lineages. Here we will demonstrate in a true multilocus analysis that each

lineage has diversified into ecologically distinct populations in spite of recombination between populations.

Single-locus analyses may suffer from the effects of recombination, such that the evolutionary history of the gene may deviate from that of the organisms (Feil et al., 2001, 2004). Thus, we developed a novel multi-locus sequence analysis (MLSA) approach for cultivation-free sampling and analysis of population structure. MLSA provides a buffer against the effects of recombination in any single gene, increases molecular resolution, and allows detection of recombination events that involve both whole genes and parts of genes because the genes investigated are known to be linked on the same genome. MLSA was developed for population genetics studies of cultivated pathogenic isolates (Maiden et al., 1998; Feil et al., 2000a; Salerno et al., 2007; Vitorino et al., 2008; Cesarini et al., 2009) and has also been applied to nonpathogenic isolates (Papke et al., 2004, 2007; Whitaker et al., 2005; Koeppel et al., 2008; Mazard et al., 2012). Furthermore, the development of methods that permit access to large segments of genomes has extended its application to uncultivated organisms (Kashtan et al., 2014). Our cultivation-independent MLSA approach was based on the use of bacterial artificial chromosome (BAC) libraries (Shizuya et al., 1992; Tao et al., 2002; Liles et al., 2008) to sample multiple genes from individual genomes of *Synechococcus* inhabiting the microbial mat of Mushroom Spring.

BACs were derived from libraries constructed from DNA that was extracted from samples collected at either a 60°C site or a 65°C site. Consequently, like the other studies mentioned above, our focus populations have diverged into two major lineages (i.e., the A and B' lineages of *Synechococcus*, defined by 16S rRNA sequence variants A and B', see above) inferred to rarely recombine between lineages and known to be ecologically distinct (Ward et al., 1998, 2006; Klatt et al., 2011). BACs were screened to identify clones containing a *Synechococcus* A/B lineage-specific 16S rRNA region. Multiple loci were selected and PCR-amplified from these BAC clones and the sequence data obtained were analyzed using Ecotype Simulation of both concatenated MLSA and single-gene phylogenies, and alternatively, using eBURST analysis, which has routinely been used in MLSA studies to demarcate variants into clusters (see Methods; Feil et al., 2004).

Ecotype Simulation and eBURST use very different approaches to infer populations from sequence variation. Ecotype Simulation is a theory-based algorithm demarcating clades that are consistent with the dynamics of ecotype formation and purging of diversity within ecotypes; eBURST clusters variants on the basis of a pre-determined cutoff—that members of a cluster must be identical at all or all but one of the loci studied; however, concatenated MLSA sequences have been used in phylogenetic analyses (independent from eBURST analyses) to assist in demarcating species clusters (Maiden et al., 1998; Hanage et al., 2005). In previous analyses of this type, suspected recombinant sequences have simply been removed from Ecotype Simulation analyses, on the assumption that these recombinant sequences do not reflect the history of the organism at the locus undergoing recombination and, if not removed, might lead to overestimation of PEs (Koeppel et al., 2008). In this

study, however, we address the ability of Ecotype Simulation to predict PEs when recombined sequences are included.

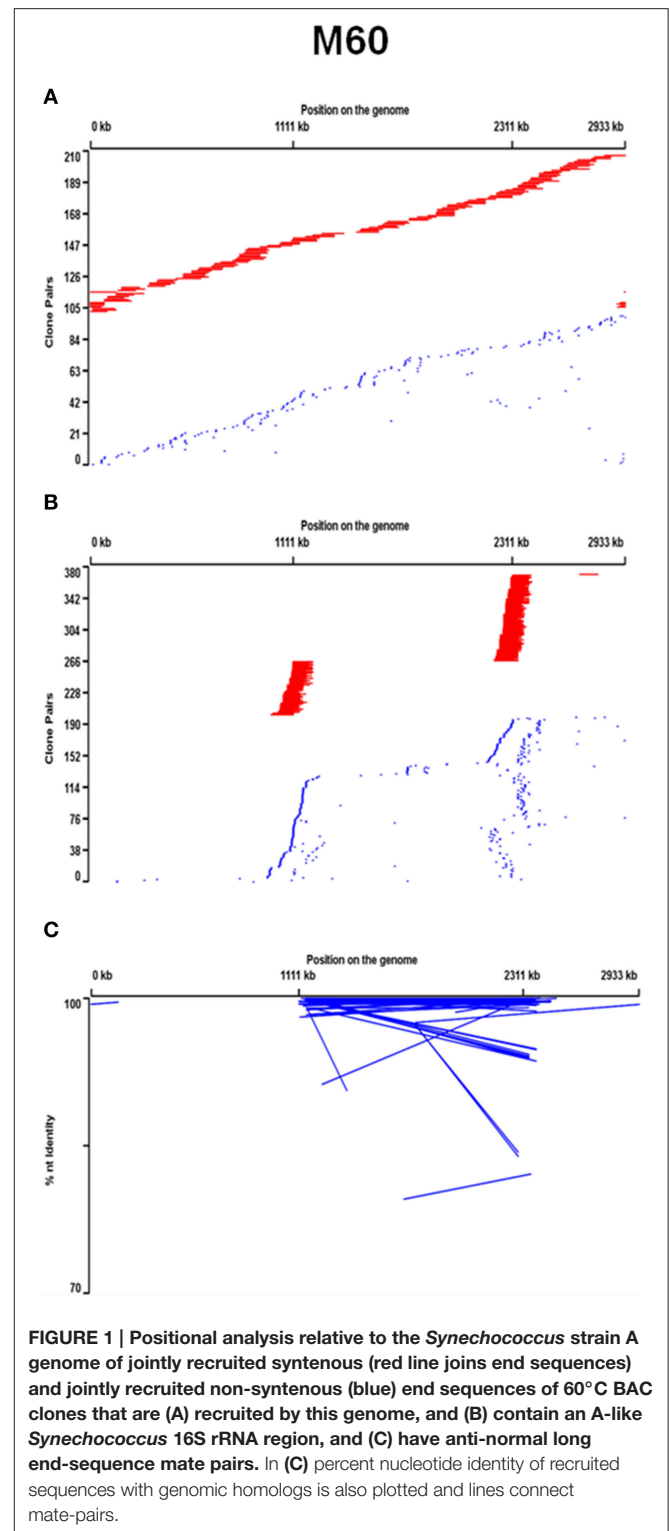
The extent of recombination was assessed in single-gene and concatenated MLSA alignments using programs designed to detect recombination events and phylogenetic incongruity (also assessed by visual comparisons), and by SNP pattern analyses. The ecological distinctness of PEs, predicted either by MLSA or single-locus analysis, was determined through association with the temperature (60° or 65°) from which the BACs were obtained. We also tested for finer-scale habitat associations by tracking the distributions of genetic variants of an MLSA locus using pyrosequencing of DNA from samples collected over a range of vertical microenvironments in the 63–65°C mat (Becraft et al., 2015). In some cases genomic sequences were available for isolates representative of PEs demarcated in MLSA analyses (Olsen et al., 2015). This permitted comparison of distribution of the MLSA locus with *psaA* distributions that had previously been determined on the same samples (Becraft et al., 2011).

We will demonstrate not only that recombination has occurred more frequently within than between the A and B' lineages, but that it has neither prevented ecological diversification within each of these lineages nor our ability to detect ecotypes. We suggest that an ecology-based model of speciation is more appropriate than the biological species concept for bacterial speciation in hot spring *Synechococcus*, and possibly many other bacteria and archaea in diverse environments.

## RESULTS

### BAC Clone Libraries

Metagenomic libraries constructed from the 60° and 65° mat samples from the Mushroom Spring effluent channel contained 304,128 and 64,512 BAC clones with average insert sizes of 90 and 120 kb, respectively (see Supplemental Data Sheet Section I). BLAST analyses of paired-end sequences of 9216 randomly selected clones from each BAC library showed that the BAC libraries contained the same predominant taxonomic composition as small-insert metagenomes previously produced from the same DNA (Klatt et al., 2011; also see Supplemental Data Sheet Section II, Supplemental Data Tables 3, 4, and Supplemental Data Presentation Figure 2). While the BACs yielded poorer recovery of *Synechococcus* genes than the small-insert metagenomes, they provided broad coverage of *Synechococcus* strain JA-3-3Ab [accession: CP000239.1] and JA-2-3B'a(2-13) [accession: CP000240.1] reference genomes, which are representative of A-like and B'-like *Synechococcus* 16S rRNA lineages (Bhaya et al., 2007; **Figure 1A**, Supplemental Data Presentation Figure 3). BAC clones containing a *Synechococcus* strain A-like or B'-like 16S rRNA sequence were identified by oligonucleotide probe screening and sequence analysis (Supplemental Data Sheet Section I). Mapping the distribution of the paired-end sequences of each BAC clone relative to reference genomes suggested nearly equal and random coverage of the two unlinked 16S rRNA loci of these genomes (**Figure 1B**, Supplemental Data Presentation Figure



3). Interestingly, many *Synechococcus* A-like or B'-like BACs containing a 16S rRNA sequence were non-syntenous when compared with the respective genome sequence. Syntenous sequences are considered here to be those whose mate pairs were of the same orientation as the reference genome and were

separated by a distance that was similar to the size of the DNA fragments used to construct the metagenomic library. Non-syntenous sequences are considered here to be those whose mate pairs deviated from the insert length and/or orientation of the reference genome (See Supplemental Data Sheet Section II and reference, Klatt et al., 2011). Such cases were revealed by the paired-end sequences of the same clone matching regions near both 16S rRNA loci, as opposed to one. The percentage of normal- and anti-normal long orientations of paired-end sequences in these non-syntenous clones was greater than in randomly sampled BACs (Figure 1C, Supplemental Data Sheet Section II, Supplemental Data Table 5, and Supplemental Data Presentation Figure 3). This suggested that non-syntenous BACs may have been associated with genomic inversions (Rusch et al., 2007).

## MLSA Databases

BACs containing A-like and B'-like *Synechococcus* 16S rRNA genes were screened by PCR amplification of loci targeted for MLSA analysis (Tables 1, 2; Supplemental Data Tables 1, 2). MLSA loci were selected on the basis of their being (i) single-copy genes, (ii) under neutral or purifying selection, that (iii) represented a range of degrees of divergences and distances from

the 16S rRNA locus and (iv) were not adjacent to potential mobile elements (see Supplemental Data Sheet Sections I, III).

The distributions of MLSA loci among the 267 A-like and 237 B'-like BACs containing the targeted 16S rRNA locus and at least one of the other MLSA loci are shown in Supplemental Data Sheet Section III and Supplemental Data Tables 6, 7. The majority of BACs (94 and 66% of *Synechococcus* A- and B'-like BACs, respectively) exhibited locus combinations consistent with the gene order of the reference genomes. The number of BACs positive for various loci decreased as the distance separating them from the 16S rRNA locus increased, providing additional evidence of genome rearrangements in these lineages (Supplemental Data Sheet Section III and Supplemental Data Presentation Figure 4). There was no obvious pattern of decaying synteny with increasing phylogenetic divergence (see end of legends in Figure 2 and Supplemental Data Presentation Figure 10 identifying syntenous and non-syntenous clones in the dataset). There were 71 *Synechococcus* A-like BACs that contained the total set of 7 selected loci (*rbsK*, *PK* [locus tag *CYA\_2262*], *hisF*, *lepB*, *CHP* [locus tag *CYA\_2291*], *aroA* and *dnaG*) in addition to the 16S rRNA/16S-23S rRNA internal transcribed spacer (ITS) region (Supplemental Data Table 6). However, only two *Synechococcus* B'-like BACs contained 7 of

TABLE 1 | Results from recombination and mutation rate and ratio analyses for A-like *Synechococcus* BACs.

Locus (No. of Loci)	No. of STs in Analysis	No. of nts <sup>b</sup>	No. of Segregating Sites	LDHat					ClonalFrame					
				$\theta^c$	R <sup>d</sup>	R <sup>k</sup>	R <sup>l</sup>	Ave PWD <sup>i</sup>	Var PWD <sup>j</sup>	R/ $\theta^e$	$\theta^c$ (CI)	R <sup>d</sup> (CI)	$\rho/\theta^e$ (CI)	r/m <sup>f</sup> (CI)
7 <sup>m</sup>	50	4008	183	40.86	41	13	1.6	33.14	580.03	0.04–1.0	33.94	20.365 (12.92– 30.29)	0.600 (0.38– 0.892)	2.596 (1.57– 4.01)
5a. <sup>m</sup>	69	2760	222	45.67	44	16	2.8	39.19	706.5	0.06–0.96	42.59	24.76 (16.75– 34.65)	0.581 (0.39– 0.81)	3.396 (2.21– 4.92)
<i>rbsK</i>	h	520	119	24.48	5	9	0	23.24	509.7	0–0.368	h	h	h	h
<i>PK<sup>m</sup></i>	h	584	30	6.17	11	1	0	3.63	18.85	0–1.7	h	h	h	h
<i>hisF</i>	h	429	0	g	g					g	g	g	g	g
<i>lepB<sup>m</sup></i>	h	420	30	6.17	0	2	0	2.11	18.58	0–0.324	h	h	h	h
<i>CHP<sup>m</sup></i>	h	629	28	5.76	7	1	0	9.13	93.59	0–1.2	h	h	h	h
<i>aroA</i>	h	607	15	3.09	0	0	0	1.10	2.67	0.0	h	h	h	h
<i>dnaG<sup>m</sup></i>	h	547	26	5.80	0	0	0	1.49	20.48	0.0	h	h	h	h

CI: 95% credibility interval.

<sup>a</sup>*rbsK*, *CHP*, *PK*, *lepB*, *aroA*.

<sup>b</sup>Sum of all single gene lengths (number of nucleotides) and analysis pertains to a 73-sequence (145 sequence de-duplicated) 5-locus alignment except for *hisF* and *dnaG* which pertain to 7-locus alignment.

<sup>c</sup>Watterson's theta.

<sup>d</sup>Maximum at 4Ner(region); composite likelihood method (LDHat; pairwise) finite sites model (McVean et al., 2002, 2004).

<sup>e</sup>R/ $\theta$  from LDHat is equivalent to the  $\rho/\theta$  measure from Clonal Frame and define the ratio of the rates of recombination (R or  $\rho$ ) to mutation ( $\theta$ ) illustrating how often recombination occurs relative to mutation (McVean et al., 2002, 2004; Didelot and Falush, 2007; Didelot and Maiden, 2010). For LDHat-pairwise analysis, R/ $\theta$  range includes calculations from composite-likelihood, Rmin and Wakeleys moment method (McVean et al., 2002, 2004).

<sup>f</sup>Ratio of the probabilities that a given site is altered through recombination (r) and mutation (m) illustrating how important the effect of recombination was in the diversification of the samples relative to mutation (Didelot and Falush, 2007; Didelot and Maiden, 2010).

<sup>g</sup>There were no segregating sites in the sequence dataset.

<sup>h</sup>Clonal Frame analysis is designed for concatenated multi-locus alignments (Didelot and Falush, 2007; Didelot and Maiden, 2010).

<sup>i</sup>avePWD: average pairwise distance (LDHat pairwise).

<sup>j</sup>varPWD: variance in pairwise distance (LDHat pairwise).

<sup>k</sup>Rmin value (LDHat pairwise); minimum number of recombination events describing evidence for recombination in region (McVean et al., 2002, 2004) infinite sites model.

<sup>l</sup>Population scaled 4Ner (recombination estimate) by Wakeley Moment method (McVean et al., 2002, 2004).

<sup>m</sup>The look up table for LDHat pairwise not generated from data but from existing *lkgen* table provided in LDHat distribution (*lk\_n100\_t0.01*; <https://github.com/auton1/LDhat>).

**TABLE 2 | Results from recombination and mutation rate and ratio analyses for B'-like *Synechococcus* BACs.**

Locus (No. of Loci)– PE	No. of STs in Analysis	No. of Nts	No. of Segregating Sites	LDHat					ClonalFrame			
				$\theta^a$	$R^b$	R <sup>h</sup>	R <sup>i</sup>	Ave PWD <sup>f</sup>	Var PWD <sup>g</sup>	R/ $\theta^c$	$\theta^a$	R <sup>b</sup> (CI)
4 <sup>j</sup>	51	2448	361	80.24	85 0 22.3	66.14	905.36	0–1.06	63.34	23.53 (15.18– 33.89)	0.371 (0.24– 0.535)	2.42 (1.58– 3.44)
<i>aroA</i> <sup>i</sup>	e	550	101	22.45	0 13 0	14.42	219.48	0–0.579	e	e	e	e
<i>rbsK</i>	e	535	122	27.12	15 15 2.9	34.05	539.83	0.44–0.55	e	e	e	e
<i>pcrA</i> <sup>i</sup>	e	628	62	13.78	38 11 0.5	11.06	75.06	0.36–2.8	e	e	e	e
16S rRNA/ITS <sup>j</sup>	e	733	76	16.89	15 0 0	6.725	43.46	0–0.889	e	e	e	e

CI: 95% credibility interval.

<sup>a</sup>Watterson's theta.

<sup>b</sup>Maximum at 4Ner(region); composite likelihood method (LDHat; pairwise) finite sites model (McVean et al., 2002, 2004).

<sup>c</sup>R/ $\theta$  from LDHat is equivalent to the  $\rho/\theta$  measure from Clonal Frame and define the ratio of the rates of recombination (R or  $\rho$ ) to mutation ( $\theta$ ) illustrating how often recombination occurs relative to mutation (McVean et al., 2002, 2004; Didelot and Falush, 2007; Didelot and Maiden, 2010). For LDHat-pairwise analysis, R/ $\theta$  range includes calculations from composite-likelihood, Rmin and Wakeleys moment method (McVean et al., 2002, 2004).

<sup>d</sup>Ratio of the probabilities that a given site is altered through recombination (r) and mutation (m) illustrating how important the effect of recombination was in the diversification of the samples relative to mutation (Didelot and Falush, 2007; Didelot and Maiden, 2010).

<sup>e</sup>Clonal Frame analysis is designed for concatenated multi-locus alignments (Didelot and Falush, 2007; Didelot and Maiden, 2010).

<sup>f</sup>avePWD: average pairwise distance (LDHat pairwise).

<sup>g</sup>varPWD: variance in pairwise distance (LDHat pairwise).

<sup>h</sup>Rmin value (LDHat pairwise); minimum number of recombination events describing evidence for recombination in region (McVean et al., 2002, 2004) infinite sites model.

<sup>i</sup>Population scaled 4Ner (recombination estimate) by Wakeley Moment method (McVean et al., 2002, 2004).

<sup>j</sup>The look up table for LDHat pairwise **not** generated from data but from existing lkgen table provided in LDHat distribution (lk\_n100\_t0.01; <https://github.com/auton1/LDhat>).

the targeted MSLA loci (Supplemental Data Table 7). In order to obtain a comparable sampling of *Synechococcus* B'-like and A-like BAC clones, the number of loci for the *Synechococcus* B'-like population was reduced to three protein-encoding loci (*rbsK*, *aroA* and *pcrA*) plus the 16S rRNA/16S-23S rRNA ITS sequence. The amount of nucleotide divergence at the 16S rRNA locus within A-like and B'-like BACs averaged 0.31% ( $\pm 0.036\%$  SE) and 0.71% ( $\pm 0.064\%$  SE), respectively, much less than that between BACS of the different lineages, which averaged 2.73% ( $\pm 0.024\%$  SE), which was somewhat lower than the 3.6% divergence reported for the *Synechococcus* strain A and B' genomes (Bhaya et al., 2007). We compared the *rbsK* sequences of A-like and B'-like BACs to *rbsK* sequences recovered by direct PCR amplification from the same mat samples and found that the BAC library sequences sampled broadly across B'-like and A-like lineages (Supplemental Data Sheet Section IV and Supplemental Data Presentation Figures 6, 7). All multi-locus sequence datasets were assembled into sequence types (STs) comprised of individual BACs with identical sequences at all loci (Supplemental Data Sheet Section V and Supplemental Data Tables 8, 9).

## Recombination and Mutation within and Between A and B' *Synechococcus* Lineages

Evidence of recombination within the A- and B'-lineages was readily detected by various analyses of both single genes and multiple loci. The ability to detect recombination events was influenced by the number and length of sequences analyzed and

by the number of genes included in the analysis. Furthermore, different methods detected different events. For instance, as shown in **Table 3**, RDP4 analysis of 7 loci in 71 A-like BACs detected 11 unique events. Clonal Frame detected 7 of the same events, and manual inspection of SNPs (using the definition from (Feil et al., 2000a), where  $>1$  SNP within any single locus is indicative of recombination) suggested 24 additional unique putative events. Hence, 11–35 unique events were detected. However, in an analysis in which we more than doubled the number of sequences by removing 2 of the 7 genes (see below), RDP4 detected only 5 events; Clonal Frame detected 1 additional event and SNP analysis suggested 2 more events (range 6–8 events). Similarly, in an analysis of 4 genes in 72 B'-like BACs RDP4 detected 4 events, Clonal Frame detected an additional 9 events and SNP inspection suggested 11 additional unique events (range 13–24 events).

The majority of recombination events were detected in the *rbsK* locus in both lineages; to a lesser extent recombination events were also detected in *PK*, *CHP*, and *lepB* for A-like *Synechococcus* and in the 16S rRNA/ITS region and *pcrA* gene for B'-like *Synechococcus* (Supplemental Data Tables 10–13). Phylogenies for *rbsK*, constructed using RDP4 with sequence data from either side of the predicted breakpoints, were shown to be incongruent providing additional evidence of recombination at this locus in both lineages (Supplemental Data Presentation Figures 8, 9).

In contrast, evidence of recombination between the A-like and B'-like lineages was rare. Blast analyses of 7 MLSA loci on 71 A-like BACs and 4 MLSA loci on 72 B'-like BACs revealed only three examples, all involving *rbsK* loci on A-like ( $n =$

**TABLE 3 | The number of unique (u) and overlapping (ovl; supported by multiple methods) recombination events recorded by RDP4, Clonal Frame (CF), and single nucleotide polymorphism (SNP) analysis of MLSA datasets.**

Organism	Dataset	No. Sequences	RDP4u <sup>a,b</sup>	CFu	CFovl	SNPu	SNPovl	All Unique <sup>e</sup>
<i>Synechococcus</i> A-like BACs	MLSA7 <sup>d</sup>	71	11	0 <sup>a</sup>	7 <sup>a</sup>	24 <sup>a</sup>	7 <sup>a</sup>	35
	MLSA5	49	5	0 <sup>a</sup>	0 <sup>a</sup>	0 <sup>a</sup>	0 <sup>a</sup>	5
	MLSA5	145	5	1 <sup>a</sup>	8 <sup>a</sup>	2 <sup>a</sup>	6 <sup>a</sup>	8
<i>Synechococcus</i> B'-like BACs	MLSA4	72	4	g <sup>b,c</sup>	1g <sup>b</sup>	11 <sup>b,c</sup>	14 <sup>b,c</sup>	24

All loci were considered in analysis.

<sup>a</sup>Overlapping RDP4 events with CF or SNP analyses were not recorded in CFu or SNPu columns, only the RDP4u column.

<sup>b</sup>See Supplemental Data Table 10.

<sup>c</sup>See Supplemental Data Table 11.

<sup>d</sup>See Supplemental Data Presentation Figure 10.

<sup>e</sup>See **Figure 2**.

<sup>e</sup>Sum of "u" columns only.

1) or B'-like ( $n = 2$ ) BACs that were associated with the genome of the other lineage (Supplemental Data Sheet Section VI). Similarly, of the loci used to study both A-like and B'-like *Synechococcus* lineages, *rbsK* was the only gene for which RDP4 analysis detected evidence of recombination. Only 3 unique recombination events were identified among 123 combined A-like and B'-like *rbsK* sequences in the 511 nt overlapping region (all within B'-like BACs; Supplemental Data Table 14).

The importance of recombination relative to mutation for the evolution of A-like and B'-like *Synechococcus* lineages was estimated independently in two ways: (i)  $R/\theta$ , which is the ratio at which recombination and mutation occur (McVean et al., 2002, 2004; Didelot and Falush, 2007) using LDHAT analysis (reported as a range depending on LDHAT method annotated in footnotes of **Tables 1, 2** and equivalent to  $\rho/\theta$  in Clonal Frame analysis), and (ii)  $r/m$ , which is a ratio of the probabilities that a given site was altered through recombination or mutation (i.e., how important the effect of recombination was in the diversification of the sample relative to mutation in terms of the number of resulting nucleotide substitutions) as defined by Clonal Frame analysis (Didelot and Falush, 2007; Didelot and Maiden, 2010). For MLSA concatenated datasets, the ratios ( $R/\theta$ ,  $\rho/\theta$ , and  $r/m$ ) differed somewhat in the two lineages. Recombination events were generally less frequent than mutation events ( $\rho/\theta$  ranging from 0.38 to 0.89 for A-like BACs and 0.24 to 0.54 for B'-like BACs, in Clonal frame analysis;  $R/\theta$  ranging from 0.4 to 1.0 for A-like BACs and 0.44 to 1.06 for B'-like BACs in LDHAT analysis; see **Tables 1, 2**). It was also clear from Clonal frame analysis that recombination had a greater impact than mutation on diversification of the lineage ( $r/m$  ratio ranging from 2.60 to 3.40 depending on number of loci for *Synechococcus* A-like BACs, and 2.42 for *Synechococcus* B'-like BACs; **Tables 1, 2**).

## Ecotype Simulation Analyses of Concatenated A-like *Synechococcus* MLSA Datasets

We focus in the main text on the A-like *Synechococcus* lineage, which offered a greater number of genes for MLSA analyses (7 loci, hence termed MLSA7). Also, A-like *Synechococcus* BACs were recovered from both mat samples, thus enabling

analysis of habitat association. Comparable results for a 4-locus MLSA analysis (MLSA4) of B'-like lineage variants, which were recovered only from the 60°C sample, are presented in Supplemental Data Sheet Section VII. For clarity, PEs demarcated by Ecotype Simulation are named according to whether they are based on MLSA data (MLSA7 or MLSA4 followed by the PE designation; e.g., MLSA7 PEA1; MLSA4 PEB'4) or single-locus data (specified by the gene analyzed followed by the PE designation; e.g., *rbsK* PEA2).

All individual-locus sequences sampled by BACs and multi-locus concatenations constructed from them (STs) were analyzed using Ecotype Simulation (**Figure 2A, Table 4**). STs predicted by Ecotype Simulation to be members of the same putative ecotype in the MLSA7 analysis are given the same color, but members of different PEs are colored differently, and colors are maintained throughout all MLSA7 Figures. The MLSA7 concatenated phylogeny and the single-locus phylogeny for *rbsK* sequences sampled by the same BACs are compared in **Figures 2A,B** respectively, which also show PEs predicted by Ecotype Simulation. Phylogenetic comparisons with other loci (*CHP*, *lepB*, *dnaG* PK, *aroA*, and *hisF*) are discussed in Supplemental Data Sheet Section VIII and are shown in Supplemental Data Presentation Figure 14. Ecotype Simulation predicted 2–7 A-like PEs from individual BAC loci, depending on the locus analyzed. Among individual loci, the greatest number of PEs was predicted from the *rbsK* gene (**Figure 2B**), which had the greatest average evolutionary divergence among the loci studied (**Table 4**). Ecotype Simulation predicted 13 A-like MLSA7 PEs from concatenated MLSA sequence data (**Figure 2A**), though five of these PEs were based on a single ST sequence (i.e., singletons) and one was based on two occurrences of the same ST (i.e., a doubleton). MLSA7 PE clades contained from 1 to 28 BACs. Three of the 13 MLSA7 PE clades for *Synechococcus* A-like BACs contained a dominant variant (i.e., 2–14 clones that were identical at all MLSA7 loci) and singleton variants. In two cases, MLSA7 PEs A4 and A7, subdominant variants were also observed, along with singletons. Supplemental Data Table 23 shows how STs, dominant variants and subdominant variants were distributed among MLSA7 PEs.

Only one case of complete correspondence between *rbsK* PEs and MLSA7 PEs was observed (i.e., MLSA7 PE A9 = *rbsK*

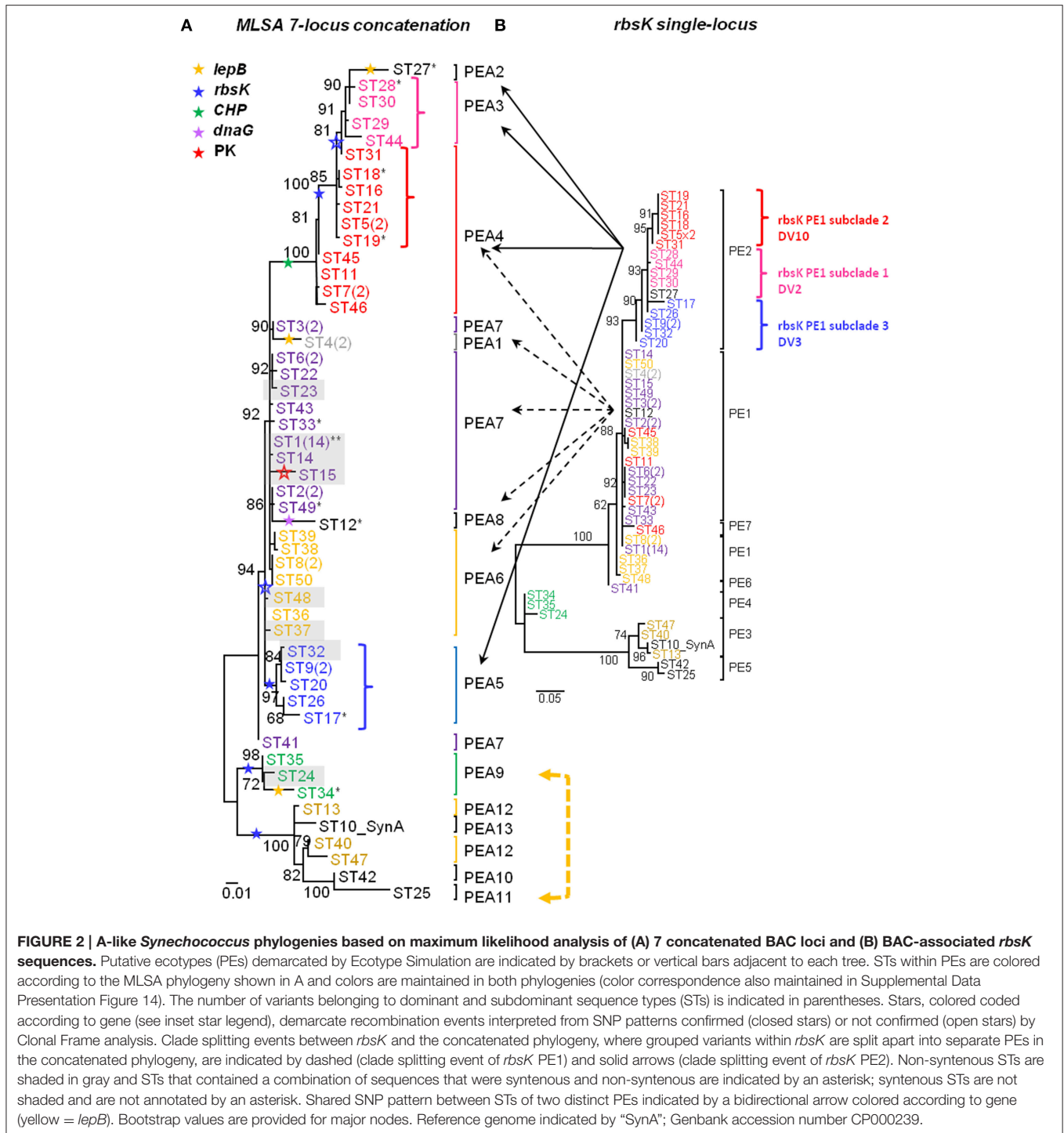


**FIGURE 2 | A-like *Synechococcus* phylogenies based on maximum likelihood analysis of (A) 7 concatenated BAC loci and (B) BAC-associated *rbsK* sequences.** Putative ecotypes (PEs) demarcated by Ecotype Simulation are indicated by brackets or vertical bars adjacent to each tree. STs within PEs are colored according to the MLSA phylogeny shown in A and colors are maintained in both phylogenies (color correspondence also maintained in Supplemental Data Presentation Figure 14). The number of variants belonging to dominant and subdominant sequence types (STs) is indicated in parentheses. Stars, colored coded according to gene (see inset star legend), demarcate recombination events interpreted from SNP patterns confirmed (closed stars) or not confirmed (open stars) by Clonal Frame analysis. Clade splitting events between *rbsK* and the concatenated phylogeny, where grouped variants within *rbsK* are split apart into separate PEs in the concatenated phylogeny, are indicated by dashed (clade splitting event of *rbsK* PE1) and solid arrows (clade splitting event of *rbsK* PE2). Non-synonymous STs are shaded in gray and STs that contained a combination of sequences that were syntenous and non-syntenous are indicated by an asterisk; syntenous STs are not shaded and are not annotated by an asterisk. Shared SNP pattern between STs of two distinct PEs indicated by a bidirectional arrow colored according to gene (yellow = *lepB*). Bootstrap values are provided for major nodes. Reference genome indicated by "SynA"; Genbank accession number CP000239.

PEA 4) (green colored STs in **Figure 2**). Otherwise, the *rbsK* and MLSA7 phylogenies were mainly incongruent, providing further evidence that recombination complicates single-locus analyses of PEs (compare **Figures 2A,B**). For instance, some members of MLSA7 PE A4 were classified into three *rbsK* PEs (A1, A2, and A7; red colored sequences in **Figure 2**). Ecotype Simulation analysis of concatenated MLSA7 loci mainly split individual PEs

demarcated by *rbsK* analysis into multiple MLSA7 PEs, as shown by dashed and solid black arrows in **Figure 2** (e.g., *rbsK* PE2 was split into MLSA PEs 3 (pink), 4 (red), and 5 (blue)).

### Evidence of Habitat Association

In order to obtain a greater number of A-like BACs from samples collected at both temperatures sufficient to observe

**TABLE 4 | Ecotype Simulation and eBURST output for 71 A-like *Synechococcus* BACs that contained all 7 loci assayed for the study.**

Locus	Average evolutionary divergence (BACs)	Ecotype Simulation (ES)				eBURST <sup>b</sup>	
		PEs Demarcated-ES (95% CI)	Omega (95% CI)	Sigma (95% CI)	Sample-specific PEs	No. of alleles or sequence types	No. of clonal complexes
<i>rbsK</i>	0.03	7 (4–16)	0.05 (0.01–0.14)	3.5 (0.33–42)	Yes	24	d
<i>PK</i>	0.002	2 (2–60)	0.052 (0.04–66)	13 (1.2–12.2)	No	11	d
<i>hisF</i> <sup>a</sup>	< 0.0001	2 (2–71)	3113 ( $<2e^{-7}$ – $\rightarrow 100$ )	48,000 (0.7– $\rightarrow 100$ )	No	2	d
<i>lepB</i>	0.005	2 (2–6)	0.09 (0.003–0.6)	26.9 (1.7–99.8)	No	6	d
<i>CHP</i>	0.01	2 (2–5)	0.03 (0.001–0.23)	564 (5.4– $\rightarrow 100$ )	No	4	d
<i>aroA</i>	0.001	3 (2–71)	1.86 (0.03–99.6)	22.7 (0.07–100)	No	7	d
<i>dnaG</i>	0.002	4 (3–22)	0.3 (0.07–2.5)	180 (3.8– $\rightarrow 100$ )	No	7	d
Concatenation <sup>b</sup>	0.01	13 (9–44)	0.05 (0.03–0.12)	1.11 (0.07–100)	c	50	3

<sup>a</sup>Molecular resolution of *hisF* was not significant enough for Ecotype Simulation to effectively predict ecotypes.

<sup>b</sup>Calculated from concatenated sequence datasets only.

<sup>c</sup>Not enough 65° sequences to determine sample specificity of demarcated PEs.

<sup>d</sup>Clonal complexes only apply to concatenated sequence datasets.

habitat associations, we performed two separate MLSA analyses of 5 of the 7 loci (*rbsK*, *lepB*, *aroA*, *CHP*, and *PK*; MLSA5, see Supplemental Data Sheet Section VIII). One included 49 concatenated sequences with nearly equal representation of sequences from 60 and 65°C (Supplemental Data Presentation Figure 15). The other included the full dataset of 145 concatenated sequences that could be compared at these 5 loci (Supplemental Data Presentation Figure 16). Fisher's exact tests of contingency on both sets of BACs from 60 and 65°C yielded significant evidence of heterogeneity in habitat associations (i.e., collection temperatures;  $p$ -value = 0.001). Additionally, several MLSA5 PEs were comprised of multiple BACs obtained only from one of the two temperatures.

In order to investigate vertical distributions of alleles we pyrosequenced the *rbsK* locus in DNAs extracted from 80  $\mu$ m-thick cryotome sections from different depths in the top green layer of the 63–65°C mat, where A-like PEs predominate. Pyrosequencing analysis of the *rbsK* locus resulted in a phylogeny (Supplemental Data Sheet Section IX; Supplemental Data Presentation Figure 19) that closely resembled the *rbsK* phylogeny based on sequences sampled by BAC clones (compare **Figure 2B** and Supplemental Data Presentation Figure 19). In cases where pyrosequences matched only STs of the same PE or subclade, we could test the hypothesis that these PEs represent ecologically distinct populations. As shown in **Figure 3A**, the subclade representing MLSAs PE A4 and A5 (red and blue STs in **Figure 2A**), which were grouped together into *rbsK* PE A2 (**Figure 2B**), were shown to exhibit different vertical distributions (Fisher's exact test, ANOVA and  $G$ -tests  $p < 0.001$ ). *rbsK* sequences representative of MLSA PE A4 declined with depth, whereas those representative of MLSA PE A5 increased with depth. This provides an example of how a single-locus analysis can lump populations that are ecologically distinct, giving the impression of a clade containing ecologically heterogeneous members. Additionally, the availability of genome sequences of

isolates representative of MLSA7 PEs A5 and A9 (Olsen et al., 2015; and see Supplemental Data Sheet Section X) allowed us to associate *rbsK* and *psaA* sequences corresponding to the same PEs. In these cases we could demonstrate correspondence between *rbsK* distributions and the *psaA* distributions observed in single-locus analysis of the same samples by Becraft et al. (2015) (see also **Figures 3B,C**, where MLSA7 PE 5 = *psaA* PE A6 and MLSA7 PE 9 = *psaA* PE A14). Both of these PEs have been shown to be most prevalent toward the bottom portion of the upper green layer of the mat at this temperature (Becraft et al., 2015), and representative isolates have been shown to possess genes that enable harvesting of lower amounts of light, characteristic of *in situ* light conditions (Becraft et al., 2015; Nowack et al., 2015; Olsen et al., 2015; also see Supplemental Data Sheet Section X).

## eBURST Analyses

The eBURST algorithm assembles STs into clonal complexes (Maiden et al., 1998; Feil et al., 1999, 2000a, 2004) that are typically composed of a single predominant genotype (consensus group or here, dominant variant), plus variants that are identical to the predominant genotype at all but one locus (single-locus variants; Feil and Spratt, 2001; Feil et al., 2004). Single-locus variants can differ from the dominant variant by any number of SNPs as long as those SNPs occur in only one locus (Feil et al., 1999, 2000b, 2003). Only 3 clonal complexes were observed with eBURST analyses of the MLSA7 dataset (**Figure 4**, **Table 5**), and the correspondence between eBURST's clonal complexes and Ecotype Simulation's PEs was imprecise (see **Figure 4** and Supplemental Data Sheet Section VIII for details of these analyses and results). In the eBURST analyses of the MLSA5 datasets, Fisher's exact tests did not indicate differences among clonal complexes in their habitat associations (Supplemental Data Presentation Figure 17,  $p$ -value 0.943; Supplemental Data Presentation Figure 18,  $p$ -value 0.734).

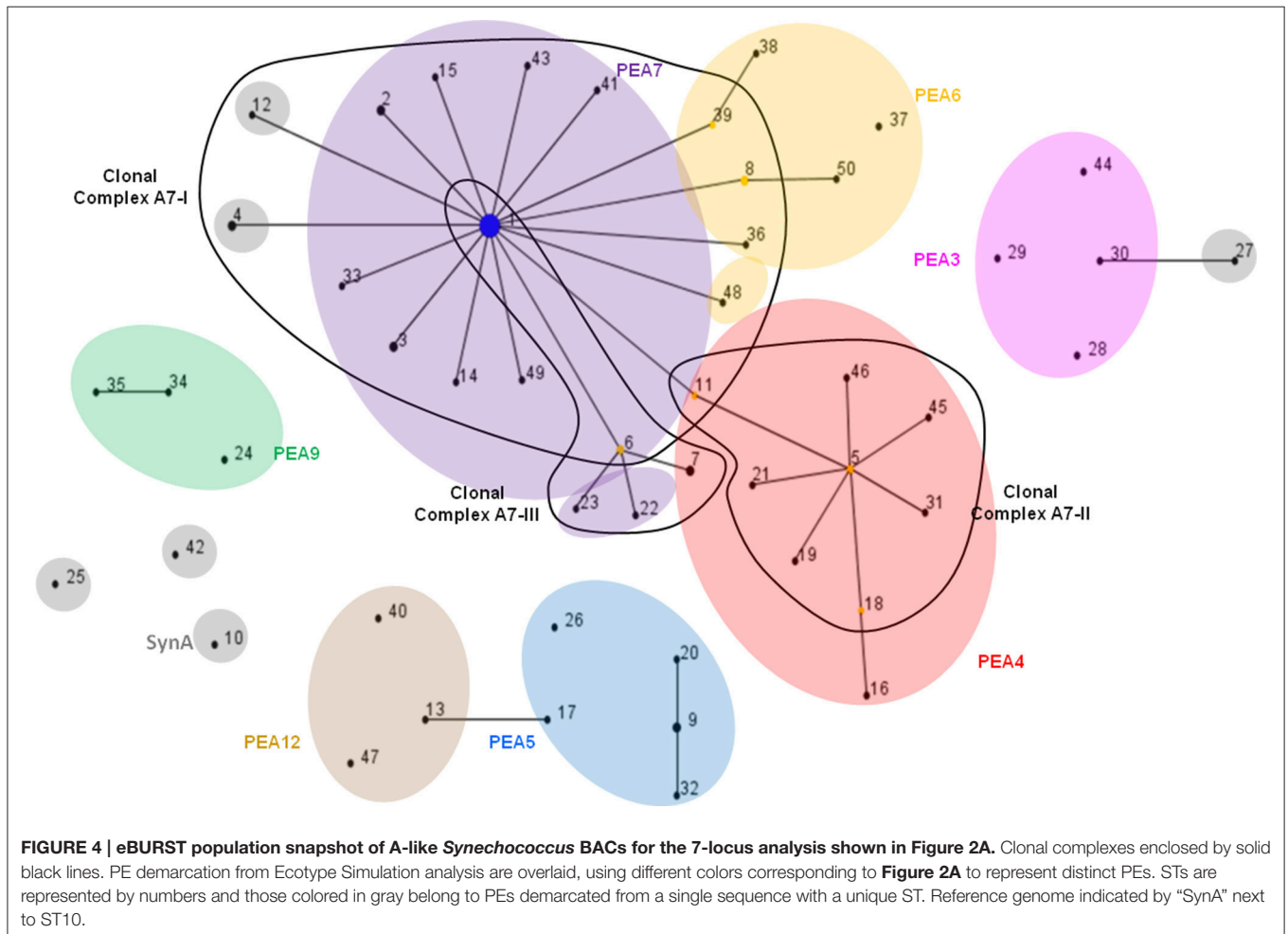
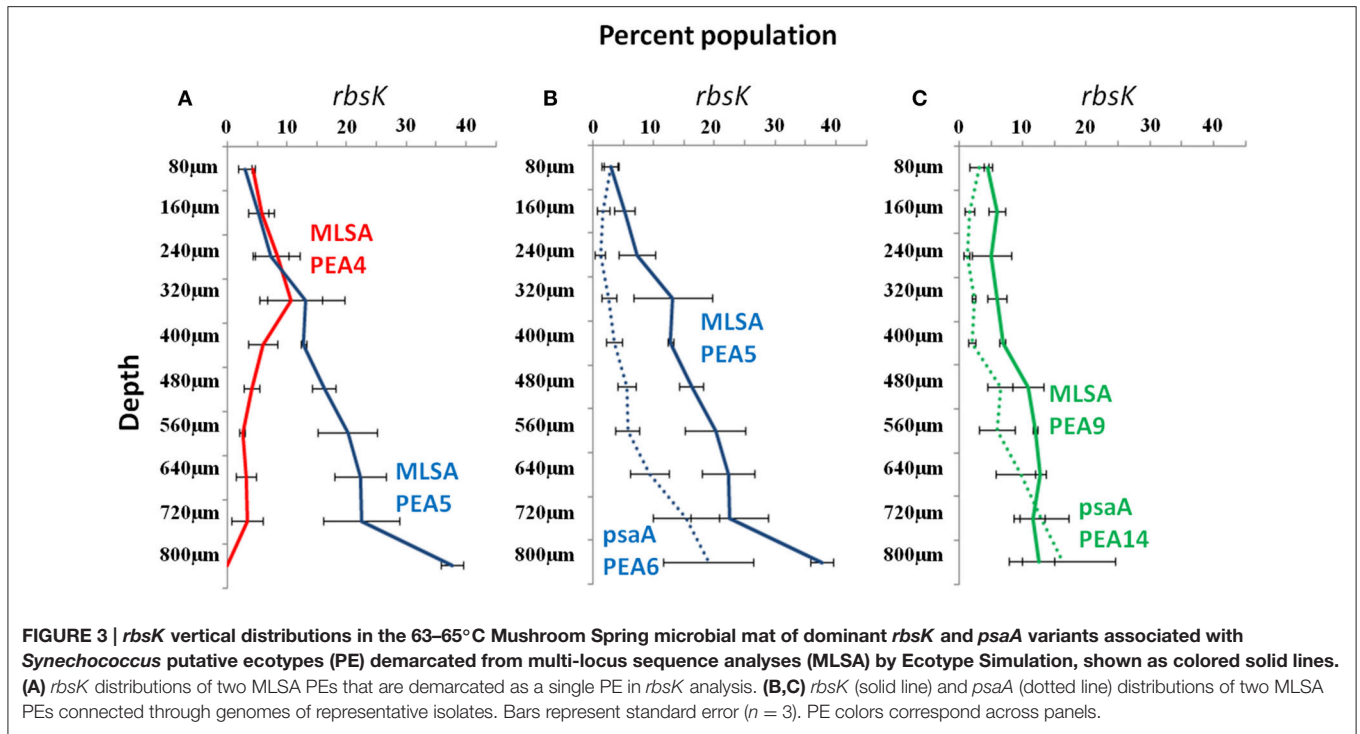


**TABLE 5 | eBURST analysis of clonal complexes for the 7-locus MLSA of A-like *Synechococcus* BACs.**

Clonal Complex A7-I																	
Locus	Consensus DV-ST1 (14)	ST2	ST3	ST4	ST6	ST8	ST11	ST12	ST14	ST15	ST33	ST36	ST39	ST41	ST43	ST48	ST49
<i>rbsK</i>	1	1	1	1	3 <sup>1</sup>	1	1	1	1	1	1	7 <sup>2</sup>	8 <sup>2</sup>	10 <sup>5</sup>	12 <sup>1</sup>	17 <sup>2</sup>	1
<i>PK</i>	1	1	1	1	1	2 <sup>1</sup>	1	1	8 <sup>1</sup>	10 <sup>11</sup>	1	1	1	1	1	1	1
<i>hisF</i>	1	1	1	1	1	1	1	1	1	1	1	1	1	1	1	1	1
<i>lepB</i>	1	1	2 <sup>1</sup>	3 <sup>13</sup>	1	1	1	1	1	1	1	1	1	1	1	1	1
<i>CHP</i>	1	1	1	1	1	1	2 <sup>20</sup>	1	1	1	1	1	1	1	1	1	1
<i>aroA</i>	1	1	1	1	1	1	1	1	1	1	7 <sup>2</sup>	1	1	1	1	1	1
<i>dnaG</i>	1	2 <sup>1</sup>	1	1	1	1	1	5 <sup>19</sup>	1	1	1	1	1	1	1	1	3 <sup>2</sup>

Clonal Complex A7-II								
Locus	Consensus DV-ST5 (2)	ST11	ST18	ST19	ST21	ST31	ST45	ST46
<i>rbsK</i>	2	1 <sup>20</sup>	2	2	2	18 <sup>2</sup>	14 <sup>8</sup>	15 <sup>13</sup>
<i>PK</i>	1	1	1	1	8 <sup>1</sup>	1	1	1
<i>hisF</i>	1	1	1	1	1	1	1	1
<i>lepB</i>	1	1	2 <sup>1</sup>	1	1	1	1	1
<i>CHP</i>	2	2	2	3 <sup>1</sup>	2	2	2	2
<i>aroA</i>	1	1	1	1	1	1	1	1
<i>dnaG</i>	1	1	1	1	1	1	1	1

Clonal Complex A7-III						
Locus	Consensus DV-ST6 (2)	ST1	ST7	ST22	ST23	
<i>rbsK</i>	3	1 <sup>1</sup>	3	3	3	
<i>PK</i>	1	1	1	1	1	
<i>hisF</i>	1	1	1	1	1	
<i>lepB</i>	1	1	1	1	1	
<i>CHP</i>	1	1	2 <sup>20</sup>	1	1	
<i>aroA</i>	1	1	1	1	5 <sup>2</sup>	
<i>dnaG</i>	1	1	1	4 <sup>1</sup>	1	

The number of BACs within an ST is in parentheses when greater than 1. Superscripts next to the allele number denote number of nucleotide differences compared to the consensus sequence. Corresponding to **Figure 4**. DV, dominant variant.

## Evidence of Historic and Recent Recombination Events

The presence of historic recombination events was further investigated after it was initially found through SNP analysis that identical SNP differences were observed in two different MLSA7 PEs. **Figure 5** shows SNP differences between variants that were grouped into MLSA7 PEs and clonal complexes sharing the same dominant variant. Most differences resulted either from the exclusion of STs containing SNPs in multiple loci from clonal complexes by eBURST, or from the exclusion of STs containing a large number of SNPs from phylogenetic clusters demarcated as PEs by Ecotype Simulation. Of particular interest, however, was the observation of identical SNP differences in the *CHP* locus in two different MLSA7 PE A4 STs relative to two different dominant variants of MLSA7 PE A7 (ST7 vs. ST6 and ST11 vs. ST1). This prompted us to consider the possibility that these SNP patterns were clade-specific. We investigated recombination events occurring on internal nodes

(suggestive of historic recombination) using Clonal Frame. Clonal Frame predicted several internal nodes in both the *Synechococcus* A-like and B'-like lineages where there was a high probability of recombination having occurred in one or more loci (closed colored stars in **Figure 2A** and Supplemental Data Presentation Figure 10). This revealed a historical record of the impact recombination has had on the diversification of these organisms. Detailed manual inspection of SNP patterns in all clades allowed us to suggest additional putative recombination events in the phylogeny of these *Synechococcus* lineages (open colored stars in **Figure 2A** and Supplemental Data Presentation Figure 10; also see Supplemental Data Sheet Section XI and Supplemental Data Presentation Figure 21). For instance, all variants grouped into the clade containing MLSA7 PEs A2-A4 appear to have vertically inherited a recombinant *CHP* gene after an early recombination event (closed green star) and variants within MLSA7 PEs A2, A3, and a portion of PEA4, appear to have vertically inherited an *rbsK* sequence from a

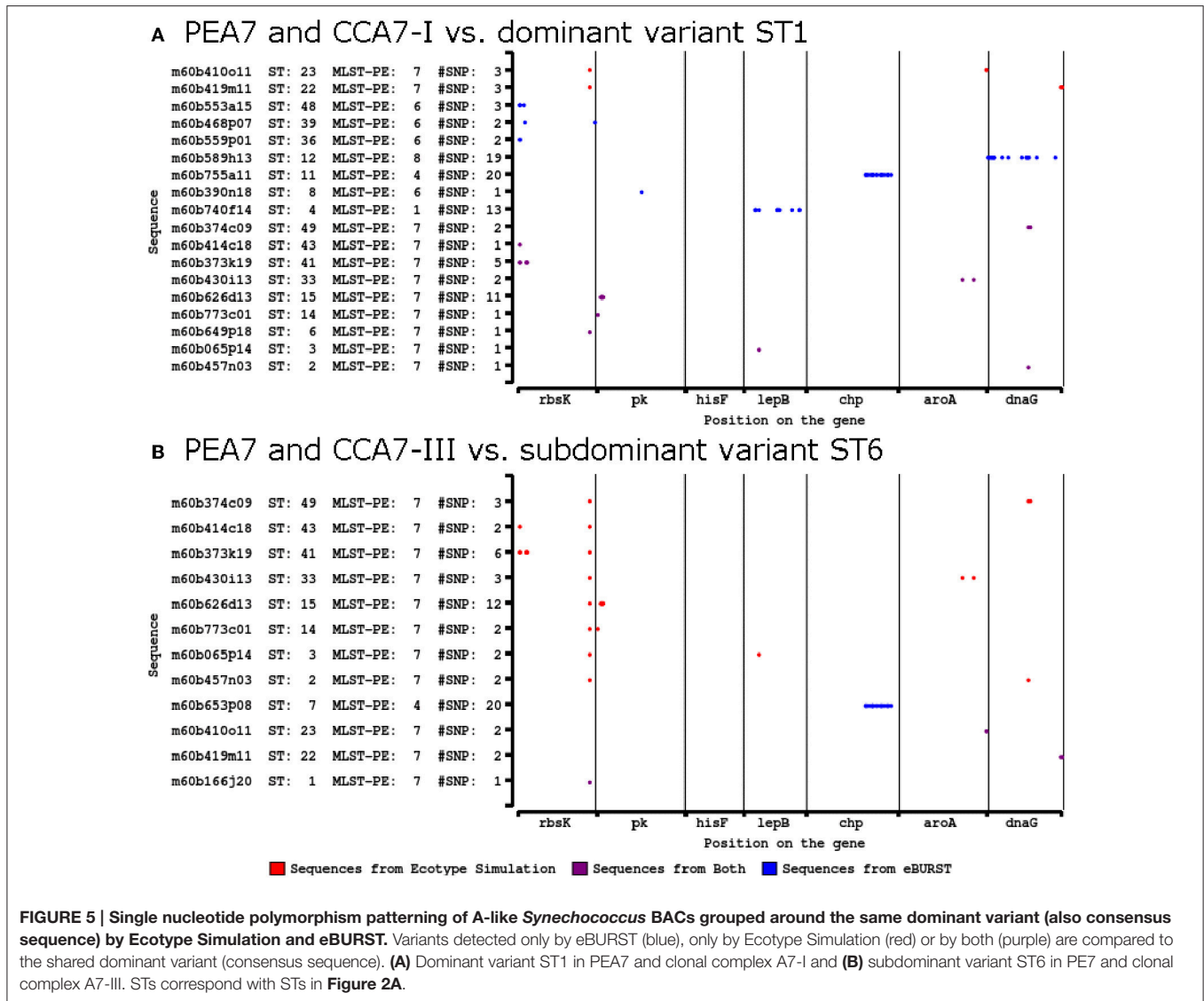


**FIGURE 5 |** Single nucleotide polymorphism patterning of A-like *Synechococcus* BACs grouped around the same dominant variant (also consensus sequence) by Ecotype Simulation and eBURST. Variants detected only by eBURST (blue), only by Ecotype Simulation (red) or by both (purple) are compared to the shared dominant variant (consensus sequence). **(A)** Dominant variant ST1 in PEA7 and clonal complex A7-I and **(B)** subdominant variant ST6 in PE7 and clonal complex A7-III. STs correspond with STs in **Figure 2A**.

subsequent recombination event (closed blue star). A third putative recombination event involving the *rbsK* locus (open blue star) may distinguish MLSA7 PEs A2 and A3 from MLSA7 PE A4.

These SNP analyses also revealed several examples of singleton MLSA7 PEs associated with recombination patterns involving a large number of SNPs [MLSA7 PEs A1 (ST4), A2 (ST27), A8 (ST12), and A11 (ST25); see **Figure 2A**]. These singleton-PE variants formed long-branches and were closely related to sister PEs comprised of multiple variants, but different in many SNPs from the dominant variant of that PE. For example, in **Figures 2A, 5A**, singleton-PE A8 (ST12) was closely related to PE A7, but differed by 19 SNPs in the *dnaG* locus, suggesting that a recent recombination event might have caused enough sequence difference to prevent its accurate demarcation by Ecotype Simulation. There was only one case in which an identical SNP pattern shared by two STs (ST25 in singleton MLSA7 PE A11 and ST 34 in MLSA7 PE A9; *lepB*) was not

clade-specific (**Figure 2** and Supplemental Data Presentation Figure 21 panel I).

Similar analysis was performed on the *Synechococcus* B'-like BACs with the interesting result that 2–3 recombination events were associated with some divergences, even though only 4 loci were included in the B'-like MLSA4 phylogeny (Supplemental Data Sheet Section VIII and Supplemental Data Presentation Figures S10, S12, S13).

## DISCUSSION

### Recombination within and Between Lineages of *Synechococcus*

There is abundant evidence that genomic rearrangements and recombination have influenced the evolution of the *Synechococcus* populations inhabiting the Mushroom Spring microbial mat. As in previous investigations of *Sulfolobus*

*islandicus* (Cadillo-Quiroz et al., 2012), *Wolbachia* (Ellegaard et al., 2013), and *Vibrio cyclitrophicus* (Shapiro et al., 2012) mentioned above, recombination between the divergent A and B' lineages of *Synechococcus* appears to be less frequent than recombination within each lineage. Specifically, only approximately 2% of BACs exhibited evidence of recombination between A- and B'-like *Synechococcus* BACs (see Results, Supplemental Data Sheet Section VI and Supplemental Data Table 14). This corroborates our previous metagenomic analyses, in which we found a low percentage of metagenomic clones with end sequences stemming from both the A-like and B'-like lineages (Klatt et al., 2011) (Supplemental Data Sheet Section VI). In contrast, within-lineage recombination was greater, with 5.5% of A-like and 33.3% of B'-like *Synechococcus* BACs exhibiting evidence of recombination for approximately equal numbers of loci analyzed (MLSA5, 145 sequences and MLSA4, 72 sequences for *Synechococcus* A- and B'-like BACs respectively; **Table 3**).

Recombination events have occurred at various times in the history of the A-like and B'-like clades: some recombinant segments are fixed in large subclades (i.e., evidenced by clustering of SNPs in MLSA PEs 2, 3, and 4 in Supplemental Data Presentation Figures 21A,D,G or MLSA PEs 10, 11, 12, and 13 in Supplemental Data Presentation Figures 21C,E,I; for analogous B'-like fixed recombinant segments see Supplemental Data Presentation Figure 13), indicating a recombination event early in the clade's history followed by vertical inheritance of the recombined gene, while others are specific only to singleton (one doubleton) variants demarcated as PEs based on recent recombination in single loci (i.e., MLSA PEs 1, 2, 8, 10, 11, and 13 in **Figure 2A**). These results suggest that recent recombination events might cause overestimation of PEs by Ecotype Simulation. That is, a single recombination event, if involving a long enough fragment, can cause Ecotype Simulation to split a PE. In the case of eBURST, a single recombination event of any size cannot split a consensus group; however, two or more recombinants of any size will separate a recipient organism into a different consensus group.

The rates of recombination within the A and B' lineages were estimated to be less than or about the same as that of mutation (**Tables 1, 2**). However, we determined that recombination had a somewhat greater impact than mutation on sequence change within these populations (**Tables 1, 2**; Clonal Frame,  $r/m$  range 1.58–4.92). The impact of recombination ( $r/m$ ) was estimated at 2.6 and 2.4, for the *Synechococcus* A-like and B'-like lineages, respectively. These  $r/m$  ratios are similar to values reported for other cyanobacteria (Vos and Didelot, 2009) and are in the same range as those reported for *S. islandicus*, *Wolbachia*, and *Halorubrum* (Papke et al., 2004; Whitaker et al., 2005; Ellegaard et al., 2013). The recent study on *Synechococcus* by Rosen et al. (2015), did not provide  $r/m$ , but their estimate of the ratio of recombination to mutation rates ( $\rho/\theta$ ) was close to 1, which fell within the  $R/\theta$  range provided by our LDHAT analysis (**Tables 1, 2**). Why do such different interpretations arise from such similar results? Although, Rosen et al. interpreted from a very similar recombination/mutation ratio that recombination is “ubiquitous,” we note that this ratio is not extraordinarily high when compared against the many groups of bacteria whose

recombination rates were quantified by Vos and Didelot (2009). Furthermore, Rosen et al. have not considered the theoretical work of Haldane (1932), which shows that such low rates of recombination cannot prevent ecological diversification.

Given the rates of mutation estimated for various bacteria (Drake, 2009; Vos and Didelot, 2009), we may conclude that a typical gene in the *Synechococcus* populations is experiencing recombination at an extremely low *absolute* rate, so that recombination between nascent species is unlikely to hinder their divergence (Haldane, 1932; Vos, 2011; Wiedenbeck and Cohan, 2011). Low-frequency recombination may allow shuffling of niche-neutral alleles, which do not determine ecological niche, but low-frequency recombination of *niche-determining* alleles from other populations can be countered by natural selection (Haldane, 1932). Maladaptive niche-determining alleles from other populations will be kept at negligible levels, maintaining the integrity of populations' adaptations (Wiedenbeck and Cohan, 2011). Rates of recombination observed in *Synechococcus* should not lead us to dismiss *a priori* the possibility of ecological diversification within either clade.

We therefore disagree with Rosen et al.'s conclusion (Rosen et al., 2015) that frequent recombination has caused each of the A and B' clades of *Synechococcus* to be a “quasisexual population,” where close relatives are prevented from diversifying into long-standing, ecologically homogeneous populations, or ecotypes. While Rosen et al. (2015) have shown a shuffling of alleles (really gene segments) within the A and B' clades, they have not shown that the recombination has randomized associations between niche-determining alleles, which are responsible for ecotype divergence. Moreover, we do not see how they could rule out ecological diversification without studying ecology. As we have shown in many previous papers, as well as in the present study, there is ample evidence for the coexistence of long-standing, ecologically divergent populations within both the A and B' clades, as we discuss below. Rosen et al. mentioned some of these studies, but did not use an ecological model in their work, as we have done here.

As with most (if not all) bacteria, recombination has been sufficient in *Synechococcus* to create new ecological diversity. Within the A lineage, for example, low-light PEs differ from high-light PEs in having acquired a gene cluster likely coding for an additional photoreceptor (Olsen et al., 2015). It does not take a recombination rate much higher than that of mutation to transfer a gene that is adaptive in a new niche. Only one adaptive transfer of a gene (or one mutation event); see Bantinaki et al. (2007) is required to found a new ecotype and thereby bring about ecological diversification. On the other hand, a much higher rate of recombination is required to prevent adaptive divergence between nascent populations; this requires recurrent inter-population transfer of genes poorly adapted to their new niche (Wiedenbeck and Cohan, 2011).

## Ecological Diversification within the A-like and B'-like *Synechococcus* Lineages

The Ecotype Simulation analysis of concatenated MLSA sequences hypothesized 13 and 29 PEs within the A-like and B'-like clades, respectively. This was greater than the

number of PEs predicted from single-locus analyses of the most divergent locus, *rbsK*. This is likely because of greater resolution provided by MLSA7 (as well as MLSA4; see Supplemental Data Presentation Figure 10), as evidenced by the fact that MLSA7 split numerous PEs that were lumped by *rbsK* analysis. We were able to demonstrate the ecological distinctness of some of the A-like putative ecotypes, first with respect to the two habitat types investigated in this study (60 and 65°C). That is, some hypothesized A-like ecotypes were sampled entirely from different habitats, while others were quantitatively different in their habitat associations. Also, pyrosequencing of PCR-amplified *rbsK* genes typical of different MLSA7 PEs demonstrated fine-scale distribution differences of MLSA7 PEs along vertical gradients. Additionally, the availability of genomes of isolates representative of MLSA7 PEs permitted us to demonstrate correspondence of *rbsK* distributions with distributions observed earlier in *psaA* analyses (Becraft et al., 2015). This led to demonstration of adaptation consistent with distribution patterns (Nowack et al., 2015) and genomic evidence of mechanisms likely to underlie these adaptations (Olsen et al., 2015). For instance, MLSA PEs 5 and 9 correspond to *psaA* PEs A6 and A14, whose distribution deep in the upper green layer of the mat (Becraft et al., 2015) is consistent with the presence of auxiliary photosystem genes that are likely to be associated with the ability to acclimate to low irradiance (Nowack et al., 2015; Olsen et al., 2015); and see Supplemental Data Sheet Section X). Becraft et al. (2011, 2015) also describe the existence and ecological distinction of B'-like *Synechococcus* ecotypes, as well as the ecological interchangeability of the members of each ecotype.

We conclude that both the A-like and B'-like *Synechococcus* lineages have clearly diversified into many younger species populations, whose niches correspond in part to differences along temperature and vertical gradients (Becraft et al., 2015). Our approach did not permit us to evaluate the role of positive selection within our dataset as our genes were under neutral/purifying selection. Evaluation of full genomes of strains of closely related species will allow us to further examine the roles that recombination, mutation, selection and neutral processes have played in the diversification of *Synechococcus*.

## Whither the Biological Species Concept?

That recombination has occurred more frequently within closely related clades than between them has previously been taken as support for the Biological Species Concept in bacteria and archaea (Cadillo-Quiroz et al., 2012; Shapiro et al., 2012; Ellegaard et al., 2013). However, the quintessential idea of the Biological Species Concept is that sexual isolation is required for irreversible divergence and ecological distinctness in the origin of species (Cohan, 2013). Support for the Biological Species Concept requires more than a correlation between sexual isolation and divergence among clades; one must demonstrate that reduced recombination was necessary for their divergence.

We argue that such evidence is lacking in the above-cited studies on *Vibrio*, *Wolbachia*, and *Sulfolobus*. As seen in the present work, *Synechococcus* lineages have been noted to have

recombination levels similar to those reported for *Halorubrum* and *Sulfolobus*. Like these organisms, major *Synechococcus* clades that are highly divergent (3.6% diverged at the 16S rRNA locus and 18% diverged in average nucleotide identity (ANI), Bhaya et al., 2007) are ecologically distinct. However, our high-resolution analysis of closest relatives within each clade has shown ecological speciation among organisms that have identical or nearly identical 16S rRNA sequences and have diverged only on the order of 1% ANI (Olsen et al., 2015; also see Supplemental Data Table 25) and show minimal sexual isolation. Similarly, in work on another system we have found ecotype differentiation among *Bacillus* clades that show very little sexual isolation (Majewski and Cohan, 1999; Connor et al., 2010). We hypothesize that analysis of fine-scale ecological divergence within *Halorubrum* or *Sulfolobus* may yield similar results (Papke et al., 2007; Cadillo-Quiroz et al., 2012). Recombination does not appear to have impeded ecological diversification among close relatives that are not sexually isolated. Thus, sexual isolation, in this context, is unnecessary for the origin of species (Wiedenbeck and Cohan, 2011).

Instead, sexual isolation is more likely to be the result of divergence among closely related groups than the cause. Not only do ecologically distinct populations tend to diverge over time into separate sequence clusters (Cohan and Perry, 2007), but ecological divergence may also cause occupancy of different microhabitats, reducing opportunities for genetic exchange (Shapiro et al., 2012); in addition, functional divergence may result in reduced fitness of recombinants (Retchless and Lawrence, 2010). For other mechanisms of sexual isolation, also see Wiedenbeck and Cohan (2011). Regarding evidence for the Biological Species Concept provided by previous bacterial and archaeal studies, we note that two of these studies have provided no direct evidence that the groups of sequences studied have distinct ecological properties (Cadillo-Quiroz et al., 2012; Ellegaard et al., 2013), and rely primarily on the coexistence of sequence clusters as evidence that they utilize different resources. A third study by Shapiro et al looking at genetic exchange between two recently diverged populations of *Vibrio* (Shapiro et al., 2012) reported similar patterns of sub-clustering within the *Vibrio* populations (their Figure S2), and we predict that these sub-clusters would show ecological diversification if the authors were to test this. We predict each subgroup would represent an ecotype, subject to genomic sweeps. The fourth study (Rosen et al., 2015) claimed that there cannot be discrete ecotypes within the *Synechococcus* A and B' clades, owing to recombination, yet the existence of such discrete ecotypes has been amply demonstrated here and in many earlier papers (Becraft et al., 2015; Nowack et al., 2015; Olsen et al., 2015).

Most importantly, an argument for the Biological Species Concept should provide evidence that ecological diversification was prevented among groups hypothesized to recombine more frequently. This would require a search for ecological diversification among the close relatives recombining at the highest rates. While previous studies have not attempted to search for ecological diversity among closest relatives (within the major clades); this has been a principal aim of our study.

## CONCLUSION

In conclusion, it appears that we have found some of the most newly divergent ecotypes of hot spring *Synechococcus*. They do recombine, and recombination has not prevented their divergence, as had been suggested by Doolittle and Zhaxybayeva (2009). Because a reduction in recombination does not appear necessary for ecological divergence, and because ecological patterning of bacterial and archaeal diversity is common, the Biological Species Concept does not appear appropriate for bacterial and archaeal speciation. While recombination has not hindered speciation, ongoing genomic and metagenomic analyses have begun to reveal evidence suggesting that (i) horizontal genetic transfer and recombination have likely led to ecological diversification by introducing niche-transcending adaptations to new lineages (Gogarten et al., 2002; Lawrence, 2002; Doolittle and Zhaxybayeva, 2009; Wiedenbeck and Cohan, 2011; Olsen et al., 2015), and (ii) mutation and selection have also played a role in the evolutionary ecology of *Synechococcus* ecological species (Olsen et al., 2015). Sub-clustering within major clades predicted to be ecologically distinct has been observed across a variety of taxa and habits (Smith et al., 2006; Zinser et al., 2006; Hunt et al., 2008; Connor et al., 2010; Deneff et al., 2010; Mazard et al., 2012), suggesting that our observations may have general importance to the issue of species and speciation in bacteria and archaea. It is important to keep in mind that the molecular dimension of microbial species may be smaller than we have previously thought, and that it is important to understand theories underlying species and speciation.

## MATERIALS AND METHODS

Samples were collected on 2 October 2003 from the effluent channel of Mushroom Spring (44.5386°N, 110.7979°W), an alkaline siliceous hot spring in the Lower Geyser Basin of Yellowstone National Park, WY, at two temperatures, 60 and 65°C. DNA extraction and construction of bacterial artificial chromosome (BAC) clones and oligonucleotide probe screening to identify BACs containing a *Synechococcus* A/B lineage-specific 16S rRNA gene are described in the Supplemental Data Sheet Section I. DNA from parallel samples was used for analyses of the 16S rRNA and ITS region on the BACs (Ward et al., 2006) and PCR-amplified single protein-encoding loci (*rbsK*, *aroA*, and *apcAB*) (Melendrez et al., 2011), as well as for construction of small-insert (2–12 kb) metagenomic libraries (Bhaya et al., 2007; Klatt et al., 2011).

### Locus Selection

From one hundred genes that were upstream and downstream of the two unlinked 16S rRNA genes in the *Synechococcus* strain A and B' genomes, loci were selected based on the following characteristics: (i) presence in both genomes, (ii) range of distances from the 16S rRNA locus, (iii) high degree of nucleotide divergence between *Synechococcus* strain A and B' homologs, (iv) high average nucleotide divergence and variance of metagenomic homologs from *Synechococcus* strain A and B' homologs, (v) not under positive evolutionary selection (dN/dS values < 1) and (vi)

functionally useful for gene expression studies. In addition, loci adjacent to transposons or mobile elements were avoided due to the greater possibility of co-migration of adjacent loci. Loci used in this study are presented in Supplemental Data Tables 1, 2.

### PCR Amplification and Sequencing of BAC MLSA Loci

Primers for the separate amplification of *Synechococcus* A-like and B'-like BAC target genes (Supplemental Data Tables 1, 2) were designed and tested as described for amplification of *rbsK*, *aroA*, and *apcAB* gene segments by Melendrez et al. (2011), which also provides details of PCR conditions and gel-based size verification and purification of amplicons. Cycling conditions for the *dnaG*, *pcrA*, *ispE*, *sufB*, and *argD* genes were the same used for *aroA* and *rbsK* genes, and cycling conditions for the protein kinase (*PK*), *lepB*, and *accC* genes were the same as for the *apcAB* gene, except for the use of 40 cycles instead of 30 cycles. Cycling conditions for *hisF* and the conserved hypothetical protein (*CHP* [locus tag CYA\_2291]) gene were: an initial denaturing step at 94°C (2 min) followed by 20 cycles of 94°C (1 min), 60°C (1 min), and 72°C (1 min); then 20 cycles of 94°C (1 min), 55°C (1 min), and 72°C (1 min) with a final extension at 72°C for 10 min and storage at 4°C. BAC clones exhibiting no PCR product for any gene were amplified two more times (directly from the BAC clone sample) to increase confidence that the gene was absent.

### Sequencing

Purified PCR products were sequenced using the forward and reverse primers for each gene described in Supplemental Data Tables 1, 2 and the BigDye v.3.1 cycle sequencing kit (Applied Biosystems) at the University of Nevada-Reno Sequence Center (Reno, NV). The sequences have been submitted to GenBank, via the BankIt submission tool; Accession numbers: *pcrA*; KT425377-KT425447, *rbsK*; HQ662694-HQ662843, HQ187926-187996, KT425519-KT425589, and KT426096-KT426240, 16S rRNA; KT425590-KT425660, *PK* (protein kinase); KT425661-KT425805, *CHP* (conserved hypothetical protein); KT425806-KT425950, *lepB*; KT425951-KT426095, *aroA*; HQ187854-HQ187925, KT425447-KT425518, and KT426241-426385, *dnaG*; KT426386-KT426455, *hisF*; KT426456-KT426525.

### Sequence Alignment and Phylogenetic Analysis

Bidirectional sequence data for each locus were analyzed using Sequencher v.4.8. Sequence data were then analyzed with NCBI-BLAST nr/nt (Altschul et al., 1990) to determine whether the top match was with genomic homologs of *Synechococcus* strains JA-3-3Ab [accession: CP000239.1], JA-2-3B'a(2-13) [accession: CP000240.1], or neither. Sequences used in MLSA were concatenated using a custom perl script (available from J.M. Wood) and uploaded in MEGA4. Alignments were made using the ClustalW algorithm in the MEGA4 software (Tamura et al., 2007) or the MUSCLE (Edgar, 2004) algorithm implemented in Seaview (Gouy et al., 2010). The *Synechococcus* strain A and B' genomes were included as references (Bhaya et al.,

2007). MLSA including newly obtained isolates are described in Supplemental Data Sheet Section X. Alignments were analyzed using jModeltest2 (Darriba et al., 2012) to determine the best model fit for maximum likelihood tree construction. Maximum likelihood trees were constructed using PhyML (Guindon et al., 2010) as implemented in Seaview (Gouy et al., 2010) with aLRT support and edited using MEGA4 (Tamura et al., 2007) or Figtree (Rambaut, 2009). Estimates of average evolutionary divergence for single and multi-locus phylogenies were computed over all sequence pairs using the Maximum Composite Likelihood method in MEGA4 as previously described (Tamura et al., 2004, 2007; Melendrez et al., 2011).

## Ecotype Simulation and Demarcation

Concatenated and single-locus sequence alignments were analyzed using Ecotype Simulation to predict the number of PEs ( $n$ ), rates of periodic selection ( $\sigma$ ), ecotype formation ( $\omega$ ), and 95% confidence intervals (CI) for all parameters at the best precision match between observed and simulated data for that sequence dataset (between 1.25x and 2x). Ecotypes were manually demarcated conservatively as previously described (Cohan and Perry, 2007; Koeppl et al., 2008; Becraft et al., 2011; Melendrez et al., 2011) (<http://fcohan.web.wesleyan.edu/ecosim/>). Statistical tests were conducted using the R statistical package (<http://cran.r-project.org/>). Groups (rows) were defined as PEs that contained >5 sequences. The variables being tested were temperature (60 and 65°C) and vertical (80  $\mu$ m intervals) distributions. Significance level was set at 0.05.

## Multi-Locus and eBURST Analyses

Alignments for each gene used in MLSA were organized into groups that were 100% identical at the nucleotide level using Sequencher v 4.8. Allele types were assigned for each unique sequence and were used to generate allelic profiles; BACs with identical allelic profiles at all loci were assigned as unique sequence types (STs), as described in Supplemental Data Tables 8, 9, 19, 20. Allelic profiles and their unique ST designation were uploaded into eBURST (Feil et al., 2004; Spratt et al., 2004) and population snapshots were generated to view A-like and B'-like *Synechococcus* diversity. Clonal complexes (CC) were defined as a consensus group of BACs and at least 3 single-locus variants, as suggested (Feil et al., 2004). Population snapshots to visualize CCs with less stringent criteria were generated by defining CCs as a consensus group with at least 2 single-locus variants and/or allowing for double-locus variants to be included in the CC and are defined as sub-clonal complexes (see Supplemental Data Sheet Section XII).

## Single Nucleotide Polymorphism Analysis

SNPs were analyzed by comparing sequences of PE clade variants and single-locus variants with that of the dominant variant of the same PE clade or consensus group of the same CC (often the same as the dominant variant) using the Perl program, Pigeon (<https://github.com/sandain/pigeon>). Pigeon reads in the FASTA file and compares each nucleotide in the dominant variant to the corresponding nucleotide in each PE variant

(or single-locus variant), locating and reporting the position of SNPs.

## Detection of Recombination Signals

Five methods were utilized to detect recombination in single-gene and concatenated datasets; (i) outlier detection on phylogeny followed by BLAST (<http://blast.ncbi.nlm.nih.gov/Blast.cgi>), (ii) RDP version 4 (RDP4) (Martin et al., 2015), (iii) Clonal Frame version 1.1 (Didelot and Falush, 2007), (iv) SNP analysis (PIGEON; <https://github.com/sandain/pigeon>), and (v) LDHAT v2.2 (McVean et al., 2002).

- (i) BLAST. Phylogenies were manually inspected for long branch lengths. Those STs/clones which fell on long branch lengths were analyzed using BLAST (bl2seq program) against isolate genomes (CP000239.1 and CP000240.1) to ensure that all genes within the concatenation had the highest match to the appropriate isolate genome as determined by 16S rRNA analysis (also see Supplemental Data Sheet Section VI).
- (ii) RDP identifies recombinants in either multi-locus or single-gene sequence datasets. All loci for A-like and B'-like *Synechococcus* populations were tested for putative recombination events using Recombination Detection Program, version 4 (RDP4) (Martin et al., 2015). The loci were tested individually and as concatenated sequences. In the RDP suite of programs a number of different methods are implemented. The methods used for recombination detection in this study included the RDP method (Martin et al., 2005), GENECONV (Sawyer, 1989), Maximum Chi Square (Smith, 1992; Posada and Crandall, 2001), Chimera (Posada and Crandall, 2001), Sister Scanning (Siscan) (Gibbs et al., 2000), 3SEQ (Boni et al., 2007), and Likelihood Assisted Recombination Detection (LARD), which constitute some of the most powerful methods currently available (RDP4 manual, Martin et al., 2005). The general settings within RDP4 were as follows: the highest acceptable  $p$ -value was set to 0.05 with Bonferroni corrections. For the individual methods default parameters were used for all methods with the following exceptions:
 

In RDP, the window size was set to 30 as recommended (RDP4 Instruction Manual, available at <http://web.cbio.uct.ac.za/~darren/RDP4Manual.pdf>). In MaxChi and Chimera the 'variable window size' was used. In Siscan the window size was set to 200 bp with a step size of 20.

Recombination signals were considered present if they could be detected by at least 3 methods within the RDP4 package at significant  $p$ -values as suggested (RDP4 manual).
- (iii) Clonal Frame identifies evidence of recombination in multi-locus sequence datasets (Didelot and Falush, 2007). Extended multi-FASTA formatted alignments (XMFA) were generated using the MAUVE program (Darling et al., 2004, 2007) and given file extensions of.dat. DAT files were loaded into Clonal Frame and analyzed using default settings with 1,000,000 iterations after burn in, 250,000 burnin,

sampling every 100 iterations and verbose mode (-v,-x,-y,-z options). OUT files with phylogenies and statistics (mutation events, recombination events, rho/theta and r/m) were visualized using the *cfgui.bat* program included in the Clonal Frame installation. Recombination events identified along branches are noted with closed stars for MLSA datasets in **Figure 2A** and Supplemental Data Presentation Figure 10.

- (iv) SNP analysis. The patterning of PE variant and single-locus variant SNPs against the dominant variant sequence was also considered in interpreting possible evidence of recombination events (method described above). Recombination events inferred by SNP analysis are noted with open stars on branches for MLSA datasets in **Figure 2A** and Supplemental Data Presentation Figure 10.
- (v) LDHAT estimates a per-locus population recombination parameter (R), the average per-site population mutation rate (Watterson's  $\theta$ ), average pairwise distance (avePWD) and variance within the average pairwise difference (varPWD). These were determined using three methods within the LDHAT v2.2a package (McVean et al., 2002); the composite-likelihood method, Rmin calculation and Wakeley's moment method (all implemented using *convert*, pairwise and associated lookup tables generated either from precompiled tables included with package distribution or generated directly from the sequence data). All analyses were run using default parameters. The recombination rate calculated by LDHAT assumes a constant recombination rate over the region and a gene conversion model with either a finite sites model (composite likelihood) or infinite sites model (Rmin calculation). We note that the linkage of our loci caused by sampling a portion of the genome as well as sequencing only a portion of each gene may possibly cause underestimation or large range of recombination ratios if recombined segments tend to span several genes or if the recombined segment was larger than the amplified gene segment thereby capturing one 'breakpoint' but not the other (see Supplemental Data Sheet Section VI).

## Pyrosequencing

PCR primers and protocols described by Melendrez et al. (2011) or in Supplemental Data Table 1 were used to amplify *rbsK* sequences from Mushroom Spring samples collected at ~63–65°C and sectioned along vertical gradients (~80  $\mu$ m intervals using a cryotome). Samples were collected on 13 and 14 September 2008 and DNA was extracted as described in Becraft et al. (2011). Barcoding and Ti454-sequencing were completed at the J. Craig Venter Institute according to the GS FLX Titanium Series Rapid Library Preparation Method. DNA was

sheared using the Covaris S2 System, and qPCR was used to accurately estimate the number of molecules needed for emPCR. BAC clone MLSA sequences were trimmed at the 5' and 3' ends to match the average sequence length, which collapsed some SNP variation contained in the *rbsK* single-locus analysis and caused a decrease in molecular resolution. Homopolymer inserts were removed by aligning sequences to the *rbsK* reading frame of genomes from the A or B' *Synechococcus* isolates. High-frequency sequences (sequences totaling  $\geq 50$  identical copies in all combined samples) were then identified and PEs were demarcated from high-frequency sequences using Ecotype Simulation. Population percentages based on high-frequency sequences that matched STs of a single MLSA PE were calculated as described in Becraft et al. (2015). Sequence data for *rbsK* was deposited into the MG-RAST version 4 database (<https://metagenomics.anl.gov/>) under accession numbers 4642340.3-4642367.3.

## FUNDING

This research was supported by the National Science Foundation Frontiers in Integrative Biology Research Program (EF-0328698), the National Aeronautics and Space Administration Exobiology Program (NAG5-8807 and NX09AM87G), and the U.S. Department of Energy (DOE), Office of Biological and Environmental Research (BER), as part of BER's Genomic Science Program (GSP). This contribution originates from the GSP Foundational Scientific Focus Area (FSFA) at the Pacific Northwest National Laboratory (PNNL), contract no. 112443. It was also supported by Montana Agricultural Experiment Station project 911352.

## ACKNOWLEDGMENTS

We appreciate the assistance from National Park Service personnel at Yellowstone National Park. Special thanks to Darren Martin from the University of Cape Town, South Africa for assistance with the RDP4 software suite, Dr. Timothy McDermott from Montana State University, USA for use of equipment required for radioactive probing of BAC clones and the laboratory of Dr. Al Jesaitis from Montana State University, USA for use of the phosphoimager to identify BACs containing 16S rRNA loci.

## SUPPLEMENTAL DATA

The Supplemental Data for this article can be found online at: <http://journal.frontiersin.org/article/10.3389/fmicb.2015.01540>

## REFERENCES

- Allewalt, J. P., Bateson, M. M., Revsbech, N. P., Slack, K., and Ward, D. M. (2006). Effect of temperature and light on growth of and photosynthesis by *Synechococcus* isolates typical of those predominating in the octopus spring microbial mat community of Yellowstone National Park. *Appl. Environ. Microb.* 72, 544–550. doi: 10.1128/AEM.72.1.544-550.2006
- Altschul, S. F., Gish, W., Miller, W., Myers, E. W., and Lipman, D. J. (1990). Basic local alignment search tool. *J. Mol. Biol.* 215, 403–410. doi: 10.1016/S0022-2836(05)80360-2

- Bantinaki, E., Kassen, R., Knight, C. G., Robinson, Z., Spiers, A. J., and Rainey, P. B. (2007). Adaptive divergence in experimental populations of *Pseudomonas fluorescens*. III. Mutational origins of wrinkly spreader diversity. *Genetics* 176, 441–453. doi: 10.1534/genetics.106.069906
- Becraft, E. D., Cohan, F. M., Kühl, M., Jensen, S. I., and Ward, D. M. (2011). Fine-scale distribution patterns of *Synechococcus* ecological diversity in microbial mats of Mushroom Spring, Yellowstone National Park. *Appl. Environ. Microb.* 77, 7689–7697. doi: 10.1128/AEM.05927-11
- Becraft, E. D., Wood, J. M., Rusch, D. B., Kühl, M., Jensen, S. I., Bryant, D. A., et al. (2015). The molecular dimension of microbial species: 1. Ecological distinctions among, and homogeneity within, putative ecotypes of *Synechococcus* inhabiting the cyanobacterial mat of Mushroom Spring, Yellowstone National Park. *Front. Microbiol.* 6:590. doi: 10.3389/fmicb.2015.00590
- Bhaya, D., Grossman, A. R., Steunou, A. S., Khuri, N., Cohan, F. M., Hamamura, N., et al. (2007). Population level functional diversity in a microbial community revealed by comparative genomic and metagenomic analyses. *ISME J.* 1, 703–713. doi: 10.1038/ismej.2007.46
- Boni, M. F., Posada, D., and Feldman, M. W. (2007). An exact nonparametric method for inferring mosaic structure in sequence triplets. *Genetics* 176, 1035–1047. doi: 10.1534/genetics.106.068874
- Cadillo-Quiroz, H., Didelot, X., Held, N. L., Herrera, A., Darling, A., Reno, M. L., et al. (2012). Patterns of gene flow define species of thermophilic Archaea. *PLoS Biol.* 10:e1001265. doi: 10.1371/journal.pbio.1001265
- Cesarini, S., Bevivino, A., Tabacchioni, S., Chiarini, L., and Dalmastrì, C. (2009). RecA gene sequence and Multilocus Sequence Typing for species-level resolution of *Burkholderia cepacia* complex isolates. *Lett. Appl. Microbiol.* 49, 580–588. doi: 10.1111/j.1472-765X.2009.02709.x
- Cohan, F. M. (2013). “Species,” in *Brenner’s Encyclopedia of Genetics, 2nd Edn.*, eds S. Maloy and K. Hughes (Amsterdam: Elsevier), 506–511.
- Cohan, F. M. (2016). “Prokaryotic species concepts,” in *Encyclopedia of Evolutionary Biology*, ed R. M. Kliman (Oxford: Elsevier).
- Cohan, F. M., and Perry, E. B. (2007). A systematics for discovering the fundamental units of bacterial diversity. *Curr. Biol.* 17, R373–R86. doi: 10.1016/j.cub.2007.03.032
- Connor, N., Sikorski, J., Rooney, A. P., Kopac, S., Koeppl, A. F., Burger, A., et al. (2010). Ecology of speciation in the genus *Bacillus*. *Appl. Environ. Microb.* 76, 1349–1358. doi: 10.1128/AEM.01988-09
- Coyne, J. A., and Orr, H. A. (2004). *Speciation*. Sunderland: Sinauer Associates.
- Darling, A. C., Mau, B., Blattner, F. R., and Perna, N. T. (2004). Mauve: multiple alignment of conserved genomic sequence with rearrangements. *Genome Res.* 14, 1394–1403. doi: 10.1101/gr.2289704
- Darling, A. E., Treangen, T. J., Messguier, X., and Perna, N. T. (2007). Analyzing patterns of microbial evolution using the mauve genome alignment system. *Methods Mol. Biol.* 396, 135–152. doi: 10.1007/978-1-59745-515-2\_10
- Darriba, D., Taboada, G. L., Doallo, R., and Posada, D. (2012). jModelTest 2: more models, new heuristics and parallel computing. *Nat. Methods.* 9, 772. doi: 10.1038/nmeth.2109
- Denef, V. J., Kalnejais, L. H., Mueller, R. S., Wilmes, P., Baker, B. J., Thomas, B. C., et al. (2010). Proteogenomic basis for ecological divergence of closely related bacteria in natural acidophilic microbial communities. *Proc. Natl. Acad. Sci. U.S.A.* 107, 2383–2390. doi: 10.1073/pnas.0907041107
- Didelot, X., and Falush, D. (2007). Inference of bacterial microevolution using multilocus sequence data. *Genetics* 175, 1251–1266. doi: 10.1534/genetics.106.063305
- Didelot, X., and Maiden, M. C. (2010). Impact of recombination on bacterial evolution. *Trends Microbiol.* 18, 315–322. doi: 10.1016/j.tim.2010.04.002
- Dobzhansky, T. (1951). *Genetics and the Origin of Species, 3rd Edn.* New York, NY: Columbia University Press.
- Doolittle, W. F., and Zhaxybayeva, O. (2009). On the origin of prokaryotic species. *Genome Res.* 19, 744–756. doi: 10.1101/gr.086645.108
- Drake, J. W. (2009). Avoiding dangerous missense: thermophiles display especially low mutation rates. *PLoS Genet.* 5:e1000520. doi: 10.1371/journal.pgen.1000520
- Edgar, R. C. (2004). MUSCLE: a multiple sequence alignment method with reduced time and space complexity. *BMC Bioinformatics* 5:113. doi: 10.1186/1471-2105-5-113
- Ellegaard, K. M., Klasson, L., Naslund, K., Bourtzis, K., and Andersson, S. G. (2013). Comparative genomics of *Wolbachia* and the bacterial species concept. *PLoS Genet.* 9:e1003381. doi: 10.1371/journal.pgen.1003381
- Eren, A. M., Maignien, L., Sul, W. J., Murphy, L. G., Grim, S. L., Morrison, H. G., et al. (2013). Oligotyping: differentiating between closely related microbial taxa using 16S rRNA gene data. *Methods Ecol. Evol.* 4, 1111–1119. doi: 10.1111/2041-210X.12114
- Feil, E. J., Cooper, J. E., Grundmann, H., Robinson, D. A., Enright, M. C., Berendt, T., et al. (2003). How clonal is *Staphylococcus aureus*? *J. Bacteriol.* 185, 3307–3316. doi: 10.1128/JB.185.11.3307-3316.2003
- Feil, E. J., Enright, M. C., and Spratt, B. G. (2000a). Estimating the relative contributions of mutation and recombination to clonal diversification: a comparison between *Neisseria meningitidis* and *Streptococcus pneumoniae*. *Res. Microbiol.* 151, 465–469. doi: 10.1016/S0923-2508(00)00168-6
- Feil, E. J., Holmes, E. C., Bessen, D. E., Chan, M. S., Day, N. P. J., Enright, M. C., et al. (2001). Recombination within natural populations of pathogenic bacteria: short-term empirical estimates and long-term phylogenetic consequences. *Proc. Natl. Acad. Sci. U.S.A.* 98, 182–187. doi: 10.1073/pnas.98.1.182
- Feil, E. J., Li, B. C., Aanensen, D. M., Hanage, W. P., and Spratt, B. G. (2004). eBURST: Inferring patterns of evolutionary descent among clusters of related bacterial genotypes from multilocus sequence typing data. *J. Bacteriol.* 186, 1518–1530. doi: 10.1128/JB.186.5.1518-1530.2004
- Feil, E. J., Maiden, M. C. J., Achtman, M., and Spratt, B. G. (1999). The relative contributions of recombination and mutation to the divergence of clones of *Neisseria meningitidis*. *Mol. Biol. Evol.* 16, 1496–1502. doi: 10.1093/oxfordjournals.molbev.a026061
- Feil, E. J., Smith, J. M., Enright, M. C., and Spratt, B. G. (2000b). Estimating recombinational parameters in *Streptococcus pneumoniae* from multilocus sequence typing data. *Genetics* 154, 1439–1450. Available online at: <http://www.genetics.org/content/154/4/1439.long>
- Feil, E. J., and Spratt, B. G. (2001). Recombination and the population structures of bacterial pathogens. *Annu. Rev. Microbiol.* 55, 561–590. doi: 10.1146/annurev.micro.55.1.561
- Ferris, M. J., Kühl, M., Wieland, A., and Ward, D. M. (2003). Cyanobacterial ecotypes in different optical microenvironments of a 68 degrees C hot spring mat community revealed by 16S-23S rRNA internal transcribed spacer region variation. *Appl. Environ. Microb.* 69, 2893–2898. doi: 10.1128/AEM.69.5.2893-2898.2003
- Ferris, M. J., and Ward, D. M. (1997). Seasonal distributions of dominant 16S rRNA-defined populations in a hot spring microbial mat examined by denaturing gradient gel electrophoresis. *Appl. Environ. Microb.* 63, 1375–1381.
- Gibbs, M. J., Armstrong, J. S., and Gibbs, A. J. (2000). Sister-Scanning: a monte carlo procedure for assessing signals in recombinant sequences. *Bioinformatics* 16, 573–582. doi: 10.1093/bioinformatics/16.7.573
- Gogarten, J. P., Doolittle, W. F., and Lawrence, J. G. (2002). Prokaryotic evolution in light of gene transfer. *Mol. Biol. Evol.* 19, 2226–2238. doi: 10.1093/oxfordjournals.molbev.a004046
- Gouy, M., Guindon, S., and Gascuel, O. (2010). SeaView version 4: a multiplatform graphical user interface for sequence alignment and phylogenetic tree building. *Mol. Biol. Evol.* 27, 221–224. doi: 10.1093/molbev/msp259
- Guindon, S., Dufayard, J. F., Lefort, V., Anisimova, M., Hordijk, W., and Gascuel, O. (2010). New algorithms and methods to estimate maximum-likelihood phylogenies: assessing the performance of PhyML 3.0. *Syst. Biol.* 59, 307–321. doi: 10.1093/sysbio/syq010
- Haldane, J. B. S. (1932). *The Causes of Evolution*. London: Longmans, Green and Co.
- Hanage, W. P., Fraser, C., and Spratt, B. G. (2005). Fuzzy species among recombinogenic bacteria. *BMC Biol.* 3:6. doi: 10.1186/1741-7007-3-6
- Hunt, D. E., David, L. A., Gevers, D., Preheim, S. P., Alm, E. J., and Polz, M. F. (2008). Resource partitioning and sympatric differentiation among closely related bacterioplankton. *Science* 320, 1081–1085. doi: 10.1126/science.1157890
- Kashtan, N., Roggensack, S. E., Rodrigue, S., Thompson, J. W., Biller, S. J., Coe, A., et al. (2014). Single-cell genomics reveals hundreds of coexisting subpopulations in wild *Prochlorococcus*. *Science* 344, 416–420. doi: 10.1126/science.1248575
- Klatt, C. G., Wood, J. M., Rusch, D. B., Bateson, M. M., Hamamura, N., Heidelberg, J. F., et al. (2011). Community ecology of hot spring cyanobacterial mats:

- predominant populations and their functional potential. *ISME J.* 5, 1262–1278. doi: 10.1038/ismej.2011.73
- Koepfel, A., Perry, E. B., Sikorski, J., Krizanc, D., Warner, A., Ward, D. M., et al. (2008). Identifying the fundamental units of bacterial diversity: a paradigm shift to incorporate ecology into bacterial systematics. *Proc. Natl. Acad. Sci. U.S.A.* 105, 2504–2509. doi: 10.1073/pnas.0712205105
- Kopac, S., and Cohan, F. M. (2011). “A theory-based pragmatism for discovering and classifying newly divergent bacterial species,” in *Genetics and Evolution of Infectious Diseases*, ed M. Tibayrenc (London: Elsevier), 21–41.
- Kopac, S., Wang, Z., Wiedenbeck, J., Sherry, J., Wu, M., and Cohan, F. M. (2014). Genomic heterogeneity and ecological speciation within one subspecies of *Bacillus subtilis*. *Appl. Environ. Microb.* 80, 4842–4853. doi: 10.1128/AEM.00576-14
- Lawrence, J. G. (2002). Gene transfer in bacteria: speciation without species? *Theor. Popul. Biol.* 61, 449–460. doi: 10.1006/tpbi.2002.1587
- Levin, B. R., and Bergstrom, C. T. (2000). Bacteria are different: observations, interpretations, speculations, and opinions about the mechanisms of adaptive evolution in prokaryotes. *Proc. Natl. Acad. Sci. U.S.A.* 97, 6981–6985. doi: 10.1073/pnas.97.13.6981
- Liles, M. R., Williamson, L. L., Rodbumer, J., Torsvik, V., Goodman, R. M., and Handelsman, J. (2008). Recovery, purification, and cloning of high-molecular-weight DNA from soil microorganisms. *Appl. Environ. Microb.* 74, 3302–3305. doi: 10.1128/AEM.02630-07
- Maiden, M. C. J., Bygraves, J. A., Feil, E., Morelli, G., Russell, J. E., Urwin, R., et al. (1998). Multilocus sequence typing: a portable approach to the identification of clones within populations of pathogenic microorganisms. *Proc. Natl. Acad. Sci. U.S.A.* 95, 3140–3145. doi: 10.1073/pnas.95.6.3140
- Majewski, J., and Cohan, F. M. (1999). DNA sequence similarity requirements for interspecific recombination in *Bacillus*. *Genetics* 153, 1525–1533.
- Mallet, J. (2008). Hybridization, ecological races and the nature of species: empirical evidence for the ease of speciation. *Philos. Trans. R. Soc. Lond. B. Biol. Sci.* 363, 2971–2986. doi: 10.1098/rstb.2008.0081
- Martin, D. P., Murrell, B., Golden, M., Khoosal, A., and Muhire, B. (2015). RDP4: detection and analysis of recombination patterns in virus genomes. *Virus Evolution*. 1:vev003. doi: 10.1093/ve/vev003
- Martin, D. P., Williamson, C., and Posada, D. (2005). RDP2: recombination detection and analysis from sequence alignments. *Bioinformatics* 21, 260–262. doi: 10.1093/bioinformatics/bth490
- Mayr, E. (1942). *Systematics and the Origin of Species from the Viewpoint of a Zoologist*. New York, NY: Columbia University.
- Mayr, E. (1963). *Animal Species and Evolution*. Cambridge, MA: Belknap Press of Harvard University Press.
- Mazard, S., Ostrowski, M., Partensky, F., and Scanlan, D. J. (2012). Multi-locus sequence analysis, taxonomic resolution and biogeography of marine *Synechococcus*. *Environ. Microbiol.* 14, 372–386. doi: 10.1111/j.1462-2920.2011.02514.x
- McVean, G. A. T., Myers, S. R., Hunt, S., Deloukas, P., Bentley, D. R., and Donnelly, P. (2004). The fine-scale structure of recombination rate variation in the human genome. *Science* 304, 581–584. doi: 10.1126/science.1092500
- McVean, G., Awadalla, P., and Fearnhead, P. (2002). A coalescent-based method for detecting and estimating recombination from gene sequences. *Genetics* 160, 1231–1241. Available online at: <http://www.genetics.org/content/160/3/1231.long>
- Melendrez, M. C., Lange, R. K., Cohan, F. M., and Ward, D. M. (2011). Influence of molecular resolution on sequence-based discovery of ecological diversity among *Synechococcus* populations in an alkaline siliceous hot spring microbial mat. *Appl. Environ. Microb.* 77, 1359–1367. doi: 10.1128/AEM.02032-10
- Nowack, S., Olsen, M. T., Schaible, G., Becraft, E. D., Shen, G., Klapper, I., et al. (2015). The molecular dimension of microbial species: 2. *Synechococcus* isolates representative of putative ecotypes inhabiting different depths in the Mushroom Spring microbial mat exhibit different adaptive and acclimative responses to light. *Front. Microbiol.* 6:626. doi: 10.3389/fmicb.2015.00626
- Olsen, M. T., Nowack, S., Wood, J. M., Becraft, E. D., LaButti, K., Lipzen, A., et al. (2015). The molecular dimension of microbial species: 3. Comparative genomics of *Synechococcus* isolates with different light responses and *in situ* diel transcription patterns of associated putative ecotypes in the Mushroom Spring microbial mat. *Front. Microbiol.* 6:604. doi: 10.3389/fmicb.2015.00604
- Papke, R. T., Koenig, J. E., Rodriguez-Valera, F., and Doolittle, W. F. (2004). Frequent recombination in a saltern population of *Halorubrum*. *Science* 306, 1928–1929. doi: 10.1126/science.1103289
- Papke, R. T., Zhaxybayeva, O., Feil, E. J., Sommerfeld, K., Muise, D., and Doolittle, W. F. (2007). Searching for species in haloarchaea. *Proc. Natl. Acad. Sci. U.S.A.* 104, 14092–14097. doi: 10.1073/pnas.0706358104
- Polz, M. F., Alm, E. J., and Hanage, W. P. (2013). Horizontal gene transfer and the evolution of bacterial and archaeal population structure. *Trends Genet.* 29, 170–175. doi: 10.1016/j.tig.2012.12.006
- Posada, D., and Crandall, K. A. (2001). Evaluation of methods for detecting recombination from DNA sequences: computer simulations. *Proc. Natl. Acad. Sci. U.S.A.* 98, 13757–13762. doi: 10.1073/pnas.241370698
- Rambaut, A. (2009). *FigTree v1.3.1: Tree Figure Drawing Tool*. Available online at: <http://treebioedacuk/software/figtree/>
- Ramsing, N. B., Ferris, M. J., and Ward, D. M. (2000). Highly ordered vertical structure of *Synechococcus* populations within the one-millimeter-thick photic zone of a hot spring cyanobacterial mat. *Appl. Environ. Microb.* 66, 1038–1049. doi: 10.1128/AEM.66.3.1038-1049.2000
- Retchless, A. C., and Lawrence, J. G. (2010). Phylogenetic incongruence arising from fragmented speciation in enteric bacteria. *Proc. Natl. Acad. Sci. U.S.A.* 107, 11453–11458. doi: 10.1073/pnas.1001291107
- Rosen, M. J., Davison, M., Bhaya, D., and Fisher, D. S. (2015). Microbial diversity. Fine-scale diversity and extensive recombination in a quasisexual bacterial population occupying a broad niche. *Science* 348, 1019–1023. doi: 10.1126/science.aaa4456
- Rusch, D. B., Halpern, A. L., Sutton, G., Heidelberg, K. B., Williamson, S., Yooseph, S., et al. (2007). The sorcerer II global ocean sampling expedition: Northwest Atlantic through Eastern Tropical Pacific. *PLoS Biol.* 5, 398–431. doi: 10.1371/journal.pbio.0050077
- Salerno, A., Delétolle, A., Lefevre, M., Ciznar, I., Krovacek, K., Grimont, P., et al. (2007). Recombining population structure of *Plesiomonas shigelloides* (Enterobacteriaceae) revealed by multilocus sequence typing. *J. Bacteriol.* 189, 7808–7818. doi: 10.1128/JB.00796-07
- Sawyer, S. (1989). Statistical tests for detecting gene conversion. *Mol. Biol. Evol.* 6, 526–538.
- Schluter, D. (2009). Evidence for ecological speciation and its alternative. *Science* 323, 737–741. doi: 10.1126/science.1160006
- Shapiro, B. J., Friedman, J., Cordero, O. X., Preheim, S. P., Timberlake, S. C., Szabó, G., et al. (2012). Population genomics of early events in the ecological differentiation of bacteria. *Science* 336, 48–51. doi: 10.1126/science.1218198
- Shizuya, H., Birren, B., Kim, U. J., Mancino, V., Slepak, T., Tachiiri, Y., et al. (1992). Cloning and stable maintenance of 300-kilobase-pair fragments of human DNA in *Escherichia coli* using an F-factor-based vector. *Proc. Natl. Acad. Sci. U.S.A.* 89, 8794–8797. doi: 10.1073/pnas.89.18.8794
- Smith, J. M. (1992). Analyzing the mosaic structure of genes. *J. Mol. Evol.* 34, 126–129. doi: 10.1007/BF00182389
- Smith, N. H., Gordon, S. V., de la Rúa-Domenech, R., Clifton-Hadley, R. S., and Hewinson, R. G. (2006). Bottlenecks and broomsticks: the molecular evolution of *Mycobacterium bovis*. *Nat. Rev. Microbiol.* 4, 670–681. doi: 10.1038/nrmicro1472
- Spratt, B. G., Hanage, W. P., Li, B., Aanensen, D. M., and Feil, E. J. (2004). Displaying the relatedness among isolates of bacterial species - the eBURST approach. *Fems Microbiol. Lett.* 241, 129–134. doi: 10.1016/j.femsle.2004.11.015
- Tamura, K., Dudley, J., Nei, M., and Kumar, S. (2007). MEGA4: molecular evolutionary genetics analysis (MEGA) software version 4.0. *Mol. Biol. Evol.* 24, 1596–1599. doi: 10.1093/molbev/msm092
- Tamura, K., Nei, M., and Kumar, S. (2004). Prospects for inferring very large phylogenies by using the neighbor-joining method. *Proc. Natl. Acad. Sci. U.S.A.* 101, 11030–11035. doi: 10.1073/pnas.0404206101
- Tao, Q., Wang, A., and Zhang, H. B. (2002). One large-insert plant-transformation-competent BIBAC library and three BAC libraries of Japonica rice for genome research in rice and other grasses. *Theor. Appl. Genet.* 105, 1058–1066. doi: 10.1007/s00122-002-1057-3
- Van Valen, L. (1976). Ecological species, multispecies, and oaks. *Taxon* 25, 233–239. doi: 10.2307/1219444
- Vitorino, L. R., Margos, G., Feil, E. J., Collares-Pereira, M., Zé-Zé, L., and Kurtenbach, K. (2008). Fine-scale phylogeographic structure of borrelia

- lusitaniae revealed by multilocus sequence typing. *PLoS ONE* 3:e4002. doi: 10.1371/journal.pone.0004002
- Vos, M. (2011). A species concept for bacteria based on adaptive divergence. *Trends Microbiol.* 19, 1–7. doi: 10.1016/j.tim.2010.10.003
- Vos, M., and Didelot, X. (2009). A comparison of homologous recombination rates in bacteria and archaea. *Isme J.* 3, 199–208. doi: 10.1038/ismej.2008.93
- Ward, D. M., Bateson, M. M., Ferris, M. J., Köhl, M., Wieland, A., Koeppl, A., et al. (2006). Cyanobacterial ecotypes in the microbial mat community of Mushroom Spring (Yellowstone National Park, Wyoming) as species-like units linking microbial community composition, structure and function. *Philos. Trans. R. Soc. Lond. B. Biol. Sci.* 361, 1997–2008. doi: 10.1098/rstb.2006.1919
- Ward, D. M., Ferris, M. J., Nold, S. C., and Bateson, M. M. (1998). A natural view of microbial biodiversity within hot spring cyanobacterial mat communities. *Microbiol. Mol. Biol. Rev.* 62, 1353–1370.
- Whitaker, R. J., Grogan, D. W., and Taylor, J. W. (2005). Recombination shapes the natural population structure of the hyperthermophilic archaeon *Sulfolobus islandicus*. *Mol. Biol. Evol.* 22, 2354–2361. doi: 10.1093/molbev/msi233
- Wiedenbeck, J., and Cohan, F. M. (2011). Origins of bacterial diversity through horizontal genetic transfer and adaptation to new ecological niches. *FEMS Microbiol. Rev.* 35, 957–976. doi: 10.1111/j.1574-6976.2011.00292.x
- Zinser, E. R., Coe, A., Johnson, Z. I., Martiny, A. C., Fuller, N. J., Scanlan, D. J., et al. (2006). *Prochlorococcus* ecotype abundances in the North Atlantic Ocean as revealed by an improved quantitative PCR method. *Appl. Environ. Microb.* 72, 723–732. doi: 10.1128/AEM.72.1.723-732.2006

**Conflict of Interest Statement:** The authors declare that the research was conducted in the absence of any commercial or financial relationships that could be construed as a potential conflict of interest.

Copyright © 2016 Melendrez, Becraft, Wood, Olsen, Bryant, Heidelberg, Rusch, Cohan and Ward. This is an open-access article distributed under the terms of the Creative Commons Attribution License (CC BY). The use, distribution or reproduction in other forums is permitted, provided the original author(s) or licensor are credited and that the original publication in this journal is cited, in accordance with accepted academic practice. No use, distribution or reproduction is permitted which does not comply with these terms.



# Characterization of a single mutation in TraQ in a strain of *Escherichia coli* partially resistant to Q $\beta$ infection

Akiko Kashiwagi\*, Hikari Kitamura and Fumie Sano Tsushima

Faculty of Agriculture and Life Science, Hirosaki University, Hirosaki, Japan

## Edited by:

Hiroyuki Futamata, Shizuoka University, Japan

## Reviewed by:

Evelien M. Adriaenssens, University of Pretoria, South Africa

Hailan Piao, Washington State University in Tri-Cities, USA

## \*Correspondence:

Akiko Kashiwagi, Faculty of Agriculture and Life Science, Hirosaki University, 3 Bunkyo-cho, Hirosaki, Aomori 036-8561, Japan  
e-mail: kashi\_a1@cc.hirosaki-u.ac.jp

Bacteria and virulent bacteriophages are in a prey–predator relationship. Experimental models under simplified conditions with the presence of bacteria and bacteriophages have been used to elucidate the mechanisms that have enabled both prey and predator to coexist over long periods. In experimental coevolution conducted with *Escherichia coli* and the virulent RNA bacteriophage Q $\beta$  in serial transfer, both coexisted for at least for 54 days, during which time they continued to change genetically and phenotypically. By day 16, an *E. coli* strain partially resistant to Q $\beta$  appeared and caused an approximately 10<sup>4</sup>-fold decrease in Q $\beta$  amplification. Whole-genome analysis of this strain suggested that a single mutation in TraQ was responsible for the partially resistant phenotype. TraQ interacts with propilin, encoded by the *traA* gene and a precursor of pilin, which is a component of the F pilus. The present study was performed to elucidate the mechanism underlying the coexistence of *E. coli* and Q $\beta$  by investigating how a mutation in TraQ altered the physiological state of *E. coli*, and thus the amplification of Q $\beta$ . Overexpression of wild-type TraQ in the partially resistant *E. coli* strain resulted in recovery of both TraA protein content, including propilin and pilin, and Q $\beta$  amplification to levels comparable to those observed in the susceptible strain. Intriguingly, overexpression of the mutant TraQ in the partially resistant strains also increased the levels of TraA protein and Q $\beta$  amplification, but these increases were smaller than those observed in the wild-type strain or the partially resistant strain expressing wild-type TraQ. The results of this study represent an example of how *E. coli* can become partially resistant to RNA bacteriophage infection via changes in a protein involved in maturation of a receptor rather than in the receptor itself and of how *E. coli* can stably coexist with virulent RNA bacteriophages.

**Keywords:** coevolution, prey–predator, experimental evolution, virulent phage, partial resistance

## INTRODUCTION

There have long been ecological and theoretical investigations regarding why predators do not eradicate their prey (Murdoch and Oaten, 1975; Anderson and May, 1978; Alexander, 1981; Berryman, 1992; Abrams, 2000; Briggs and Hoopes, 2004; Pettorelli et al., 2011; Brockhurst and Koskella, 2013). Bacteria and bacteriophages have been used as model systems of prey–predator interactions to elucidate the fundamental mechanism underlying this issue. Due to their short generation time, large population size, and ease of analyzing phenotypic and genomic changes, theoretical and experimental evolutionary research have been conducted extensively using these systems (Campbell, 1961; Levin et al., 1977; Lenski and Levin, 1985; Lenski, 1988; Schrag and Mittler, 1995; Sasaki, 2000; Paterson et al., 2010; Dennehy, 2012; Brockhurst and Koskella, 2013; Bull et al., 2014). The stable coexistence of bacteria and virulent phages has been widely observed in experimental evolution (Horne, 1970; Chao et al., 1977; Levin et al., 1977; Buckling and Rainey, 2002; Lythgoe and Chao, 2003; Kerr et al., 2006; Kashiwagi and Yomo, 2011; Marston et al., 2012), even though virulent phages kill the host bacteria to release progeny phages.

The existence of refuges for sensitive bacteria or the occurrence of endless arms races were suggested to be necessary to

explain the coexistence of bacteria and bacteriophages (Chao et al., 1977; Lenski, 1988; Schrag and Mittler, 1995; Brockhurst et al., 2006). The numerical refuge in which density-dependent protection of susceptible cells from over-predation (Chao et al., 1977), spatial refuges such as wall populations on flasks in continuous culture or solid media used in serial passage (Chao et al., 1977; Lenski, 1988; Schrag and Mittler, 1995), and physiological refuges in which cells become transiently resistant or susceptible have been discussed (Lenski, 1988). In most of these previous studies, DNA bacteriophages, such as T2, T5, T7,  $\lambda$ , and  $\Phi$ 2, were used (Bohannan and Lenski, 2000; Buckling and Rainey, 2002; Dennehy, 2012). Although a great deal of knowledge has been accumulated regarding DNA bacteriophages, little is known about RNA bacteriophages in terms of stable coexistence.

In our previous study, *Escherichia coli* and the lytic RNA bacteriophage Q $\beta$  (Q $\beta$ ) were shown to coevolve for at least 54 days, equivalent to 165 generations, under conditions of serial passage with shaking (Kashiwagi and Yomo, 2011). Q $\beta$  is a bacteriophage with a single-stranded RNA genome that specifically infects and lyses *E. coli* cells to release progeny phages (Van Duin and Tsareva, 2006). Phenotypic and genomic analyses indicated the coevolution of both *E. coli* and Q $\beta$ . In the course of experimental coevolution,

partially resistant *E. coli* appeared in the 54th generation (16th day). Detailed analysis of the partially resistant *E. coli* is necessary to determine how *E. coli* and Q $\beta$  coexist in this experimental coevolution system. Genetic analysis revealed a single mutation in the *traQ* gene in the day-16 *E. coli* population (Kashiwagi and Yomo, 2011). It was reported that TraQ protein is a chaperone for insertion of propilin encoded by the *traA* gene (Moore et al., 1982; Kathir and Ippen-Ihler, 1991), and propilin was also reported to be unstable in *traQ*<sup>-</sup> cells (Maneewannakul et al., 1993). The 13-kDa propilin is processed by peptidase to a 7-kDa pilin and pilin proteins are assembled into filaments (i.e., the F pilus). Q $\beta$  adsorbs the F pilus of *E. coli* at the first step of infection (Van Duin and Tsareva, 2006), and the adsorption rate of Q $\beta$  on partially resistant cells estimated by first-order kinetics decreased markedly (Kashiwagi and Yomo, 2011). Therefore, the partially resistant phenotype of *E. coli* to Q $\beta$  infection observed in coevolution may be correlated with F pilus biosynthesis, especially TraA, and we focused on the relationships among mutation in TraQ, TraA content, and Q $\beta$  amplification.

Here, we report that a single amino acid change in TraQ was linked to the reduction of TraA content in the *E. coli* population. In addition, this decrease was recovered by supplying ancestral (wild-type) or mutant-type TraQ from an expression vector, and the ability of Q $\beta$  to amplify in the cell also recovered. These results represent one example of how *E. coli* can become partially resistant to RNA bacteriophage infection, which involves changes in a protein related to the maturation of a receptor, in this case the F pilus, rather than changes to the receptor itself. These results suggest that the mutation in TraQ may cause heterogeneity within the *E. coli* population, with a small number of cells supporting the phage population and a large number of cells supporting the *E. coli* population without Q $\beta$  infection, even though the *E. coli* cells were genetically identical.

## MATERIALS AND METHODS

### STRAINS, CULTURE MEDIA, AND PLASMID DNA

*Escherichia coli* Anc(C), the partially Q $\beta$  infection-resistant mutant strain, M54(C) (Kashiwagi and Yomo, 2011), and DH1  $\Delta$ leuB::(*gfpuv5-Km<sup>r</sup>*) (hereafter called LKG; Kishimoto et al., 2010) were used to characterize the effects of S21P mutation in TraQ protein and a control F<sup>-</sup> strain. *E. coli* A/ $\lambda$  (Watanabe et al., 1979) was used as the host strain for titer assay. LB medium (10 g/L tryptone, 5 g/L yeast extract, 10 g/L NaCl; Nakalai Tesque, Kyoto, Japan) was used.

To construct TraQ with a Strep-tag II sequence (Schmidt and Skerra, 2007) at the C-terminus of the ancestral-type TraQ (TraQ<sub>AncTag</sub>) and mutant-type TraQ (TraQ<sub>S21Ptag</sub>), the *traQ* gene was amplified by PCR with Anc(C) and M54(C) genome as the template, the primers traQ\_XbaI and traQ\_strep\_HindIII, and Phusion<sup>®</sup> High-Fidelity DNA polymerase (New England Biolabs, Ipswich, MA, USA). The oligonucleotide DNAs used in this study are listed in **Table 1**. The *traQ*<sub>AncTag</sub> and *traQ*<sub>S21Ptag</sub> genes with XbaI and HindIII sites at both ends were subcloned into the XbaI/HindIII sites of pASK-IBA3plus (IBA Biologics GmbH, Goettingen, Germany). The resulting plasmid DNAs were designated as pASK-traQ<sub>AncTag</sub> and pASK-traQ<sub>S21Ptag</sub>, respectively.

**Table 1 | Oligonucleotide DNA sequence.**

Primer name	Sequence (5'→3')
F_4f_2	ATCAGCGCAATAATTGCCGC
F_4r_2	CGATTATCCCGTCACGATG
Linker_r	ATTGATGGTGCCTACAG
pACYC_rev2	CCACACATTATACGAGCCG
traA1	GACGAGTGAATTTGGAAAA AACGACTTCTTTTTGACGGCC GCAGAAGCACCTGAACAC
traA_f	ATGAATGCTGTTTTAAGTGT
traA_r	TCAGAGGCCAACGACGGCCA
traA_r2	GGCCATACCCACAGCAATAA
traQ_XbaI	TCTAGAAGGAGATATACAATG ATAAGTAAACGCAGATT
traQ_strep_HindIII	AAGCTTATTATTTTTCGAACTG CGGGTGGCTCCAGTGAGAGA CATGTCCGCCCT
5PpACYC_rev	pTCGGCTCGTATAATGTGTGG
16SrRNA_1	GCTGCCTCCCGTAGGAGT

### DNA SEQUENCING OF THE *traQ* GENE OF ANCESTRAL AND PARTIALLY RESISTANT *E. coli*

To determine the *traQ* gene sequences of Anc(C) and M54(C), the *traQ* region in 10 colonies each of Anc(C) and M54(C) was amplified by PCR with the primers F\_4f\_2 and F\_4r\_2 and Phusion<sup>®</sup> High-Fidelity DNA polymerase (New England BioLabs), and PCR products were directly sequenced by the dideoxynucleotide chain termination sequencing method (Sanger et al., 1977).

### ESTIMATION OF Q $\beta$ AMPLIFICATION

Anc(C)/pASK-traQ<sub>AncTag</sub>, Anc(C)/pASK-traQ<sub>S21Ptag</sub>, Anc(C)/pASK-IBA3plus, M54(C)/pASK-traQ<sub>AncTag</sub>, M54(C)/pASK-traQ<sub>S21Ptag</sub>, and M54(C)/pASK-IBA3plus were cultured in 5 mL of LB with 100  $\mu$ g/mL ampicillin overnight and 50  $\mu$ L of the culture was inoculated into 5 mL of LB with 100  $\mu$ g/mL ampicillin for approximately 2 h. Aliquots of 1 mL of the culture were transferred into 4 mL of LB medium with 100  $\mu$ g/mL ampicillin and 100 nM doxycycline-HCl (Dox) and cultured for a further 2 h. Q $\beta$  was added to infect the bacterial cells and the free phage was separated immediately or 4 h after infection by centrifugation at 13400  $\times$  g for 1 min. The free phage in the supernatant was diluted, the number of plaque forming units per milliliter was determined (PFU/mL), and the amplification ratio was calculated as  $x = N_4/N_0$ , where  $N_4$  and  $N_0$  represent 4 h after and initial (0 h) free phage density, respectively. The titer assay was conducted according to the standard method described previously (Carlson, 2005).

### WESTERN BLOTTING ANALYSIS

A polyclonal antibody to TraA protein raised against the keyhole limpet hemocyanin-conjugated peptide (CDLMASGNTTVKATFGKDSS) was obtained from Sigma-Aldrich Japan (Tokyo, Japan).

Cell preculture was conducted as described in the Section “Estimation of Q $\beta$  Amplification.” For induction with 100 nM Dox, Dox was added to the 2-h culture and cells were cultured for a further 5.75 h. Without Dox induction, the cells were cultured for 7.25 h in LB medium. Proteins from the cells obtained from 0.1 mL of culture with OD<sub>600</sub> = 2.0 were subjected to SDS-PAGE using Any kD™ Mini-PROTEAN® TGX™ precast gels (Bio-Rad Laboratories, Hercules, CA, USA), and the TraA protein was determined by Western blotting analysis with anti-TraA antibody and HRP-conjugated goat anti-rabbit polyclonal antibody (Santa Cruz Biotechnology, Inc., Santa Cruz, CA, USA) as the primary and secondary antibodies, respectively, diluted with Can Get Signal® immunoreaction enhancer solution (Toyobo Co. Ltd., Osaka, Japan). TraQ with a Strep-tag II at the C-terminus was detected using Precision Protein™ Strep-Tactin-HRP conjugate (Bio-Rad Laboratories). The signals were detected with Chemi-Lumi One L (Nakalai Tesque).

#### NORTHERN HYBRIDIZATION ANALYSIS

To compare the *traA* mRNA contents by Northern hybridization, Anc(C), M54(C), and LKG with pASK-IBA3plus were cultured in LB medium and total RNA was extracted from the cells in logarithmic phase using the SV Total RNA isolation system (Promega, Madison, WI, USA) according to the manufacturer’s instructions. Total RNA from cells obtained from 0.16 mL of culture with OD<sub>600</sub> = 0.27 was subjected to Northern hybridization using a digoxigenin-labeled single-stranded DNA probe, i.e., *traA1* for *traA* and 16SrRNA\_1 for 16SrRNA, as an indicator of the amount of total RNA used (Moran et al., 1995). The signals were detected with CDP-Star (GE Healthcare UK Ltd., Little Chalfont, UK). DynaMarker® Prestain Marker for RNA High (BioDynamics Laboratory Inc., Tokyo, Japan) was used to obtain the standard curve for RNA length.

#### DETERMINATION OF 5'- AND 3'-TERMINAL SEQUENCES OF *traA* mRNA

To determine the 5'-terminal sequence of *traA* mRNA, cDNA was synthesized using total RNA of Anc(C) as the template, SuperScript® III reverse transcriptase (Life Technologies, Carlsbad, CA, USA), and *traA\_r* primer. The 5'-phosphorylated DNA linker 5PpACYC\_rev was ligated at the 3'-terminus of the first strand cDNA with T4 RNA ligase 1 (New England Biolabs). PCR was performed using the resultant cDNA as the template, PrimeSTAR® HS DNA polymerase (Takara Bio Inc., Shiga, Japan), and the primers pACYC\_rev2 and *traA\_r2*. To determine the 3'-terminal sequence of *traA* mRNA, universal miRNA cloning linker (5'-rAppCTGTAGGCACCATCAAT-NH2-3'; New England Biolabs) was ligated with the 3'-terminus of total RNA of Anc(C) using T4 RNA ligase 1 (New England Biolabs). The first strand cDNA was synthesized using the primer Linker\_r and SuperScript® III reverse transcriptase (Life Technologies), and then purified cDNA was subjected to PCR using the primers Linker\_r and *traA\_f*. Three and two bands of PCR products for 5'- and 3'-terminal sequence determination, respectively, were sliced from the gel and subcloned using a Zero Blunt® TOPO® PCR Cloning Kit for Sequencing (Life Technologies). Three to six clones were randomly picked and sequenced by the dideoxynucleotide chain termination sequencing method.

#### STATISTICAL ANALYSIS

Amplification ratios were compared by one-way ANOVA with the *post hoc* Tukey’s test (Zar, 2010). In all analyses, values of log<sub>10</sub> (N<sub>4t</sub>/N<sub>0t</sub>) of each strain were used for statistical analysis. The Studentized range, *q*, is shown in the text. In all analyses, *P* < 0.01 was taken to indicate statistical significance.

## RESULTS

### RECOVERY OF Q $\beta$ AMPLIFICATION IN RESISTANT *E. coli* BY SUPPLYING TraQ

We first analyzed the *traQ* gene sequences from 10 single colonies derived from the coevolved *E. coli* population to confirm that the majority harbored the T61C mutation. We picked 10 single colonies from each of Anc(C) and M54(C) populations, which were the initial and day-16 *E. coli* populations in the coevolution experiment (Kashiwagi and Yomo, 2011). All 10 colonies of Anc(C) had T and all 10 colonies of M54(C) had C at position 61, and this T61C mutation resulted in S21P in the TraQ protein.

We analyzed the amplification ratio of Q $\beta$  on Anc(C) and M54(C) that harbored only the vector (pASK-IBA3plus) to determine the extent of reduction in the amplification ratio of Q $\beta$  on M54(C). Anc(C) and M54(C) expressed inherent ancestral-type TraQ protein and mutant-type TraQ protein from the F plasmid, respectively. The amplification ratio of Q $\beta$  was calculated as described in the Section “Materials and Methods.” The amplification ratios of Q $\beta$  on Anc(C)/pASK-IBA3plus and M54(C)/pASK-IBA3plus were  $3.5 \times 10^4$  and 1.8, respectively (Figure 1). Although the amplification ratio on M54(C) was much lower than that on Anc(C), Q $\beta$  could undergo amplification on M54(C), indicating that M54(C) had a partially rather than fully resistant phenotype.

To analyze whether ancestral-type TraQ expression in M54(C) could compensate for Q $\beta$  amplification in this strain, ancestral-type TraQ with the Strep-tag II sequence at the C-terminus

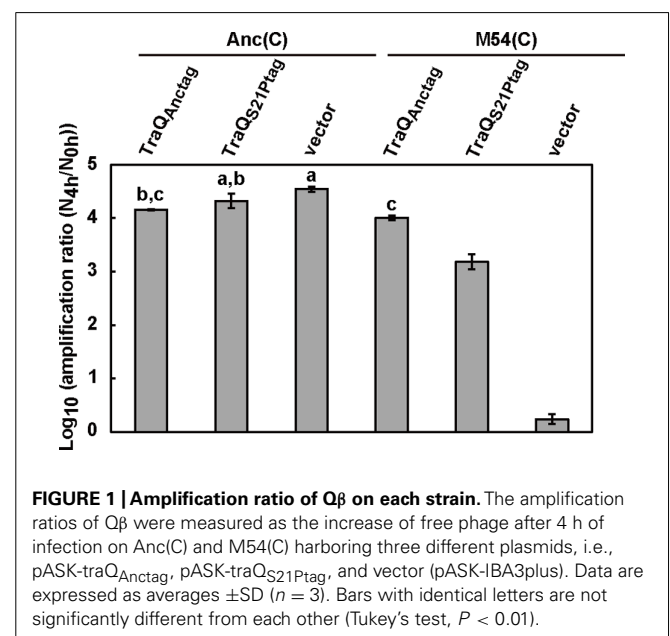


**FIGURE 1 | Amplification ratio of Q $\beta$  on each strain.** The amplification ratios of Q $\beta$  were measured as the increase of free phage after 4 h of infection on Anc(C) and M54(C) harboring three different plasmids, i.e., pASK-*traQ*<sub>Ancctag</sub>, pASK-*traQ*<sub>S21Ptag</sub>, and vector (pASK-IBA3plus). Data are expressed as averages  $\pm$ SD (*n* = 3). Bars with identical letters are not significantly different from each other (Tukey’s test, *P* < 0.01).

was expressed from the P<sub>tetA</sub> promoter by doxycycline (Dox) induction. We designated ancestral and mutant-type TraQ with Strep-tag II sequence at the C-terminus expressed from the expression vector as TraQ<sub>Anctag</sub> and TraQ<sub>S21Ptag</sub> to allow them to be distinguished from the inherent TraQ<sub>Anc</sub> and TraQ<sub>S21P</sub> derived from the F plasmid, respectively. First, to examine whether TraQ<sub>Anctag</sub> overexpression altered the amplification ratio of Q $\beta$  on Anc(C), we compared the amplification ratios of Q $\beta$  on Anc(C)/pASK-traQ<sub>Anctag</sub> and Anc(C)/pASK-IBA3plus under conditions of Dox induction. The amplification ratio of Q $\beta$  on Anc(C) overexpressing TraQ<sub>Anctag</sub> was  $1.4 \times 10^4$ , which was lower than that on Anc(C) harboring only the vector,  $3.5 \times 10^4$ , suggesting that overexpression of TraQ may be slightly deleterious for Q $\beta$  amplification (one-way ANOVA  $F_{5,12} = 920$ ,  $P < 0.01$ ; *post hoc* Tukey's test  $q = 7.3$ ,  $P < 0.01$ ; **Figure 1**). Second, the amplification ratio of Q $\beta$  on M54(C) overexpressing TraQ<sub>Anctag</sub> was  $1.0 \times 10^4$ , which was greater than the value of 1.8 on M54(C) carrying only the vector (one-way ANOVA  $F_{5,12} = 920$ ,  $P < 0.01$ ; *post hoc* Tukey's test  $q = 70.5$ ,  $P < 0.01$ ), and the amplification ratio of M54(C) overexpressing TraQ<sub>Anctag</sub> was comparable to that of Anc(C)/pASK-TraQ<sub>Anctag</sub> (one-way ANOVA  $F_{5,12} = 920$ ,  $P < 0.01$ ; *post hoc* Tukey's test  $q = 2.76$ ,  $P = 0.42$ ; **Figure 1**). These results showed that the amplification ratio of Q $\beta$  on M54(C) was recovered by supplying TraQ<sub>Anctag</sub>. Intriguingly, supplying mutant-type TraQ, TraQ<sub>S21Ptag</sub>, to M54(C) also rescued the amplification of Q $\beta$  on this strain. When TraQ<sub>S21Ptag</sub> was overexpressed by Dox induction in M54(C), the amplification ratio of Q $\beta$  on the strain was  $1.6 \times 10^3$ , which was greater than that of M54(C) with the vector alone (one-way ANOVA  $F_{5,12} = 920$ ,  $P < 0.01$ ; *post hoc* Tukey's test  $q = 55.1$ ,  $P < 0.01$ ), but was lower than that of M54(C) overexpressing TraQ<sub>Anctag</sub> (one-way ANOVA  $F_{5,12} = 920$ ,  $P < 0.01$ ; *post hoc* Tukey's test  $q = 15.4$ ,  $P < 0.01$ ; **Figure 1**). These results indicated that overexpression of mutant-type TraQ in M54(C) could partially, but not completely, compensate for the decrease in amplification of Q $\beta$  on the partially resistant cells.

#### RECOVERY OF Q $\beta$ AMPLIFICATION LINKED TO AN INCREASE IN TraA

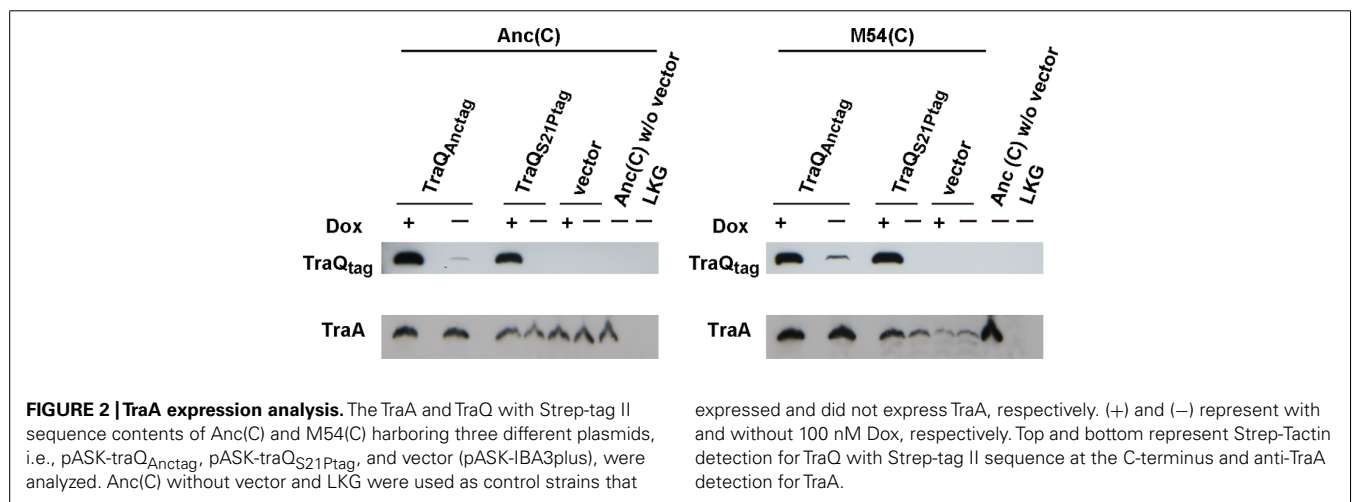
We analyzed the TraA content by Western blotting to investigate the links between the mutation in TraQ and TraA content.

Proteins derived from the same cell numbers calculated by the values of OD<sub>600</sub> were subjected to SDS-PAGE. When we compared the levels of TraA produced by Anc(C) and M54(C) with vector (pASK-IBA3plus) and Anc(C) without the vector, the signal strength of TraA of Anc(C) with vector was almost the same as that of Anc(C) without the vector independent of Dox induction (**Figure 2**), but the TraA content of M54(C) with vector was extremely low independent of Dox induction (**Figure 2**). As no signal was detected in the lane for the F<sup>-</sup> control strain, LKG, M54(C) had not entirely lost TraA. These results showed that M54(C) had markedly decreased propilin and/or pilin content.

The expression levels of ancestral and mutant-type TraQ with the Strep-tag II sequence at its C-terminus were determined with Strep-Tactin. When TraQ<sub>Anctag</sub> was expressed in M54(C), the signal level for TraA was almost the same as that of Anc(C); (**Figure 2**). In this case, the TraA contents were independent of Dox induction. Next, we supplied TraQ<sub>S21Ptag</sub> to M54(C) with and without Dox induction. The TraA content in M54(C) increased with Dox induction, but the level was lower than that in M54(C) supplied with TraQ<sub>Anctag</sub> (**Figure 2**). The TraA content of M54(C) also increased without Dox induction, but the strength of the signal was smaller than that under conditions of Dox induction. With supply of TraQ<sub>S21Ptag</sub>, the TraA content was dependent on the expression level of TraQ<sub>S21Ptag</sub>. These observations indicated that a small amount of ancestral-type TraQ in the partially resistant cells was sufficient to recover the TraA content, and a large amount of mutant-type TraQ protein increased the TraA content but the level was lower than that of the ancestral cells. Therefore, these results showed that a single mutation in TraQ resulted in a decrease of TraA content in the partially resistant cells.

#### traA mRNA EXPRESSION LEVEL IN M54(C)

To determine whether the decrease of TraA protein content in the partially resistant cells was due to a decrease in *traA* mRNA content, we analyzed the *traA* mRNA level by Northern hybridization. No signal was detected in the lane for the F<sup>-</sup> control strain LKG (**Figure 3A**), while signals were observed in the lanes for the Anc(C) and M54(C) strains (**Figure 3A**). The difference in



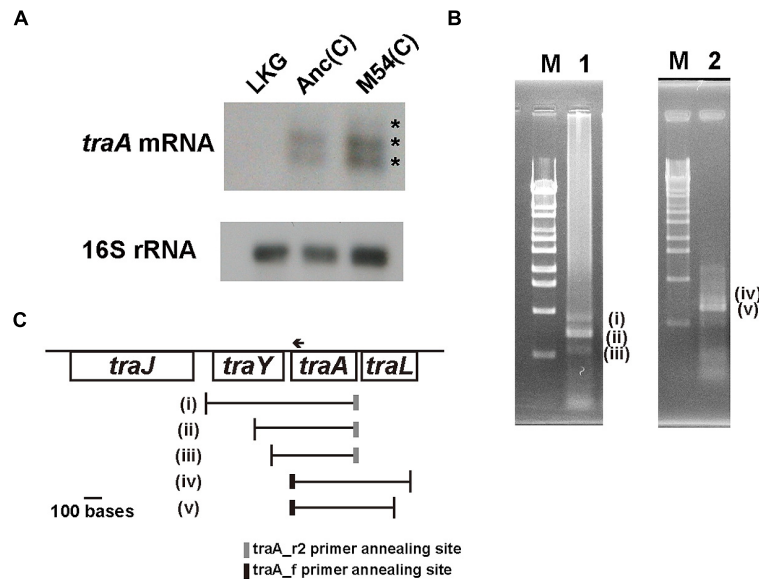


**FIGURE 3 | mRNA of *traA* gene analysis. (A)** Northern hybridization for *traA* mRNA and 16S rRNA using the total RNA of LKG/pASK-IBA3plus; left, Anc(C)/pASK-IBA3plus; middle, M54(C)/pASK-IBA3plus; right. The upper and lower figures are X-ray films of *traA* mRNA and 16S rRNA, respectively. The asterisks (\*) indicate the three signals (one weak and two strong). **(B)** RT-PCR for Anc(C)/pASK-IBA3plus to determine the 5'- and 3'-terminal sequences of *traA* mRNA. Lambda DNA digested with *StyI* was used as a molecular size marker; lane M. RT-PCR products for determination of the 5'-terminus. The

three bands were designated as (i), (ii), and (iii), respectively; lane 1. RT-PCR products for determination of the 3'-terminus. The two bands were designated as (iv) and (v), respectively; lane 2. **(C)** Schematic representations of the start and end positions of *traA* mRNA. The vertical lines represent the positions of 5'- and 3'-terminal sequences of (i)–(v) shown in **(B)**. The gray and black boxes represent the positions of *traA\_r2* and *traA\_f* primer annealing sites in RT-PCR. The arrow represents the position of the *traA1* probe annealing site for Northern hybridization.

signal strength of *traA* mRNA between Anc(C) and M54(C) may have been due to differences in the amount of total RNA loaded per lane, which was determined based on the 16S rRNA signal strength, although equal amounts of total RNA were loaded in each lane as calculated from the OD<sub>600</sub>. Therefore, we assumed that the mRNA levels were the almost the same for Anc(C) and M54(C).

As shown in **Figure 3A**, three bands were observed on Northern hybridization; one was weak and two were strong. The three bands corresponded to approximately 800, 610, and 460 bases, respectively, calculated using the standard curve obtained with the molecular weight markers. As the *traA* gene is 366 bases in length, the mRNA may contain upstream and/or downstream sequences. To determine the 5'- and 3'-terminal sequences of *traA* mRNA, RT-PCR was performed as described in the Section “Materials and Methods.” For 5'-terminal analysis of mRNA, we added a linker to the 3'-terminus of the first strand cDNA and conducted PCR. At least three PCR products, two of which were clear and the remaining one was weak, were obtained (**Figure 3B**, left). For 3'-terminal analysis of mRNA, we added a linker at the 3'-terminus of the mRNA and conducted RT-PCR. At least two PCR products were obtained, one of which was clearly observed and the other was weak (**Figure 3B**, right). The sequences of these PCR products, designated as (i)–(v), were analyzed and the starting and termination positions of the mRNA including *traA* were determined (**Figure 3C**). The starting and terminating positions described below are numbered according to GenBank accession number AP001918.1. Analysis of six clones of (i) showed that mRNAs

started from a position upstream of the *traY* gene; five started at position 67808 and one started at position 67754. Analysis of six clones of (ii) showed that it started from within the *traY* gene; four started at position 68000 and two started at position 67999. Analysis of five clones of (iii) showed that mRNAs started from within the *traY* gene; one started at position 68165, two at 68166, one at 68167, and one at 68189 (**Figure 3C**). Analysis of five clones of (v) showed that mRNAs terminated within the *traL* gene; four terminated at 68818 and one at 68819. Analysis of three clones of (iv) also showed that the mRNAs terminated within the *traL* gene; all three terminated at position 68902. These results indicated that the total RNA included mRNAs encoding *traA* of various lengths with different upstream and downstream sequences. Therefore, all three bands observed on Northern hybridization should contain the *traA* gene sequence.

## DISCUSSION

We reported previously that *E. coli* and Q $\beta$  coexisted in serial passage and both continued to change genetically and phenotypically (Kashiwagi and Yomo, 2011). Here, we characterized partially resistant *E. coli* obtained in the previous study and demonstrated links among TraQ content, TraA content, and amplification of Q $\beta$ .

In this study, overexpression of mutant-type TraQ<sub>S21Ptag</sub> was shown to result in an increase in TraA content and recovery of Q $\beta$  amplification. These observations indicated that TraQ<sub>S21P</sub> had not entirely lost its function. The S21P mutation may alter the activity of TraQ, such as changing the binding affinity between TraQ and TraA, and may result in a decrease of TraA content in the

M54(C) population and reduce the possibility of Q $\beta$  infection by decreasing either the number of cells with F pili or the amount of F pili in each cell in the population, as TraQ protein binds propilin that is a precursor of mature TraA and the first 21 amino acids are important for this binding (Harris et al., 1999). In this study, not only TraQ<sub>AncTag</sub> but also the TraQ<sub>S21Ptag</sub> increased the TraA contents of M54(C) without Dox induction. The copy numbers of pASK-TraQ<sub>S21Ptag</sub>, which has the ColE1 replication origin, and F plasmid in the cell are 15–20 and 1, respectively (Snyder and Champness, 2007). Therefore, introduction of pASK-TraQ<sub>S21Ptag</sub> into the cell increased the copy number of the *traQ* (T61C) gene and therefore may have increased the concentration of mutant-type TraQ in the cell.

It has been reported that F<sup>+</sup> cells in *E. coli* populations are heterogeneous in the number of F pili per cell and in the length of F pili through the cycles of extension and retraction (Clarke et al., 2008; Silverman and Clarke, 2010). In addition, it is widely accepted that even *E. coli* with the same genotype show phenotypic diversity due to the stochasticity in living organisms (Elowitz et al., 2002; Kashiwagi et al., 2006; Bressloff, 2014). Therefore, even in Anc(C), the population would be heterogeneous in both number and length of F pili per cell. The single mutation of TraQ would decrease the percentage of cells that could be infected by Q $\beta$  in the population, even though the M54(C) population was genetically identical throughout the community. The mutation was introduced into the region involved in binding with propilin (Harris et al., 1999) and protein–protein binding is one of the stochastic processes in a cell because it is a collision reaction and reducing numbers of interacting molecules in a cell would increase the fluctuation in number of bound proteins (Bressloff, 2014). Therefore, there would be at least three types of players in the community: a small proportion of cells supporting the phage population, a large proportion of cells supporting the *E. coli* population due to escape from Q $\beta$  infection, and Q $\beta$  itself. This heterogeneity would result in the partially resistant phenotype of the M54(C) population, as we assessed the phenotype based on the amplification ratio of Q $\beta$  in the population and not in single infected cells. As we evaluated the TraA and TraQ contents and Q $\beta$  amplification of the population and not of single cells, there are at least two plausible explanations for the partial resistance. The first is that every cell had low levels of TraA or F pili, and the second is that only a small portion of cells in the population had sufficient F pili for Q $\beta$  adsorption. In both cases, at least two types of cell—a minor population infected by Q $\beta$  and a major population that was not infected by Q $\beta$ —may emerge from *E. coli* with the identical genotype.

The physiological refuge hypothesis has been reported as one of the mechanisms allowing the coexistence of bacteria and bacteriophages by providing phenotypic heterogeneity in resistance within the bacterial population (Lenski, 1988; Schrag and Mittler, 1995). The results of the present study suggested that the coevolved *E. coli* in experimental evolution would generate phenotypic heterogeneity with both resistant and susceptible cells, as suggested by the physiological refuge hypothesis.

Many resistance mechanisms of bacteria for DNA bacteriophages have been reported, such as preventing phage adsorption, preventing phage DNA entry, cutting phage nucleic acids, abortive

infection, and phase variation (Hancock and Reeves, 1975; Labrie et al., 2010; Bikard and Marraffini, 2012). In preventing phage adsorption, surface receptors of bacteria for phage infection were modified, masked by proteins, or blocked by exopolysaccharide (Labrie et al., 2010). However, there have been few discussions regarding the mechanisms of resistance to RNA bacteriophages. Here, we first reported one of the mechanisms underlying partial resistance of *E. coli* to the RNA bacteriophage Q $\beta$  that would be included in preventing phage adsorption: a decrease in chance of phage adsorption by reducing the receptor contents in the host population by changing a single amino acid on the protein related to production of the mature receptor (F pilus), not the receptor itself. In addition, the results of this study also suggested that the phenotypic fluctuation caused by changing a single amino acid on the protein would facilitate long-term coexistence of both predator (Q $\beta$  phage) and prey (*E. coli*).

## AUTHOR CONTRIBUTIONS

AK designed the research. AK, HK, and FST carried out the experiments and analyzed the data. AK wrote the manuscript.

## ACKNOWLEDGMENTS

We are grateful to Dr. Tetsuya Yomo (Osaka University) and Dr. Kotaro Mori (Ishihara Sangyo Kaisha, Ltd.) for valuable discussions, and Ms. Hiroko Tohyama for excellent technical assistance. We thank Dr. Takahiro Toba and the members of RNA Research Center (Hirosaki University) for their cooperation. This work was supported in part by MEXT KAKENHI (21770255 and 23570268), Kato Memorial Bioscience Foundation, Hirosaki University Grant for Exploratory Research by Young Scientists, Priority Research Grant for Young Scientists Designated by the President of Hirosaki University, and Hirosaki University Institutional Research Grant for Young Scientists.

## REFERENCES

- Abrams, P. A. (2000). The evolution of predator-prey interactions: theory and evidence. *Annu. Rev. Ecol. Syst.* 31, 79–105. doi: 10.1146/annurev.ecolsys.31.1.79
- Alexander, M. (1981). Why microbial predators and parasites do not eliminate their prey and hosts. *Annu. Rev. Microbiol.* 35, 113–133. doi: 10.1146/annurev.mi.35.100181.000553
- Anderson, R. M., and May, R. M. (1978). Regulation and stability of host-parasite population interactions I. Regulatory processes. *J. Anim. Ecol.* 47, 219–247. doi: 10.2307/3933
- Berryman, A. A. (1992). The origins and evolution of predator-prey theory. *Ecology* 73, 1530–1535. doi: 10.2307/1940005
- Bikard, D., and Marraffini, L. A. (2012). Innate and adaptive immunity in bacteria: mechanisms of programmed genetic variation to fight bacteriophages. *Curr. Opin. Immunol.* 24, 15–20. doi: 10.1016/j.coi.2011.10.005
- Bohannan, B. J., and Lenski, R. E. (2000). Linking genetic change to community evolution: insights from studies of bacteria and bacteriophage. *Ecol. Lett.* 3, 362–377. doi: 10.1046/j.1461-0248.2000.00161.x
- Bressloff, P. C. (2014). *Stochastic Processes in Cell Biology*. Heidelberg: Springer. doi: 10.1007/978-3-319-08488-6
- Briggs, C. J., and Hoopes, M. F. (2004). Stabilizing effects in spatial parasitoid-host and predator-prey models: a review. *Theor. Popul. Biol.* 65, 299–315. doi: 10.1016/j.tpb.2003.11.001
- Brockhurst, M. A., Buckling, A., and Rainey, P. B. (2006). Spatial heterogeneity and the stability of host-parasite coexistence. *J. Evol. Biol.* 19, 374–379. doi: 10.1111/j.1420-9101.2005.01026.x
- Brockhurst, M. A., and Koskella, B. (2013). Experimental coevolution of species interactions. *Trends Ecol. Evol.* 28, 367–375. doi: 10.1016/j.tree.2013.02.009

- Buckling, A., and Rainey, P. B. (2002). Antagonistic coevolution between a bacterium and a bacteriophage. *Proc. Biol. Sci.* 269, 931–936. doi: 10.1098/rspb.2001.1945
- Bull, J. J., Vegge, C. S., Schmerer, M., Chaudhry, W. N., and Levin, B. R. (2014). Phenotypic resistance and the dynamics of bacterial escape from phage control. *PLoS ONE* 9:e94690. doi: 10.1371/journal.pone.0094690
- Campbell, A. (1961). Conditions for the existence of bacteriophage. *Evolution* 15, 153–165. doi: 10.2307/2406076
- Carlson, K. (2005). “Working with bacteriophages: common techniques and methodological approaches,” in *Bacteriophages, Biology and Applications*, eds E. Kutter and A. Sulakvelidze (Boca Raton, FL: CRC Press), 437–494.
- Chao, L., Levin, B. R., and Stewart, F. M. (1977). A complex community in a simple habitat: an experimental study with bacteria and phage. *Ecology* 58, 369–378. doi: 10.2307/1935611
- Clarke, M., Maddera, L., Harris, R. L., and Silverman, P. M. (2008). F-pili dynamics by live-cell imaging. *Proc. Natl. Acad. Sci. U.S.A.* 105, 17978–17981. doi: 10.1073/pnas.0806786105
- Dennehy, J. J. (2012). What can phages tell us about host-pathogen coevolution? *Int. J. Evol. Biol.* 2012, 12. doi: 10.1155/2012/396165
- Elowitz, M. B., Levine, A. J., Siggia, E. D., and Swain, P. S. (2002). Stochastic gene expression in a single cell. *Science* 297, 1183–1186. doi: 10.1126/science.1070919
- Hancock, R. E., and Reeves, P. (1975). Bacteriophage resistance in *Escherichia coli* K-12: general pattern of resistance. *J. Bacteriol.* 121, 983–993.
- Harris, R. L., Sholl, K. A., Conrad, M. N., Dresser, M. E., and Silverman, P. M. (1999). Interaction between the F plasmid TraA (F-pilin) and TraQ proteins. *Mol. Microbiol.* 34, 780–791. doi: 10.1046/j.1365-2958.1999.01640.x
- Horne, M. T. (1970). Coevolution of *Escherichia coli* and bacteriophages in chemostat culture. *Science* 168, 992–993. doi: 10.1126/science.168.3934.992-a
- Kashiwagi, A., Urabe, I., Kaneko, K., and Yomo, T. (2006). Adaptive response of a gene network to environmental changes by fitness-induced attractor selection. *PLoS ONE* 1:e49. doi: 10.1371/journal.pone.0000049
- Kashiwagi, A., and Yomo, T. (2011). Ongoing phenotypic and genomic changes in experimental coevolution of RNA bacteriophage Q $\beta$  and *Escherichia coli*. *PLoS Genet.* 7:e1002188. doi: 10.1371/journal.pgen.1002188
- Kathir, P., and Ippen-Ihler, K. (1991). Construction and characterization of derivatives carrying insertion mutations in F plasmid transfer region genes, trbA, artA, traQ, and trbB. *Plasmid* 26, 40–54. doi: 10.1016/0147-619X(91)90035-U
- Kerr, B., Neuhauser, C., Bohannan, B. J., and Dean, A. M. (2006). Local migration promotes competitive restraint in a host-pathogen ‘tragedy of the commons.’ *Nature* 442, 75–78. doi: 10.1038/nature04864
- Kishimoto, T., Iijima, L., Tatsumi, M., Ono, N., Oyake, A., Hashimoto, T., et al. (2010). Transition from positive to neutral in mutation fixation along with continuing rising fitness in thermal adaptive evolution. *PLoS Genet.* 6:e1001164. doi: 10.1371/journal.pgen.1001164
- Labrie, S. J., Samson, J. E., and Moineau, S. (2010). Bacteriophage resistance mechanisms. *Nat. Rev. Microbiol.* 8, 317–327. doi: 10.1038/nrmicro2315
- Lenski, R. E. (1988). “Dynamics of interactions between bacteria and virulent bacteriophage,” in *Advances in Microbial Ecology*, ed. K. C. Marshall (New York: Plenum Publishing Corporation), 1–44.
- Lenski, R. E., and Levin, B. R. (1985). Constraints on the coevolution of bacteria and virulent phage: a model, some experiments, and predictions for natural communities. *Am. Nat.* 125, 585–602. doi: 10.1086/284364
- Levin, B. R., Stewart, F. M., and Chao, L. (1977). Resource-limited growth, competition, and predation: a model and experimental studies with bacteria and bacteriophage. *Am. Nat.* 111, 3–24. doi: 10.1086/283134
- Lythgoe, K. A., and Chao, L. (2003). Mechanisms of coexistence of a bacteria and a bacteriophage in a spatially homogeneous environment. *Ecol. Lett.* 6, 326–334. doi: 10.1046/j.1461-0248.2003.00433.x
- Maneewannakul, K., Maneewannakul, S., and Ippen-Ihler, K. (1993). Synthesis of F pilin. *J. Bacteriol.* 175, 1384–1391.
- Marston, M. F., Pierciey, F. J. Jr., Shepard, A., Gearin, G., Qi, J., Yandava, C., et al. (2012). Rapid diversification of coevolving marine *Synechococcus* and a virus. *Proc. Natl. Acad. Sci. U.S.A.* 109, 4544–4549. doi: 10.1073/pnas.1120310109
- Moore, D., Sowa, B. A., and Ippen-Ihler, K. (1982). A new activity in the Ftra operon which is required for F-pilin synthesis. *Mol. Gen. Genet.* 188, 459–464. doi: 10.1007/BF00330049
- Moran, M. A., Rutherford, L. T., and Hodson, R. E. (1995). Evidence for indigenous *Streptomyces* populations in a marine environment determined with a 16S rRNA probe. *Appl. Environ. Microbiol.* 61, 3695–3700.
- Murdoch, W. W., and Oaten, A. (1975). “Predation and population stability,” in *Advances in Ecological Research*, ed. A. Macfadyen (London: Academic press Inc.), 1–131.
- Paterson, S., Vogwill, T., Buckling, A., Benmayor, R., Spiers, A. J., Thomson, N. R., et al. (2010). Antagonistic coevolution accelerates molecular evolution. *Nature* 464, 275–278. doi: 10.1038/nature08798
- Pettorelli, N., Coulson, T., Durant, S. M., and Gaillard, J. M. (2011). Predation, individual variability and vertebrate population dynamics. *Oecologia* 167, 305–314. doi: 10.1007/s00442-011-2069-y
- Sanger, F., Nicklen, S., and Coulson, A. R. (1977). DNA sequencing with chain-terminating inhibitors. *Proc. Natl. Acad. Sci. U.S.A.* 74, 5463–5467. doi: 10.1073/pnas.74.12.5463
- Sasaki, A. (2000). Host-parasite coevolution in a multilocus gene-for-gene system. *Proc. Biol. Sci.* 267, 2183–2188. doi: 10.1098/rspb.2000.1267
- Schmidt, T. G., and Skerra, A. (2007). The Strep-tag system for one-step purification and high-affinity detection or capturing of proteins. *Nat. Protoc.* 2, 1528–1535. doi: 10.1038/nprot.2007.209
- Schrag, S. J., and Mittler, J. E. (1995). Host-parasite coexistence: the role of spatial refuges in stabilizing bacteria-phage interactions. *Am. Nat.* 148, 348–377. doi: 10.1086/285929
- Silverman, P. M., and Clarke, M. B. (2010). New insights into F-pilus structure, dynamics, and function. *Integr. Biol.* 2, 25–31. doi: 10.1039/B917761B
- Snyder, L., and Champness, W. (2007). “Plasmids,” in *Molecular Genetics of Bacteria* (Washington, DC: ASM Press), 197–242.
- Van Duin, J., and Tsareva, N. (2006). “Single-stranded RNA phages,” in *The Bacteriophages*, ed. R. Calendar (New York: Oxford University Press), 175–196.
- Watanabe, I., Sakurai, T., Furuse, K., and Ando, A. (1979). “Pseudolysogenization” by RNA phage Q $\beta$ . *Microbiol. Immunol.* 23, 1077–1083. doi: 10.1111/j.1348-0421.1979.tb00539.x
- Zar, J. H. (2010). *Biostatistical Analysis*, 5th Edn, Upper Saddle River, NJ: Pearson education Inc.

**Conflict of Interest Statement:** The authors declare that the research was conducted in the absence of any commercial or financial relationships that could be construed as a potential conflict of interest.

Received: 26 November 2014; accepted: 02 February 2015; published online: 20 February 2015.

Citation: Kashiwagi A, Kitamura H and Sano Tsushima F (2015) Characterization of a single mutation in TraQ in a strain of *Escherichia coli* partially resistant to Q $\beta$  infection. *Front. Microbiol.* 6:124. doi: 10.3389/fmicb.2015.00124

This article was submitted to *Systems Microbiology*, a section of the journal *Frontiers in Microbiology*.

Copyright © 2015 Kashiwagi, Kitamura and Sano Tsushima. This is an open-access article distributed under the terms of the Creative Commons Attribution License (CC BY). The use, distribution or reproduction in other forums is permitted, provided the original author(s) or licensor are credited and that the original publication in this journal is cited, in accordance with accepted academic practice. No use, distribution or reproduction is permitted which does not comply with these terms.

# Complexities of cell-to-cell communication through membrane vesicles: implications for selective interaction of membrane vesicles with microbial cells

Yusuke Hasegawa, Hiroyuki Futamata and Yosuke Tashiro\*

Department of Applied Chemistry and Biochemical Engineering, Graduate School of Engineering, Shizuoka University, Hamamatsu, Japan

**Keywords:** membrane vesicles, cell-to-cell communication, predation, horizontal gene transfer, quorum-sensing

## OPEN ACCESS

### Edited by:

Yo Suzuki,  
J. Craig Venter Institute, USA

### Reviewed by:

Bogumil Jacek Karas,  
Designer Microbes Inc./J. Craig  
Venter Institute, USA  
Yoshiteru Aoi,  
Hiroshima University, Japan

### \*Correspondence:

Yosuke Tashiro,  
tashiro.yosuke@shizuoka.ac.jp

### Specialty section:

This article was submitted to  
Systems Microbiology,  
a section of the journal  
Frontiers in Microbiology

**Received:** 27 January 2015

**Accepted:** 11 June 2015

**Published:** 03 July 2015

### Citation:

Hasegawa Y, Futamata H and Tashiro  
Y (2015) Complexities of cell-to-cell  
communication through membrane  
vesicles: implications for selective  
interaction of membrane vesicles with  
microbial cells.  
*Front. Microbiol.* 6:633.  
doi: 10.3389/fmicb.2015.00633

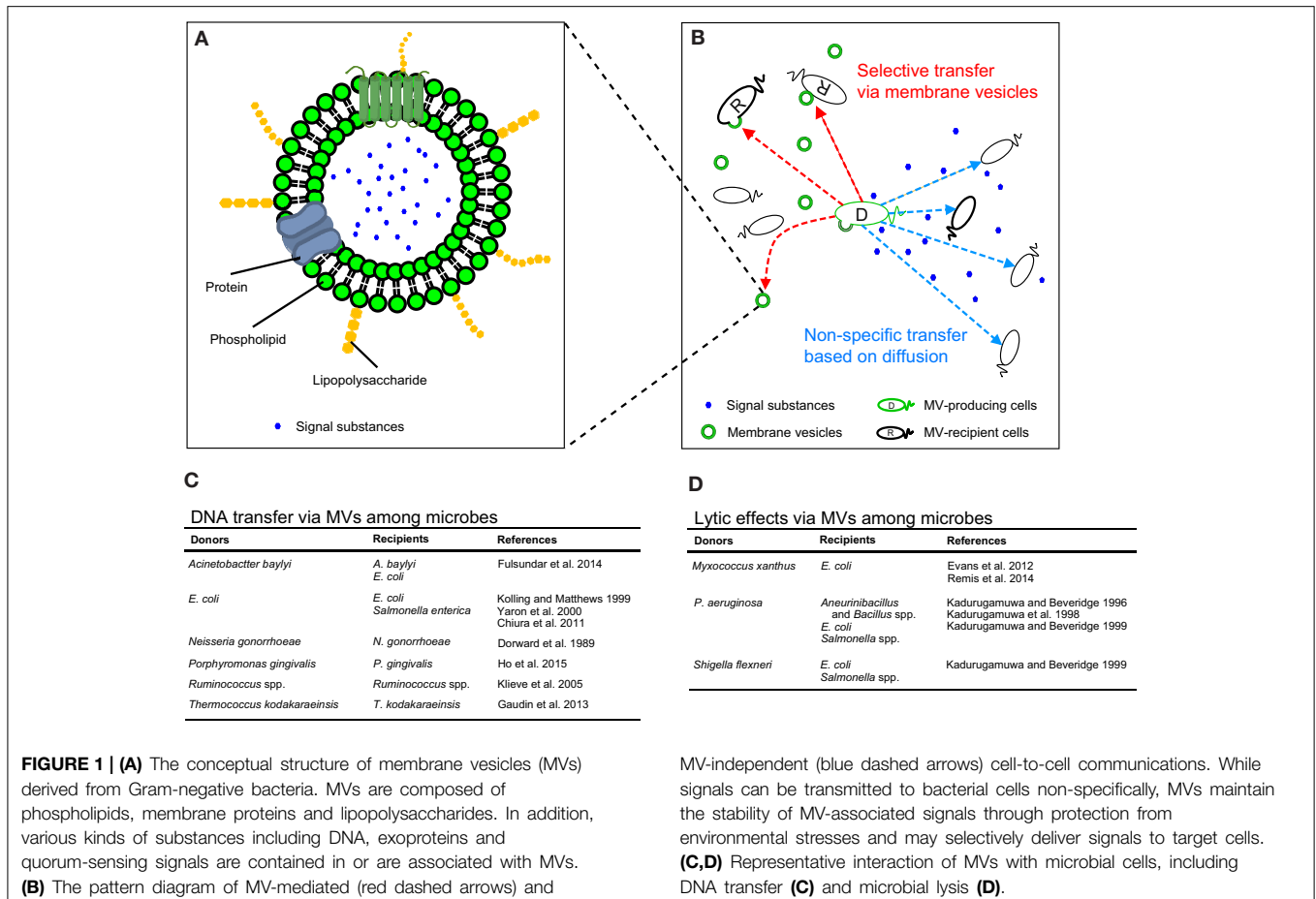
## Introduction

Interaction between microbes in multicellular communities contributes to the development of complex microbial ecosystems. The secretion of various substances such as extracellular toxic compounds for combatting predation, extracellular DNA for horizontal gene transfer (HGT) and quorum-sensing (QS) signals for cell density-dependent cooperation, greatly influences microbial interactions (Hibbing et al., 2010; Tashiro et al., 2013). Study of the diffusion of substances secreted from donor cells to the extracellular environment and their uptake by recipient cells offers valuable insights for understanding microbial interactions.

The existence of membrane vesicles (MVs) increases the complexity involved in the diffusion of secreted substances during microbial interactions. MVs are extracellular particle-like liposome structures ranging from 20 to 200 nm in diameter (Figure 1A) and are pinched off from the external membrane of the microbe. The phenomenon of MV secretion has been observed in Gram-negative bacteria; however, recent studies have indicated that MVs are also produced by other prokaryotes including Gram-positive bacteria and archaea (Beveridge, 1999; Tashiro et al., 2010a, 2012; Haurat et al., 2015). MVs encapsulate membranous, periplasmic, and cytoplasmic components and play a role in the transfer of several compounds to organisms including both prokaryotic and eukaryotic cells. MVs contain proteins, DNA, RNA and in some cases, quorum sensing signals, and these substances are transferred to cells. Compared with freely-diffused chemical compounds secreted from bacteria, MVs have the following unique characteristics: (1) several chemical substances are highly concentrated in MVs, (2) interior substances in MVs are protected against environmental stresses, and (3) MVs play a role in effectively delivering these substances to cells. In this opinion article, we highlight the characteristics of MVs stated above and discuss the possibility of MV-mediated selective delivery to target cells (Figure 1B).

## Highly Concentrated Substances in MVs

The significant characteristic of MVs is their ability to encapsulate specific substances. Interior substances are maintained at high concentration and are protected from degradation by exterior stresses and enzymes. In the case of *Pseudomonas aeruginosa*, which is not only known as an



opportunistic pathogen but also known to inhabit a variety of environments, a total of 68% of phospholipase C and 50% of alkaline phosphatase in the supernatant are localized in MVs along with the highly concentrated murein hydrolase (Kadurugamuwa and Beveridge, 1995, 1996). The encapsulation of toxic proteins provides an effective means for toxic transfer to not only eukaryotic cells but also other bacteria to counteract predation in the environment (Li et al., 1998; Evans et al., 2012). Furthermore, 86% of the *Pseudomonas* quinolone signal, which is one of the QS signals of *P. aeruginosa*, is localized in MVs, although smaller percentages (<1%) of other QS signals, including acyl-homoserine lactones, are localized in MVs (Mashburn and Whiteley, 2005). Such a highly concentrated QS signal is likely to effectively facilitate rapid alteration of gene expression in recipient cells. DNA is also highly concentrated in MVs, and MV-associated DNA is protected against extracellular DNase (Renelli et al., 2004). Several studies indicated that encapsulation of DNA contributes to HGT (Kolling and Matthews, 1999; Yaron et al., 2000; Fulsundar et al., 2014). Thus, the encapsulation of various signals in MVs plays an important role in microbial communications including QS and HGT, and increases effectiveness compared with diffusion-based interactions.

## Association of Vesicles in Eukaryotic Cells

Whether MVs associate with a specific cellular surface remains unknown. In studies of eukaryotic intracellular vesicles, it has been shown that membrane-enveloped vesicles travel in between organelles in the cytoplasm, playing a role in transporting specific cargos to programmed locations via membrane fusion (Balch et al., 1984; Wilson et al., 1989; Sollner et al., 1993; Mcnew et al., 2000). In particular, a specific pairing between ligand and receptor allows vesicles to recognize the target compartment. In addition, the association between MVs and eukaryotic cells has been comprehensively studied in pathogenic bacteria, and MVs secreted from pathogens transfer virulent factors to cells (Parker et al., 2010; Chatterjee and Chaudhuri, 2011; Elmi et al., 2012; Rompikuntal et al., 2012; Bielaszewska et al., 2013). In particular, specific proteins localized on the surface of MVs increase the association with epithelial cells. For example, a heat-labile enterotoxin associated with MVs derived from enterotoxigenic *Escherichia coli* increases the association of MVs with cells (Kesty et al., 2004). The aminopeptidase of *P. aeruginosa* PaAP similarly increases the association of *P. aeruginosa* MVs with lung epithelial cells (Bauman and Kuehn, 2009). In addition, bacterial cytotoxin VacA increases

the adhesion of MVs with cells, most likely by increasing the association of MV lipopolysaccharide with cells (Parker et al., 2010). Thus, MVs can contribute to the virulence of eukaryotic cells, but little is understood regarding whether such associations are promoted by specific interactions between a ligand and a receptor. Understanding the specific association of MVs with cells would enable the development of applications involving MVs as vehicles for cell-specific drug delivery (Gujrati et al., 2014).

## Selective Association between MVs and Microbial Cells

The association of MVs and microbial cells has been a subject of several studies on electric charge and hydrophobicity of cellular surfaces. The surfaces of bacterial cells are usually negatively charged and rich in divalent cations that stabilize surface charges such as  $Mg^{2+}$  or  $Ca^{2+}$ . When freely floating MVs encounter bacterial cells, these divalent cations act as a bridge between the negative charged surfaces, and the adhesion of negatively charged MVs on a bacterial cellular surface is stabilized (Kadurugamuwa and Beveridge, 1996; Tashiro et al., 2010b).

Hydrophobicity of a cellular surface is also an important factor for adhesion of MVs on bacterial cells. It has been shown that *P. aeruginosa* MVs can more easily attach to the hydrophilic surface of *Bacillus subtilis* than to other Gram-positive bacteria (Macdonald and Beveridge, 2002), indicating that liberated MVs from bacterial cells can selectively interact with bacterial cells. Nakao et al. developed a novel method to purify MVs derived from *Porphyromonas gingivalis* using epoxy-coated magnetic beads (Nakao et al., 2014) and the authors suggested that binding between MVs and epoxy beads is facilitated via a hydrophobic interaction.

In another report, MVs derived from *Myxococcus xanthus* adhered not only to the cells but also to MVs to form vesicle chains between cells (Remis et al., 2014). The detailed mechanism of the connection has not yet been elucidated, but it has been suggested that lipopolysaccharides (LPS) plays a role in MV-cell recognition because the distance between MVs and cellular surface was 5–10 nm, corresponding to the LPS.

Thus, MVs secreted from bacteria have characteristic surfaces and possess variable potential to attach to certain surfaces. Because specific proteins are selectively assimilated into MVs from bacterial cells, it is possible that the association of MVs with bacterial cells is a highly specific process based on a specific ligand-receptor interaction.

## Transfer of MV Interior Substances to Microbial Cells

The importance of the contents of MVs has been exemplified by the critical role the transported material plays in the transfer of DNA (Figure 1C) (Dorward et al., 1989; Kolling and Matthews,

1999; Yaron et al., 2000; Klieve et al., 2005; Chiura et al., 2011; Gaudin et al., 2013; Fulsundar et al., 2014; Ho et al., 2015), bacterial lysis (Figure 1D) (Kadurugamuwa and Beveridge, 1996, 1999; Kadurugamuwa et al., 1998; Li et al., 1998; Evans et al., 2012; Remis et al., 2014) and QS-regulated gene expression (Tashiro et al., 2010b). It should be noted that membrane fusion does not always occur when interior substances in MVs are transferred to bacterial cells.

With regard to DNA transfer via MVs, the adhesion of MVs with bacterial cellular surface but not membrane fusion has been confirmed by transmission electron microscope observation in *E. coli* O157:H7 (Kolling and Matthews, 1999). Recently, however, it has been shown that MVs are integrated to recipient cells and DNA is transferred from *Acinetobacter baylyi* to *E. coli* and *A. baylyi* (Fulsundar et al., 2014).

Microbial predation using MVs occurs when virulent factors or peptidoglycan hydrolytic enzymes contained in MVs are transferred to other bacterial cells. It has been suggested that the mechanism of bacterial lysis via MVs secreted from Gram-negative bacteria differs in whether recipient cells are Gram-negative or positive. MVs derived from *P. aeruginosa* can attach to the surface of *E. coli* and *Staphylococcus aureus*, while they are able to fuse with *E. coli* but not *S. aureus* (Kadurugamuwa and Beveridge, 1996). The authors have suggested a possible mechanism described below. Because MVs have high curvature, negatively charged O-side chains of LPS are loosely packaged and they could form salt-bridging by cations such as  $Ca^{2+}$  and  $Mg^{2+}$ , with bacterial surfaces on which such cations are rich. For the association of MVs with a Gram-positive bacterial surface, this event would break apart the high curvature of MVs, and thereby open MVs, resulting in the liberation of interior lytic enzymes and the digestion of the cell wall. This event would enable the transition of the content from MVs to cells, possibly through permeation of the cellular membrane without fusion. On the other hand, MVs fuse into outer membrane of Gram-negative bacteria because they possess a compatible bilayer surface. Thus, it is considered that selective MV integration with recipient cells occurs, but interior substances in MVs can be transferred to microbial cells even when MVs just adhere on the cellular surfaces.

## Concluding Remarks and Perspectives

Therefore, MVs encapsulate signaling substances secreted from cells, protect these substances from environmental stresses and maintain these substances at high concentrations. In addition, signals associated with MVs are likely transferred to specific bacterial cells. Such signal transfer via MVs is considerably different from diffusion-based cell-to-cell communication (Figure 1B). The transfer of substances via MVs increases accuracy, swiftness and effectiveness of responses in combating predation, HGT and QS. Thus, cell-to-cell communications are comprised of not only a simple method based on diffusive substances but also very complicated

aspects. Microbes intricately communicate through as-yet-unknown methods using MVs, thereby influencing interspecies networks, microbial community organization and ecosystem dynamics.

## References

- Balch, W. E., Glick, B. S., and Rothman, J. E. (1984). Sequential intermediates in the pathway of intercompartmental transport in a cell-free system. *Cell* 39, 525–536. doi: 10.1016/0092-8674(84)90459-8
- Bauman, S. J., and Kuehn, M. J. (2009). *Pseudomonas aeruginosa* vesicles associate with and are internalized by human lung epithelial cells. *BMC Microbiol* 9:26. doi: 10.1186/1471-2180-9-26
- Beveridge, T. (1999). Structures of gram-negative cell walls and their derived membrane vesicles. *J. Bacteriol.* 181, 4725–4733.
- Bielaszewska, M., Rüter, C., Kunsmann, L., Greune, L., Bauwens, A., Zhang, W., et al. (2013). Enterohemorrhagic *Escherichia coli* hemolysin employs outer membrane vesicles to target mitochondria and cause endothelial and epithelial apoptosis. *PLoS Pathog.* 9:e1003797. doi: 10.1371/journal.ppat.1003797
- Chatterjee, D., and Chaudhuri, K. (2011). Association of cholera toxin with *Vibrio cholerae* outer membrane vesicles which are internalized by human intestinal epithelial cells. *FEBS Lett.* 585, 1357–1362. doi: 10.1016/j.febslet.2011.04.017
- Chiura, H. X., Kogure, K., Hagemann, S., Ellinger, A., and Velimirov, B. (2011). Evidence for particle-induced horizontal gene transfer and serial transduction between bacteria. *FEMS Microbiol. Ecol.* 76, 576–591. doi: 10.1111/j.1574-6941.2011.01077.x
- Dorward, D. W., Garon, C. F., and Judd, R. C. (1989). Export and intercellular transfer of DNA via membrane blebs of *Neisseria gonorrhoeae*. *J. Bacteriol.* 171, 2499–2505.
- Elmi, A., Watson, E., Sandu, P., Gundogdu, O., Mills, D. C., Inglis, N. F., et al. (2012). *Campylobacter jejuni* outer membrane vesicles play an important role in bacterial interactions with human intestinal epithelial cells. *Infect. Immun.* 80, 4089–4098. doi: 10.1128/IAI.00161-12
- Evans, A. G. L., Davey, H. M., Cookson, A., Currinn, H., Cooke-Fox, G., Stanczyk, P. J., et al. (2012). Predatory activity of *Myxococcus xanthus* outer-membrane vesicles and properties of their hydrolase cargo. *Microbiology* 158, 2742–2752. doi: 10.1099/mic.0.060343-0
- Fulsundar, S., Harms, K., Flaten, G. E., Johnsen, P. J., Chopade, B. A., and Nielsen, K. M. (2014). Gene transfer potential of outer membrane vesicles of *Acinetobacter baylyi* and effects of stress on vesiculation. *Appl. Environ. Microbiol.* 80, 3469–3483. doi: 10.1128/AEM.04248-13
- Gaudin, M., Gaulliard, E., Schouten, S., Houel-Renault, L., Lenormand, P., Marguet, E., et al. (2013). Hyperthermophilic archaea produce membrane vesicles that can transfer DNA. *Environ. Microbiol. Rep.* 5, 109–116. doi: 10.1111/j.1758-2229.2012.00348.x
- Gujrati, V., Kim, S., Kim, S.-H., Min, J. J., Choy, H. E., Kim, S. C., et al. (2014). Bioengineered bacterial outer membrane vesicles as cell-specific drug-delivery vehicles for cancer therapy. *ACS Nano* 8, 1525–1537. doi: 10.1021/n405724x
- Haurat, M. F., Elhenawy, W., and Feldman Mario, F. (2015). Prokaryotic membrane vesicles: new insights on biogenesis and biological roles. *Biol. Chem.* 396, 95. doi: 10.1515/hsz-2014-0183
- Hibbing, M. E., Fuqua, C., Parsek, M. R., and Peterson, S. B. (2010). Bacterial competition: surviving and thriving in the microbial jungle. *Nat. Rev. Microbiol.* 8, 15–25. doi: 10.1038/nrmicro2259
- Ho, M.-H., Chen, C.-H., Goodwin, J. S., Wang, B.-Y., and Xie, H. (2015). Functional advantages of *Porphyromonas gingivalis* vesicles. *PLoS ONE* 10:e0123448. doi: 10.1371/journal.pone.0123448
- Kadurugamuwa, J., Mayer, A., Messner, P., Sára, M., Sleytr, U., and Beveridge, T. (1998). S-layered *Aneurinibacillus* and *Bacillus* spp. are susceptible to the lytic action of *Pseudomonas aeruginosa* membrane vesicles. *J. Bacteriol.* 180, 2306–2311.
- Kadurugamuwa, J. L., and Beveridge, T. J. (1995). Virulence factors are released from *Pseudomonas aeruginosa* in association with membrane vesicles during normal growth and exposure to gentamicin: a novel mechanism of enzyme secretion. *J. Bacteriol.* 177, 3998–4008.
- Kadurugamuwa, J. L., and Beveridge, T. J. (1996). Bacteriolytic effect of membrane vesicles from *Pseudomonas aeruginosa* on other bacteria including pathogens: conceptually new antibiotics. *J. Bacteriol.* 178, 2767–2774.
- Kadurugamuwa, J. L., and Beveridge, T. J. (1999). Membrane vesicles derived from *Pseudomonas aeruginosa* and *Shigella flexneri* can be integrated into the surfaces of other gram-negative bacteria. *Microbiology* 145, 2051–2060. doi: 10.1099/13500872-145-8-2051
- Kesty, N., Mason, K., Reedy, M., Miller, S., and Kuehn, M. (2004). Enterotoxigenic *Escherichia coli* vesicles target toxin delivery into mammalian cells. *EMBO J.* 23, 4538–4549. doi: 10.1038/sj.emboj.7600471
- Klieve, A. V., Yokoyama, M. T., Forster, R. J., Ouwkerk, D., Bain, P. A., and Mawhinney, E. L. (2005). Naturally occurring DNA transfer system associated with membrane vesicles in cellulolytic *Ruminococcus* spp. of ruminal origin. *Appl. Environ. Microbiol.* 71, 4248–4253. doi: 10.1128/AEM.71.8.4248-4253.2005
- Kolling, G. L., and Matthews, K. R. (1999). Export of virulence genes and Shiga toxin by membrane vesicles of *Escherichia coli* O157:H7. *Appl. Environ. Microbiol.* 65, 1843–1848.
- Li, Z., Clarke, A. J., and Beveridge, T. J. (1998). Gram-negative bacteria produce membrane vesicles which are capable of killing other bacteria. *J. Bacteriol.* 180, 5478–5483.
- Macdonald, K. L., and Beveridge, T. J. (2002). Bactericidal effect of gentamicin-induced membrane vesicles derived from *Pseudomonas aeruginosa* PAO1 on gram-positive bacteria. *Can. J. Microbiol.* 48, 810–820. doi: 10.1139/w02-077
- Mashburn, L. M., and Whiteley, M. (2005). Membrane vesicles traffic signals and facilitate group activities in a prokaryote. *Nature* 437, 422–425. doi: 10.1038/nature03925
- Mcnew, J. A., Parlati, F., Fukuda, R., Johnston, R. J., Paz, K., Paumet, F., et al. (2000). Compartmental specificity of cellular membrane fusion encoded in SNARE proteins. *Nature* 407, 153–159. doi: 10.1038/35025000
- Nakao, R., Kikushima, K., Higuchi, H., Obana, N., Nomura, N., Bai, D., et al. (2014). A novel approach for purification and selective capture of membrane vesicles of the periodontopathic bacterium, *Porphyromonas gingivalis*: membrane vesicles bind to magnetic beads coated with epoxy groups in a noncovalent, species-specific manner. *PLoS ONE* 9:e95137. doi: 10.1371/journal.pone.0095137
- Parker, H., Chitcholtan, K., Hampton, M. B., and Keenan, J. I. (2010). Uptake of *Helicobacter pylori* outer membrane vesicles by gastric epithelial cells. *Infect. Immun.* 78, 5054–5061. doi: 10.1128/IAI.00299-10
- Remis, J. P., Wei, D., Gorur, A., Zemla, M., Haraga, J., Allen, S., et al. (2014). Bacterial social networks: structure and composition of *Myxococcus xanthus* outer membrane vesicle chains. *Environ. Microbiol.* 16, 598–610. doi: 10.1111/1462-2920.12187
- Renelli, M., Matias, V., Lo, R. Y., and Beveridge, T. J. (2004). DNA-containing membrane vesicles of *Pseudomonas aeruginosa* PAO1 and their genetic transformation potential. *Microbiology* 150, 2161–2169. doi: 10.1099/mic.0.26841-0
- Rompikuntal, P. K., Thay, B., Khan, M. K., Alanko, J., Penttinen, A.-M., Asikainen, S., et al. (2012). Perinuclear localization of internalized outer membrane vesicles carrying active cytolethal distending toxin from *Aggregatibacter actinomycetemcomitans*. *Infect. Immun.* 80, 31–42. doi: 10.1128/IAI.06069-11
- Sollner, T., Whiteheart, S. W., Brunner, M., Erdjument-Bromage, H., Geromanos, S., Tempst, P., et al. (1993). SNAP receptors implicated in vesicle targeting and fusion. *Nature* 362, 318–324. doi: 10.1038/362318a0
- Tashiro, Y., Ichikawa, S., Nakajima-Kambe, T., Uchiyama, H., and Nomura, N. (2010a). *Pseudomonas* quinolone signal affects membrane vesicle production

- in not only Gram-negative but also Gram-positive bacteria. *Microb. Environ.* 25, 120–125. doi: 10.1264/jsme2.ME09182
- Tashiro, Y., Ichikawa, S., Shimizu, M., Toyofuku, M., Takaya, N., Nakajima-Kambe, T., et al. (2010b). Variation of physicochemical properties and cell association activity of membrane vesicles with growth phase in *Pseudomonas aeruginosa*. *Appl. Environ. Microbiol.* 76, 3732–3739. doi: 10.1128/AEM.02794-09
- Tashiro, Y., Uchiyama, H., and Nomura, N. (2012). Multifunctional membrane vesicles in *Pseudomonas aeruginosa*. *Environ. Microbiol.* 14, 1349–1362. doi: 10.1111/j.1462-2920.2011.02632.x
- Tashiro, Y., Yawata, Y., Toyofuku, M., Uchiyama, H., and Nomura, N. (2013). Interspecies interaction between *Pseudomonas aeruginosa* and other microorganisms. *Microb. Environ.* 28, 13–24. doi: 10.1264/jsme2.ME12167
- Wilson, D. W., Wilcox, C. A., Flynn, G. C., Chen, E., Kuang, W.-J., Henzel, W. J., et al. (1989). A fusion protein required for vesicle-mediated transport in both mammalian cells and yeast. *Nature* 339, 355–359. doi: 10.1038/339355a0
- Yaron, S., Kolling, G., Simon, L., and Matthews, K. (2000). Vesicle-mediated transfer of virulence genes from *Escherichia coli* O157:H7 to other enteric bacteria. *Appl. Environ. Microbiol.* 66, 4414–4420. doi: 10.1128/AEM.66.10.4414-4420.2000

**Conflict of Interest Statement:** The authors declare that the research was conducted in the absence of any commercial or financial relationships that could be construed as a potential conflict of interest.

Copyright © 2015 Hasegawa, Futamata and Tashiro. This is an open-access article distributed under the terms of the Creative Commons Attribution License (CC BY). The use, distribution or reproduction in other forums is permitted, provided the original author(s) or licensor are credited and that the original publication in this journal is cited, in accordance with accepted academic practice. No use, distribution or reproduction is permitted which does not comply with these terms.

# Mathematical modeling of dormant cell formation in growing biofilm

Kotaro Chihara<sup>1†</sup>, Shinya Matsumoto<sup>2†</sup>, Yuki Kagawa<sup>3†</sup> and Satoshi Tsuneda<sup>1,3\*</sup>

<sup>1</sup> Department of Life Science and Medical Bioscience, Waseda University, Tokyo, Japan, <sup>2</sup> Center for Biofilm Engineering, Montana State University, Bozeman, MT, USA, <sup>3</sup> Institute for Nanoscience and Nanotechnology, Waseda University, Tokyo, Japan

## OPEN ACCESS

### Edited by:

Hiroyuki Futamata,  
Shizuoka University, Japan

### Reviewed by:

Roy D. Welch,  
Syracuse University, USA  
Takeshi Miki,  
National Taiwan University, Taiwan

### \*Correspondence:

Satoshi Tsuneda,  
Department of Life Science and  
Medical Bioscience, Waseda  
University, 2-2 Wakamatsu-cho,  
Shinjuku, Tokyo 162-8480, Japan  
stsuneda@waseda.jp

<sup>†</sup>These authors have contributed  
equally to this work.

### Specialty section:

This article was submitted to  
Systems Microbiology,  
a section of the journal  
Frontiers in Microbiology

**Received:** 10 February 2015

**Accepted:** 14 May 2015

**Published:** 28 May 2015

### Citation:

Chihara K, Matsumoto S, Kagawa Y  
and Tsuneda S (2015) Mathematical  
modelling of dormant cell formation in  
growing biofilm.  
Front. Microbiol. 6:534.  
doi: 10.3389/fmicb.2015.00534

Understanding the dynamics of dormant cells in microbial biofilms, in which the bacteria are embedded in extracellular matrix, is important for developing successful antibiotic therapies against pathogenic bacteria. Although some of the molecular mechanisms leading to bacterial persistence have been speculated in planktonic bacterial cell, how dormant cells emerge in the biofilms of pathogenic bacteria such as *Pseudomonas aeruginosa* remains unclear. The present study proposes four hypotheses of dormant cell formation; stochastic process, nutrient-dependent, oxygen-dependent, and time-dependent processes. These hypotheses were implemented into a three-dimensional individual-based model of biofilm formation. Numerical simulations of the different mechanisms yielded qualitatively different spatiotemporal distributions of dormant cells in the growing biofilm. Based on these simulation results, we discuss what kinds of experimental studies are effective for discriminating dormant cell formation mechanisms in biofilms.

**Keywords:** biofilm, dormancy, persistence, individual-based modeling, mathematical model

## Introduction

In natural environments or within the tissues of living organisms, some bacterial species form biofilms to ensure their long-term survival (Costerton et al., 1999; Hall-Stoodley et al., 2004). Bacteria attached to solid surfaces form mature biofilms by proliferating and producing extracellular polymeric substance (EPS), which captures planktonic bacteria (Stewart and Franklin, 2008). The EPS is composed of DNA molecules, proteins and polysaccharide. The thick biofilm structure impedes antibiotic diffusion and reduces the mobility of immune cells. Therefore, biofilms are responsible for the chronic and intractable characteristics of bacterial infectious disease (Stewart and Costerton, 2001; Stewart, 2002), which increase the morbidity and mortality of infections in immunocompromised patients. For example, intractable *Pseudomonas aeruginosa* infections have been reported in cystic fibrosis patients (Harrison, 2007).

One aspect of chronic characteristics of bacterial infectious disease is persister cells, which can tolerate sublethal concentrations of antibiotics. Unlike antibiotic resistant cells that carry genetic mutations, persister cells are nonheritable phenotypic variants. Some persister cells suppress their metabolism, including cell membrane formation, protein synthesis, and DNA replications (Lewis, 2007; Lewis et al., 2010). Such dormant bacteria can survive antibiotic exposure because their antibiotic target sites are deactivated. Actually, Balaban et al. (2004) investigated the single cell dynamics of the high persistence (*hip*) mutants (Moyed and Bertrand, 1983) of *Escherichia coli* by using microfluidic devices and found that preexisting subpopulations having reduced growth rates showed persistence under ampicillin exposure.

Several mechanisms of dormant cell formation have been proposed (Maisonneuve and Gerdes, 2014). Elowitz et al. (2002) posited that bacterial gene expressions related to physiological states are stochastically activated or inactivated. Expansion of this stochastic gene noise induces the formation of the stable subpopulation of some different bacterial phenotypes, such as dormant cell and active cell (Balaban et al., 2004). However, whether dormant cell is formed stochastically in a biofilm is unclear because previous studies were conducted by use of planktonic bacterial cell. Other researchers indicated that low nutrient concentration and diauxic shift of carbon initiate the ppGpp-controlled stress response, which activates the signal pathways for cell dormancy in planktonic bacterial cell (Nguyen et al., 2011; Amato et al., 2013). In a more recent study, Wakamoto et al. (2013) investigated persister cell dynamics of *Mycobacterium smegmatis* at a single cell level by microfluidic device in the presence of the drug isoniazid (INH) and time-lapse microscopy measurement. They showed that all persister cells did not necessarily repress their division, and persister cell did not always include dormant cell in the INH disposal of *M. smegmatis*, whereas dormant cell always included persister cell. Moreover, they showed that persister cells appeared due to the genetic stochastic expression encoded catalase-peroxidase (KatG), which activates INH.

During the biofilm formation, bacteria consume nutrients and oxygen, creating oxygen and nutrient concentration gradients within the developing biofilm (Stewart and Franklin, 2008). Therefore, dormant cells will emerge from the bottom of the biofilms, where the nutrient and oxygen are depleted to induce the dormant state due to the direct effect of nutrient or oxygen limitation, or the indirect effect of time-dependent growth arrest. To prevent the emergence of dormant cells, we need to elucidate the dynamics of dormant cell formation in growing biofilms. However, the spatiotemporal dynamics by which dormant cells emerge in growing biofilms are difficult to investigate, because experimental methods for specifically detecting dormant cells are not sufficiently developed. Consequently, which mechanisms of dormancy; stochastic, nutrient limitation, oxygen limitation, and time-dependent growth arrest, has a major impact against the bacterial dormancy within growing biofilm is unknown.

Experiments can be complemented by mathematical modeling, which has become one of the most promising tools for studying the emergence of dormant cells in growing biofilms. Many mathematical models of biofilm formation in specific environments have been developed. Multi-species biofilm formation has been modeled by one-dimensional partial differential equations describing a reaction–diffusion system (Rittmann et al., 2002). Other researchers have adopted two- and three-dimensional cellular automaton algorithms that replicate the complex structures of porous biofilms, such as mushroom-like structures with many voids and channels (Picioreanu et al., 1998a,b). An individual-based modeling (IbM) approach originally proposed for bacterial colony growth (Kreft et al., 1998), in which bacterial cells were represented as hard spheres, has been adapted to biofilms and microbial granule modeling by allowing continuous displacements and directions of the biomass

particles (Picioreanu et al., 2004; Matsumoto et al., 2010; Kagawa et al., 2015). The IbM algorithm is considered as a suitable basis for describing the dynamics of rare species such as dormant cells in growing biofilms.

Therefore, in the present study, we develop three-dimensional biofilm models based on the IbM algorithm to understand and predict the formation of dormant cells within growing biofilms. We propose four hypothetical mechanisms of dormant cell formation. Using the proposed model, we then simulate the spatiotemporal dynamics of dormant cell emergence under each hypothesis. Finally, we discuss what kinds of potential experimental design are effective for verifying the given hypotheses.

## Methods

We first constructed a three-dimensional biofilm model based on the IbM algorithm. Next, we implemented four hypothetical mechanisms of dormant cell formation in the model. Here we proposed that dormant cells were formed by stochastic, nutrient-dependent, oxygen-dependent, or time-dependent processes. Using the developed model, we numerically simulated the spatiotemporal formation of dormant cells in a growing biofilm. Particularly, we perturbed the bulk nutrient or oxygen concentration, and observed the changes in the dormant cell distribution throughout the biofilm. Finally, based on these simulation results, we discussed what kinds of experimental approaches are effective for discriminating the above-mentioned hypotheses. The discussed experiments should provide new insights into the mechanisms of dormant cell formation.

### Construction of a Three-dimensional Biofilm Model

Our three-dimensional (3D) mathematical model of biofilm formation is based on the IbM algorithm (Picioreanu et al., 2007). Parameter values used in this model are summarized in **Table 1**. Each bacterial cell is represented as a sphere of radius  $R$  positioned at  $(x, y, z)$  in 3D space. The radius is given by:

$$R = (3m/4\pi c)^{1/3}, \quad (1)$$

where  $m$  and  $c$  are the mass and density of the cells, respectively. Each particle undergoes the following three behaviors of real bacteria (Supplementary Figure 1A):

(i) *Growth*: Each bacterial cell consumes nutrient at a rate given by:

$$q = q^{\max} \cdot [S_S/(S_S + K_S)] \cdot [S_O/(S_O + K_O)], \quad (2)$$

where  $q^{\max}$  is the maximum consumption rate,  $S_S$  and  $S_O$  are the local concentrations of the nutrient and oxygen, respectively, and  $K_S$  and  $K_O$  are the half-saturation constants of the nutrient and oxygen, respectively. Cells consume oxygen along with nutrient, and increase their masses according to the stoichiometric ratios defined in **Tables 2, 3**.

(ii) *Division*: When a cell reaches its maximum mass, it divides into two uniform daughter cells. The daughter cells do not

**TABLE 1 | Parameter values used in 3D biofilm model.**

Parameter	Symbol	Value	Unit	References
Time step	$\Delta t$	0.2	h	
System size	$L_x, L_y, L_z$	$2.0 \times 10^{-4}$	m	Picioreanu et al., 2007
Grid number	$N, M, L$	33		
Thickness of boundary layer	$N_{bl}$	3	$\Delta x (= L_x/N)$	This study
Maximum consumption rate of active cell	$q_A^{max}$	75	(gCOD/gCOD)/day	Picioreanu et al., 2007
Maximum consumption rate of dormant cell	$q_D^{max}$	15	(gCOD/gCOD)/day	This study
Maximum cell density	$C$	$1.5 \times 10^5$	gCOD/m <sup>3</sup>	Picioreanu et al., 2007
Maximum cell mass	$m_{max}$	$9.60 \times 10^{-12}$	gCOD	This study
Initial cell mass	$m_{min}$	$4.80 \times 10^{-12}$	gCOD	This study
Bulk concentration of oxygen	$C_O^{bulk}$	4.0	g/m <sup>3</sup>	Xavier et al., 2005
Bulk concentration of nutrient	$C_S^{bulk}$	100	gCOD/m <sup>3</sup>	Xavier et al., 2005
Diffusion coefficient of oxygen	$D_O$	$2.0 \times 10^{-4}$	m <sup>2</sup> /day	Xavier et al., 2005
Diffusion coefficient of nutrient	$D_S$	$4.5 \times 10^{-6}$	m <sup>2</sup> /day	Picioreanu et al., 2007
Half saturation constant of oxygen	$K_O$	0.35	g/m <sup>3</sup>	Xavier et al., 2005
Half saturation constant of nutrient	$K_S$	20	gCOD/m <sup>3</sup>	Picioreanu et al., 2007

**TABLE 2 | Stoichiometric matrix and kinetic rate expressions.**

Process	Solute species		Particle species		Rate
	$S_S$	$S_O$	$X_A$	$X_D$	
Growth of active cell	-1	$-(1-Y_A)$	$Y_A$		$q_A^{max} \cdot [S_S/(S_S+K_S)] \cdot [S_O/(S_O+K_O)] \cdot X_A$
Growth of dormant cell	-1	$-(1-Y_D)$		$Y_D$	$q_D^{max} \cdot [S_S/(S_S+K_S)] \cdot [S_O/(S_O+K_O)] \cdot X_D$

overlap but remain attached, as described previously (Picioreanu et al., 2004).

(iii) *Shoving*: The growth and division processes cause overlapping of the spherical particles. To minimize these overlaps, each particle pushes its neighboring particles multiple times in the shoving algorithm (Picioreanu et al., 2004). Kagawa et al. (2014) related the number of shoves to the area of the overlap region in two-dimensional (2D) space. In the present study, the number of shoves was fixed at 200. Previous models considered bacterial decay, death and detachment processes (Xavier et al., 2005); these factors were excluded in the present model.

Movement of the particles obeys the following two boundary conditions: (a) particles cannot penetrate into the bottom surface of the system, and (b) periodic boundary conditions are imposed at the lateral boundaries.

The spatial distributions of the nutrient and oxygen concentrations were calculated by the following reaction-diffusion equations:

$$\partial_t S_S = D_S(\partial_x^2 S_S + \partial_y^2 S_S + \partial_z^2 S_S) + r_S, \quad (3)$$

$$\partial_t S_O = D_O(\partial_x^2 S_O + \partial_y^2 S_O + \partial_z^2 S_O) + r_O, \quad (4)$$

where  $D_S$  and  $D_O$  are the diffusion coefficients of the nutrient and oxygen, respectively.  $r_S$  and  $r_O$  are the net reaction rates of the nutrient and oxygen respectively, obtained by summing the

**TABLE 3 | Stoichiometric parameters for microbial reactions.**

Parameters	Symbol	Value	Unit	Reference
Yield on nutrient at active cell	$Y_A$	0.5	gCOD/gCOD	Xavier et al., 2005
Yield on nutrient at dormant cell	$Y_D$	0	gCOD/gCOD	This study

rates of all processes involving these respective growth factors. Explicitly,  $r_S$  and  $r_O$  are expressed by the following equations:

$$r_S = -q_A \cdot X_A - q_D \cdot X_D, \quad (5)$$

$$r_O = -(1 - Y_A)q_A \cdot X_A - (1 - Y_D)q_D \cdot X_D, \quad (6)$$

where  $X_A$  and  $X_D$  are the local biomass densities of active and dormant cells, respectively.

The 3D reaction-diffusion Equations (3–6) are numerically solved under the following three boundary conditions (the coordinate system of the cubic computational space is defined in Supplementary Figure 1B): (a) A Dirichlet boundary condition is imposed along the top boundary, i.e., the concentration remains constant at the interface between boundary layer and bulk liquid. The boundary is defined as the plane  $x = (N_{bf} + N_{bl}) \Delta x$ , where  $N_{bf}$  and  $N_{bl}$  are the maximum biofilm thickness and the boundary layer thickness, respectively, expressed in units of grid size (integer), defined as  $\Delta x = L_x/N$ . Note that this boundary moves upwards as the biofilm grows over time. This boundary

**TABLE 4 | Parameter values of simulated dormant cells.**

Mechanism of dormancy	Parameter	Symbol	Values used in simulation	Unit
(i) Stochastic process	Frequency of dormancy	$R_{a \rightarrow d}$	0.01, 0.02, 0.04	day <sup>-1</sup>
(ii.a) Nutrient-dependent process*	Half saturation constant of nutrient	$K_S$	2, 20, 200	gCOD/m <sup>3</sup>
(ii.b) Oxygen-dependent process*	Half saturation constant of oxygen	$K_O$	0.035, 0.35, 3.5	g/m <sup>3</sup>
(iii) Time-dependent process	Threshold time to become dormancy	$T_{a \rightarrow d}$	10, 12, 14	h

\*In these mechanisms, the maximum frequency of dormancy  $R_{a \rightarrow d}^{\max}$  was set to 0.12 day<sup>-1</sup>.

condition is expressed as:

$$S_S(x, y, z) = S_S^{\text{bulk}} \text{ and } S_O(x, y, z) = S_O^{\text{bulk}},$$

$$\text{for } x \geq (N_{\text{bf}} + N_{\text{bl}})\Delta x. \quad (7)$$

(b) Neumann boundary conditions are imposed at the bottom of the system, where the nutrient and oxygen fluxes are zero:

$$\partial_x S_S(x = 0, y, z) = 0 \text{ and } \partial_x S_O(x = 0, y, z) = 0, \quad (8)$$

and (c) periodic boundary conditions are imposed at the lateral boundaries:

$$S_S(x, y = 0, z) = S_S(x, y = L_y, z),$$

$$S_O(x, y = 0, z) = S_O(x, y = L_y, z),$$

$$S_S(x, y, z = 0) = S_S(x, y, z = L_z),$$

$$\text{and } S_O(x, y, z = 0) = S_O(x, y, z = L_z). \quad (9)$$

### Implementation of Dormant Cell Formation Mechanisms

Four possible mechanisms of dormant cell formation were implemented in the 3D biofilm model. These mechanisms are briefly described below.

- (i) Dormant cell formation by stochastic process: Bacterial cells stochastically enter the dormant state anywhere in the biofilm at constant frequency  $R_{a \rightarrow d}$  (unit = day<sup>-1</sup>) (Chambless et al., 2006).
- (ii) Dormant cell formation by a nutrient-dependent process or an oxygen-dependent process: Bacterial cells rarely become dormant cells at high nutrient or oxygen concentration, but readily become dormant at low nutrient or oxygen concentration. The frequency of dormant cell formation by a nutrient-dependent or an oxygen-dependent process is respectively given by:

$$R_{a \rightarrow d} = R_{a \rightarrow d}^{\max} \exp(-S/K). \quad (10)$$

where  $S$  (g/m<sup>3</sup>) is the concentration of nutrient ( $S_S$ ) or oxygen ( $S_O$ ),  $K$  (g/m<sup>3</sup>) is the half saturation constant of nutrient ( $K_S$ ) or oxygen ( $K_O$ ), and  $R_{a \rightarrow d}^{\max}$  (day<sup>-1</sup>) is the maximum frequency of dormancy.

- (iii) Dormant cell formation by a time-dependent process: Bacterial cells become dormant when the duration from the last division exceeds some threshold time  $T_{a \rightarrow d}$  (h).

Each mechanism was simulated using the parameter values specified in **Table 4**. In the simulation, dormant cells are shown in red to visualize their distribution through the biofilm. Dormant cells consume a small amount of nutrient and oxygen for their maintenance without growing. We did not implement the resuscitation of dormant cells in this model because the molecular mechanisms behind the switching back to growth after dormancy are largely unknown.

### Numerical Simulations

The simulation flow is detailed elsewhere (Picioreanu et al., 2004). Briefly, the initial condition of each simulation ( $t = 0$ ) is ten particles with mass  $m_{\text{min}}$  randomly inoculated along the bottom surface ( $x = 0$ ). In each time step, the spatial distributions of the nutrient and oxygen in the system were obtained by solving Equations (3–9) in steady state. The particles grew, divided, or entered the dormant state as described above. Biofilm formation was simulated for 1 day, or 2 days in cases of slow-growing biofilms. Three simulations with different seeds were conducted for each hypothesis.

### Quantitative Analysis of the Distribution of Dormant Cells in Biofilm

The composition ratio of the dormant cells along the  $x$  direction of the biofilm, i.e., the height from the bottom surface, was derived from the simulation results. First, the particles residing at  $x = 0.8H$ , where  $H$  is the maximum biofilm thickness (in  $\mu\text{m}$ ), were collected, and the positions ( $x$ ) and states (dormant or active) of all particles below the collected particle were investigated. Precisely, if the collected particle was located at ( $x_p, y_p, z_p$ ), all particles with centers positioned at ( $x_l, y_l, z_l$ ) satisfying the following criteria were investigated;

$$(y_l - y_p)^2 + (z_l - z_p)^2 < R_l^2, \quad (11)$$

where  $R_l$  is the radius of the particle. Note that  $x_l$  can be less than  $0.8H$ . For each run of the simulation, fifty to two-hundred particles were collected (i.e., these particles resided at  $x = 0.8H$ ). Position data of dormant cells below the collected particles were accumulated in three runs of simulations and calculated the abundance of dormant cells for each height level.

### Results and Discussion

Representative examples of the simulated growing biofilms, assuming each hypothesis of dormant cell formation, are shown

in Movies 1–4 (Supplementary Material). **Figure 1** shows cross-sections of the biofilms 24 h after inoculation. As shown in this figure, the morphologies of the formed biofilms are very similar under the different hypotheses. Moreover, spatiotemporal dynamics of nutrient and oxygen concentrations within growing biofilms are shown in Movies 5–12 (Supplementary Material). As shown in these Movies, the spatial distributions of nutrient and oxygen are also very similar under the different hypotheses. However, nutrient was completely depleted at the bottom of the biofilm whereas oxygen remained even at the bottom of the biofilm (the value of the oxygen concentration at the bottom of the biofilm was about  $2.9 \text{ g/m}^3$ ). Therefore, concentration gradients of nutrient and oxygen were different within growing biofilms.

On the other hand, **Figure 1** reveals prominent differences in the spatial distributions of dormant cells among the four models. For example, when the cells become dormant by a time-dependent process (**Figure 1D**), they are restricted to the bottom of the biofilm, whereas they are widely distributed throughout the biofilms in the other three models. This reflects the low growth rate of bacterial cells residing near the bottom of the biofilm, where the nutrient and/or oxygen concentrations are substantially reduced. In fact, when the threshold value  $T_{a \rightarrow d}$  was decreased in the simulations, the region of dormant cells expanded toward the upper region of the biofilm (data not shown). Thus, the size of the dormant region strongly depends on the model parameter values. Moreover, when the half saturation constant of the nutrient  $K_S$  was decreased and the maximum frequency of dormant cell formation  $R_{a \rightarrow d}^{\max}$  was increased in the nutrient-dependent hypothesis, the dormant cell distribution was similar to that of **Figure 1D**, i.e., dormant cells distributed exclusively near the bottom of the biofilm (Supplementary

Figure 2). Thus, the shape of the dormant region is sensitive to the model parameter values.

Because the parameter values related to dormant cell formation alter the spatial distributions of dormant cells both qualitatively (the shape of the dormant region) and quantitatively (the size of the dormant region), the four hypotheses cannot be discriminated merely from the spatial distributions of dormant cells at a given time. Therefore, we simulated time evolution of the spatial distribution of dormant cells in each of the four proposed models (**Figure 2**). In this investigation, when dormancy was driven by a time-dependent process (**Figure 2D**), dormant cells emerged 20 h after inoculation. This process of dormant cell formation was very different from those of the other three models.

All three of the remaining models underwent similar processes of dormant cell formation. Dormant cells were widely distributed throughout the biofilms, and their abundances decreased with increasing height from the bottom of the biofilm (**Figures 2A–C**).

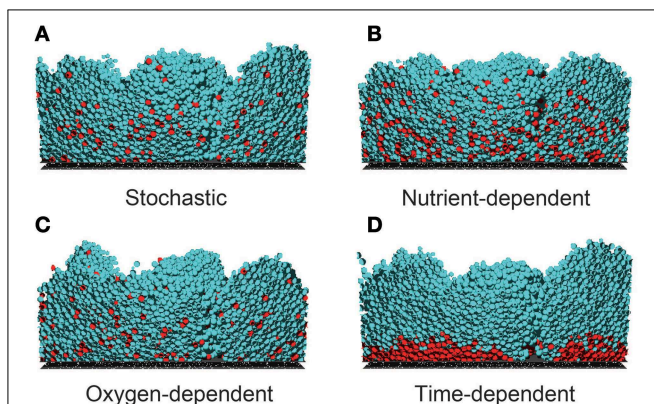


**FIGURE 1 | Cross sections of biofilms 24 h post-inoculation, developed under four dormancy mechanisms.** Dormancy was induced by (A) stochastic process ( $R_{a \rightarrow d} = 0.04 \text{ day}^{-1}$ ), (B) nutrient-dependent process ( $K_S = 20 \text{ gCOD/m}^3$ ), (C) oxygen-dependent process ( $K_O = 3.5 \text{ g/m}^3$ ), and (D) a time-dependent process ( $T_{a \rightarrow d} = 14 \text{ h}$ ). In the stochastic, nutrient-dependent and oxygen-dependent processes, the dormant cells are widely distributed through the biofilm. In the time-dependent process, dormant cells reside near the bottom of the biofilm. These spatial distributions of dormant cells largely depend on the parameter values related to the dormant cell formation mechanism (see Supplementary Figure 2).

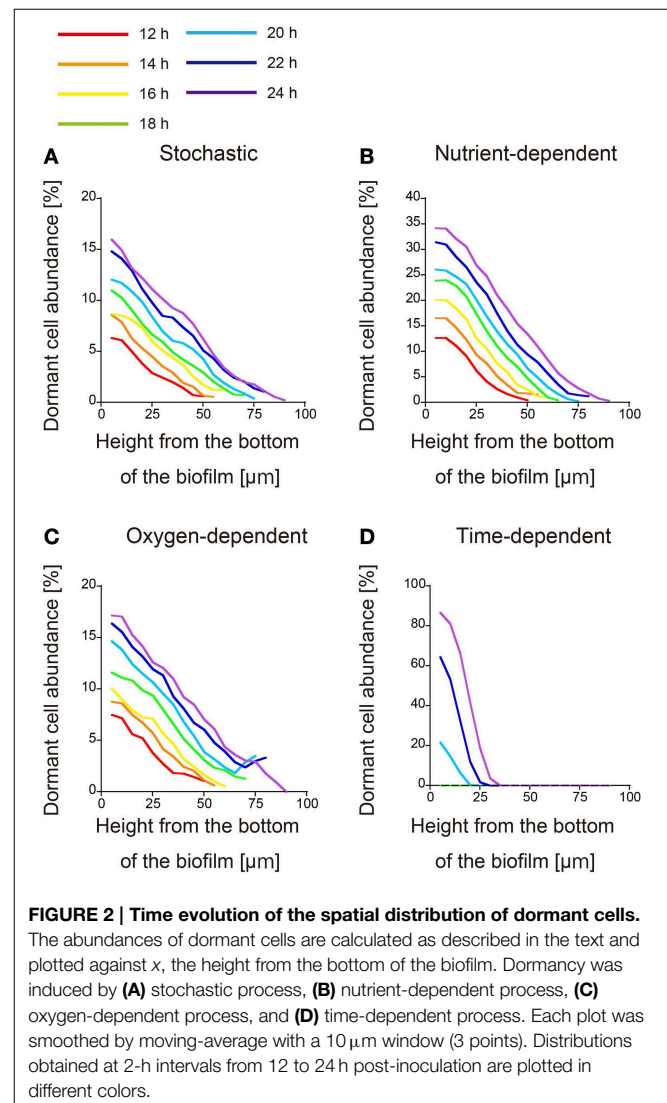


**FIGURE 2 | Time evolution of the spatial distribution of dormant cells.** The abundances of dormant cells are calculated as described in the text and plotted against  $x$ , the height from the bottom of the biofilm. Dormancy was induced by (A) stochastic process, (B) nutrient-dependent process, (C) oxygen-dependent process, and (D) time-dependent process. Each plot was smoothed by moving-average with a  $10 \mu\text{m}$  window (3 points). Distributions obtained at 2-h intervals from 12 to 24 h post-inoculation are plotted in different colors.

Counter-intuitively, the abundance of dormant cells established a gradient along the  $x$  direction in the stochastically driven dormancy model, although the probability of dormant cell formation is position-independent in this model (Figure 2A). This gradient probably resulted from the cell velocity gradient along  $x$ , which was driven by the cell division process. Namely, the velocity in deeper biofilm regions was lower than in higher regions because of the low nutrient and oxygen concentrations. To test this, we conducted the additional simulation under the condition that dormant cells are formed by stochastic process as described below. In the simulation, to cancel the variation in cell velocities along the  $x$  direction, we reset  $K_S$  and  $K_O$  to be very small values. The results showed that the abundance of dormant cells did not establish a gradient along the  $x$  direction (Supplementary Figure 3). Therefore, the variation in the cell velocities along the  $x$  direction is responsible for the gradient of the abundance of dormant cells in the stochastically driven dormancy model.

To confirm the difference between these three models, we can investigate how the dormant cell distribution responds to an increase or decrease in the nutrient and oxygen concentrations in the bulk liquid. Such an investigation should be simple and straightforward. Thus, biofilm formation was simulated under three conditions of nutrient and oxygen concentrations in the bulk liquid (expressed in units of  $\text{gCOD}/\text{m}^3$  and  $\text{g}/\text{m}^3$ , respectively): (condition I)  $10 \text{ gCOD}/\text{m}^3$  and  $0.4 \text{ g}/\text{m}^3$ , (condition II)  $10 \text{ gCOD}/\text{m}^3$  and  $8 \text{ g}/\text{m}^3$ , and (condition III)  $200 \text{ gCOD}/\text{m}^3$  and  $0.4 \text{ g}/\text{m}^3$ . When dormant cell formation was induced by stochastic or time-dependent processes, the dormant cell distribution was not qualitatively affected by altering the bulk concentrations of nutrient and oxygen, i.e., there was a height gradient in the abundance of dormant cells under all three conditions (Figures 3A,D). Conversely, if dormancy was induced by a nutrient-dependent process, dormant cells rarely emerged in the biofilm at very high nutrient concentration ( $200 \text{ gCOD}/\text{m}^3$ ; condition III) (Figure 3B). Similarly, in the oxygen-dependent model, dormant cells rarely emerged when the oxygen concentration was high ( $8 \text{ g}/\text{m}^3$ ; condition II) (Figure 3C). Therefore, these three models can be discriminated by investigating their qualitative responses to altered bulk concentrations of nutrient and oxygen.

As shown in Figures 1, 2, the dormant cells resided in the deeper region of biofilms in the present four simulation models. There were several previous studies investigating the actual spatial distributions of dormant cells within biofilms. In one study, colony biofilms of *P. aeruginosa* PAO1 containing a plasmid with an isopropylthio- $\beta$ -D-galactoside (IPTG) inducible GFP gene were cultured on polycarbonate membranes placed on LB agar plates. After 48 h cultivation, the membranes were transferred to an LB plate containing IPTG for an additional 4 h. The IPTG induced GFP expression in the active cells. The GFP-expressing cells were observed only in the upper region of the colony biofilm, although the nutrient was supplied through the membrane at the bottom of the colony biofilm (Kim et al., 2009). Williamson et al. (2012) also performed similar experiments using a continuous-drip flow biofilm system which nutrient enter from above and obtained similar results. This result implies that

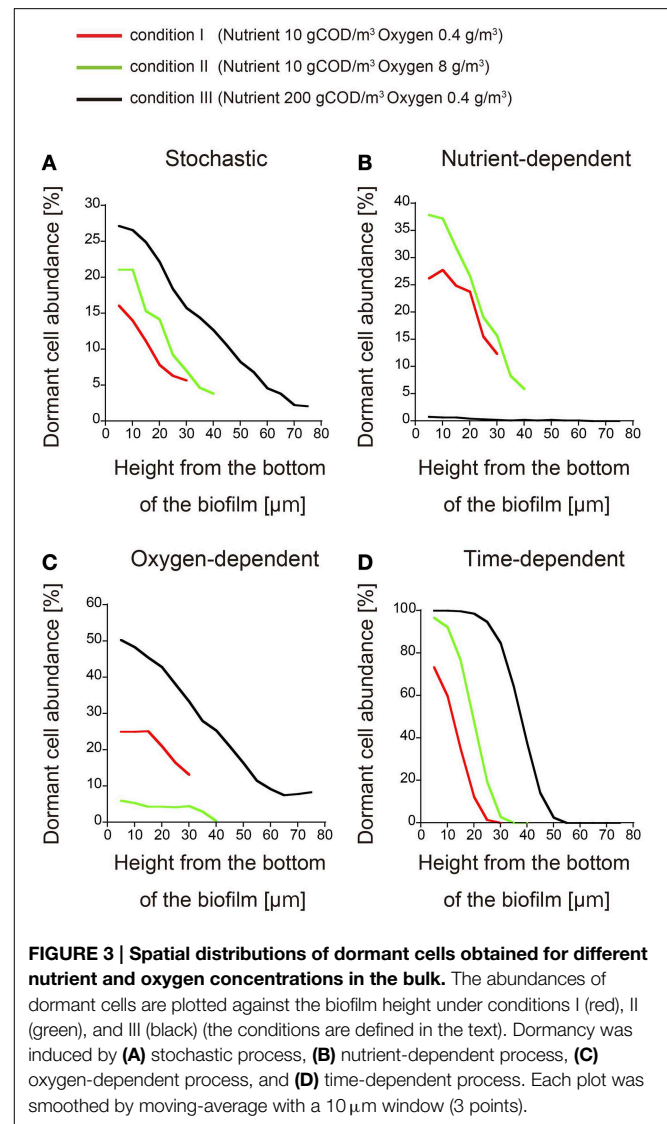


**FIGURE 3 | Spatial distributions of dormant cells obtained for different nutrient and oxygen concentrations in the bulk.** The abundances of dormant cells are plotted against the biofilm height under conditions I (red), II (green), and III (black) (the conditions are defined in the text). Dormancy was induced by (A) stochastic process, (B) nutrient-dependent process, (C) oxygen-dependent process, and (D) time-dependent process. Each plot was smoothed by moving-average with a  $10 \mu\text{m}$  window (3 points).

dormant cells reside in the deeper regions of biofilms, which is consistent with our simulation results. The spatial distribution of dormant cells in biofilms obtained in the above reports can reject none of the four hypotheses on the mechanisms of dormant cell formation implemented into the computational models developed in the present study. As stated above, time evolution of the distribution and/or the responses to the increase/decrease of the substrate/oxygen may provide novel insights about the mechanism of dormancy.

## Conclusions

To predict the formation of dormant cells in growing biofilms, we proposed four hypotheses of dormant cell formation and implemented them in a 3D biofilm model based on the IbM algorithm. In numerical simulations of the model, we found that (i) in the stochastic hypothesis of dormant cell formation, an unexpected gradient appeared in the abundance of dormant cells along the depth direction; thus (ii) investigating the

spatial distributions of dormant cells at a specific time cannot discriminate among the four suggested dormancy mechanisms; however, (iii) all four hypotheses were discriminated in spatiotemporal studies of the dormant cell distributions while varying the bulk concentrations of nutrient and/or oxygen. The proposed simulation methodology could guide experiments for efficiently elucidating the mechanisms of dormant cell formation in growing biofilms.

The following steps are the method to determine what kinds of experimental studies are effective for discriminating dormant cell formation mechanisms in biofilms. First, we will establish the biofilm into which nutrients enter from above in liquid medium, for example, a continuous-drip flow biofilm system, and should investigate the spatial distribution of the dormant cell within growing biofilm. At that time, we should use the detecting system of dormant cell, such as degradable GFP (half-life < 1 h) under the control of the ribosomal *rrnB*P1 promoter, which normally controls expression of the *rrnB* gene which codes for 16S rRNA (Shah et al., 2006; Maisonneuve et al., 2013), or TIMER<sup>bac</sup> fluorescence system in which both rapidly maturing green and slowly maturing orange TIMER molecules can accumulate, whereas in dividing cells, rapidly maturing green molecules dominate over orange molecules that are diluted by cell division (Claudi et al., 2014). Second, we will observe time evolution of the spatial distribution of dormant cells in growing biofilm by measurement with the use of microscopy. In this observation, if dormant cell arise near the bottom of the biofilm good long time after inoculation, a time-dependent process will be a plausible mechanism of dormancy (Figure 2D). Third, if dormant cells are widely distributed throughout the biofilm, we should investigate the responses to the increase/decrease of the nutrient/oxygen. If

the mechanism of dormant cell formation was caused by stochastic process, the distribution of dormant cells in biofilms was not affected qualitatively by the change in the bulk concentrations of the nutrient and oxygen (Figure 3A). On the other hand, if the mechanism was caused by the nutrient-dependent process, dormant cells rarely emerged in the biofilm when the concentration of the nutrient was very high (condition III) (Figure 3B). Similarly, if the mechanism was caused by oxygen-dependent process, dormant cells rarely emerged when the concentration of oxygen is high (condition II) (Figure 3C). As stated above, we could find a clue of the dynamics of dormant cell formation within growing biofilm by comparing the simulation results provided in present study with experimental results.

In summary, the simulation results of this study suggest that, by experimentally investigating the spatiotemporal dormant cell distributions while varying the nutrient and oxygen concentrations in the bulk, we could gain new insights into how dormant cell populations establish in biofilms.

## Acknowledgments

We appreciate Dr. Cristian Picioreanu (Delft University of Technology, Delft, The Netherlands) for permitting us to use and modify the source code of his original biofilm model.

## Supplementary Material

The Supplementary Material for this article can be found online at: <http://journal.frontiersin.org/article/10.3389/fmicb.2015.00534/abstract>

## References

- Amato, S., Orman, M., and Brynildsen, M. (2013). Metabolic control of persister formation in *Escherichia coli*. *Mol. Cell.* 50, 475–487. doi: 10.1016/j.molcel.2013.04.002
- Balaban, N., Merrin, J., Chait, R., Kowalik, L., and Leibler, S. (2004). Bacterial persistence as a phenotypic switch. *Science* 305, 1622–1625. doi: 10.1126/science.1099390
- Chambless, J., Hunt, S., and Stewart, P. (2006). A three-dimensional computer model of four hypothetical mechanisms protecting biofilms from antimicrobials. *Appl. Environ. Microbiol.* 72, 2005–2013. doi: 10.1128/AEM.72.3.2005-2013.2006
- Claudi, B., Sprote, P., Chirkova, A., Personnic, N., Zankl, J., Schurmann, N., et al. (2014). Phenotypic variation of *Salmonella* in host tissues delays eradication by antimicrobial chemotherapy. *Cell* 158, 722–733. doi: 10.1016/j.cell.2014.06.045
- Costerton, J., Stewart, P., and Greenberg, E. (1999). Bacterial biofilms: a common cause of persistent infections. *Science* 284, 1318–1322. doi: 10.1126/science.284.5418.1318
- Elowitz, M., Levine, A., Siggia, E., and Swain, P. (2002). Stochastic gene expression in a single cell. *Science* 297, 1183–1186. doi: 10.1126/science.1070919
- Hall-Stoodley, L., Costerton, J., and Stoodley, P. (2004). Bacterial biofilms: from the natural environment to infectious diseases. *Nat. Rev. Microbiol.* 2, 95–108. doi: 10.1038/nrmicro821
- Harrison, F. (2007). Microbial ecology of the cystic fibrosis lung. *Microbiology* 153, 917–923. doi: 10.1099/mic.0.2006/004077-0
- Kagawa, Y., Horita, N., Taniguchi, H., and Tsuneda, S. (2014). Modeling of stem cell dynamics in human colonic crypts *in silico*. *J. Gastroenterol.* 49, 263–269. doi: 10.1007/s00535-013-0887-x
- Kagawa, Y., Tahata, J., Kishida, N., Matsumoto, S., Picioreanu, C., van Loosdrecht, M., et al. (2015). Modeling the nutrient removal process in aerobic granular sludge system by coupling the reactor- and granule-scale models. *Biotechnol. Bioeng.* 112, 53–64. doi: 10.1002/bit.25331
- Kim, J., Hahn, J., Franklin, M., Stewart, P., and Yoon, J. (2009). Tolerance of dormant and active cells in *Pseudomonas aeruginosa* PA01 biofilm to antimicrobial agents. *J. Antimicrob. Chemother.* 63, 129–135. doi: 10.1093/jac/dkn462
- Kreft, J., Booth, G., and Wimpenny, J. (1998). BacSim, a simulator for individual-based modelling of bacterial colony growth. *Microbiology* 144, 3275–3287. doi: 10.1099/00221287-144-12-3275
- Lewis, K. (2007). Persister cells, dormancy and infectious disease. *Nat. Rev. Microbiol.* 5, 48–56. doi: 10.1038/nrmicro1557
- Lewis, K., Gottesman, S., and Harwood, C. (2010). Persister cells. *Ann. Rev. Microbiol.* 64, 357–372. doi: 10.1146/annurev.micro.112408.134306
- Maisonneuve, E., Castro-Camargo, M., and Gerdes, K. (2013). (p)ppGpp controls bacterial persistence by stochastic induction of toxin-antitoxin activity. *Cell* 154, 1140–1150. doi: 10.1016/j.cell.2013.07.048
- Maisonneuve, E., and Gerdes, K. (2014). Molecular mechanisms underlying bacterial persisters. *Cell* 157, 539–548. doi: 10.1016/j.cell.2014.02.050
- Matsumoto, S., Katoku, M., Saeki, G., Terada, A., Aoi, Y., Tsuneda, S., et al. (2010). Microbial community structure in autotrophic nitrifying granules

- characterized by experimental and simulation analyses. *Environ. Microbiol.* 12, 192–206. doi: 10.1111/j.1462-2920.2009.02060.x
- Moyed, H., and Bertrand, K. (1983). HipA, A newly recognized gene of *Escherichia coli* K-12 that affects frequency of persistence after inhibition of murein synthesis. *J. Bacteriol.* 155, 768–775.
- Nguyen, D., Joshi-Datar, A., Lepine, F., Bauerle, E., Olakanmi, O., Beer, K., et al. (2011). Active starvation responses mediate antibiotic tolerance in biofilms and nutrient-limited bacteria. *Science* 334, 982–986. doi: 10.1126/science.1211037
- Picioreanu, C., Kreft, J., Haagensen, J., Tolker-Nielsen, T., and Molin, S. (2007). Microbial motility involvement in biofilm structure formation—a 3D modelling study. *Water Sci. Technol.* 55, 337–343. doi: 10.2166/wst.2007.275
- Picioreanu, C., Kreft, J., and van Loosdrecht, M. (2004). Particle-based multidimensional multispecies biofilm model. *Appl. Environ. Microbiol.* 70, 3024–3040. doi: 10.1128/AEM.70.5.3024-3040.2004
- Picioreanu, C., van Loosdrecht, M., and Heijnen, J. (1998a). A new combined differential-discrete cellular automaton approach for biofilm modeling: application for growth in gel beads. *Biotechnol. Bioeng.* 57, 718–731.
- Picioreanu, C., van Loosdrecht, M., and Heijnen, J. (1998b). Mathematical modeling of biofilm structure with a hybrid differential-discrete cellular automaton approach. *Biotechnol. Bioeng.* 58, 101–116.
- Rittmann, B., Stilwell, D., and Ohashi, A. (2002). The transient-state, multiple-species biofilm model for biofiltration processes. *Water Res.* 36, 2342–2356. doi: 10.1016/S0043-1354(01)00441-9
- Shah, D., Zhang, Z., Khodursky, A., Kaldalu, N., Kurg, K., and Lewis, K. (2006). Persisters: a distinct physiological state of *E. coli*. *BMC Microbiol.* 6:53. doi: 10.1186/1471-2180-6-53
- Stewart, P. (2002). Mechanisms of antibiotic resistance in bacterial biofilms. *Int. J. Med. Microbiol.* 292, 107–113. doi: 10.1078/1438-4221-00196
- Stewart, P., and Costerton, J. (2001). Antibiotic resistance of bacteria in biofilms. *Lancet* 358, 135–138. doi: 10.1016/S0140-6736(01)05321-1
- Stewart, P., and Franklin, M. (2008). Physiological heterogeneity in biofilms. *Nat. Rev. Microbiol.* 6, 199–210. doi: 10.1038/nrmicro1838
- Wakamoto, Y., Dhar, N., Chait, R., Schneider, K., Signorino-Gelo, F., Leibler, S., et al. (2013). Dynamic persistence of antibiotic-stressed mycobacteria. *Science* 339, 91–95. doi: 10.1126/science.1229858
- Williamson, K., Richards, L., Perez-Osorio, A., Pitts, B., McInerney, K., Stewart, P., et al. (2012). Heterogeneity in *Pseudomonas aeruginosa* biofilms includes expression of ribosome hibernation factors in the antibiotic-tolerant subpopulation and hypoxia-induced stress response in the metabolically active population. *J. Bacteriol.* 194, 2062–2073. doi: 10.1128/JB.00022-12
- Xavier, J., Picioreanu, C., and van Loosdrecht, M. (2005). A general description of detachment for multidimensional modelling of biofilms. *Biotechnol. Bioeng.* 91, 651–669. doi: 10.1002/bit.20544

**Conflict of Interest Statement:** The authors declare that the research was conducted in the absence of any commercial or financial relationships that could be construed as a potential conflict of interest.

Copyright © 2015 Chihara, Matsumoto, Kagawa and Tsuneda. This is an open-access article distributed under the terms of the Creative Commons Attribution License (CC BY). The use, distribution or reproduction in other forums is permitted, provided the original author(s) or licensor are credited and that the original publication in this journal is cited, in accordance with accepted academic practice. No use, distribution or reproduction is permitted which does not comply with these terms.



# Interspecies interactions are an integral determinant of microbial community dynamics

Fatma A. A. Aziz<sup>1,2\*</sup>, Kenshi Suzuki<sup>2</sup>, Akihiro Ohtaki<sup>3</sup>, Keita Sagegami<sup>3</sup>, Hidetaka Hirai<sup>2</sup>, Jun Seno<sup>2</sup>, Naoko Mizuno<sup>2</sup>, Yuma Inuzuka<sup>2</sup>, Yasuhisa Saito<sup>4</sup>, Yosuke Tashiro<sup>2</sup>, Akira Hiraishi<sup>3</sup> and Hiroyuki Futamata<sup>2\*</sup>

## OPEN ACCESS

### Edited by:

Jochen Ait Mueller,  
Helmholtz Centre for Environmental  
Research - UFZ, Germany

### Reviewed by:

Prasun Ray,  
The Samuel Roberts Noble  
Foundation, USA  
Paul Richard Himes,  
University of Louisville, USA

### \*Correspondence:

Fatma A. A. Aziz  
fatma.hjaziz@yahoo.com;  
Hiroyuki Futamata  
thfutam@ipc.shizuoka.ac.jp

### Specialty section:

This article was submitted to  
Systems Microbiology,  
a section of the journal  
Frontiers in Microbiology

**Received:** 29 June 2015

**Accepted:** 05 October 2015

**Published:** 20 October 2015

### Citation:

Aziz FAA, Suzuki K, Ohtaki A,  
Sagegami K, Hirai H, Seno J,  
Mizuno N, Inuzuka Y, Saito Y,  
Tashiro Y, Hiraishi A and Futamata H  
(2015) Interspecies interactions are an  
integral determinant of microbial  
community dynamics.  
*Front. Microbiol.* 6:1148.  
doi: 10.3389/fmicb.2015.01148

<sup>1</sup> Laboratory of Food Crops, Institute of Tropical Agriculture, Universiti Putra Malaysia, Serdang, Malaysia, <sup>2</sup> Department of Applied Chemistry and Biochemical Engineering, Graduate School of Engineering, Shizuoka University, Hamamatsu, Japan, <sup>3</sup> Department of Environmental and Life Sciences, Toyohashi University of Technology, Toyohashi, Japan, <sup>4</sup> Department of Mathematics, Shimane University, Matsue, Japan

This study investigated the factors that determine the dynamics of bacterial communities in a complex system using multidisciplinary methods. Since natural and engineered microbial ecosystems are too complex to study, six types of synthetic microbial ecosystems (SMEs) were constructed under chemostat conditions with phenol as the sole carbon and energy source. Two to four phenol-degrading, phylogenetically and physiologically different bacterial strains were used in each SME. Phylogeny was based on the nucleotide sequence of 16S rRNA genes, while physiologic traits were based on kinetic and growth parameters on phenol. Two indices,  $J$  parameter and “interspecies interaction,” were compared to predict which strain would become dominant in an SME. The  $J$  parameter was calculated from kinetic and growth parameters. On the other hand, “interspecies interaction,” a new index proposed in this study, was evaluated by measuring the specific growth activity, which was determined on the basis of relative growth of a strain with or without the supernatant prepared from other bacterial cultures. Population densities of strains used in SMEs were enumerated by real-time quantitative PCR (qPCR) targeting the gene encoding the large subunit of phenol hydroxylase and were compared to predictions made from  $J$  parameter and interspecies interaction calculations. In 4 of 6 SEMs tested the final dominant strain shown by real-time qPCR analyses coincided with the strain predicted by both the  $J$  parameter and the interspecies interaction. However, in SMEII-2 and SMEII-3 the final dominant *Variovorax* strains coincided with prediction of the interspecies interaction but not the  $J$  parameter. These results demonstrate that the effects of interspecies interactions within microbial communities contribute to determining the dynamics of the microbial ecosystem.

**Keywords:** microbial ecosystem, population dynamics, interaction, self-organization, chemostat, phenol

## INTRODUCTION

Microbial populations influence each other during the development of their ecosystems, while at the same time the microbial ecosystem is affected by its surrounding environments and vice versa (Fernández et al., 2000; Hashsham et al., 2000; Little et al., 2008; Klitgord and Segrè, 2010). It is predicted that the sustainability of an ecosystem will be maintained by dynamic changes of the bacterial community (dynamic equilibrium) (Ishii et al., 2012; Yamamoto et al., 2014). Comprehensive understanding of the principles of microbial ecosystems is not only central to research in microbial ecology but also important for efficient bioremediation, wastewater treatment, agriculture and human health but has been a challenging subject for microbial ecologists (Fernández et al., 1999, 2000; Futamata et al., 2005; El-Chakhtoura et al., 2015).

We previously observed a unique phenomenon of bacterial population dynamics in a chemostat soil bioreactor enriched with phenol (Futamata et al., 2005). Usually, since the chemostat culture is enriched with a low concentration of a sole substrate, bacteria exhibiting the highest affinity for this substrate eventually come to dominate the culture (Watanabe et al., 1998a). However, members of *Variovorax* exhibiting lower affinities for phenol constituted the final dominant population in this soil bioreactor (Futamata et al., 2005). This result indicated that kinetic parameters are not necessarily the sole determinant for predicting bacterial community dynamics in a chemostat culture. Therefore, further research is necessary to unveil the mechanism by which the *Variovorax* species became dominant in a complex chemostat ecosystem despite exhibiting lower affinity for phenol.

Kinetic and growth parameters have been used to predict bacterial population dynamics and the “*J* parameter” has been reported as a useful predictor for which strain will become dominant in a mixed culture (Hansen and Hubbell, 1980). Additionally, interactions between bacterial cells is also thought to be an important mechanism that plays a major role in biofilm formation through quorum sensing and other biological processes (Tashiro et al., 2013; DeSalvo et al., 2015; Inaba et al., 2015). Here, we investigated whether kinetic and growth parameters or interactions between populations of different species are more important for determining the composition of a microbial ecosystem.

The complete set of all possible interactions between many species of bacteria has to be investigated in order to fully understand a natural microbial ecosystem. However, microbial ecosystems in natural and engineered systems (including the soil bioreactor described above), are far too complex to be described by a single determinant and/or law. Currently, the factors and processes that influence the behavior and functionality of bacterial ecosystems remain largely unknown. Due to the high complexity of natural systems, an approach known as the synthetic microbial ecosystem (SME) has gained much interest of late (Narisawa et al., 2008; Mee et al., 2014; De Roy et al., 2014). Because of their reduced complexity and increased controllability, synthetic communities are often preferred over complex communities when examining ecological theories. The possible factors that influence the microbial community are

reduced to a minimum, allowing the factors that affect specific community dynamics to be managed and identified.

The objective of this study was to understand the surprising bacterial community dynamics observed in the soil bioreactor. To this end, we determined the *J* parameter (based on kinetic and growth parameters) (Hansen and Hubbell, 1980) and the interspecies interactions (based on the specific growth activity) of several phenol degrading bacterial strains. These data were used to predict which strain would become dominant in different SMEs and the results were compared to real-time qPCR quantification of each strain. From this work we have determined that interactions between species, in addition to kinetic and growth parameters, are integral in determining bacterial community dynamics.

## MATERIALS AND METHODS

### Bacterial Strains Used in This Study

Phenol-degrading bacteria isolated from a phenol-degrading soil bioreactor and its inoculum (Futamata et al., 2001a, 2005) were used in this study (Table 1). *Pseudomonas putida* strains P-2, P-5, P-6, and P-8, and *Ralsotonia* sp. strain P-10 were isolated from trichloroethene (TCE) -contaminated aquifer soil (Futamata et al., 2001a). Other strains were isolated from chemostat enrichment cultures grown on phenol with pristine aquifer soil sampled from near the TCE-contaminated site. These bacteria were grown at 25°C in BSM medium supplemented with phenol at 2.0 mM (Futamata et al., 2001a) or MP medium (Watanabe et al., 1998a) supplemented with phenol at 2.0 mM.

### Kinetic Analyses

Isolated strains or SMEs were grown in a chemostat reactor with BSM medium and phenol as the sole carbon and energy source. The phenol or catechol-oxygenating activity (phenol or catechol-consumption rate) was measured at various substrate concentrations using an oxygen electrode (DO METER TD-51, Toko Chemical Lab. Co., Ltd) after the respiratory oxygen consumption was suppressed by adding potassium cyanide (Watanabe et al., 1996). Kinetic parameters were calculated using the initial phenol-oxygenating velocities at more than 10 different substrate concentrations. The data were fitted to the Michaelis-Menten's equation or the Haldane's equation (Folsom et al., 1990; Watanabe et al., 1998b; Futamata et al., 2005) using JMP statistical visualization software (SAS Institute Inc.). The apparent kinetic constants,  $K_S$  (affinity constant),  $K_I$  (inhibition constant), and  $V_{max}$  (theoretical maximum activity) were determined using the nonlinear regression method as described previously (Watanabe et al., 1996, 1998a). Following Folsom et al. (1990), the term  $K_S$  was employed instead of  $K_m$  because the activity was measured using intact cells rather than purified enzymes.

### Construction of Synthetic Microbial Ecosystem

Six kinds of SMEs, differing based on their strain composition and flow rate, were constructed with phenol as sole carbon

**TABLE 1 | Kinetic parameters for phenol-degradation of strains isolated from the soil-bioreactor.**

Isolated strains	$K_S$ ( $\mu\text{M}$ )	$K_I$ ( $\mu\text{M}$ )	$V_{max}$ ( $\mu\text{mol min}^{-1} \text{g}^{-1}$ of dry cells)	No. <sup>a</sup>	Accession number
<i>Acinetobacter</i> sp. c1 <sup>b</sup>	1.1 ± 0.40	4800 ± 1600	31 ± 1.4	3	AB167183
<i>Acinetobacter</i> sp. c26 <sup>b</sup>	2.4 ± 1.8	80 ± 30	16 ± 2.4	30	AB167203
<i>Acinetobacter</i> sp. c40	11 ± 3.1	530 ± 92	50 ± 4.9	15	AB167208
<i>Arthrobacter</i> sp. c106	3.1 ± 0.11	110 ± 12	39 ± 1.2	29	AB167237
<i>Pseudomonas</i> sp. LAB-06	2.3 ± 0.31	4800 ± 800	21 ± 0.84	2	AB051693
<i>Pseudomonas</i> sp. LAB-08	2.2 ± 0.23	3200 ± 370	30 ± 0.73	4	AB051694
<i>Pseudomonas</i> sp. LAB-20	2.8 ± 0.55	1500 ± 290	28 ± 1.5	10	AB051697
<i>Pseudomonas</i> sp. LAB-23	2.3 ± 0.23	2700 ± 450	16 ± 0.50	6	AB051699
<i>Pseudomonas putida</i> P-2 <sup>c</sup>	4.1 ± 1.2	3100 ± 1300	13 ± 1.1	5	AB038136
<i>Pseudomonas putida</i> P-5 <sup>c</sup>	3.0 ± 0.66	1100 ± 260	48 ± 2.8	12	AB038140
<i>Pseudomonas putida</i> P-6 <sup>c</sup>	3.9 ± 1.7	460 ± 260	16 ± 2.9	17	AB038141
<i>Pseudomonas putida</i> P-8 <sup>c</sup>	5.3 ± 1.6	6900 ± 1600	23 ± 1.2	1	AB038142
<i>Pseudomonas</i> sp. LAB-26	2.5 ± 0.55	2300 ± 520	33 ± 1.6	7	AB051700
<i>Ralstonia</i> sp. P-10 <sup>c</sup>	4.4 ± 0.89	580 ± 200	100 ± 20	14	AB016860
<i>Ralstonia</i> sp. c5	7.9 ± 1.6	220 ± 60	49 ± 5.3	22	AB167187
<i>Ralstonia</i> sp. chemo32	5.1 ± 0.60	470 ± 110	57 ± 3.4	16	LC086859
<i>Ralstonia</i> sp. c41	3.2 ± 1.0	200 ± 15	60 ± 10	24	AB167209
<i>Ralstonia</i> sp. HAB-01	5.6 ± 0.74	260 ± 46	60 ± 3.5	20	AB051680
<i>Ralstonia</i> sp. HAB-02	9.6 ± 1.6	180 ± 37	75 ± 7.5	25	AB051681
<i>Ralstonia</i> sp. HAB-11	2.2 ± 0.29	850 ± 120	14 ± 0.45	13	AB051683
<i>Ralstonia</i> sp. HAB-18	6.2 ± 0.93	310 ± 70	56 ± 3.7	18	AB051684
Unidentified strain TUT-005	2.9 ± 0.60	1600 ± 350	62 ± 2.8	9	NR <sup>d</sup>
Unidentified strain TUT-006	3.4 ± 0.50	1600 ± 200	130 ± 4.7	8	NR
<i>Variovorax</i> sp. c24 <sup>b</sup>	8.2 ± 1.2	220 ± 45	93 ± 6.5	21	AB622239
<i>Variovorax</i> sp. c52	1.7 ± 0.4	270 ± 20	16 ± 3.1	19	AB167215
<i>Variovorax</i> sp. HAB-24 <sup>b</sup>	7.6 ± 1.5	180 ± 47	106 ± 12	26	AB051688
<i>Variovorax</i> sp. HAB-27	7.1 ± 1.6	120 ± 47	96 ± 15	28	AB051689
<i>Variovorax</i> sp. HAB-29	7.4 ± 1.2	150 ± 38	108 ± 11	27	AB051690
<i>Variovorax</i> sp. HAB-30 <sup>b</sup>	5.8 ± 0.94	200 ± 40	160 ± 12	23	AB051691
<i>Variovorax</i> sp. YN07 <sup>b</sup>	12 ± 1.4	1200 ± 120	66 ± 2.5	11	AB622227

<sup>a</sup>Number links the number shown in **Figure 1**.

<sup>b</sup>These data were reported in Futamata et al. (2005).

<sup>c</sup>These data were reported in Futamata et al. (2001a).

<sup>d</sup>The strain was not registered in Genbank.

and energy source under chemostat conditions. The SMEI series had 2–4 strains present and a high flow rate while the SMEII series had a lower flow rate and had different combinations of three strains. SMEI-1 consisted of *P. putida* P-8 (Futamata et al., 2001a) and *Variovorax* sp. HAB-24 (Futamata et al., 2001b). SMEI-2 consisted of *P. putida* strains P-8, *Variovorax* sp. HAB-24 and *Acinetobacter* sp. c26 (Futamata et al., 2005). SMEI-3 included *Ralstonia* sp. c41 in addition to the above-noted 3 strains. It was previously demonstrated that strains P-8 and HAB-24 belong to High- $K_S$  (Group III) and Low- $K_S$  (Group I) types according to their nucleotide sequences of the gene coding large subunit of multicomponent phenol hydroxylase (Futamata et al., 2001b). Furthermore, it was shown that the population density of Group III is approximately 10-fold higher than that of Group I. Therefore, initial population density of strain P-8 was set to be 10-fold higher than that of strain HAB-24. The same strains used in SMEI-2 were used in SMEII-1

to investigate the effect of medium flow rate on population dynamics. SMEII-2 consisted of *P. putida* LAB-06 (Futamata et al., 2001b), *Acinetobacter* sp. c26 and *Variovorax* sp. HAB24. SMEII-3 consisted of strain LAB-06, *Ralstonia* sp. chemo32, and *Variovorax* sp. HAB-30 (Futamata et al., 2001b). Prior to inoculation into the chemostat, all strains were precultured at 25°C in BSM medium supplemented with 2 mM phenol as the sole carbon source. Cultures were harvested at the early- or mid-exponential growth phase and then were transferred into 1.5 L of BSM medium containing 0.2 mM of phenol [in a chemostat reactor [(2 L in capacity)]. The initial cell density of each strain was adjusted to approximately  $1.0 \times 10^5$  cells  $\text{mL}^{-1}$  by measuring the optical density at 600 nm ( $\text{OD}_{600 \text{ nm}}$ ). An  $\text{OD}_{600 \text{ nm}}$  of 0.1 corresponded to  $1.0 \times 10^9$  cells  $\text{mL}^{-1}$  for strains HAB-24 and HAB-30 and to  $5.0 \times 10^8$  cells  $\text{mL}^{-1}$  for the other bacteria. After the initially added phenol was almost completely degraded (start-up phase), the SMEI series cultures were supplied

continuously with BSM medium containing phenol (1500 mg L<sup>-1</sup>) at a flow rate of 31.5 mL h<sup>-1</sup>, corresponding to a dilution rate ( $D$ ) of 0.5 d<sup>-1</sup> (31.5 mL h<sup>-1</sup> × 24 h/1500 mL). The hydraulic residence time (HRT), calculated as 1/ $D$ , was 2 days. The SMEII series cultures were supplied continuously with BSM medium containing phenol (1500 mg L<sup>-1</sup>) at a flow rate of 10.4 mL h<sup>-1</sup> (HRT was 6 days). The culture volume was maintained at 1.5 L. The culture was stirred at 150 rpm, and the temperature and pH were maintained at 25°C and 7.0, respectively. Air was filtered through 0.2 μm-pore-size membrane filters (Millipore) and supplied to the culture at 1.5 L min<sup>-1</sup>. The concentration of phenol in the culture was measured using a colorimetric assay with a Phenol Test Wako kit (Wako Pure Chemicals) (Futamata et al., 2001b). The detection limit of this method was around 1.0 μM.

## Monitoring of Strains in Synthetic Microbial Ecosystems

The population density of each strain was monitored using real-time qPCR targeting the gene encoding the large subunit of phenol hydroxylase (LmPH). Specific sets of primers were designed by the alignment of various LmPH genes (Supplemental Table 1). A specific PCR-product amplified with each specific primer set was used as a standard DNA fragment in a real-time qPCR analysis. For the monitoring of the *P. putida* P-8, *Variovorax* sp. HAB-24, and *Ralstonia* sp. c41, the PCR profile consisted of preheating at 95°C for 10 min, followed by 40 cycles of denaturation at 95°C for 10 s, annealing at 62°C for 5 s, and extension at 72°C for 15 s. The annealing temperature was set to 56°C and 68°C for the monitoring of strains *Acinetobacter* sp. c26 and *Variovorax* sp. HAB30, respectively. Annealing temperature was set to 58°C for the monitoring of strains *P. putida* LAB-06 and *R. sp.* chemo32. The fluorescence signal was detected at 72°C in each cycle, and a melting curve was obtained by heating the product to 95°C and cooling to 40°C. The reaction was performed using a LightCycler FastStart DNA Master SYBR GREEN I kit (Roche Molecular Biochemicals, Indianapolis, IN, USA) and a LightCycler system (Roche Diagnostics, Mannheim, Germany) according to the manufacturer's instructions. The copy number of each of the amplicons was calculated using the LightCycler software version 3.52.

## Simulation

We performed computer simulations about SMEI-1 (strains P-8 and HAB-24) using the Runge-Kutta method (Saito et al., 1999; Saito, 2002), with important modifications described in the equations below.

$$S' = (S^{(0)} - S)D - \mu_1 S / (K_{S1} + S)x_1 / r_1 - \mu_2 S / (K_{S2} + S)x_2 / r_2$$

$x_1' = x_1 \{ \mu_1 S / (K_{S1} + S) - D \}$  and  $x_2' = x_2 \{ \mu_2 S / (K_{S2} + S) - D \}$  where  $S$  is the substrate (phenol in this study) concentration (mg L<sup>-1</sup>),  $D$  is the dilution rate (h<sup>-1</sup>),  $\mu$  is the growth rate constant (h<sup>-1</sup>),  $x$  is the dried cell density (mg L<sup>-1</sup>),  $r$  is the cell yield (g [cell] g<sup>-1</sup> [substrate]) and  $K_S$  is the half-saturation constant (μM). Here "1" and "2" mean strains P-8 and HAB-24, respectively.

## Specific Growth Activity

Since it is known that supernatants of microbial culture can affect the metabolic processes of other microbes (Tanaka et al., 2005; Tashiro et al., 2013; Inaba et al., 2015), the effect of interspecies communication was investigated using a supernatant collected from a pure chemostat culture and was evaluated as specific growth activity. Growth curves were recorded to estimate the physiological changes that occurred after the addition of a supernatant. Each strain was incubated in the BSM medium under the conditions of the chemostat culture supplemented with phenol as the sole carbon source. After the culture was stable, which means that phenol was not detected and OD<sub>600nm</sub> of the culture reached plateau, the culture was centrifuged at 4°C and 5800 × g. The supernatant was sterilized by filtration through a Steriflip-GP Filter ([pore size is 0.22 μm], Millipore). The supernatant was stored at -20°C after filtration. Frozen supernatant was thawed for each use. We empirically knew that the growth inhibiting activity of supernatant was kept for approximate 6 month at least. The effect of a single supernatant on growth of all strains was always assessed at the same time as a control. Cells precultured in the BSM medium supplemented with 2.0 mM phenol (BSM2.0phe) and 0.3 mL of filter-sterilized supernatant were transferred into 2.7 mL of fresh BSM2.0phe medium. The initial amount of cells was adjusted to an OD<sub>600nm</sub> of 0.01. As the control condition, 0.3 mL of BSM medium without phenol was added instead of the supernatant. The growth curve was automatically measured using a Bio-photorecorder (TVS062CA, ADVANTEC). Growth parameters, including a lag time (h), growth rate constant (μ [h<sup>-1</sup>]) and amount of growth at a stationary phase (OD<sub>max</sub>), were calculated using the growth curve. Here, we defined the specific growth activity as the surviving activity maintaining the cell density over 1.0 × 10<sup>9</sup> cells mL<sup>-1</sup> in a chemostat culture under the condition of a dilution rate. Therefore, 1 unit (U) of specific growth activity was calculated using the following equations: 1 U = 0.021 (h<sup>-1</sup>) × 10<sup>9</sup> (cells mL<sup>-1</sup>) under the HRT condition of 2 days (in SMEI series) or 1 U = 0.0069 (h<sup>-1</sup>) × 10<sup>9</sup> (cells mL<sup>-1</sup>) under the HRT condition of 6 days (in SMEII series). As mentioned above, the cell density of *Variovorax* sp. strains HAB-24 and HAB-30 were 1.0 × 10<sup>9</sup> cells mL<sup>-1</sup> at an OD<sub>600nm</sub> of 0.1, whereas the other strains had cell densities of 5.0 × 10<sup>8</sup> cells mL<sup>-1</sup> at an OD<sub>600nm</sub> of 0.1. The OD<sub>max</sub> was then converted to cell density. Thus, one unit of specific growth activity changes according to the strain and the dilution rate of the chemostat. Units of specific growth activity for the tested strains were calculated according to the following equation:

$$U = (\mu \times \text{cell density from ODmax}) / (1 \text{ U} \times \text{lag time}).$$

## J parameter

$J$  parameter was calculated according to the following equation (Hansen and Hubbell, 1980):  $J = (K_S \times D) / (\mu - D)$ , where  $K_S$  is the half-saturation constant (μM),  $D$  is the dilution rate (h<sup>-1</sup>), and  $\mu$  is the growth rate constant (h<sup>-1</sup>). Parameters of  $D$  in SMEI and SMEII series were 0.021 (h<sup>-1</sup>) and 0.0069 (h<sup>-1</sup>), respectively. Based on the equation, the strain exhibiting a lower  $J$  parameter should out-grow strains exhibiting higher  $J$  parameters.

## RESULTS

### Kinetic Parameters for Phenol of Strains

Kinetic parameters for phenol of 30 strains isolated from the soil bioreactor and its inoculum are shown in **Table 1** and plotted in **Figure 1**. Overall, *Pseudomonas* sp. strains, with the exception of *Pseudomonas* sp. P-6, exhibited lower  $K_S$ -values ( $3.0 \pm 1.1 \mu\text{M}$ ) and higher  $K_I$ -values ( $3200 \pm 1900 \mu\text{M}$ ) than the other strains. The *Ralstonia* sp. strains exhibited middle  $K_S$ -values ( $4.9 \pm 1.9 \mu\text{M}$ ) and  $K_I$ -values ( $410 \pm 240 \mu\text{M}$ ) with the exception of *Ralstonia* sp. HAB-02. The *Variovorax* sp. strains exhibited higher  $K_S$ -values ( $7.2 \pm 0.86 \mu\text{M}$ ) and lower  $K_I$ -values ( $170 \pm 40 \mu\text{M}$ ) with the exception of *Variovorax* sp. strains YN07 and chemo52. Almost all of the kinetic parameters for phenol of the individual strains were similar to those from the soil bioreactor as described previously (Haruta et al., 2013). The  $K_S$ -values varied within one order of magnitude (from 1 to  $10 \mu\text{M}$ ), whereas the  $K_I$ -values varied within two orders of magnitude (from 100 to  $1000 \mu\text{M}$ ). Furthermore, kinetic parameters ( $K_S$ - and  $K_I$ -values) of the strains and the soil bioreactor changed one-thirtieth fold decrease in the  $K_I$ -values with a three-fold increase in the  $K_S$ -value.

### Population Dynamics in the Mixed Chemostat Reactor SMEI-1

To understand the previous observation that high  $K_S$ -type bacteria eventually became dominant in the soil bioreactor, we attempted to reproduce the result in an SME constructed with the isolated strains *P. putida* P-8 (No. 1 shown in **Figure 1**) and *Variovorax* sp. HAB-24 (No. 26 shown in **Figure 1**). The SME was run at a flow rate of  $31.5 \text{ mL h}^{-1}$  (an HRT of 2.0 days) and the population densities were monitored by the real-time qPCR technique (**Figure 2A**). It was previously shown that *Pseudomonas* and *Variovorax* strains were the dominant genera in, respectively, the early and final stages of reactor operation (Futamata et al., 2005). The kinetic parameters of strains P-8

and HAB-24 were similar to those of the soil bioreactor. From these phylogenetic and kinetic data, it was predicted that strain HAB-24 would be the final dominant strain. However, in the SME strain P-8 overcame strain HAB-24 (**Figure 2A**); the population densities of strains P-8 and HAB-24 were stable at  $3.6 \pm 1.1 \times 10^9$  cells  $\text{mL}^{-1}$  and  $1.3 \pm 0.84 \times 10^7$  cells  $\text{mL}^{-1}$ , respectively. The result of a simulation showed that only strain P-8 would survive and be maintained at  $9.8 \times 10^9$  cells  $\text{mL}^{-1}$  (**Figure 2B**), whereas strain HAB-24 would be eradicated (**Figure 2C**).

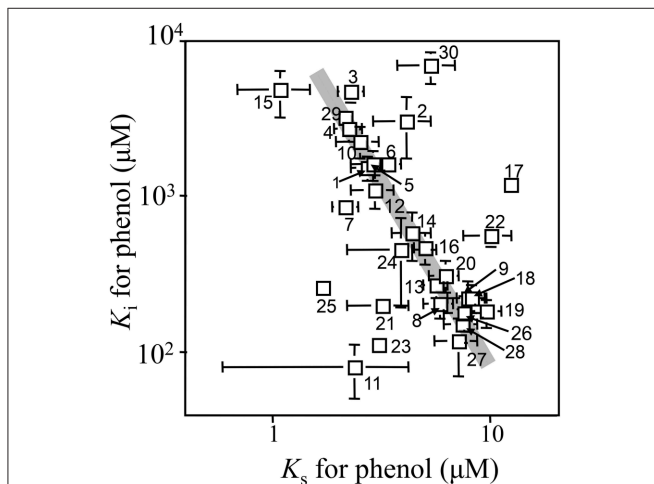


**FIGURE 1 | Kinetic parameters of isolated strains and the soil bioreactor for phenol.** Number indicates the strain shown in **Table 1**.

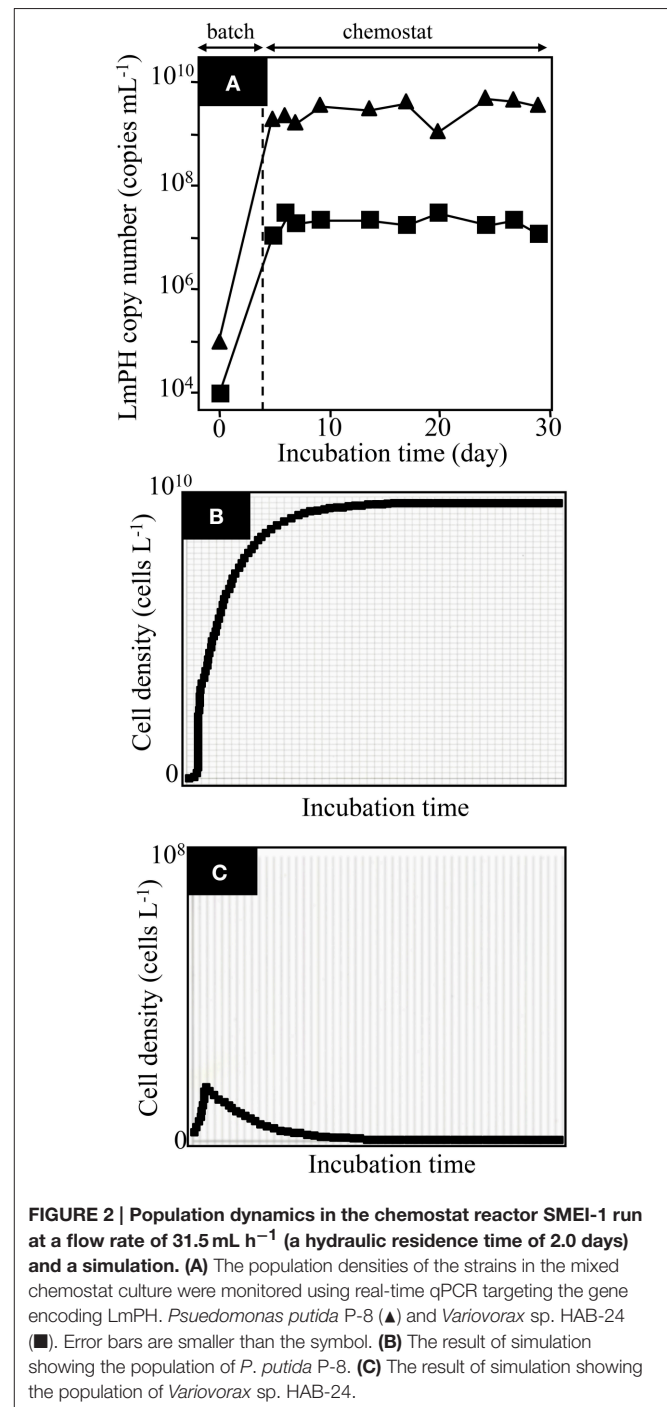


**FIGURE 2 | Population dynamics in the chemostat reactor SMEI-1 run at a flow rate of  $31.5 \text{ mL h}^{-1}$  (a hydraulic residence time of 2.0 days) and a simulation. (A)** The population densities of the strains in the mixed chemostat culture were monitored using real-time qPCR targeting the gene encoding LmPH. *Pseudomonas putida* P-8 (▲) and *Variovorax* sp. HAB-24 (■). Error bars are smaller than the symbol. **(B)** The result of simulation showing the population of *P. putida* P-8. **(C)** The result of simulation showing the population of *Variovorax* sp. HAB-24.

## SMEI-2

SMEI-2, which consisted of strains *P. putida* P-8, *Acinetobacter* sp. c26 (No. 30 shown in **Figure 1**), and *Variovorax* sp. HAB-24, was run at a flow rate of  $31.5 \text{ mL h}^{-1}$  (an HRT of 2.0 days) and the population densities were monitored using real-time qPCR (**Figure 3A**). The genera *Pseudomonas*, *Acinetobacter*, and *Variovorax* corresponded respectively to the first, second, and third dominant genera in the soil bioreactor. According to the affinity dynamics of the soil bioreactor for phenol and catechol, the affinity parameters of strain c26 for phenol and catechol were located at an inflection point from low  $K_S$  for phenol and high  $K_S$  for catechol to high  $K_S$  for phenol and low  $K_S$  for catechol of the soil bioreactor (Supplemental Figure 1). It was thought that a strain located at this inflection point would be needed for strain HAB-24 to become dominant. Strains P-8 and c26, rather than strain HAB-24, grew quickly in the batch mode because of their higher  $\mu$ -values (**Table 2**). The population density of strain c26 was maintained at around  $1.1 \pm 0.073 \times 10^9 \text{ cells mL}^{-1}$

after day 5. Although strain P-8 grew well at a similar level to strain c26 under batch mode, the population density of strain P-8 decreased gradually from  $6.1 \times 10^8 \text{ cells mL}^{-1}$  to  $4.7 \times 10^7 \text{ cells mL}^{-1}$ . On the other hand, the population density of strain HAB-24 remained stable at about  $4.11 \pm 0.24 \times 10^5 \text{ cells mL}^{-1}$  after day 5. Small amounts of phenol were detected in the effluent from the SMEI-2 around day 7 as well as from day 17 to 20 (data not shown).

## SMEI-3

SMEI-3, which consisted of *P. putida* P-8, *Acinetobacter* sp. c26, *Ralstonia* sp. c41 (No. 24 shown in **Figure 1**), and *Variovorax* sp. HAB-24, was run at a flow rate of  $31.5 \text{ mL h}^{-1}$  (an HRT of 2.0 days) and the population densities were again monitored (**Figure 3B**). According to the affinity dynamics of the soil bioreactor for phenol and catechol, it was predicted that strain c41 would be an intermediate between strains P-8, HAB-24, and c26 (Supplemental Figure 1). The amount of growth of the four strains corresponded to their  $\mu$ -values under batch conditions. Their population densities were roughly maintained under chemostat conditions of this experiment; the population densities of strains c26, P-8, c41, and HAB-24 were  $1.3 \pm 0.21 \times 10^9 \text{ cells mL}^{-1}$ ,  $2.3 \pm 0.26 \times 10^8 \text{ cells mL}^{-1}$ ,  $7.6 \pm 0.81 \times 10^6 \text{ cells mL}^{-1}$ , and  $2.9 \pm 1.71 \times 10^5 \text{ cells mL}^{-1}$ , respectively. Again, small amounts of phenol were detected in the effluent from the SMEI-3 on days 7–10 and days 16–20 (data not shown).

## SMEII-1

SMEII-1 consisted of *P. putida* P-8, *Acinetobacter* sp. c26, and *Variovorax* sp. HAB-24, which were the same strains as used in SMEI-2). The purpose of SMEII-1 was to investigate the effect of flow rate on population dynamics. Here the flow rate was decreased from  $31.5 \text{ mL h}^{-1}$  (HRT = 2.0 days) to  $10.4 \text{ mL h}^{-1}$  (HRT = 6.0 days). The population densities were monitored using real-time QPCR with specific sets of primers (**Figure 4A**). Strains P-8 and c26 grew faster than strain HAB-24 in the batch mode, as was the case in SMEI-2. The population density of strain P-8 was stable at  $6.2 \pm 0.78 \times 10^9 \text{ cells mL}^{-1}$  from day 10 to day 48, after which the population density decreased below  $1.0 \times 10^7 \text{ cells mL}^{-1}$  by the end of the experiment. Conversely, the population density of strain c26 was stable at  $8.2 \pm 0.16 \times 10^7 \text{ cells mL}^{-1}$  from day 15 to day 30, after which the population density increased to approximately  $4.2 \pm 0.32 \times 10^9 \text{ cells mL}^{-1}$  by the end of the experiment. The population density of strain HAB-24 was stable at around  $6.2 \pm 0.76 \times 10^5 \text{ cells mL}^{-1}$  after day 5. The population dynamics of SMEII-1 were similar to that of SMEI-2, showing that the final dominant bacterium was *Acinetobacter* sp. c26. Phenol was never detected in the effluent during this experiment. Therefore, all subsequent SMEII series chemostats were run with a flow rate at  $10.4 \text{ mL h}^{-1}$  (HRT = 6.0 days).

## SMEII-2

SMEII-2 was constructed with *Pseudomonas* sp. LAB-06 (No. 2 shown in **Figure 1**), *Acinetobacter* sp. c26 and *Variovorax* sp. HAB-24, and run with a flow rate of  $10.4 \text{ mL h}^{-1}$  (an HRT of 6.0 days) (**Figure 4B**). Strain c26, but not strains LAB-06 and HAB-24, grew quickly in the batch mode because of higher  $\mu$ -value

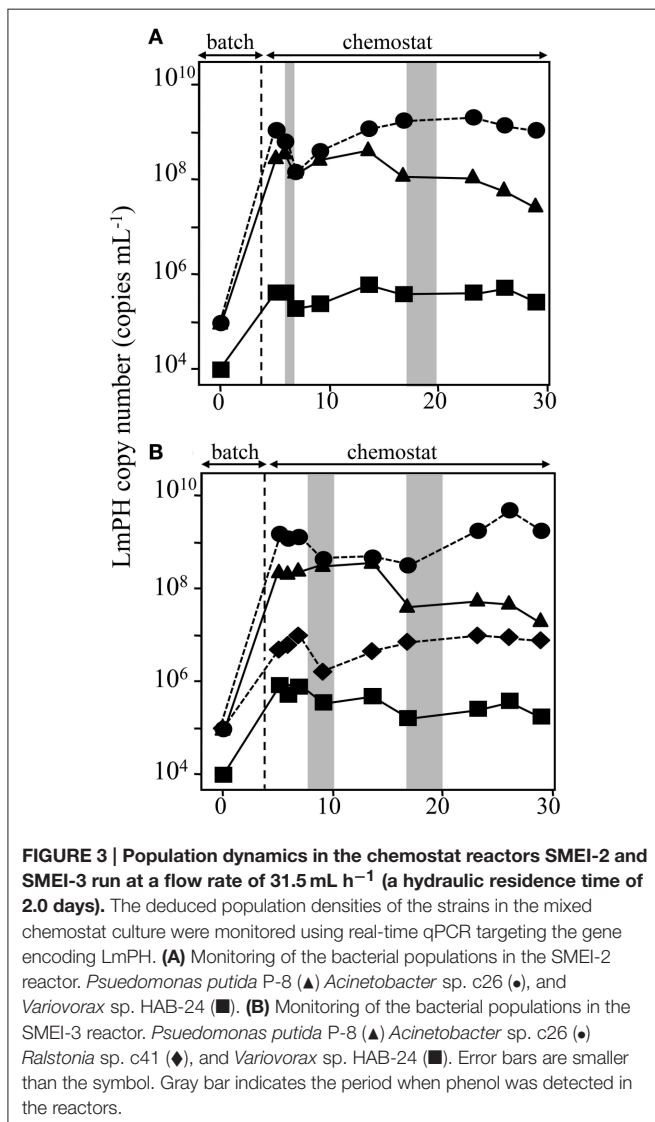


**TABLE 2 | Kinetic and growth parameters on phenol of isolates used in mixed chemostat culture.**

Strains	$\mu$ ( $\text{h}^{-1}$ )	Maximum OD	J parameter ( $\mu\text{M}$ ) <sup>a</sup>	J parameter ( $\mu\text{M}$ ) <sup>b</sup>
<i>Acinetobacter</i> sp. c26	$0.63 \pm 0.13$	$0.18 \pm 0.046$	$0.086 \pm 0.025$	$0.027 \pm 0.0077$
<i>Ralstonia</i> sp. chemo32	$0.22 \pm 0.089$	$0.27 \pm 0.11$	$0.59 \pm 0.17$	$0.18 \pm 0.048$
<i>Ralstonia</i> sp. c41	$0.17 \pm 0.029$	$0.32 \pm 0.043$	$0.46 \pm 0.096$	$0.14 \pm 0.026$
<i>Pseudomonas</i> sp. LAB-06	$0.39 \pm 0.14$	$0.23 \pm 0.0084$	$0.41 \pm 0.20$	$0.13 \pm 0.060$
<i>Pseudomonas</i> sp. P-8	$0.37 \pm 0.054$	$0.24 \pm 0.0093$	$0.33 \pm 0.059$	$0.10 \pm 0.018$
<i>Variovorax</i> sp. HAB-24	$0.11 \pm 0.012$	$0.25 \pm 0.020$	$1.7 \pm 0.21$	$0.49 \pm 0.052$
<i>Variovorax</i> sp. HAB-30	$0.13 \pm 0.021$	$0.20 \pm 0.084$	$1.2 \pm 0.19$	$0.33 \pm 0.050$

<sup>a</sup>Dilution rate was  $0.021 \text{ h}^{-1}$  (HRT = 2 days). It was a chemostat condition of BRI-series.

<sup>b</sup>Dilution rate was  $0.0069 \text{ h}^{-1}$  (HRT = 6 days). It was a chemostat condition of BRII-series.

(Table 2). Strain c26 remained dominant until day 10. On day 15, the population densities of the three strains were all close to  $2.8 \pm 2.5 \times 10^6$  cells  $\text{mL}^{-1}$ , after which the population density of HAB-24 increased and was stable at  $2.5 \pm 1.1 \times 10^9$  cells  $\text{mL}^{-1}$  after day 35. Conversely, the population density of LAB-06 and c26 were  $2.6 \pm 1.8 \times 10^6$  cells  $\text{mL}^{-1}$  and  $2.7 \pm 1.6 \times 10^7$  cells  $\text{mL}^{-1}$  after day 30, respectively. Bacterial community succession was observed, resulting in the dominance of HAB-24.

### SMEII-3

SMEII-3 was constructed with *Pseudomonas* sp. LAB-06 (No. 2 shown in Figure 1), *Ralstonia* sp. chemo32 (No. 16 shown in Figure 1), and *Variovorax* sp. HAB-30 (No. 23 shown in Figure 1) and run at a flow rate of  $10.4 \text{ mL h}^{-1}$  (an HRT of 6.0 days) (Figure 4C). Strains LAB-06 and chemo32 grew faster than strain HAB-30 in the batch mode because of their higher  $\mu$ -values (Table 2). Strain LAB-06 became dominant at a cell density of  $1.6 \pm 0.89 \times 10^8$  cells  $\text{mL}^{-1}$  until day 20. The population densities of strains LAB-06 and chemo32 decreased to  $9.1 \pm 8.9 \times 10^5$  cells  $\text{mL}^{-1}$  and  $8.6 \pm 8.2 \times 10^4$  cells  $\text{mL}^{-1}$ , respectively, after day 40. Conversely, the population density of HAB-30 remained stable at around  $1.3 \pm 1.3 \times 10^7$  cells  $\text{mL}^{-1}$  from days 10 to 60. Thus, SMEII-3 exhibited a bacterial community succession, where strain HAB-30 became dominant. Small amounts of phenol were detected in the effluent from the SMEII on days 65–70 (data not shown).

## Interspecies Interactions

### Strains Used in the SMEI Series SMEs

Interactions among the four strains used in the SMEI series SEMs, *P. putida* P-8, *Variovorax* sp. HAB-24, *Acinetobacter* sp. c26, and, *Ralstonia* sp. c41, were investigated by measuring their specific growth activities (Table 3). The supernatant of strain P-8 culture enhanced the growth activities of strains P-8 and c26 to approximately 140 and 180%, respectively but repressed those of strains c41 and HAB-24 to approximately 6.5 and 7.4%, respectively. The supernatant of strain c26 did not affect the growth activities of strains P-8 and c26, but repressed those of strains c41 and HAB-24 to approximately 25 and 38%, respectively. The supernatant of strain c41 enhanced the growth activities of strains P-8 and c26 to approximately 120% but did not affect the growth activities

of strains c41 and HAB-24. The supernatant of strain HAB-24 enhanced the growth activities of strains c26 and HAB-24 to approximately 160 and 150%, respectively, but repressed those of strains P-8 and c41 to approximately 40 and 11%, respectively.

### Strains Used in the SMEII Series SMEs

Interactions among the three strains used in SMEII-2 (Table 4) and SMEII-3 (Table 5) were investigated by measuring their specific growth activities. The supernatant of strain LAB-06 did not affect its own growth activity but it repressed that of strain c26 to approximately 71% and enhanced that of strain HAB-24 to approximately 180% (Table 4). Supernatant of strain c26 did not affect the growth activity of strain LAB-06 and itself but repressed that of strain HAB-24 to approximately 38%. Supernatant of strain HAB-24 repressed the growth activity of strain LAB-06 to approximately 40% but enhanced those of strains c26 and HAB-24 to approximately 160 and 153%, respectively. The supernatant of strain LAB-06 repressed those of strains chemo32 and HAB-30 to approximately 75 and 22%, respectively (Table 5). The supernatant of strain chemo32 did not affect the growth activities of strains LAB-06 and chemo32 but enhanced that of strain HAB-30 to approximately 160%. The supernatant of strain HAB-30 enhanced its own growth activity to approximately 140% but repressed those of strains LAB-06 and chemo32 to approximately 87 and 48%, respectively. The mixed supernatant of strains chemo32 and HAB-30 did not affect the growth activity of LAB-06. Similarly, the mixed supernatant of strains LAB-06 and chemo32 did not affect the growth activity of HAB-30. The mixed supernatant of strain LAB-06 and HAB-30 repressed the growth activity of chemo32 to approximately 85%.

## Dynamics of Kinetics Parameters in the SMEII-3 SME

The kinetic parameters ( $K_S$ - and  $K_I$ -values) of the SMEII-3 SME for phenol and catechol were monitored (Figure 5). The  $K_S$ - and  $K_I$ -values for phenol shifted from  $2.6 \pm 0.17 \mu\text{M}$  and  $2060 \pm 200 \mu\text{M}$  at day 10 to  $0.42 \pm 0.037 \mu\text{M}$  and  $1060 \pm 28 \mu\text{M}$  at day 30, which indicated that the affinity for phenol of the SMEII-3 reactor increased. However, these kinetic parameters changed dramatically and exhibited a dynamic equilibrium at higher  $K_S$ -values ( $4.0 \pm 1.8 \mu\text{M}$ ) and lower  $K_I$ -values ( $275 \pm$

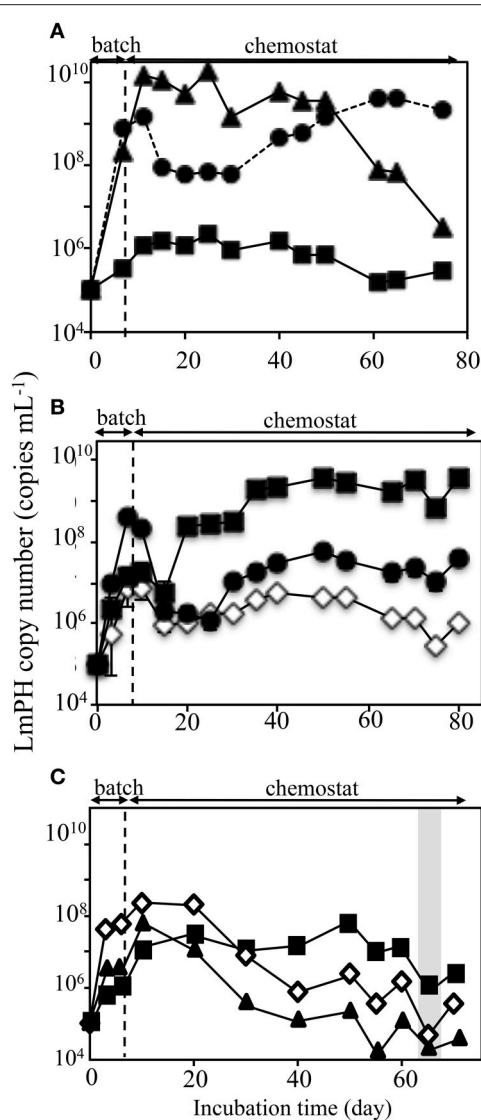


**FIGURE 4 | Population dynamics in the chemostat reactors SMEI series run at a flow rate of  $10.4 \text{ mL h}^{-1}$  (a hydraulic residence time of 6.0 days).** The deduced population densities of the strains in the mixed chemostat culture were monitored using real-time qPCR targeting the gene encoding LmPH. **(A)** Monitoring of the bacterial populations used in the SMEI-1 reactor. *Pseudomonas putida* P-8 (▲), *Acinetobacter* sp. c26 (●), and *Variovorax* sp. HAB-24 (■). **(B)** Monitoring of the bacterial populations used in the SMEI-2 reactor. *Pseudomonas* sp. LAB-06 (◇), *Acinetobacter* sp. c26 (●), and *Variovorax* sp. HAB-24 (■). **(C)** Monitoring of the bacterial populations used in the SMEI-3 reactor. *Pseudomonas* sp. LAB-06 (◇), *Acinetobacter* sp. chemo32 (▲), and *Variovorax* sp. HAB-24 (■). The gray bar indicates the period when phenol was detected in the reactors. The error bars indicate standard deviations and some bars were hidden with symbols.

$180 \mu\text{M}$ ) from days 40 to 70. The  $K_S$ -value for catechol shifted more dynamically than that for phenol (Figure 5B). The  $K_S$ - and  $K_I$ -values for catechol were stable at  $25 \pm 13 \mu\text{M}$  and  $3000 \pm 170 \mu\text{M}$ , respectively, from days 10 to 30. However, these kinetic parameters fluctuated dynamically from  $9.9 \pm 0.56 \mu\text{M}$  and  $11500 \pm 860 \mu\text{M}$  at day 40 to  $100 \pm 6.2 \mu\text{M}$  and  $540 \pm$

**TABLE 3 | Relative specific growth among strains used in SMEI-series and SMEI-1<sup>a</sup>.**

Strains	Supernatant of strains			
	P-8	c26	chemo41	HAB-24
<i>Pseudomonas</i> sp. P-8	$140 \pm 35$	$105 \pm 11$	$120 \pm 16$	$40 \pm 5.0$
<i>Acinetobacter</i> sp. c26	$180 \pm 90$	$100 \pm 3.0$	$120 \pm 58$	$160 \pm 90$
<i>Ralstonia</i> sp. c41	$6.5 \pm 0.5$	$25 \pm 9.3$	$97 \pm 39$	$1 \pm 9.1$
<i>Variovorax</i> sp. HAB-24	$7.4 \pm 1.3$	$38 \pm 8.6$	$90 \pm 12$	$153 \pm 8.9$

<sup>a</sup>The specific growth activity without supernatant (control condition) was calculated as 100%.

**TABLE 4 | Relative specific growth among strains used in SMEI-2<sup>a</sup>.**

Strains	Supernatant of strains		
	LAB-06	c26	HAB-24
<i>Pseudomonas</i> sp. LAB-06	$93 \pm 7.3$	$105 \pm 11$	$77 \pm 8.4$
<i>Acinetobacter</i> sp. c26	$71 \pm 6.8$	$100 \pm 3.0$	$160 \pm 90$
<i>Variovorax</i> sp. HAB-24	$180 \pm 90$	$38 \pm 8.6$	$153 \pm 8.9$

<sup>a</sup>Specific growth activity without supernatant was calculated as 100% (control condition).

**TABLE 5 | Relative specific growth among strains used in SMEI-3<sup>a</sup>.**

Strains	Supernatant of strains			
	LAB-06	chemo32	HAB-30	Mixed supernatant
<i>Pseudomonas</i> sp. LAB-06	$93 \pm 7.3$	$103 \pm 41$	$87 \pm 12$	$103 \pm 8.5^b$
<i>Ralstonia</i> sp. chemo32	$75 \pm 6.3$	$100 \pm 50$	$48 \pm 17$	$85 \pm 16^c$
<i>Variovorax</i> sp. HAB-30	$22 \pm 6.4$	$160 \pm 35$	$140 \pm 33$	$105 \pm 4.8^d$

<sup>a</sup>Specific growth activity without supernatant (control condition) was calculated as 100%.

<sup>b</sup>Supernatants obtained from strain c32 and HAB-30 were used.

<sup>c</sup>Supernatants obtained from strain LAB-06 and HAB-30 were used.

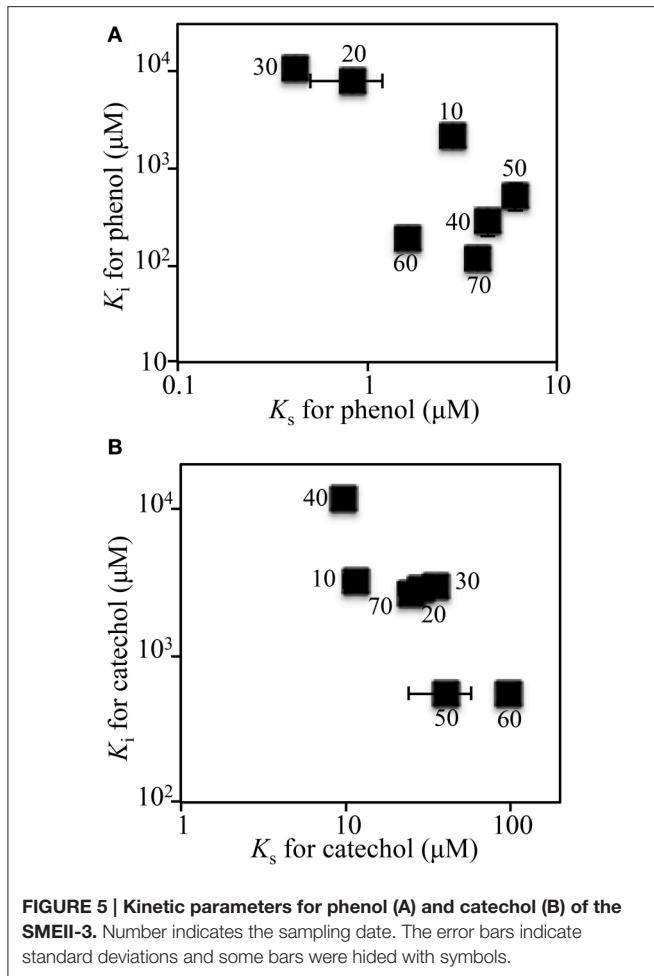
<sup>d</sup>Supernatants obtained from strain LAB-06 and c32 were used.

$47 \mu\text{M}$  at day 60 and then returned to their initial values at day 70.

## DISCUSSION

In a soil bioreactor fed with phenol we previously observed a unique phenomenon where the kinetic parameters shifted toward higher  $K_S$  and lower  $K_I$ -values (Futamata et al., 2005; Haruta et al., 2013). In the present study, to understand this unique phenomenon, SMEs were constructed using isolated strains exhibiting different phenotypic features. By observing changes in population densities we have developed a better understanding of population dynamics in SMEs and soil bioreactors.

Kinetic parameters have been thought to be one of the most important determinants for predicting the competitiveness of strains grown on a single substrate (Watanabe et al., 1996, 1998a). Since the  $J$  parameter is calculated using not only the  $K_S$ -value (affinity) but also  $\mu$  (growth rate constant) and



$D$  (dilution rate), it is especially useful for predicting what strain will become dominant in a chemostat culture (Hansen and Hubbell, 1980). Additionally, cell-to-cell interactions are important for understanding the microbial ecosystem (Watts and Strogatz, 1998; Flagan et al., 2003; Kato et al., 2005; Narisawa et al., 2008). To the best of our knowledge this study presents the first attempt to use both the  $J$  parameter and interspecies interaction information simultaneously for understanding the dynamics of microbial community in a complex system.

It is reported that *Variovorax* strains are capable of utilizing or producing acyl-homoserine lactones which are quorum signaling molecules in many species of the class *Proteobacteria* (Leadbetter and Greenberg, 2000; d'Angelo-Picard et al., 2005; Yang et al., 2006; Satola et al., 2013). We hypothesized that the *Variovorax* spp. became dominant in the soil bioreactor through the use of quorum signaling. The SMEI series and SMEII-1 were expected to reproduce the unique phenomenon of the soil bioreactor, however, *Variovorax* sp. strain HAB-24 exhibiting highest  $K_S$ -value among strains used in SMEs did not become dominant (Figures 2, 3, 4A). Therefore, it was demonstrated that either the  $J$  parameter or interspecies interactions data were capable of predicting the experimentally observed population dynamics

and it was natural that *Acinetobacter* sp. strain c26 became dominant.

It remained unknown whether the  $J$  parameter or interspecies interactions were more important for predicting population dynamics in a chemostat culture. Therefore, SMEII-2 was constructed with *Acinetobacter* sp. strain c26, *Variovorax* sp. strain HAB-24, and *Pseudomonas* sp. strain LAB-06 instead of *P. putida* strain P-8. Based on their  $J$  parameters (Table 2), *Acinetobacter* sp. strain c26 was predicted to become dominant. However, from these interspecies interactions (Table 4), it was predicted that *Variovorax* sp. strain HAB-24 would become dominant as strain LAB-06 would repress strain c26 and enhance strain HAB-24. In actuality the final dominant organism was strain HAB-24 not strain c26 (Figure 4B), suggesting that the interspecies interactions did indeed play a more important role in bacterial community dynamics than the  $J$  parameter. To confirm this possibility, SMEII-3 was constructed with *Pseudomonas* sp. strain LAB-06, *Ralstonia* sp. strain chemo32, and *Variovorax* sp. strain HAB-30. Although strain LAB-06 exhibited the lowest  $J$  parameter (indicating it should be the most competitive) among these three strains (Table 2), the final dominant was strain HAB-30. While interspecies interaction data (Table 5) indicated that strain LAB-06 inhibited HAB-30, the addition of chemo32 was also expected to rescue this inhibition. Thus, the complexity of this three-way interaction resulted in strain HAB-30 becoming dominant after community succession and fluctuation of kinetic parameters (Figure 5). Importantly it was also demonstrated that this SME reproduced the unique phenomenon previously observed in the soil bioreactor (Futamata et al., 2005; Haruta et al., 2013).

Since it is recognized that interactive networks develop among diverse microbes in natural ecosystems (Gilbert et al., 2012), it was expected that understanding these complex interactions would be important for understanding how microbial ecosystems develop. Striking a balance between the enhancing and repressing relationships was considered to be essential for maintaining the stable coexistence of the five bacterial strains in a cellulose-degrading community (Kato et al., 2005). While it is possible to qualitatively understand such interspecies interactions, it remains difficult to quantify their outcome. As a physiological process with defined, quantifiable output, cell growth was expected to be an ideal indicator for understanding the effects of interspecies interactions. Here, using relative growth in the presence of supernatants of other strains, we have demonstrated that the specific growth activity was indeed useful for understanding the dynamics of microbial ecosystems and for predicting the dominant species in a mixed, SME.

In this study we characterized both kinetic, physiological traits of multiple phenol-degrading strains as well as their binary interactions with each other. Using this quantitative method for evaluating interspecies interactions we have developed a method for predicting microbial community dynamics and demonstrated that the complex interactions between species are a more significant determinant for microbial community dynamics than the  $J$  parameter is for predicting which species will

become dominant. Interestingly, although bacterial community succession was observed, all strains still co-existed in all SMEs and none were eradicated, suggesting that these strains shared a role in phenol degradation. Further work still needs to be done as it was thought that these strains shared a role in degradation of phenol by changing metabolic process. A novel biomathematical theory is also required to fully understand dynamic microbial ecosystems. Research subjects that attract attention with respect to microbial community dynamics are relevant to the identification of growth-repressing compounds, mechanisms of interspecies interactions and comparison of metabolism under the conditions of pure and complex cultures.

## REFERENCES

- d'Angelo-Picard, C., Faure, D., Penot, I., and Dessaux, Y. (2005). Diversity of *N*-acyl homoserine lactone-producing and -degrading bacteria in soil and tobacco rhizosphere. *Environ. Microbiol.* 7, 1796–1808. doi: 10.1111/j.1462-2920.2005.00886.x
- De Roy, K., Marzorati, M., den Abbeele, P. V., de Wiele, T. V., and Boon, N. (2014). Synthetic microbial ecosystems: an exciting tool to understand and apply microbial communities. *Environ. Microbiol.* 16, 1472–1481. doi: 10.1111/1462-2920.12343
- DeSalvo, S. C., Liu, Y., Choudhary, G. S., Ren, D., Nangia, S., Sureshkumar, R., et al. (2015). Signaling factor interactions with polysaccharide aggregates of bacterial biofilms. *Langmuir* 31, 1958–1966. doi: 10.1021/la504721b
- El-Chakhtoura, J., Prest, E., Saikaly, P., van Loosdrecht, M., Hammers, F., and Vrouwenvelder, H. (2015). Dynamics of bacterial communities before and after distribution in a full-scale drinking water network. *Water Res.* 74, 180–190. doi: 10.1016/j.watres.2015.02.015
- Fernández, A., Juang, S., Seston, S., Xing, J., Hickey, R., Criddle, C., et al. (1999). How stable is stable? Function versus community composition. *Appl. Environ. Microbiol.* 65, 3697–3704.
- Fernández, A. S., Hashsham, S. A., Dollhopf, S. L., Raskin, L., Glagoleva, O., Dazzo, F. B., et al. (2000). Flexible community structure correlates with stable community function in methanogenic bioreactor communities perturbed by glucose. *Appl. Environ. Microbiol.* 66, 4058–4067. doi: 10.1128/AEM.66.9.4058-4067.2000
- Flagan, S., Chign, W. K., and Leadbetter, J. R. (2003). *Arthrobacter* strain VAI-A utilizes acyl-homoserine lactone inactivation products and stimulates quorum signal biodegradation by *Variovorax paradoxus*. *Appl. Environ. Microbiol.* 69, 909–916. doi: 10.1128/AEM.69.2.909-916.2003
- Folsom, B. R., Chapman, P. J., and Pritchard, P. H. (1990). Phenol and trichloroethylene degradation by *Pseudomonas cepacia* G4: kinetics and interactions between substrates. *Appl. Environ. Microbiol.* 56, 1279–1285.
- Futamata, H., Harayama, S., and Watanabe, K. (2001a). Diversity in kinetics of trichloroethylene-degrading activities exhibited by phenol-degrading bacteria. *Appl. Microbiol. Biotechnol.* 55, 248–253. doi: 10.1007/s00253000500
- Futamata, H., Harayama, S., and Watanabe, K. (2001b). Group-specific monitoring of phenol hydroxylase genes for a functional assessment of phenol-stimulated trichloroethylene bioremediation. *Appl. Environ. Microbiol.* 67, 4671–4677. doi: 10.1128/AEM.67.10.4671-4677.2001
- Futamata, H., Nagano, Y., Watanabe, K., and Hiraishi, A. (2005). Unique kinetic properties of phenol-degrading *Variovorax* strains responsible for efficient trichloroethylene degradation in a chemostat enrichment culture. *Appl. Environ. Microbiol.* 71, 904–911. doi: 10.1128/AEM.71.2.904-911.2005
- Gilbert, J. A., Steele, J. A., Gaporaso, J. G., Steinbrück, L., Reeder, J., Temperton, B., et al. (2012). Defining seasonal marine microbial community dynamics. *ISME J.* 6, 298–308. doi: 10.1038/ismej.2011.107
- Hansen, S. R., and Hubbell, S. P. (1980). Single-nutrient microbial competition: qualitative agreement between experimental and theoretically forecast outcomes. *Science* 207, 1491–1493. doi: 10.1126/science.6767274

## ACKNOWLEDGMENTS

We thank Sean Booth for assistance in preparation of the manuscript. This study was carried out as grant KAKENHI 15K12228, Japan. It was also supported partially by ALCA project, Japan Science and Technology Agency.

## SUPPLEMENTARY MATERIAL

The Supplementary Material for this article can be found online at: <http://journal.frontiersin.org/article/10.3389/fmicb.2015.01148>

- Haruta, S., Yoshida, T., Aoi, Y., Kaneko, K., and Futamata, H. (2013). Challenges for complex microbial ecosystems: combination of experimental approaches with mathematical modeling. *Microbes Environ.* 28, 285–294. doi: 10.1264/jsme2.ME13034
- Hashsham, S. A., Fernandez, A. S., Dollhopf, S. L., Dazzo, F. B., Hickey, R. F., Tiedje, J. M., et al. (2000). Parallel processing of substrate correlates with greater functional stability in methanogenic bioreactor communities perturbed by glucose. *Appl. Environ. Microbiol.* 66, 4050–4057. doi: 10.1128/AEM.66.9.4050-4057.2000
- Inaba, T., Oura, H., Morinaga, K., Toyofuku, M., and Nomura, N. (2015). The *Pseudomonas* quinolone signal inhibits biofilm development of *Streptococcus* mutants. *Microbes Environ.* 30, 189–191. doi: 10.1264/jsme2.ME14140
- Ishii, S., Suzuki, S., Norden-Krichmar, T. M., Neelson, K. H., Sekiguchi, Y., Gorby, Y. A., et al. (2012). Functionally stable and phylogenetically diverse microbial enrichments from microbial fuel cells during wastewater treatment. *PLoS ONE* 7:e30495. doi: 10.1371/journal.pone.0030495
- Kato, S., Haruta, S., Cui, Z. J., Ishii, M., and Igarashi, Y. (2005). Stable coexistence of five bacterial strains as a cellulose-degrading community. *Appl. Environ. Microbiol.* 71, 7099–7107. doi: 10.1128/AEM.71.11.7099-7106.2005
- Klitgord, N., and Segrè, D. (2010). Environments that induce synthetic microbial ecosystems. *PLoS Comput. Biol.* 6:e1001002. doi: 10.1371/journal.pcbi.1001002
- Leadbetter, J. R., and Greenberg, E. P. (2000). Metabolism of acyl-homoserine lactone quorum-sensing signals by *Variovorax paradoxus*. *J. Bacteriol.* 182, 6921–6926. doi: 10.1128/JB.182.24.6921-6926.2000
- Little, A. E. F., Robinson, C. J., Peterson, S. B., Raffa, K. E., and Handelsman, J. (2008). Rules of engagement: interspecies interactions that regulate microbial communities. *Annu. Rev. Microbiol.* 62, 375–401. doi: 10.1146/annurev.micro.030608.101423
- Mee, M. T., Collins, J. J., Church, G. M., and Wang, H. H. (2014). Synthrophic exchange in synthetic microbial communities. *Proc. Natl. Acad. Sci. U.S.A.* 111, E2149–E2156. doi: 10.1073/pnas.1405641111
- Narisawa, N., Haruta, S., Arai, H., Ishii, M., and Igarashi, Y. (2008). Coexistence of antibiotic-producing and antibiotic-sensitive bacteria in biofilm is mediated by resistant bacteria. *Appl. Environ. Microbiol.* 74, 3887–3894. doi: 10.1128/AEM.02497-07
- Saito, Y. (2002). The necessary and sufficient condition for global stability of a Lotka-Volterra cooperative or competition system with delays. *J. Math. Anal. Appl.* 268, 109–124. doi: 10.1006/jmaa.2001.7801
- Saito, Y., Hara, T., and Ma, W. (1999). Necessary and sufficient conditions for permanence and global stability of a Lotka-Volterra system with two delays. *J. Math. Anal. Appl.* 236, 534–556. doi: 10.1006/jmaa.1999.6464
- Satola, B., Wübbeler, J. H., and Steinbüchel, A. (2013). Metabolic characteristics of the species *Variovorax paradoxus*. *Appl. Microbiol. Biotechnol.* 97, 541–560. doi: 10.1007/s00253-012-4585-z
- Tanaka, Y., Hanada, S., Tamaki, H., Nakamura, K., and Kamagata, Y. (2005). Isolation and identification of bacterial strains producing diffusible growth factor(s) for *Catellibacterium nectariphilium* strain AST4<sup>T</sup>. *Microbes Environ.* 20, 110–116. doi: 10.1264/jsme2.20.110
- Tashiro, Y., Yawata, Y., Toyofuku, M., Uchiyama, H., and Nomura, N. (2013). Interspecies interaction between *Pseudomonas aeruginosa* and

- other microorganisms. *Microbes Environ.* 28, 13–24. doi: 10.1264/jsme2.ME12167
- Watanabe, K., Hino, S., Onodera, K., Kajie, S., and Takahashi, N. (1996). Diversity in kinetics of bacterial phenol-oxygenating activity. *J. Ferment. Bioeng.* 81, 560–563. doi: 10.1016/0922-338X(96)81481-4
- Watanabe, K., Teramoto, M., Futamata, H., and Harayama, S. (1998a). Molecular detection, isolation, and physiological characterization of functionally dominant phenol-degrading bacteria in activated sludge. *Appl. Environ. Microbiol.* 64, 4396–4402.
- Watanabe, K., Yamamoto, S., Hino, S., and Harayama, S. (1998b). Population dynamics of phenol-degrading bacteria in activated sludge determined by *gyrB*-targeted quantitative PCR. *Appl. Environ. Microbiol.* 64, 1203–1209.
- Watts, D. J., and Strogatz, S. H. (1998). Collective dynamics of ‘small-world’ networks. *Nature* 393, 440–442. doi: 10.1038/30918
- Yamamoto, S., Suzuki, K., Araki, Y., Mochihara, H., Hosokawa, T., Kubota, H., et al. (2014). Dynamics of different bacterial communities are capable of generating sustainable electricity from microbial fuel cell with organic waste. *Microbes Environ.* 29, 145–153. doi: 10.1264/jsme2.ME13140
- Yang, W. W., Han, J. I., and Leadbetter, J. R. (2006). Utilization of homoserine lactone as a sole source of carbon and energy by soil *Arthrobacter* and *Burkholderia* species. *Arch. Microbiol.* 185, 47–54. doi: 10.1007/s00203-005-0065-5

**Conflict of Interest Statement:** The authors declare that the research was conducted in the absence of any commercial or financial relationships that could be construed as a potential conflict of interest.

Copyright © 2015 Aziz, Suzuki, Ohtaki, Sagegami, Hirai, Seno, Mizuno, Inuzuka, Saito, Tashiro, Hiraiishi and Futamata. This is an open-access article distributed under the terms of the Creative Commons Attribution License (CC BY). The use, distribution or reproduction in other forums is permitted, provided the original author(s) or licensor are credited and that the original publication in this journal is cited, in accordance with accepted academic practice. No use, distribution or reproduction is permitted which does not comply with these terms.

# Estimating and mapping ecological processes influencing microbial community assembly

James C. Stegen\*, Xueju Lin, Jim K. Fredrickson and Allan E. Konopka

Fundamental and Computational Sciences Directorate, Biological Sciences Division, Pacific Northwest National Laboratory, Richland, WA, USA

## OPEN ACCESS

### Edited by:

Shin Haruta,  
Tokyo Metropolitan University, Japan

### Reviewed by:

Ross Carlson,  
Montana State University, USA  
Takeshi Miki,  
National Taiwan University, Taiwan

### \*Correspondence:

James C. Stegen,  
Fundamental and Computational  
Sciences Directorate, Biological  
Sciences Division, Pacific Northwest  
National Laboratory, 902 Battelle  
Boulevard, Richland, WA, USA  
james.stegen@pnnl.gov

### Specialty section:

This article was submitted to  
Systems Microbiology,  
a section of the journal  
Frontiers in Microbiology

Received: 14 November 2014

Accepted: 11 April 2015

Published: 01 May 2015

### Citation:

Stegen JC, Lin X, Fredrickson JK  
and Konopka AE (2015) Estimating  
and mapping ecological processes  
influencing microbial community  
assembly.  
*Front. Microbiol.* 6:370.  
doi: 10.3389/fmicb.2015.00370

Ecological community assembly is governed by a combination of (i) selection resulting from among-taxa differences in performance; (ii) dispersal resulting from organismal movement; and (iii) ecological drift resulting from stochastic changes in population sizes. The relative importance and nature of these processes can vary across environments. Selection can be homogeneous or variable, and while dispersal is a rate, we conceptualize extreme dispersal rates as two categories; dispersal limitation results from limited exchange of organisms among communities, and homogenizing dispersal results from high levels of organism exchange. To estimate the influence and spatial variation of each process we extend a recently developed statistical framework, use a simulation model to evaluate the accuracy of the extended framework, and use the framework to examine subsurface microbial communities over two geologic formations. For each subsurface community we estimate the degree to which it is influenced by homogeneous selection, variable selection, dispersal limitation, and homogenizing dispersal. Our analyses revealed that the relative influences of these ecological processes vary substantially across communities even within a geologic formation. We further identify environmental and spatial features associated with each ecological process, which allowed mapping of spatial variation in ecological-process-influences. The resulting maps provide a new lens through which ecological systems can be understood; in the subsurface system investigated here they revealed that the influence of variable selection was associated with the rate at which redox conditions change with subsurface depth.

**Keywords:** ecological niche theory, ecological neutral theory, Hanford Site 300 Area, microbial biogeography, null modeling, phylogenetic beta-diversity, phylogenetic signal, Raup-Crick

## Introduction

In his conceptual synthesis, Vellend (2010) proposed that ecological communities are influenced by a combination of ecological selection, organismal dispersal, ecological drift, and speciation (see also Hanson et al., 2012). This is a useful perspective that places all ecological communities within the same conceptual framework, thereby facilitating cross-system comparisons. While there is some knowledge of what causes shifts in the relative influences of governing processes (e.g., Horner-Devine and Bohannan, 2006; Chase, 2007, 2010; Stegen et al., 2012), turning Vellend's conceptual framework into an operational framework is a significant challenge. As an initial

attempt, Stegen et al. (2013) proposed a null modeling approach that estimates the relative influences of ecological components within Vellend's framework at the scale of a metacommunity. To provide context, we next introduce the concepts synthesized in Vellend (2010).

Ecological selection results from different organisms having different levels of fitness for a given set of environmental conditions; here we consider 'environmental conditions' to include both abiotic variables (e.g., temperature) and biotic factors related to organismal interactions. If environmental conditions are homogeneous through space, the selective environment will also be homogeneous (Vellend, 2010). The scenario in which a consistent selective pressure—that results from consistent environment conditions—is the primary cause of low compositional turnover is referred to as 'homogeneous selection' (Figure 1), as in Dini-Andreote et al. (2015). On the other hand, if environmental conditions change through space, among-taxa fitness differences can change (Vellend, 2010). The scenario in which a shift in selective pressure—that results from a shift in environment conditions—is the primary cause of high compositional turnover is referred to as 'variable selection' (Figure 1).

Organismal dispersal refers to the movement of organisms through space (Vellend, 2010). High dispersal rates have the potential to homogenize community composition such that there is low turnover in composition (Leibold et al., 2004). High dispersal rates can, in principle, overwhelm selection-based influences, a scenario at the population level known as source-sink dynamics (Dias, 1996). The scenario in which a high dispersal rate—between a given pair of communities—is the primary cause of low compositional turnover is referred to as 'homogenizing dispersal' (Stegen et al., 2013).

On the other hand, when selection is relatively weak and organisms rarely move between communities, ecological drift (i.e., stochastic changes in population sizes) can lead to marked differences in community composition (Hubbell, 2001; Vellend, 2010). The scenario in which high turnover in composition is primarily due to a low rate of dispersal enabling community composition to drift apart is referred to here as 'dispersal limitation.' To be clear, our use of the term 'dispersal limitation' does not directly refer to a low rate of dispersal between a given pair of communities. We use 'dispersal limitation' to indicate a situation in which a low dispersal rate is the *primary cause* of high compositional turnover; differences in selective environments may be the primary cause of high compositional turnover even when dispersal rates are low, which would fall within the conceptualization of 'variable selection.'

It is important to consider that the rate of dispersal and strength of selection are continuous variables with context-dependent magnitudes and that these processes simultaneously influence ecological communities. The above-summarized scenarios assume relatively extreme levels of dispersal and/or selection, but it is likely that some natural systems (or parts of systems) are characterized by moderate levels of dispersal and selection. In this case, neither process may dominate, leading to compositional differences between communities that are due to a mixture of stochastic organismal movements and stochastic birth–death events. Stegen et al. (2013) used the term 'ecological drift' to refer

to this scenario, but here we use the term 'undominated' to refer more directly to the scenario in which neither dispersal nor selection is the primary cause of between-community compositional differences.

Here we first develop and test an extended version of the Stegen et al. (2013) framework and, in turn, apply the extended framework to subsurface microbial communities distributed across two geologic formations within the 300 Area of the U.S. Department of Energy's Hanford Site in southcentral Washington State. Our framework uses null models to estimate the degree to which compositional turnover between a single focal community and all other sampled communities is governed by different ecological processes (homogeneous selection, variable selection, homogenizing dispersal, and dispersal limitation). The framework also estimates the portion of compositional turnover that is not dominated by a single process. To evaluate this framework we simulated community assembly under different scenarios; the analytical framework was applied to simulated communities to ask how robust the framework was in detecting the dominance of specific ecological processes. In turn, process estimates were generated for the field-sampled subsurface communities; these estimates were combined with environmental data and community spatial locations to identify environmental drivers and to characterize spatial variation in the relative influence of each ecological process.

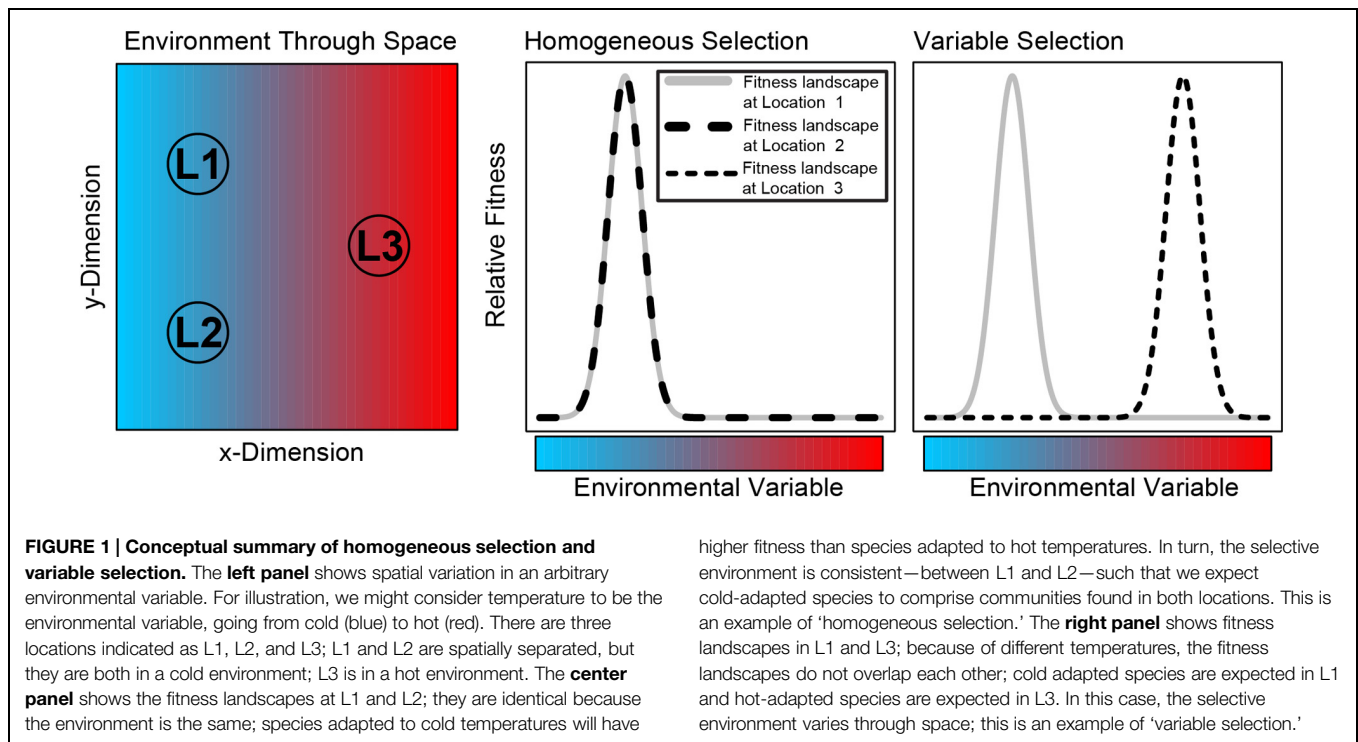
## Materials and Methods

### Subsurface Sampling

The dataset used here is the same as in Stegen et al. (2013) such that here we provide a brief summary of methods used to generate those data. We analyzed sediment-associated bacterial communities found within two subsurface geologic formations roughly 250 m from the Columbia River in Richland, WA, USA. The sampled communities were within the Hanford Integrated Field Research Challenge (IFRC) site<sup>1</sup>, and were sampled during the drilling of 26 IFRC wells (Bjornstad et al., 2009); supplemental material in Stegen et al. (2013) provides details on sample locations. The sampled formations are structurally and hydrologically distinct, are separated vertically, but are in the same horizontal location; 16 communities were sampled within the deeper-lying Ringold Formation, which has restricted water flow and finer-grain sediments; 28 communities were sampled within the shallower Hanford formation, which has less restricted water flow and coarser-grain sediments (Bjornstad et al., 2009). In addition, the Ringold formation changes with depth from oxidized to reduced conditions (Bjornstad et al., 2009). Microbial communities were characterized through pyrosequencing of the 16S rRNA gene (see Lin et al., 2012a,b), DNA sequences were processed using QIIME (Caporaso et al., 2010), and statistical analyses were done using R<sup>2</sup> (for molecular and bioinformatics methods see Stegen et al., 2013). Each microbial community was associated with environmental metadata including its spatial position, its

<sup>1</sup><http://ifchanford.pnnl.gov/>

<sup>2</sup><http://cran.r-project.org/>



horizontal distance from the Columbia River, the elevations of reduced and oxidized portions of the Ringold Formation, and the vertical thickness of the oxidized portion of the Ringold. Vertically structured features were obtained from Bjornstad et al. (2009).

### Statistical Approach

Our statistical framework uses phylogenetic turnover between communities to infer ecological selection (Stegen et al., 2013). This approach requires significant ‘phylogenetic signal’ (Losos, 2008) whereby there is a relationship between phylogenetic relatedness and ecological similarity (Kraft et al., 2007; Cavender-Bares et al., 2009; Fine and Kembel, 2011); as in other microbial systems (e.g., Wang et al., 2013) this was found to be true such that more closely related taxa were more similar ecologically (see Figure 2 in Stegen et al., 2013).

To quantify phylogenetic turnover between communities we used the between-community mean-nearest-taxon-distance ( $\beta$ MNTD) metric (Fine and Kembel, 2011; Webb et al., 2011), which quantifies the phylogenetic distance between each species in one community ( $k$ ) and its closest relative in a second community ( $m$ ):

$$\beta MNTD = 0.5 \left[ \sum_{ik=1}^{n_k} f_{ik} \min(\Delta_{ikjm}) + \sum_{im=1}^{n_m} f_{im} \min(\Delta_{imjk}) \right],$$

where  $f_{ik}$  is the relative abundance of species  $i$  in community  $k$ ,  $n_k$  is the number of species in  $k$ , and  $\min(\Delta_{ikjm})$  is the minimum phylogenetic distance between species  $i$  in community  $k$  and all species  $j$  in community  $m$ .  $\beta$ MNTD was calculated using the R function ‘comdistnt’ (abundance.weighted = TRUE; package ‘picante’).

For each pair of communities within each geologic formation we generated the value of  $\beta$ MNTD expected if ecological selection was *not* the primary factor governing compositional differences by randomly shuffling species across the tips of the phylogeny and, recalculating  $\beta$ MNTD. This procedure was repeated 999 times to provide a distribution of null values. If the observed  $\beta$ MNTD value was significantly (a) less or (b) greater than the null expectation, we inferred that (a) homogeneous selection or (b) variable selection was responsible for the similarity or differences, respectively, between the pair of communities. Significance was evaluated via the  $\beta$ -Nearest Taxon Index ( $\beta$ NNTI), which expresses the difference between observed  $\beta$ MNTD and the mean of the null distribution in units of SDs;  $\beta$ NNTI values  $< -2$  or  $> +2$  indicate significance (Stegen et al., 2012). These interpretations of the  $\beta$ NNTI metric were evaluated and supported via simulation modeling, as described below.

If observed  $\beta$ MNTD does not significantly deviate from the null expectation it indicates that the observed compositional difference is not due to selection (Hardy, 2008), and should therefore be due to very low rates of dispersal (i.e., dispersal limitation), very high rates of dispersal (i.e., homogenizing dispersal), or a lack of dominance between selection and dispersal (i.e., the ‘undominated’ scenario described in the Introduction). To distinguish among these possibilities, we used the Raup–Crick metric (Chase et al., 2011) extended to incorporate species’ relative abundances (as in Stegen et al., 2013); referred to as  $RC_{\text{bray}}$ . Like  $\beta$ NNTI,  $RC_{\text{bray}}$  was based on a comparison between observed and expected levels of turnover, but without using phylogenetic information.

To generate an expected degree of turnover—for use in quantifying  $RC_{\text{bray}}$ —we drew species into each local community until

empirically observed local species richness was reached. The probability of drawing a given species was proportional to the number of local sites occupied by that species (as in Chase et al., 2011). In turn, we drew individuals into each selected species until total abundance—summed across species—was equal to observed total abundance. The probability of drawing an individual into a given species was proportional to the relative abundance of that species across all local communities (as in Stegen et al., 2013). This procedure represented stochastic assembly of local communities under the assumptions of weak selection and random dispersal. Compositional differences were quantified with Bray–Curtis (Bray and Curtis, 1957). Repeating stochastic assembly 999 times for each pair of communities provided a null distribution of Bray–Curtis dissimilarities.

To compare observed Bray–Curtis to the null distribution we followed Chase et al. (2011). The number of comparisons between randomly assembled communities that had a Bray–Curtis value greater than the empirical Bray–Curtis was added to half the number of ties. This sum was standardized to range from  $-1$  to  $+1$  by subtracting  $0.5$  and multiplying by  $2$ ; the resulting value is  $RC_{\text{bray}}$ ; values between  $-0.95$  and  $+0.95$  indicate that compositional turnover between a given pair of communities is ‘undominated.’ In turn, we infer that  $RC_{\text{bray}}$  values  $< -0.95$  or  $> +0.95$  indicate that selection, dispersal limitation, or homogenizing dispersal govern observed compositional differences. Furthermore, dispersal limitation is expected to increase differences in community composition and should therefore result in  $RC_{\text{bray}}$  values greater than  $+0.95$ . Homogenizing dispersal, in contrast, increases compositional similarity and should therefore result in  $RC_{\text{bray}}$  values less than  $-0.95$  (Stegen et al., 2013). These interpretations of the  $RC_{\text{bray}}$  metric were evaluated and supported via simulation modeling, as described below.

## Quantifying Influences of Ecological Processes

The composition of each community was compared to the composition of all other sampled communities within the same geologic formation. For a given community we estimated the relative influence of variable selection or homogeneous selection as the fraction of its comparisons with  $\beta\text{NTI} > +2$  or  $\beta\text{NTI} < -2$ , respectively. Selection is excluded as the dominant process when  $|\beta\text{NTI}| < 2$ ; in these cases  $RC_{\text{bray}} > +0.95$  or  $< -0.95$  were taken as evidence that dispersal limitation or homogenizing dispersal, respectively, was the dominant process. For a given local community the relative influence of dispersal limitation was therefore estimated as the fraction of its between-community comparisons with  $|\beta\text{NTI}| < 2$  and  $RC_{\text{bray}} > +0.95$ . Similarly, the relative influence of homogenizing dispersal was estimated as the fraction of comparisons with  $|\beta\text{NTI}| < 2$  and  $RC_{\text{bray}} < -0.95$ . The scenario where  $|\beta\text{NTI}| < 2$  and  $|RC_{\text{bray}}| < 0.95$  indicates that neither selection nor dispersal strongly drive compositional turnover; this is the ‘undominated’ scenario and its relative contribution was estimated as the fraction of comparisons characterized by  $|\beta\text{NTI}| < 2$  and  $|RC_{\text{bray}}| < 0.95$ . These interpretations of the  $\beta\text{NTI}$  and  $RC_{\text{bray}}$  metrics were

evaluated and supported via simulation modeling, as described below.

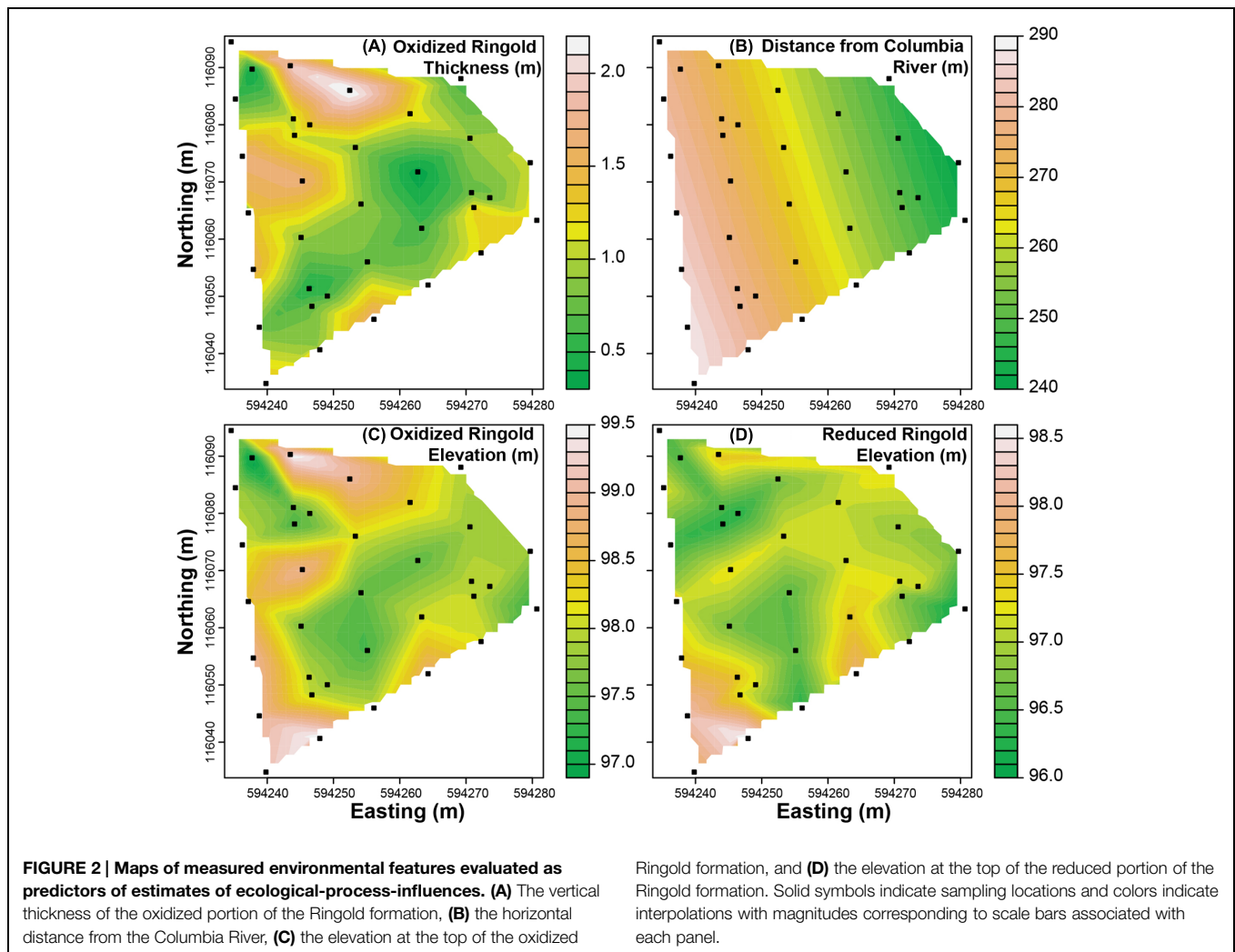
## Statistical Models of Ecological-Process-Influences

In addition to estimating ecological-process-influences we aimed to map spatial variation in those influences. In the subsurface system studied here there were spatial locations where environmental features were characterized but where microbial communities were not. To predict ecological-process-influences across the entire system we first characterized explanatory variables using spatial and environmental data from all sampled locations.

The spatial positions of sampled locations were used with Principal Coordinates of Neighbor Matrices’ (PCNM, now referred to as ‘Moran’s Eigenvector Maps’) to describe spatial eigenvectors (function ‘pcnm’ in R package ‘vegan’; Borcard and Legendre, 2002; Borcard et al., 2011). The horizontal positions of locations at which microbial communities were sampled were unique to each formation such that spatial eigenvectors (referred to as PCNM axes) were generated independently for each formation. We also examined horizontally structured environmental features that included horizontal distance from the Columbia River, the elevations of the reduced and oxidized portions of the Ringold Formation, and the vertical thickness of the oxidized Ringold. Spatial eigenvectors and the four environmental features were used to construct statistical models for each ecological process in each formation; in all cases the statistical models were linear, multiple regression models.

For each ecological process we used environmental features and formation-specific PCNM axes as explanatory variables to construct all possible models with up to seven independent variables. Explanatory variables were described using data from all locations for which there were environmental data (Figure 2), but ecological-process estimates were only available from locations where microbial communities were sampled (Figures 3 and 4). While three of the environmental variables characterize the Ringold Formation, they were used as potential explanatory variables in models for both formations. Doing so evaluated the hypothesis that features of the Ringold Formation influence ecological processes in one or both formations.

Microbial communities were characterized at 16 and 28 locations in the Ringold and Hanford, respectively. We therefore chose the statistical (i.e., the linear, multiple regression) model with the lowest small-sample-size-corrected Akaike Information Criterion (AICc; Burnham and Anderson, 2002). Prior to the construction of statistical models some explanatory variables were removed to avoid strong co-variation. The set of retained explanatory variables was unique to each ecological process in each formation, and was determined as follows. First, explanatory variables were prioritized; a primary goal was to determine the influence of measured environmental features over spatial patterns in ecological processes; measured environmental features had higher priority than the spatial PCNM axes. In addition, ranking within each class of variable—environmental or



PCNM—was based on the strength of correlation to the ecological process being evaluated. If two explanatory variables were significantly correlated ( $R$  function ‘cor.test’), only the explanatory variable with higher priority was retained. Using this approach, lower priority variables that were strongly correlated with higher priority variables were removed prior to model selection.

Models with the lowest AICc for each ecological process in each formation were used to construct spatial maps of ecological-process-influences. For each ecological process in each formation, estimates of explanatory variables from each sampled location were fed into the selected models to generate predictions of ecological-process-influences. This was done for all sampled locations, which included locations where microbial communities were characterized and locations where microbial communities were not characterized. The statistical models were therefore used to extrapolate to locations without microbial data. In turn, the predicted ecological-process-influences were spatially interpolated (function ‘interp’ in R library ‘akima’) and visualized (function ‘filled.contour’ in R package ‘graphics’).

To help determine which environmental features are most likely to have a causal effect on ecological-process-influences,

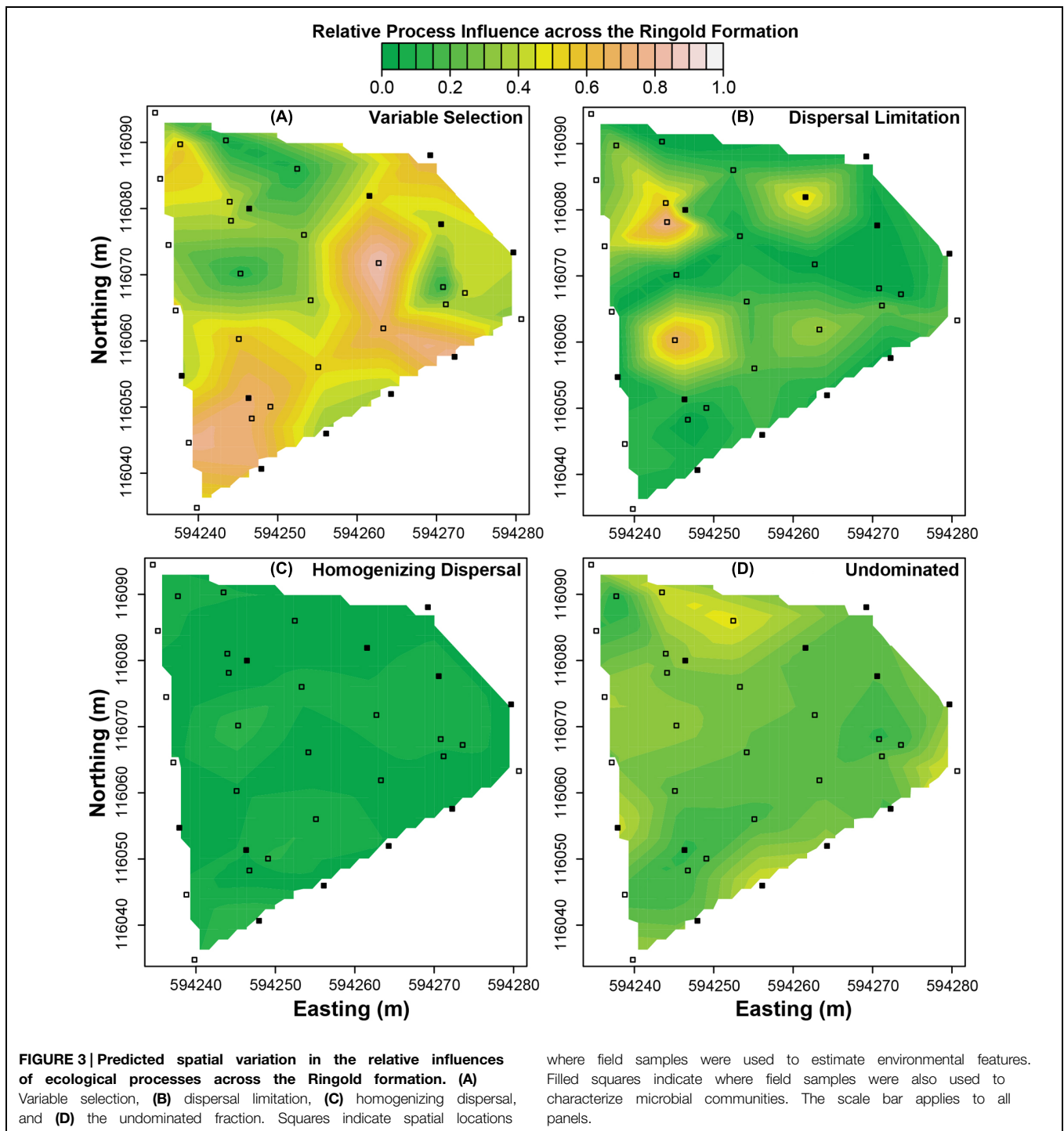
environmental features were related to ecological-process-influences using univariate linear regression. This was only done when a measured environmental feature was the most important component within the multiple regression model of a given ecological process; the most important variable had the largest absolute standardized regression parameter.

## Simulation Model

### Overview

The preceding two subsections contain a number of assertions regarding the interpretation of  $\beta$ NTI and  $RC_{\text{bray}}$  that need to be evaluated to refine interpretations and better understand limitations. For an initial evaluation we developed a purposely simple simulation model that uses idealized cases of specific ecological scenarios to generate a set of ecological communities that are used to evaluate our proposed interpretations.

The simulation model has two components; the first evolves a regional pool of species, tracking species’ evolutionary relationships and evolution in species’ optimal environments; the

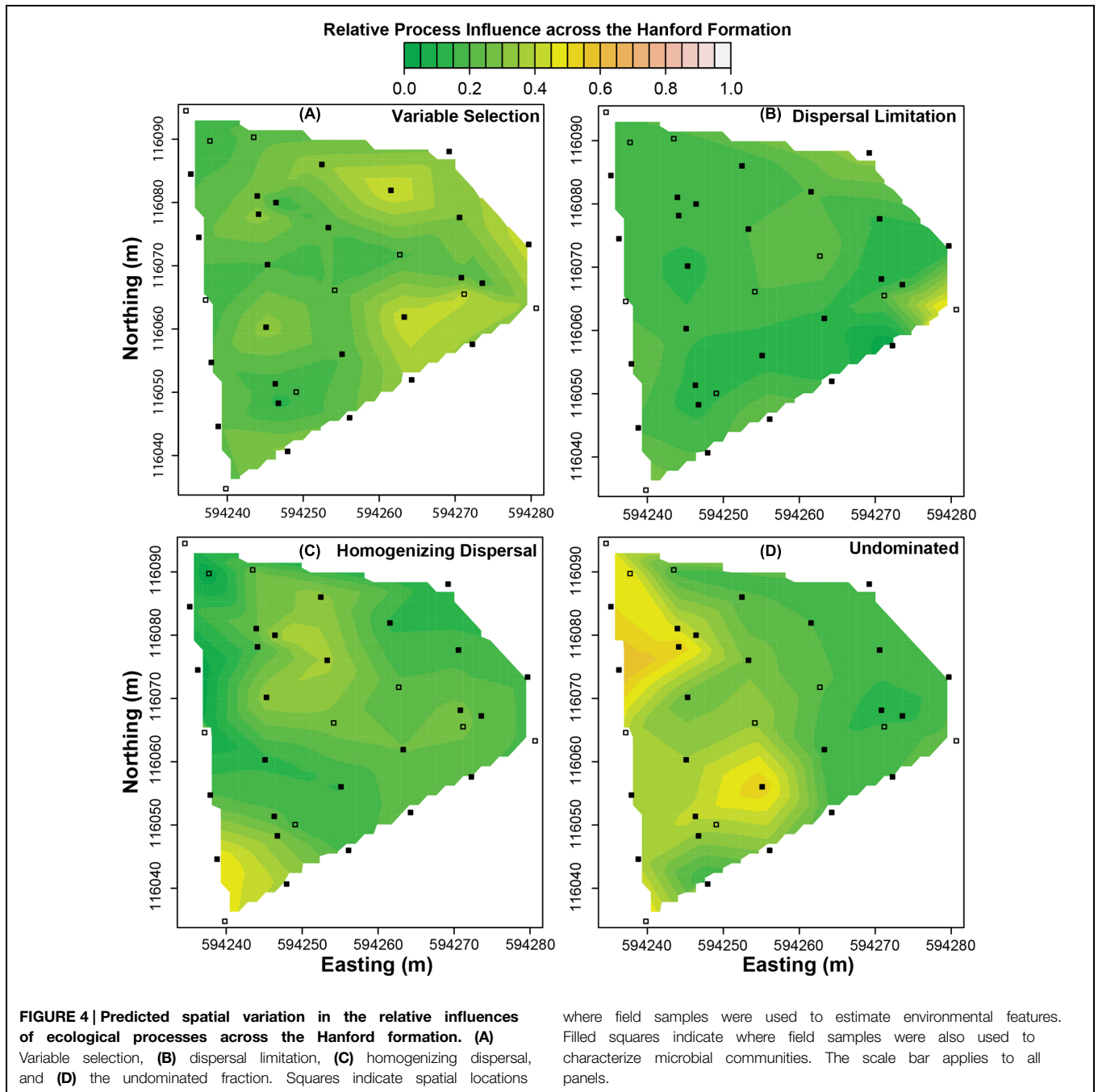


second uses this regional pool to assemble local communities based on scenarios that reflect our conceptualization of how each ecological process influences community composition (Figure 5).

The first component of the model simulates diversification in which new species arise asexually through mutations in the environmental optima of ancestral species. Environmental optima evolve and diversify along an arbitrary environmental axis that takes on values from 0 to 1. Evolution is effectively Brownian

due to no variation in fitness across the environmental axis. The number of species in the regional pool reaches equilibrium due to the following constraints, which are similar to those imposed in Hurlbert and Stegen (2014): there is a maximum total number of individuals (2 million) summed across all species such that population sizes (equal across species) decline with increasing number of species, and the probability of species extinction increases with decreasing population size following a

due to no variation in fitness across the environmental axis. The number of species in the regional pool reaches equilibrium due to the following constraints, which are similar to those imposed in Hurlbert and Stegen (2014): there is a maximum total number of individuals (2 million) summed across all species such that population sizes (equal across species) decline with increasing number of species, and the probability of species extinction increases with decreasing population size following a



negative exponential function [population extinction probability  $\propto \exp(-0.001 \cdot \text{population size})$ ].

The system was initiated with one ancestor that had a randomly chosen environmental optimum. The maximum number of individuals in the system was always achieved such that the ancestor had an initial population size of 2 million. The probability of mutation increased with population size, and a descendant's environmental optimum deviated from its ancestor's by a quantity selected from a Gaussian distribution with mean of 0 and SD of 0.15. Following mutation, population sizes were adjusted so that the total number of individuals was 2 million. Within a time

step, mutation and extinction occurred probabilistically and population sizes were adjusted. The simulation was run for 250 time steps, which was sufficient to reach equilibrium species richness. This simulation procedure, which included tracking of evolutionary relationships among species, provided significant phylogenetic signal (Supplementary Figure S1) for a regional species pool comprised of 1140 species with environmental optima that spanned the environmental axis (Supplementary Figure S2).

In the ecological component of our model, species were drawn from the simulated regional pool to assemble four communities under relatively weak ecological selection (blue environment,

step, mutation and extinction occurred probabilistically and population sizes were adjusted. The simulation was run for 250 time steps, which was sufficient to reach equilibrium species richness. This simulation procedure, which included tracking of evolutionary relationships among species, provided significant phylogenetic signal (Supplementary Figure S1) for a regional species pool comprised of 1140 species with environmental optima that spanned the environmental axis (Supplementary Figure S2).

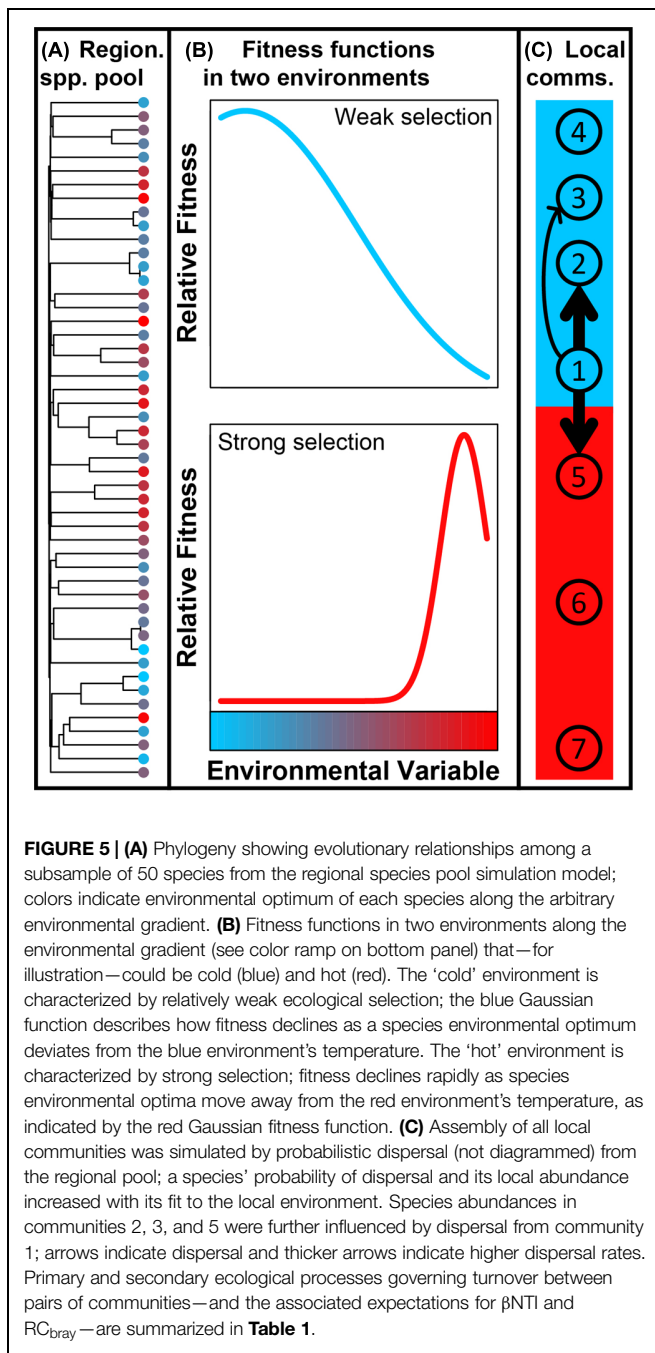


**Figure 5)** and three communities under stronger ecological selection (red environment, **Figure 5**). All communities had 100 species and 10,000 individuals, drawn probabilistically from the regional species pool using ecological rules summarized below. The ecological rules enabled development of *a priori* expectations (summarized in **Table 1**) for the magnitudes of  $\beta$ NTI and  $RC_{\text{bray}}$ , under the assumption that greater fitness translates into higher relative abundance. Following community assembly these expectations were evaluated by comparing one focal community to five other simulated communities, with one exception discussed below.

To characterize the degree of support for our proposed interpretations of  $\beta$ NTI and  $RC_{\text{bray}}$ , the ecological assembly model was run 1000 times. Each iteration used the same regional pool, which was evolved once, and  $\beta$ NTI and  $RC_{\text{bray}}$  were quantified following community assembly. This approach generated a distribution of both metrics for each pairwise community comparison. These distributions were used to characterize the degree of support for our *a priori* expectations, which were tied directly to our proposed conceptual interpretations of  $\beta$ NTI and  $RC_{\text{bray}}$ . We next describe the different ecological rules imposed within the assembly model.

### The Focal Community (Community 1)

Hundred species were drawn without replacement from the regional species pool with probabilities proportional to their fitness in an environment of 0.05; fit was quantified with a Gaussian function centered on 0.05 and with variance of 0.175 (blue curve, **Figure 5**); the arbitrary environmental variable used in the simulations took on values between 0 and 1. Individuals were probabilistically drawn into the 100 selected species until reaching 10,000 individuals. Note that the strength of selection is relatively weak in the blue environment as indicated by the relatively broad fitness function; for comparison, note that selection is relatively strong in the red environment as indicated by the narrower fitness function (**Figure 5**).

### Homogenizing Dispersal (Community 2)

Species and individuals were probabilistically drawn as for community 1, but the probabilities were altered to reflect a high rate of dispersal from community 1. More specifically, species’ probabilities based on the Gaussian fitness function (within the blue environment) were modified by adding a quantity equal to  $0.05^*$  (species abundance in the focal community<sup>1,1</sup>); the exponent controls the rate of dispersal and was selected through preliminary exploration of parameter-space. Given a high rate of dispersal between communities 1 and 2, compositional turnover between communities 1 and 2 will be primarily governed by homogenizing dispersal; the expectations are  $|\beta\text{NTI}| < 2$  and  $RC_{\text{bray}} < -0.95$ .

### Undominated (Community 3)

In our conceptualization, an ‘undominated’ scenario arises when there is a moderate rate of dispersal and the strength of selection is relatively weak; high dispersal leads to homogenizing dispersal, low dispersal leads to dispersal limitation, and strong selection will constrain community composition. To generate this scenario, species were drawn into community 3 as for community 2, but with a lower dispersal rate; species’ probabilities based on the Gaussian fitness function were modified by adding a quantity equal to  $0.05^*$  (species abundance in the focal community<sup>0,8</sup>); this smaller exponent caused a lower rate of dispersal. Compositional turnover between communities 2 and 3 should be undominated such that  $|\beta\text{NTI}| < 2$  and  $|RC_{\text{bray}}| < 0.95$  are expected.

### Dispersal Limitation (Community 4)

Species were drawn into community 4 using only probabilities based on fit to the environment (as for community 1 assembly).

**TABLE 1 | Ecological processes primarily, and secondarily, responsible for turnover between indicated pairs of communities within the simulation model (Figure 1 depicts relationships among communities).**

Communities	Primary factor	Primary expectation	Primary supported	Secondary factor	Secondary expectation	Secondary supported	Fraction unexpected
1 and 2	Homogenizing dispersal	$ \beta\text{NTI}  < 2$ $\text{RC}_{\text{bray}} < -0.95$	91%	Homogeneous selection	$\beta\text{NTI} < -2$	8%	1%
1 and 3	Undominated	$ \beta\text{NTI}  < 2$ $ \text{RC}_{\text{bray}}  < 0.95$	87%	Homogeneous selection	$\beta\text{NTI} < -2$	11%	2%
1 and 4	Dispersal limitation	$ \beta\text{NTI}  < 2$ $\text{RC}_{\text{bray}} > +0.95$	88%	Homogeneous selection	$\beta\text{NTI} < -2$	12%	1%
1 and 5	Homogenizing dispersal	$ \beta\text{NTI}  < 2$ $\text{RC}_{\text{bray}} < -0.95$	83%	Variable selection	$\beta\text{NTI} > +2$	16%	1%
1 and (6 or 7)	Variable selection	$\beta\text{NTI} > +2$	91%	Dispersal limitation	$ \beta\text{NTI}  < 2$ $\text{RC}_{\text{bray}} > +0.95$	9%	0%
6 and 7	Homogeneous selection	$\beta\text{NTI} < -2$	90%	Dispersal limitation	$ \beta\text{NTI}  < 2$ $\text{RC}_{\text{bray}} > +0.95$	0%	10%

Primary and secondary ecological processes are inputs to the simulation model and the associated expectations are patterns that our statistical framework should reveal if it is properly parsing the influences of those ecological processes. The degree of support is summarized as the percentage of replicate simulations for which the statistical framework generates the expected magnitudes of  $\beta\text{NTI}$  and  $\text{RC}_{\text{bray}}$ . The frequency of observing combinations of these two metrics that depart from both the primary and secondary expectations is the scenario-specific error (Fraction unexpected).

This reflects dispersal limitation in the sense that the abundance of a given species in community 1 had no influence on its abundance in community 4 because there is no direct dispersal between the communities. Given weak selection in the blue environment and a low dispersal rate between communities 1 and 4, compositional turnover between communities 1 and 4 should be dominated by dispersal limitation;  $|\beta\text{NTI}| < 2$  and  $\text{RC}_{\text{bray}} > +0.95$  are expected.

### Homogenizing Dispersal Overwhelms Variable Selection (Community 5)

To generate this scenario a second selective environment was required, and was represented as the red environment in **Figure 5**, (environmental value of 0.95). Community 5 was assembled in the red environment such that species' probabilities of occurrence were influenced by their fitness as determined by a Gaussian fitness function centered on 0.95 and with a variance of 0.0075 (red curve, **Figure 5**). The red Gaussian fitness function had lower variance than the blue Gaussian fitness function, which reflected stronger selection. To draw species and individuals into community 5, the fitness-based probabilities were modified as for community 2 assembly such that there was a high rate of dispersal from community 1 to community 5; species' probabilities based on the Gaussian fitness function (within the red environment) were modified by adding a quantity equal to  $0.05 \times (\text{species abundance in the focal community})^{1.1}$ . Given a high rate of dispersal between communities 1 and 5, compositional turnover between communities 1 and 5 should be governed by homogenizing dispersal even though the selective environments are different;  $|\beta\text{NTI}| < 2$  and  $\text{RC}_{\text{bray}} < -0.95$  are expected.

### Variable Selection (Community 6)

Community 6 was assembled as for community 1, but instead using species' probabilities based on fitness within the red environment. In this case, large compositional differences should

arise between communities 1 and 6 due to these communities being assembled in different selective environments; variable selection should dominate such that  $\beta\text{NTI} > +2$  is expected.

### Homogeneous Selection (Community 7)

Homogeneous selection can dominate if communities occur in the same selective environment and if selection is relatively strong. Ecological selection in the blue environment is relatively weak such that homogeneous selection is unlikely to arise; as selection becomes weaker, species become demographically equivalent so that selection does not govern community composition (as in Hubbell, 2001). Selection in the red environment is relatively strong, however, such that homogeneous selection will emerge when assembly is governed principally by environmentally determined fitness. Community 7 was therefore assembled as for community 6;  $\beta\text{NTI} < -2$  is expected.

### Secondary Expectations

As summarized above, our proposed conceptual interpretations of  $\beta\text{NTI}$  and  $\text{RC}_{\text{bray}}$  provide *a priori* expectations for patterns of these metrics in each simulated scenario (**Table 1**). Ecological systems are, however, inherently probabilistic (as is our simulation model). While there is a high probability that species in community (1) disperse to community (2), for example, this is not guaranteed to occur—in the model or in natural systems—and it is therefore expected that homogenizing dispersal will not always dominate. Given that communities (1) and (2) are assembled under the same selective environment, we suggest that when homogenizing dispersal fails to dominate it is most likely because homogeneous selection has constrained community composition; on average, selection is relatively weak in the blue environment (**Figure 5**), but occasionally selection will strongly constrain community composition. The comparison between communities (1) and (2) in a relatively small fraction of replicate simulations should therefore be characterized by  $\beta\text{NTI} < -2$ ; we consider this to be a 'secondary expectation.' For each pairwise community comparison we derived secondary expectations, which

are summarized in **Table 1**. The percentage of replicate simulations showing patterns of  $\beta$ NTI and  $RC_{\text{bray}}$  consistent with those expectations are summarized in **Table 1**.

## Results

Analysis of simulation model outputs showed strong correspondence between expected and observed patterns of  $\beta$ NTI and  $RC_{\text{bray}}$  (**Table 1**). Five of the six scenarios showing error rates of 2% or less. The scenario with the highest error rate (10%) invoked strong homogeneous selection and was associated with the comparison between communities (6) and (7). The statistical framework was therefore applied to the data on microbial communities across the Hanford and Ringold formations.

In both geologic formations there was substantial variation across local communities in the relative influences of the ecological processes (Supplementary Figure S3). Using environmental features and PCNM axes to describe spatial variation in ecological-process-influences showed that each process within each formation was associated with a distinct set of features/axes (**Tables 2 and 3**). In most cases the best models were highly significant, contained at least one environmental feature, and explained up to 83% of spatial variation in ecological-process-influences (**Tables 2 and 3**).

Within the Ringold Formation, the model for homogeneous selection was not significant ( $p = 0.11$ ), but the thickness of the oxidized Ringold was the most important feature retained in the model for variable selection (**Table 2**). A significant relationship

**TABLE 2 | Chosen models for each ecological process within the Ringold Formation.**

Variable	Coefficient	SE	t-value	p-value
<b>Ringold homogeneous selection:</b> model $R^2 = 0.17$ , $p = 0.11$				
PCNM22	0.023	0.014	1.694	0.112
<b>Ringold variable selection:</b> model $R^2 = 0.81$ , $p = 0.0007$				
Oxidized Ringold Thick	-0.164	0.035	-4.637	0.001
PCNM21	0.103	0.026	3.955	0.002
PCNM2	0.065	0.029	2.241	0.047
PCNM8	0.093	0.034	2.710	0.020
<b>Ringold undominated:</b> model $R^2 = 0.3847$ , $p = 0.04257$				
Oxidized Ringold Thick	0.088	0.039	2.258	0.042
PCNM17	0.063	0.033	1.893	0.081
<b>Ringold dispersal limitation:</b> model $R^2 = 0.8298$ , $p = 0.001333$				
Oxidized Ringold Elevation	-0.196	0.038	-5.228	0.0004
PCNM22	-0.176	0.026	-6.802	0.0000
PCNM1	0.125	0.025	4.944	0.0006
PCNM13	-0.039	0.015	-2.669	0.0235
PCNM8	0.171	0.036	4.790	0.0007
<b>Ringold homogenizing dispersal:</b> model $R^2 = 0.7029$ , $p = 0.001742$				
Reduced Ring. Elevation	0.044	0.009	4.911	0.0004
PCNM8	-0.034	0.010	-3.378	0.0055
PCNM16	-0.033	0.010	-3.449	0.0048

All explanatory variables were standardized as standard normal deviates prior to analysis such that coefficient magnitudes are directly comparable.

**TABLE 3 | Chosen models for each ecological process within the Hanford formation.**

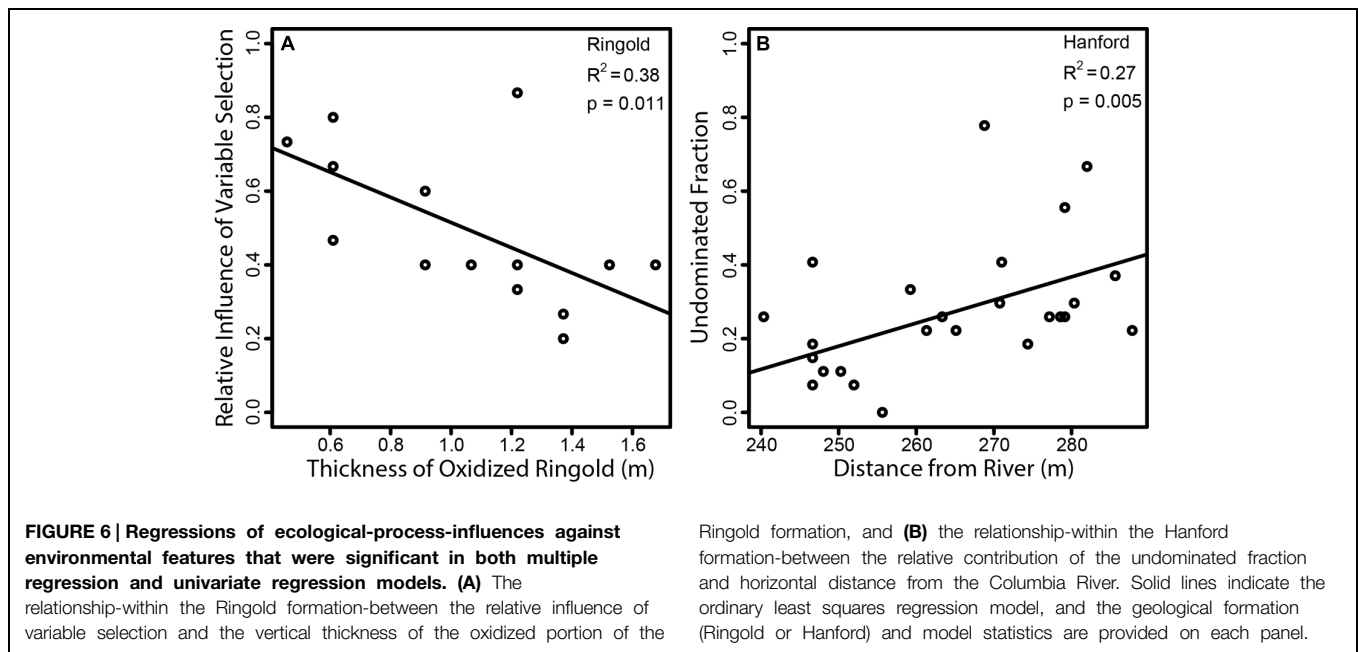
Variable	Coefficient	SE	t-value	p-value
<b>Hanford homogeneous selection:</b> model $R^2 = 0.65$ , $p = 0.0002$				
Distance to River	-0.013	0.007	-1.787	0.0877
Oxidized Ringold Thick.	-0.015	0.008	-1.957	0.0632
PCNM22	0.019	0.006	3.023	0.0063
PCNM6	0.019	0.009	2.138	0.0439
PCNM21	0.013	0.007	1.903	0.0702
<b>Hanford variable selection:</b> model $R^2 = 0.29$ , $p = 0.04$				
Distance to River	-0.061	0.027	-2.252	0.0337
PCNM22	-0.058	0.025	-2.269	0.0325
PCNM8	0.049	0.031	1.611	0.1204
<b>Hanford undominated:</b> model $R^2 = 0.5271$ , $p = 0.0003783$				
Distance to River	0.114	0.025	4.558	0.0001
Reduced Ring. Elevation	-0.075	0.028	-2.686	0.0129
PCNM11	-0.070	0.027	-2.572	0.0167
<b>Hanford dispersal limitation:</b> model $R^2 = 0.3908$ , $p = 0.00696$				
PCNM17	0.067	0.028	2.425	0.023
PCNM7	-0.042	0.023	-1.801	0.084
PCNM13	-0.044	0.024	-1.844	0.078
<b>Hanford homogenizing dispersal:</b> model $R^2 = 0.6128$ , $p = 3.664e-05$				
Oxidized Ringold Elevation	0.042	0.026	1.625	0.1172
PCNM10	-0.075	0.018	-4.103	0.0004
PCNM4	0.069	0.021	3.275	0.0032

All explanatory variables were standardized as standard normal deviates prior to analysis such that coefficient magnitudes are directly comparable.

between the influence of variable selection and the thickness of the oxidized Ringold was also observed by univariate regression ( $p = 0.01$ ,  $R^2 = 0.38$ , **Figure 6A**). Oxidized Ringold thickness was also the most important feature retained in the model of the undominated fraction (**Table 2**), but this relationship was not significant when evaluated by univariate regression ( $p = 0.07$ ). The upper elevation of the oxidized Ringold was the most important feature retained in the model of dispersal limitation (**Table 2**), but this relationship was not significant when evaluated by univariate regression ( $p = 0.75$ ). The elevation at the top of the reduced Ringold was the most important feature in the homogenizing dispersal model (**Table 2**), but this relationship was not significant when evaluated with univariate regression ( $p = 0.09$ ).

Within the Hanford formation, homogeneous selection was most strongly related to PCNM axes and variable selection was most strongly related to distance from the Columbia River (**Table 3**). Variable selection in the Hanford was not, however, significantly related to distance from the Columbia River, by univariate regression ( $p = 0.12$ ). Distance from the Columbia River was the most important feature in the model of the undominated fraction (**Table 3**), and this relationship was also observed by univariate regression ( $p = 0.005$ ,  $R^2 = 0.27$ , **Figure 6B**). No environmental features were retained in the dispersal limitation model (**Table 3**). Homogenizing dispersal was most strongly related to PCNM axes (**Table 3**).

In the Ringold, process-influence-maps revealed spatial patterns of variable selection and in the undominated fraction (**Figure 3**) that showed similarities to spatial patterns of oxidized



Ringold thickness (cf. **Figures 2A** and **3A,D**). Dispersal limitation also showed marked spatial variation across the Ringold Formation, with some congruence with spatial patterns in the elevation of the oxidized Ringold (cf. **Figures 2C** and **3B**). In contrast, homogenizing dispersal was characterized by relatively little spatial variation across the Ringold Formation (**Figure 3C**). The model for homogeneous selection was not significant within the Ringold Formation (see above) such that a map was not generated and, in turn, spatial variation was not evaluated.

Process-influence-maps in the Hanford revealed increases in variable selection and decreases in the undominated fraction in regions closest to the Columbia River and complex patterns across regions further from the river (cf. **Figures 2B** and **4A,D**). Homogeneous selection was relatively consistent through space (Supplementary Figure S4). The influence of dispersal limitation in the Hanford appears to be greatest near the eastern corner of the investigated spatial domain (**Figure 4B**), with no obvious correspondence to environmental features, which is consistent with no environmental variables being retained in the associated multiple regression model (**Table 3**). Homogenizing dispersal across the Hanford was characterized by a complex spatial pattern without any obvious correspondence to environmental features.

## Discussion

Here we worked to improve understanding of the ecological processes that influence microbial community composition. A major component of our approach was extending the statistical framework developed in Stegen et al. (2013), which generated process estimates at the scale of a metacommunity and lumped variable and homogeneous selection into a single estimate. Our extension of their framework distinguished homogeneous selection

from variable selection and estimated the influences of ecological processes for local communities. This extended framework revealed a dominant influence of variable selection—relative to homogeneous selection—and enabled an evaluation of subsurface environmental features related to ecological-process-influences. In turn, we generated process-influence-maps across two geologic formations. Also distinct from Stegen et al. (2013), we evaluated the statistical framework via simulation, which showed close correspondence between expected and observed patterns of  $\beta$ NTI and  $RC_{\text{bray}}$  (**Table 1**). This provides confidence that our statistical framework generates reasonable estimates of ecological-process-influences.

The comparison between communities 6 and 7—in which homogeneous selection was invoked—resulted in the highest error rate (10%). We hypothesize that increasing the strength of selection would reduce this error rate. Simulation studies that continuously vary the strength of selection could be used to evaluate this hypothesis. Such studies could also be used to go beyond the discrete ecological scenarios studied here. These scenarios were used to enable a tractable evaluation of our approach to inferring ecological processes from null modeling results, but selection strength and dispersal rate are continuous variables (e.g., Stegen and Hurlbert, 2011). If our approach is robust, null modeling results should change continuously with the strength of selection and rate of dispersal. Follow-on simulation studies will be needed to fully understand this coupling.

Direct comparison between our results and those from other systems is not currently feasible; we are not aware of previous work that parses homogeneous selection, variable selection, dispersal limitation, and homogenizing dispersal. We note, however, that our results are consistent with dispersal limitation having an important influence over microbial community composition. This aligns with the emerging perspective that microbes have

biogeography (Green et al., 2004, 2008; Martiny et al., 2006) and suggests that in the subsurface all microbes are not everywhere, in contrast to the classic perspective (De Wit and Bouvier, 2006; Martiny et al., 2006).

### Conceptual Inferences

In both formations variable selection and the undominated fraction showed opposing, spatially structured patterns while dispersal limitation and homogenizing dispersal showed more idiosyncratic patterns. To a first approximation variable selection in the Ringold was maximized along a Southwest to Northeast axis, but was maximized in the Eastern corner of the Hanford formation. Spatial patterns of dispersal limitation and homogenizing dispersal were also different between formations. Environmental features governing the relative influences of ecological processes therefore appear to be formation-specific.

The influence of variable selection in the Ringold was most strongly related to oxidized Ringold thickness; variable selection became increasingly weak with increasing thickness (**Figure 6A**). If one defines the rate at which redox conditions change with depth as the vertical distance between oxidized and reduced conditions, redox conditions must change more rapidly with depth in locations with a thinner oxidized Ringold layer. In turn, our results suggest that variable selection increases as the vertical redox gradient becomes steeper (i.e., when redox conditions change more rapidly with depth).

The influence of variable selection may increase with steeper redox gradients if a small number of microbial taxa take advantage of rapidly changing redox conditions. This hypothesis could be directly tested by evaluating the response of microbial communities to experimentally manipulated redox patterns within laboratory flow cells. Such an approach would leverage the strengths of comparative and experimental techniques to provide a deeper level of understanding than otherwise possible (Weber and Agrawal, 2012).

In the Hanford formation the undominated fraction decreased toward the Columbia River (**Figure 4D**; **Table 3**), and there was a modest increase in the influence of variable selection toward the Columbia River (**Figure 4A**; **Table 3**). These patterns suggest an important environmental shift as one moves toward the river, which may be related to spatially structured river-water intrusion.

Elevation of the Columbia River increases annually in the spring, causing river-water intrusion into the studied subsurface system (Peterson et al., 2008; Lin et al., 2012b). To a first approximation, regions of the system that are closer to the river (**Figure 2B**) receive more river-water (Lin et al., 2012b). It may be that an annually repeated pattern of more river-water in the eastern portion of the Hanford formation has resulted in a shift in environmental conditions that cause a stronger influence of variable selection in that region. As a first test of this hypothesis it would be useful to sample a broader spatial domain that contains regions of the subsurface closer to and further from the river, relative to what has been sampled here. Coupling this expanded sampling with laboratory flow cell experiments would provide powerful hypothesis tests.

The undominated fraction should increase with decreases in the strength of selection and/or with a shift toward moderate dispersal rates. In both formations the undominated fraction generally showed patterns opposite those of variable selection. This suggests that a shift toward undominated compositional turnover is due primarily to weaker selection, as opposed to a change in dispersal rates. It is also interesting to note that both formations were characterized by relatively weak influences of homogeneous selection. This result is expected as selection is unlikely to be consistent across spatially heterogeneous systems such as the subsurface system studied here.

Dispersal limitation and homogenizing dispersal both have complex spatial structure, and it is difficult to discern which environmental features (if any) drive these spatial patterns. Dispersal limitation across both formations was unrelated to environmental features when evaluated with univariate regression, suggesting that the environmental features used in our analyses do not strongly determine the influence of dispersal limitation. Similarly, homogenizing dispersal in the Hanford was more strongly related to PCNM axes than to environmental features (**Table 3**). Instead of being driven by relatively simple environmental features, the influences of dispersal limitation and homogenizing dispersal may be governed more by complex and spatially inconsistent features that influence hydrologic transport.

### Comparison to Variation Partitioning

While it may appear that variation partitioning (Legendre and Legendre, 1998) was used here to estimate ecological-process-influences, there are substantial differences between variation partitioning and our approach. In variation partitioning, variation in community composition is explained using features deemed *a priori* to reflect spatial relationships or environmental differences among communities (e.g., Tuomisto et al., 2003; Cottenie, 2005; Legendre et al., 2009; Heino et al., 2011). Intuitively, the more variation in community composition explained by spatial or environmental features, the greater the influence of dispersal limitation or selection, respectively (Stegen and Hurlbert, 2011). At least three studies have shown that this intuitive expectation is not valid and that variation partitioning cannot be used to infer the influences of ecological processes (Gilbert and Bennett, 2010; Smith and Lundholm, 2010; Stegen and Hurlbert, 2011). Variation partitioning can, at best, determine whether dispersal limitation has more or less influence than selection (Stegen and Hurlbert, 2011).

With variation partitioning it is tempting to infer that variation in community composition not explained by spatial or environmental features results from ecological drift. Unexplained variation will, however, increase artificially if any of the following occur: (i) important environmental features have not been measured; (ii) spatial axes fail to capture idiosyncratic patterns in spatial isolation among communities; or (iii) community composition is non-linearly related to explanatory variables (see discussions in Laliberte et al., 2009; Legendre et al., 2009; Anderson et al., 2011).

In contrast to variation partitioning we used null models to estimate the influences of ecological processes; our approach

does not relate community composition to explanatory variables. Our approach therefore solves a primary shortcoming of variation partitioning, but like all statistical frameworks has its own limitations.

### Limitations, Caveats, and the Path Forward

With respect to the framework used here, two important considerations are sample size and error from sampling, DNA sequencing and data processing. Ecological process estimates likely approach their true values as sample size increases and this should be considered in cross-system comparisons.

It is not obvious that sources of error will systematically increase or decrease any particular process estimate such that we assume errors contribute equally to estimates of all ecological processes. Nonetheless, future simulation studies need to evaluate the potential for bias related to sample size and sources of error.

On the conceptual side, we note that our framework does not account for influences of *in situ* diversification, which is the evolutionary component in Vellend's (2010) synthesis (see also Hanson et al., 2012). This may be relevant as high rates of *in situ* diversification could increase compositional turnover in terms of OTU presence/absence; if dispersal rates are low, new OTUs that evolve *in situ* may only be found in one community. On the other hand, among-community dispersal will minimize influences of *in situ* diversification; if newly evolved OTUs disperse away from their community-of-origin, the influence of *in situ* diversification on compositional turnover will be minimal. Outcomes are therefore influenced by the balance between dispersal and diversification rates.

Extending our framework to characterize the influence of *in situ* diversification on patterns of compositional turnover represents an important challenge. Pattern-oriented simulation modeling (e.g., Grimm et al., 2005; Rangel et al., 2007; Stegen and Hurlbert, 2011; McClain et al., 2012) is one approach that could be leveraged to meet this challenge. In the context of species richness gradients, for example, Hurlbert and Stegen (2014) recently developed a pattern-oriented simulation model that provides 'multi-metric fingerprints' that indicate the operation of specific underlying processes. A similar approach could be added to our framework to identify multi-metric fingerprints indicating the influence of *in situ* diversification on patterns of compositional turnover.

We further suggest that a pattern-oriented simulation modeling approach could be used to draw additional inferences from the undominated fraction provided by our current framework. The undominated fraction is tied to a conceptual inference—selection is too weak and dispersal rates are not extreme enough for either process to drive compositional turnover. It would be

useful, however, to parse the relative influences of ecological processes within the undominated fraction. To this end, pattern-oriented simulations similar to those in Stegen and Hurlbert (2011) could be used to study compositional turnover patterns expected across a two-dimensional process-space defined by the strength of selection and the rate of dispersal. Observed turnover patterns within the undominated fraction could then be related back to simulated turnover patterns and, in turn, the balance between selection and dispersal (similar to McClain et al., 2012).

In summary, we have provided spatial projections for the relative influences of ecological processes on subsurface microbial community composition. Doing so has revealed key features of our system unrecognized through application of existing statistical frameworks. We suggest that for many systems a similar outcome is likely and that novel insights can be gained through broad application of a framework that couples the approach used here with that of Stegen et al. (2013). We look forward to these statistical frameworks being improved through additional simulation-based evaluations, to experimental tests of the hypotheses they generate, and to a coupling between the information they provide and process-based models aimed at predicting community composition across environmental conditions.

### Acknowledgments

A portion of the research described in this paper was conducted under the Laboratory Directed Research and Development Program at Pacific Northwest National Laboratory (PNNL), a multiprogram national laboratory operated by Battelle for the U.S. Department of Energy. JS is grateful for the support of the Linus Pauling Distinguished Postdoctoral Fellowship program at PNNL. A portion of the research was performed using Institutional Computing at PNNL. This research was further supported by the U.S. Department of Energy (DOE), Office of Biological and Environmental Research (BER), as part of Subsurface Biogeochemistry Research Program's Scientific Focus Area (SFA), and Integrated Field-Scale Research Challenge (IFRC) at the Pacific Northwest National Laboratory (PNNL). PNNL is operated for DOE by Battelle under contract DE-AC06-76RLO 1830.

### Supplementary Material

The Supplementary Material for this article can be found online at: <http://journal.frontiersin.org/article/10.3389/fmicb.2015.00370/abstract>

### References

- Anderson, M. J., Crist, T. O., Chase, J. M., Vellend, M., Inouye, B. D., Freestone, A. L., et al. (2011). Navigating the multiple meanings of (diversity): a roadmap for the practicing ecologist. *Ecol. Lett.* 14, 19–28. doi: 10.1111/j.1461-0248.2010.01552.x
- Bjornstad, B. N., Horner, J. A., Vermeul, V. R., Lanigan, D. C., and Thorne, P. D. (2009). *Borehole Completion and Conceptual Hydrogeologic Model for the IFRC Well Field, 300 Area, Hanford Site*, Richland, WA: Pacific Northwest National Laboratory.
- Borcard, D., Gillet, F., and Legendre, L. (2011). *Numerical Ecology with R*, New York, NY: Springer.
- Borcard, D., and Legendre, P. (2002). All-scale spatial analysis of ecological data by means of principal coordinates of neighbour matrices. *Ecol. Model.* 153, 51–68. doi: 10.1016/S0304-3800(01)00501-4

- Bray, J. R., and Curtis, J. T. (1957). An ordination of the upland forest communities of southern wisconsin. *Ecol. Monogr.* 27, 326–349. doi: 10.2307/1942268
- Burnham, K. P., and Anderson, D. (2002). *Model Selection and Multi-Model Inference*. New York, NY: Springer-Verlag.
- Caporaso, J. G., Kuczynski, J., Stombaugh, J., Bittinger, K., Bushman, F. D., Costello, E. K., et al. (2010). QIIME allows analysis of high-throughput community sequencing data. *Nat. Methods* 7, 335–336. doi: 10.1038/Nmeth.F.303
- Cavender-Bares, J., Kozak, K. H., Fine, P. V. A., and Kembel, S. W. (2009). The merging of community ecology and phylogenetic biology. *Ecol. Lett.* 12, 693–715. doi: 10.1111/j.1461-0248.2009.01314.x
- Chase, J. M. (2007). Drought mediates the importance of stochastic community assembly. *Proc. Natl. Acad. Sci. U.S.A.* 104, 17430–17434. doi: 10.1073/pnas.0704350104
- Chase, J. M. (2010). Stochastic community assembly causes higher biodiversity in more productive environments. *Science* 328, 1388–1391. doi: 10.1126/science.1187820
- Chase, J. M., Kraft, N. J. B., Smith, K. G., Vellend, M., and Inouye, B. D. (2011). Using null models to disentangle variation in community dissimilarity from variation in  $\alpha$ -diversity. *Ecosphere* 2:art24. doi: 10.1890/es10-00117.1
- Cottenie, K. (2005). Integrating environmental and spatial processes in ecological community dynamics. *Ecol. Lett.* 8, 1175–1182. doi: 10.1111/j.1461-0248.2005.00820.x
- De Wit, R., and Bouvier, T. (2006). Everything is everywhere, but, the environment selects; what did Baas Becking and Beijerinck really say? *Environ. Microbiol.* 8, 755–758. doi: 10.1111/j.1462-2920.2006.01017.x
- Dias, P. C. (1996). Sources and sinks in population biology. *Trends Ecol. Evol.* 11, 326–330. doi: 10.1016/0169-5347(96)10037-9
- Dini-Andreote, F., Stegen, J. C., Van Elsas, J. D., and Salles, J. F. (2015). Disentangling mechanisms that mediate the balance between stochastic and deterministic processes in microbial succession. *Proc. Natl. Acad. Sci. U.S.A.* 112, E1326–E1332. doi: 10.1073/pnas.1414261112
- Fine, P. V. A., and Kembel, S. W. (2011). Phylogenetic community structure and phylogenetic turnover across space and edaphic gradients in western Amazonian tree communities. *Ecography* 34, 552–565. doi: 10.1111/j.1600-0587.2010.06548.x
- Gilbert, B., and Bennett, J. R. (2010). Partitioning variation in ecological communities: do the numbers add up? *J. Appl. Ecol.* 47, 1071–1082. doi: 10.1111/j.1365-2664.2010.01861.x
- Green, J. L., Bohannan, B. J. M., and Whitaker, R. J. (2008). Microbial biogeography: from taxonomy to traits. *Science* 320, 1039–1043. doi: 10.1126/science.1153475
- Green, J. L., Holmes, A. J., Westoby, M., Oliver, I., Briscoe, D., Dangerfield, M., et al. (2004). Spatial scaling of microbial eukaryote diversity. *Nature* 432, 747–750. doi: 10.1038/Nature03034
- Grimm, V., Revilla, E., Berger, U., Jeltsch, F., Mooij, W. M., Railsback, S. F., et al. (2005). Pattern-oriented modeling of agent-based complex systems: lessons from ecology. *Science* 310, 987–991. doi: 10.1126/science.1116681
- Hanson, C. A., Fuhrman, J. A., Horner-Devine, M. C., and Martiny, J. B. H. (2012). Beyond biogeographic patterns: processes shaping the microbial landscape. *Nat. Rev. Microbiol.* 10, 497–506. doi: 10.1038/Nrmicro2795
- Hardy, O. J. (2008). Testing the spatial phylogenetic structure of local communities: statistical performances of different null models and test statistics on a locally neutral community. *J. Ecol.* 96, 914–926. doi: 10.1111/j.1365-2745.2008.01421.x
- Heino, J., Grönroos, M., Soininen, J., Virtanen, R., and Muotka, T. (2011). Context dependency and metacommunity structuring in boreal headwater streams. *Oikos* 121, 537–544. doi: 10.1111/j.1600-0706.2011.19715.x
- Horner-Devine, M. C., and Bohannan, B. J. M. (2006). Phylogenetic clustering and overdispersion in bacterial communities. *Ecology* 87, 100–108. doi: 10.1890/0012-9658(2006)87[100:PCAOIB]2.0.CO;2
- Hubbell, S. P. (2001). *The Unified Neutral Theory of Biodiversity and Biogeography*. Princeton, NJ: Princeton University Press.
- Hurlbert, A. H., and Stegen, J. C. (2014). When should species richness be energy limited, and how would we know? *Ecol. Lett.* 17, 401–413. doi: 10.1111/ele.12240
- Kraft, N. J. B., Cornwell, W. K., Webb, C. O., and Ackerly, D. D. (2007). Trait evolution, community assembly, and the phylogenetic structure of ecological communities. *Am. Nat.* 170, 271–283. doi: 10.1086/519400
- Laliberte, E., Paquette, A., Legendre, P., and Bouchard, A. (2009). Assessing the scale-specific importance of niches and other spatial processes on beta diversity: a case study from a temperate forest. *Oecologia* 159, 377–388. doi: 10.1007/s00442-008-1214-1218
- Legendre, P., and Legendre, L. (1998). *Numerical Ecology*. Amsterdam, The Netherlands: Elsevier Science.
- Legendre, P., Mi, X. C., Ren, H. B., Ma, K. P., Yu, M. J., Sun, I. F., et al. (2009). Partitioning beta diversity in a subtropical broad-leaved forest of China. *Ecology* 90, 663–674. doi: 10.1890/07-1880.1
- Leibold, M. A., Holyoak, M., Mouquet, N., Amarasekare, P., Chase, J. M., Hoopes, M. F., et al. (2004). The metacommunity concept: a framework for multi-scale community ecology. *Ecol. Lett.* 7, 601–613. doi: 10.1111/j.1461-0248.2004.00608.x
- Lin, X., Kennedy, D., Peacock, A., McKinley, J., Resch, C. T., Fredrickson, J., et al. (2012a). Distribution of microbial biomass and potential for anaerobic respiration in Hanford Site 300 Area subsurface sediment. *Appl. Environ. Microbiol.* 78, 759–767. doi: 10.1128/aem.07404-7411
- Lin, X., McKinley, J., Resch, C. T., Lauber, C., Fredrickson, J., and Konopka, A. E. (2012b). Spatial and temporal dynamics of microbial community in the Hanford unconfined aquifer. *ISME J.* 6, 1665–1676. doi: 10.1038/ismej.2012.26
- Losos, J. B. (2008). Phylogenetic niche conservatism, phylogenetic signal and the relationship between phylogenetic relatedness and ecological similarity among species. *Ecol. Lett.* 11, 995–1003. doi: 10.1111/j.1461-0248.2008.01229.x
- Martiny, J. B. H., Bohannan, B. J. M., Brown, J. H., Colwell, R. K., Fuhrman, J. A., Green, J. L., et al. (2006). Microbial biogeography: putting microorganisms on the map. *Nat. Rev. Micro.* 4, 102–112. doi: 10.1038/nrmicro1341
- McClain, C. R., Stegen, J. C., and Hurlbert, A. H. (2012). Dispersal, environmental niches and oceanic-scale turnover in deep-sea bivalves. *Proc. R. Soc. Biol. Sci. U.S.A.* 279, 1993–2002. doi: 10.1098/rspb.2011.2166
- Peterson, R. E., Rockhold, M. L., Serne, R. J., Thorne, P. D., and Williams, M. D. (2008). *Uranium Contamination in the Subsurface Beneath the 300 Area, Hanford site, Washington*. Richland, WA: Pacific Northwest National Laboratory. doi: 10.2172/925719
- Rangel, T. F. L. V. B., Diniz-Filho, J. A. F., and Colwell, R. K. (2007). Species richness and evolutionary niche dynamics: a spatial pattern-oriented simulation experiment. *Am. Nat.* 170, 602–616. doi: 10.1086/521315
- Smith, T. W., and Lundholm, J. T. (2010). Variation partitioning as a tool to distinguish between niche and neutral processes. *Ecography* 33, 648–655. doi: 10.1111/j.1600-0587.2009.06105.x
- Stegen, J. C., and Hurlbert, A. H. (2011). Inferring ecological processes from taxonomic, phylogenetic and functional trait  $\beta$ -diversity. *PLoS ONE* 6:e20906. doi: 10.1371/journal.pone.0020906
- Stegen, J. C., Lin, X., Fredrickson, J. K., Chen, X., Kennedy, D. W., Murray, C. J., et al. (2013). Quantifying community assembly processes and identifying features that impose them. *ISME J.* 7, 2069–2079. doi: 10.1038/ismej.2013.93
- Stegen, J. C., Lin, X., Konopka, A. E., and Fredrickson, J. K. (2012). Stochastic and deterministic assembly processes in subsurface microbial communities. *ISME J.* 6, 1653–1664. doi: 10.1038/ismej.2012.22
- Tuomisto, H., Ruokolainen, K., and Yli-Halla, M. (2003). Dispersal, environment, and floristic variation of western amazonian forests. *Science* 299, 241–244. doi: 10.1126/science.1078037
- Vellend, M. (2010). Conceptual synthesis in community ecology. *Q. Rev. Biol.* 85, 183–206. doi: 10.1086/652373

- Wang, J., Shen, J., Wu, Y., Tu, C., Soininen, J., Stegen, J. C., et al. (2013). Phylogenetic beta diversity in bacterial assemblages across ecosystems: deterministic versus stochastic processes. *ISME J.* 7, 1310–1321. doi: 10.1038/ismej.2013.30
- Webb, C. O., Ackerly, D. D., and Kembel, S. (2011). *Phylocom: Software for the Analysis of Phylogenetic Community Structure and Character Evolution (with Phylomatic and Ecoevolve). User's Manual, Version 4.2.* Available at: <http://www.phylodiversity.net/phylocom/>
- Weber, M. G., and Agrawal, A. A. (2012). Phylogeny, ecology, and the coupling of comparative and experimental approaches. *Trends Ecol. Evol.* 27, 394–403. doi: 10.1016/j.tree.2012.04.010

**Conflict of Interest Statement:** The authors declare that the research was conducted in the absence of any commercial or financial relationships that could be construed as a potential conflict of interest.

Copyright © 2015 Stegen, Lin, Fredrickson and Konopka. This is an open-access article distributed under the terms of the Creative Commons Attribution License (CC BY). The use, distribution or reproduction in other forums is permitted, provided the original author(s) or licensor are credited and that the original publication in this journal is cited, in accordance with accepted academic practice. No use, distribution or reproduction is permitted which does not comply with these terms.

# What difference does it make if viruses are strain-, rather than species-specific?

T. Frede Thingstad\*, Bernadette Pree, Jarl Giske and Selina Våge

Department of Biology, Hjort Centre for Marine Ecosystem Dynamics, University of Bergen, Bergen, Norway

## OPEN ACCESS

### Edited by:

Shin Haruta,  
Tokyo Metropolitan University, Japan

### Reviewed by:

Angel Valverde,  
University of Pretoria, South Africa  
Takeshi Miki,  
National Taiwan University, Taiwan  
Andreas Florian Haas,  
San Diego State University, USA

### \*Correspondence:

T. Frede Thingstad,  
Department of Biology, Hjort Centre  
for Marine Ecosystem Dynamics,  
University of Bergen, PO Box 7803,  
5020 Bergen, Norway  
frede.thingstad@uib.no

### Specialty section:

This article was submitted to  
Systems Microbiology,  
a section of the journal  
Frontiers in Microbiology

**Received:** 26 November 2014

**Accepted:** 31 March 2015

**Published:** 20 April 2015

### Citation:

Thingstad TF, Pree B, Giske J and  
Våge S (2015) What difference does it  
make if viruses are strain-, rather than  
species-specific?  
*Front. Microbiol.* 6:320.  
doi: 10.3389/fmicb.2015.00320

Theoretical work has suggested an important role of lytic viruses in controlling the diversity of their prokaryotic hosts. Yet, providing strong experimental or observational support (or refutation) for this has proven evasive. Such models have usually assumed “host groups” to correspond to the “species” level, typically delimited by 16S rRNA gene sequence data. Recent model developments take into account the resolution of species into strains with differences in their susceptibility to viral attack. With strains as the host groups, the models will have explicit viral control of abundance at strain level, combined with explicit predator or resource control at community level, but the direct viral control at species level then disappears. Abundance of a species therefore emerges as the combination of how many strains, and at what abundance, this species can establish in competition with other species from a seeding community. We here discuss how species diversification and strain diversification may introduce competitors and defenders, respectively, and that the balance between the two may be a factor in the control of species diversity in mature natural communities. These models can also give a dominance of individuals from strains with high cost of resistance; suggesting that the high proportion of “dormant” cells among pelagic heterotrophic prokaryotes may reflect their need for expensive defense rather than the lack of suitable growth substrates in their environment.

**Keywords:** killing-the-winner model, biodiversity control, biodiversity–ecosystem functioning relationships, Weinbauer’s Paradox, fractal similarity, microevolution

## Introduction

Classical discussions of diversity-maintaining mechanisms in microbiology had a tendency to focus on competition, with the works of Hutchinson (1961) and Tilman (1977) in phytoplankton ecology as influential examples. With competitive exclusion as the theoretical outcome for species competing for the same limiting substrate, this created a need for additional hypotheses to explain observed microbial biodiversity. With the huge microbial diversity revealed by modern metagenomics (Venter et al., 2004), this gap between observation and theory is now perhaps wider than ever.

The list of mechanisms thought to maintain diversity includes, among others, substrate diversity (Tilman, 1977), environmental variability in time and/or space (Connell, 1979; Beninca et al., 2008; Dini-Andreote et al., 2014; Jankowski et al., 2014; Staley et al., 2014; Uksa et al., 2014), chaotic dynamics (Beninca et al., 2008), and selective loss (Thingstad and Lignell, 1997; Thingstad, 2000), presumably working together in a more or less additive manner in

complex natural environments. In the prokaryotic world, the issue of species diversity is further complicated not only by the problem of defining what constitutes a species (Fraser et al., 2009), but also by the fact that strains from the same species contain non-conserved, non-core genes that are sporadically distributed among members of the population (Avrani et al., 2011).

Quite different from a picture of natural communities as assemblages of clonal species populations, this suggests that a prokaryote “species” consists of a set of strains where some traits characterize the set, while other traits vary between strains. Any comparison between model and data then needs to take into account whether the experimental data resolves the genetic information at species or at strain level.

As a kind of minimum model to describe the effect of top-down control, one can combine size-selective predators with host specific viruses. This creates a two-level model where the same basic “killing-the winner” (KtW) principle (Figure 1A) is applied at both levels: Grazing control of the community size of heterotrophic prokaryotes allows for phytoplankton coexistence with heterotrophic bacteria (Figure 1B), even when bacteria are superior competitors for a shared limiting mineral nutrient (Pengerud et al., 1987). Applying the KtW principle inside the community (Figure 1C) allows competitive host-groups with high growth rate to coexist with defensive host-groups with a low loss to viral lysis, even if this defense comes at the expense of a slower growth rate (Bohannan and Lenski, 2000).

A lot of the experimental and observational work in the field has tried to relate their findings to this KtW model, but clear support (or rebuttal) of the theory has so far been evasive (see e.g., Winter et al., 2010). We recently suggested (Thingstad et al., 2014) that part of this problem might be rooted in the often implicitly made assumption that this model’s “host groups” correspond to observational information contained in 16S rRNA gene sequence data. Since such data are more relevant to the species than to a strain level, it means that the KtW model in this case is interpreted with host groups representing species.

Models that incorporate the possibility for viral strain specificity have recently been introduced (Jover et al., 2013; Thingstad et al., 2014). In these, the explicit top-down control on species abundances disappears as illustrated in Figure 1D. This obviously is important for discussions of community “species” composition such as e.g., recent attempts to combine the high abundance of the SAR11 clade with its susceptibility to viral infection (Giovannoni et al., 2013; Våge et al., 2013; Zhao et al., 2013).

In the model of Figure 1D, the abundance of individuals belonging to a species is the sum of individuals belonging to each of its strains, with no other explicit control on species size than the maximum value given by the community size. As a consequence, abundance at the species level becomes a combination of its ability to establish many strains, and the virus-controlled abundance of individuals within each of these strains. Since establishment of a strain and abundance within this strain are functions of its competitive and its defensive abilities, respectively, abundance at species level becomes a combined function

of a species’ competitive and defensive abilities (Thingstad et al., 2014).

To illustrate the ecological consequences of these models we have arranged the subsequent discussion in sections devoted to a set of questions picked from the list of themes announced for this special issue.

## How Does a Foreign Microbe Become a Member of the Ecosystem?

In a system at steady state, specific growth rate ( $\mu$ ) must equal specific loss rate ( $\delta$ ) for all populations and all subpopulations, so that their net growth rate  $\mu - \delta$  is zero. This system can then be invaded by any new organism type  $x$ , be it a mutant or an immigrant species, for which  $\mu_x - \delta_x > 0$  when it enters the established community (Symbols summarized in Table 1). The invasion changes the growth conditions in the established community. How numerous the invader will become in the new steady state (if this exists) depends on a new set of equilibrium conditions. This set includes the new  $\mu_x - \delta_x = 0$  condition, while the equivalent condition for now excluded members in the previous state of the community has disappeared. Although, both invasion and final community size for the invader depend on how  $\mu$  and  $\delta$  vary with the state of the community, the conditions for invasion and population size are thus different.

Two cases are of particular interest for our subsequent discussion, (1) a mutant that can use some unexploited resource in the system and therefore has a large  $\mu_x$ ; and (2) an organism that has few/no enemies in the system or is good in defending itself against those already present, and therefore has a low  $\delta_x$ .

## How Do Microbes in Ecosystems Evolve?

The importance of the somewhat abstract reasoning above can be illustrated by considering the idealized environment of a chemostat, frequently used to study simplified virus-host systems (e.g., Bohannan and Lenski, 1997, 2000; Middelboe et al., 2009; Marston et al., 2012). This simple environment is characterized by two parameters: the dilution rate  $D$ , and the reservoir concentration  $S_R$  of limiting substrate (for simplicity assumed here to be a non-respired substance like e.g., phosphate).

In the traditional theoretical case of a clonal bacterial population, the chemostat will have a resource-controlled population size proportional to  $S_R$  and a growth rate equal to the dilution rate:  $\mu(S_C) = D$ . The steady-state culture concentration  $S_C$  is thus linked to dilution rate through the growth characteristics of the organism. This clonal community is invadable only by a better competitor, i.e., one that has a higher growth rate at the given  $S_C$ . If, however, the established population is infected with a lytic virus, the original susceptible clone becomes virus-controlled and is reduced to a low population level. Part of the available reservoir substrate  $S_R$  will then remain unused in the culture, i.e., leading to a high  $S_C$ . With a high  $S_C$ , this one host-one virus community will be easily invadable by a resistant host mutant, even if the mutation comes at a price (a cost of resistance, COR). With higher  $S_C$ , the original parent strain will now grow faster than  $D$ , it can

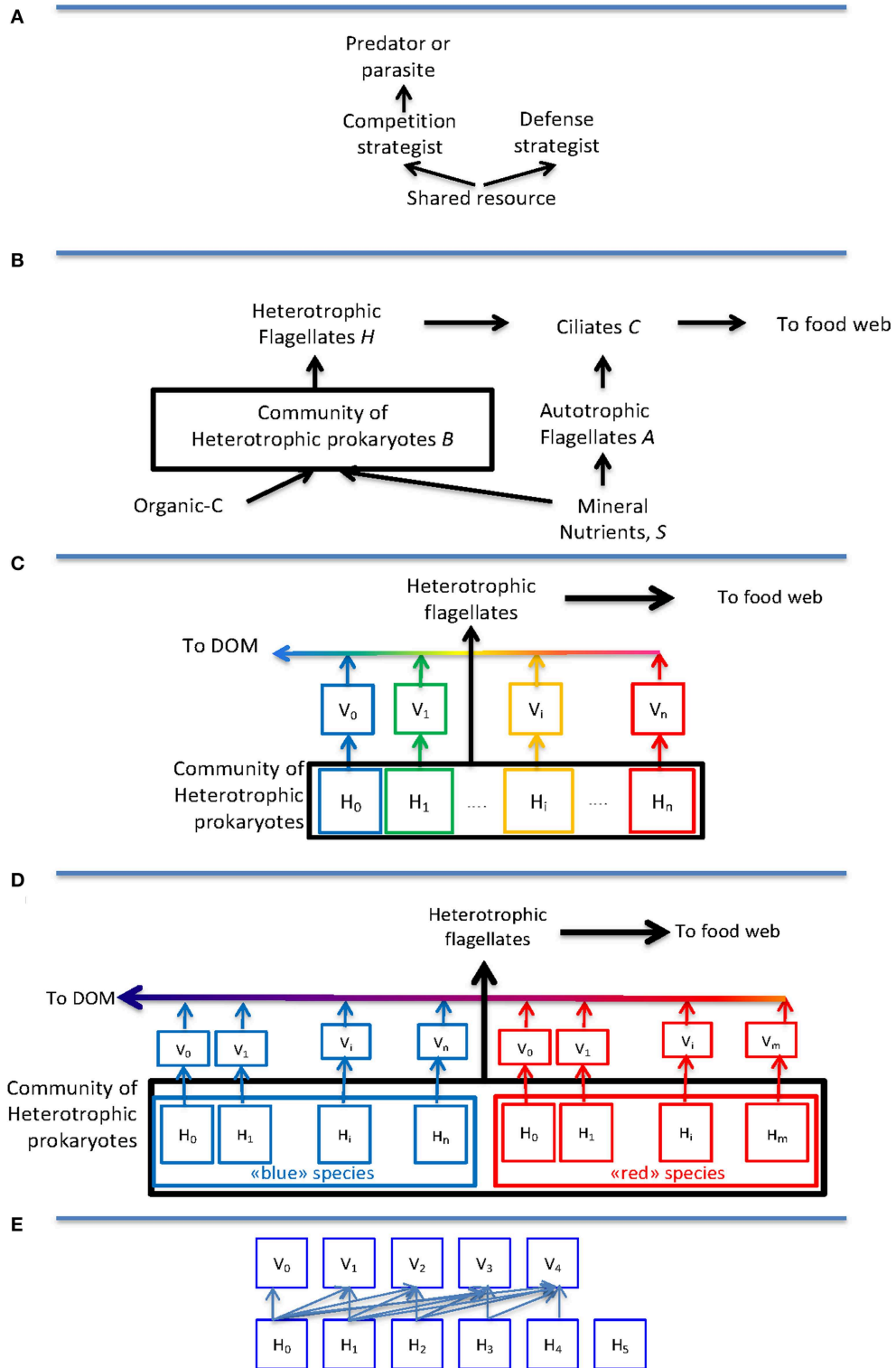


**FIGURE 1 | Idealized models for trophic interactions discussed: (A) The “Killing-the-Winner” structure where abundance of the competition strategist is top-down controlled by a predator or parasite, thereby leaving resources for a resource-limited defense strategist. (B) An idealized model of the microbial food web based on the**

principles from (A), illustrating how ciliates influence both biomass and growth conditions of heterotrophic flagellates through their grazing on heterotrophic and autotrophic flagellates, respectively. (C) The original one host-one virus model interpreted as host-groups corresponding to species (Continued)

**FIGURE 1 | Continued**  
 (“blue,” “green,” “yellow,” “red”) and species abundance therefore being top-down controlled. In this model, the application of the KtW principle at the predator-prey creates a transport “up” the food chain, while applying the same principle to viruses sends material “down” to dissolved organic material (DOM). **(D)** Modification of **(C)** by the assumption that host groups correspond to strains belonging to either a “blue” or a “red” species, illustrating how the direct top-down control of abundance disappears at the intermediate level of species. **(E)** Modification of the host-virus interaction from the one host–one virus relationship in **(D)** to a nested structure. This is the structure used in drawing **Figure 2C**.

**TABLE 1 | List of symbols.**

DESCRIPTION OF HOST SPECIES <i>x</i>	
$xH_i$	Abundance of host strain <i>i</i> belonging to species <i>x</i>
$x\mu_i$	Specific growth rate for host strain <i>i</i> of species <i>x</i> . For the graphs in <b>Figure 2</b> this is calculated from the Michaelis-Menten relationship: $x\mu_i(S) = \frac{x\alpha S}{1 + \frac{x\alpha S}{x\mu^{max}_x v}}$
$x\delta$	Specific loss rate host <i>x</i>
Competitive abilities of host species <i>x</i> influencing the number of strains it can establish	
$x\alpha$	Nutrient affinity
$x\mu^{max}$	Maximum specific growth rate
$xv$	Fractional reduction in $x\mu^{max}$ for each mutational step in the host
Defensive properties of host species <i>x</i> influencing the abundance of individuals within strains	
$x\beta$	Adsorption coefficient
$x\rho$	Parameter $0 < \rho < 1$ representing the loss in effective adsorption coefficient for each new host strain added to the arms race
$x\sigma$	Parameter $0 < \sigma < 1$ representing the fractional loss in effective adsorption coefficient to previous hosts for each new virus strain added to the arms race
VIRUS PROPERTIES	
$\delta_V$	Specific loss rate virus
<i>m</i>	Burst size virus
PHYSICAL, CHEMICAL, AND BIOLOGICAL PARAMETERS DEFINING THE ENVIRONMENT AND THE FOOD WEB EFFECTS	
<i>D</i>	Chemostat dilution rate
<i>S<sub>R</sub></i>	Concentration of limiting element in the chemostat reservoir
<i>S<sub>C</sub></i>	Concentration of limiting substrate in the culture
<i>A</i>	Population size autotrophic flagellates
<i>C</i>	Population size ciliates
<i>H</i>	Population size heterotrophic flagellates
$\alpha_A$	Affinity for uptake of limiting nutrient, autotrophic flagellates
$\alpha_C$	Clearance rate for ciliate grazing on flagellates
$\alpha_H$	Clearance rate for heterotrophic flagellates grazing on bacteria
$\delta_B$	Non-viral bacterial loss rate
<i>Y<sub>H</sub></i>	Yield of heterotrophic flagellates on bacterial prey

therefore compensate for both dilution and viral loss and can therefore remain in the culture at a low, virus-controlled, density in coexistence with the now abundant, resource-controlled, immune mutant. The abundant mutant population represents a resource exploitable for a mutant of the virus. Establishment of such a mutant virus gives a new situation with two low-abundant host strains and high *S<sub>C</sub>*, again representing a resource for a new host mutant, and so on. This evolutionary sequence is thus characterized by a “remaining resource” that alternates in form between free limiting nutrients facilitating a successful mutation in the host, and an immune host strain facilitating successful mutation in the virus. This is a model of the “Red Queen” dynamics observed in chemostat experiments of this type (Little, 2002; Martiny et al., 2014). Importantly, the remaining free resource is diminishing for each turn of the arms race until the final resistant host strain has a population size too small to carry a new virus mutant. In a more generalized analysis, Härter et al. (2014)

describe such maturation processes as “narrowing staircase(s) of coexistence.” Since the size of the “free resource” would affect the probability that a random mutation is successful, this could explain why antagonistic evolution is fast, but would also suggest that the rate diminishes as the process approaches maturation. The mature state in this arms race model is characterized by many virus-susceptible strains, while the initial stages are dominated by a resistant strain and have a small virus population. Interestingly, these are the two situations forming what has been termed Weinbauer’s Paradox (Weinbauer, 2004), where the question is why the few virus—many resistant hosts situation is observed when trying to construct simple host-virus systems in the laboratory, while natural systems are characterized by high viral numbers and many susceptible hosts. In the arms race model above, this apparent paradox is explained simply as the differences between an early and a late stage in the maturation process of strain diversification (Thingstad et al., 2014). How long time is needed for

such strain diversifications to mature, and to what extent the speed of the arms race diminishes with the decrease in remaining resource, remain as open questions.

In their analysis of phage-bacteria infection networks, Weitz et al. (2013) defined four basic types: random, one-to-one, nested, and modular. The arms race model outlined for the chemostat example above leads to the nested type with communities that are connected as illustrated in **Figure 1E**, corresponding to an upper-triangular interaction matrix (Weitz et al., 2013; Thingstad et al., 2014). Such upper-triangular interaction matrices have been found in analysis of published host-virus networks (Flores et al., 2011; Beckett and Williams, 2013), providing some evidence that the highly idealized chemostat analysis used here may bear some relevance to natural systems. The validity of such an extrapolation to natural systems is not self-evident since each species does not evolve independently in a complex community: There, the free resource will be available to all competing species and a high-abundant immune host strain would be available to mutants from many different viruses, opening for models that could lead to more complex structures. With the assumption that no viruses infect hosts belonging to more than one species, the interaction matrix for the community will consist of upper-triangular sub-matrices, one for each species, arranged along the diagonal (Thingstad et al., 2014), very similar to the modularity found in an existing dataset (Beckett and Williams, 2013). The potentially more complex interactions of multispecies communities would be represented by non-zero elements in the void spaces of such a community interaction matrix. A search for the consequences of such complications would require a systematic approach to how to fill in these void spaces and has not been attempted here.

## How Is Microbial Community Composition Determined?

### The Richness Component

In the chemostat example discussed above, the mechanism generating strain richness in the mature community can be visualized by the set of growth curves for the strains shown in **Figure 2A**, where a cost of resistance (COR) is assumed in the form of a reduction in maximum growth rate for each successive mutation. The community will consist of all strains for which  $\mu_i(S_C) \geq D$  where  $D$  and  $S_C$  are represented by the horizontal and the vertical lines in **Figure 2A**, respectively. As discussed above, the culture concentration  $S_C$  will increase as the arms race proceeds, illustrated by a shifting of the vertical line in **Figure 2A** one step to the right for each turn of the arms race, adding subsequently less competitive strains to the established host community. This will continue until either (1) the COR has become too large for a new mutant to compensate for dilution, or (2) the community size reaches the carrying capacity defined by the reservoir concentration  $S_R$ . In this chemostat model, viral loss is the only mechanism compensating for growth that exceeds dilution loss. The amount of viruses in the mature situation is thus the amount needed to give each strain  $i$  a loss rate by viral lysis equal to  $\mu_i(S_C) - D$ .

The main viral loss is thus associated with the fastest growing strains, which, as we will see later, are not the same as the dominant strains.

This graphical representation is easily extrapolated to a multi-species situation with grazing control of community size. This is illustrated for a 3-species case in **Figure 2B**, where the horizontal line now represents a non-selective grazing loss.

Application of the KtW principle at the food web level allows for models that contain a shift between mineral nutrient limited and carbon limited growth of the heterotrophic prokaryotes (Thingstad and Pengerud, 1985). The nature of the limiting element represented on the x-axis of **Figure 2B** may therefore change with the environmental conditions with at least organic carbon, nitrogen, phosphorous and iron as expected possibilities. If trade-offs at the species level are mainly between the three parameters defining the topology of **Figure 2B** ( $\mu^{max}$ ,  $\alpha$ , and  $\nu$ ) one could conceive a situation where the topology of **Figure 2B**, and therefore the community structure, is invariant to such qualitative shifts in limitation. If, however, there is trade-off between specializations so that e.g., a good competitor under C-limitation is a poor competitor under P-limitation, the growth curves would reshuffle as the type of limitation changes, thereby inducing shifts in species/strain composition.

### The Evenness Component

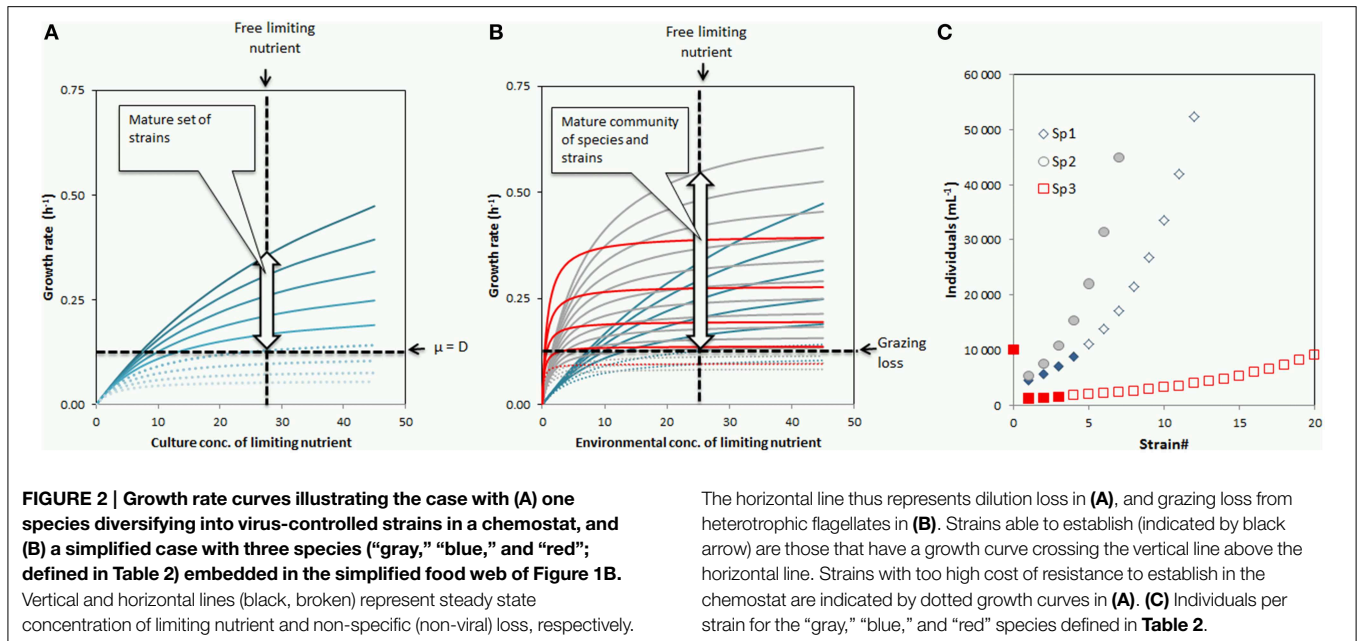
**Figure 2B** does not provide an answer to the evenness aspect of strain diversity since it does not constrain the abundance of individuals within each established strain. This abundance is controlled by the virus host-interactions, i.e., by the structure of the interaction matrix. For the nested structure in **Figure 1E**, the abundance of the undefended parent strain of species  $x$  is given as Thingstad et al. (2014):

$${}_xH_0 = \frac{\delta_V + D}{(m - 1)\beta}. \quad (1a)$$

While abundance of subsequent mutant strains are given by:

$${}_xH_i = {}_xH_0 \frac{1 - \sigma\rho}{\rho^i}, \quad i \geq 1. \quad (1b)$$

Equation 1a arises from the equilibrium condition for the first virus which only can infect the parent strain. Abundance of the parent strain thus depends on the decay rate of the virus ( $\delta_V$ ), the burst size ( $m$ ), and the effective adsorption rate ( $\beta$ ) between the undefended parent strain and the original virus. For the subsequent strains, this is modified by the two factors  $\rho$ , that represents a fractional loss in  $\beta$  for each new host mutant, and  $\sigma$  which represents a fractional loss in infectivity for previous hosts for each mutational step in the virus. The model thus contains mechanism where there is a cost in the form of reduced infectivity for viruses having a broad host range (Symbols summarized in **Table 1**, see Thingstad et al., 2014 for further details). Abundance within strains is thus related to the species' defensive properties, in particular the parameter  $0 < \rho < 1$ , where values of  $\rho \ll 1$  give a very rapid increase in strain size for large  $i$  (Equation 1b). Since all the parameters  $\beta$ ,  $m$ ,  $\delta_V$ ,  $\rho$ , and  $\sigma$  may vary between host species and between viruses, both the abundance of



the parent host strain (Equation 1a) and the modification of this with subsequent strains (Equation 1b) will vary between species. The set of parameters defining a species can thus be divided into two sets: one ( $\alpha$ ,  $\mu^{max}$ , and  $v$ , see Table 1) that describes the species' competitive properties and determining how many strains it can establish, and another ( $\beta$ ,  $\rho$ , and  $\sigma$ ) that defines its defensive properties and, together with the properties of its virus ( $m$ ,  $\delta_V$ ), determines the abundance within strains. Since abundance at species level is the sum over established strains, this will depend on both the competitive and the defensive properties of the species.

Such a combination of high competitive with high defensive abilities requires a low trade-off between the two. With this insight, the question of SAR11 abundance should probably not be focused on whether this is a competition or a defense strategist, but rather whether there is something particular in the lifestyle of this organism that leads to a low trade-off between the two traits (Thingstad et al., 2014). This leads to the intriguing question of whether there is any link between the minimalistic genome design of SAR11 (Giovannoni et al., 2013, 2014) and the potential for a low trade-off between competition and defense. The answer to this is not immediately obvious from the analysis done here.

In the arms race scenario above, a host mutant needs to develop resistance to a virus community that already has co-evolved with the established host community, and it has to do so without losing too much in competitive ability. This could seem like a comparably more difficult task than the "rabbits in Australia" analogy with invasion of a foreign species not recognized by the established virus community and therefore initially not necessarily handicapped by high COR. Although viral attack on invading organisms has been demonstrated experimentally (Sano et al., 2004), such mature communities could thus theoretically seem prone to invasion. Including invasion in the models would create a new maturation process where species richness increases at a rate driven by a combination of the invasion rate and the

distribution of competitive abilities within the seeding community. The result would be an interaction between processes occurring at, at least, five characteristic time scales: the population dynamics (linked to the  $\mu$  and  $\delta$  functions), the time scale of the host-virus arms races driving strain diversification, the time scale of the species invasion process, and the time scale of environmental disturbances disrupting these maturation processes. On top of this comes the presumably longer time scale of evolution of new species, changing the properties of the seeding community. An important question is whether there is a theoretical balance between these processes, leading to a steady state combination of species and strains somewhere between the two extremes of (1) a single species with many strains on one side and (2) many species, each with only one strain, on the other. The problem is easiest to illustrate in the chemostat example (Figure 2A) where the position of the horizontal line is fixed by the value of  $D$ . As discussed above, the maturation in strain diversification that establishes new defense specialists will drive the vertical line representing  $S$  to the right. A successful invasion (or evolution) of a new species will establish a new competition strategist competing better than the last established strain in the existing community. This would exchange previously established strains with low competitive ability (high COR) for a strain from the more competitive newcomer, and thereby drive the vertical line to the left. With species and strain diversification introducing new competition and new defense strategists as assumed here, one therefore gets two opposing processes, suggesting that there is a theoretical balancing point, and therefore a theoretical steady state somewhere between the two extremes outlined above.

This gets a bit more complicated in Figure 2B where the position of the horizontal line is a dynamic variable coupled to grazing loss. Using the simple food web model in Figure 1B, the state with mineral nutrient limited bacteria is, however, still relatively transparent: Assuming steady state in the mineral nutrients (S)—autotrophic flagellates (A)—ciliates (C)—food chain, the

**TABLE 2 | Numerical values used to draw the growth curves and the abundance per strain for the three species in Figures 2B,C.**

	Competitive traits			Defensive traits			Trade-off index	Species abundance mL <sup>-1</sup>	% of community abundance
	$\alpha$ nM-P <sup>-1</sup> h <sup>-1</sup>	$\mu^{max}$ h <sup>-1</sup>	$\nu$	$H_0$ mL <sup>-1</sup>	$\sigma$	$\rho$			
Sp#1 <<blue>>	0.2	1	0.7	1 10 <sup>4</sup>	0.8	0.8	1.5	3.6 10 <sup>4</sup>	10
Sp#2 <<gray>>	0.1	0.7	0.85	1 10 <sup>4</sup>	0.9	0.7	0.35	3.0 10 <sup>5</sup>	86
Sp#3 <<red>>	0.5	0.4	0.7	1 10 <sup>4</sup>	0.99	0.9	1.2	1.4 10 <sup>4</sup>	4
Community abundance:								3.5 10 <sup>5</sup>	

Trade-off index calculated as described in Thingstad et al. (2014).

autotrophic flagellates must grow as fast as they are grazed. With the simplifying assumption that food intake is proportional to food concentration, the growth = loss condition for autotrophic flagellates becomes  $\alpha_A SA = \alpha_C AC$ , or:

$$S = \frac{\alpha_C}{\alpha_A} C. \tag{2a}$$

The position of the vertical line (S) is therefore now constrained by ciliate abundance (C) and not directly controlled by introduction of new species or strains as in the chemostat example above. Instead, it is now the position of the horizontal line that becomes a function of strains and species diversity. Using a similar steady state argument for heterotrophic flagellates, the size of the bacterial community becomes proportional to ciliate abundance:

$$B = \frac{\alpha_C}{Y_H \alpha_H} C. \tag{2b}$$

in a non-mature community, the strain diversification process will thus fill the community with successively less competitive strains, thereby driving the horizontal line downwards until the community size given by Equation (2b) is reached. A new species, sufficiently competitive to invade and initially without viral loss, will outcompete existing strains and thereby drive the horizontal line upwards. Since the horizontal line represents the bacterial loss rate to grazing:

$$\delta_B = \alpha_H H, \tag{2c}$$

its position reflects the amount (H) of bacterial grazers. The strain diversification process thus drives the system toward a smaller population of heterotrophic flagellates and reduced food chain efficiency, thus favoring the viral shunt of bacterial production back to dissolved material. The invasion (or mutation) of new, more competitive species drives the system in the other direction toward less viruses, a smaller virus-bacteria ratio and a more efficient food chain. As the two diversification processes drive the system in opposite directions, this raises the question of whether there is an equilibrium point where the two processes balance?

Equations (2b) and (2c) link the abundance of heterotrophic flagellates (H) to the abundance of ciliates (C), through the internal population structure of the bacterial community. Stated differently, they suggest a theory where the internal diversity of the bacterial community and the structure of the predator food chain are intimately connected. The analysis above thus suggests

a mechanistic basis for a biodiversity—ecosystem functioning (BEF) theory for the pelagic microbial community. It is noteworthy that these relationships were derived without any assumption of host diversity being linked to substrate specialization in the hosts, and are therefore quite different from arguments where a high biodiversity is needed to perform a large set of required biochemical reactions. The food web framework used for this analysis (Figure 1B) may appear unrealistically simple, but its ability to capture essential aspects of mesocosm perturbation experiments recently been demonstrated (Larsen et al., 2015). This includes the demonstration of a central controlling role for ciliates as assumed in the arguments for Equations (2b) and (2c).

The fundamental set of trophic interactions driving the arms races discussed here is summarized in the idealized structure of the KtW principle (Figure 1A). With this basic mechanism being the same at the predator-prey as at the host-parasite level, similar lines of argument can be applied for food web evolution as those used in the above discussion of community composition. The difference in time scale is, however, vast: Whereas the modern pelagic food web can be seen as the present (mature?) state of a 3.5 10<sup>9</sup> year old arms race with a characteristic time scale in the order of 0.5 10<sup>9</sup> years (Thingstad et al., 2010) between major new inventions in weapon technology; Red Queen dynamics of prokaryote hosts and viruses seem to occur more over time scale of days to weeks (Martiny et al., 2014).

In such a geological perspective, there may have been strong couplings between these arms races and the global climate systems as for example the rapid evolution of eukaryotic forms in the Neoproterozoic has been suggested to affect the biological pump and therefore may have been a driving force for rather than a response to extreme climatic fluctuations in this period (Lenton et al., 2014).

## How Is the Physiological State of Microbes Affected by the Environment and Other Microbes?

The viral top-down control in this model does not only allow competitively inferior microbes to become members of the ecosystem, it rather suggests that the prokaryote community should be dominated by slow-growing, high-defensive strains. This opens for a possible “sieged city” re-interpretation of the old “dormant or dead” (Zweifel and Hagstrom, 1995; Jones and Lennon, 2010) debate in marine microbiology: The dominance of low-active cells found in aquatic environments is perhaps not

a sign of starvation caused by a lack of suitable substrates in their environment; it may be more because they have “shut the gates to keep the enemy out.”

## How Do (Apparently) Inferior Microbes Persist in the Ecosystem?

The KtW structure (Figure 1A) was originally designed to provide an answer to this question at the food web level, where the discovery of systems with apparent persistent phosphorus-limitation of bacteria (Pengerud et al., 1987; Vadstein et al., 1988; Cotner et al., 1997) raised the question of why their supposedly inferior phytoplankton competitors were not outcompeted to a level where bacteria would become C-limited. The same basic theory has also been applied to the fish-jellyfish dichotomy at higher levels in the pelagic food chain (Haraldsson et al., 2012). It is also a basic mechanism in size-structured plankton models where the intense grazing and rapid response of flagellates explains the (relatively) constant  $10^6 \text{ mL}^{-1}$  abundance of prokaryotes as predator (top-down) control (Azam et al., 1983). Adding nutrients to the system allows large-celled phytoplankton species to establish that are less competitive but also less grazed (resource controlled). Such models thus produce a gradient from small-celled, top-down controlled, “competition strategist” species dominating in oligotrophic regions to large-celled, resource controlled, “defense strategist” phytoplankton dominating nutrient rich upwelling areas (e.g., Ward et al., 2012). As a principle recognizable at many (all?) trophic levels, the KtW structure of Figure 1A generates self-similarity in pelagic ecosystems (Thingstad et al., 2010). This provides at least an analogy to fractal systems where complexity can be generated through the repetition of a simple, scale-independent, rule (Mandelbrot, 1982).

## How Are Microbes Distributed in Their Ecosystems?

The models discussed above use the simplifying assumptions of a stable steady-state in an environment homogenous in time and space. This is an approximation that should be treated with caution since it means that some important aspects of host-virus interactions are lost. There are at least two relevant examples of microbial competitive and defensive behavior that seem to work only if an evolutionary adaptation to micro scale patchiness in aquatic environments is invoked: motility and altruistic suicide.

Motility is usually argued to have little effect on bacterial nutrient acquisition in homogenous environments because of the high efficiency of molecular diffusion at the  $1 \mu\text{m}$ -scale (Jumars et al., 1993). Motility is thus believed only to be of any advantage in patchy environments. Since the diffusivity of viruses is about 2 orders of magnitude lower ( $0.2\text{--}3.10^{-7} \text{ cm}^2\text{s}^{-1}$ ) (Murray and Jackson, 1992) than that of small nutrient molecules ( $\sim 10^{-5} \text{ cm}^2\text{s}^{-1}$ ), one can turn this around to argue that the collision frequency with viruses should increase significantly with motility. One should thus expect to find motile bacteria only in patchy environments (Blackburn et al., 1997). One can speculate whether this means that the fraction of motile bacteria may be

used as a proxy for environmental patchiness, and also whether this is linked to the COR since the foraging gain from swimming must outweigh the COR associated with the increased defense needed by motile hosts.

A somewhat similar argument is linked to the enigma of altruistic suicide, where some species induce apoptosis when infected (Ackermann et al., 2008; Blower et al., 2012). If this kills the host before new viruses are released, it would protect the neighbors from infection. From an evolutionary perspective, this poses the problem that altruistic suicide may not seem like an evolutionary stable strategy since the genes of the altruist are obviously not passed on to any offspring. If, however, the neighbors are close relatives, the patch becomes a kind of super-organism consisting of cells having the same genes, and altruistic suicide becomes evolutionarily stable (Smith et al., 2010), as has also been shown experimentally (Berngruber et al., 2013). With lytic events creating centers of release for both viruses and DOM, viral lysis is in itself a patchiness-generating mechanism with an interesting geometry consisting of two concentric spheres of food and danger expanding at different rates.

## Concluding Comments

The consequences of applying the KtW principles at strain rather than species level are both practical and conceptual. The practical part is that the models then no longer constrain species diversity in the same manner as in the case of pure top-down control of species size, with direct consequences for model comparison with e.g., 16S rRNA gene sequence data. A main conceptual consequence, at least in the model of Thingstad et al. (2014), is the separation of the two aspects of abundance control: The number of strains being controlled by the competitive properties of the host, and the number of individuals per strain by the host's defensive abilities and the host-virus interactions. This separation may seem like a relatively robust feature transferable to models with more complicated interaction matrices. The structure of the interaction matrix would then primarily affect the abundance within strains feature of the system.

The Thingstad et al. (2014) model also involves a seeding community. While this can be approached from a descriptive side with a laborious description of the competitive and defensive properties of “all” existing host species; the intriguing challenge is to try to understand the trade-offs between traits in this population. One can visualize this problem in an n-dimensional strategy space formed by the n relevant life-history traits of hosts and viruses. Trade-offs represent correlations in this n-dimensional space and would confine the subset of feasible strategies. With a slight rephrasing of Baas Becking and Beijerinck's famous statement (de Wit and Bouvier, 2006), this would give models where “The feasible is everywhere, the environment selects.”

## Acknowledgments

This work was financed by the European Union FP7 through the European Research Council Advanced Grant 250254 Microbial Network Organisation (MINOS), and by the Department of Biology, University of Bergen.

## References

- Ackermann, M., Stecher, B., Freed, N. E., Songhet, P., Hardt, W.-D., and Doebeli, M. (2008). Self-destructive cooperation mediated by phenotypic noise. *Nature* 454, 987–990. doi: 10.1038/nature07067
- Avrani, S., Wurtzel, O., Sharon, I., Sorek, R., and Lindell, D. (2011). Genomic island variability facilitates *Prochlorococcus*-virus coexistence. *Nature* 474, 604–608. doi: 10.1038/nature10172
- Azam, F., Fenichel, T., Field, J. G., Gray, J. S., Meyer-Reil, L. A., and Thingstad, T. F. (1983). The ecological role of water-column microbes in the sea. *Mar. Ecol. Prog. Ser.* 10, 257–263. doi: 10.3354/meps010257
- Beckett, S. J., and Williams, H. T. P. (2013). Coevolutionary diversification creates nested-modular structure in phage-bacteria interaction networks. *Interface Focus* 3:20130033. doi: 10.1098/rsfs.2013.0033
- Benincà, E., Huisman, J., Heerkloss, R., Johnk, K. D., Branco, P., Van Nes, E. H., et al. (2008). Chaos in a long-term experiment with a plankton community. *Nature* 451, 822–827. doi: 10.1038/nature06512
- Berngruber, T. W., Lion, S., and Gandon, S. (2013). Evolution of suicide as a defence strategy against pathogens in a spatially structured environment. *Ecol. Lett.* 16, 446–453. doi: 10.1111/ele.12064
- Blackburn, N., Azam, F., and Hagstrom, A. (1997). Spatially explicit simulations of a microbial food web. *Limnol. Oceanogr.* 42, 613–622. doi: 10.4319/lo.1997.42.4.0613
- Blower, T. R., Evans, T. J., Przybilski, R., Fineran, P. C., and Salmond, G. P. C. (2012). Viral evasion of a bacterial suicide system by RNA-based molecular mimicry enables infectious altruism. *PLoS Genet.* 8:e1003023. doi: 10.1371/journal.pgen.1003023
- Bohannan, B. J. M., and Lenski, R. E. (1997). Effect of resource enrichment on a chemostat community of bacteria and bacteriophage. *Ecology* 78, 2303–2315. doi: 10.1890/0012-9658(1997)078[2303:EOEOA]2.0.CO;2
- Bohannan, B. J. M., and Lenski, R. E. (2000). The relative importance of competition and predation varies with productivity in a model community. *Am. Nat.* 156, 329–340. doi: 10.1086/303393
- Connell, J. H. (1979). Intermediate-disturbance hypothesis. *Science* 204, 1345–1345. doi: 10.1126/science.204.4399.1345
- Cotner, J. B., Ammerman, J. W., Peele, E. R., and Bentzen, E. (1997). Phosphorus-limited bacterioplankton growth in the Sargasso Sea. *Aquat. Microb. Ecol.* 13, 141–149. doi: 10.3354/ame013141
- de Wit, R., and Bouvier, T. (2006). 'Everything is everywhere, but, the environment selects'; what did Baas Becking and Beijerinck really say? *Environ. Microbiol.* 8, 755–758. doi: 10.1111/j.1462-2920.2006.01017.x
- Dini-Andreote, F., de Cássia Pereira e Silva, M., Triado-Margarit, X., Casamayor, E. O., van Elsas, J. D., and Salles, J. F. (2014). Dynamics of bacterial community succession in a salt marsh chronosequence: evidences for temporal niche partitioning. *ISME J.* 8, 1989–2001. doi: 10.1038/ismej.2014.54
- Flores, C. O., Meyer, J. R., Valverde, S., Farr, L., and Weitz, J. S. (2011). Statistical structure of host-phage interactions. *Proc. Natl. Acad. Sci. U.S.A.* 108, E288–E297. doi: 10.1073/pnas.1101595108
- Fraser, C., Alm, E. J., Polz, M. F., Spratt, B. G., and Hanage, W. P. (2009). The bacterial species challenge: making sense of genetic and ecological diversity. *Science* 323, 741–746. doi: 10.1126/science.1159388
- Giovannoni, S., Temperton, B., and Zhao, Y. (2013). SAR11 viruses and defensive host strains reply. *Nature* 499, E4–E5. doi: 10.1038/nature12388
- Giovannoni, S. J., Thrash, J. C., and Temperton, B. (2014). Implications of streamlining theory for microbial ecology. *ISME J.* 8, 1553–1565. doi: 10.1038/ismej.2014.60
- Haraldsson, M., Tonnesson, K., Tiselius, P., Thingstad, T. F., and Aksnes, D. L. (2012). Relationship between fish and jellyfish as a function of eutrophication and water clarity. *Mar. Ecol. Prog. Ser.* 471, 73–85. doi: 10.3354/meps10036
- Härter, J. O., Mitarai, N., and Sneppen, K. (2014). Phage and bacteria support mutual diversity in a narrowing staircase of coexistence. *ISME J.* 8, 2317–2326. doi: 10.1038/ismej.2014.80
- Hutchinson, G. E. (1961). The paradox of the plankton. *Am. Nat.* 95, 137–145. doi: 10.1086/282171
- Jankowski, K., Schindler, D. E., and Horner-Devine, M. C. (2014). Resource availability and spatial heterogeneity control bacterial community response to nutrient enrichment in lakes. *PLoS ONE* 9:e8699. doi: 10.1371/journal.pone.0086991
- Jones, S. E., and Lennon, J. T. (2010). Dormancy contributes to the maintenance of microbial diversity. *Proc. Natl. Acad. Sci. U.S.A.* 107, 5881–5886. doi: 10.1073/pnas.0912765107
- Jover, L. F., Cortez, M. H., and Weitz, J. S. (2013). Mechanisms of multi-strain coexistence in host-phage systems with nested infection networks. *J. Theor. Biol.* 332, 65–77. doi: 10.1016/j.jtbi.2013.04.011
- Jumars, P., Deming, J., Hill, P., Karp-Boss, L., Yager, P., and Dade, W. (1993). Physical constraints on marine osmotrophy in an optimal foraging context. *Mar. Microb. Food Webs* 7, 121–159.
- Larsen, A., Egge, J. K., Nejtgaard, J. C., Di Capua, I., Thyrrhaug, R., Bratbak, G., et al. (2015). Contrasting response to nutrient manipulation in Arctic mesocosms are reproduced by a minimum microbial food web model. *Limnol. Oceanogr.* 60, 360–374. doi: 10.1002/lno.10025
- Lenton, T. M., Boyle, R. A., Poulton, S. W., Shields-Zhou, G. A., and Butterfield, N. J. (2014). Co-evolution of eukaryotes and ocean oxygenation in the Neoproterozoic era. *Nat. Geosci.* 7, 257–265. doi: 10.1038/ngeo2108
- Little, T. J. (2002). The evolutionary significance of parasitism: do parasite-driven genetic dynamics occur *ex silico*? *J. Evol. Biol.* 15, 1–9. doi: 10.1046/j.1420-9101.2002.00366.x
- Mandelbrot, B. B. (1982). *The Fractal Geometry of Nature*. New York, NY: W.H. Freeman and Company.
- Marston, M. F., Pierciey, F. J. Jr., Shepard, A., Gearin, G., Qi, J., Yandava, C., et al. (2012). Rapid diversification of coevolving marine *Synechococcus* and a virus. *Proc. Natl. Acad. Sci. U.S.A.* 109, 4544–4549. doi: 10.1073/pnas.1120310109
- Martiny, J. B. H., Riemann, L., Marston, M. F., and Middelboe, M. (2014). Antagonistic coevolution of marine planktonic viruses and their hosts. *Ann. Rev. Mar. Sci.* 6, 393–414. doi: 10.1146/annurev-marine-010213-135108
- Middelboe, M., Holmfeldt, K., Riemann, L., Nybroe, O., and Haaber, J. (2009). Bacteriophages drive strain diversification in a marine Flavobacterium: implications for phage resistance and physiological properties. *Environ. Microbiol.* 11, 1971–1982. doi: 10.1111/j.1462-2920.2009.01920.x
- Murray, A. G., and Jackson, G. A. (1992). Viral dynamics - A model of the effects of size, shape, motion and abundance of single-celled planktonic organisms and other particles. *Mar. Ecol. Prog. Ser.* 89, 103–116. doi: 10.3354/meps089103
- Pengerud, B., Skjoldal, E. F., and Thingstad, T. F. (1987). The reciprocal interaction between degradation of glucose and ecosystem structure - studies in mixed chemostat cultures of marine bacteria, algae, and bacterivorous nanoflagellates. *Mar. Ecol. Prog. Ser.* 35, 111–117. doi: 10.3354/meps035111
- Sano, E., Carlson, S., Wegley, L., and Rohwer, F. (2004). Movement of viruses between biomes. *Appl. Environ. Microbiol.* 70, 5842–5846. doi: 10.1128/AEM.70.10.5842-5846.2004
- Smith, J., Van Dyken, J. D., and Zee, P. C. (2010). A generalization of Hamilton's rule for the evolution of microbial cooperation. *Science* 328, 1700–1703. doi: 10.1126/science.1189675
- Staley, C., Gould, T. J., Wang, P., Phillips, J., Cotner, J. B., and Sadowsky, M. J. (2014). Bacterial community structure is indicative of chemical inputs in the Upper Mississippi River. *Front. Microbiol.* 5:524. doi: 10.3389/fmicb.2014.00524
- Thingstad, T. F. (2000). Elements of a theory for the mechanisms controlling abundance, diversity, and biogeochemical role of lytic bacterial viruses in aquatic systems. *Limnol. Oceanogr.* 45, 1320–1328. doi: 10.4319/lo.2000.45.6.1320
- Thingstad, T. F., and Lignell, R. (1997). Theoretical models for the control of bacterial growth rate, abundance, diversity and carbon demand. *Aquat. Microb. Ecol.* 13, 19–27. doi: 10.3354/ame013019
- Thingstad, T. F., and Pengerud, B. (1985). Fate and effect of allochthonous organic material in aquatic microbial ecosystems - an analysis based on chemostat theory. *Mar. Ecol. Prog. Ser.* 21, 47–62. doi: 10.3354/meps021047
- Thingstad, T. F., Strand, E., and Larsen, A. (2010). Stepwise building of plankton functional type (PFT) models: a feasible route to complex models? *Prog. Oceanogr.* 84, 6–15. doi: 10.1016/j.pocean.2009.09.001
- Thingstad, T. F., Våge, S., Storesund, J. E., Sandaa, R.-A., and Giske, J. (2014). A theoretical analysis of how strain-specific viruses can control microbial species diversity. *Proc. Natl. Acad. Sci. U.S.A.* 111, 7813–7818. doi: 10.1073/pnas.1400909111
- Tilman, D. (1977). Resource competition between planktonic algae - Experimental and theoretical approach. *Ecology* 58, 338–348. doi: 10.2307/1935608
- Uksa, M., Fischer, D., Welzl, G., Kautz, T., Koepke, U., and Schlöter, M. (2014). Community structure of prokaryotes and their functional potential in subsoils

- is more affected by spatial heterogeneity than by temporal variations. *Soil Biol. Biochem.* 75, 197–201. doi: 10.1016/j.soilbio.2014.04.018
- Vadstein, O., Jensen, A., Olsen, Y., and Reinertsen, H. (1988). Growth and phosphorus status of limnetic phytoplankton and bacteria. *Limnol. Oceanogr.* 33, 489–503. doi: 10.4319/lo.1988.33.4.0489
- Våge, S., Storesund, J. E., and Thingstad, T. F. (2013). SAR11 viruses and defensive host strains. *Nature* 499, E3–E4. doi: 10.1038/nature12387
- Venter, J. C., Remington, K., Heidelberg, J. F., Halpern, A. L., Rusch, D., Eisen, J. A., et al. (2004). Environmental genome shotgun sequencing of the Sargasso Sea. *Science* 304, 66–74. doi: 10.1126/science.1093857
- Ward, B. A., Dutkiewicz, S., Jahn, O., and Follows, M. J. (2012). A size-structured food-web model for the global ocean. *Limnol. Oceanogr.* 57, 1877–1891. doi: 10.4319/lo.2012.57.6.1877
- Weinbauer, M. G. (2004). Ecology of prokaryotic viruses. *FEMS. Microbiol. Ecol.* 28, 127–181. doi: 10.1016/j.femsre.2003.08.001
- Weitz, J. S., Poisot, T., Meyer, J. R., Flores, C. O., Valverde, S., Sullivan, M. B., et al. (2013). Phage-bacteria infection networks. *Trends Microbiol.* 21, 82–91. doi: 10.1016/j.tim.2012.11.003
- Winter, C., Bouvier, T., Weinbauer, M. G., and Thingstad, T. F. (2010). Trade-Offs between competition and defense specialists among unicellular planktonic organisms: the “killing the winner” hypothesis revisited. *Microbiol. Mol. Biol. Rev.* 74, 42–57. doi: 10.1128/MMBR.00034-09
- Zhao, Y., Temperton, B., Thrash, J. C., Schwalbach, M. S., Vergin, K. L., Landry, Z. C., et al. (2013). Abundant SAR11 viruses in the ocean. *Nature* 494, 357–360. doi: 10.1038/nature11921
- Zweifel, U. L., and Hagstrom, A. (1995). Total counts of marine bacteria include a large fraction of non-nucleoid-containing bacteria (ghosts). *Appl. Environ. Microbiol.* 61, 2180–2185.

**Conflict of Interest Statement:** The authors declare that the research was conducted in the absence of any commercial or financial relationships that could be construed as a potential conflict of interest.

Copyright © 2015 Thingstad, Pree, Giske and Våge. This is an open-access article distributed under the terms of the Creative Commons Attribution License (CC BY). The use, distribution or reproduction in other forums is permitted, provided the original author(s) or licensor are credited and that the original publication in this journal is cited, in accordance with accepted academic practice. No use, distribution or reproduction is permitted which does not comply with these terms.



# A Generalized Spatial Measure for Resilience of Microbial Systems

Ryan S. Renslow<sup>1</sup>, Stephen R. Lindemann<sup>2</sup> and Hyun-Seob Song<sup>2\*</sup>

<sup>1</sup> Environmental Molecular Sciences Laboratory, Pacific Northwest National Laboratory, Richland, WA, USA, <sup>2</sup> Biological Sciences Division, Earth and Biological Sciences Directorate, Pacific Northwest National Laboratory, Richland, WA, USA

The emergent property of resilience is the ability of a system to return to an original state after a disturbance. Resilience may be used as an early warning system for significant or irreversible community transition; that is, a community with diminishing or low resilience may be close to catastrophic shift in function or an irreversible collapse. Typically, resilience is quantified using recovery time, which may be difficult or impossible to directly measure in microbial systems. A recent study in the literature showed that under certain conditions, a set of spatial-based metrics termed *recovery length*, can be correlated to recovery time, and thus may be a reasonable alternative measure of resilience. However, this spatial metric of resilience is limited to use for step-change perturbations. Building upon the concept of recovery length, we propose a more general form of the spatial metric of resilience that can be applied to any shape of perturbation profiles (for example, either sharp or smooth gradients). We termed this new spatial measure “perturbation-adjusted spatial metric of resilience” (PASMORE). We demonstrate the applicability of the proposed metric using a mathematical model of a microbial mat.

**Keywords:** resilience, microbial communities, recovery, ecology, emergent properties

## INTRODUCTION

Complex networks of interacting components produce outcomes that cannot be easily predicted, even when the state of the network components and the inputs to the network are known. These difficult-to-determine outcomes have come to be known as emergent phenomena or higher-order properties, which emerge from the functioning of the whole network, rather than as a simple sum of the individual states of the parts (De La Fuente et al., 2008; Schubert, 2014). Emergent properties arise in complex networks that impact our lives, such as in the communities of microbes and higher organisms that compose ecosystems (Tilman et al., 2001), social networks (Lusseau, 2003; Mitrovic and Tadic, 2010), military-political structures (Porter et al., 2005), commercial systems (Carey and Carville, 2003; Cimellaro et al., 2010), and climate and weather systems (Higgins et al., 2002; Easterling and Kok, 2003). Consequently, developing the ability to understand and predict emergent properties from complex networks is of great importance.

Microorganisms are commonly found physically associated with one another in spatially structured communities such as biofilms or microbial mats (Curtis and Sloan, 2004; Wagner et al., 2006; Fuhrman, 2009; Robinson et al., 2010; Renslow et al., 2011). These communities may range from monocultures to highly diverse assemblages of species; however, in either case, individual members operate and interact in ways governed by their individual functional

## OPEN ACCESS

### Edited by:

Hiroyuki Futamata,  
Shizuoka University, Japan

### Reviewed by:

Steven Singer,  
Lawrence Berkeley National  
Laboratory, USA  
Yoshiteru Aoi,  
Hiroshima University, Japan

### \*Correspondence:

Hyun-Seob Song  
hyunseob.song@pnnl.gov

### Specialty section:

This article was submitted to  
Systems Microbiology,  
a section of the journal  
Frontiers in Microbiology

**Received:** 31 August 2015

**Accepted:** 18 March 2016

**Published:** 07 April 2016

### Citation:

Renslow RS, Lindemann SR  
and Song H-S (2016) A Generalized  
Spatial Measure for Resilience  
of Microbial Systems.  
Front. Microbiol. 7:443.  
doi: 10.3389/fmicb.2016.00443

responses and local microenvironmental conditions (Schramm et al., 1996; Hibiya et al., 2003; Bernstein et al., 2013, 2014). Formation of a biofilm matrix composed of extracellular polymeric substances confers significant fitness advantages on the microbes it shelters, including physical protection, such as from predation or shearing forces, reduction of environmental stresses, such as from rapid changes in environmental conditions or exposure to antibiotics, facilitation of beneficial interspecies relationships, and rapid exchange of genetic material (Flemming and Wingender, 2001; Lapidou and Rittmann, 2002; Czarczyk and Myszk, 2007; Cao et al., 2011). It is likely that emergent properties arise from the spatial organization of microbes, forming microenvironments and promoting interconnectedness of a multi-species metabolic network through resource exchange and intercellular communication (Xavier and Foster, 2007; Konopka, 2009; Wintermute and Silver, 2010).

Resilience is a higher-order property in microbial communities, characterized by the ability to recover from a perturbation or disturbance (Allison and Martiny, 2008; Shade et al., 2012; Griffiths and Philippot, 2013; Hawkes and Keitt, 2015). While resilience is not yet conclusively defined in microbial communities, we use this term to imply the rate of recovery of a given *function* in a community (or, more generally, their *functional* relationship with environmental variables) after perturbation. The concept of functional resilience in both engineered and ecological microbial systems, and the relationship between state and functional properties is examined in detail in our companion paper (Song et al., 2015). Attempts at quantifying resilience have primarily been done by monitoring functional recovery over time, with resilience being negatively correlated to recovery time (i.e., the time required for function to recover a defined percent of original function), or being correlated to recovery speed (i.e., the rate of recovery of function with units of slope). Faster recovery of function is therefore an indicator of higher resilience. These ideas have been explored theoretically and experimentally (Wissel, 1984). For example, recovery rate was monitored for cyanobacterial cultures exposed to a dilution perturbation by flushing out 10% of the population volume; the recovery rate decreased as the population lost resilience and approached a tipping point where function became irrecoverable (Veraart et al., 2012). In this experiment where the recovery over time was readily observable over a relevant timescale, assessing the system's resilience is straightforward. Such quantification of recovery time is important because it is known that systems nearing the verge of collapse or those trending toward unstable dynamics frequently exhibit reduced rates of recovery, or decreasing resilience (van Nes and Scheffer, 2007). This is known as "critical slowing down," meaning that, as a system nears a tipping point, recovery of function after a perturbation slackens (Scheffer et al., 2009, 2012). Thus quantitative measures of resilience are essential for early warning of impending system collapse, from which function cannot be regained.

Although recovery rate provides a direct measurement of resilience, in some systems it is not possible or practical to measure recovery time on time scales relevant to the perturbation. Additionally, some systems do not allow for

measurement of resilience because the experiments needed for quantify recovery time are impossible, unethical (e.g., when imposing a perturbation and monitoring function would endanger ecosystems or humans), or otherwise detrimental to the function of neighboring systems. In such cases not amenable to temporal analysis, resilience can alternatively be quantified in terms of *spatial* recovery as a proxy for temporal recovery (Dai et al., 2013). This means that resilience may still be predicted by observing spatial, rather than temporal, features of the system in cases where temporal and spatial recovery are reasonably correlated. The ability to monitor microbial function over relevant spatial scales has become increasingly possible due to advances in imaging and sensor capabilities, enabling a link between function, structure, and microbial identity (Behrens et al., 2008; Li et al., 2008; Pett-Ridge and Weber, 2012; Babauta et al., 2014; Vanwonterghem et al., 2014).

Recently, Dai et al. (2013) put forward recovery length as a measure for resilience. Recovery length is characterized by the distance required for function to recover from a spatial perturbation, and it was initially based on the observation that recovery length, which was correlated to recovery time, increased when a yeast system was on the verge of collapse. In their experiment, populations of *Saccharomyces cerevisiae* were connected spatially along a one-dimensional array through discrete dispersal events. Population stability was measured as the dilution factor was increased, imposing a perturbation. Recovery length was quantified by measuring the population density across distance, which provided a warning signal of imminent population collapse as the dilution factor approached unsustainable levels. Furthermore, these indicators increased with gradual increases in dilution factor, revealing deterioration of resilience in the system in real time. The recovery length concept proposed by Dai and coworkers faithfully quantified resilience to perturbations with sharp boundaries (such as step-change perturbations). As the authors pointed out, however, the same may not be effective for more realistic forms of perturbations that follow gradients or which are blurred across the spatial dimension. In reality, perturbation may come as gradients across both time and space. For example, spatial perturbations that form gradients include the intrusion of substrate or toxins into soil and its subsequent removal (Cao et al., 2012; Moran et al., 2014) or sunlight penetrating into a microbial mat (Bhaya et al., 2001; Häder and Lebert, 2001; Lindemann et al., 2013).

In this study we propose a perturbation-independent resilience metric, termed perturbation-addjusted spatial metric of resilience (PASMORE), to be applicable to perturbations that may be either step-change or gradient-based, and thus extending the recovery length work by Dai et al. (2013). To test this new metric, we developed a simple model of a microbial mat containing species with differing resilience. We discuss cases where the previously proposed metric fails to faithfully measure resilience under gradient perturbations, and then demonstrate how PASMORE provides an appropriate assessment of resilience for the same and other types of perturbation profiles. We also explored the impact of limited knowledge about the shape of

perturbation profiles on the effectiveness of PASMORE. Finally, we investigated a test application of PASMORE to systems of two interacting species, and observed how resilience is affected by interspecies competition.

## MODEL SYSTEM

We considered a simple mathematical model, which simulates a microbial mat with populations of microbial species: one with faster motility, and another with slower motility (see **Figure 1** for illustration). Each species responds to a perturbation (e.g., light) with movement proportional and opposite to the perturbation; during perturbation, both species move away from the perturbation toward a region where the perturbation is not present. The key aspect of this simulation is that the motility allows the microbial species to recover their initial population density after the perturbation occurs, with the more motile species recovering more quickly, and thus displaying higher resilience. While resilience is bestowed by motility rate in our model system, there are many other properties of a microbial species that can confer resilience beyond motility, and these features may present themselves within spatial constructions besides microbial mats. Furthermore, our proposed resilience measure has been formulated to be agnostic to the type of function being monitored. As discussed in Song et al. (2015), it is the researcher's job to identify the function of interest that is measured in a spatially defined community. Function may be defined as any trait or variable of interest, and resilience of the chosen function must be relative to a specific perturbation (Felix and Wagner, 2008). This is the cardinal "What to What?" question discussed by Carpenter et al. (2001) and Lesne (2008). For an in-depth discussion on the biological features that contribute to microbial resilience see the review by Shade et al. (2012). For the sake of evaluating our proposed resilience

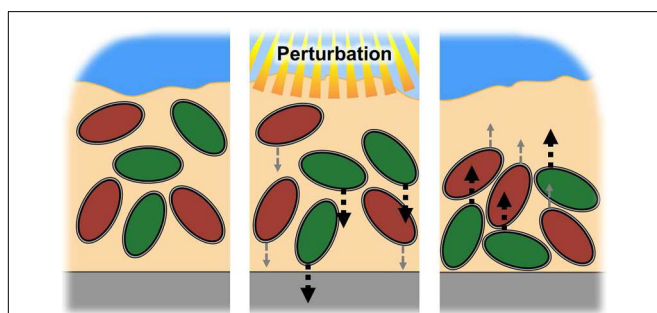


**FIGURE 1 | Schematic of model system.** A microbial mat has a population of species with differing resilience. In this system, resilience is conferred by movement, with rapid movement (green) having higher resilience than slower movement (red). Both cells respond to a perturbation, in this case light penetration into the mat, by moving out of the zone affected by the perturbation. After the perturbation concludes, the cells recover their initial cell density by moving back into the previously affected region. The faster moving cell has a higher resilience, i.e., the ability to recover population density more quickly, as it is capable of returning more quickly to the previously vacated space.

measure, motility suffices to provide a good working model, with population density as the example function of interest (or as a proxy for community functions that are closely linked to it).

The simulation was built using Comsol Multiphysics (v. 5.0.1.276) finite element analysis software with the chemical reaction engineering module. The microbial mat model was implemented using the diffusion application mode, with a one-dimensional geometry, similar to models previously described by our group (Renslow et al., 2013a,b,c).

## THE CONCEPT OF THE RECOVERY LENGTH AND PROPOSED EXTENSION

Dai et al. (2013) proposed the half-point recovery length definition of spatial recovery, which increases in proportion to the loss of resilience. The half-point recovery length is defined as  $L^{\text{half}}$  in Equation 1:

$$f(L^{\text{half}}) = \frac{1}{2}[f(x^{\text{b}}) + f(x^{\text{eq}})] \quad (1)$$

where  $f$  is the function of interest,  $x^{\text{b}}$  is the spatial distance at the boundary of the perturbation,  $f(x^{\text{eq}})$  is the functional value at the corresponding equilibrium (e.g., unperturbed) condition (a diagram of these terms is provided in Dai et al. (2013) supplementary information). For our simulation, we define  $f(x^{\text{eq}})$  as the functional value when it has reached 99% of its true equilibrium value, similar to how we calculate temporal recovery, described below. The equilibrium condition may also be considered to be  $f(x^{\text{eq}})$  where the function is fully perturbed, especially in the case where recovery length is measured at a boundary or where a full recovery profile (i.e., one that includes both perturbed and unperturbed equilibrium regions) may not be available (see Dai et al., Supplementary Figures 6 and 8 for a more detailed discussion on this special case). In cases where the perturbation boundary is not well defined or unknown, such as during a gradient perturbation, we assign  $x^{\text{b}}$  to be the spatial distance at the start of the perturbation. This does not alter the recovery length–resilience correlation for step-change perturbations in our model, but simply allows for quantifying  $L^{\text{half}}$  in gradient perturbation cases. Also note that, as described in Dai et al., function profiles are normalized by  $f(x^{\text{eq}})$ , and all results are shown on normalized scales for clarity and ease of comparison.

A new measure proposed in this work, PASMORE takes into account the shape of the perturbation, whether it follows a sharp step-change or a gradient. PASMORE is defined as a weighted integral, where the perturbation profile is the weighting function:

$$\text{PASMORE} = \int_S p(x)f(x)dx \quad (2)$$

where  $f$  is the function of interest,  $p$  is the perturbation profile, and PASMORE is the integral of  $pf$  over the defined system space,  $S$ . In our simulation, the defined system space is the microbial mat where the perturbation has effect.

## COMPARISON OF RECOVERY LENGTH AND PASMORE IN MICROBIAL MATS WITH NON-INTERACTING SPECIES

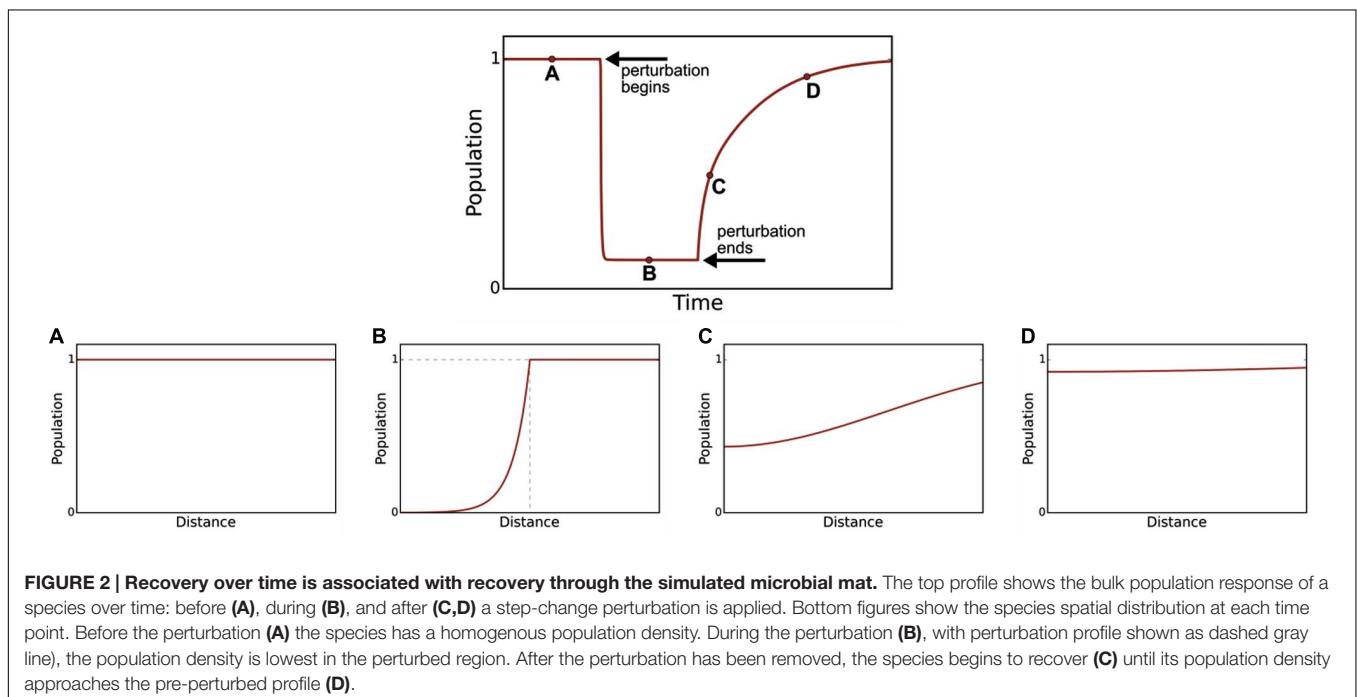
In **Figure 2**, we demonstrate how a microbial population responds to the application and removal of a perturbation. It is possible to see the relationship between temporal recovery and spatial recovery. Temporal recovery is defined as the time required for the recovery of function, in this case population density, to 99% of its original value. In cases where spatial recovery is correlated to temporal recovery, such as in our simulation (Pearson product-moment correlation coefficient, i.e., Pearson's  $r$ , of 1.0), spatial recovery metrics may be used as a proxy for quantifying resilience.

It is known that perturbations, whether occurring over time or over spatial domains, will occur frequently across gradients of varying sharpness. For example, using the example of light as the source of perturbation, attenuation follows an exponential decay profile. Even when the perturbation occurs across a gradient, rapidly motile species exhibit high resilience, meaning in this case that they recover population density more quickly than species with slow motility. However, as discussed by Dai et al. (2013), half-point recovery length may fail to accurately quantify resilience under conditions of a blurred or gradient perturbation. We tested step-change, linear, polynomial, and exponential perturbation gradients (data shown only for the exponential case) (**Figure 3**). The ability for spatial recovery to correlate to temporal recovery decreases as the perturbation profiles approaches an exponential function, where all correlation is lost (Pearson's  $r$  of 0.0). **Figure 4** demonstrates that PASMORE is able to accurately quantify spatial recovery and maintain the correlation to temporal recovery (Pearson's  $r$  of 1.0) regardless

of the perturbation profile. This was true for all perturbation gradients that we tested. Resilience arises due to the motility of the population, thus the metric should maintain its relationship to motility regardless of the perturbation to which it is exposed.

## QUANTIFYING RESILIENCE WITH LIMITED PERTURBATION INFORMATION

Properly quantifying resilience using spatial metrics requires information about the perturbation's shape. This is true whether PASMORE or other metrics like half-point recovery length are used. However, in experimental systems, it may not be possible to obtain the entire profile of a perturbation gradient. Here we wanted to quantify the effect of limited information about the gradient. Therefore, we examined PASMORE for use when the exact shape of the gradient imposed by a perturbation was uncertain. As shown in **Figure 5**, we compared two cases against the full-profile PASMORE: (1) a two-point dataset to generate a linear approximation between the start and end of the observed perturbation and (2) a three-point dataset to generate two linear approximations between the start and middle and between the middle and end of the observed perturbation. Note that only the perturbation profile was approximated, not the population density, since it is assumed that the function of interest, for which resilience is to be evaluated, is quantifiable. Using sensitive measurement instruments in real systems, it is likely that more than two or three data points of the perturbation profile could be obtained, for example by using microelectrodes (Nguyen et al., 2012) or NMR imaging (Renslow et al., 2010). However, as will be demonstrated, even using a three-point



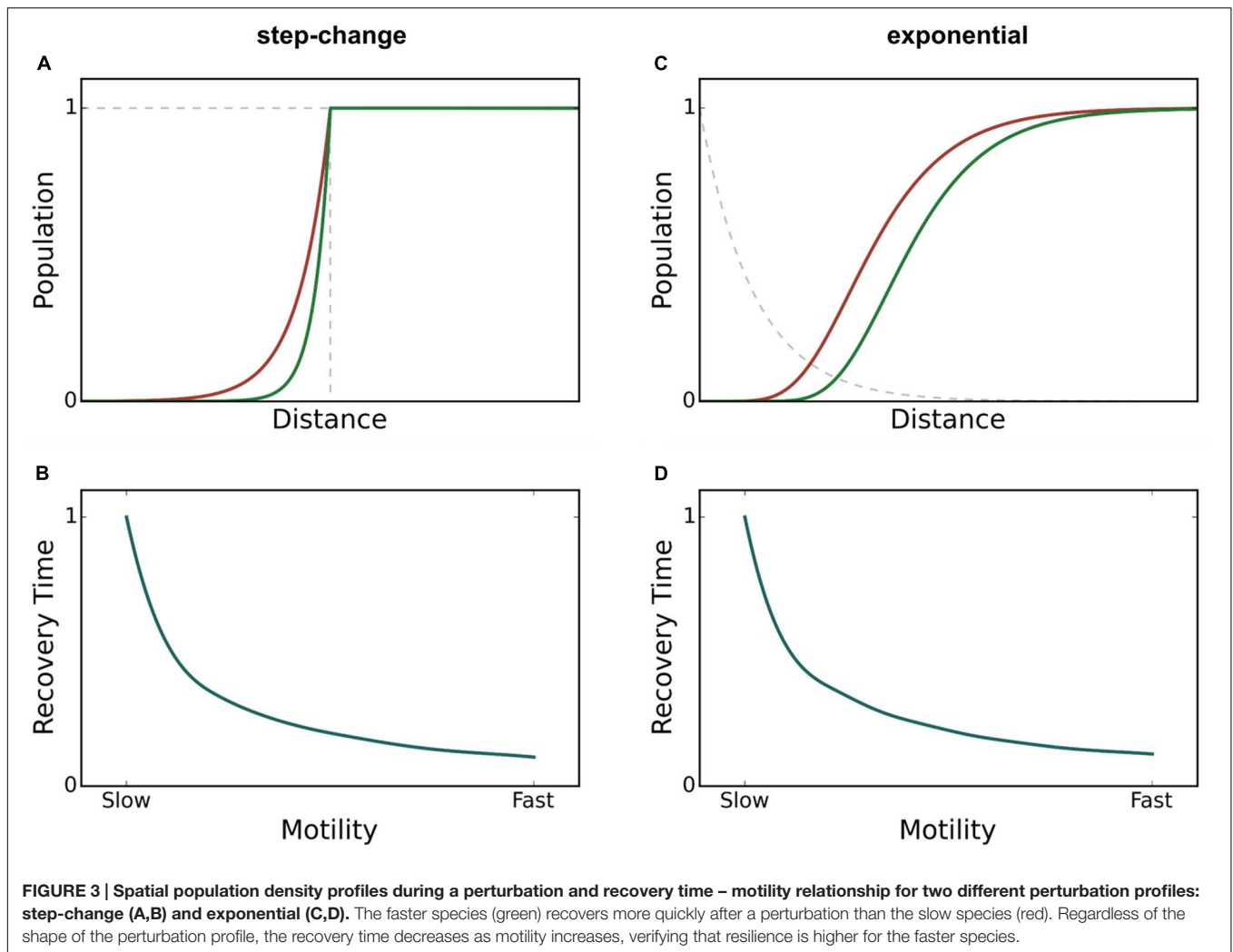


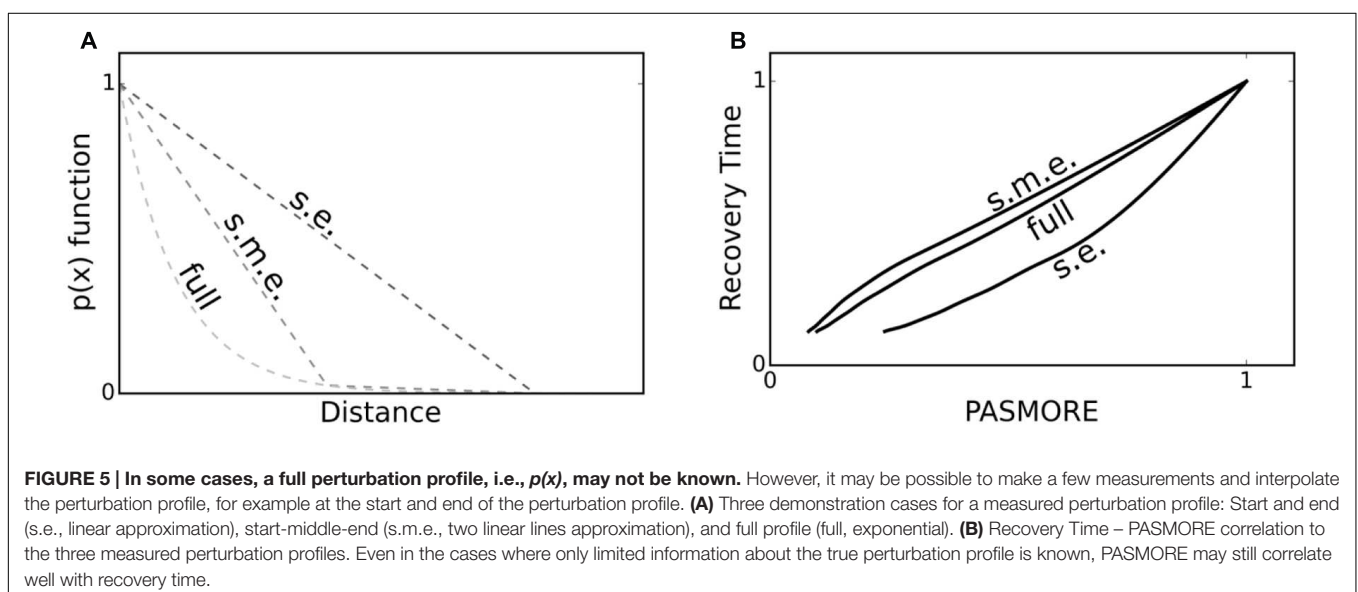
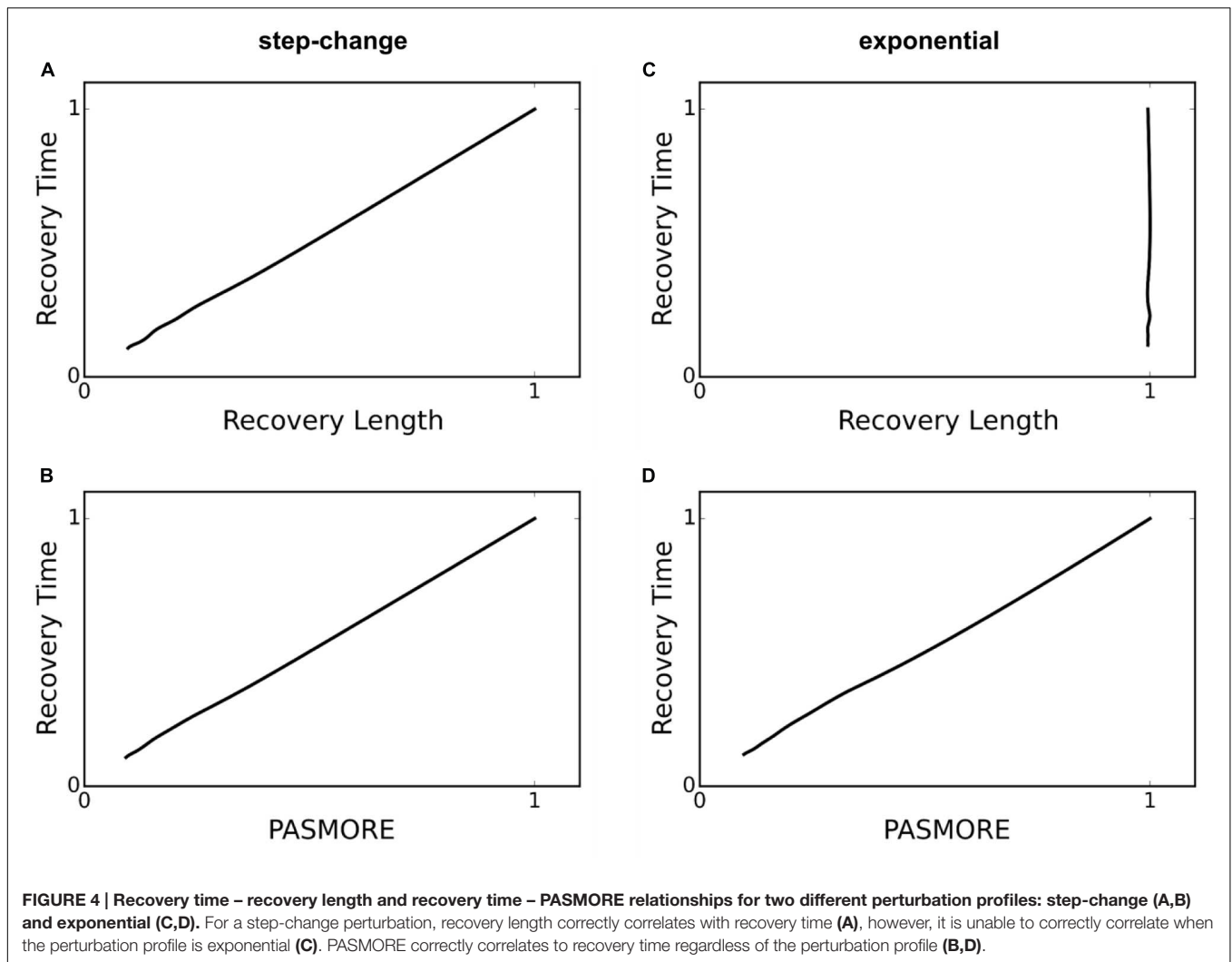
**FIGURE 3 | Spatial population density profiles during a perturbation and recovery time – motility relationship for two different perturbation profiles: step-change (A,B) and exponential (C,D).** The faster species (green) recovers more quickly after a perturbation than the slow species (red). Regardless of the shape of the perturbation profile, the recovery time decreases as motility increases, verifying that resilience is higher for the faster species.

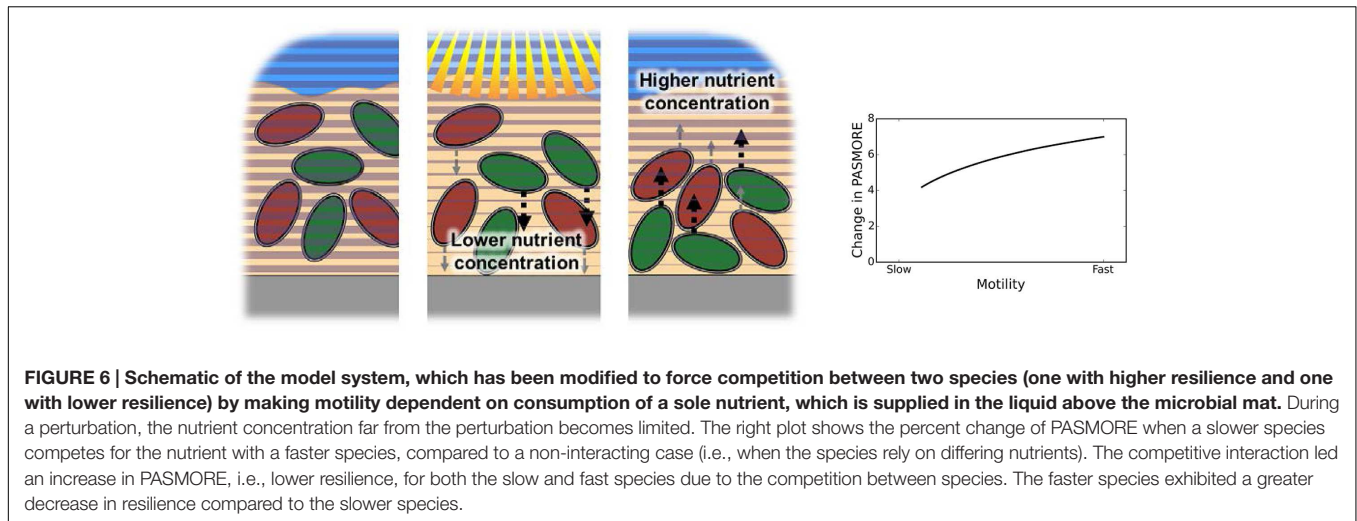
approximation, the calculation of PASMORE quickly approaches the full-profile PASMORE. **Figure 5** shows that PASMORE is able to maintain the correlation to temporal recovery with a two-point approximation (Pearson's  $r$  of 0.96), and this correlation improved with a three-point dataset (Pearson's  $r$  of 0.99).

## ANALYSIS OF A MICROBIAL MAT WITH INTERACTING SPECIES

We investigated how resilience as measured by PASMORE would change if two species in the mat interacted with each other. Therefore, we modified the model to simultaneously include two motile species that exhibited a difference in their rate of motility, but which was dependent on the consumption of a substrate. The substrate diffused from the top of the mat and consumption followed Monod-type kinetics, based on the diffusion and reaction parameters and setup of a previous model (Renslow et al., 2013b). Such a configuration broadly approximates the structure of a cyanobacterial mat, where the

carbon fixation upon which heterotrophs depend is maximal near the mat surface (Lindemann et al., 2013). The case where both species competed for the same substrate was compared to the case where the species consumed two independent substrates noncompetitively. **Figure 6** shows the percent change of PASMORE comparing the non-interacting to competitive interaction cases. Compared to the non-interacting case, the interacting species displayed an increase in PASMORE, and thus were found to have lower resilience. Furthermore, the species with the faster motility exhibited a larger loss of resilience compared to the slower species. This is due to the fact that, during perturbation, the species with higher resilience occupy a lower nutrient zone, while the species with lower resilience are closer to the nutrient source and are thus less affected. As such, the model illustrates a trade-off between resource availability and stress avoidance in these motile species; we anticipate that similar trade-offs will exist in many spatially organized communities where local interactions lead to gains in fitness. Finally, this simple simulation demonstrates how PASMORE can help quantify resilience in a case where previous metrics would not have been meaningful.





## PASMORE IN THE BROADER CONTEXT OF SPATIAL RESILIENCE MEASURES

The capability to monitor spatial patterns of microbial function can help elucidate the resilience of a community in cases where temporal measurements may not have previously been practical. Spatial measures remove the need to monitor a given function over time, and thus a snapshot of the present community stability can be gauged. This type of analysis may have implications beyond the microbial world, as there are many forms of complex networks and communities that display properties of emergent phenomena with spatially-relevant functions. For example, the spatial effects of social dilemmas have been investigated for several decades (Nowak and May, 1992; Hauert, 2006) and the frequency of human cooperation and collaboration or selfishness and exploitation across spatial dimensions impacts the resilience of groups of peoples and their ability to maintain high productivity (Alvard, 2004; Jimenez et al., 2008). Furthermore, spatial patterns of human settlements and population densities may be related to community stability in the face of perturbation events such as loss of water, tillable soil, hunting ground, food, energy and other resources, as well as the related incidents of overpopulation and politico-military conflicts (Tir and Diehl, 1998; Vandam et al., 2013). In this context, densities of refugee settlements across countries and subsequent patterns of repopulation of cities after wars may reveal human community and ethno-regional group stability properties in the face of significant devastation. Other possible application areas for spatial measures of resilience could include aquifer-groundwater recharge rates (Guglielmi and Mudry, 1996; Katic and Grafton, 2011), soil and vegetation health (Seybold et al., 1999; van de Koppel and Rietkerk, 2004; Alongi, 2008; Jiang et al., 2012), permafrost vulnerability (Jorgenson et al., 2010), coral reef habitats (Nystrom and Folke, 2001; Cheal et al., 2013), and fishery management (Carpenter and Brock, 2004; Kerr et al., 2010). Indeed, understanding the resilience of biological and non-biological systems will be critical for determining the impact of climate change and the necessary policy changes to alleviate

negative consequences (Bloetscher et al., 2010; Cumming, 2011). Future experiments and observations will need to be done to determine the extent to which spatial measures of resilience, such as PASMORE, may be used to provide insight into stability of complex systems beyond microbial communities. Furthermore, the ability of PASMORE to measure resilience in highly heterogeneous, discontinuous, or physically-restricted systems will need to be tested. It is unclear how barriers that constrain functional recovery, whether social, cultural, financial, political, or physical (e.g., soil and minerals at the microbial scale), will impact the capacity of PASMORE to measure resilience.

## CONCLUSION

'Perturbation-adjusted spatial metric of resilience' (PASMORE) is capable of accurately quantifying spatial recovery and maintaining the correlation to temporal recovery regardless of the perturbation profile. In many environmental and ecological systems, the gradient shape of the perturbation may not be quantifiable and even the identity or type of perturbation may not be known. However, even with limited information, PASMORE can be calculated with approximation of the perturbation profile to reveal a close estimate of the system's resilience. We envision that establishing the concept of PASMORE as a practically useful metric of resilience requires further studies, including investigation of the limits of using spatial recovery in lieu of temporal recovery to quantify resilience in real natural and engineered microbial communities and relating these measurements to predictions of when systems are on the verge of collapse or nearing an irreversible transition across a tipping point. The present work provides initial foundations along this direction.

## AUTHOR CONTRIBUTIONS

All authors listed have made substantial, direct, and intellectual contribution to the work, and approved it for publication.

## ACKNOWLEDGMENTS

This research was supported by the Genomic Science Program (GSP), Office of Biological and Environmental Research (OBER), U.S. Department of Energy (DOE), and is a contribution of

the Pacific Northwest National Laboratory (PNNL) Foundational Scientific Focus Area (SFA) and Subsurface Biogeochemistry Research Program's SFA. R. Renslow was supported by a Linus Pauling Distinguished Postdoctoral Fellowship at PNNL.

## REFERENCES

- Allison, S. D., and Martiny, J. B. H. (2008). Resistance, resilience, and redundancy in microbial communities. *Proc. Natl. Acad. Sci. U.S.A.* 105, 11512–11519. doi: 10.1073/pnas.0801925105
- Alongi, D. M. (2008). Mangrove forests: resilience, protection from tsunamis, and responses to global climate change. *Estuar. Coast. Shelf Sci.* 76, 1–13. doi: 10.1016/j.eccs.2007.08.024
- Alvard, M. (2004). Good hunters keep smaller shares of larger pies. *Behav. Brain Sci.* 27, 560–561. doi: 10.1017/S0140525X0422012X
- Babauta, J. T., Atci, E., Ha, P. T., Lindemann, S. R., Ewing, T., Call, D. R., et al. (2014). Localized electron transfer rates and microelectrode-based enrichment of microbial communities within a phototrophic microbial mat. *Front. Microbiol.* 5:11. doi: 10.3389/fmicb.2014.00011
- Behrens, S., Losekann, T., Pett-Ridge, J., Weber, P. K., Ng, W. O., Stevenson, B. S., et al. (2008). Linking microbial phylogeny to metabolic activity at the single-cell level by using enhanced element labeling-catalyzed reporter deposition fluorescence in situ hybridization (EL-FISH) and NanoSIMS. *Appl. Environ. Microbiol.* 74, 3143–3150. doi: 10.1128/AEM.00191-08
- Bernstein, H. C., Beam, J. P., Kozubal, M. A., Carlson, R. P., and Inskeep, W. P. (2013). In situ analysis of oxygen consumption and diffusive transport in high-temperature acidic iron-oxide microbial mats. *Environ. Microbiol.* 15, 2360–2370. doi: 10.1111/1462-2920.12109
- Bernstein, H. C., Kesaano, M., Moll, K., Smith, T., Gerlach, R., Carlson, R. P., et al. (2014). Direct measurement and characterization of active photosynthesis zones inside wastewater remediation and biofuel producing microalgal biofilms. *Bioresour. Technol.* 156, 206–215. doi: 10.1016/j.biortech.2014.01.001
- Bhaya, D., Takahashi, A., and Grossman, A. R. (2001). Light regulation of type IV pilus-dependent motility by chemosensor-like elements in *Synechocystis* PCC6803. *Proc. Natl. Acad. Sci. U.S.A.* 98, 7540–7545. doi: 10.1073/pnas.131201098
- Bloetscher, F., Meeroff, D. E., Heimlich, B. N., Brown, A. R., Bayler, D., and Loucraft, M. (2010). Improving resilience against the effects of climate change. *J. Am. Water Works Assoc.* 102, 36–46. doi: 10.1007/s00572-014-0595-2
- Cao, B., Ahmed, B., Kennedy, D. W., Wang, Z., Shi, L., Marshall, M. J., et al. (2011). Contribution of extracellular polymeric substances from *Shewanella* sp. HRCR-1 biofilms to U (VI) immobilization. *Environ. Sci. Technol.* 45, 5483–5490. doi: 10.1021/es200095j
- Cao, B., Majors, P. D., Ahmed, B., Renslow, R. S., Silvia, C. P., Shi, L., et al. (2012). Biofilm shows spatially stratified metabolic responses to contaminant exposure. *Environ. Microbiol.* 14, 2901–2910. doi: 10.1111/j.1462-2920.2012.02850.x
- Carey, M., and Carville, S. (2003). Scheduling and platforming trains at busy complex stations. *Transp. Res. Part A Policy Pract.* 37, 195–224. doi: 10.1016/S0965-8564(02)00012-5
- Carpenter, S., Walker, B., Anderies, J. M., and Abel, N. (2001). From metaphor to measurement: resilience of what to what? *Ecosystems* 4, 765–781. doi: 10.1007/s10021-001-0045-9
- Carpenter, S. R., and Brock, W. A. (2004). Spatial complexity, resilience, and policy diversity: fishing on lake-rich landscapes. *Ecol. Soc.* 9, 31.
- Cheal, A. J., Emslie, M., Macneil, M. A., Miller, I., and Sweatman, H. (2013). Spatial variation in the functional characteristics of herbivorous fish communities and the resilience of coral reefs. *Ecol. Appl.* 23, 174–188. doi: 10.1890/11-2253.1
- Cimellaro, G. P., Reinhorn, A. M., and Bruneau, M. (2010). Seismic resilience of a hospital system. *Struct. Infrastruct. Eng.* 6, 127–144. doi: 10.1080/15732470802663847
- Cumming, G. S. (2011). Spatial resilience: integrating landscape ecology, resilience, and sustainability. *Landsc. Ecol.* 26, 899–909. doi: 10.1007/s10980-011-9623-1
- Curtis, T. P., and Sloan, W. T. (2004). Prokaryotic diversity and its limits: microbial community structure in nature and implications for microbial ecology. *Curr. Opin. Microbiol.* 7, 221–226. doi: 10.1016/j.mib.2004.04.010
- Czaczyk, K., and Myszka, K. (2007). Biosynthesis of extracellular polymeric substances (EPS) and its role in microbial biofilm formation. *Pol. J. Environ. Stud.* 16, 799–806.
- Dai, L., Korolev, K. S., and Gore, J. (2013). Slower recovery in space before collapse of connected populations. *Nature* 496, 355–358. doi: 10.1038/nature12071
- De La Fuente, I. M., Martínez, L., Pérez-Samartín, A. L., Ormaetxea, L., Amezaga, C., and Vera-López, A. (2008). Global self-organization of the cellular metabolic structure. *PLoS ONE* 3:e3100. doi: 10.1371/journal.pone.0003100
- Easterling, W. E., and Kok, K. (2003). “Emergent properties of scale in global environmental modeling: are there any?,” in *Scaling in Integrated Assessment*, eds J. Rotmans and D. S. Rothman (Lisse: Swets and Zeitlinger Group BV), 263–292.
- Felix, M. A., and Wagner, A. (2008). Robustness and evolution: concepts, insights and challenges from a developmental model system. *Heredity* 100, 132–140. doi: 10.1038/sj.hdy.6800915
- Flemming, H. C., and Wingender, J. (2001). Relevance of microbial extracellular polymeric substances (EPSs) – Part I: structural and ecological aspects. *Water Sci. Technol.* 43, 1–8.
- Fuhrman, J. A. (2009). Microbial community structure and its functional implications. *Nature* 459, 193–199. doi: 10.1038/nature08058
- Griffiths, B. S., and Philippot, L. (2013). Insights into the resistance and resilience of the soil microbial community. *FEMS Microbiol. Rev.* 37, 112–129. doi: 10.1111/j.1574-6976.2012.00343.x
- Guglielmi, Y., and Mudry, J. (1996). Estimation of spatial and temporal variability of recharge fluxes to an alluvial aquifer in a fore land area by water chemistry and isotopes. *Ground Water* 34, 1017–1023. doi: 10.1111/j.1745-6584.1996.tb02167.x
- Häder, D.-P., and Lebert, M. (2001). *Photomovement*. Amsterdam: Elsevier Science.
- Hauert, C. (2006). Spatial effects in social dilemmas. *J. Theor. Biol.* 240, 627–636. doi: 10.1016/j.jtbi.2005.10.024
- Hawkes, C. V., and Keitt, T. H. (2015). Resilience vs. historical contingency in microbial responses to environmental change. *Ecol. Lett.* 18, 612–625. doi: 10.1111/ele.12451
- Hibiya, K., Terada, A., Tsuneda, S., and Hirata, A. (2003). Simultaneous nitrification and denitrification by controlling vertical and horizontal microenvironment in a membrane-aerated biofilm reactor. *J. Biotechnol.* 100, 23–32. doi: 10.1016/S0168-1656(02)00227-4
- Higgins, P. A. T., Mastrandrea, M. D., and Schneider, S. H. (2002). Dynamics of climate and ecosystem coupling: abrupt changes and multiple equilibria. *Philos. Trans. R. Soc. Lond. B Biol. Sci.* 357, 647–655. doi: 10.1098/rstb.2001.1043
- Jiang, J., Gao, D. Z., and Deangelis, D. L. (2012). Towards a theory of ecotone resilience: coastal vegetation on a salinity gradient. *Theor. Popul. Biol.* 82, 29–37. doi: 10.1016/j.tpb.2012.02.007
- Jimenez, R., Lugo, H., Cuesta, J. A., and Sanchez, A. (2008). Emergence and resilience of cooperation in the spatial prisoner's dilemma via a reward mechanism. *J. Theor. Biol.* 250, 475–483. doi: 10.1016/j.jtbi.2007.10.010
- Jorgenson, M. T., Romanovsky, V., Harden, J., Shur, Y., O'donnell, J., Schuur, E. A. G., et al. (2010). Resilience and vulnerability of permafrost to climate change. *Can. J. For. Res.* 40, 1219–1236. doi: 10.1139/X10-060
- Katic, P., and Grafton, R. Q. (2011). Optimal groundwater extraction under uncertainty: resilience versus economic payoffs. *J. Hydrol.* 406, 215–224. doi: 10.1016/j.jhydrol.2011.06.016
- Kerr, L. A., Cadrin, S. X., and Secor, D. H. (2010). The role of spatial dynamics in the stability, resilience, and productivity of an estuarine fish population. *Ecol. Appl.* 20, 497–507. doi: 10.1890/08-1382.1
- Konopka, A. (2009). What is microbial community ecology? *ISME J.* 3, 1223–1230. doi: 10.1038/ismej.2009.88
- Laspidou, C. S., and Rittmann, B. E. (2002). A unified theory for extracellular polymeric substances, soluble microbial products, and active and inert biomass. *Water Res.* 36, 2711–2720. doi: 10.1016/S0043-1354(01)00414-6

- Lesne, A. (2008). Robustness: confronting lessons from physics and biology. *Biol. Rev.* 83, 509–532. doi: 10.1111/j.1469-185X.2008.00052.x
- Li, T., Wu, T. D., Mazeas, L., Toffin, L., Guerquin-Kern, J. L., Leblon, G., et al. (2008). Simultaneous analysis of microbial identity and function using NanoSIMS. *Environ. Microbiol.* 10, 580–588. doi: 10.1111/j.1462-2920.2007.01478.x
- Lindemann, S. R., Moran, J. J., Stegen, J. C., Renslow, R. S., Hutchison, J. R., Cole, J. K., et al. (2013). The epsomitic phototrophic microbial mat of Hot Lake, Washington: community structural responses to seasonal cycling. *Front. Microbiol.* 4:323. doi: 10.3389/fmicb.2013.00323
- Lusseau, D. (2003). The emergent properties of a dolphin social network. *Proc. R. Soc. B Biol. Sci.* 270, S186–S188. doi: 10.1098/rsbl.2003.0057
- Mitrovic, M., and Tadic, B. (2010). Bloggers behavior and emergent communities in Blog space. *Eur. Phys. J. B* 73, 293–301. doi: 10.1140/epjb/e2009-00431-9
- Moran, J. J., Doll, C. G., Bernstein, H. C., Renslow, R. S., Cory, A. B., Hutchison, J. R., et al. (2014). Spatially tracking C-13-labelled substrate (bicarbonate) accumulation in microbial communities using laser ablation isotope ratio mass spectrometry. *Environ. Microbiol. Rep.* 6, 786–791. doi: 10.1111/1758-2229.12211
- Nguyen, H. D., Renslow, R., Babauta, J., Ahmed, B., and Beyenal, H. (2012). A voltammetric flavin microelectrode for use in biofilms. *Sens. Actuators B Chem.* 161, 929–937. doi: 10.1016/j.snb.2011.11.066
- Nowak, M. A., and May, R. M. (1992). Evolutionary games and spatial chaos. *Nature* 359, 826–829. doi: 10.1038/359826a0
- Nystrom, M., and Folke, C. (2001). Spatial resilience of coral reefs. *Ecosystems* 4, 406–417. doi: 10.1007/s10021-001-0019-y
- Pett-Ridge, J., and Weber, P. K. (2012). “NanoSIP: nanoSIMS applications for microbiology,” in *Springer Protocols*, ed. A. Navid (New York, NY: Humana Press), 375–408.
- Porter, M. A., Mucha, P. J., Newman, M. E. J., and Warmbrand, C. M. (2005). A network analysis of committees in the US House of Representatives. *Proc. Natl. Acad. Sci. U.S.A.* 102, 7057–7062. doi: 10.1073/pnas.0500191102
- Renslow, R., Babauta, J., Kuprat, A., Schenk, J., Ivory, C., Fredrickson, J., et al. (2013a). Modeling biofilms with dual extracellular electron transfer mechanisms. *Phys. Chem. Chem. Phys.* 15, 19262–19283. doi: 10.1039/c3cp53759e
- Renslow, R., Lewandowski, Z., and Beyenal, H. (2011). Biofilm image reconstruction for assessing structural parameters. *Biotechnol. Bioeng.* 108, 1383–1394. doi: 10.1002/bit.23060
- Renslow, R. S., Babauta, J. T., Dohnalkova, A. C., Boyanov, M. I., Kemner, K. M., Majors, P. D., et al. (2013b). Metabolic spatial variability in electrode-respiring *Geobacter sulfurreducens* biofilms. *Energy Environ. Sci.* 6, 1827–1836. doi: 10.1039/c3ee40203g
- Renslow, R. S., Babauta, J. T., Majors, P. D., and Beyenal, H. (2013c). Diffusion in biofilms respiring on electrodes. *Energy Environ. Sci.* 6, 595–607. doi: 10.1039/C2EE23394K
- Renslow, R. S., Majors, P. D., Mclean, J. S., Fredrickson, J. K., Ahmed, B., and Beyenal, H. (2010). In situ effective diffusion coefficient profiles in live biofilms using pulsed-field gradient nuclear magnetic resonance. *Biotechnol. Bioeng.* 106, 928–937. doi: 10.1002/bit.22755
- Robinson, C. J., Bohannon, B. J. M., and Young, V. B. (2010). From structure to function: the ecology of host-associated microbial communities. *Microbiol. Mol. Biol. Rev.* 74, 453–476. doi: 10.1128/MMBR.00014-10
- Scheffer, M., Bascompte, J., Brock, W. A., Brovkin, V., Carpenter, S. R., Dakos, V., et al. (2009). Early-warning signals for critical transitions. *Nature* 461, 53–59. doi: 10.1038/nature08227
- Scheffer, M., Carpenter, S. R., Lenton, T. M., Bascompte, J., Brock, W., Dakos, V., et al. (2012). Anticipating critical transitions. *Science* 338, 344–348. doi: 10.1126/science.1225244
- Schramm, A., Larsen, L. H., Revsbech, N. P., Ramsing, N. B., Amann, R., and Schleifer, K. H. (1996). Structure and function of a nitrifying biofilm as determined by in situ hybridization and the use of microelectrodes. *Appl. Environ. Microbiol.* 62, 4641–4647.
- Schubert, W. (2014). Systematic, spatial imaging of large multimolecular assemblies and the emerging principles of supramolecular order in biological systems. *J. Mol. Recognit.* 27, 3–18. doi: 10.1002/jmr.2326
- Seybold, C. A., Herrick, J. E., and Brejda, J. J. (1999). Soil resilience: a fundamental component of soil quality. *Soil Sci.* 164, 224–234. doi: 10.1097/00010694-199904000-00002
- Shade, A., Peter, H., Allison, S. D., Baho, D. L., Berga, M., Burgmann, H., et al. (2012). Fundamentals of microbial community resistance and resilience. *Front. Microbiol.* 3:417. doi: 10.3389/fmicb.2012.00417
- Song, H.-S., Renslow, R. S., Fredrickson, J. K., and Lindemann, S. R. (2015). Integrating ecological and engineering concepts of resilience in microbial communities. *Front. Microbiol.* 6:1298. doi: 10.3389/fmicb.2015.01298
- Tilman, D., Reich, P. B., Knops, J., Wedin, D., Mielke, T., and Lehman, C. (2001). Diversity and productivity in a long-term grassland experiment. *Science* 294, 843–845. doi: 10.1126/science.1060391
- Tir, J., and Diehl, P. F. (1998). Demographic pressure and interstate conflict: linking population growth and density to militarized disputes and wars, 1930–89. *J. Peace Res.* 35, 319–339. doi: 10.1177/0022343398035003004
- van de Koppel, J., and Rietkerk, M. (2004). Spatial interactions and resilience in arid ecosystems. *Am. Nat.* 163, 113–121. doi: 10.1086/380571
- van Nes, E. H., and Scheffer, M. (2007). Slow recovery from perturbations as a generic indicator of a nearby catastrophic shift. *Am. Nat.* 169, 738–747. doi: 10.1086/516845
- Vandam, R., Kaptijn, E., and Vanschoenwinkel, B. (2013). Disentangling the spatio-environmental drivers of human settlement: an eigenvector based variation decomposition. *PLoS ONE* 8:e67726. doi: 10.1371/journal.pone.0067726
- Vanwonterghem, I., Jensen, P. D., Ho, D. P., Batstone, D. J., and Tyson, G. W. (2014). Linking microbial community structure, interactions and function in anaerobic digesters using new molecular techniques. *Curr. Opin. Biotechnol.* 27, 55–64. doi: 10.1016/j.copbio.2013.11.004
- Veraart, A. J., Faassen, E. J., Dakos, V., Van Nes, E. H., Lurling, M., and Scheffer, M. (2012). Recovery rates reflect distance to a tipping point in a living system. *Nature* 481, 357–359. doi: 10.1038/nature10723
- Wagner, M., Nielsen, P. H., Loy, A., Nielsen, J. L., and Daims, H. (2006). Linking microbial community structure with function: fluorescence in situ hybridization-microautoradiography and isotope arrays. *Curr. Opin. Biotechnol.* 17, 83–91. doi: 10.1016/j.copbio.2005.12.006
- Wintermute, E. H., and Silver, P. A. (2010). Emergent cooperation in microbial metabolism. *Mol. Syst. Biol.* 6, 407. doi: 10.1038/msb.2010.66
- Wissel, C. (1984). A universal law of the characteristic return time near thresholds. *Oecologia* 65, 101–107. doi: 10.1007/BF00384470
- Xavier, J. B., and Foster, K. R. (2007). Cooperation and conflict in microbial biofilms. *Proc. Natl. Acad. Sci. U.S.A.* 104, 876–881. doi: 10.1073/pnas.0607651104

**Conflict of Interest Statement:** The authors declare that the research was conducted in the absence of any commercial or financial relationships that could be construed as a potential conflict of interest.

Copyright © 2016 Renslow, Lindemann and Song. This is an open-access article distributed under the terms of the Creative Commons Attribution License (CC BY). The use, distribution or reproduction in other forums is permitted, provided the original author(s) or licensor are credited and that the original publication in this journal is cited, in accordance with accepted academic practice. No use, distribution or reproduction is permitted which does not comply with these terms.



# Integrating Ecological and Engineering Concepts of Resilience in Microbial Communities

Hyun-Seob Song<sup>1</sup>, Ryan S. Renslow<sup>2</sup>, Jim K. Fredrickson<sup>1</sup> and Stephen R. Lindemann<sup>1\*</sup>

<sup>1</sup> Biological Sciences Division, Earth and Biological Sciences Directorate, Pacific Northwest National Laboratory, Richland, WA, USA, <sup>2</sup> Environmental Molecular Sciences Laboratory, Pacific Northwest National Laboratory, Richland, WA, USA

## OPEN ACCESS

### Edited by:

Matthias Hess,  
University of California, Davis, USA

### Reviewed by:

Angel Valverde,  
University of Pretoria, South Africa  
Steven Singer,  
Lawrence Berkeley National  
Laboratory, USA

### \*Correspondence:

Stephen R. Lindemann  
stephen.lindemann@pnl.gov

### Specialty section:

This article was submitted to  
Systems Microbiology,  
a section of the journal  
Frontiers in Microbiology

**Received:** 03 August 2015

**Accepted:** 06 November 2015

**Published:** 01 December 2015

### Citation:

Song H-S, Renslow RS,  
Fredrickson JK and Lindemann SR  
(2015) Integrating Ecological and  
Engineering Concepts of Resilience in  
Microbial Communities.  
*Front. Microbiol.* 6:1298.  
doi: 10.3389/fmicb.2015.01298

Many definitions of resilience have been proffered for natural and engineered ecosystems, but a conceptual consensus on resilience in microbial communities is still lacking. We argue that the disconnect largely results from the wide variance in microbial community complexity, which range from compositionally simple synthetic consortia to complex natural communities, and divergence between the typical practical outcomes emphasized by ecologists and engineers. Viewing microbial communities as elasto-plastic systems that undergo both recoverable and unrecoverable transitions, we argue that this gap between the engineering and ecological definitions of resilience stems from their respective emphases on elastic and plastic deformation, respectively. We propose that the two concepts may be fundamentally united around the resilience of function rather than state in microbial communities and the regularity in the relationship between environmental variation and a community's functional response. Furthermore, we posit that functional resilience is an intrinsic property of microbial communities and suggest that state changes in response to environmental variation may be a key mechanism driving functional resilience in microbial communities.

**Keywords:** microbial communities, microbial ecology, resilience, resistance, robustness, stability, networks

## INTRODUCTION

Microorganisms collectively exceed the biomass of all macrobiota on the planet (Whitman et al., 1998). Communities of microbes control the biogeochemical cycles upon which all macrobiota depend (Falkowski et al., 2008; Strom, 2008; Nazaries et al., 2013), and the role of microbial communities in shaping human health and physiology is also increasingly appreciated (Song et al., 2014a; Braundmeier et al., 2015; Lone et al., 2015; Sassone-Corsi and Raffatellu, 2015). Although natural microbial communities continually respond to perturbations (Konopka et al., 2014), their functioning can exhibit remarkable stability over time (Fuhrman et al., 2015), even under extreme environmental variation (Shade et al., 2012b; Lindemann et al., 2013). Comprehending the processes governing the responses of microbial communities to perturbation is critical both to ecologists concerned with predicting effects on ecosystem function (Hooper et al., 2005) and engineers designing communities for stable biotechnological processes (Lucas et al., 2015).

Though there is widespread interest in factors driving microbial community stability, the conceptual bases of stability measures, like resilience, are poorly defined. A report by the Community and Regional Resilience Institute (CARRI Report, 2013) summarized 47 definitions of resilience used in diverse scientific areas including engineering, ecology, sociology, economics,

and psychology. Ambiguity is found even within disciplines: in ecology, resilience has been discussed alongside, and sometimes interchangeably with, ~70 other terms describing various stability measures (e.g., resistance, sustainability, and vulnerability; Grimm and Wissel, 1997). The conceptual variability in ecology surrounding stability, and resilience in particular, likely stems from system-specificity. Microbial communities span orders of magnitude in the diversity of their interacting components, from experimental or engineered systems to diverse natural communities. The metrics employed to evaluate each system's stability are largely idiosyncratic. The diversity of environments in which communities are investigated, the large array of functions of interest, and the range of research objectives concerning stability beg the question of whether a single definition of resilience can be universally applied across systems and scales for microbial communities.

Seeking an integrated concept applicable to all microbial communities, we herein compare engineering and ecological resilience and reconcile them by arguing that resilience is an intrinsic property of complex adaptive systems which, after perturbation, recover their system-level functions and interactions with the environment, rather than their endogenous state.

## ENGINEERING AND ECOLOGICAL CONCEPTS OF RESILIENCE

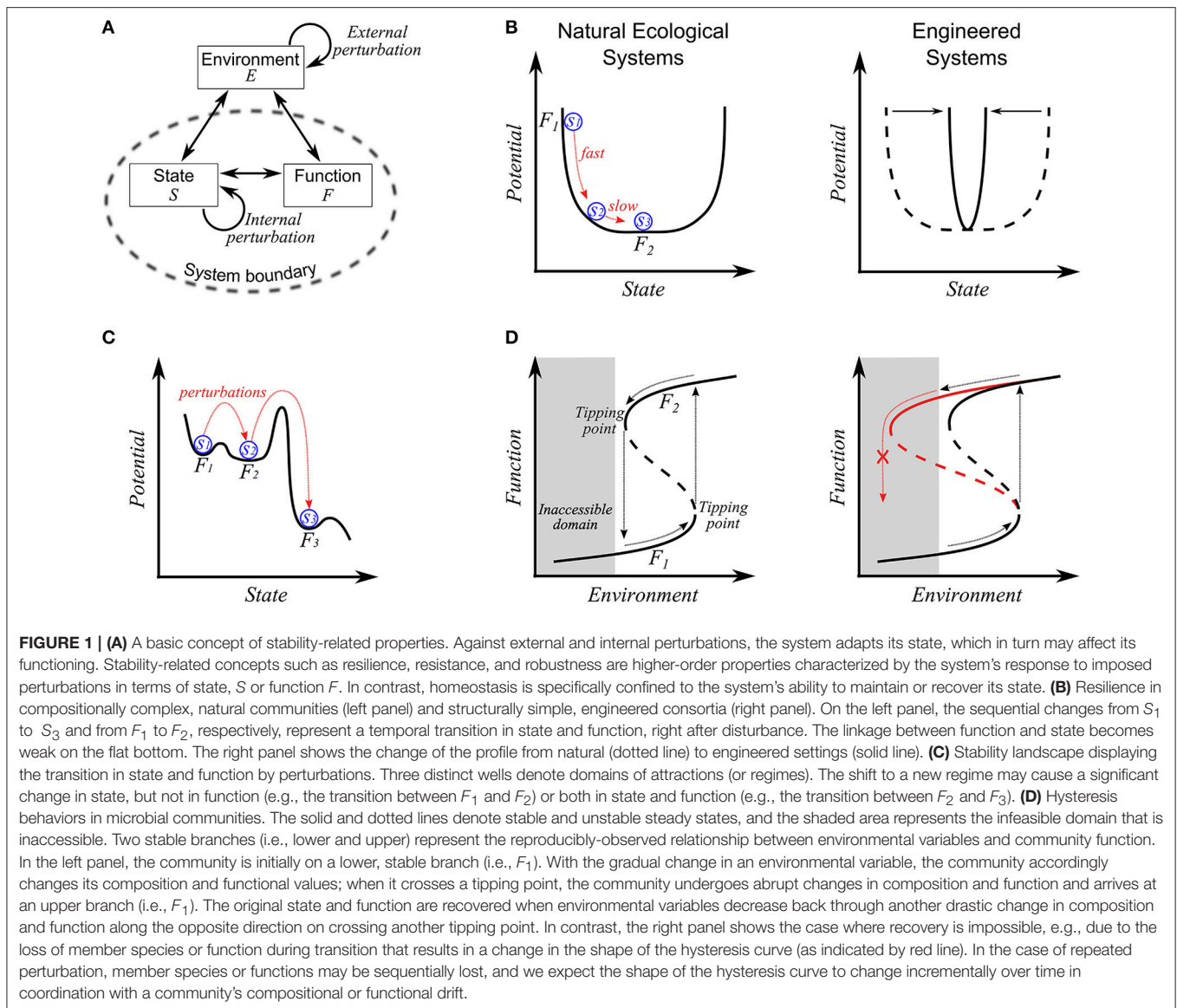
Discussion of resilience in the literature often involves the related concepts of resistance and robustness. These stability-related properties are all concerned with the relationship between an imposed perturbation and a system's response (**Figure 1A**). Resilience has been broadly articulated as a system's *ability to recover* from disturbance. Diverse interpretations emerge, however, depending on what is considered "recovery" and how that recovery is quantified. In contrast, resistance has been defined with relatively less confusion, e.g., as the degree to which a system's state or function is insensitive to disturbance (Konopka et al., 2014). As a simple distinction, resilience is concerned with the system's ability to *recover* its function post-disturbance, while resistance is concerned with the system's ability to *maintain* its function against a perturbation. In these contexts, resilience (or resistance) denotes the degree to which the *quantitative* value of any function of interest is recovered to (or maintained at) an initial or reference condition. As illustrated elsewhere (Carpenter et al., 2001), systems may display significant resilience but not appreciable resistance and vice versa. In some cases, resilience has also been used as a synonym of robustness, described as the system's ability to maintain function post-disturbance (Levin and Lubchenco, 2008). Herein we consider robustness as a more general concept of stability that is comprised of resilience, resistance, and other complementary properties (Shade et al., 2012b), i.e., resilience and resistance are key components of a system's overall robustness.

The literature provides rich discussions of resilience, which can be subdivided into two categories: engineering and ecological

concepts. As discriminated by Holling in his seminal paper (Holling, 1973), engineering resilience denotes the system's ability to recover its pre-perturbed equilibrium state as measured by the *rate* of return. The ecological concept considers a system's tolerance against disturbance without shifting to a new regime governed by fundamentally different processes and mechanisms (i.e., a domain of attraction), as quantified by the overall area of the domain of attraction or the depth of the basin. A domain of attraction represents a set of states converging to a given equilibrium point (such as S3 in **Figure 1B**, left panel). Both concepts of resilience have been invoked in microbial ecology. Faithful translation of the etymon of resilience, the Latin word *resalire* (literally, "to jump back") (CARRI Report, 2013), interprets resilience as a property of elastic systems (as in physics/material sciences) that recover their original shape after disturbance. In this regard, Grimm and Calabrese (2011) equated elasticity with engineering resilience. Indeed, microbial communities share some features with elastic systems in that they sometimes undergo internal or structural deformation (e.g., changes of composition or gene expression patterns) under disturbance, yet eventually recover their original performance (e.g., recovery of microbe-driven biogeochemical processes after a forest fire; Tas et al., 2014). However, microbial communities lose elasticity (i.e., fail to recover) if the applied environmental stress exceeds a threshold, a phenomenon termed plastic deformation. The threshold across which plastic deformation occurs is variously called a tipping, yield, or bifurcation point (Veraart et al., 2012). Plastic deformation is better captured by the ecological concept of resilience. Obviously, microbial communities are neither perfectly elastic nor plastic, but are elasto-plastic systems. Thus, engineering and ecological concepts that reflect these aspects of microbial communities are complementary.

Variation in complexity between engineered and natural communities provides rationale for both the engineering and ecological concepts. Microbial communities in non-extreme natural settings typically have high compositional diversity and functional redundancy among species. As illustrated in **Figure 1B** (left panel), the community composition may vary over a certain range without affecting the function. The flat bottom of the profile implies *slow* dynamics in compositional change around a low-energy state, even in a rarely-perturbed or constant environment. Konopka et al. (2014) hypothesized that endogenous dynamics contribute to a community-level functional resilience. Relating resilience to the system's ability to persist within a domain of attraction after disturbance (i.e., ecological resilience), rather than the rate of return to the initial state, makes more sense in this circumstance. In contrast, microbial consortia with relatively lower diversity and functional redundancy should display a sharper curve (right panel of **Figure 1B**), meaning that (1) consortium-level function is maintained only at a specific compositional state and, (2) that the recovery to the original state after disturbance is relatively fast. In this second case, the rate of recovery may be a better measure of resilience (i.e., the engineering concept).

The distinction between engineering and ecological concepts of resilience fundamentally lies in their different foci: equilibrium



vs. domain of attraction; numerical values of state variables vs. relationship between structure and function; rate of recovery after perturbation vs. ability to absorb the effect of disturbance (Grimm and Calabrese, 2011). In addition, we propose that the engineering and ecological concepts represent optimization for different objectives. Microbial consortia used for bioprocessing are, in essence, a set of biocatalysts that convert substrates into products. In well-designed bioreactors, where environmental conditions are tightly controlled, collapse across a tipping point may not be the major concern. Instead, rapid recovery after minor disturbances (i.e., engineering resilience) is critical to ensure consistent product quality and profit maximization. In contrast, with respect to natural communities with complex structure and dynamics, it would be of greater importance to proactively identify threats to ecosystem functioning by predicting how much additional stress a system can absorb

without failure, a main concern in ecological resilience. In this regard, we add “maximizing system performance” vs. “preserving desirable system function” or “optimal control” vs. “monitoring and predicting” to the list of differences between engineering and ecological concepts.

The distinction in categorization of communities as “engineered” or “natural” becomes blurred in some cases. Wastewater treatment facilities (Adrados et al., 2014; Bernstein et al., 2014) and algal ponds (Park et al., 2011), for example, are engineered systems designed for a specific goal (i.e., water purification, biofuel production, or both) but are subject to environmental variations and influx of invasive species. Therefore, communities in natural and engineered environments, albeit structurally different, could be regarded as similar systems (subject to regular or episodic perturbations) to which an integrated concept of resilience could be applied.

Toward this end, the theoretical underpinnings of the engineering and ecological concepts need to be understood more fundamentally.

## RESILIENCE OF COMPOSITION, FUNCTION, AND THE COMMUNITY-ENVIRONMENT RELATIONSHIP

In principle, though the resilience of any system variable could be evaluated, a more fundamental question is at what level resilience is an intrinsic property of microbial communities (i.e., endogenous state or system function) and how state changes feed back to function. This issue has been extensively addressed by Kitano in regards to the robustness of biological systems (Kitano, 2004, 2007). He made a clear distinction between homeostasis and robustness, highlighting functional robustness as a property ubiquitously observed in biological systems, which often change in internal structure and mode of operation to preserve specific system functions against perturbation. We posit that Kitano's assertion, formulated to describe the behavior of single organisms, can be extended to describe the behavior of microbial communities. Thus, the translation of Rölting et al. (2007) can be extended from enzymes in the cell to microbial species in a community.

In contrast to single organisms, microbial communities rarely have obvious *physical* boundaries that circumscribe the system, although locality of interactions is a hallmark of such communities (*sensu* Konopka) (Konopka, 2009). We could, however, assume a *hypothetical* boundary encompassing all interacting species and treat the community as a supra-organism, though, in practice, community boundaries are operationally defined. The individual components that constitute such a supra-organism can then, *in toto*, be considered to be the system's state variables, which include relative abundances of individual species, energy and material exchange across species (i.e., interspecies metabolic interactions), organismal gene expression patterns, and so forth. Community-level functions are then aggregate properties, such as the total growth rate and net uptake or production rates of metabolites. In practical terms, when discussing the resilience of microbial communities, it is the observer's task to unambiguously define both the system boundary and the function of interest measured in the community within that boundary. Theoretically, any variable or component of the community may be defined as the function of interest, and resilience of that function is necessarily relative to a specific perturbation. This is the "What to What?" approach detailed by Carpenter et al. (2001), which alleviates confusion of what quantified resilience signifies by supplying details regarding the system, the observed function, the cause and scale of perturbation, and the dimension of recovery.

Following Kitano, we argue that resilience is an intrinsic property of microbial communities that recover system-level functions after perturbation, instead of recovering a given endogenous state. Two related sub-hypotheses (SH) can be distinguished. SH1: the probability of a given community

function being resilient (that is, capable of regaining its pre-perturbation value) is *hierarchical* (i.e.,  $p_{comm} > p_{spec} > p_{subcell}$ , where  $p_{comm}$ ,  $p_{spec}$ , and  $p_{subcell}$  denote those probabilities of community-level, species-level, and subcellular variables, respectively), and SH2: the probability gap for functional resilience at different levels of organization is unequal (i.e.,  $p_{comm} - p_{spec} < p_{spec} - p_{subcell}$ ). Together, these hypotheses imply that: (1) the intracellular state of an organism may change without affecting organism-level functions; (2) the function of organisms may change without impacting community-level functions; and (3) changes in community-level function happen at a relatively lower frequency than in organism-level function, which occur at lower frequency than intracellular state changes. While cases where this does not hold exist (e.g., Faith et al., 2011), examples for SH1 are commonly observed, e.g., changes in gene expression patterns are more susceptible to environmental variation than microbial growth rates and metabolic flux distributions (Ishii et al., 2007; Tang et al., 2009; Song et al., 2014b, 2015). Likewise, the resilience and functional stability in communities often arise as a result of significant compositional changes (Konopka et al., 2014). SH2 examples include cases where resilience of a community's composition and its function are closely linked, i.e., the gap between  $p_{comm}$  and  $p_{spec}$  is small. In a number of cases reported in the literature, the compositional resilience in microbial communities is shown to be comparable to functional resilience (Allison and Martiny, 2008; Shade et al., 2012a). Indeed, overall community function would be affected by compositional change even in cases where the role of one species can be replaced by other functionally-redundant members, unless the loss is not *quantitatively* compensated. It should be noted, however, that composition-function relationships depend on many factors including the specific function of interest, how many taxa perform the chosen function, and in what regime experimental data were collected. Thus, although we uphold the position that microbial communities are more likely to recover function, rather than composition, we regard compositional change as a potential governing mechanism of the whole system's resilience. To illustrate how community-level function can be maintained by changing internal state, we constructed a tutorial network representing a microbial community and simulated its responses to changes in environmental variables (Supplementary Material).

With a focus on the community-level performance, we restate the engineering concept of resilience as the rate of the system's recovery of its pre-perturbation *function*. This function-centered concept is linked to the ecological concept because the latter tolerates state changes that do not impact the overall function of interest. While exceptions exist, the tolerable magnitude of disturbance (the ecological concept) and the system dynamics (the engineering concept) are correlated around tipping points, i.e., systems nearing tipping points display peculiar behaviors such as slow recovery and magnified variations of state and functions (Dai et al., 2013). Thus, slow recovery of the ecosystem from disturbance may be an indicator of approaching a tipping point (Van Nes and Scheffer, 2007; Dai et al., 2012; Griffiths and Philippot, 2013; Dakos and Bascompte, 2014). The function-based view also expands the concept of a domain of attraction

in ecological resilience. The stability landscape in **Figure 1C**, for example, shows three distinct domains of attraction. Suppose that the community performance at each regime is measured as  $F_1$ ,  $F_2$ , and  $F_3$  ( $F_1 \approx F_2 > F_3$ ), and its initial state is  $S_1$ . In this case, we can consider the community to display resilience if the system returns (after perturbation) either to Regime 1 or to Regime 2. In this regard, Regimes 1 and 2 may be taken together as essentially the same functional domain.

Assessing resilience is challenging when microbial communities are subject to slow, chronic perturbation (e.g., climate change), or periodic environmental disturbances (e.g., temperature change during diel or seasonal cycles). Under such circumstances where the system's state, functions, and stability landscape are continually changing, it becomes unclear how to define a "pre-perturbed" condition for engineering resilience and a domain of attraction for ecological resilience. With respect to environmental variations that are much slower than the system's intrinsic dynamics, microbial communities may have sufficient time to adapt their endogenous state to the environment. We argue that this is the reason why some communities develop a stable relationship with their environment. Furthermore, the regularity in the relationship between environmental variation and the community's functional response is a fundamental aspect of resilience in that it applies to both fluctuating and constant environments. That is, microbial communities can be said to exhibit resilience as long as their functional interactions with the environment are reproducibly observed (Fuhrman et al., 2015). This idea of *relational resilience* (i.e., resilience of the relationship between environmental conditions and community function) provides fresh insight into system behavior at and around tipping points. On the left panel of **Figure 1D**, two stable branches of the hysteresis curve denote two unique relationships between the community function and environment. A tipping point is then defined as the condition across which a shift in the community-environment interaction occurs. Such non-linear hysteresis behavior has been observed in laboratory (Kim et al., 2012; Song and Ramkrishna, 2013) and ecological systems, e.g., coral reef-dominated vs. macroalgae-dominated state (Hughes et al., 2010); tropical forest vs. savanna vs. treeless state (Hirota et al., 2011). Early detection of nearby tipping points in ecosystems is therefore of practical importance before transition to an undesirable state and potentially permanent loss of critical functions. It may happen that key member species are lost during steady or abrupt change in environmental conditions. The resulting reduced diversity may lead to the change of stability landscape and subsequently the shape of the hysteresis curve so that catastrophic transition is very slow to recover or even *irreversible* (the right panel of **Figure 1D**). In this case, directly restoring lost members could be required to recover the systems' original functionalities. For example, pseudomembranous colitis is a condition in which *Clostridium difficile* dominates the gut microbiome after antibiotic treatment suppresses the normal, commensal microbiota. The measurable diversity of the *C. difficile*-dominated gut community is reduced compared with healthy controls (Song et al., 2013; Schubert et al., 2014), and large populations of *C. difficile* are difficult for normal commensal organisms to displace as these organisms enter

the gut. Restoring members lost from the community through fecal transplantation has been effective in rapidly restoring the dysbiotic gut community to a more normal microbiome (Weingarden et al., 2015). Although restoring lost diversity imparts resilience to the community, similar approaches may be difficult for large-scale ecosystems, highlighting the importance of detecting diversity loss through continual monitoring and predicting the effects of environmental changes on community- and ecosystem-level responses.

## CONCLUSIONS AND FUTURE RESEARCH NEEDS

Moving toward an integrated framework for understanding microbial community resilience, we propose reconciling concepts of engineering and ecological resilience through (1) consideration of microbial communities as systems that undergo both elastic and plastic deformation, and (2) defining resilience as the rate of recovery of a function of interest. Refocusing on the system's fundamental characteristics (such as the community-level functions and community-environment relationships) not only minimizes conceptual variation across different resilience definitions, but also provides a deeper understanding of the intrinsic community properties. In parallel, from a practical point of view, it is also of great importance to develop rational methods for quantifying microbial community resilience and predicting approaching tipping points.

Future research will need to address several important, unresolved issues—primarily, the identification of fundamental mechanisms responsible for microbial community resilience. For example, redundancy, diversity, and modularity are frequently advanced as mechanisms for robustness in complex systems (Kitano, 2004), but in some cases, and particularly in structurally simple consortia, they may not be directly related to resilience. The question remains: what unifying mechanisms impart resilience across both structurally simple and complex microbial communities? While the concept of networked buffering offers a potential mechanism (Whitacre and Bender, 2010; Konopka et al., 2014), rigorous analysis of microbial communities has yet to be performed. Another issue is the possible occurrence of trade-offs between system robustness (or resilience) and performance (Kitano, 2007) or trade-offs between robustness with respect to distinct perturbations (e.g., the conservation principle as discussed by Doyle and colleagues; Carlson and Doyle, 1999; Csete and Doyle, 2002). One major question is to what degree do resilience mechanisms identified for microbial communities overcome such trade-offs? Finally, the principles for structural organization of microbial communities as robust networks need to be further examined, as little is known about the general topological characteristics of microbial association networks and their relationships to resilience. Critical questions include: how does the compartmentalization of genes into a network of species affect the structural and higher-order properties of microbial communities; and are microbial community properties better understood as networks of species or networks of genes? Future research focusing on

these issues will significantly advance our capability for the design, prediction, and control of microbial communities and maintenance of the critical ecosystem services they provide.

## ACKNOWLEDGMENTS

This research was supported by the Genomic Science Program (GSP), Office of Biological and Environmental Research (OBER), U.S. Department of Energy (DOE), and is a contribution of the Pacific Northwest National Laboratory (PNNL)

## REFERENCES

- Adrados, B., Sánchez, O., Arias, C. A., Becares, E., Garrido, L., Mas, J., et al. (2014). Microbial communities from different types of natural wastewater treatment systems: vertical and horizontal flow constructed wetlands and biofilters. *Water Res.* 55, 304–312. doi: 10.1016/j.watres.2014.02.011
- Allison, S. D., and Martiny, J. B. H. (2008). Resistance, resilience, and redundancy in microbial communities. *Proc. Natl. Acad. Sci. U.S.A.* 105, 11512–11519. doi: 10.1073/pnas.0801925105
- Bernstein, H. C., Kesaano, M., Moll, K., Smith, T., Gerlach, R., Carlson, R. P., et al. (2014). Direct measurement and characterization of active photosynthesis zones inside wastewater remediating and biofuel producing microalgal biofilms. *Bioresour. Technol.* 156, 206–215. doi: 10.1016/j.biortech.2014.01.001
- Braundmeier, A. G., Lenz, K. M., Inman, K. S., Chia, N., Jeraldo, P., Walther-Antônio, M. R., et al. (2015). Individualized medicine and the microbiome in reproductive tract. *Front. Physiol.* 6:97. doi: 10.3389/fphys.2015.00097
- Carlson, J. M., and Doyle, J. (1999). Highly optimized tolerance: a mechanism for power laws in designed systems. *Phys. Rev. E* 60, 1412–1427. doi: 10.1103/PhysRevE.60.1412
- Carpenter, S., Walker, B., Anderies, J. M., and Abel, N. (2001). From metaphor to measurement: resilience of what to what? *Ecosystems* 4, 765–781. doi: 10.1007/s10021-001-0045-9
- CARRI Report (2013). *Definitions of Community Resilience: An Analysis*. Available online at: <http://www.resilientus.org/wp-content/uploads/2013/08/definitions-of-community-resilience.pdf>
- Csete, M. E., and Doyle, J. C. (2002). Reverse engineering of biological complexity. *Science* 295, 1664–1669. doi: 10.1126/science.1069981
- Dai, L., Korolev, K. S., and Gore, J. (2013). Slower recovery in space before collapse of connected populations. *Nature* 496, 355–358. doi: 10.1038/nature12071
- Dai, L., Vorselen, D., Korolev, K. S., and Gore, J. (2012). Generic indicators for loss of resilience before a tipping point leading to population collapse. *Science* 336, 1175–1177. doi: 10.1126/science.1219805
- Dakos, V., and Bascompte, J. (2014). Critical slowing down as early warning for the onset of collapse in mutualistic communities. *Proc. Natl. Acad. Sci. U.S.A.* 111, 17546–17551. doi: 10.1073/pnas.1406326111
- Faith, J. J., McNulty, N. P., Rey, F. E., and Gordon, J. I. (2011). Predicting a human gut microbiota's response to diet in gnotobiotic mice. *Science* 333, 101–104. doi: 10.1126/science.1206025
- Falkowski, P. G., Fenchel, T., and Delong, E. F. (2008). The microbial engines that drive Earth's biogeochemical cycles. *Science* 320, 1034–1039. doi: 10.1126/science.1153213
- Fuhrman, J. A., Cram, J. A., and Needham, D. M. (2015). Marine microbial community dynamics and their ecological interpretation. *Nat. Rev. Microbiol.* 13, 133–146. doi: 10.1038/nrmicro3417
- Griffiths, B. S., and Philippot, L. (2013). Insights into the resistance and resilience of the soil microbial community. *FEMS Microbiol. Rev.* 37, 112–129. doi: 10.1111/j.1574-6976.2012.00343.x
- Grimm, V., and Calabrese, J. M. (2011). "What is resilience? A short introduction," in *Viability and Resilience of Complex Systems: Concepts, Methods, and Case Studies from Ecology and Society*, eds G. Deffuant and N. Gilbert (New York, NY: Springer), 3–13.
- Grimm, V., and Wissel, C. (1997). Babel, or the ecological stability discussions: an inventory and analysis of terminology and a guide for avoiding confusion. *Oecologia* 109, 323–334. doi: 10.1007/s004420050090
- Hirota, M., Holmgren, M., Van Nes, E. H., and Scheffer, M. (2011). Global resilience of tropical forest and savanna to critical transitions. *Science* 334, 232–235. doi: 10.1126/science.1210657
- Holling, C. S. (1973). Resilience and stability of ecological systems. *Annu. Rev. Ecol. Syst.* 4, 1–23. doi: 10.1146/annurev.es.04.110173.000245
- Hooper, D. U., Chapin, F. S., Ewel, J. J., Hector, A., Inchausti, P., Lavorel, S., et al. (2005). Effects of biodiversity on ecosystem functioning: a consensus of current knowledge. *Ecol. Monogr.* 75, 3–35. doi: 10.1890/04-0922
- Hughes, T. P., Graham, N. A. J., Jackson, J. B.C., Mumby, P. J., and Steneck, R. S. (2010). Rising to the challenge of sustaining coral reef resilience. *Trends Ecol. Evol.* 25, 633–642. doi: 10.1016/j.tree.2010.07.011
- Ishii, N., Nakahigashi, K., Baba, T., Robert, M., Soga, T., Kanai, A., et al. (2007). Multiple high-throughput analyses monitor the response of *E. coli* to perturbations. *Science* 316, 593–597. doi: 10.1126/science.1132067
- Kim, J. I., Song, H. S., Sunkara, S. R., Lali, A., and Ramkrishna, D. (2012). Exacting predictions by cybernetic model confirmed experimentally: steady state multiplicity in the chemostat. *Biotechnol. Prog.* 28, 1160–1166. doi: 10.1002/btpr.1583
- Kitano, H. (2004). Biological robustness. *Nat. Rev. Genet.* 5, 826–837. doi: 10.1038/nrg1471
- Kitano, H. (2007). Towards a theory of biological robustness. *Mol. Syst. Biol.* 3, 137. doi: 10.1007/978-3-540-31339-7\_4
- Konopka, A. (2009). What is microbial community ecology? *ISME J.* 3, 1223–1230. doi: 10.1038/ismej.2009.88
- Konopka, A., Lindemann, S., and Fredrickson, J. (2014). Dynamics in microbial communities: unraveling mechanisms to identify principles. *ISME J.* 9, 1488–1495. doi: 10.1038/ismej.2014.251
- Levin, S. A., and Lubchenco, J. (2008). Resilience, robustness, and marine ecosystem-based management. *Bioscience* 58, 27–32. doi: 10.1641/B580107
- Lindemann, S. R., Moran, J. J., Stegen, J. C., Renslow, R. S., Hutchison, J. R., Cole, J. K., et al. (2013). The epsomitic phototrophic microbial mat of Hot Lake, Washington: community structural responses to seasonal cycling. *Front. Microbiol.* 4:323. doi: 10.3389/fmicb.2013.00323
- Lone, A. G., Atci, E., Renslow, R., Beyenal, H., Noh, S., Fransson, B., et al. (2015). *Staphylococcus aureus* induces hypoxia and cellular damage in porcine dermal explants. *Infect. Immun.* 83, 2531–2541. doi: 10.1128/IAI.03075-14
- Lucas, R., Kuchenbuch, A., Fetzer, I., Harms, H., and Kleinstueber, S. (2015). Long-term monitoring reveals stable and remarkably similar microbial communities in parallel full-scale biogas reactors digesting energy crops. *FEMS Microbiol. Ecol.* 91:fiv004. doi: 10.1093/femsec/fiv004
- Nazaries, L., Pan, Y., Bodrossy, L., Baggs, E. M., Millard, P., Murrell, J. C., et al. (2013). Evidence of microbial regulation of biogeochemical cycles from a study on methane flux and land use change. *Appl. Environ. Microbiol.* 79, 4031–4040. doi: 10.1128/AEM.00095-13
- Park, J. B. K., Craggs, R. J., and Shilton, A. N. (2011). Wastewater treatment high rate algal ponds for biofuel production. *Bioresour. Technol.* 102, 35–42. doi: 10.1016/j.biortech.2010.06.158
- Röling, W. F. M., Van Breukelen, B. M., Bruggeman, F. J., and Westerhoff, H. V. (2007). Ecological control analysis: being(s) in control of mass flux and metabolite concentrations in anaerobic degradation processes. *Environ. Microbiol.* 9, 500–511. doi: 10.1111/j.1462-2920.2006.01167.x

## SUPPLEMENTARY MATERIAL

The Supplementary Material for this article can be found online at: <http://journal.frontiersin.org/article/10.3389/fmicb.2015.01298>

- Sassone-Corsi, M., and Raffatellu, M. (2015). No vacancy: how beneficial microbes cooperate with immunity to provide colonization resistance to pathogens. *J. Immunol.* 194, 4081–4087. doi: 10.4049/jimmunol.1403169
- Schubert, A. M., Rogers, M. A. M., Ring, C., Mogle, J., Petrosino, J. P., and Schloss, P.D. (2014). Microbiome data distinguish patients with *Clostridium difficile* infection and non-*C. difficile*-associated diarrhea from healthy controls. *MBio* 5:e01021. doi: 10.1128/mBio.01021-14
- Shade, A., Peter, H., Allison, S. D., Baho, D. L., Berga, M., Bürgmann, H., et al. (2012a). Fundamentals of microbial community resistance and resilience. *Front. Microbiol.* 3:417. doi: 10.3389/fmicb.2012.00417
- Shade, A., Read, J. S., Youngblut, N. D., Fierer, N., Knight, R., Kratz, T. K., et al. (2012b). Lake microbial communities are resilient after a whole-ecosystem disturbance. *ISME J.* 6, 2153–2167. doi: 10.1038/ismej.2012.56
- Song, H.-S., Cannon, W. R., Beliaev, A. S., and Konopka, A. (2014a). Mathematical modeling of microbial community dynamics: a methodological review. *Processes* 2, 711–752. doi: 10.3390/pr2040711
- Song, H.-S., McClure, R. S., Bernstein, H. C., Overall, C. C., Hill, E. A., and Beliaev, A. S. (2015). Integrated *in silico* analyses of regulatory and metabolic networks of *Synechococcus* sp. PCC 7002 reveal relationships between gene centrality and essentiality. *Life* 5, 1127–1140. doi: 10.3390/life5021127
- Song, H.-S., and Ramkrishna, D. (2013). Complex nonlinear behavior in metabolic processes: global bifurcation analysis of *Escherichia coli* growth on multiple substrates. *Processes* 1, 263–278. doi: 10.3390/pr1030263
- Song, H.-S., Reifman, J., and Wallqvist, A. (2014b). Prediction of metabolic flux distribution from gene expression data based on the flux minimization principle. *PLoS ONE* 9:e112524. doi: 10.1371/journal.pone.0112524
- Song, Y., Garg, S., Girotra, M., Maddox, C., Von Rosenvinge, E. C., Dutta, A., et al. (2013). Microbiota dynamics in patients treated with fecal microbiota transplantation for recurrent *Clostridium difficile* infection. *PLoS ONE* 8:e81330. doi: 10.1371/journal.pone.0081330
- Strom, S. L. (2008). Microbial ecology of ocean biogeochemistry: a community perspective. *Science* 320, 1043–1045. doi: 10.1126/science.1153527
- Tang, Y. J., Martin, H. G., Deutschbauer, A., Feng, X. Y., Huang, R., Llorca, X., et al. (2009). Invariability of central metabolic flux distribution in *Shewanella oneidensis* MR-1 under environmental or genetic perturbations. *Biotechnol. Prog.* 25, 1254–1259. doi: 10.1002/btpr.227
- Tas, N., Prestat, E., McFarland, J. W., Wickland, K. P., Knight, R., Berhe, A. A., et al. (2014). Impact of fire on active layer and permafrost microbial communities and metagenomes in an upland Alaskan boreal forest. *ISME J.* 8, 1904–1919. doi: 10.1038/ismej.2014.36
- Van Nes, E. H., and Scheffer, M. (2007). Slow recovery from perturbations as a generic indicator of a nearby catastrophic shift. *Am. Nat.* 169, 738–747. doi: 10.1086/516845
- Veraart, A. J., Faassen, E. J., Dakos, V., van Nes, E. H., Lürling, M., and Scheffer, M. (2012). Recovery rates reflect distance to a tipping point in a living system. *Nature* 481, 357–359. doi: 10.1038/nature11029
- Weingarden, A., González, A., Vázquez-Baeza, Y., Weiss, S., Humphry, G., Berg-Lyons, D., et al. (2015). Dynamic changes in short- and long-term bacterial composition following fecal microbiota transplantation for recurrent *Clostridium difficile* infection. *Microbiome* 3, 10. doi: 10.1186/s40168-015-0070-0
- Whitacre, J. M., and Bender, A. (2010). Networked buffering: a basic mechanism for distributed robustness in complex adaptive systems. *Theor. Biol. Med. Model.* 7:20. doi: 10.1186/1742-4682-7-20
- Whitman, W. B., Coleman, D. C., and Wiebe, W. J. (1998). Prokaryotes: the unseen majority. *Proc. Natl. Acad. Sci. U.S.A.* 95, 6578–6583. doi: 10.1073/pnas.95.12.6578

**Conflict of Interest Statement:** The authors declare that the research was conducted in the absence of any commercial or financial relationships that could be construed as a potential conflict of interest.

Copyright © 2015 Song, Renslow, Fredrickson and Lindemann. This is an open-access article distributed under the terms of the Creative Commons Attribution License (CC BY). The use, distribution or reproduction in other forums is permitted, provided the original author(s) or licensor are credited and that the original publication in this journal is cited, in accordance with accepted academic practice. No use, distribution or reproduction is permitted which does not comply with these terms.



# Incorporating the soil environment and microbial community into plant competition theory

Po-Ju Ke<sup>1,2\*</sup> and Takeshi Miki<sup>2,3</sup>

<sup>1</sup> Department of Biology, Stanford University, Stanford, CA, USA, <sup>2</sup> Institute of Oceanography, National Taiwan University, Taipei, Taiwan, <sup>3</sup> Research Center for Environmental Changes, Academia Sinica, Taipei, Taiwan

## OPEN ACCESS

### Edited by:

Yasuhisa Saito,  
Shimane University, Japan

### Reviewed by:

James C. Stegen,  
Pacific Northwest National Lab, USA  
Satoshi Tsuneda,  
Waseda University, Japan

### \*Correspondence:

Po-Ju Ke,  
Department of Biology, Stanford  
University, 371 Serra Mall, Stanford,  
CA 94305, USA  
pojuke@stanford.edu

### Specialty section:

This article was submitted to  
Systems Microbiology,  
a section of the journal  
Frontiers in Microbiology

**Received:** 04 January 2015

**Accepted:** 17 September 2015

**Published:** 08 October 2015

### Citation:

Ke P-J and Miki T (2015) Incorporating  
the soil environment and microbial  
community into plant competition  
theory. *Front. Microbiol.* 6:1066.  
doi: 10.3389/fmicb.2015.01066

Plants affect microbial communities and abiotic properties of nearby soils, which in turn influence plant growth and interspecific interaction, forming a plant-soil feedback (PSF). PSF is a key determinant influencing plant population dynamics, community structure, and ecosystem functions. Despite accumulating evidence for the importance of PSF and development of specific PSF models, different models are not yet fully integrated. Here, we review the theoretical progress in understanding PSF. When first proposed, PSF was integrated with various mathematical frameworks to discuss its influence on plant competition. Recent theoretical models have advanced PSF research at different levels of ecological organizations by considering multiple species, applying spatially explicit simulations to examine how local-scale predictions apply to larger scales, and assessing the effect of PSF on plant temporal dynamics over the course of succession. We then review two foundational models for microbial- and litter-mediated PSF. We present a theoretical framework to illustrate that although the two models are typically presented separately, their behavior can be understood together by invasibility analysis. We conclude with suggestions for future directions in PSF theoretical studies, which include specifically addressing microbial diversity to integrate litter- and microbial-mediated PSF, and apply PSF to general coexistence theory through a trait-based approach.

**Keywords:** coexistence, litter-mediated feedback, Lotka-Volterra model, microbial-mediated feedback, invasibility analysis, spatial-explicit model

## Introduction

One of the fundamental goals of plant ecology is to understand the maintenance mechanisms of plant species coexistence (Chesson, 2000). Many hypotheses have been proposed, including the resource competition theory (Hsu et al., 1977; Tilman et al., 1981), two-way trade-off models (Tilman, 1994), and the three-way trade-off strategy model (Grime, 1977). Other theories, such as the neutral theory (Hubbell, 1997) and the metacommunity theory (Leibold et al., 2004), address stochastic and spatial processes as well as deterministic processes. These theoretical frameworks and subsequent accepted viewpoints in plant ecology implicitly rely on environmental determinism (i.e., a unidirectional effect of the abiotic environment on the plant community and unidirectional adaptation of organisms to the given environment). This concept is widely accepted despite the fact Tansley (1935), a plant ecologist, first proposed the term “ecosystem” precisely to address feedback among organisms and the abiotic environment. The resource competition theory (Tilman, 1982) examines the effect of individuals on environmental resource availability, however its competitive

outcome depends on rates of external resource supply. An alternative investigative approach in plant community ecology, plant-soil-feedback (PSF), emphasizes the bidirectional interaction between growth limiting factors in soil and plant population and community dynamics (Berendse, 1994; Bever et al., 1997). Plants can affect soil properties, which in turn alter plant growth, survival, reproduction, and competition, subsequently acting as the driving forces for community composition and function. In this sense, Jones et al. (1994) appropriately characterized plants as fundamental ecosystem engineers.

Theoretical advances in PSF research have primarily focused on two major drivers: soil microbes and soil nutrients (see Ehrenfeld et al., 2005 for other factors, and van der Putten et al., 2013 for a comprehensive empirical review). Soil microbes interact with plants, providing diverse functional roles and are responsible for “microbial-mediated” PSF. Plants ‘cultivate’ local microbial communities surrounding plant roots (i.e., species-specific root-associated microbes, including beneficial and detrimental groups), which in turn affects plant performance (Bever et al., 1997; Bever, 2003). On the other hand, the feedback mechanisms mediating soil nutrient availability and the subsequent nutrient cycling between above- and below-ground ecosystem components are often referred to as “litter-mediated” PSF. Soil nutrient availability is determined by organic carbon and plant litter mineralization, which is controlled by plant species specific traits (e.g., litter production rate and its chemistry, Binley and Giardina, 1998) and can influence plant competition outcome (Berendse et al., 1987, 1989; Berendse, 1994). Although, the two mechanisms are commonly discussed individually, under some scenarios, the two main mechanisms are shown to interact and are in fact tightly linked. For example, litter-mediated PSF is also mediated by soil microbial decomposers such as saprophytic bacteria and fungi (Miki et al., 2010; Miki, 2012).

Although, empirical studies have increased our general understanding of PSF, many ecological models are constructed to examine PSF processes for specific species or ecosystems. General PSF mathematical theory remains under-explored, thus hindering comprehensive understanding of the importance of PSF and the roles of belowground microbial-mediated processes in structuring terrestrial ecosystems. Clearly, PSF theory requires development to better understand various plant community properties, including the number of coexisting species (e.g., Molofsky and Bever, 2002; Mazzoleni et al., 2010), species abundance and distribution (e.g., Mack and Bever, 2014), transient successional patterns (e.g., Fukami and Nakajima, 2013), and species spatial and temporal distribution (e.g., Molofsky et al., 2002).

In this article, we summarize how PSF concepts have been integrated into ecological modeling studies, with particular focus on topics related to plant species coexistence and spatio-temporal dynamics (see **Table 1** for a list of theoretical studies along with their corresponding modeling framework category). We subsequently reanalyzed two fundamental mechanistic PSF models (i.e., Berendse, 1994; Bever et al., 1997), which are the foundation of current theoretical models, and compared

them with the classic Lotka-Volterra competition model. Our results demonstrated how the application of invasibility analysis elucidated behaviors of different PSF models by generating coexistence criteria with similar ecological interpretation. Moreover, invasibility analysis provided superior ideas for soil-centered (or microbe-centered) views in PSF studies, resulting in a revised PSF metric which will aid in future theoretical development in microbial ecology. Finally, we proposed new research directions to integrate litter- and microbial-mediated PSF, and apply trait-based modeling approaches to predict species’ PSF and coexistence.

## Theoretical Development and Modeling Achievements for PSF

### PSF Effects on Plant Competition Outcome and Species Coexistence

Theoretical PSF studies were first proposed to examine how PSF contributes to the coexistence of competing plant species. Bever et al. (1997) (hereafter Bever’s model) conducted pioneering research leading to the microbial-mediated PSF model, which incorporated reciprocal interactions and frequency dependency among plants and soil microbial communities. Bever’s model proposed that the final fate of a plant community can be predicted by the overall effect of soil microbial communities on both plant species (i.e., an interaction coefficient,  $I_S$ ). Bever’s model predicted that two plant species can coexist cyclically due to microbial-mediated PSF when both species generate PSF which decreases its relative growth rate (i.e., negative microbial-mediated PSF in terms of negative  $I_S$ ). However, the model predicted that single species dominance is reached when both plants species generate PSF which increases its relative growth rate (i.e., positive microbial-mediated PSF in terms of positive  $I_S$ ). It is important to note that the community-level outcome of PSF (i.e., predicted by the sign of  $I_S$ ) cannot be directly inferred by the interaction type between soil microbes and its host (Bever et al., 1997). For example, if the mycorrhizal fungi delivers more benefit to the competitor compared to that to its host, competing plant species can coexist as PSF would decrease the relative growth rate of its host (i.e., negative  $I_S$  despite positive plant-microbe interaction; Bever, 1999, 2002; Umbanhowar and McCann, 2005). Likewise, pathogens can increase the relative growth rate of its host and result in single species dominance if it has stronger suppression on the growth of the competitor (i.e., positive  $I_S$  despite negative interaction with its host). A later version of Bever’s model incorporated PSF into a two species Lotka-Volterra model and demonstrated coexistence can be promoted by a negative PSF, even under strong competitive interactions and fitness differences between the two plant species (Bever, 2003). Individual-based simulation models incorporating the PSF concept made similar predictions (Bonanomi et al., 2005; Petermann et al., 2008), and further suggested that the magnitude of population oscillations depends on negative PSF strength. However, Revilla et al. (2013) performed a complete analysis of Bever’s model and suggested population cycling under negative PSF (i.e., in terms of negative  $I_S$ , a modified

**TABLE 1 | Theoretical plant-soil feedback models reviewed in this article.**

Author (year)	Main PSF mechanisms (model type) <sup>†</sup>	Study detail (plant community processes) <sup>§</sup>
Adler and Muller-Landau, 2005	Microbial-PSF <sup>a</sup>	Plant and natural enemy dispersal distance (SS, SD)
Aguilera, 2011	Microbial-PSF <sup>b</sup>	Density-dependency of plant microbe interactions (PI)
Berendse et al., 1987	Litter-PSF <sup>b</sup>	Species-specific litter chemistry (SC)
Berendse et al., 1989	Litter-PSF <sup>b</sup>	Species-specific litter chemistry (SC)
Berendse, 1994	Litter-PSF <sup>b</sup>	Species-specific litter chemistry (SC)
Bever et al., 1997	Microbial-PSF <sup>b</sup>	LV-type plant-microbe interactions (SC)
Bever, 1999	Microbial-PSF <sup>b</sup>	LV-type plant-microbe interactions (SC)
Bever, 2003	Microbial-PSF <sup>b</sup>	LV-type plant-microbe interactions (SC)
Bever et al., 2010	Microbial-PSF <sup>b</sup>	Microbial-mediated plant niche partitioning and PSF (SC)
Bonanomi et al., 2005	No specific mechanism <sup>a</sup>	Negative PSF and population dynamics (SC, SD)
Clark et al., 2005	Litter-PSF <sup>b</sup>	Species-specific litter chemistry (SC)
Daufresne and Hedin, 2005	Litter-PSF <sup>b</sup>	Resource ratio hypothesis and nutrient cycling (SC)
Dickie et al., 2005	Microbial-PSF <sup>a</sup>	Distance-dependent interaction strength (SS)
Eppinga et al., 2006	Microbial-PSF <sup>b</sup>	Nonlinear LV-type plant-microbe interactions (PI)
Eppinga et al., 2011	Litter-PSF <sup>b</sup>	Species-specific litter chemistry and trait evolution (PI)
Eppstein et al., 2006	No specific mechanism <sup>a</sup>	Community dynamics and frequency dependency (SS, SC)
Eppstein and Molofsky, 2007	No specific mechanism <sup>b</sup>	Invasion dynamics and frequency dependency (PI, SC)
Fukami and Nakajima, 2013	No specific mechanism <sup>a</sup>	Transient dynamics and delayed convergence (SD)
Fukano et al., 2013	Microbial-PSF <sup>c</sup>	Disturbance regime (PI)
Kulmatiski et al., 2011	Microbial-PSF <sup>b</sup>	Multi-species LV-type plant microbe interaction (SC)
Kulmatiski et al., 2012	Microbial-PSF <sup>c</sup>	Multi-species biomass-explicit plant-microbe interaction (BEF)
Loeuille and Leibold, 2014	No specific mechanism <sup>a</sup>	Species diversification and macro-ecological patterns (SD)
Levine et al., 2006	Microbial-PSF <sup>d</sup>	Spatial scale and invasion velocity (PI, SS)
Mack and Bever, 2014	Microbial-PSF <sup>a</sup>	Plant dispersal and PSF interactions scale (SRA, SS)
Mangan et al., 2010	Microbial-PSF <sup>a</sup>	Negative PSF and Janzen-Connell hypothesis (SD, SRA)
Mazzoleni et al., 2010	Litter-PSF <sup>b</sup>	Autotoxicity and latitudinal diversity gradient (SD)
Miki and Kondoh, 2002	Litter-PSF <sup>b</sup>	Species-specific litter chemistry (PI, SC)
Miki et al., 2010	Litter- and microbial- PSF <sup>b</sup>	Decomposer diversity (SC)
Miki, 2012	Litter- and microbial- PSF <sup>b</sup>	Decomposer diversity (PI)
Molofsky et al., 2001	No specific mechanism <sup>a</sup>	Coexistence under positive PSF (SS, SC)
Molofsky and Bever, 2002	No specific mechanism <sup>a</sup>	Positive PSF and unsuitable habitats (SS, SD)
Molofsky et al., 2002	No specific mechanism <sup>a</sup>	Plant dispersal and PSF interactions scale (SS, SC)
Mordecai, 2013a	Microbial-PSF <sup>c</sup>	Generalist pathogen and pathogen spillover (SC)
Mordecai, 2013b	Microbial-PSF <sup>c</sup>	Generalist pathogen and pathogen spillover (SC)
Mordecai, 2015	Microbial-PSF <sup>c</sup>	Generalist pathogen and storage effect (SC)
Petermann et al., 2008	Microbial-PSF <sup>a</sup>	Janzen-Connell hypothesis (SD)
Revilla et al., 2013	Microbial-PSF <sup>b</sup>	LV-type plant-microbe interactions (SC)
Schnitzer et al., 2011	No specific mechanism <sup>b</sup>	LV-type plant-microbe interactions (BEF)
Sedio and Ostling, 2013	Microbial-PSF <sup>a</sup>	Natural enemy host specificity and Janzen-Connell hypothesis (SD)
Suding et al., 2013	No specific mechanism <sup>a</sup>	Invasion dynamics and enemy release (PI)
Turnbull et al., 2010	Microbial-PSF <sup>c</sup>	Invasive species spread (PI)
Umbanhowar and McCann, 2005	Microbial-PSF <sup>b</sup>	Plant-mycorrhizal fungi interactions (SC)
Zee and Fukami, 2015	No specific mechanism <sup>a</sup>	Species loss following habitat fragmentation (SD)

Studies are selected if it considers the effect of microbial-mediated PSF and/or litter-mediated PSF on plant competition outcome or community structure. As a result, models investigating the effect of plant-microbial interaction and nutrient cycling on the growth of a single plant species, as well as those focusing on disease dynamics, are not included.

<sup>†</sup> Model type: <sup>a</sup>stochastic cellular automata; <sup>b</sup>ordinary differential equations; <sup>c</sup>difference equations; <sup>d</sup>integrodifference equations. <sup>§</sup>Plant community process: SC, species coexistence; PI, plant invasion; BEF, biodiversity-ecosystem functioning relationship; SRA, species relative abundance; SD, species diversity; SS, spatial structure.

version of  $I_S$  in Bever's model) might occur in the form of heteroclinic cycles, which can enable stochastic extinction in real empirical systems. Recent theoretical studies with an emphasis on microbial-mediated PSF have also extended Bever's

model to multiple species (Bonanomi et al., 2005; Petermann et al., 2008; Kulmatiski et al., 2011, 2012). For example, a three-species version of Bever's model showed PSF played a critical role in predicting rank order abundance of experimental

plant communities, and the PSF model made better predictions compared with a pure competition model (Kulmatiski et al., 2011).

Theoretical studies on litter-mediated PSF investigated the influence of plant litter quality on soil nutrient availability, and how changes in soil nutrient availability alter plant competition (pioneered by Berendse et al., 1987, 1989; Berendse, 1994). When plants compete for a single growth limiting factor in the soil (e.g., inorganic nitrogen), a difference in plant growth response to different nutrient levels (i.e., a tradeoff) is often necessary for litter-mediated PSF to alter competitive outcomes (Miki and Kondoh, 2002; Clark et al., 2005). Berendse (1994) used ordinary differential equations to build simple ecosystem models to demonstrate community-level outcomes depended on a combination of the plant species' litter quality and nutrient uptake strategies. Plant species with growth advantages in nutrient-rich soils reinforced their dominance by producing rapidly decomposing litter. Similarly, plant species more competitive in nutrient-poor sites increased their dominance by producing slowly decomposing litter. Both trait combinations resulted in nutrient availability that favors the resident plant (i.e., positive litter-mediated PSF), leading to competitive exclusion of its competitor (Berendse, 1994), or alternative stable states differing in species composition (Clark et al., 2005) or species richness (Miki and Kondoh, 2002; Miki et al., 2010). In contrast, coexistence was facilitated if plant species influenced the nutrient cycle to reinforce the persistence of its competitor (i.e., negative litter-mediated PSF). Some studies integrated litter-mediated PSF with Tilman's (1982) resource ratio theory to consider multiple limiting factors in the soil and plant stoichiometry (Daufresne and Hedin, 2005; Eppinga et al., 2011). This theoretical framework also demonstrated that whether litter-mediated PSF enhances or suppresses coexistence was dependent on the trait combination of competing plants species (Daufresne and Hedin, 2005). Simple litter-mediated PSF models were also extended to examine more detailed nutrient cycling, emphasizing the importance of environmental factors (Miki and Kondoh, 2002), litter quality attributes other than decomposition rates (e.g., the recycled proportion, Clark et al., 2005), different plant-available nutrient types (Clark et al., 2005; Daufresne and Hedin, 2005), and litter effects other than soil nutrient availability (Eppinga et al., 2011) on community outcomes driven by litter-mediated PSF.

### PSF Models that Go Beyond Species Coexistence

Recent theoretical studies go beyond discussing coexistence of few plant species, and have applied PSF as a mechanism to explain other macro-scale community patterns (see Bever et al., 2010; van der Putten et al., 2013 and references therein). The relationship between PSF and plant diversity is one topic that has received a great deal of interest. Many empirical studies revealed negative microbial-mediated PSF acted as a mechanism for the Janzen-Connell hypothesis (Janzen, 1970; Connell, 1971), contributing to negative density-dependent (Bell et al., 2006; Yamazaki et al., 2008; Bagchi et al., 2010, 2014) and distance-dependent (Augspurger, 1983; Packer and Clay, 2000; Swamy and Terborgh, 2010) seedling mortality. These mortality patterns resulted from

negative PSF, which enhanced plant diversity; and simulation models suggested the greatest diversity was attained when natural enemies were host-specific (Sedio and Ostling, 2013). Furthermore, a species' relative abundance in a community was predicted by the PSF strength it experienced; plant species with lower abundance suffered stronger negative PSF (Klironomos, 2002; Mangan et al., 2010; but see Reinhart, 2012). Mangan et al. (2010) applied a spatially explicit cellular automata model to confirm the positive relationship between species' PSF strength and species relative abundance by parameterizing the model with field-measured PSF strength. Additional work on the model confirmed the positive relationship was robust for different forms of life-history tradeoffs (e.g., tradeoffs between mortality and establishment rates) (Mangan et al., 2010; Mack and Bever, 2014).

Large-scale studies suggested that the stronger negative microbial-mediated PSF at lower latitude regions contributed to its higher plant species richness (Johnson et al., 2012). Mazzoleni et al. (2010) constructed an ecosystem model considering "resource-waste" (i.e., "autotoxicity" via intra-specific toxic compounds, Mazzoleni et al., 2007) during litter decomposition as a source for negative litter-mediated PSF. Autotoxicity has the potential to suppress plant growth directly by harming plant tissue or indirectly by exacerbating detrimental pathogen effects (Mazzoleni et al., 2007, 2010; Bonanomi et al., 2010). The ecosystem model indicated that as litter decomposition rate increased from higher to lower latitude, so did the level of autotoxicity, generating stronger negative density-dependency and supporting higher species richness at lower latitudes. The model also showed that washing of autotoxicity removed negative PSF effects and decreased species richness, a potential mechanism to explain differences in plant species richness between flooded and non-flooded communities at the same latitude (Mazzoleni et al., 2010).

At the interface between community and ecosystem ecology, PSF was also proposed to contribute to the biodiversity-ecosystem functioning relationship, with particular focus on productivity (i.e., higher plant diversity leads to increased productivity, also known asoveryielding). Loreau and Hector (2001) attributed an asymptotic productivity increase to either sampling effect or niche complementary due to a rise in species diversity (Loreau and Hector, 2001; but see Hector et al., 1999; Miki, 2009; Cardinale et al., 2012 for diversity-productivity patterns other than asymptotically increase). Soil microbes, particularly host-specific pathogens, were recently proposed as another potential mechanism involved in the diversity-productivity relationship. Studies showed that negative density-dependent effect of pathogens were diluted as plant species diversity increased since the proportion of self-cultivated soil decreased, resulting in higher plant productivity (Maron et al., 2011; Schnitzer et al., 2011). Empirical studies supported this mechanism; compared with monocultures, plants overyield when grown in a soil mixture cultivated with different plant species (Kulmatiski et al., 2012; Hendriks et al., 2013), while sterilizing the soil eliminated the positive relationship (Maron et al., 2011; Schnitzer et al., 2011). In addition, Hendriks et al. (2015) found spatial heterogeneity in soil biota created by highly diverse

communities also contributed to plant avoidance of host-specific pathogens. Schnitzer et al. (2011) used a simple Lotka-Volterra type model to illustrate that the classic asymptotic diversity-productivity relationship appeared only in the presence of host-specific pathogens. The pathogen effects were stronger, and the plant productivity saturation point occurred at higher plant diversity, when operating together with niche complementary (i.e., comparing neutral and non-neutral models). Based on Bever's PSF model, Kulmatiski et al. (2012) developed a biomass-explicit multi-species PSF model to directly examine the influence of PSF on biomass production. Their model suggested that dilution of species-specific soil biota effects, resulting from increased plant diversity, can result in over- and under-yielding, depending on the sign of species' PSF (i.e., negative or positive, respectively). In addition, the negative relationship between PSF strength and over-yielding became stronger with increasing species richness. Empirical results supported model predictions, however results also indicated further information regarding plant community structure (e.g., presence or absence of nitrogen-fixing plants) would provide useful information for future studies (Kulmatiski et al., 2012). Although, theoretical studies linking microbial-mediated PSF and diversity-productivity relationships are growing, to our knowledge models related to this topic have not explicitly considered litter-mediated PSF and nutrient cycling.

Finally, the impact of PSF on invasion success has been another rapidly growing research area (empirical studies reviewed in Mitchell et al., 2006; Reinhart and Callaway, 2006; Inderjit and van der Putten, 2010; Suding et al., 2013). In general, PSF facilitates invasion when exotic plant species experience weaker negative PSF (or benefit from stronger positive PSF) compared to native plant species (Reinhart and Callaway, 2006). Keane and Crawley (2002) proposed the "enemy-release hypothesis," which stated that by migrating from their native range, exotic species escaped species-specific specialized natural pathogens. Consequently, exotic species experienced reduced negative microbial-mediated PSF in the new region and became successful invaders (Keane and Crawley, 2002; Klironomos, 2002; Mitchell and Power, 2003; Callaway et al., 2004). Further, theoretical studies suggested the effectiveness of enemy-release depended on the diversity of the native community (Turnbull et al., 2010), the functional response between plant growth and soil microbial density (Aguilera, 2011), the disturbance regime (Fukano et al., 2013), and the invader competitive ability on the native species' cultivated soil environment (Eppstein and Molofsky, 2007; Turnbull et al., 2010; Suding et al., 2013). In some cases, soil-borne pathogens might still facilitate invasion, even if the invader is not enemy-released. This happens when the invader attracts generalist pathogens, which have stronger negative effects on native plant species, a scenario termed the "enemy-accumulation hypothesis." This scenario was first proposed by Eppinga et al. (2006) using a non-linear extension of Bever's model to explain the success of *Ammophila arenaria* invasion in California, which was a successful invader despite suffering similar pathogen suppression as that in its native European range (Bever et al., 1997; Beckstead and Parker, 2003). The effects of generalist pathogens on plant

invasion have also been studied under the "pathogen spillover" hypothesis, where invasive plant species with greater pathogen tolerance gain advantage by transmitting the shared pathogens to less tolerant native plant species (Beckstead et al., 2010). Pathogen spillover can lead to competitive exclusion of natives, coexistence, or priority effects (Mordecai, 2013a,b). In addition to microbial-mediated PSF, litter-mediated PSF can also influence the outcome of exotic plant invasion. Specific combinations of litter decomposability and nutrient uptake strategies will generate positive litter-mediated PSF for the invader (Miki and Kondoh, 2002). When linking litter-mediated PSF with invasion, studies have also discussed its effect on resources other than soil nutrient. The effect of invader's litter on the local light environment has been of particular interest. Results of studies indicated that invaders' litter accumulation will decrease light availability by shading, while simultaneously increasing soil nutrient availability via litter decomposition. Studies suggested that the combined impact of invader litter facilitated invasion non-additively when the invader is a weaker competitor for soil nutrients but a better competitor for light (Farrer and Goldberg, 2009; Eppinga et al., 2011).

### The Importance of Spatial Scale on PSF Effects

One simplification made in many PSF models is the assumption of a well-mixed soil environment, which neglects the fact that plant dispersal and PSF usually operate locally. However, empirical evidence often revealed that the interaction between plants and soil microbes are highly distance-dependent and can influence plant spatial patterning (Augsburger, 1983; Packer and Clay, 2000; Reinhart et al., 2003; Dickie et al., 2005; Swamy and Terborgh, 2010). Eppstein et al. (2006) applied spatially explicit models to investigate the importance of space on PSF outcomes; results differed from the well-mixed models and provided new insights into the value of PSF and plant spatial patterning. In addition, the prediction from Bever's model regarding PSF sign and plant competition outcome had been extensively studied (Bever et al., 1997; Molofsky et al., 2001, 2002; Molofsky and Bever, 2002; also reviewed in Bever, 2003 and Bever et al., 2012). Molofsky et al. (2002) showed that under a spatially explicit modeling framework the prediction that negative PSF facilitated plant coexistence was generally not altered (but see Bever et al., 1997 for the case when two plants exhibited different dispersal ability). Plant coexistence was maintained by negative PSF, while a large array of different spatial patterns was observed, ranging from near random, clumped, to band formation distributions. The spatial patterning of competing plant species depends on the relative spatial scale of dispersal and PSF, as well as the negative PSF strength (Molofsky et al., 2002). However, the prediction that positive PSF leads to single species dominance was altered when considering the spatial aspects of PSF. Studies demonstrated that under certain initial conditions, positive PSF can lead to the formation of self-maintained monomorphic patches, promoting long-term coexistence at the regional scale via the maintenance of spatial heterogeneity (Molofsky et al., 2001; Molofsky and Bever, 2002). Moreover, the probability of species coexistence was greater when positive PSF existed compared with the absence of PSF (i.e., a neutral case), and coexistence was

more effectively maintained when positive PSF operated at a local scale (Molofsky et al., 2001; Molofsky and Bever, 2002). This unique prediction was maintained even when the model was generalized to consider asymmetric frequency-dependent strength between competing plant species (Eppstein et al., 2006). Dickie et al. (2005) demonstrated that mycorrhizal-generated positive PSF and plant-plant competition showed different distance-dependent patterns. By integrating empirical evidence into a spatially explicit model, results indicated a net mycorrhizal effect facilitating seedling growth occurred only at low plant densities, thus potentially promoting species coexistence and diversity (Dickie et al., 2005). These theoretical achievements suggested that when spatial structure of interactions was considered, the predicted species monoculture associated with positive PSF was mitigated and coexistence was maintained at larger spatial scales.

In addition to the coexistence patterns between two plant species, other macro-scale community patterns generated by PSF have also been examined under a spatial framework. By considering spatial structure and heterogeneous landscape (i.e., with unsuitable habitats conditions), Molofsky and Bever (2002) suggested that positive PSF can maintain community species diversity for a much longer time period if PSF operated at a local scale. For negative microbial-mediated PSF to effectively promote species richness, local microbial and plant dispersal was required to generate clumped adult distribution and strong negative density-dependency for seedling survival (Adler and Muller-Landau, 2005; Petermann et al., 2008). The positive relationship between species' PSF strength and its relative abundance (Mack and Bever, 2014), as well as evolutionary diversification (Loeuille and Leibold, 2014), were also only observed when the scale of negative PSF and plant dispersal were local. For exotic plant invasion, positive PSF created by the invader can promote its invasiveness when operating at a local scale, despite the counteracting positive PSF created by natives (Eppstein et al., 2006). However, Levine et al. (2006) showed for positive PSF to accelerate invasion velocity, the spatial scale of soil modification must be larger than that of the plant-plant competition.

Former studies typically considered positive or negative PSF separately, however recent models have begun to consider the spatial consequences of a complex PSF scenario (Fukami and Nakajima, 2013), where PSF affects plant growth positively for some species-pair, and negatively for others. Fukami and Nakajima (2013) evaluated compositional variation between patches with different initial compositions, and suggested a complex PSF scenario could maintain the initial variability in species composition for a longer period of time, contributing to regional plant diversity compared to a simpler PSF scenario. A complex PSF scenario also alleviated diversity loss caused by habitat fragmentation, and such buffering effects were greatest when plants dispersed locally. The mechanisms for such a buffering effect is because complex PSF decreased both spatial clustering of species distribution prior to habitat fragmentation and extinction probability after fragmentation, which would both be pronounced in the absence of PSF if plants dispersed locally (Zee and Fukami, 2015). In conclusion,

spatially explicit PSF models generated many useful predictions that cannot be revealed if a well-mixed soil environment was assumed, and suggested that the structuring ability of PSF strongly depends on the spatial scale of PSF and plant dispersal.

## Temporal Dynamics of PSF and its Effect on Plant Community Succession

The influence of PSF has primarily been examined in studies that focused on community properties in a single temporal snapshot, or implicitly assumed the community is at equilibrium (but see Mordecai, 2015, for the effects of generalist pathogens on plant species coexistence through a temporal storage effect). However, PSF also contributes to temporal dynamics and the development of plant communities. Most of our current knowledge in this area derives from successional studies (reviewed in Kardol et al., 2013; van der Putten et al., 2013). The following two concepts were proposed for the roles of PSF during succession: (i) the predictable and directional changes in PSF sign and strength (Kardol et al., 2006); and (ii) random-emergence of PSF (Fukami and Nakajima, 2013). The first dominant concept suggested that during succession, negative PSF was experienced by early-successional plant species and facilitated replacement by late-successional plant species (van der Putten et al., 1993; Berendse, 1994; Bonanomi et al., 2005; Clark et al., 2005). In a well-known empirical example, Kardol et al. (2006) demonstrated that during secondary succession of abandoned grasslands, directional changes in PSF strength occurred and early-successional plant species mainly experienced negative PSF, while late-successional species primarily experienced positive PSF, which stabilized the plant community composition. This directional sequence of PSF occurrence resulted from nonrandom linkage between plants' above- and below-ground PSF-related traits; early-arriving plant species generally exhibited fast growth rates, but poor defense against pathogens, while late-arriving species were typically slow growing and mycorrhizal-associated species (Kardol et al., 2006, 2007, 2013).

While directional change in PSF strength across plant succession (i.e., from negative to positive PSF) has attracted much attention, empirical evidence supporting other hypotheses has also been reported (e.g., Reynolds et al., 2003; Sikes et al., 2012). A new idea proposed by Fukami and Nakajima (2013) focused on the priority effects generated by PSF, and how different PSF scenarios would influence community trajectories among patches with different immigration histories. Their main conclusion was when PSF operated in a complex manner such that the direction and strength of species' PSF was not determined by its successional stage (e.g., PSF for early-successional species were not necessarily negative), initial species variation among patches would be maintained, and more plant species could colonize a patch and persist longer before local extinction. This results in a long-lasting transient phase characterized by high species turnover (i.e., a large number of local colonization and extinction events) and high regional diversity before reaching the final community structure (Fukami and Nakajima, 2013). Therefore, the model indicated that when PSF occurred idiosyncratically, with a weak correlation between its strength and the species'

successional stage, PSF delayed succession and the speed for local communities to converge to a late successional stage community. The different successional trajectories resulting from different PSF scenarios represented alternative transient states in plant community development, which is defined as communities varying in structure or function before reaching a stable state (Fukami and Nakajima, 2011). A promising direction for future research is to integrate the directional and random-emergence paradigm for changes in PSF during succession, and test predictions for successional trajectories using chronosequences from different ecosystems.

## Linkage Between Mechanistic-PSF Models and the Lotka-Volterra Competition Model

The influence of PSF on plant community dynamics has been incorporated into theoretical ecological modeling, however many of these models are phenomenological and not restricted to specific PSF mechanisms (Table 1). In terms of specific PSF mechanisms, it can be traced back to two fundamental models: microbial- (Bever et al., 1997) and litter-mediated PSF (Berendse, 1994). Here, we reintroduce these two mechanistic-PSF models with more unified formulations. We reanalyzed both models using invasibility analysis (Bever, 2003; Revilla et al., 2013) to show how the final community state can be classified into four possible outcomes, a scenario comparable to the classic Lotka-Volterra competition model. We believe this method provides a systematic way to evaluate PSF models, regardless of the specific topics which they originally focused on.

### Lotka-Volterra Competition Model and Invasibility Analysis for PSF Models

Our analytical framework can first be illustrated by considering the phenomenological Lotka-Volterra competition model for two plant species (with species density represented by  $P_A$  and  $P_B$ , respectively), which is written as follows:

$$\frac{dP_A}{dt} = r_A P_A \left( 1 - \frac{P_A + c_B P_B}{T_P} \right) \quad (1)$$

$$\frac{dP_B}{dt} = r_B P_B \left( 1 - \frac{c_A P_A + P_B}{T_P} \right). \quad (2)$$

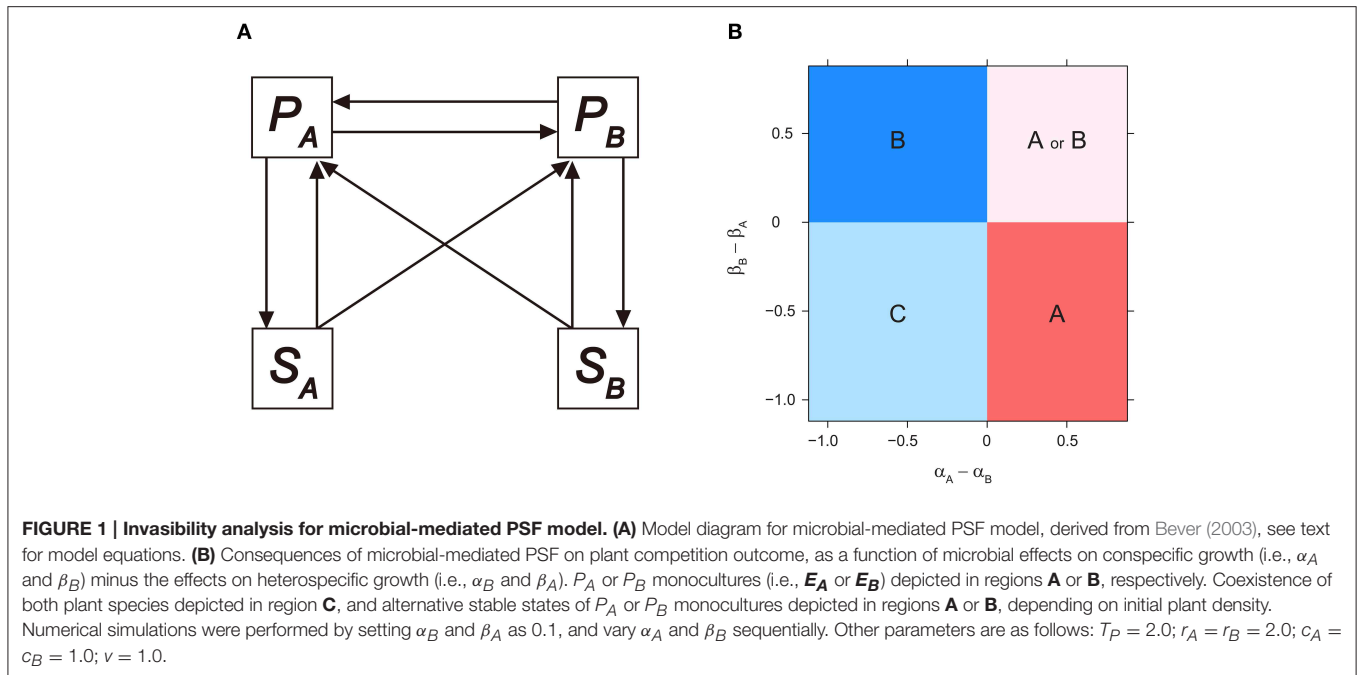
Here,  $r_i$  represents intrinsic population growth rate for plant species  $i$  ( $i = A$  or  $B$ ),  $T_P$  denotes the carrying capacity for plants (for simplicity, we assumed identical parameter values for both species). Coefficient  $c_j$  measures the negative effects of space competition from heterospecies  $j$  relative to the negative density dependent effect of conspecific  $i$  (i.e.,  $j = B$  or  $A$  when  $i = A$  or  $B$ , respectively). If  $c_j = 1$ , species are identical in terms of competition for space (i.e., a neutral case when intra- and interspecific competition have similar magnitudes). The final outcome in Lotka-Volterra type competition can be predicted by applying invasibility analysis. That is, evaluating species' per capita growth rate (i.e., invader fitness) when its density is low while the competitor is at its monoculture equilibrium (Chesson, 2000). When invader fitness is positive, the invasibility criteria is fulfilled

and population size increases (or recovers) from low density. A plant species monoculture occurs when only one species can invade the other. Coexistence is achieved when two plant species are mutually invasive (i.e., each species can invade the habitat dominated by the other species and no species can competitively exclude the other), while founder control (i.e., competition outcome depends on the initial plant density conditions) occurs when both invader species are unable to invade the other. From Equations (1) and (2), the invasibility criterion for  $P_A$  to invade a monoculture of  $P_B$  (i.e.,  $E_B(P_A^* = 0, P_B^* = T_P)$ ) is  $c_B < 1$ , while that for  $P_B$  to invade monoculture of  $P_A$  (i.e.,  $E_A(P_A^* = T_P, P_B^* = 0)$ ) is  $c_A < 1$ . Here,  $E_i$  is the mathematical notation for the plant monoculture equilibrium of  $P_i$ , and  $P_i^*$  within the parenthesis represents the density of  $P_i$  at the specific equilibrium. Therefore, the parameter space of  $c_A$  and  $c_B$  can be partitioned into the following four regions: (i)  $P_A$  monocultures ( $c_B < 1$  but  $c_A > 1$ ); (ii)  $P_B$  monocultures ( $c_B > 1$  but  $c_A < 1$ ); (iii) coexistence (both  $c_B$  and  $c_A < 1$ ); (iv) founder control (i.e., alternative stable state of either  $P_A$  or  $P_B$  monoculture; both  $c_B$  and  $c_A > 1$ ). These results are consistent with those obtained from local stability analysis; coexistence was possible when impacts on heterospecific growth are weaker than those on conspecific growth (i.e.  $c_B$  and  $c_A < 1$ ; Chesson, 2000).

The framework of invasibility analysis can be applied to mechanistic-PSF models. Consider a two plant species (i.e.,  $P_A$  and  $P_B$ ) and two corresponding soil components (e.g., either soil nutrients or microbial communities) that influence plant population dynamics. When the community is at equilibrium for the  $P_A$  monoculture (i.e.  $E_A(P_A^* > 0, P_B^* = 0)$ ), the corresponding soil component is determined by the parameters related to the dominant resident species (in this case  $P_A$ ), but is independent of the invader ( $P_B$ ) parameters. The invasion criterion for  $P_B$  to invade the  $P_A$  monoculture can be derived from its invader fitness. Importantly, this invasibility criterion includes parameters determining how  $P_B$  is affected directly by  $P_A$  and indirectly by  $P_A$ -cultivated soil components, but does not include parameters related to how  $P_B$  affects the soil. The criterion implies that the important invasion determinants are interactions between resident species and resident-cultivated soil. Therefore, by combining mutual invasibility conditions for PSF models, we can categorize the trait parameter space related to  $P_A$ - and  $P_B$ -soil interactions into different consequences of monoculture and/or coexistence.

### Microbial-mediated PSF Models and Invasibility Analyses

Microbial-mediated PSF was first incorporated into the Lotka-Volterra model by Bever et al. (1997) and Bever (2003), and further extended by other studies (Eppinga et al., 2006; Bever et al., 2010; Aguilera, 2011; Kulmatiski et al., 2011; Revilla et al., 2013). Bever's groundbreaking models (Bever et al., 1997; Bever, 2003) captured the bidirectional interaction of PSF; different plant species interacted with the soil microbial community differently and developed a species-specific microbial community association, and changes in microbial communities had differential influences on different plant species (Bever et al., 1997; see Figure 1A for model diagram adapted from



Bever, 2003). The microbial community density specifically associated with  $P_A$  and  $P_B$  was represented by  $N_\alpha$  and  $N_\beta$ , respectively. The dimensionality of the soil microbial community was reduced by focusing on the relative abundance of different soil microbial communities, which were represented by  $S_A = N_\alpha / (N_\alpha + N_\beta)$  and  $S_B = N_\beta / (N_\alpha + N_\beta)$  for  $P_A$ - and  $P_B$ -associated soil microbial communities, respectively (Bever et al., 1997). The model also assumed linear frequency dependency between plants and soil microbial communities (but see Eppinga et al., 2006 and Aguilera, 2011 for a non-linear case). When integrating microbial-mediated PSF in the Lotka-Volterra model, the population dynamics for plants can be written as follows (Bever, 2003):

$$\frac{dP_A}{dt} = r_A P_A \left( 1 + \alpha_A S_A + \beta_A S_B - \frac{P_A + c_B P_B}{T_P} \right) \quad (3)$$

$$\frac{dP_B}{dt} = r_B P_B \left( 1 + \alpha_B S_A + \beta_B S_B - \frac{c_A P_A + P_B}{T_P} \right). \quad (4)$$

The parameters  $\alpha_A$  and  $\alpha_B$  measure how  $S_A$  influences the per-capita growth rate of  $P_A$  and  $P_B$ , respectively, while  $\beta_A$  and  $\beta_B$  measure how  $S_B$  influences the per-capita growth rates of  $P_A$  and  $P_B$ , respectively. The feedback parameters  $\alpha_A$  and  $\beta_B$  denote the effect of microbial community on its associated host and are termed direct (or intraspecific) PSF. Alternatively, the microbial community can affect its associated host by influencing the growth of competing plant species. Such interactions are termed indirect (or interspecific) PSF, and are indicated by  $\alpha_B$  and  $\beta_A$ . The sign and magnitude of these feedback parameters are determined by both plant and microbial traits that influence microbial composition (e.g., detrimental pathogens or beneficial mycorrhiza), and

interaction strength between plants and microbes (e.g., host specificity of microbes) (Bever et al., 1997, 2010; Bever, 2002).

Under the assumption of linear frequency dependency, the sizes of soil microbial communities (i.e.,  $N_\alpha$  and  $N_\beta$ ) were assumed to increase linearly with the relative abundance of its associated host plant as:

$$\frac{dN_\alpha}{dt} = \frac{P_A}{P_A + P_B} \cdot N_\alpha \quad (5)$$

$$\frac{dN_\beta}{dt} = v \frac{P_B}{P_A + P_B} \cdot N_\beta, \quad (6)$$

where  $v$  represents the relative influence of  $P_B$  on the microbial community against that of  $P_A$ . One way to interpret  $v$  is the rate that  $P_B$ , relative to  $P_A$ , converts the microbial community to its specific associated composition (Kulmatiski et al., 2011), which can be determined by plant exudate and microbial response (reviewed in Bais et al., 2006; Bever et al., 2012). Since,  $S_A + S_B = 1$ , the dynamics of relative abundance in different microbial communities can be derived by applying the quotient rule of calculus to Equation (5) as follows:

$$\frac{dS_A}{dt} = S_A (1 - S_A) \left( \frac{P_A}{P_A + P_B} - v \frac{P_B}{P_A + P_B} \right). \quad (7)$$

In regard to plant species composition, monoculture equilibrium of either  $P_A$  or  $P_B$  are derived from Equations (3), (4), and (7) as  $E_A(P_A^* = T_P (1 + \alpha_A), P_B^* = 0)$  and  $E_B(P_A^* = 0, P_B^* = T_P (1 + \beta_B))$ , respectively. The corresponding soil equilibrium states are  $S_A^* = 1$  and  $S_A^* = 0$ , respectively. Based on local stability analysis, Bever et al. (1997) proposed that the community outcome was predicted by the sign of an interaction coefficient,  $I_S$ , which was

defined as  $I_S = \alpha_A - \beta_A - \alpha_B + \beta_B$ . The necessary condition for coexistence to be maintained by PSF was  $I_S < 0$ . In contrast, PSF resulted in a monoculture of either plant species when  $I_S > 0$ . Here, applying a similar invasibility analysis used in Bever (2003) and Revilla et al. (2013), we calculated plant  $P_A$  would invade the  $P_B$  monoculture (i.e.,  $E_B$ ) when:

$$\lim_{P_A \rightarrow +0} \frac{1}{P_A} \frac{dP_A}{dt} \Big|_{E_B} = r_A \left[ 1 + \beta_A - \frac{c_B T_P (1 + \beta_B)}{T_P} \right] > 0. \quad (8)$$

As we were interested in the effects of PSF strength on the invasion criteria, we assume  $c_A = c_B = 1$  (i.e., a neutral case such that the two plants are identical in terms of competition for space). The invasibility criterion for  $P_A$  can be written as  $\beta_B - \beta_A < 0$ . This criterion implies that  $P_A$  can invade  $E_B$  if the dominating  $P_B$ -cultivated soil has less facilitative (or more negative) effects on  $P_B$  compared to that on the invading  $P_A$  (i.e.,  $P_B$ -cultivated soil has a relatively negative effect on  $P_B$  compared to that on  $P_A$ ). On the other hand, plant  $P_B$  can invade the monoculture of  $P_A$  (i.e.,  $E_A$ ) when:

$$\lim_{P_B \rightarrow +0} \frac{1}{P_B} \frac{dP_B}{dt} \Big|_{E_A} = r_B \left[ 1 + \alpha_B - \frac{c_A T_P (1 + \alpha_A)}{T_P} \right] > 0, \quad (9)$$

which gives the invasion criterion as  $\alpha_A - \alpha_B < 0$  when  $c_A = c_B = 1$ . Consequently,  $P_B$  can invade  $E_A$  if the dominant  $P_A$ -cultivated soil has a relatively negative effect on  $P_A$ . Note that these criteria are determined by the sign of direct PSF (i.e.,  $\alpha_A$  and  $\beta_B$ ) minus indirect PSF (i.e.,  $\alpha_B$  and  $\beta_A$ ), and can be interpreted as the differential effect of the cultivated soil on its host compared to the effects on the other plant species. The parameter space of  $\alpha_A - \alpha_B$  and  $\beta_B - \beta_A$  can therefore be partitioned into four regions based on these invasibility criteria (also confirmed by numerical simulations, **Figure 1B**). Coexistence (region C in **Figure 1B**) is possible when both plant species support a microbial community which has stronger facilitative effects on the competitor compared to that on itself, or stronger suppressive effects on itself than on the competitor (i.e., both  $\alpha_A - \alpha_B$  and  $\beta_B - \beta_A < 0$ ). Alternatively, microbial-mediated PSF leads to a plant species monoculture (region A and B in **Figure 1B**) when only one plant cultivates the microbial community to have a positive effect on itself (i.e., only  $\beta_B - \beta_A$  or  $\alpha_A - \alpha_B < 0$  for  $P_A$ - and  $P_B$ -monoculture, respectively). Finally, when both plant species experience positive feedback from its associated microbial community (i.e., both  $\alpha_A - \alpha_B$  and  $\beta_B - \beta_A > 0$ ), the system generates alternative stable state of monoculture of either plant species (region A or B in **Figure 1B**). Note that by relaxing the  $c_A = c_B = 1$  assumption, similar simple boundaries are produced, although the invasion criteria becomes  $\beta_B - \beta_A < 1 - c_B$  for  $P_A$  and  $\alpha_A - \alpha_B < 1 - c_A$  for  $P_B$  (see also Bever, 2003 and Revilla et al., 2013 for model analysis when relaxing this assumption).

We argue that applying the invasibility analysis to Bever's fundamental microbial-mediated PSF model (Bever, 2003) provides a more transparent interpretation of PSF. For example, consider conditions where  $\alpha_A > \alpha_B$  and  $\beta_A > \beta_B$  (i.e.,  $P_A$  has

greater growth advantages compared to  $P_B$ , despite competitive equivalence for space). Dominance of  $P_A$  can be successfully predicted by criteria derived from invasibility analysis, but not by the sign of  $I_S$  (e.g., positive coexistence equilibrium does not exist under some parameter region despite  $I_S < 0$ ). In addition, unlike local stability analysis, which can only pinpoint the local asymptotically stable criteria of the coexistence equilibrium, invasibility analysis relies on species' per capita growth rate when rare (i.e., at low population density) and identifies the criteria for either stable or fluctuating coexistence (Chesson, 2000).

## Litter-mediated PSF Models and Invasibility Analysis

In addition to microbial-mediated PSF, another branch of mechanistic-PSF models focus on plants ability to alter soil biochemical properties through litter-mediated PSF (Binley and Giardina, 1998). Berendse (1994, see also Berendse et al., 1987, 1989) proposed the litter-mediated PSF model, which was further extended by other studies (Miki and Kondoh, 2002; Clark et al., 2005; Miki et al., 2010; Eppinga et al., 2011). A simplified version of the model (**Figure 2A**, modified from Berendse, 1994) incorporates plant growth limitations by soil nutrients and nutrient cycling processes into the Lotka-Volterra model as follows:

$$\frac{dP_A}{dt} = \frac{v_A N}{K_A + N} \left( 1 - \frac{P_A + c_B P_B}{T_P} \right) P_A - m_A P_A \quad (10)$$

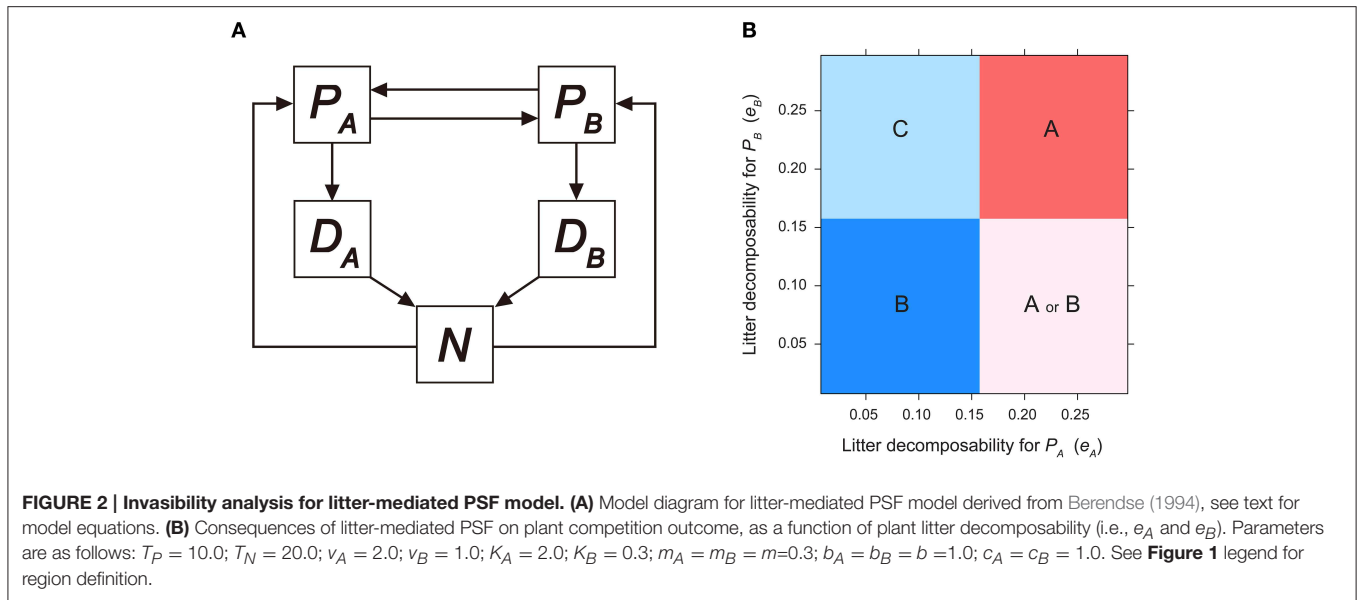
$$\frac{dP_B}{dt} = \frac{v_B N}{K_B + N} \left( 1 - \frac{c_A P_A + P_B}{T_P} \right) P_B - m_B P_B \quad (11)$$

Here,  $v_i$  and  $K_i$  ( $i = A$  or  $B$ ) represent the maximum rate and half-saturation constant for plant species  $i$  ( $i = A$  or  $B$ ) to uptake plant-available nutrients in the soil,  $N$ . The term  $v_i N / (K_i + N)$  in Equations (10) and (11) represent how the per capita growth rate of  $P_i$  is influenced by nutrient availability; the term in the parenthesis denotes growth limitation due to space competition, and the last term represents plant mortality (with species-specific mortality rate,  $m_i$ ). To ensure potential coexistence of plant species, in the following analysis we considered trade-offs between nutrient uptake strategies:  $P_A$  (or  $P_B$ ) tends to be competitively superior with high nutrient (low nutrient) levels (Miki and Kondoh, 2002; Clark et al., 2005). When parameterizing the model, we set  $v_A > v_B$  while  $v_A / K_A < v_B / K_B$ .

Dead plant materials from  $P_A$  and  $P_B$  enter the plant-unavailable litter pool, with nutrient content denoted by  $D_A$  and  $D_B$ , respectively. The amount of nutrient transferred was calculated by the number of dead individuals multiplied by nutrient content per individual,  $b_i$  (i.e., the first term in Equations (12) and (13)).

$$\frac{dD_A}{dt} = b_A m_A P_A - e_A D_A \quad (12)$$

$$\frac{dD_B}{dt} = b_B m_B P_B - e_B D_B \quad (13)$$



$$\frac{dN}{dt} = e_A D_A + e_B D_B - \frac{b_A v_A N}{K_A + N} \left(1 - \frac{P_A + c_B P_B}{T_P}\right) P_A - \frac{b_B v_B N}{K_B + N} \left(1 - \frac{c_A P_A + P_B}{T_P}\right) P_B. \quad (14)$$

$$N_A^* < \frac{K_A v_A - K_B v_B}{v_A - v_B} \equiv \hat{N}, \quad (15)$$

while the condition for  $P_A$  to invade  $E_B$  is calculated as follows:

$$N_B^* > \hat{N}. \quad (16)$$

The second term in Equations (12) and (13) represents nutrient release from biological components through plant litter decomposition, with species-specific decomposition rate,  $e_i$ . For simplicity, it is assumed that litter chemical quality determines its decomposition rate (Cornwell et al., 2008), excluding the role of saprophytic microbes (but see Knops et al., 2002; Miki et al., 2010; Miki, 2012). Mineralized nutrients are returned to the plant-available nutrient pool and taken up by plants for population growth. Under this simple framework, the dynamic system was assumed to be closed, such that  $b_A P_A(t) + b_B P_B(t) + D_A(t) + D_B(t) + N(t) = const. \equiv T_N$ , where  $T_N$  represents the system's total nutrient content (but see Menge et al., 2009 for an opened ecosystem model).

The community outcome of the litter-mediated PSF model can be characterized by combining local stability analysis and

To solve  $N_i^*$  (and corresponding plant litter decomposition rate), which fulfill Equations (15) and (16), we substitute Equations (10–13) into Equation (14) to derive the quadratic equation of  $N_i^*$  for each monoculture equilibrium as follows:

$$f_i(N_i^*) \equiv (e_i v_i) N_i^{*2} + [(e_i + m)(v_i - m) b T_P - e_i v_i T_N] N_i^* + [-K_i b m T_P (e_i + m)] = 0. \quad (17)$$

The above equation has one unique positive root due to the positive quadratic coefficient but negative constant term. The inequality  $f_A(\hat{N}) > 0$  must be satisfied to obtain the  $N_A^*$  fulfilling the invasibility criterion for  $P_B$  (i.e., Equation (15)), resulting in the following:

$$e_A < \frac{m b T_P v_A [(K_A v_B - K_B v_A) - m (K_A - K_B)]}{v_A (K_A v_B - K_B v_A) \left\{ T_N - \left[ (v_A - m) - \frac{(v_A - v_B) K_A m}{(K_A v_B - K_B v_A)} \right] \frac{b T_P}{v_A} - \left[ \frac{K_A v_B - K_B v_A}{v_A - v_B} \right] \right\}} \equiv e_A^*, \quad (18)$$

invasibility analysis. We set  $c_A = c_B = 1$ ,  $m_A = m_B = m$ , and  $b_A = b_B = b$  to examine the effects of litter decomposition rates,  $e_A$  and  $e_B$ . The monoculture equilibrium of plant species  $i$  exhibits the following form:  $E_i (P_i^* = T_P - T_P m (K_i + N_i^*) / (v_i N_i^*), P_j^* = 0)$ , where  $N_i^*$  is the corresponding equilibrium for soil nutrient pool when the system is at monoculture of  $P_i$  ( $i = A$  or  $B$ ). By applying invasibility analysis to the litter-mediated PSF model, we derive that plant  $P_B$  can invade the  $P_A$ -monoculture (i.e.,  $E_A$ ) when:

assuming that  $T_N$  is sufficiently large and  $m < (K_A v_B - K_B v_A) / (K_A - K_B)$ . This indicates when litter decomposition rate of  $P_A$  is sufficiently low, the soil nutrient pool size of  $P_A$ -cultivated soils is not maintained at higher levels, and consequently cannot prevent  $P_B$  invasion (which is assumed to be competitively superior under low soil nutrients). Similarly,  $f_B(N_B^*)$  has a root satisfying Equation (16), and thus  $P_A$  can invade, when  $f_B(\hat{N}) < 0$ . This leads to the following inequality:

$$e_B > \frac{mbT_{PVB} [(K_{AVB} - K_{BVA}) - m(K_A - K_B)]}{v_B (K_{AVB} - K_{BVA}) \left\{ T_N - \left[ (v_B - m) - \frac{(v_A - v_B)K_B m}{(K_{AVB} - K_{BVA})} \right] \frac{bT_P}{v_B} - \left[ \frac{K_{AVB} - K_{BVA}}{v_A - v_B} \right] \right\}} \equiv e_B^*, \quad (19)$$

suggesting that  $P_A$  can invade  $E_B$  when litter decomposition rate of  $P_B$  is sufficiently fast (i.e.,  $e_B > e_B^*$ ). When  $e_B > e_B^*$ , the soil nutrient pool size of  $P_B$ -cultivated soil is maintained at higher levels and provides  $P_A$  a growth advantage during invasion. When the two invasibility criteria are combined, the parameter space of  $e_A$  and  $e_B$  is categorized into four regions (Figure 2B). Coexistence (region C in Figure 2B) is possible when litter produced by  $P_A$  decomposes at a sufficiently slower rate, but litter of  $P_B$  decomposes sufficiently faster (i.e.,  $e_A < e_A^*$ , and  $e_B > e_B^*$ ). Dominance of  $P_A$  (region A in Figure 2B) occurs when  $e_A < e_A^*$ , and dominance of  $P_B$  (region B in Figure 2B) occurs when  $e_B > e_B^*$ . When litter produced by  $P_A$  decomposes at a sufficiently faster rate and  $P_B$  litter decomposes sufficiently slow (i.e.,  $e_A > e_A^*$ , and  $e_B < e_B^*$ ), the system has alternative stable states of either  $E_A$  or  $E_B$ , depending on the initial plant species density (region A or B in Figure 2B).

### The Effectiveness of Invasion Analysis and a Revised PSF Index

Based on invasibility analysis, we derived coexistence criteria for both microbial- and litter-mediated PSF models. Invasiveness of one plant species depends on how the resident-cultivated soil affects the growth of the invader compared to the resident, and the competition outcome is then assessed by the mutual invasion between plant species. Invasion is possible when the resident-cultivated soil microbial community has less positive effect on the resident species (e.g.,  $\alpha_A - \alpha_B < 0$  for microbial-mediated PSF), or when nutrient cycling has reduced benefit for the resident species (e.g.,  $e_A < e_A^*$  for litter-mediated PSF). The rationale for these criteria is consistent with theoretical models, which indicate invasiveness is determined by the growth response of the invader in resident soil (Eppstein and Molofsky, 2007; Turnbull et al., 2010; Suding et al., 2013).

PSF strength for a target plant species is commonly quantified in empirical studies by comparing the growth response of the target plant species in soils cultivated by different species (i.e., a “plant-centered PSF index”). For example, let  $M_{ij}$  represent the growth response of plant species  $i$  in plant species  $j$  soil; the plant-centered PSF index is commonly calculated as  $\log(M_{ii}/M_{ij})$ . The invasibility analysis result provided here, which suggested that the competition outcome depended on how the resident-cultivated soil influenced the invader’s growth compared with that of the resident, indicated the need for a revision of this metric. Based on the analytical results provided in the previous section, we argue the PSF quantified by comparing the competing plant species’ growth responses in the target plant-cultivated soil were a better predictor for competition outcomes (i.e., a “soil-centered PSF index” for plant species  $i$ , calculated as  $\log(M_{ii}/M_{ji})$ ). These soil-centered indices have been used in studies regarding a home-field advantage in litter decomposition (e.g., Ayres et al., 2009;

Milcu and Manning, 2011), but to the best of our knowledge, not yet in empirical PSF studies. Figure 3 provides an illustrative example why the revised metric should be considered. Application of the commonly used PSF metric indicated that PSF for  $P_A$  was negative (i.e.,  $\log(M_{AA}/M_{AB}) < 0$ ), while that for  $P_B$  was positive (i.e.,  $\log(M_{BB}/M_{BA}) > 0$ ), predicting a  $P_B$  monoculture. However, in this example  $P_A$  was outcompeting  $P_B$  in soil environment cultivated by both  $P_A$  and  $P_B$ . The actual competition outcome should be the competitive exclusion of  $P_B$  by  $P_A$ , which can be accurately predicted by the soil-centered PSF index derived from the invasibility analysis (i.e., soil-centered PSF index for  $P_A$  was  $\log(M_{AA}/M_{BA}) > 0$ , while that for  $P_B$  was  $\log(M_{BB}/M_{AB}) < 0$ ). In fact, out of all 24 possible plant growth response outcomes of a two-plant transplant experiment, the traditional plant-centered PSF index only correctly predicted half of the competitive outcomes, while the soil-centered PSF index correctly predicted all outcomes (see Figures S1–S4). However, we noted that when comparing growth response of different plants, biomass should first be normalized against their growth in uncultivated soils lacking plant growth (e.g., field-collected bare soil or autoclaved soils) to examine intrinsic biomass differences between different plant species. This reference soil choice can be critical, and sometimes challenging, however we believe studies can reveal a higher controlling power of PSF on community structure by quantifying PSF strength using a revised PSF index.

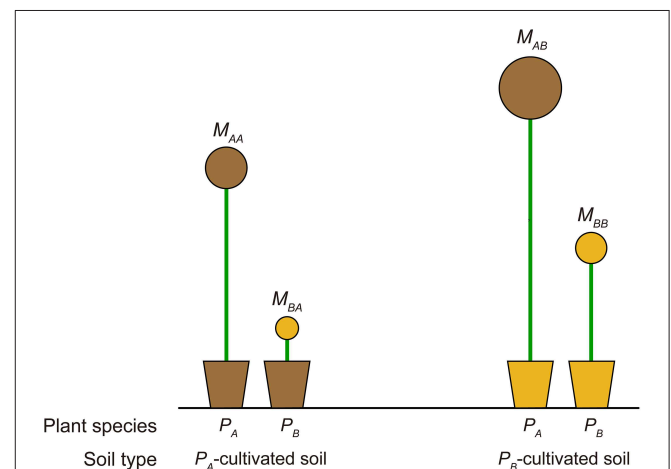


**FIGURE 3 | Schematic diagram for a comparison between a traditional “plant-centered PSF index” and the revised “soil-centered PSF index,” which was an extension of invasibility analysis.**

Plant-centered PSF index for plant species A (i.e.,  $P_A$ ) is calculated as  $\log(M_{AA}/M_{AB})$ , which compares growth response of  $P_A$  in  $P_A$ - and  $P_B$ -cultivated soils. The soil-centered PSF index for  $P_A$  is calculated as  $\log(M_{AA}/M_{BA})$ , which compares the growth response of  $P_A$  and  $P_B$  in  $P_A$ -cultivated soil.  $M_{ij}$  represents the growth response of plant species  $i$  in soil cultivated by plant species  $j$  (see main text).

## Future Directions

### Toward an Integration of Microbial- and Litter-mediated PSF

The majority of PSF modeling papers to date has specifically addressed a single PSF mechanism or were phenomenological studies and did not assume a specific mechanism. The influence of PSF on plant and microbial communities can be better predicted by integrating microbial- and litter-mediated PSF in future research (de Deyn et al., 2004; Manning et al., 2008). Bever et al. (2010) reviewed the role of root-associated microbes in structuring plant resource partitioning, however plant nutrient uptake was not coupled with nutrient cycling in their framework. The role of saprophytic microbes in litter-mediated PSF is an interesting and important starting point to combine the two mechanisms, as microbial decomposers ultimately drive litter decomposition (Knops et al., 2002; Miki et al., 2010; Miki, 2012). The microbial decomposer community has been emphasized during discussions of differential litter decomposition rates at different sites (Ayres et al., 2009; Austin et al., 2014), and predictions of carbon storage in response to climate change (Allison et al., 2010; Wieder and Allison, 2013). However, the effects of decomposer community structure on plant competition outcomes are rarely explicitly discussed within the context of PSF. Recent theoretical studies revealed that community structure of microbial decomposers had critical consequences when predicting plant community structure and their responses to anthropogenic disturbance via litter-mediated PSF (Miki et al., 2010; Miki, 2012). In particular, Miki et al. (2010) demonstrated that functional diversity of microbial decomposers can weaken the positive litter-mediated PSF controlled by plant litter quality, thus facilitating plant coexistence.

Microbial decomposers are engaged in a broad range of interactions, which also provides linkages between litter- and microbial-mediated PSF. For example, in addition to providing nutrients via their active control on litter decomposition, microbial decomposers are directly involved in nutrient competition with plants (i.e., through immobilization). The competition strength depends on the plant's nutrient uptake strategies and litter quality (Daufresne and Loreau, 2001; Schimel and Bennett, 2004; Ushio et al., 2009). Miki et al. (2010) demonstrated these traits therefore influence the outcome of litter-mediated PSF, other than simply altering decomposition rates. Root-associated microbes, which were more commonly discussed in microbial-mediated PSF, might also indirectly influence litter-mediated PSF. For example, the competition between plants and microbial decomposers could be modified when mycorrhizal fungi have the ability to take up organic nutrients. Studies have reported nutrient uptake by ectomycorrhizal and ericoid mycorrhizal fungi, which resulted in decomposer carbon starvation and hence slower litter decomposition rates accompanied by increased soil carbon storage (Read and Perez-Moreno, 2003; Orwin et al., 2011; Averill et al., 2014). In addition to indirect modification of litter decomposition rates, root-associated microbes also altered plant litter input through their effects on plant productivity (Mitchell, 2003; van der Heijden et al., 2008; Orwin et al., 2011; Ke et al.,

2015). In conclusion, the functional composition and community dynamics of microbes can interact with litter-mediated PSF, even when the microbes themselves are not directly engaged in litter decomposition. Our studies support an explicit consideration of the interdependency between the two PSF mechanisms, which can provide new predictions related to both plant and microbial community dynamics.

### Predicting Species' PSF Strength through a Trait-based Ecological Approach

PSF acts as a structuring force in plant and microbial communities, therefore one important task for ecologists is to improve our prediction of species' PSF strength. The trait-based approach is a promising new approach, which has been widely applied to study plant community assembly via aboveground interactions (McGill et al., 2006; de Bello et al., 2010; Adler et al., 2013). Recent studies also applied trait-based approaches to elucidate microbial community assembly and the evolution of microbial life forms (Aguilar-Trigueros et al., 2014; Crowther et al., 2014). However, attempts to apply such approach remain scarce for PSF studies (van der Putten et al., 2013) (but see Baxendale et al., 2014). Ke et al. (2015) employed a trait-based approach to a theoretical PSF study, which assessed the sensitivity of PSF strength to various plant and microbial traits. Results revealed that the relative importance of litter decomposability compared to other plant demographic traits in determining PSF strength changes with the community composition of root-associated microbes. Baxendale et al. (2014) provided the first empirical data that associated PSF with plant foliar traits mentioned by the leaf economic spectrum (Wright et al., 2004). Results suggested that trait-based plant classification was most informative when plants are grown in mixtures (i.e., under interspecific competition), and plants responded positively to nutrient environments cultivated by plants with similar traits. One ultimate goal for trait-based studies is to predict shifts in ecological processes, such as PSF along abiotic gradients (McGill et al., 2006). The above studies suggested some traits might lose their impact along the abiotic gradient, as trait influence was also determined by biotic interactions with other plant and microbial species. We propose that additional studies linking plant and microbial traits to PSF strength or predicting species' PSF under different conditions are warranted.

### Combining PSF with General Coexistence Theory

Empirical and theoretical ecologists have long puzzled over the maintenance mechanisms of plant species coexistence. Chesson (2000) proposed that species coexistence was maintained by a combination of equalizing and stabilizing forces. This can be defined as equalizing forces that minimize differences in species' intrinsic growth rates, while stabilizing forces that limit species' per capita growth rates as species become common (Chesson, 2000; Adler et al., 2007). The establishment of a theoretical link between PSF-driven coexistence and classic coexistence theories is our final suggestion for future PSF research. Under Chesson's (2000) coexistence framework, PSF has been most commonly thought to act as a stabilizing mechanism by generating negative density-dependence (Bell et al., 2006;

Yamazaki et al., 2008; Bagchi et al., 2010, 2014) or nutrient usage differentiation (Clark et al., 2005; Daufresne and Hedin, 2005; Bever et al., 2010). However, PSF can also facilitate plant coexistence through equalizing mechanisms. For example, if the competitive inferior species can form mutualistic associations with beneficial microbes (e.g., mycorrhizal fungi), which act in a density-independent manner, the presence of PSF can decrease fitness differences between competing species. Similar, equalizing examples in pathogens were also thoroughly reviewed (Mordecai, 2011, 2013a). If such equalizing forces of PSF are strong, plant coexistence can be maintained despite weak stabilizing forces by host specific pathogens or resource partitioning (Adler et al., 2007; Bever et al., 2010). The invasibility analysis provided in the present review is a viable starting point, as the invader's long-term low-density growth rate was one most important metric in Chesson's framework (Chesson, 2000). Future theoretical studies can continue separating the equalizing and stabilizing forces in current PSF models, and mechanistically link plant and microbial traits to the two coexistence mechanisms.

In conclusion, PSF research has attracted attention from many empirical ecologists and demonstrated notable success

in using PSF to predict plant community patterns. Theoretical models, based on fundamental mechanistic-PSF models, have also substantially contributed to our knowledge. We believe the integration of multiple PSF mechanisms into the well-developed theoretical framework in ecology, such as stage-structure (e.g., Ke et al., 2015) and metacommunity (e.g., Loeuille and Leibold, 2014) models will produce new insights to understand plant and microbial community structure and dynamics.

## Acknowledgments

The authors thank Tadashi Fukami and Kabir Peay for their useful comments on the manuscript. This study is supported by National Taiwan University and Ministry of Science and Technology of Taiwan (NSC101-2621-B-002-004-MY3).

## Supplementary Material

The Supplementary Material for this article can be found online at: <http://journal.frontiersin.org/article/10.3389/fmicb.2015.01066>

## References

- Adler, F. R., and Muller-Landau, H. C. (2005). When do localized natural enemies increase species richness? *Ecol. Lett.* 8, 438–447. doi: 10.1111/j.1461-0248.2005.00741.x
- Adler, P. B., Fajardo, A., Kleinhesselink, A. R., and Kraft, N. J. B. (2013). Trait-based tests of coexistence mechanisms. *Ecol. Lett.* 16, 1294–1306. doi: 10.1111/ele.12157
- Adler, P. B., HilleRisLambers, J., and Levine, J. M. (2007). A niche for neutrality. *Ecol. Lett.* 10, 95–104. doi: 10.1111/j.1461-0248.2006.00996
- Aguilar-Trigueros, C. A., Powell, J. R., Anderson, I. C., Antonovics, J., and Rillig, M. C. (2014). Ecological understanding of root-infecting fungi using trait-based approaches. *Trends Plant Sci.* 19, 432–438. doi: 10.1016/j.tplants.2014.02.006
- Aguilera, A. G. (2011). The influence of soil community density on plant-soil feedbacks: an important unknown in plant invasion. *Ecol. Model.* 222, 3413–3420. doi: 10.1016/j.ecolmodel.2011.06.018
- Allison, S. D., Wallenstein, M. D., and Bradford, M. A. (2010). Soil-carbon response to warming dependent on microbial physiology. *Nat. Geosci.* 3, 336–340. doi: 10.1038/ngeo846
- Augsburger, C. K. (1983). Seed dispersal of the tropical tree, *Platypodium Elegans*, and the escape of its seedlings from fungal pathogens. *J. Ecol.* 71, 759–771. doi: 10.2307/2259591
- Austin, A. T., Vivanco, L., González-Arzac, A., and Pérez, L. I. (2014). There's no place like home? An exploration of the mechanisms behind plant litter-decomposer affinity in terrestrial ecosystems. *New Phytol.* 204, 307–314. doi: 10.1111/nph.12959
- Averill, C., Turner, B. L., and Finzi, A. C. (2014). Mycorrhiza-mediated competition between plants and decomposers drives soil carbon storage. *Nature* 505, 543–545. doi: 10.1038/nature12901
- Ayres, E., Steltzer, H., Simmons, B. L., Simpson, R. T., Steinweg, J. M., Wallenstein, M. D., et al. (2009). Home-field advantage accelerates leaf litter decomposition in forests. *Soil Biol. Biochem.* 41, 606–610. doi: 10.1016/j.soilbio.2008.12.022
- Bagchi, R., Gallery, R. E., Gripenberg, S., Gurr, S. J., Narayan, L., Addis, C. E., et al. (2014). Pathogens and insect herbivores drive rainforest plant diversity and composition. *Nature* 506, 85–88. doi: 10.1038/nature12911
- Bagchi, R., Swinfield, T., Gallery, R. E., Lewis, O. T., Gripenberg, S., Narayan, L., et al. (2010). Testing the Janzen-Connell mechanism: pathogens cause overcompensating density dependence in a tropical tree. *Ecol. Lett.* 13, 1262–1269. doi: 10.1111/j.1461-0248.2010.01520.x
- Bais, H. P., Weir, T. L., Perry, L. G., Gilroy, S., and Vivanco, J. M. (2006). The role of root exudates in rhizosphere interactions with plants and other organisms. *Annu. Rev. Plant Biol.* 57, 233–266. doi: 10.1146/annurev.arplant.57.032905.105159
- Baxendale, C., Orwin, K. H., Poly, F., Pommier, T., and Bardgett, R. D. (2014). Are plant-soil feedback responses explained by plant traits? *New Phytol.* 204, 408–423. doi: 10.1111/nph.12915
- Beckstead, J., Meyer, S. E., Connolly, B. M., Huck, M. B., and Street, L. E. (2010). Cheatgrass facilitates spillover of a seed bank pathogen onto native grass species. *J. Ecol.* 98, 168–177. doi: 10.1111/j.1365-2745.2009.01599.x
- Beckstead, J., and Parker, I. M. (2003). Invasiveness of *Ammophila arenaria*: release from soil-borne pathogens? *Ecology* 84, 2824–2831. doi: 10.1890/02-0517
- Bell, T., Freckleton, R. P., and Lewis, O. T. (2006). Plant pathogens drive density-dependent seedling mortality in a tropical tree. *Ecol. Lett.* 9, 569–574. doi: 10.1111/j.1461-0248.2006.00905.x
- Berendse, F. (1994). Litter decomposability – a neglected component of plant fitness. *J. Ecol.* 82, 187–190. doi: 10.2307/2261398
- Berendse, F., Bobbink, R., and Rouwenhorst, G. (1989). A comparative study on nutrient cycling in wet heathland ecosystems II. Litter decomposition and nutrient mineralization. *Oecologia* 78, 338–348. doi: 10.1007/BF00379107
- Berendse, F., Oudhof, H., and Bol, J. (1987). A comparative study on nutrient cycling in wet heathland ecosystems I. Litter production and nutrient losses from the plant. *Oecologia* 74, 174–184. doi: 10.1007/BF00379357
- Bever, J. D. (1999). Dynamics within mutualism and the maintenance of diversity?: inference from a model of interguild frequency dependence. *Ecol. Lett.* 2, 52–62. doi: 10.1046/j.1461-0248.1999.21050.x
- Bever, J. D. (2002). Negative feedback within a mutualism: host-specific growth of mycorrhizal fungi reduces plant benefit. *Proc. Biol. Sci.* 269, 2595–2601. doi: 10.1098/rspb.2002.2162
- Bever, J. D. (2003). Soil community feedback and the coexistence of competitors: conceptual frameworks and empirical tests. *New Phytol.* 157, 465–473. doi: 10.1046/j.1469-8137.2003.00714.x
- Bever, J. D., Dickie, I. A., Facelli, E., Facelli, J. M., Klironomos, J., Moora, M., et al. (2010). Rooting theories of plant community ecology in microbial interactions. *Trends Ecol. Evol.* 25, 468–478. doi: 10.1016/j.tree.2010.05.004
- Bever, J. D., Platt, T. G., and Morton, E. R. (2012). Microbial population and community dynamics on plant roots and their feedbacks on plant community. *Annu. Rev. Microbiol.* 66, 265–283. doi: 10.1146/annurev-micro-092611-150107
- Bever, J. D., Westover, K. M., and Antonovics, J. (1997). Incorporating the soil community into plant population dynamics: the utility of the feedback approach. *J. Ecol.* 85, 561–573. doi: 10.2307/2960528

- Binley, D., and Giardina, C. (1998). Why do tree species affect soil? the warp and woof of tree-soil interaction. *Biogeochemistry* 42, 89–106. doi: 10.1023/A:1005948126251
- Bonanomi, G., Antignani, V., Capodilupo, M., and Scala, F. (2010). Identifying the characteristics of organic soil amendments that suppress soilborne plant diseases. *Soil Biol. Biochem.* 42, 136–144. doi: 10.1016/j.soilbio.2009.10.012
- Bonanomi, G., Giannino, F., and Mazzoleni, S. (2005). Negative plant-soil feedback and species coexistence. *Oikos* 111, 311–321. doi: 10.1111/j.0030-1299.2005.13975.x
- Callaway, R. M., Thelen, G. C., Rodriguez, A., and Holben, W. E. (2004). Soil biota and exotic plant invasion. *Nature* 427, 731–733. doi: 10.1038/nature02322
- Cardinale, B. J., Duffy, J. E., Gonzalez, A., Hooper, D. U., Perrings, C., Venail, P., et al. (2012). Biodiversity loss and its impact on humanity. *Nature* 489, 326–326. doi: 10.1038/nature11373
- Chesson, P. (2000). Mechanisms of maintenance of species diversity. *Annu. Rev. Ecol. Syst.* 31, 343–366. doi: 10.1146/annurev.ecolsys.31.1.343
- Clark, B. R., Hartley, S. E., Suding, K. N., and de Mazancourt, C. (2005). The effect of recycling on plant competitive hierarchies. *Am. Nat.* 165, 609–622. doi: 10.1086/430074
- Connell, J. H. (1971). “On the role of natural enemies in preventing competitive exclusion in some marine animals and in rain forest trees,” in *Dynamics of Populations*, eds P. J. den Boer and G. R. Gradwell (Wageningen: Centre for Agricultural Publishing and Documentation), 298–312.
- Cornwell, W. K., Cornelissen, J. H. C., Amatangelo, K., Dorrepaal, E., Eviner, V. T., Godoy, O., et al. (2008). Plant species traits are the predominant control on litter decomposition rates within biomes worldwide. *Ecol. Lett.* 11, 1065–1071. doi: 10.1111/j.1461-0248.2008.01219.x
- Crowther, T. W., Maynard, D. S., Crowther, T. R., Peccia, J., Smith, J. R., and Bradford, M. A. (2014). Untangling the fungal niche: the trait-based approach. *Front. Microbiol.* 5:579. doi: 10.3389/fmicb.2014.00579
- Daufresne, T., and Hedin, L. O. (2005). Plant coexistence depends on ecosystem nutrient cycles: extension of the resource-ratio theory. *Proc. Natl. Acad. Sci. U.S.A.* 102, 9212–9217. doi: 10.1073/pnas.0406427102
- Daufresne, T., and Loreau, M. (2001). Ecological stoichiometry, primary producer-decomposer interactions, and ecosystem persistence. *Ecology* 82, 3069–3082. doi: 10.1890/0012-9658(2001)082[3069:ESPPDI]2.0.CO;2
- de Bello, F., Lavorel, S., Diaz, S., Harrington, R., Cornelissen, J. H. C., Bardgett, R. D., et al. (2010). Towards an assessment of multiple ecosystem processes and services via functional traits. *Biodivers. Conserv.* 19, 2873–2893. doi: 10.1007/s10531-010-9850-9
- de Deyn, G. B., Raaijmakers, C. E., and van der Putten, W. H. (2004). Plant community development is affected by nutrients and soil biota. *J. Ecol.* 824–834. doi: 10.1111/j.0022-0477.2004.00924.x
- Dickie, I. A., Schnitzer, S. A., Reich, P. B., and Hobbie, S. E. (2005). Spatially disjunct effects of co-occurring competition and facilitation. *Ecol. Lett.* 8, 1191–1200. doi: 10.1111/j.1461-0248.2005.00822.x
- Ehrenfeld, J. G., Ravit, B., and Elgersma, K. (2005). Feedback in the plant-soil system. *Annu. Rev. Environ. Resour.* 30, 75–115. doi: 10.1146/annurev.energy.30.050504.144212
- Eppinga, M. B., Kaproth, M. A., Collins, A. R., and Molofsky, J. (2011). Litter feedbacks, evolutionary change and exotic plant invasion. *J. Ecol.* 99, 503–514. doi: 10.1111/j.1365-2745.2010.01781.x
- Eppinga, M. B., Rietkerk, M., Dekker, S. C., and de Ruiter, P. C. (2006). Accumulation of local pathogens: a new hypothesis to explain exotic plant invasion. *Oikos* 114, 168–176. doi: 10.1111/j.2006.0030-1299.14625.x
- Epstein, M. J., Bever, J. D., and Molofsky, J. (2006). Spatio-temporal community dynamics induced by frequency dependent interactions. *Ecol. Modell.* 197, 133–147. doi: 10.1016/j.ecolmodel.2006.02.039
- Epstein, M. J., and Molofsky, J. (2007). Invasiveness in plant communities with feedbacks. *Ecol. Lett.* 10, 253–263. doi: 10.1111/j.1461-0248.2007.01017.x
- Farrer, E. C., and Goldberg, D. E. (2009). Litter drives ecosystem and plant community changes in cattail invasion. *Ecol. Appl.* 19, 398–412. doi: 10.1890/08-0485.1
- Fukami, T., and Nakajima, M. (2011). Community assembly: alternative stable states or alternative transient states? *Ecol. Lett.* 14, 973–984. doi: 10.1111/j.1461-0248.2011.01663.x
- Fukami, T., and Nakajima, M. (2013). Complex plant-soil interactions enhance plant species diversity by delaying community convergence. *J. Ecol.* 101, 316–324. doi: 10.1111/1365-2745.12048
- Fukano, Y., Tachiki, Y., Yahara, T., and Iwasa, Y. (2013). Soil disturbances can suppress the invasion of alien plants under plant-soil feedback. *Ecol. Model.* 260, 42–49. doi: 10.1016/j.ecolmodel.2013.03.022
- Grime, J. P. (1977). Evidence for the existence of three primary strategies in plants and its relevance of ecological and evolutionary theory. *Am. Nat.* 111, 1169–1194. doi: 10.1086/283244
- Hector, A., Schmid, B., Beierkuhnlein, C., Caldeira, M. C., Diemer, M., Dimitrakopoulos, P. G., et al. (1999). Plant diversity and productivity experiments in European grassland. *Science* 286, 1123–1127. doi: 10.1126/science.286.5442.1123
- Hendriks, M., Mommer, L., de Caluwe, H., Smit-tiekstra, A. E., van der Putten, W. H., and de Kroon, H. (2013). Independent variations of plant and soil mixtures reveal soil feedback effects on plant community overyielding. *J. Ecol.* 101, 287–297. doi: 10.1111/1365-2745.12032
- Hendriks, M., Visser, E. J. W., Visschers, I. G. S., Aarts, B. H. J., de Caluwe, H., Smit-Tiekstra, A. E., et al. (2015). Root responses of grassland species to spatial heterogeneity of plant-soil feedback. *Funct. Ecol.* 29, 177–186. doi: 10.1111/1365-2435.12367
- Hsu, S. B., Hubbell, S., and Waltman, P. (1977). A mathematical theory for single-nutrient competition in continuous cultures of micro-organisms. *SIAM J. Appl. Math.* 32, 366–383. doi: 10.1137/0132030
- Hubbell, S. (1997). A unified theory of biogeography and relative species abundance and its application to tropical rain forests and coral reefs. *Coral Reefs* 16, S9–S21. doi: 10.1007/s003380050237
- Inderjit, and van der Putten, W. H. (2010). Impacts of soil microbial communities on exotic plant invasions. *Trends Ecol. Evol.* 25, 512–519. doi: 10.1016/j.tree.2010.06.006
- Janzen, D. H. (1970). Herbivores and the number of tree species in tropical forest. *Am. Nat.* 104, 501–528
- Johnson, D. J., Beaulieu, W. T., Bever, J. D., and Clay, K. (2012). Conspecific negative density dependence and forest diversity. *Science* 336, 904–907. doi: 10.1126/science.1220269
- Jones, C. G., Lawton, J. H., and Schachak, M. (1994). Organisms as ecosystems engineers. *Oikos* 69, 373–386. doi: 10.2307/3545850
- Kardol, P., Bezemer, T. M., and van der Putten, W. H. (2006). Temporal variation in plant-soil feedback controls succession. *Ecol. Lett.* 9, 1080–1088. doi: 10.1111/j.1461-0248.2006.00953.x
- Kardol, P., Cornips, N. J., van Kempen, M. M. L., Bakx-Schotman, J. M. T., and van der Putten, W. H. (2007). Microbe-mediated plant-soil feedback causes historical contingency effects in plant community assembly. *Ecol. Monogr.* 77, 147–162. doi: 10.1890/06-0502
- Kardol, P., De Dyne, G. B., Laliberte, E., Mariotte, P., and Hawkes, C. V. (2013). Biotic plant-soil feedbacks across temporal scales. *J. Ecol.* 101, 309–315. doi: 10.1111/1365-2745.12046
- Ke, P.-J., Miki, T., and Ding, T.-S. (2015). The soil microbial community predicts the importance of plant traits in plant-soil feedback. *New Phytol.* 206, 349–341. doi: 10.1111/nph.13215
- Keane, R. M., and Crawley, M. J. (2002). Exotic plant invasion and the enemy release hypothesis. *Trends Ecol. Evol.* 17, 164–170. doi: 10.1016/S0169-5347(02)02499-0
- Klironomos, J. N. (2002). Feedback with soil biota contributes to plant rarity and invasiveness in communities. *Nature* 417, 67–70. doi: 10.1038/417067a
- Knops, J. M. H., Bradley, K. L., and Wedin, D. A. (2002). Mechanisms of plant species impact on ecosystem nitrogen cycling. *Ecol. Lett.* 5, 454–466. doi: 10.1046/j.1461-0248.2002.00332.x
- Kulmatiski, A., Beard, K. H., and Heavilin, J. (2012). Plant-soil feedbacks provide an additional explanation for diversity-productivity relationships. *Proc. Biol. Sci.* 279, 3020–3026. doi: 10.1098/rspb.2012.0285
- Kulmatiski, A., Heavilin, J., and Beard, K. H. (2011). Testing predictions of a three-species plant-soil feedback model. *J. Ecol.* 99, 542–550. doi: 10.1111/j.1365-2745.2010.01784.x
- Leibold, M. A., Holyoak, M., Mouquet, N., Amarasekare, P., Chase, J. M., Hoopes, M. F., et al. (2004). The metacommunity concept: a framework for multi-scale community ecology. *Ecol. Lett.* 7, 601–613. doi: 10.1111/j.1461-0248.2004.00608.x

- Levine, J. M., Pachepsky, E., Kendall, B. E., Yelenik, S. G., and Lambers, J. H. R. (2006). Plant-soil feedbacks and invasive spread. *Ecol. Lett.* 9, 1005–1014. doi: 10.1111/j.1461-0248.2006.00949.x
- Loeuille, N., and Leibold, M. A. (2014). Effects of local negative feedbacks on the evolution of species within metacommunities. *Ecol. Lett.* 17, 563–573. doi: 10.1111/ele.12258
- Loreau, M., and Hector, A. (2001). Partitioning selection and complementarity in biodiversity experiments. *Nature* 412, 72–76. doi: 10.1038/35083573
- Mack, K. M. L., and Bever, J. D. (2014). Coexistence and relative abundance in plant communities are determined by feedbacks when the scale of feedback and dispersal is local. *J. Ecol.* 102, 1195–1201. doi: 10.1111/1365-2745.12269
- Mangan, S. A., Schnitzer, S. A., Herre, E. A., Mack, K. M. L., Valencia, M. C., Sanchez, E. I., et al. (2010). Negative plant-soil feedback predicts tree-species relative abundance in a tropical forest. *Nature* 466, 752–755. doi: 10.1038/nature09273
- Manning, P., Morrison, S. A., Bonkowski, M., and Bardgett, R. D. (2008). Nitrogen enrichment modifies plant community structure via changes to plant-soil feedback. *Oecologia* 157, 661–673. doi: 10.1007/s00442-008-1104-0
- Maron, J. L., Marler, M., Klironomos, J. N., and Cleveland, C. C. (2011). Soil fungal pathogens and the relationship between plant diversity and productivity. *Ecol. Lett.* 14, 36–41. doi: 10.1111/j.1461-0248.2010.01547.x
- Mazzoleni, S., Bonanomi, G., Giannino, F., Incerti, G., Dekker, S. C., and Rietkerk, M. (2010). Modelling the effects of litter decomposition on tree diversity patterns. *Ecol. Modell.* 221, 2784–2792. doi: 10.1016/j.ecolmodel.2010.08.007
- Mazzoleni, S., Bonanomi, G., Giannino, F., Rietkerk, M., Dekker, S. C., and Zucconi, F. (2007). Is plant biodiversity driven by decomposition processes? An emerging new theory on plant diversity. *Community Ecol.* 8, 103–109. doi: 10.1556/ComEc.8.2007.1.12
- McGill, B. J., Enquist, B. J., Weiher, E., and Westoby, M. (2006). Rebuilding community ecology from functional traits. *Trends Ecol. Evol.* 21, 178–185. doi: 10.1016/j.tree.2006.02.002
- Menge, D. N. L., Pacala, S. W., and Hedin, L. O. (2009). Emergence and maintenance of nutrient limitation over multiple timescales in terrestrial ecosystems. *Am. Nat.* 173, 164–175. doi: 10.1086/595749
- Miki, T. (2009). A new graphical model for untangling complex relationships among environment, biodiversity, and ecosystem functioning. *Ecol. Res.* 24, 937–941. doi: 10.1007/s11284-008-0552-7
- Miki, T. (2012). Microbe-mediated plant-soil feedback and its roles in a changing world. *Ecol. Res.* 27, 509–520. doi: 10.1007/s11284-012-0937-5
- Miki, T., and Kondoh, M. (2002). Feedbacks between nutrient cycling and vegetation predict plant species coexistence and invasion. *Ecol. Lett.* 5, 624–633. doi: 10.1046/j.1461-0248.2002.00347.x
- Miki, T., Ushio, M., Fukui, S., and Kondoh, M. (2010). Functional diversity of microbial decomposers facilitates plant coexistence in a plant-microbe-soil feedback model. *Proc. Nat. Acad. Sci. U.S.A.* 107, 14251–14256. doi: 10.1073/pnas.0914281107
- Milcu, A., and Manning, P. (2011). All size classes of soil fauna and litter quality control the acceleration of litter decay in its home environment. *Oikos* 120, 1366–1370. doi: 10.1111/j.1600-0706.2010.19418.x
- Mitchell, C. E. (2003). Trophic control of grassland production and biomass by pathogens. *Ecol. Lett.* 6, 147–155. doi: 10.1046/j.1461-0248.2003.00408.x
- Mitchell, C. E., Agrawal, A. A., Bever, J. D., Gilbert, G. S., Hufbauer, R. A., Klironomos, J. N., et al. (2006). Biotic interactions and plant invasions. *Ecol. Lett.* 9, 726–740. doi: 10.1111/j.1461-0248.2006.00908.x
- Mitchell, C. E., and Power, A. G. (2003). Release of invasive plants from fungal and viral pathogens. *Nature* 421, 625–627. doi: 10.1038/nature01317
- Molofsky, J., and Bever, J. D. (2002). A novel theory to explain species diversity in landscapes: positive frequency dependence and habitat suitability. *Proc. Biol. Sci.* 269, 2389–2393. doi: 10.1098/rspb.2002.2164
- Molofsky, J., Bever, J. D., and Antonovics, J. (2001). Coexistence under positive frequency dependence. *Proc. Biol. Sci.* 268, 273–277. doi: 10.1098/rspb.2000.1355
- Molofsky, J., Bever, J. D., Antonovics, J., and Newman, T. J. (2002). Negative frequency dependence and the importance of spatial scale. *Ecology* 83, 21–27. doi: 10.2307/2680117
- Mordecai, E. A. (2011). Pathogen impacts on plant communities: unifying theory, concepts, and empirical work. *Ecology* 81, 429–441. doi: 10.1890/10-2241.1
- Mordecai, E. A. (2013a). Consequences of pathogen spillover for cheatgrass-invaded grassland coexistence, competitive exclusion, or priority effects. *Am. Nat.* 181, 737–747. doi: 10.1086/670190
- Mordecai, E. A. (2013b). Despite spillover, a shared pathogen promotes native plant persistence in a cheatgrass-invaded grassland. *Ecology* 94, 2744–2753. doi: 10.1890/13-0086.1
- Mordecai, E. A. (2015). Pathogens impact on plant diversity in variable environments. *Oikos* 124, 414–420. doi: 10.1111/oik.01328
- Orwin, K. H., Kirschbaum, M. U. F., St John, M. G., and Dickie, I. A. (2011). Organic nutrient uptake by mycorrhizal fungi enhances ecosystem carbon storage: a model-based assessment. *Ecol. Lett.* 14, 493–502. doi: 10.1111/j.1461-0248.2011.01611.x
- Packer, A., and Clay, K. (2000). Soil pathogens and spatial patterns of seedling mortality in a temperate tree. *Nature* 404, 278–281. doi: 10.1038/35005072
- Petermann, J. S., Fergus, A. J. F., Turnbull, L. A., and Schmid, B. (2008). Janzen-Connell effects are widespread and strong enough to maintain diversity. *Ecology* 89, 2399–2406. doi: 10.1890/07-2056.1
- Read, D. J., and Perez-Moreno, J. (2003). Mycorrhizas and nutrient cycling in ecosystems - a journey towards relevance? *New Phytol.* 157, 475–492. doi: 10.1046/j.1469-8137.2003.00704
- Reinhart, K. O. (2012). The organization of plant communities: negative plant-soil feedbacks and semiarid grasslands. *Ecology* 93, 2377–2385. doi: 10.1890/12-0486.1
- Reinhart, K. O., and Callaway, R. M. (2006). Soil biota and invasive plants. *New Phytol.* 170, 445–457. doi: 10.1111/j.1469-8137.2006.01715.x
- Reinhart, K. O., Packer, A., van der Putten, W. H., and Clay, K. (2003). Plant-soil biota interactions and spatial distribution of black cherry in its native and invasive ranges. *Ecol. Lett.* 6, 1046–1050. doi: 10.1046/j.1461-0248.2003.00539.x
- Revilla, T. A., Veen, G. F., Eppinga, M. B., and Weissing, F. J. (2013). Plant-soil feedback and the coexistence of competing plants. *Theor. Ecol.* 6, 99–113. doi: 10.1007/s12080-012-0163-3
- Reynolds, H. L., Packer, A., Bever, J. D., and Clay, K. (2003). Grassroot ecology: plant-microbe-soil interactions as drivers of plant community structure and dynamics. *Ecology* 84, 2281–2291. doi: 10.1890/02-0298
- Schimel, J. P., and Bennett, J. (2004). Nitrogen mineralization: challenges of a changing paradigm. *Ecology* 85, 591–602. doi: 10.1890/03-8002
- Schnitzer, S. A., Klironomos, J. N., HilleRisLambers, J., Kinkel, L. L., Reich, P. B., Xiao, K., et al. (2011). Soil microbes drive the classic plant diversity-productivity pattern. *Ecology* 92, 296–303. doi: 10.1890/10-0773.1
- Sedio, B. E., and Ostling, A. M. (2013). How specialised must natural enemies be to facilitate coexistence among plants? *Ecol. Lett.* 16, 995–1003. doi: 10.1111/ele.12130
- Sikes, B. A., Maherali, H., and Klironomos, J. N. (2012). Arbuscular mycorrhizal fungal communities change among three stages of primary sand dune succession but do not alter plant growth. *Oikos* 121, 1791–1800. doi: 10.1111/j.1600-0706.2012.20160.x
- Suding, K. N., Harpole, W. S., Fukami, T., Kulmatiski, A., Macdougall, A. S., Stein, C., et al. (2013). Consequences of plant-soil feedbacks in invasion. *J. Ecol.* 101, 298–308. doi: 10.1111/1365-2745.12057
- Swamy, V., and Terborgh, J. W. (2010). Distance-responsive natural enemies strongly influence seedling establishment patterns of multiple species in an Amazonian rain forest. *J. Ecol.* 98, 1096–1107. doi: 10.1111/j.1365-2745.2010.01686.x
- Tansley, A. G. (1935). The use and abuse of vegetational concepts and terms. *Ecology* 16, 284–307.
- Tilman, D. (1982). *Resource Competition and Community Structure*. Princeton, NJ: Princeton University Press.
- Tilman, D. (1994). Competition and biodiversity in spatially structured habitats. *Ecology* 75, 2–16. doi: 10.2307/1939377
- Tilman, D., Mattson, M., and Langer, S. (1981). Competition and nutrient kinetics along a temperature gradient: an experimental test of a mechanistic approach to niche theory. *Limnol. Oceanogr.* 26, 1020–1033. doi: 10.4319/lo.1981.26.6.1020
- Turnbull, L. A., Levine, J. M., Fergus, A. J. F., and Petermann, J. S. (2010). Species diversity reduces invasion success in pathogen-regulated communities. *Oikos* 119, 1040–1046. doi: 10.1111/j.1600-0706.2009.17914.x

- Umbanhowar, J., and McCann, K. (2005). Simple rules for the coexistence and competitive dominance of plants mediated by mycorrhizal fungi. *Ecol. Lett.* 8, 247–252. doi: 10.1111/j.1461-0248.2004.00714.x
- Ushio, M., Miki, T., and Kitayama, K. (2009). Phenolic control of plant nitrogen acquisition through the inhibition of soil microbial decomposition processes: a plant-microbe competition model. *Microbes Environ.* 24, 180–187. doi: 10.1264/jsme2.ME09107
- van der Heijden, M. G. A., Bardgett, R. D., and van Straalen, N. M. (2008). The unseen majority: soil microbes as drivers of plant diversity and productivity in terrestrial ecosystems. *Ecol. Lett.* 11, 296–310. doi: 10.1111/j.1461-0248.2007.01139.x
- van der Putten, W. H., Bardgett, R. D., Bever, J. D., Bezemer, T. M., Casper, B. B., Fukami, T., et al. (2013). Plant-soil feedbacks: the past, the present and future challenges. *J. Ecol.* 101, 265–276. doi: 10.1111/1365-2745.12054
- van der Putten, W. H., van Dijk, C., and Peters, B. A. M. (1993). Plant-specific soil-borne diseases contribute to succession in foredune vegetation. *Nature* 362, 53–56. doi: 10.1038/362053a0
- Wieder, W. R., and Allison, S. D. (2013). Global soil carbon projections are improved by modelling microbial processes. *Nature Clim. Change* 3, 909–912. doi: 10.1038/NCLIMATE1951
- Wright, I. J., Reich, P. B., Westoby, M., Ackerly, D. D., Baruch, Z., Bongers, F., et al. (2004). The worldwide leaf economics spectrum. *Nature* 428, 821–827. doi: 10.1038/nature02403
- Yamazaki, M., Iwamoto, S., and Seiwa, K. (2008). Distance- and density-dependent seedling mortality caused by several diseases in eight tree species co-occurring in a temperate forest. *Plant Ecol.* 201, 181–196. doi: 10.1007/s11258-008-9531-x
- Zee, P. C., and Fukami, T. (2015). Complex organism-environment feedback buffer species diversity against habitat fragmentation. *Ecography* 38, 1–10. doi: 10.1111/ecog.01027

**Conflict of Interest Statement:** The authors declare that the research was conducted in the absence of any commercial or financial relationships that could be construed as a potential conflict of interest.

Copyright © 2015 Ke and Miki. This is an open-access article distributed under the terms of the Creative Commons Attribution License (CC BY). The use, distribution or reproduction in other forums is permitted, provided the original author(s) or licensor are credited and that the original publication in this journal is cited, in accordance with accepted academic practice. No use, distribution or reproduction is permitted which does not comply with these terms.

